# Stress-Corrosion Cracking in High Strength Steels and in Titanium and Aluminum Alloys

Editor
B. F. Brown
*Physical Metallurgy Branch*
*Metallurgy Division*
*Naval Research Laboratory*

NRL Problem Order-278

1972

377 p.




NAVAL RESEARCH LABORATORY
Washington, D.C.

Sponsored by the Advanced Research Projects Agency
ARPA Order No. 878

Library of Congress Catalog Card Number: 72-600053

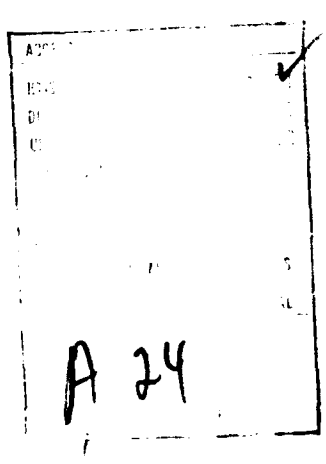


For sale by the Superintendent of Documents, U.S. Government Printing Office
Washington, D.C. 20402 - Price $3.25
Stock Number 0851-0058

# PREFACE

Stress corrosion cracking (SCC) of high strength structural alloys was one which caused numerous serious problems throughout the Department of Defense (DOD) and DOD-related NASA programs during the 1960's. Partly because of these problems, there has been a decade of unusually high research activity in the SCC field, leading to numerous conferences in which research investigators reported the results of their studies, largely for the benefit of other research investigators. Thus, we now have available a number of conference proceedings particularly useful to SCC specialists. These proceedings are not only predominantly aimed for the SCC specialist, but in addition, concentrate on basic aspects, which is indeed entirely appropriate.

The first chapter is intended to place the problem in perspective and thereby make the succeeding chapters easier for the readers and also shorter by omitting much of the material which is common to the three alloy families treated in this monograph. The second chapter treats specimens and test methods, but only those specimens provided with a preexisting crack. The reason for this seemingly one-sided presentation, all but ignoring the non-precracked specimen, is that stress analyses for smooth specimens are commonly available, whereas the stress analyses for cracked bodies (fracture mechanics) are not so widely available. Chapters 3, 4, and 5 treat each of the three high strength structural alloy families in turn. The treatment of the three families differs greatly from one to another. Part of the difference is of course a reflection of the different authors. But more importantly there are enormous differences between the status of SCC technology and of physical metallurgy of the three families. SCC has been studied far longer and more extensively in aluminum alloys than for steels or titanium alloys. Once SCC was recognized as a serious problem in some titanium alloys, a relatively higher proportion of the effort was devoted to physical metallurgy than was the case with steels and aluminum alloys. For this reason and because much of the modern physical metallurgy of titanium alloys has not diffused widely throughout the technical community and is not available in collected form, the authors of the chapter on titanium have included a much higher proportion of physical metallurgy tutorial material. A certain amount of repetition from one chapter to another has been deliberately retained on the supposition that some readers may read only one or two chapters of greatest interest, and that therefore some important thoughts if given only once would be missed.

The present monograph devotes a much smaller proportion of space to theories than do other contemporary volumes on the same subject. One reason for this is that three recent symposia were aimed exclusively at basic aspects of the problem, and there is no need to repeat here the essence of proceedings which are widely available. A second reason for emphasis upon macroscopic data rather than on theory is that theory has not arrived at the point where it can be used to predict the macroscopic SCC behavior of fundamentally new combinations of alloy and environment. This is not to say that theory is not important, nor does it imply a lesser need for developments in theory in the future. On the contrary, even before theory achieves the status of being able to have macroscopic predictive capability, it is useful in organizing what would otherwise be a vast heap of jumbled observations. But for a very long time, sound macroscopic experimental data will have to be used to avoid ugly SCC surprises in new systems. Hence the emphasis in this monograph on macroscopic test methods and the data they produce.

This monograph has been prepared not as a scientific treatise for the seasoned specialist in the field but rather primarily for the program manager's staff, the designer's staff, the materials engineer, and the newcomer to the field of SCC. Since the preparation of the monograph was supported by the Advanced Projects Research Agency of the DOD, the reader of first concern is the staff engineer of the DOD or the DOD contractor. Accordingly, the engineering data are given largely in the units most familiar to U.S. engineers, that is, stress and strength are given in pounds per square inch (psi) or thousands of pounds per square inch (ksi), stress intensities are given in ksi $\sqrt{\text{in.}}$, commercial heat-treating temperatures are commonly given in degrees Fahrenheit, whereas laboratory research temperatures are given in degrees Celsius, and some temperatures are given on both scales. The reason for this policy was again determined from a consideration of the reader interest. Although the engineer customarily sees commercial heat-treating specifications written in the Fahrenheit scale, the laboratory investigator commonly controls and records on the Celsius scale. It thus does not seem undesirably inconsistent to report the properties of a material having a commercial aging treatment at 1000°F tested in boiling magnesium chloride at 154°C.

The matter of referencing is a compromise. Inserting the names of investigators into the text interferes with the readability by the engineer, and so the attribution common in research literature is eschewed. For the benefit of the research investigator, most of the statements of fact are referenced instead by numbers only. It is characteristic of the subject and the times that many of the references are reports of contract research work supported by the Federal Government. Even the existence of many of these documents may not be widely known, and in many cases they were retained in the editing process partly on the basis of providing archive information, to help prevent the loss of research findings particularly during the period of greatly decreased research activity which may lie ahead.



I would like to record here my appreciation for the work of the other authors, some of whom made their final revisions under very difficult circumstances; for the work of R. Anastasio and B. Test who did much of the typing; to S. Curry, the production editor; to W. Ramey and I. Rudin for much advice and for physically producing the book; and to the following persons who reviewed manuscripts or provided other guidance: F. Beck, H. Bomberger, W. Boyd, R. Davis, N. Feige, M. Fontana, H. Gegel, S. Goldberg, R. Huber, G. Irwin, J. Kies, S. Ketcham, J. Krafft, J. Kruger, M. Levy, B. Lifka, H. Markus, D. Meyn, J. Mulherin, H. Paxton, E. Pugh, R. Raring, S. Rolfe, H. Rosenthal, D. Sprowls, D. Schlain, R. Schmidt, J. Scully, J. Sedriks, J. Srawley, D. van Rooyen, R. Wei, B. Wilde, and J. Williams.

B. F. BROWN

*Naval Research Laboratory*
*Washington, D. C.*

# CONTENTS

# Chapter 1

# FUNDAMENTALS

**B. F. Brown**
*Naval Research Laboratory*

**CONTENTS**

# 1. FUNDAMENTALS

## 1.1 Historical Background

Stress corrosion cracking (SCC) is a cracking process caused by the conjoint action of stress and a corrodent. The phenomenon first became of widespread technological importance in the last half of the 19th century with the adoption of the cold-drawn brass cartridge case, followed by the use of brass for condenser tubes in the rapidly growing electric power industry. During this period the phenomenon we now call SCC was termed "season cracking" because of the resemblance between stress-corrosion cracks and cracks in seasoned wood.

In 1886 a cold-drawn wire of a gold alloy containing silver and copper was shown to be susceptible to SCC in ferric chloride, thus demonstrating that the phenomenon was not confined to brass or even to base metals and drawing attention to the important role of tensile stress to the process [1]. By the end of the 19th century the role of residual stress in the SCC of brass was so widely recognized that an acidified mercurous nitrate solution, which causes liquid metal cracking of cold-worked brass, was in common use to test whether a given annealing treatment was adequate to relieve the residual stresses in cold-formed products. Also toward the end of the 19th century, "caustic cracking" (SCC) was observed in unalloyed boiler steel. In the first two decades of the 20th century SCC was reported in aluminum alloys and in high strength steel (in the latter as quench cracks). During the 1930's SCC was reported in austenitic stainless steels and in magnesium alloys. During the 1950's and 1960's SCC was reported in titanium alloys, and in 1970 in a zirconium alloy.

Thus SCC, once thought confined to a few systems (combinations of metals and environments), must now be regarded as a general phenomenon which any alloy family may experience, given the wrong combination of heat treatment and environment.

## 1.2 Characteristics of SCC

The following characteristics are common to most if not all SCC:

1. *Tensile* stress is a necessary condition, which may be provided either by cold work and stored as residual stress or by externally applied service stress. In

some systems the stress may be supplied entirely by the wedging action of corrosion products [2].

2. The alloy is usually almost inert to the environment which causes cracking. This characteristic was pointed out in an early discussion of SCC in mild steel pans used to evaporate sodium chloride and sodium nitrate solutions: "The action upon the steel is totally different in the case of the different solutions. You may go to a waste heap and pick out the pieces of steel that have come from a sodium chloride pan and those that have come from a sodium nitrate pan. Those that have come from a sodium chloride pan are all rusty, the steel rusted through, while those from the sodium nitrate pan are not rusted at all, but they are cracked" [3]. An important exception to this characteristic is low alloy high strength steel, which may experience general rusting at the same time it is cracking.

3. Only certain combinations of alloys and environments produce SCC, though this specificity is less general than is sometimes stated. The specificity of ammonia for cracking brass is often cited as an example. But brass will also crack in sulphur dioxide, in mercury, and in some organic liquids.

4. The necessary corrodent species need not be present either in large quantities or in high concentrations in the bulk environment to produce its effect. Again, brass, for example, can be cracked by ammonia concentrations in air too low to be detected by smell. SCC in austenitic stainless steels can be caused by chloride concentrations of a few parts per million in the bulk water phase, though a local chloride concentrating process may be active. In fact, *localized* concentrations of specific anions to produce in the active sites environments greatly different from the *bulk* environment is so common that it may be recognized as a separate characteristic of SCC. Thus in steels, titanium alloys, and aluminum alloys undergoing SCC in neutral or even alkaline seawater or salt water, the corrodent within the cracks is distinctly acid. Also, the corrodent within stress corrosion cracks in magnesium alloys is distinctly alkaline, and the corrodent within caustic embrittlement cracks in boiler steel is highly alkaline, in both cases differing markedly from the bulk environment.

5. Stress corrosion cracks are brittle in macroscopic appearance even though the metal may behave in a highly ductile manner in a purely mechanical fracture test. Despite their brittle macroscopic appearance, the fracture surfaces may however show evidence of considerable plastic flow on a micron scale.

6. Metallographically the stress corrosion fracture mode is usually much different from the purely mechanical plane strain ("brittle fracture") separation mode of the same metal. It was once considered that multiple branching of stress corrosion cracks was so characteristic as to be diagnostic of SCC. But it is now known that multiple branching does not always occur in SCC, as will be discussed later in this chapter.

7. There appears to be a threshold stress or stress intensity below which SCC does not occur, at least in most systems. The existence of such a threshold has

never been universally accepted. The subject is of immense practical and theoretical importance, and it is beset by complexities and difficulties, also discussed in a subsequent section of this chapter.

8. SCC does not occur in pure metals, though there may be a few technologically unimportant exceptions to this generalization.

## 1.3 Sequence of Events in SCC

SCC is a nucleation and growth process. If a metal does not have a preexisting crack or other flaw in the surface, and if it is covered by an oxide film, the sequence of events in SCC is as shown in Fig. 1. First, the oxide film is ruptured either mechanically or by the action of a chemical species, such as the chloride ion. This film rupture represents the initiation of pitting, which itself is a nucleation and growth process. The primary function of the corrosion in initiating SCC was once thought to be to provide stress concentration, and emphasis was accordingly placed on the shape and the size of the pits. Deep conical pits were said to be more serious than shallow, saucer-shaped ones.

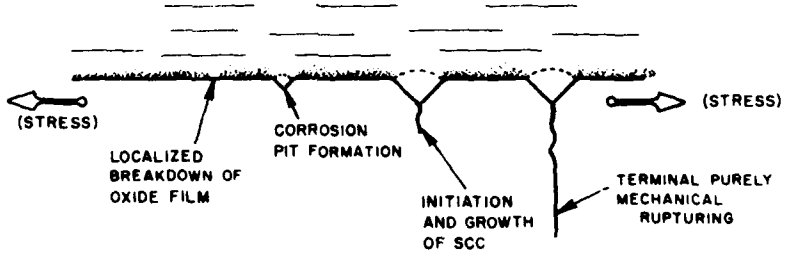


Fig. 1. Sequence of events (left to right) in a stress corrosion test on an initially smooth specimen. For low alloy steels in seawater, the rate of growth of stress corrosion cracking is faster than it is for pitting by a factor of about $10^6$, and fast fracture propagates at about $10^{10}$ times faster than stress corrosion cracking.

It has long been known that the composition of the corrodent within growing corrosion pits can differ markedly from that of the surrounding bulk corrodent, due to hydrolysis reactions producing changes in pH within the pits [4]. The porous corrosion-product cap over the pit restricts the interchange between the local environment within the pit and the bulk environment outside it. Work in recent years has demonstrated that the composition of the corrodent within growing stress corrosion cracks can also differ sharply from that of the bulk environment outside the crack, and indeed for a given system there is a great

deal of similarity between the solution within corrosion pits and that within stress-corrosion cracks. There is probably a causal relationship between the pH within the corrosion pit and the nucleation of a stress-corrosion crack, and the primary function of pitting, in those cases in which it is required to initiate SCC, is not mechanical but chemical—to permit establishment of a local environment conducive to cracking. Thus if a smooth specimen of austenitic stainless steel is stressed in (neutral) boiling NaCl, SCC does not commence until after pitting has occurred. But the same steel stressed in boiling $MgCl_2$, which is slightly acid, may commence cracking with little or no discernible pitting, presumably because now the bulk environment is conducive to cracking without requiring hydrolytic modification. Likewise SCC may commence in a high alloy high strength steel in neutral salt water at a preexisting fatigue crack, or, on an unnotched or uncracked surface, cracking will initiate immediately if the pH has been lowered locally by the addition of acid.

Referring again to Fig. 1, when the stress-corrosion crack has attained a sufficient length and if the stress has not been relaxed, we see that the critical combination of stress and crack length are met for unstable (purely mechanical "brittle fracture") crack extension, and the remaining ligament separates at a high rate—approximately one-third the speed of sound. Just how long the stress-corrosion crack grows before the onset of fast fracture depends upon the magnitude of the stress and the fracture toughness of the alloy. The chemical environment has no effect on this terminal fast fracture process.

The kinetics of the various processes shown in Fig. 1 are given schematically by curve A of Fig. 2. If the metal were somewhat more brittle, the kinetics might be represented by curve B. A very brittle material, such as the hot-work die steel designated H-11 heat treated to maximum hardness, might be represented by curve C, which shows fast fracture being initiated by a corrosion pit, with no SCC at all. The behavior of a material which does not pit (such as titanium in unheated seawater) would be represented by a line coincident with the abscissa, designated D in Fig. 2. If one measured only undifferentiated time to failure, the characterizations of the four materials of Fig. 2 would be as shown on the line above the graph. The time-to-failure order-of-merit rating would then be D (best), A, B, and C (poorest). Actually, the SCC characteristics of C and D have not been measured at all, and the true SCC order of merit of A and B is opposite to that inferred from time-to-failure data alone. Thus undifferentiated time-to-failure data can be highly misleading, particularly in high strength alloys where the brittle fracture termination of SCC can make important differences in the total time to failure.

### 1.4 Smooth and Precracked Specimens

Mechanistic studies over the past quarter-century have contributed some new ideas, but these contributions have been of limited utility in the formulation of

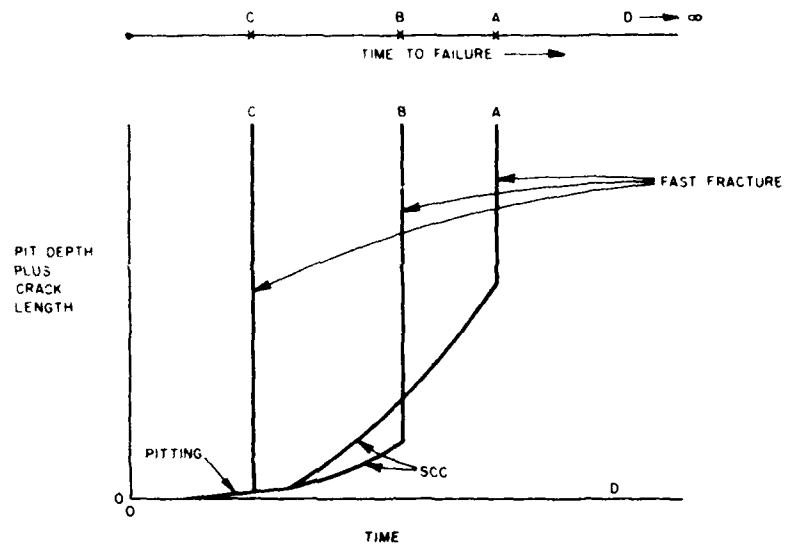


Fig. 2. Kinetics for pitting (or, in *D*, nonpitting), SCC (materials *A* and *B* only), and fast fracture (lower plot). Line at top shows how misleading time-to-failure data can be.

new alloys more resistant to SCC or to the design of structures and the selection of materials to avoid the SCC problem. Although one continues to hope for more guidance for the engineer from future fundamental studies, until that hope is fulfilled he will have to rely upon prior experience. That prior experience can be provided by structures in service, or it can be provided by laboratory tests *if* the laboratory tests adequately model real-life service. Hence, the emphasis in this monograph is upon macroscopic test methods and the information they have contributed.

A smooth specimen models a structure perfect in design and in fabrication, just as a precracked specimen models a structure with the worst kind of imperfection. All structures would therefore be expected to behave in service in a manner lying within the extremes modeled by the two types of specimens. This line of reasoning would indicate that there is justification for employing both specimens to establish the SCC characteristics of a given material under the two limiting conditions. There are two principal reasons for including the precracked specimen for characterizing the SCC properties of many materials. (a) Certain alloys, particularly titanium alloys, do not pit in fresh water or in seawater at room temperature, and a smooth specimen of such alloys does not experience SCC in these environments. One might tend to draw the inference of lack of susceptibility from such experiments. But a notched or precracked

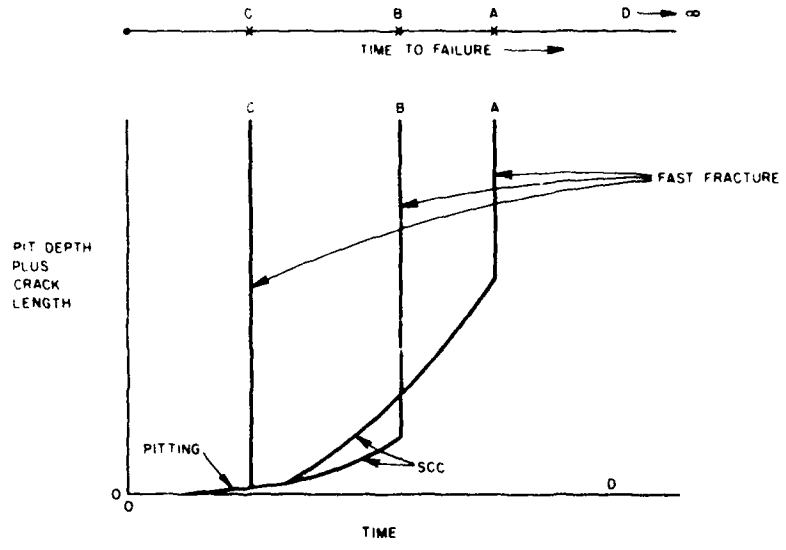


Fig. 2. Kinetics for pitting (or, in *D*, nonpitting), SCC (materials *A* and *B* only), and fast fracture (lower plot). Line at top shows how misleading time-to-failure data can be.

new alloys more resistant to SCC or to the design of structures and the selection of materials to avoid the SCC problem. Although one continues to hope for more guidance for the engineer from future fundamental studies, until that hope is fulfilled he will have to rely upon prior experience. That prior experience can be provided by structures in service, or it can be provided by laboratory tests *if* the laboratory tests adequately model real-life service. Hence, the emphasis in this monograph is upon macroscopic test methods and the information they have contributed.

A smooth specimen models a structure perfect in design and in fabrication, just as a precracked specimen models a structure with the worst kind of imperfection. All structures would therefore be expected to behave in service in a manner lying within the extremes modeled by the two types of specimens. This line of reasoning would indicate that there is justification for employing both specimens to establish the SCC characteristics of a given material under the two limiting conditions. There are two principal reasons for including the precracked specimen for characterizing the SCC properties of many materials. (a) Certain alloys, particularly titanium alloys, do not pit in fresh water or in seawater at room temperature, and a smooth specimen of such alloys does not experience SCC in these environments. One might tend to draw the inference of lack of susceptibility from such experiments. But a notched or precracked

specimen of the same titanium alloy which resisted pitting may display spectacular susceptibility to SCC. (b) Most of the important structural alloys have some degree of susceptibility to SCC in seawater, fresh water, atmospheric moisture, or other reasonably common environments, and it is not possible to label some of them "immune" and therefore acceptable without further consideration and to label the others "susceptible" and therefore to be rejected. For this gray area we need to quantify the resistance to SCC, and it will be shown that the use of a precracked specimen permits just such quantification. There is a further value of the precracked specimen, and that is that the precrack renders unnecessary the waiting period for the development of a corrosion pit, thereby saving most of the time which otherwise would be required for the initiation stage. For alloy steels this pitting stage may require half a year or more in seawater.

In the absence of a corrosion pit or of a stress corrosion crack or other surface discontinuity, classical stress analyses are of course available and valid for smooth bend beams, tensile bars, and other smooth geometries. After a stress corrosion crack commences to grow, however, or if the specimen is provided with a fatigue precrack, classical stress analysis cannot handle the situation. One attempt to treat stress at the root of a crack is to report the *nominal* membrane stress at the crack tip as if the material already cracked had been removed; that is, as if the bar were uncracked but simply thinner than originally (see Fig. 3). Such an approach equates a deep crack in a thick plate to a shallow crack in a thinner plate and equates both to an unblemished plate slightly thinner still. It should be obvious that such an "analysis" is seriously defective, and in fact it has been so demonstrated experimentally [5]. If one is therefore to quantify stress in the presence of a crack, as is needed to describe the effect of the stress factor on the SCC process, it is necessary to find an alternative to the nominal stress method. Fortunately such an analysis is available in the form of linear elastic fracture mechanics.

Since fracture mechanics can treat the stress field around a single crack, if one is employing fracture mechanics in a stress corrosion test it is customary to start with a preexisting crack so disposed as to be analyzable. This crack is commonly

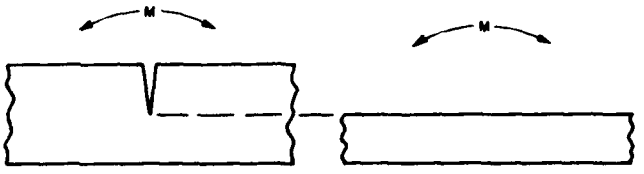


Fig. 3. Nominal stress in the presence of a crack is equivalent to replacing cracked body by a smooth body (at right) having the same depth as the unbroken ligament, obviously a defective "analysis."

produced by fatiguing a specimen containing a sharply machined groove. An alternative method suitable for the high strength aluminum alloys is described in the chapter on aluminum.

## 1.5 The Role of Fracture Mechanics

The stress at any point in the elastic region near a crack tip can be expressed by field equations containing a scaling factor $K$ [6]. This factor, the stress intensity factor, pertains to conditions of linear elastic behavior and not directly to the plastic conditions known to prevail at the site of crack extension. The value and pertinence of the factor $K$ to SCC lies in the fact that the undefined stress and strain conditions at the crack tip are caused by the elastic field quantified by $K$. Therefore if a given level of $K$ in the elastic region is found to cause a specific event, such as stress corrosion crack extension, in the plasticized crack-tip region, then any combination of geometry of solid, geometry of crack, and stress which duplicates the given level of $K$ will produce a duplication of the same crack extension if the material and the environment are the same. Thus the function of $K$ is to quantify the stress in a manner that is relatable to other geometries of body and of crack. In an infinite plate having a crack length $2a$ normal to a tensile stress field having a value of $\sigma$ remote from the crack ($K = \sigma\sqrt{\pi a}$), $K$ then has the units of stress multiplied by the square root of length. It is commonly expressed as ksi $\sqrt{\text{in.}}$ The expressions for $K$ in small bodies suitable for laboratory test specimens are discussed at length in Chapter 2.

Thus, fracture mechanics does not by itself alone provide independent new knowledge about SCC; it simply provides a usable method for treating the stress factor in the presence of a crack.

In *general*, the effect of $K$ on SCC kinetics is as shown in Fig. 4 [7]. The log crack growth is approximately linearly proportional to $K$, as denoted by region I of the figure. At higher $K$ levels some transport process becomes saturated and the crack growth rate is independent of $K$, as indicated by the horizontal segment labeled region II. At still higher $K$ levels there may be another $K$-dependent region, labeled III in Fig. 4. Region III or even both II and III may be missing in certain combinations of metals and environments if the fracture toughness is so low that fast fracture occurs at levels of $K$ lower than the onset of region III or of region II. (The $K$ level which causes fast fracture is designated $K_c$ or $K_{Ic}$, the $c$ referring to the critical value of $K$ for causing mechanical fracture.) Region I may also be missing due to an abrupt cessation of SCC as the $K$ level is lowered in region II.

In region I the plane of the growing crack tends to remain normal to the tensile axis. Any budding side branch of that crack at an angle to the original crack plane would experience a lower $K$ value and hence would have its stress field relieved by the main crack which would go shooting forward with the

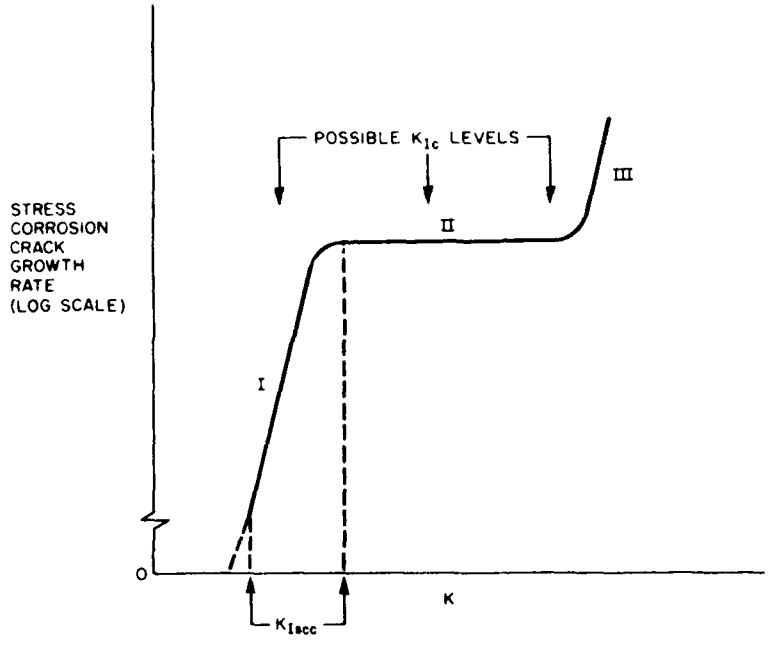


Fig. 4. Generalized SCC kinetics. Fast fracture at one of the points marked $K_{Ic}$ may preclude development of region III or of II and III. There may be a true threshold $K_{Iscc}$ or the kinetics may simply decrease continuously to ever smaller but finite values as $K$ is decreased, denoted by broken line prolongation of region I (after Ref. 7).

kinetic advantages expressed by the *log* crack growth rate vs $K$ in region I. But well out in region II a side branch would not experience a crack rate penalty because of its lower $K$, and hence one sees crack branching in this region. The crack division or branching which occurs in region II must be one of the reasons that multiple branching is often cited as a characteristic of SCC. Another reason for this citing is probably the early observations of SCC in cold-formed articles, in which the residual stress patterns were complex.

There appears to be a threshold value of $K$ below which SCC stops altogether for some metals. This is almost certainly true for titanium alloys, it appears to be true for high strength steels, but it does not appear to be true for aluminum alloys, as is discussed in Chapter 5.

The question of the existence of a true threshold is of such obvious practical and theoretical importance that the newcomer might wonder why the question is not settled almost as the first order of business. The reason is that to prove the existence of a threshold one must prove that below a certain level there is zero

crack growth, and proving negatives is often difficult. In this particular case one would want to be able to say that below the stress threshold (if one exists) a crack will not extend further no matter how sensitive the measuring technique and no matter how magnified the sensitivity by virtue of length of observation. The practical approach seems to be to provisionally accept the existence of a threshold for titanium alloys and high strength steels in natural waters unless and until a better method to quantify SCC resistance is needed and available. For aluminum alloys the $K$ level for some arbitrary but slow rate of growth would seem to be a practical way of characterizing their SCC resistance.

The threshold above which SCC has been observed but below which it has not been observed is designated $K_{Iscc}$. This symbol was derived by inserting the initial letters of stress corrosion in the symbol for the critical $K$ for plane strain mechanical fracture $K_{Ic}$. The Roman number I designates the opening mode of fracture (as in the opening of a book), distinguished from the sliding mode, for example. The numeral is superfluous in SCC because SCC occurs *only* by mode I. There is no stress corrosion analog of the shear lip, although mechanical shear lips may form as borders to a stress corrosion crack.

The corrosion scientist would like to have the full kinetic curve of $K$ vs the crack growth rate. The engineer can seldom justify obtaining the full curve, for rarely does he know either the initial algebraic sum of residual and applied stress or this same sum during the course of stress corrosion crack propagation in a large or complex structure. Hence he is more likely to settle for a simple $K_{Iscc}$ if it exists in a given system.

If one accepts a threshold designated $K_{Iscc}$ or adopts an arbitrary $K_A$ (the $K$ level for an arbitrary crack growth rate in region I of Fig. 4), one can do some useful arithmetic with the Irwin equation for the stress intensity around a crack in the surface of a metal:

$$K^2 \approx \frac{1.2\pi\sigma^2 a}{\varphi^2 - 0.212\left(\frac{\sigma}{\sigma_y}\right)^2}, \tag{1}$$

where $a$ is the depth of the crack, $\sigma$ is the stress, $\sigma_y$ is the yield strength, and $\varphi$ is a factor for the shape of the crack. If the length of the crack is $2b$, then $\varphi^2$ has the values for various crack shapes listed in Table 1. If one assumes a long, thin flaw and the existence of yield-point stress, then from Eq. (1) stress corrosion would be expected to propagate if the flaw depth exceeded $a_{cr}$, given by

$$a_{cr} = 0.2\left(\frac{K_{Iscc}}{\sigma_Y}\right)^2. \tag{2}$$

The value of $a_{cr}$ may thus be regarded as a figure of merit which incorporates both the SCC resistance $K_{Iscc}$ and the contribution which yield strength stress levels can make to SCC hazard by virtue of residual or fit-up stresses.

**Table 1.** Values of $\varphi^2$

| $\frac{a}{b}$ | | $\varphi^2$ |
|---|---|---|
| 0 | (very long, thin crack) | 1.00 |
| 0.25 | | 1.14 |
| 0.5 | | 1.46 |
| 0.75 | | 1.89 |
| 1.0 | (semicircular) | 2.46 |

One can plot Eq. (2) for various values of $a_{cr}$ as shown in Fig. 5. This plot is a convenient framework for displaying the SCC characteristics of materials. If a given material was found to have a $K_{Iscc}$ as indicated by point $x$, a surface crack 0.1 in. deep would be deeper than required to propagate a stress corrosion crack in the same environment used to determine the $K_{Iscc}$. But a crack 0.01 in. deep would not propagate a stress corrosion crack in the same material in the same environment.

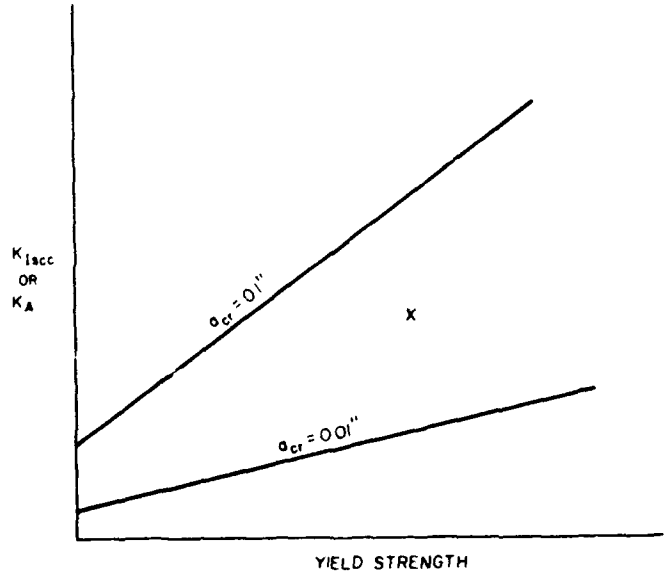


Fig. 5. Plot of Eq. (1) for two assumed values of $a_{cr}$, assuming long surface flaws and yield strength stresses operating. A material having a $K_{Iscc}$ value as indicated by $x$ would be safe from SCC in the pertinent environment if one can be sure surface flaws will be no deeper than 0.01 in.; SCC will occur if they are as deep as 0.1 in.

A plot of $K_{Iscc}$ data such as Fig. 5 can be used in a slightly different way: If one knows that he cannot detect and remove cracklike flaws less than, say, 0.01 in. deep, then if he has yield-point stresses he must select a material having a $K_{Iscc}$ above the 0.01 in. line in Fig. 5.

There are three aspects of the use of fracture mechanics in SCC where confusion is evident from statements made in the literature or at technical conferences. One of these statements might be worded as follows: "Fracture mechanics cannot be used for low strength alloys such as austenitic stainless steels because enormous specimens would be required." This statement is an incorrect inference from the requirements for purely mechanical plane strain fracture toughness. Indeed fracture mechanics would not be useful for the evaluation of mechanical brittleness in such materials because general yielding throughout any reasonable specimen prior to fracturing would invalidate the fracture mechanics analysis based on elasticity theory. SCC on the other hand occurs in austenitic stainless steel at such low stress levels that elastic fracture mechanics is applicable. The second statement, also incorrect, might be worded, "Since SCC involves a certain amount of localized plasticity, an analysis based on elastic theory (such as liner elastic fracture mechanics) is inapplicable." But there is also (even more) localized plasticity in purely mechanical fractures under circumstances in which fracture mechanics has been demonstrated as valid and useful by demonstrating predictive capabilities from one geometry to another. *This observation is not surprising* if one realizes that the *plastic* behavior in SCC is *related* to the elastic stress field which causes the plastic processes, even if we are at present unable to define precisely and in detail that relationship. Of course if there are important time-dependent plastic processes (e.g., creep), then the character of the plastic region will not be uniquely relatable to the elastic stress field. This point is one reason that, with some metals such as titanium alloys, the sequence of stressing a precracked specimen and introducing a reactive environment can make important differences in the measured value of $K_{Iscc}$. The third current but incorrect statement relating to fracture mechanics might be worded, "Corrosion reduced the fracture toughness." The confusion stems from the use of $K$ units to quantify resistance to plane strain fracture ($K_{Ic}$) and resistance to SCC ($K_{Iscc}$), wherein $K_{Iscc}$ is always less than $K_{Ic}$. No one has demonstrated any effect of chemical environment on $K_{Ic}$. Rather than lowering $K_{Ic}$, corrosion simply promotes a different fracture process (SCC) at a lower $K$ level. From such reasoning it becomes clear that phrases such as "seawater embrittlement" and "salt water fracture toughness" are confused expressions more properly phrased as SCC.

## 1.6 Environments

Much emphasis has been placed in the literature on the *specificity* of the chemical species which will cause SCC in a given alloy. This assertion of

specificity is not supported by the facts. Each of the three alloy families treated in this monograph has experienced SCC in more than one environment. Most of the data reported herein came from tests in either salt water or tap water. Both of these environments contain both hydrogen and chlorine, and indeed these two elements are so ubiquitous (inside the metal, even) that one could make a case for a causative role of whichever element he chose. Regardless of the fundamentals involved, moisture and salt water are so ubiquitous that SCC characteristics of alloys in these environments are of interest for the purposes of this monograph in addition to any special environment a given structure may experience.

It must be emphasized that a parameter like $K_{Iscc}$ or $K_A$ refers to a specific material in a specific condition of heat treatment and sometimes in a specific orientation, in a specific environment. Unfortunately a given environment may be altered by hydrolytic action within a crevice or other occluded area, and this alteration in local corrodent chemistry may produce radical changes in SCC characteristics. This is particularly true of stainless steels, in the crevices of which seawater having a bulk pH of 8.2 may be converted by hydrolytic acidification to a solution of pH less than 2 [8].

The crack provides the worst case for SCC from the standpoint of mechanics. There does not appear to be a universal worst case from the standpoint of the environment. Salt water acidified by acetic acid and saturated with $H_2S$ might be a worst-case environment for high strength steel, but it has not assumed the role in SCC studies of high strength steels that boiling $MgCl_2$ has for the austenitic stainless steels.

The theory of SCC is in such a primitive state of development that we do not have a predictive capability with respect to what SCC response a new environment will promote for a given alloy, and therefore we must resort to experimental characterization for each new environment. In fact, the $K_{Iscc}$ values for a titanium alloy used to fabricate fuel cell tankages were used to accept or reject batches of the fluids used in the tankages.

### 1.7 Mechanisms

In the early 1920's the postulate of an amorphous cement holding the grain boundaries of polycrystalline aggregates dominated physical metallurgy in Great Britain, and since SCC in both brass and mild steels is largely intergranular, it is not surprising that this "cement" (long since discredited) figured prominently in many explanations which were adduced for SCC during that era. A multitude of theories, models, and partial models has been proposed in succeeding years. The detailed mechanisms which have been put forward for various metal/corrodent systems can be grouped into the following categories:

1. Mechano-electrochemical. It has been proposed that there were paths intrinsically susceptible to anodic electrochemical dissolution, and the role of

the stress was considered to be to open the cracks enough to prevent stifling the reaction by corrosion products [9]. Whatever the role of mechanical stress may be, that role is not the effect of elastic stresses on the reversible electrode potential, which changes only about $10^{-3}$ mV from zero stress to the yield strength stress levels. A passive surface on stainless steel in boiling 42% $MgCl_2$ may be as much as 500 mV more electropositive than the bare alloy, and one can imagine bare steel being exposed by the yielding at a crack root under stress and the cracking of the oxide coating. If the bare metal is dissolved electrolytically, one can estimate the magnitude of the current required to account for the observed crack growth rates. The current density is estimated to be about one ampere per square centimeter, which would be expected to stifle the reaction by polarizing the anodic area. It has been shown, however, that under conditions of continuous yielding the polarization may be very small, perhaps due to the increase in number of active sites caused by the egress of dislocations [10].

2. *Film Rupture.* In the film rupture model, a brittle corrosion-product film is envisioned to form, which, when it becomes sufficiently thick, fractures to expose bare metal; the bare metal reacts to re-form the brittle film, and the cycle repeats. Such models have been based largely upon striation markings observed with the electron microscope. Evidence of this sort is possibly explained by other models, such as for example the rupture of a thick film well *behind* the advancing crack front but still in a location where there is a significant bending moment on the crack surface.

3. Embrittlement. A periodic electrochemical-mechanical cycle has been postulated in which the electrochemical corrosion process was pictured as embrittling the metal directly behind the corroding metal surface by an unspecified species [11]. The embrittled layer would ultimately fracture mechanically, exposing a fresh metal surface. A modified version of this model is not an unreasonable one for high strength steels in aqueous environments. It is known from measurements of local pH (pH near the crack tip) and potential that the thermodynamic conditions for hydrogen discharge are met if a stress corrosion crack is propagating in high strength steels. It is also known that these steels exhibit slow crack growth under stress if they contain hydrogen from any source. Thus it is not unreasonable to postulate that in these steels SCC occurs by corrosion-generated hydrogen cracking.

4. Adsorption. The adsorption model pictures the reduction of the energy required to form a new surface by reducing the surface energy through the adsorption of specific species [12].

The interested reader may find these models discussed in various degrees of detail elsewhere [13-19]. From time to time someone feels the urge to find a *general*, or universal, model for SCC in all systems. At a symposium in 1921, the proposal that there should be such a general model evoked the following response: "I agree with . . . that a general explanation of season cracking and

intercrystalline cracking in all metallic materials is desirable, but is it not possible that such a universal explanation is not to be found?" [20]. Currently there is growing doubt that a single detailed mechanism will ever be found to account for all manifestations of the phenomenon of SCC, though something like "activation by plastic straining at the advancing crack tip" covers the essence of most of the proposed detailed mechanisms.

The engineer new to the subject may reasonably expostulate that, "All I want is enough theory to predict which combinations of alloys and environments will cause trouble." Alas, he will not find that amount of theory in this monograph. Or elsewhere, for that matter, for it simply does not exist. At the present time all guidance for avoiding SCC in practical structures is based either on past experience with structures of the same metal in the same environment or on macroscopic tests. Hence the emphasis on *valid* test methods. This emphasis is especially important at this time because a fundamentally new philosophy of testing has emerged in recent years, concentrating upon the stress conditions for stress corrosion crack growth (and, importantly, nongrowth) from a preexisting crack.

The status of the theory of SCC is actually not far behind that of the theory of corrosion in general. It is becoming increasingly easy to *explain* observations even if only in a general way, but it is still difficult to *predict* behavior in systems which differ appreciably from those of past experience. Sometimes it is even difficult to predict behavior in systems differing only slightly from those of past experience. Who, for example, would have predicted that 1% HF added to fuming nitric acid would inhibit the SCC of martensitic stainless steel in that environment? But it did!

SCC is controlled by the metallurgy of the solid body, the chemistry of the pertinent environment, and the stress field; in other words, by effects of metallurgy, chemistry, and mechanics. Whether one is concerned with basic mechanisms or engineering applications, work with SCC requires due attention to all three factors.

## 1.8 SCC Characterization of Alloys

Much of the material presented in Chapters 3 through 5 describes the SCC characteristics of various alloys. This is not handbook material, but rather is information presented to display how good and how poor the SCC characteristics of various alloys, largely commercial ones, can be. For critical applications for a long time to come it will be prudent to conduct tests on individual lots of alloys, except for the few cases in which adequate standardization of composition and heat treatment has been achieved, such as in the more common aluminum alloys. Because of this apparent lengthy future need for continued testing, Chapter 2 is a detailed account of various specimen types and testing

procedures using precracked specimens. The methodology of SCC testing using smooth specimens is widely understood and needs no repetition here. Although the *justification* for smooth-specimen testing has already been cited, little smooth-specimen work is quoted in Chapters 3 through 5 because the reported parameter is almost always undifferentiated time to failure, the deficiencies of which have already been pointed out.

## 1.9 References


1. W. C. Roberts-Austen, *Proc. Roy. Inst. Gt. Britain*, **II**, 395 (1886).
2. N. A. Nielsen, *Physical Metallurgy of Stress Corrosion Fracture* (T. N. Rhodin, ed.), Wiley Interscience, New York, 1959, p. 121.
3. A. W. Porter, *Trans. Faraday Soc.* **17**, 150 (1921).
4. T. P. Hoar, *Trans. Faraday Soc.* **33**, 1152 (1937).
5. S. R. Novak and S. T. Rolfe, *Corrosion* **26**, 121 (1970).
6. American Society for Testing and Materials, *Fracture Toughness Testing and Its Applications*, STP 381, Philadelphia, Pa., 1965.
7. R. P. Wei et al., "Steels," in *ARPA Coupling Program on Stress Corrosion Cracking: (Seventh Quarterly Report)*, NRL Memorandum Report 1941, Naval Research Laboratory, Washington, D.C., Oct. 1968, p. 49.
8. M. H. Peterson, T. J. Lennox, Jr., and R. E. Groover, *Proc. 25th NACE Conf.*, Natl. Assoc. Corrosion Eng., Houston, Texas, 1970, 314-317.
9. E. H. Dix, *Trans. AIME* **137**, 11 (1940).
10. T. P. Hoar and J. M. West, *Proc. Roy. Soc.* **268**, 304 (1962).
11. F. H. Keating, *Symposium on Internal Stresses in Metals and Alloys*, Institute of Metals, London, 1948, p. 311.
12. E. G. Coleman et al., *Acta Met.* **9**, 491 (1961).
13. R. W. Staehle, A. J. Forty, and D. Van Rooyen, eds., *Proceedings of International Conference on Fundamental Aspects of Stress-Corrosion Cracking*, Nat. Assoc. Corrosion Eng., Houston, Texas, 1969.
14. H. L. Logan, *The Stress Corrosion of Metals*, Wiley, New York, 1966.
15. R. N. Parkins, "Stress Corrosion Cracking," *Met. Reviews* **9**, 201 (1964).
16. T. N. Rhodin, ed., *The Physical Metallurgy of Stress Corrosion Fracture*, Interscience, New York and London, 1959.
17. E. N. Pugh, et al., *Interfaces Conference Proceedings*, Melbourne, 1969, Butterworth's, London, 1969, 237.
18. J. C. Scully, ed., *The Theory of Stress Corrosion Cracking in Alloys*, Proceedings of a Research Evaluation Conference, published 1971 by NATO Science Affairs Division, Brussels.
19. W. D. Robertson, ed., *Stress Corrosion Cracking and Embrittlement*, Wiley, New York, 1956.
20. N. Moore, *Trans. Faraday Soc.* **17** 59 (1921).
21. B. F. Brown, *J. Materials* **5**, 786 (1970).

# Chapter 2

# STRESS CORROSION TESTING WITH PRECRACKED SPECIMENS

CONTENTS

# 2. STRESS CORROSION TESTING WITH PRECRACKED SPECIMENS

## 2.1 Introduction

Precracking an otherwise smooth specimen in preparation for stress corrosion testing

- Eliminates the uncertainties associated with growth of a corrosion pit.
- Provides a flaw geometry for which a stress analysis is available through fracture mechanics.
- Produces stress corrosion data that are potentially more useful for predicting the behavior of large structural components for which fracture is a critical design factor.

Expressing stress corrosion characteristics in terms of fracture mechanics provides a relationship between applied stress, crack length, and crack growth in aggressive environments. Expressing stress corrosion crack velocity in terms of fracture mechanics will aid in developing the inspection intervals necessary to avoid the catastrophic failure of components.

The significance of such data has not been fully established with respect to structural design, since it is often difficult to analyze accurately the size and distribution of stresses in components of complex geometry. However, this method offers a significant adjunct to alternative test methods employing smooth specimens. Used together, they help to overcome deficiencies in either method and prevent errors in the assessment of alloy/corrodent compatibility.

Several reviews of methods for measuring susceptibility to SCC with smooth specimens are available [1,2]. In addition, a number of task groups under ASTM Subcommittee G01.06 are now preparing recommended practices for use with the more widely employed smooth stress corrosion test specimens [3].

Specimens suitable for studying the fracture mechanics of SCC were developed originally to evaluate the resistance of high strength metallic materials to unstable opening mode crack extension. Surveys of the analytical and experimental bases for determining the plane-strain fracture toughness of metallic materials have been presented [4,5], and a recommended practice for fracture-toughness testing has been formulated [6]. The present review is concerned with specimens for use with test methods that characterize stable (subcritical) crack extension in aggressive environments rather than unstable (critical) cracking. Since practices

are based essentially on conducting a fracture test in the presence of a corrodent, the form of this review follows closely that of the texts on fracture. Two recent reports [7,8] on the application of fracture mechanics to stress corrosion testing have also contributed.

This chapter describes in detail the configurations and calibrations of precracked specimens that are suitable for use in stress corrosion testing. Limited but adequate development is given the derivation of $K_I$, the stress intensity factor for opening mode. Wherever possible, equations for $K_I$ are presented in the form $K_I = \sigma_g \sqrt{a} Y$, where $\sigma_g$ is the applied gross stress, $a$ is the crack length, and $Y$ is a polynomial factor that accounts for specimen design. In many instances, several equations for $K_I$ are included with the individual specimen configurations; however, only one form is generally recommended. To aid in visualizing the change in $K_I$ with respect to $a$ or a function of $a$, these relationships are presented graphically in many cases. Specimen preparation and testing, presentation of data, and general information about precautions and suggestions from investigators in the field of testing are discussed.

## 2.2 Glossary of Terms

| | |
|---|---|
| $a$ | crack length, in. |
| $da/dt$ | crack velocity, in./hr. |
| $a_0$ | starting crack length, in. |
| $B$ | specimen or plate thickness, in. |
| $B_n$ | specimen thickness measured between face grooves, in. |
| $C$ | compliance, in./lb. |
| $C_1, C_2, C_3, C_n$ | polynomial constants |
| $c$ | half-length of a surface flaw, in. |
| $c_0$ | beginning half-length of a surface flaw, in. |
| $D$ | major diameter of a circumferentially notched specimen, in. |
| $d$ | minor diameter of a circumferentially notched specimen, in. |
| $d_0$ | height of the crackline-loaded, single-edge-cracked plate specimen before deflection, in. |
| $d_1$ | average height of the specimen after deflection or mechanical pop-in, in. |
| $d_2$ | average height of the specimen at the end of the test period and after removal of the bolts, in. |
| $e$ | imaginary dimension of the tapered, crackline-loaded, single-edge-cracked specimen, in. |
| $E$ | tensile modulus of elasticity, psi |
| $F$ | Airy stress function |
| $f\left(\frac{a}{W}\right)$ | mathematical function of $a/W$ |

| | |
|---|---|
| $F\left(\frac{d}{D}\right)$ | mathematical function of $d/D$ |
| $g\left(\frac{B}{H}\right)$ | mathematical function of $B/H$ |
| $\mathcal{G}$ | strain-energy release rate, general, in.-lb/in.$^2$ |
| $\mathcal{G}_1$ | strain-energy release rate, opening mode, in.-lb/in.$^2$ |
| $G$ | shear modulus, psi |
| $g\left(\frac{a}{W}\right)$ | mathematical function of $(a/W)$ |
| $H$ | specimen height, in. |
| $h\left(\frac{B}{H}\right)$ | mathematical function of $B/H$ |
| $H_m$ | moment distance of a torsion-loaded specimen, in. |
| $H_a$ or $H_p$ | height of a tapered, crack-line-loaded, single-edge-cracked specimen measured at the load line, in. |
| $K$ | stress intensity factor, general, ksi $\sqrt{\text{in.}}$ |
| $K_I$ | stress intensity factor, opening mode, ksi $\sqrt{\text{in.}}$ |
| $K_{Ii}$ | initially applied stress intensity factor, ksi $\sqrt{\text{in.}}$ |
| $K_{Ic}$ | plane-strain fracture toughness, ksi $\sqrt{\text{in.}}$ |
| $K_a$ | elastic stress-concentration factor |
| $K_{Iscc}$ | stress corrosion cracking threshold stress intensity factor, ksi $\sqrt{\text{in.}}$ |
| $M$ | bending moment, in.-lb |
| $m$ | spring constant |
| $M_e$ | free surface correction factor |
| $M_p$ | plasticity correction factor |
| $n$ | general exponent |
| $P$ | load, lb |
| $Q$ | function of the elliptical integral |
| $m$ | strain-hardening coefficient |
| $r$ | radial coordinate measured from the crack tip, in. |
| $S$ | major span of a bend load fixture, in. |
| $s$ | minor span of a bend load fixture, in. |
| $u$ | $x$-direction crack-opening displacement, in. |
| $v$ | $y$-direction crack-opening displacement, in. |
| $W$ | width, in. |
| $x, y, z$ | Cartesian coordinate axes |
| $y$ | normal deflection of a torsion-loaded specimen, in. |
| $z$ | distance $(a + r)$ along the crack plane, in.; complex variable $x + iy$ |
| $\delta$ | deflection, in. |
| $\theta$ | angular coordinate at the crack tip, radians |

| | |
|---|---|
| $A$ | a slope coefficient derived for the tapered, crackline-loaded, single-edge-cracked specimen |
| $\mu$ | Poisson's ratio |
| $\rho$ | root radius of an ellipse, in. |
| $\sigma_0$ | maximum uniaxial tensile stress, ksi |
| $\sigma_{max}$ | maximum local stress, ksi |
| $\sigma_a$ | applied stress, ksi |
| $\sigma_g$ | gross section stress, ksi |
| $\sigma_n$ | net section stress, ksi |
| $\sigma_y$ | $y$-direction stress, ksi |
| $\sigma_{ys}$ | yield strength, ksi |
| $\phi$ | elliptical integral |

## 2.3 Review of Fracture Mechanics

Intensification of the stress field near the tip of a crack in a linear elastic medium can be characterized by the single parameter $K$. If the displacement of the crack surfaces is that of the opening mode (as opposed to the sliding mode) the subscript I is included in the stress intensity factor. Two methods are available for determining the opening mode stress intensity factor $K_I$; one method is based on stress analysis, and the other is based on the determination of specimen compliance.

### Derivation of $K_I$ by Stress Analysis

**Stress Analysis of a Notch.** If a crack is idealized as an infinitely sharp notch, $K_I$ is given by

$$K_I = \lim_{\rho \to 0} \frac{\sigma_{max}}{2} \sqrt{\pi \rho} \tag{1}$$

where $\sigma_{max}$ is the maximum local normal stress and $\rho$ is the root radius of the notch [9]. If the notch is contained in a panel of infinite dimensions, the expression for $\sigma_{max}$ is contained in the elastic stress-concentration factor $K_\sigma$ as

$$K_\sigma = \frac{\sigma_{max}}{\sigma_a} \tag{2}$$

where $\sigma_a$ is applied stress. In the particular case of an elliptical flaw in which the length of the major axis is $2a$,

$$K_\sigma = 1 + 2\sqrt{\frac{a}{\rho}}. \tag{3}$$

By combining Eqs. (1), (2), and (3), it can be shown that

$$K_I = \sigma_a \sqrt{\pi a} \tag{4}$$

in the limit as $\rho$ approaches zero.

A review of elastic stress-concentration factors for a number of notch problems is contained in Ref. 9.

**Stress Analysis of a Crack.** Expressions that distribute the normal stress $\sigma_y$ in the region of the crack tip can be subjected to a limiting process similar to that performed in the notch analysis to provide a solution for $K_I$. These expressions are found using elastic theory and an appropriate stress function $F$ that must satisfy equilibrium equations as well as the boundary conditions of the problem. Then $\sigma_y$ is given by the second partial derivative of $F$ with respect to $x$. This approach was used to provide the analysis of a cracked infinite panel [10] analogous to that of the notched panel described above. The normal stress obtained was

$$\sigma_y = \frac{\sigma}{\sqrt{1 - \left(\frac{a}{z}\right)^2}} = \frac{\sigma z}{\sqrt{z^2 - a^2}} \tag{5}$$

where $a$ is the half crack length, $z$ is the complex variable $x + iy$, and also equals $(a + r)$ along the crack plane. (See Fig. 1.) When $y = 0$, Eq. (5) can be written

$$\sigma_y = \frac{\sigma (a + r)}{\sqrt{(a + r)^2 - a^2}} . \tag{6}$$

Equation (5) and a number of other stress solutions for crack problems were examined [11], and it was deduced that $K_I$ was contained in the limiting case as $r$ approached zero, so that

$$K_I = \lim_{r \to 0} \sigma_y \sqrt{2\pi r} . \tag{7}$$

Combining Eqs. (6) and (7) shows that for the cracked panel in question,

$$K_I = \sigma_a \sqrt{\pi a} . \tag{8}$$

**Stress Analysis from Finite Elements.** The solutions for $K_I$ for notches and cracks are exact in the limit as $r$ or $\rho$ approaches zero. However, when structural shapes are more complicated, it is often not possible to obtain an exact solution, in which case a numerical technique that yields an approximate solution is avail-

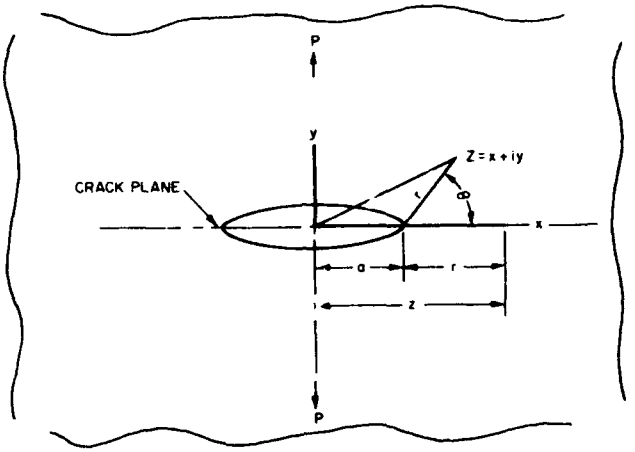


Fig. 1. Crack loaded normally and contained in an infinite body.

able [12]. This technique makes use of finite-element analysis to obtain an estimate of the $x$- and $y$-direction displacement components $u$ and $v$, respectively, in the vicinity of the crack tip. Expressions for plane strain $u$ and $v$ in terms of $K_I$ and $r$ have been derived [11] as

$$u = \frac{K_I}{G}\sqrt{\frac{r}{2\pi}}\cos\frac{\theta}{2}\left[1 - 2\mu + \sin^2\frac{\theta}{2}\right] \tag{9}$$

$$v = \frac{K_I}{G}\sqrt{\frac{r}{2\pi}}\sin\frac{\theta}{2}\left[2(1-\mu) - \cos^2\frac{\theta}{2}\right] \tag{10}$$

where $G$ is the shear modulus and $\mu$ is Poisson's ratio. By substituting in Eqs. (9) and (10) those values of $u$ and $v$ obtained by finite-element analysis at the point where $r \approx a/5$ and $\theta = \pi$, the solution for $K_I$ is found algebraically [12].

### Derivation of $K_I$ by Specimen Compliance

In the determination of $K_I$ by the compliance technique, use is made of the fact that the energy released from a growing crack is directly reflected in an increase of overall specimen compliance. A strain-energy release parameter $\mathcal{G}$ has been derived in terms of compliance and related to $K_I$ [11]. The resulting solution for $K_I$ in terms of compliance is given by

$$K_I = P\left[\frac{E}{2B} \cdot \frac{dC}{da}\right]^{1/2} \tag{11}$$

where $P$ is the applied load, $E$ is Young's modulus, $B$ is thickness, and $C$ is compliance (usually expressed as some function of the crack length $a$). In the original work [11], the relationship between $K_I$ and $\mathcal{G}_I$ contained a modifying factor $[1/(1-\mu)^2]^{1/2}$ that most investigators now delete from consideration since it amounts to less than 5% for structural materials [5]. Compliance is defined as the reciprocal of the spring constant $m$, which is the slope of a load $P$ vs deflection $\delta$ curve. The spring constant is dependent upon Young's modulus $E$ and geometry. Compliance may be measured experimentally or derived from theoretical considerations.

**Experimental Determination of Compliance.** Compliance is determined experimentally by finding the elastic load-point displacement caused by a unit of load in a specimen containing a slot (representing a crack), the length of which has been accurately measured. The slot is lengthened in some manner, for example by sawing, and a new compliance is obtained. This procedure is repeated for a sufficient number of crack length values to cover adequately and reliably the range of interest. In Fig. 2a, a number of $P-\delta$ curves for different values of $a$ are shown. The compliance $\delta/P$ for each of these is replotted as a function of $a$ in Fig. 2b. This relationship can also be presented in dimensionless form, as in Fig. 2c, by incorporating the additional terms $E$ and $B$ in the compliance and defining crack length in terms of $a/H$ or $a/W$ where $H$ is one-half the height and $W$ is the width of the specimen. It is convenient to find the equation of the compliance curve by fitting the data to a general polynomial; for example,

$$\frac{EB\delta}{P} = C_1 + C_2\left(\frac{a}{W}\right) + C_3\left(\frac{a}{W}\right)^2 + C_4\left(\frac{a}{W}\right)^3 + \cdots \tag{12}$$

The values of the constants are found by solving the appropriate number of simultaneous equations. When Eq. (12) is differentiated with respect to $a/W$, the derivative can be substituted for the term $dC/da$ in Eq. (11) to yield

$$K_I = \frac{P}{B}\left[\frac{1}{2W} \cdot \frac{d\left(\frac{EB\delta}{P}\right)}{d\left(\frac{a}{W}\right)}\right]^{1/2} \tag{13}$$

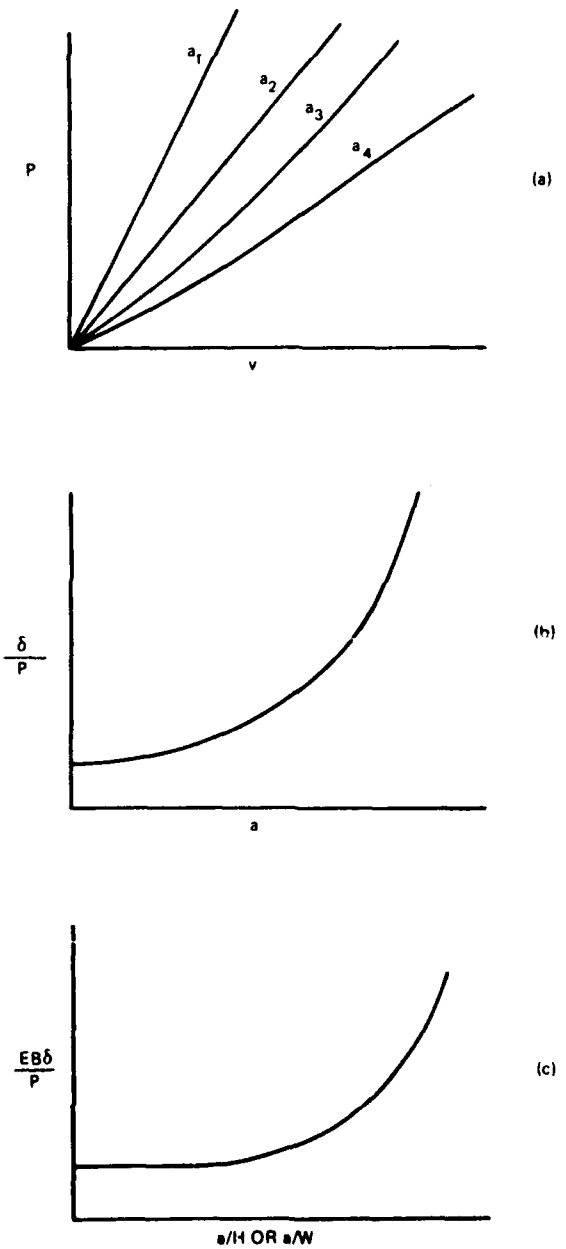


Fig. 2. Curves to develop compliance.

Variations of this equation may be given as

$$K_I = \frac{P}{B}\left[\frac{1}{2} \cdot \frac{d\left(\frac{EB\delta}{P}\right)}{da}\right]^{1/2} \tag{14}$$

and

$$K_I = \frac{P}{B}\left[\frac{1}{2H} \cdot \frac{d\left(\frac{EB\delta}{P}\right)}{d\left(\frac{a}{H}\right)}\right]^{1/2} \tag{15}$$

**Theoretical Derivation of Compliance.** Expressions for compliance as a function of crack length have been derived from strength of materials theory. However, because of the assumption involved, predicted deflections due to load do not agree very well with those actually measured. In this case, the theoretical expression can be corrected empirically by comparing it with experimental data. For example, correction has been applied to the theoretical compliance of a $(W-a)$-indifferent, single-edge-cracked specimen [13] to provide Eq. (16), which is similar in form to the general experimental derivation shown in Eq. (12). In this configuration, the crack opening displacement $v$ is identical to the total deflection $\delta$ obtained from applied cantilever loads on two beams;

$$\frac{EBv}{P} = 8\left[\left(\frac{a}{H}\right)^3 + \frac{a}{H}\right]. \tag{16}$$

### The $K_I$ Calibration

It is important to note that although $K_I$ solutions appear in many forms and degrees of complexity, it is often possible to calibrate the expression in terms of the crack length. Calibrations for $K_I$ are presented in dimensionless form so that the single expression derived for a particular test system (defined in terms of crack location and loading method) can be used to obtain $K_I$ values from specimens of different dimensions and elastic constants. As an example, the tangent expression [11] provides a $K_I$ solution for the center-cracked panel of finite width loaded remotely from the crackline as

$$K_I = \frac{P}{BW}\sqrt{\pi a}\left[\frac{W}{\pi a}\tan\frac{\pi a}{W}\right]^{1/2}. \tag{17}$$

This expression can be adjusted so that $K_I$ is calibrated in dimensionless form to $a/W$ by the function

$$\frac{K_I BW}{P\sqrt{a}} = \left[\frac{W}{a} \tan \frac{\pi a}{W}\right]^{1/2} = f\left(\frac{a}{W}\right). \tag{18}$$

When $K_I BW/P\sqrt{a}$ is plotted as a function of $a/W$, the curve so obtained can be re-expressed as an $n$th-order polynomial for which an equation can be derived in the form of

$$\frac{K_I BW}{P\sqrt{a}} = C_1 + C_2\left(\frac{a}{W}\right) + C_3\left(\frac{a}{W}\right)^2 + \ldots. \tag{19}$$

Usually an accurately obtained graph of Eq. (19) or equivalent table of values provides a convenient means of reducing data in which the process of solving the trigonometric function is avoided.

In general, the form of Eq. (19) has been used throughout this review in calibrating $K_I$ to a function of crack length. Where more than one calibration exists for a specimen, they are presented graphically for comparison.

### Critical Stress Intensity Factors

The stress intensity factor for opening mode $K_I$ is proportional to the product of the applied stress and the square root of the crack length. Considerable test experience indicates that there may exist a value of $K_I$ below which cracks are not observed to propagate *in a particular material in a specific chemical and electrochemical environment.* This value has been designated $K_{Iscc}$ [14]. In other words, $K_{Iscc}$ is the level above which SCC has been observed and below which SCC has not been observed in a given material in a specified chemical and electrochemical environment.

Stress corrosion crack growth can be monitored with suitable instrumentation and expressed as a function of the stress-intensity factor. The kinetics of crack growth have been employed extensively to characterize stress corrosion behavior.

## 2.4 Specimen Geometries

Precracked specimens are classified with respect to the relationship between the stress intensity factor $K_I$ and crack extension (Fig. 3). Depending on the method of stressing and/or the geometry of the test piece, the stress intensity factor can be made to increase, decrease, or remain constant as the crack length increases. In the first category of precracked specimen configurations, where $K_I$ increases with crack extension, specimens are most commonly stressed under constant load conditions in tension or bending. In addition, a distinction is made

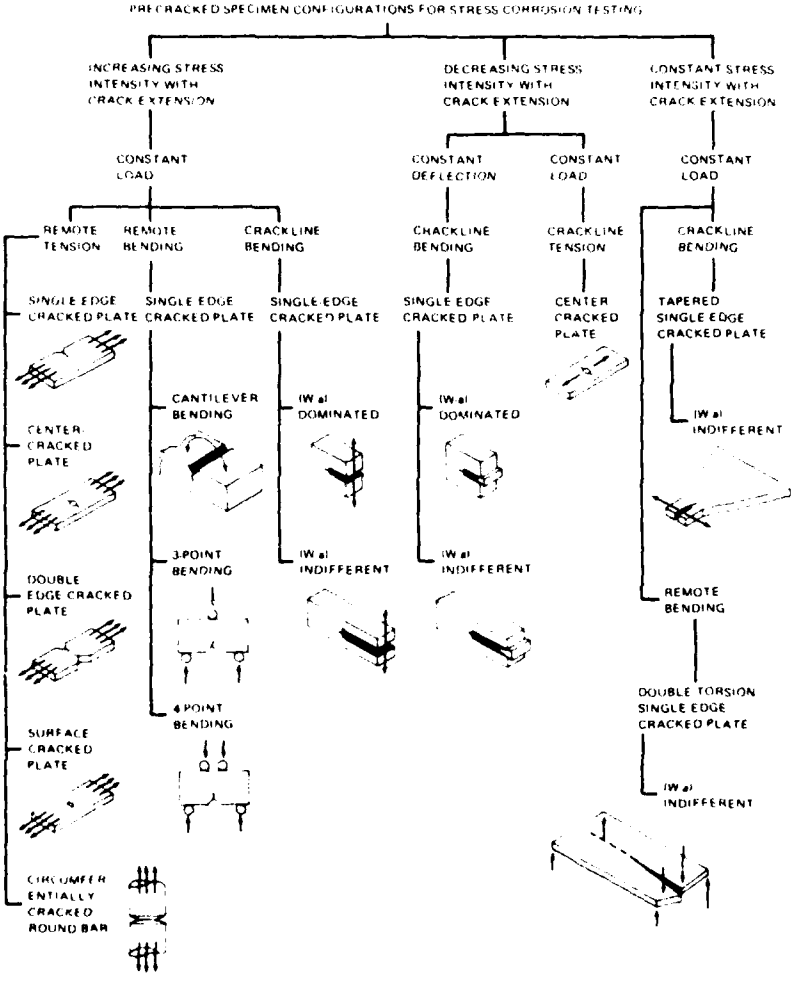


Fig. 3. Classification of precracked specimens for stress corrosion testing.

between those specimens loaded close to the precrack (crackline loaded) and at a distance from the precrack (remote loaded). Single-edge-cracked plate specimens are classified [15] according to the proximity of the boundary normal to the direction of the crack plane, the crack-tip stress field being either affected ($W-a$ dominated) or unaffected ($W-a$ indifferent) by this boundary.

In the second category of precracked specimen configurations, where $K_I$ decreases with crack extension, specimens can be stressed under conditions of constant deflection or constant load. Crackline-loaded, single-edge-cracked plate specimens are maintained at constant crack-opening displacement $v$ (measured along the line of load application) by a bolt, wedge, or other device. The overall result of this procedure is to cause the load to diminish and, consequently, the $K_I$ to decrease as the crack extends under the influence of an aggressive environment. The constant-load, crackline-tension, center-cracked plate has been commonly referred to as the wedge-force specimen.

In the third category of precracked specimens, a linear relationship between specimen compliance and crack length is obtained to produce constant $K_I$ with crack extension. The overall classification provides a useful framework for describing in more detail the use of a particular specimen or family of specimens during stress corrosion testing.

### Crackline-Loaded, Single-Edge-Cracked Plate Specimens

Crackline-loaded, single-edge-cracked specimens can be used in either increasing or decreasing $K_I$ tests performed on plate materials. However, the decreasing $K_I$ technique as applied to this configuration is probably more attractive for use in stress corrosion testing than any other specimen because a fixed crack-opening displacement can be achieved by a simple loading arrangement.

Typical crackline-loaded specimens (also known as double cantilever beam, compact tension, or wedge-opening load specimens) are shown in Figs. 4 and 5,

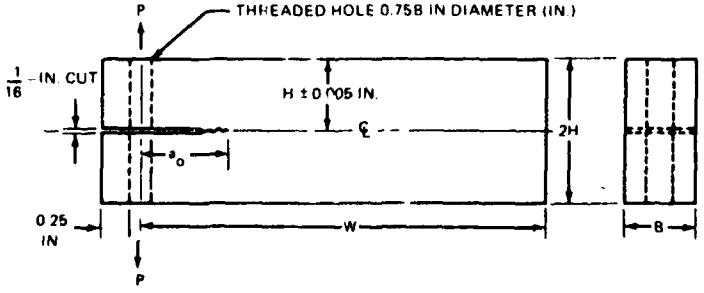


HOLE CENTERLINE MUST BE NORMAL TO SPECIMEN CENTERLINE WITHIN ± 1°
SLOT CENTERLINE MUST COINCIDE WITH CENTERLINE OF SPECIMEN WITHIN 0.005 IN.

**Fig. 4. Configuration and $K_I$ calibration of the ($W-a$)-indifferent, crackline-loaded single-edge-cracked plate specimen.**

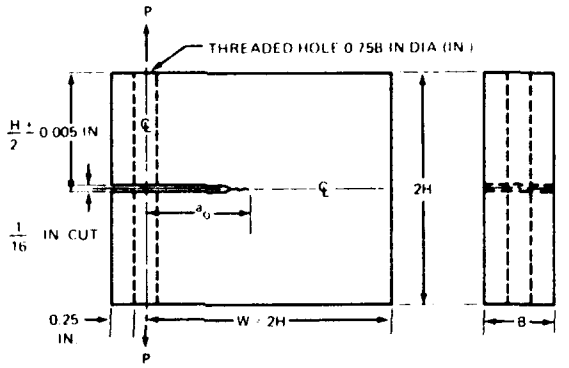


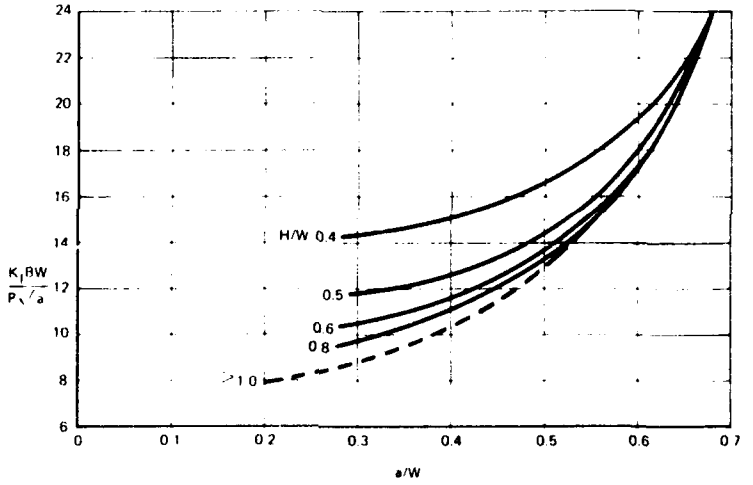


Fig. 5. Comparison of $K_I$ calibrations represented by Eqs. (24) and (25) for $(W-a)$-indifferent, crackline-loaded, single-edge-cracked plate specimens.

where dimensions are stated in ratios of $H$ to $W$ and solutions for $K_I$ are presented as calibrations in $a/W$ or $a/H$. The specimens are differentiated by the manner in which the boundary normal to the crack plane affects the crack-tip stress field. The distance of this boundary from the crack tip is given by the difference $(W-a)$, and if this dimension is small compared with $a$, the configuration is termed $(W-a)$ dominated. If $(W-a)$ is very large compared with $a$, the configuration is termed $(W-a)$ indifferent. This nomenclature was originated in Ref. 15 where $(W-a)$ indifference was shown to obtain whenever the ratio $W/H$ was not less than an amount equal to $a/H + 2$.

In these specimens all dimensions are measured either from the crackline or from the line of load application. Loads are assumed to be applied such that torsional deflection of the arms does not occur.

**Configuration and $K_I$ Calibration of the $(W-a)$-Indifferent Specimen.** The configuration of the $(W-a)$-indifferent specimen is considered solely in terms of the variable $H$, since the width $W$ by definition does not enter into the analysis of the $K_I$ calibration. Thus, a single solution represents all $(W-a)$-indifferent configurations, a factor which is extremely desirable to the testing specialist.

Calibrations for $K_I$ have been derived by both stress analysis and compliance. The stress analysis approach was used to obtain the linear relationship shown in Eq. (20) (Ref. 15), while Eq. (21) was obtained by empirically correcting an expression for compliance derived from beam theory [13];

$$\frac{K_I B H^{3/2}}{Pa} = 3.46 + 2.38\,\frac{H}{a} \tag{20}$$

$$\frac{K_I B H^{3/2}}{Pa} = 2\left[3 + 3.6\left(\frac{H}{a}\right) + 2.08\left(\frac{H}{a}\right)^2\right]^{1/2}. \tag{21}$$

To obtain the calibration for fixed crack-opening displacement $v$, the load $P$ in Eqs. (20) and (21) is replaced by its equivalent $v$ per unit of compliance (where compliance is expressed as a function of crack length). Compliance can be extracted from Eq. (20) by comparing it with the basic compliance expression, Eq. (11), adjusted to the same calibration form, Eq. (22):

$$\frac{K_I B H^{3/2}}{Pa} = \left[\frac{d\left(\frac{EBv}{P}\right)}{d\left(\frac{a}{H}\right)}\right]^{1/2} \frac{H}{\sqrt{2}\,a}. \tag{22}$$

Combining Eqs. (20) and (22) and solving the differential equation yields

$$P = \frac{EBv}{7.97\left(\frac{a}{H}\right)^3 + 16.48\left(\frac{a}{H}\right)^2 + 11.32\left(\frac{a}{H}\right)}. \tag{23}$$

Suitable substitution in Eq. (20) thus provides a calibration in terms of $K_I\sqrt{H/Ev}$, which is shown for the fixed crack-opening displacement position in

$$\frac{K_I\sqrt{H}}{Ev} = \left[\frac{3.46 + 2.38\left(\frac{H}{a}\right)}{7.8\left(\frac{a}{H}\right)^2 + 16.38\left(\frac{a}{H}\right) + 11.32}\right]. \tag{24}$$

In Eq. (21), the derivation of compliance is an integral part of the calibration procedure [13] and as such is available to replace the load $P$ for the fixed crack-opening displacement analysis. When this is done the result is

$$\frac{K_I\sqrt{H}}{Ev} = \frac{\left[3\left(\frac{a}{H}\right)^2 + 3.6\left(\frac{a}{H}\right) + 2.08\right]^{1/2}}{4\left[\left(\frac{a}{H} + 0.6\right)^3 + \frac{a}{H}\right]}. \tag{25}$$

The two decreasing $K_I$ calibrations, shown in Fig. 6, are in excellent agreement. It is important to note that the shapes of these calibration curves can be guides in preparing specimens. If it is required that the test be completed in the shortest possible time, the beginning crack length should be short to take advantage of the fact that the rate of decrease of $K_I$ with crack extension is maximum for short cracks. On the other hand, if test time is not important and maximum accuracy is desired, a longer crack can be chosen so that errors in crack length measurement do not cause appreciable errors in $K_I$.

**Configuration and $K_I$ Calibration of the ($W$–$a$)-Dominated Specimen.** Configurations of this type are described in terms of $H$ and $W$, since both parallel and normal boundaries influence the crack-tip stress field. Consequently there is a unique calibration for $K_I$ as a function of $a/W$ for each $H/W$ ratio, a factor which is somewhat undesirable from the standpoint of ease of data reduction. Calibrations for $H/W$ ratios of 0.1194, 0.444, 0.486, and 1.0 have been obtained using a stress analysis approach [16], and by the same technique [5], calibration curves for ratios of 0.4, 0.5, 0.6, 0.8, and 1.0 were derived. In only three configurations [16] have equations been published for calibration curves, and these are shown in the following equations:

$$\frac{K_I BW}{P\sqrt{a}} = 60.9 - 5.6\left(\frac{W}{a}\right) - 139.3\left(\frac{a}{W}\right) + 140.9\left(\frac{a}{W}\right)^2, \quad \frac{H}{W} = 0.444 \tag{26}$$

$$\frac{K_I BW}{P\sqrt{a}} = 30.96 - 195.8\left(\frac{a}{W}\right) + 730.6\left(\frac{a}{W}\right)^2 - 1186\left(\frac{a}{W}\right)^3 + 754.6\left(\frac{a}{W}\right)^4,$$

$$\frac{H}{W} = 0.486 \tag{27}$$

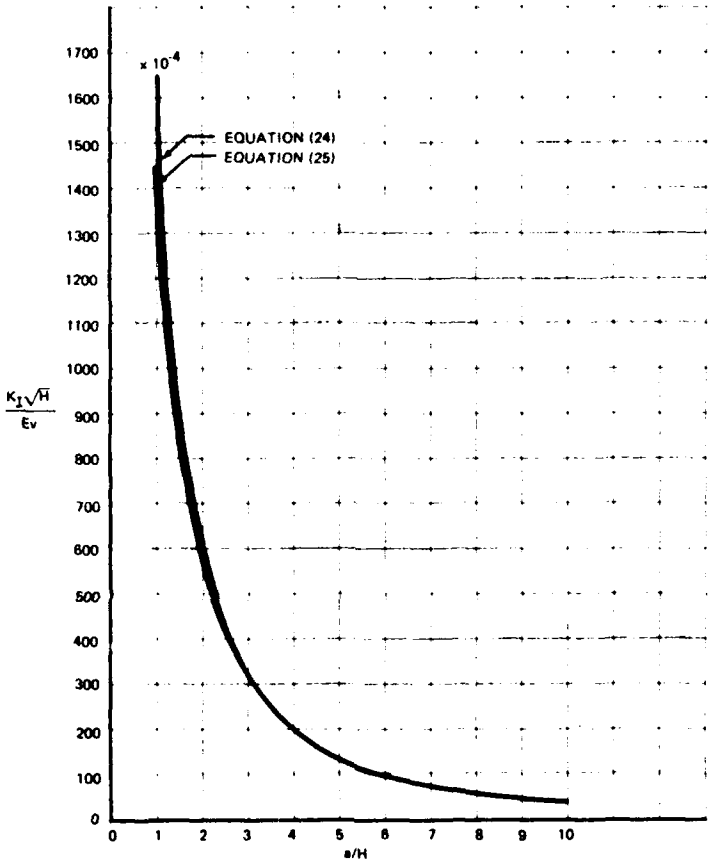


Fig. 6. Configuration and $K_I$ calibration of the ($W$–$a$)-dominated, crackline-loaded, single-edge-cracked plate specimen.

$$\frac{K_I BW}{P\sqrt{a}} = 39.7 - 294.2\left(\frac{a}{W}\right) + 1118\left(\frac{a}{W}\right)^2 - 1842\left(\frac{a}{W}\right)^3 + 1159\left(\frac{a}{W}\right)^4,$$

$$\frac{H}{W} = 0.5. \qquad (28)$$

These polynomials represent calibrat : from data obtained in the $a/W$ range from 0.25 to 0.65 and are accurate to about 0.5% in this range. It must be emphasized, however, that the slopes of the cur es increase very rapidly at the

larger values of $a/W$, which might introduce large errors in $K_I BW/P\sqrt{a}$ due to small errors in measuring $a/W$. This characteristic of the calibration is much less severe in the $(W-a)$-indifferent specimen, a factor which should be considered in the selection of specimens.

The $(W-a)$-dominated specimen can be used in the decreasing $K_I$ mode by fixing the crack-opening displacement in the same manner as described in the previous section. However, each $H/W$ configuration has its unique compliance-vs-crack-length relationship that must be determined experimentally or extracted from a $K_I$ calibration derived by stress analysis. The extraction process is arduous because the calibrations are not linear as are those for the $(W-a)$-indifferent configuration. The compliance of the $H/W = 0.486$ configuration was determined experimentally [17], and the resulting $K_I$ calibration is in good agreement with Eq. (27). It should be noted that the compliance derived from beam theory, Eq. (16), applies only to $(W-a)$-indifferent specimens and cannot be used for $(W-a)$-dominant specimens.

### Single-Edge-Cracked Plate Specimens in Remote Tension or Bending

This family of specimens has probably been used more than others in stress corrosion testing because of its popularity in fracture-toughness testing. It is well suited to obtaining $K_{Iscc}$ by the increasing $K_I$ multiple specimen test, and can also be used to obtain crack growth rate vs $K_I$ information. If these specimens are thick enough to withstand buckling tendencies, sustained loads are applied by bending; if the specimens are very thin, sustained loads are applied by tension.

**Configuration and $K_I$ Calibration of the Tension-Loaded Specimen.** Figure 7 shows the configuration, ratios of pertinent dimensions to the width $W$, and the $K_I$ calibrations of the remote-loaded, single-edge-cracked tension specimen. The calibration was initially obtained by the experimental compliance technique applied to a pin-loaded specimen where the loads were applied at distances about $1.5W$ from the crackline [18]. The pin-loaded condition approximates that of uniform tension applied at a distance $W$ from the crackline which was assumed in a later stress-analysis derivation of the calibration [19]. The stress-analysis-derived calibration

$$\frac{K_I BW}{P\sqrt{a}} = 1.99 - 0.41\left(\frac{a}{W}\right) + 18.70\left(\frac{a}{W}\right)^2 - 38.48\left(\frac{a}{W}\right)^3 + 53.85\left(\frac{a}{W}\right)^4 \quad (29)$$

agrees with the compliance-derived calibration,

$$\frac{K_I BW}{P\sqrt{a}} = \left[7.59 - 32.0\left(\frac{a}{W}\right) + 117\left(\frac{a}{W}\right)^2\right]^{1/2}, \quad (30)$$

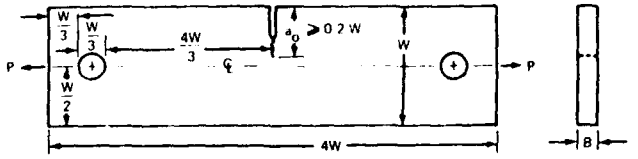


HOLE CENTERLINE MUST COINCIDE WITH SPECIMEN CENTERLINE WITHIN 0.005 IN.

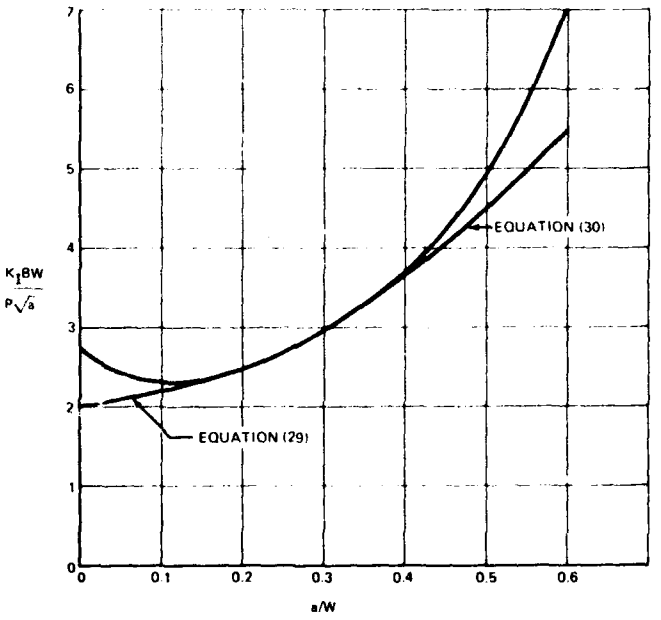


Fig. 7. Configuration and $K_I$ calibration of the remote-loaded, single-edge-cracked plate tension specimen.

within 1% for values of $a/W$ from 0.2 to 0.4, but is considered to be more accurate for larger values of $a/W$ [5].

**Configuration and $K_I$ Calibration of the Three-Point Bend Specimen.** The specimen, together with load and support points, is shown in Fig. 8, which also contains four calibrations for $K_I$ obtained from expressions originally described elsewhere [20,21]. With regard to the system described by $S/W$ ratios of 8, Eqs. (31) and (32) were obtained by stress analysis [21], whereas Eq. (33) was

$$\frac{K_I BW^2}{6M\sqrt{a}} = \left[3.52 - 7.2\left(\frac{a}{W}\right) + 23.44\left(\frac{a}{W}\right)^2\right]^{1/2}, \quad \frac{S}{W} = 8 \qquad (31)$$

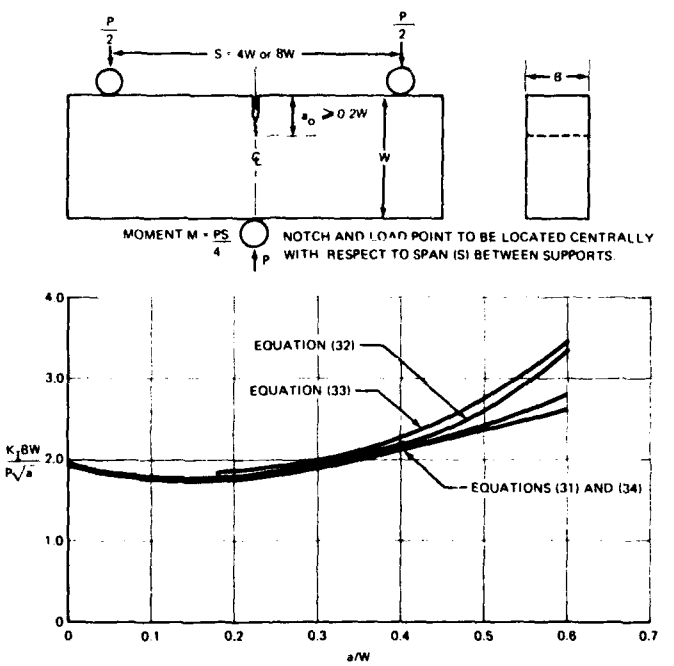


Fig. 8. Configuration and $K_I$ calibration of the three-point-loaded, single-edge-cracked plate bend specimen.

$$\frac{K_I BW^2}{6M\sqrt{a}} = 1.96 - 2.75\left(\frac{a}{W}\right) + 13.66\left(\frac{a}{W}\right)^2 - 23.98\left(\frac{a}{W}\right)^3 + 25.22\left(\frac{a}{W}\right)^4, \quad \frac{S}{W} = 8 \tag{32}$$

$$\frac{K_I BW^2}{6M\sqrt{a}} = 0.69\left[\frac{1 - \left(1 - \frac{a}{W}\right)^6}{\left(1 - \frac{a}{W}\right)^3\left(\frac{a}{W}\right)}\right]^{1/2}, \quad \frac{S}{W} = 8 \tag{33}$$

derived by the combined techniques of stress analysis and compliance [22]. Equation (32) is slightly more accurate over a range of $a/W$ values to 0.6 [5] and

is recommended for use. Equation (34) was obtained by a stress analysis performed on the system represented by an $S/W$ ratio of 4:

$$\frac{K_I BW^2}{6M\sqrt{a}} = 1.93 - 3.07\left(\frac{a}{W}\right) + 14.53\left(\frac{a}{W}\right)^2 - 25.11\left(\frac{a}{W}\right)^3 + 25.80\left(\frac{a}{W}\right)^4, \qquad \frac{S}{W} = 4. \tag{34}$$

Span-to-width ratios of less than 4 are not considered in this review because they introduce errors due to indentation and friction at the support joints.

**Configuration and $K_I$ Calibration of the Four-Point Bend Specimen.** These specimens were originally thought to yield more accurate results because they closely approximate conditions of pure bending. However, this contention is now considered to be of no consequence. Figure 9 shows the configuration, a suggested arrangement for load and support points, and calibrations for $K_I$. Equation (35) was derived for pure bending in terms of the function $g(a/W)$ according to the following table:

| $a/W$ | $g(a/W)$ | $a/W$ | $g(a/W)$ |
|---|---|---|---|
| 0.1 | 0.49 | 0.4 | 0.69 |
| 0.2 | 0.60 | 0.5 | 0.72 |
| 0.3 | 0.66 | 0.6 | 0.73 |

$$\frac{K_I(W-a)^{3/2}}{6M} = g\left(\frac{a}{W}\right). \tag{35}$$

Equations (36), (37), and (38) were obtained from expressions derived previously [20]. Of these, Eq. (37) is considered to be the most accurate over the greatest range of $a/W$. These calibrations were actually derived from pure bending considerations, but are considered to represent four-point loading if the ratio of the minor span to specimen width $W$ is greater than 2 [5].

$$\frac{K_I BW^2}{6M\sqrt{a}} = \left[3.86 - 6.15\left(\frac{a}{W}\right) + 21.7\left(\frac{a}{W}\right)^2\right]^{1/2} \tag{36}$$

$$\frac{K_I BW^2}{6M\sqrt{a}} = 1.99 - 2.47\left(\frac{a}{W}\right) + 12.97\left(\frac{a}{W}\right)^2 - 23.17\left(\frac{a}{W}\right)^3 + 24.8\left(\frac{a}{W}\right)^4 \tag{37}$$

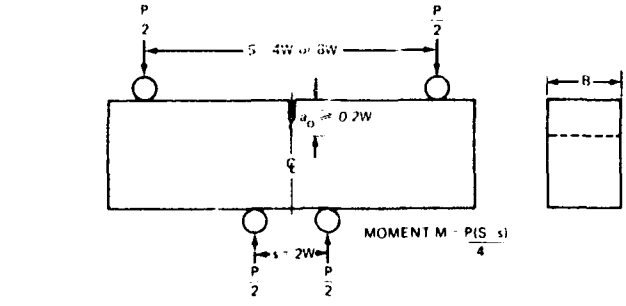


NOTCH TO BE LOCATED CENTRALLY WITH RESPECT TO MAJOR (S) AND MINOR (s) SPAN

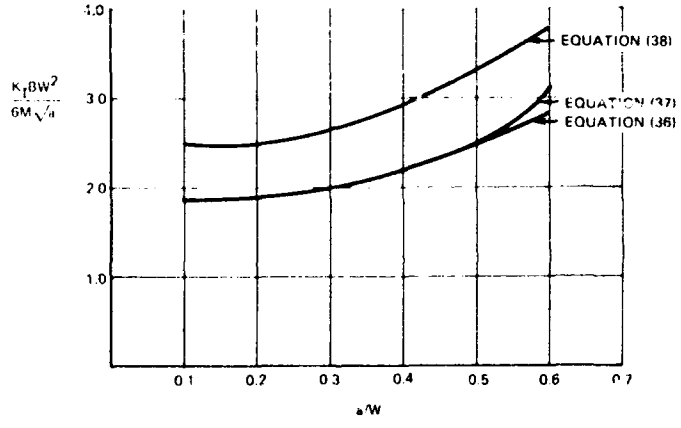


Fig. 9. Configuration and $K_I$ calibration of the four-point-loaded, single-edge-cracked plate bend specimen.

$$\frac{K_I BW^2}{6M\sqrt{a}} = \left[6.84 - 10.87\left(\frac{a}{W}\right) + 38.61\left(\frac{a}{W}\right)^2\right]^{1/2} . \qquad (38)$$

**Configuration and $K_I$ Calibration of the Cantilever Bend Specimen.** The cantilever bend configuration is the same as that of three- and four-point bend specimens and is shown in its loading position in Fig. 10. Equation (39) is Eq. (33) and has been used rather extensively to analyze results obtained by cantilever loading [14], even though it was originally derived by the combined techniques of stress analysis and compliance for three-point bending.

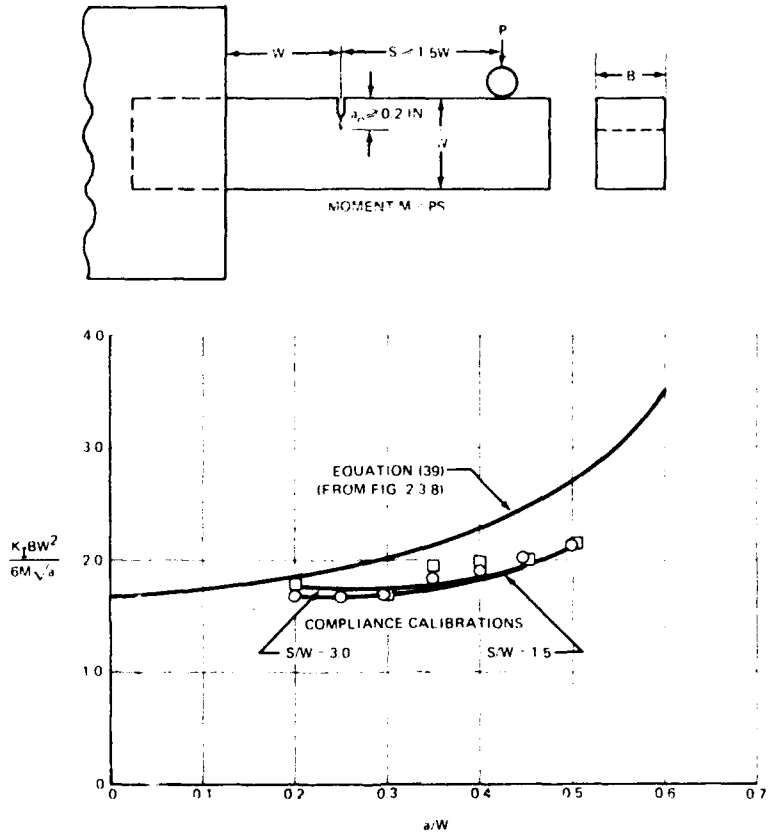


Fig. 10. Configuration and comparison of $K_I$ calibrations for cantilever-loaded, single-edge-cracked plate bend specimens.

$$\frac{K_I BW^2}{6M\sqrt{a}} = 0.69\left[\frac{1-\left(1-\frac{a}{W}\right)^6}{\left(1-\frac{a}{W}\right)^3\left(\frac{a}{W}\right)}\right]^{1/2} \quad (39)$$

The only calibration reported specifically for cantilever bending was obtained by compliance [24]. No equation was derived for the curve that may be compared graphically with the curve for Eq. (39), Fig. 11. As can be seen, there is some

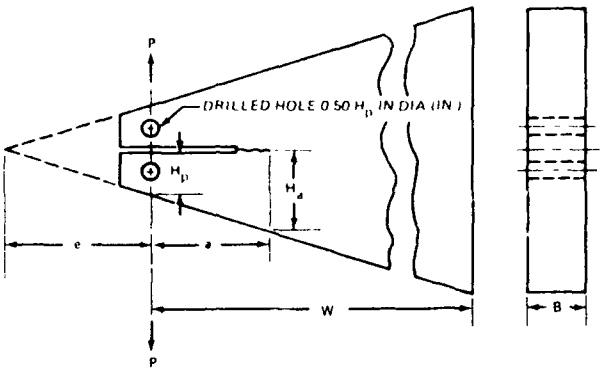


Fig. 11. Configuration and $K_I$ calibration of the $(W-a)$-indifferent tapered specimen.

difference in the two, and it is recommended that the compliance calibration be used. In assembling the specimen for testing, a distance $W$ should be allowed between the edge of the grip and the crackline to avoid end effects.

### Constant $K_I$ Specimens

The constant $K_I$ specimen is attractive for use by fundamentalists investigating mechanisms of stress corrosion cracking. The stress intensity $K_I$ is independent of crack length and can be neglected as a variable in kinetic studies. The total cost of specimen preparation and instrumentation prohibits its use during extensive stress corrosion characterization.

**Configuration and $K_I$ Calibration of the Crackline-Loaded, Single-Edge-Cracked Specimen With Tapered Sides.** This specimen, also known as the tapered double cantilever beam (*DCB*) specimen, is shown in a $(W-a)$-indifferent configuration in Fig. 11. The original work performed with this specimen [13] involved the experimental determination of the compliance as a function of crack length for a number of differently tapered configurations. These determinations showed compliance to be linearly related to crack length over a range that was governed by the angle of taper. The derivative of $EBv/P$ with respect to crack length $a$ is therefore a constant in this range; as a consequence, $K_I$ is also constant when load $P$ is maintained at a constant level. Thus Eq. (40) can be reduced to a form as simple as Eq. (41) where $C_I$ is the value of the right-hand side of Eq. (40):

$$\frac{K_I B}{P} = \left[\frac{1}{2} d \frac{\frac{EBv}{P}}{da}\right]^{1/2} \tag{40}$$

$$K_I = C_1 P \ . \tag{41}$$

Calibrations for both $(W-a)$-indifferent (where indifference for the tapered specimen is undefined as of this writing) and $(W-a)$-dominated tapered configurations have been obtained and described [25]. The result for the $(W-a)$-indifferent case is shown as the linear expression

$$\frac{K_I B \sqrt{H_a}}{P} = \Lambda \left( \frac{a}{H_a} + 0.7 \right) \tag{42}$$

where the slope coefficient $\Lambda$ depends upon the ratio $H_p/e$ as shown in the table below, and where $H_p$ is the half height of the specimen along the loadline and $H_a$ is the half height at the tip of the crack.

| $H_p/e$ | $\Lambda$ | $H_p/e$ | $\Lambda$ |
|---|---|---|---|
| 0.0 | 3.46 | 0.3 | 2.98 |
| 0.1 | 3.26 | 0.4 | 2.88 |
| 0.2 | 3.10 | | |

*Equation (42) does not show $K_I$ to be constant with crack extension simply* because the ratio $a/H_a$ is variable (whereas the ratio $(a+e)/H_a$ is constant over a range of crack length).

When the values of $H_p/e$ and either $W/e$ or $W/H_p$ are known, Eq. (42) can be converted algebraically to

$$\frac{K_I B \sqrt{W}}{P} = f\left( \frac{a}{W} \right) \tag{43}$$

which represents the $(W-a)$-dominated configuration (Fig. 12). It is claimed [25] that conversion values of $K_I B \sqrt{W}/P$ agree with those obtained directly by stress analysis in the lower range of $a/W$. Equation (43) can be restated more simply as

$$K_I = f\left( \frac{a}{W} \right) \frac{P}{B \sqrt{W}} \tag{44}$$

by using Table 1, which is also useful for selecting taper configurations to suit a particular problem. Two configurations, represented by $H_p/e$ ratios of 0.53 and 0.45, have been analyzed by the compliance technique. Later calibrations obtained by stress analysis showed that the agreement of results was excellent.

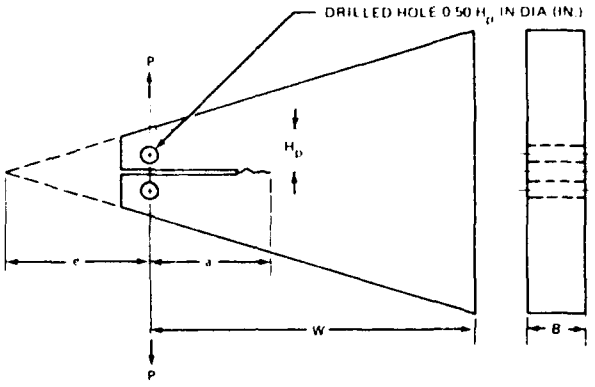


Fig. 12. Configuration and $K_I$ calibration of the $(W-a)$-dominated tapered specimen.

Therefore, when the compliance technique is used, it is considered that the disadvantage of obtaining the compliance of each configuration can be avoided by appropriate use of Table 1.

**Configuration and $K_I$ Calibration of the Torsion-Loaded Specimen.** This specimen was first described in a study of fracture in bulk glass [26]. Subsequently, its use was extended to the study of stress corrosion cracking in metals [27]. The strain-energy release rate $\mathcal{G}_J$ can be expressed as

$$\mathcal{G}_J = \frac{3}{8}\frac{P^2 H_m^2}{GB^4} \tag{45}$$

where $H_m$ is the torsional moment length as indicated in Fig. 13 and $G$ is the shear modulus. Equation (45) can be separated into parts such that

$$\mathcal{G}_J = \left[\frac{P^2}{2B}\right]\left[\frac{3}{4}\frac{H_m^2}{GB^3 H}\right]. \tag{46}$$

The constant $3/4\, H_m^2/\mathcal{G}_J B^3 H$ is $d(y/P)/da$ in the expression [11]

$$y = \left[\frac{P^2}{2B}\right]\left[\frac{d\left(\frac{y}{P}\right)}{da}\right] \tag{47}$$

where $y$ is deflection and $a$ is crack length. Because $d(y/P)/da$ is constant, $\mathcal{G}_J$ is constant for constant load.

**Table 1**

| $H_p/e$ | $W/e$ | $W/H_p$ | $a/W$ | | | | | |
|---|---|---|---|---|---|---|---|---|
| | | | 0.2 | 0.3 | 0.4 | 0.5 | 0.6 | 0.7 |
| | | | $KBW^{1/2}/P$ | | | | | |
| 0 | 0 | 1.25 | | 5.31 | 6.86 | 9.29 | 13.44 | 21.52 |
| | | 1.5 | | 5.59 | 7.10 | 9.45 | 13.52 | 21.54 |
| | | 2 | 5.32 | 6.49 | 8.01 | 10.20 | 13.92 | 21.68 |
| | | 3 | 7.65 | 9.35 | 11.34 | 13.53 | 16.64 | 23.16 |
| | | 4 | 10.20 | 13.00 | 15.76 | 18.57 | 22.35 | 26.81 |
| | | 5 | 12.90 | 16.85 | 20.72 | 24.49 | 28.61 | 33.42 |
| 0.1 | 3 | 30 | 63.4 | 70.5 | 74.0 | 75.5 | 76.1 | 75.5 |
| | 4 | 40 | 79.0 | 85.2 | 88.0 | 87.5 | 86.5 | 84.5 |
| | 5 | 50 | 92.5 | 98 | 99 | 97 | 95 | 92 |
| 0.2 | 2 | 10 | 17.65 | 20.0 | 21.3 | 22.2 | 23.3 | 27.0 |
| | 3 | 15 | 24.5 | 26.7 | 27.9 | 28.1 | 28.3 | 30.5 |
| | 3.2 | 16 | 27.0 | 28.3 | 29.0 | 29.0 | 29.1 | 31.0 |
| | 4 | 20 | 30.3 | 32.1 | 32.8 | 32.2 | 31.8 | 33.0 |
| | 5 | 25 | 35.2 | 36.2 | 36.0 | 35.3 | 34.5 | 35.0 |
| 0.3 | 3 | 10 | 14.7 | 15.7 | 16.1 | 16.4 | 18.0 | 23.5 |
| | 3.6 | 12 | 16.8 | 17.5 | 17.7 | 17.8 | 19.0 | 24.0 |
| | 4.2 | 14 | 18.6 | 19.1 | 19.2 | 18.94 | 19.77 | 24.44 |
| | 4.8 | 16 | 20.1 | 20.4 | 20.2 | 19.85 | 20.46 | 24.82 |
| | 5.4 | 18 | 21.5 | 21.6 | 21.1 | 20.6 | 21.0 | 25.14 |
| | 6 | 20 | 22.9 | 22.8 | 21.9 | 21.4 | 21.6 | 25.4 |
| 0.4 | 3 | 7.5 | 10.2 | 11.0 | 11.5 | 12.5 | 15.1 | 22.0 |
| | 4 | 10 | 12.4 | 12.8 | 12.9 | 13.6 | 15.8 | 22.3 |
| | 5 | 12.5 | 14.0 | 14.2 | 14.2 | 14.4 | 16.3 | 22.6 |
| | 6 | 15 | 15.4 | 15.5 | 15.2 | 15.1 | 16.8 | 22.8 |
| | 8 | 20 | 18.2 | 17.5 | 16.8 | 16.2 | 17.4 | 23.0 |
| 0.5 | 4 | 8 | | 9.8 | 10.3 | 11.4 | 14.5 | 21.8 |
| | 5 | 10 | | 11.2 | 11.0 | 11.9 | 14.7 | 21.9 |
| | 6 | 12 | | 12 | 11.6 | 12.5 | 15.0 | 22.0 |
| | 8 | 16 | | 14 | 12.8 | 13.2 | 15.5 | 22.1 |
| 0.6 | 3 | 5 | | 7 | | 9.8 | 13.9 | 21.5 |
| | 4 | 6.67 | | | 7.7 | 10 | 14.0 | 21.6 |
| | 5 | 8.333 | | | | 10.9 | 14.1 | 21.6 |
| | 6 | 10 | | 10 | | 11 | 14.2 | 21.7 |

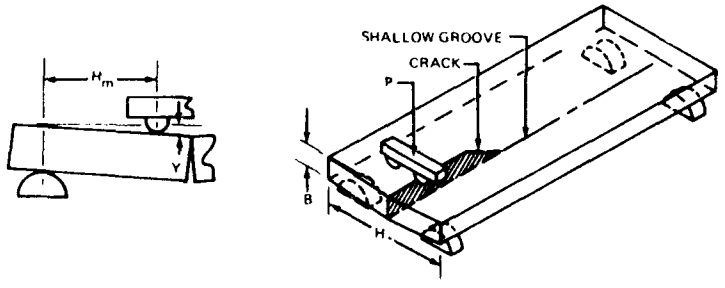


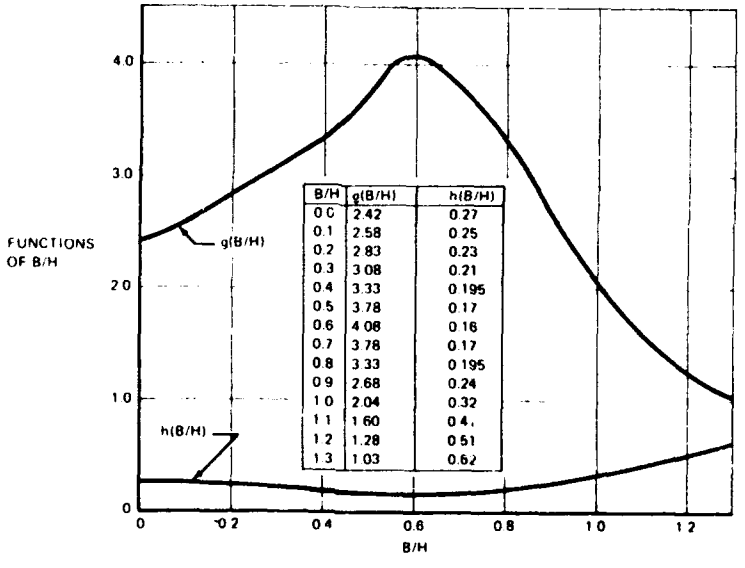


| B/H | g(B/H) | h(B/H) |
|---|---|---|
| 0.0 | 2.42 | 0.27 |
| 0.1 | 2.58 | 0.25 |
| 0.2 | 2.83 | 0.23 |
| 0.3 | 3.08 | 0.21 |
| 0.4 | 3.33 | 0.195 |
| 0.5 | 3.78 | 0.17 |
| 0.6 | 4.08 | 0.16 |
| 0.7 | 3.78 | 0.17 |
| 0.8 | 3.33 | 0.195 |
| 0.9 | 2.68 | 0.24 |
| 1.0 | 2.04 | 0.32 |
| 1.1 | 1.60 | 0.4. |
| 1.2 | 1.28 | 0.51 |
| 1.3 | 1.03 | 0.62 |

Fig. 13. Configuration and $K_1$ calibration of the torsion-loaded, single-edge-cracked plate specimen.

A solution for $\mathcal{G}$ under constant deflection is given as

$$\mathcal{G} = \frac{2GB^2y^2H}{3H_m^2a^2} \tag{48}$$

where $y$ is the deflection or displacement of an inner load point with respect to the outer load point on one of the specimen arms, and $a$ is the crack length measured from the load point position. This technique causes $\mathcal{G}$ to decrease when the crack length extends.

The expression for compliance in Eq. (46) appears to have been derived from the analysis of torsional deflection of a rectangular section; therefore, the constant 3/4 must represent one configuration only. The solutions have been extended to apply to a general configuration defined in terms of the ratio $B/H$ [28]. These are shown, for constant and decreasing $K_I$, respectively, as Eqs. (49) and (50):

$$K_I = \frac{0.845\ g\left(\frac{B}{H}\right)H_m P}{B^2\sqrt{H}} \tag{49}$$

$$K_I = \frac{EByh\left(\frac{B}{H}\right)}{H_m a}. \tag{50}$$

When face grooves are used to direct crack propagation, the actual value of $K_I$ is obtained by multiplying the value for the ungrooved specimen by $\sqrt{B/B_n}$ (see Sec. 2.6).

**Center-Cracked and Double-Edge-Cracked Plate Specimens**

The double-edge-cracked plate specimen is symmetrically similar to the center-cracked configuration, and both are suited to evaluating sheet materials. However, neither specimen is as efficient as the single-edge-cracked specimen from the standpoint of load and material requirements. When the center-cracked specimen is loaded at a distance remote from the crackline, $K_I$ increases as the crack extends; when the specimen is loaded at the crackline, $K_I$ decreases for a certain range of crack extension. In this regard, $K_I$ decreases under constant load rather than fixed crack-opening displacement, as has been discussed. The surface-cracked specimen probably simulates the majority of defective structures, but is somewhat weak from an analytical viewpoint.

**Configuration and $K_I$ Calibration of the Remote-Loaded, Center-Cracked Specimen.** The specimen shown in Fig. 14 is recommended for fracture-toughness

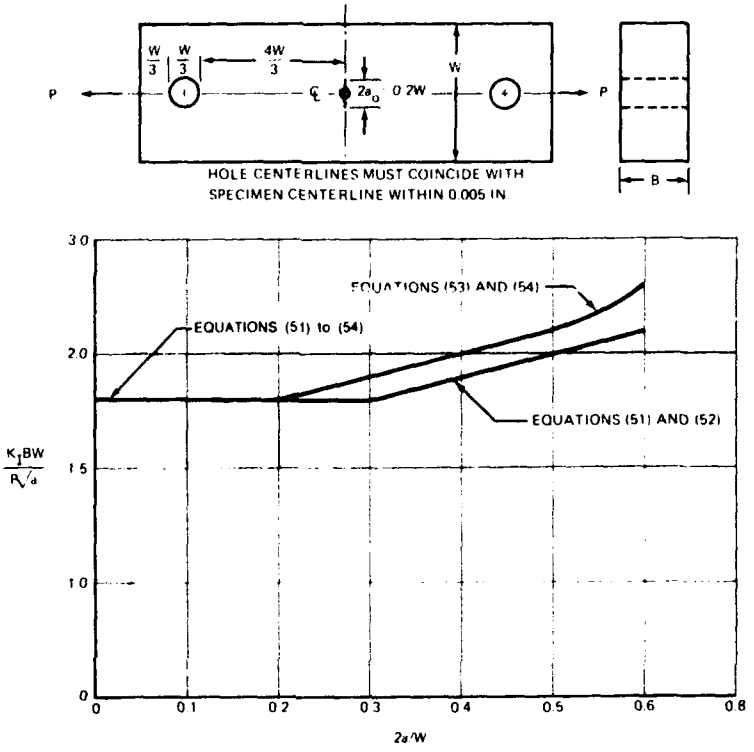


Fig. 14. Configuration and $K_I$ calibration of the remote-loaded, center-cracked plate specimen.

testing, and the details of the configuration have been reviewed at length [4]. It is claimed that the commonly used tangent expression,

$$\frac{K_I BW}{P\sqrt{a}} = \left[\frac{W}{a}\tan\frac{\pi a}{W}\right]^{1/2}, \tag{51}$$

and the equation

$$\frac{K_I BW}{P\sqrt{a}} = (\pi)^{1/2}\left[\frac{1+8\left(\frac{a}{W}\right)^4}{1-2\left(\frac{a}{W}\right)^2-8\left(\frac{a}{W}\right)^4}\right]^{1/2} \tag{52}$$

do not properly satisfy the boundary conditions of the configuration. Three other calibrations have been reviewed independently [5] which are in close agreement with each other and can be expressed by a single curve. The polynomial

$$\frac{K_I BW}{P\sqrt{a}} = 1.77 + 0.227\left(\frac{2a}{W}\right) - 0.51\left(\frac{2a}{W}\right)^2 + 2.7\left(\frac{2a}{W}\right)^3 \tag{53}$$

represents this curve to within 0.5% over the range of $2a/w$ from 0 to 0.7, while that of Eq. (54),

$$\frac{K_I BW}{P\sqrt{a}} = 1 - 0.1\left(\frac{2a}{W}\right) + \left(\frac{2a}{W}\right)^2, \tag{54}$$

is slightly less accurate (1% in the same range), but is easier to use. It is generally agreed that either Eq. (53) or (54) should be used rather than Eq. (51) or (52).

**Configuration and $K_I$ Calibration of the Crackline-Loaded, Center-Cracked Specimen.** This specimen, shown in Fig. 15, is pin loaded at a distance $S$ above and below the crackline. If $S$ is small compared with $a$ and $a$ is small compared with $W$, and the load $P$ is maintained at a constant level, $K_I$ decreases as $a/W$ increases to a limiting value and then begins to increase in accordance with [9]

$$\frac{K_I BW^{3/2}}{Pa} = \frac{3.3\left(\frac{S}{W}\right)^2 + 2\left(\frac{a}{W}\right)^2}{\left[2\sin\frac{2\pi a}{W}\right]^{1/2}\left[\left(\frac{a}{W}\right)^2 + \left(\frac{S}{W}\right)^2\right]^{3/2}}. \tag{55}$$

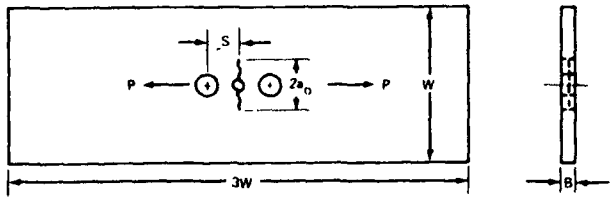


Fig. 15. Configuration and $K_I$ calibration of the crackline-loaded, center-cracked plate specimen.

**Configuration and $K_I$ Calibration of the Surface-Cracked Specimen.** The configuration is shown in Fig. 16. Two solutions for $K_I$ that do not lend themselves to presentation in calibration form are given below:

$$Q = \left[\phi^2 - 0.212\left(\frac{\sigma_g}{\sigma_{ys}}\right)^2\right] \tag{56}$$

$$\phi = \int_0^{\pi/2} \sqrt{1 - \left[\frac{C^2 - a^2}{C^2}\right] \sin^2\theta \, d\theta}. \tag{57}$$

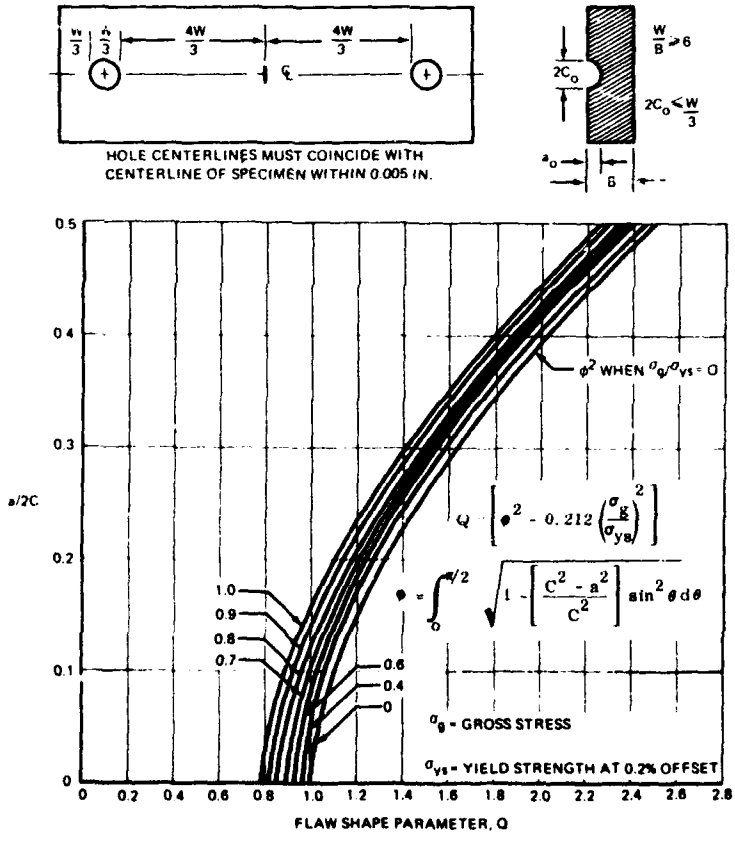


Fig. 16. Configuration and $K_I$ calibration of the surface-cracked plate specimen.

The following equation contains an estimate of the effect of plasticity on $K_I$ [29], and the factor $Q$ is found in the accompanying graph as a function of the crack geometry described in terms of the ratio of crack depth $a$ to crack length $2c$ ($a/2c$) and for different ratios of applied gross stress to yield strength ($\sigma_g/\sigma_{ys}$):

$$K_I = 1.1\ \sigma_g \sqrt{\frac{\pi a}{Q}}. \tag{58}$$

This equation is limited in use to $a/B$ ratios ($B$ is thickness) of 0.5.

The following equation was derived to extend the analysis to deeper cracks [30]:

$$K_I = M_e M_P \sigma \sqrt{\frac{\pi a}{Q^*}}, \tag{59}$$

where $Q^* = Q$ for the curve of $\sigma_g/\sigma_{ys} = 0$. The correction for free surfaces $M_e$ was obtained by a point-collocation method for $a/B$ ratios to 1.0, while for plasticity a correction $M_p$ based on a model of an extended yield zone [31] was obtained. Values of $M_e$ and $M_p$ are shown in Figs. 17 and 18, respectively. The value of $M_e$ is limited by the amount of plasticity between the crack front and the back free surface (Fig. 17). The limiting values for different ratios of $\sigma_g/\sigma_{ys}$ are shown by dashed lines at a specific value of $m$, which is a strain-hardening coefficient defined as the quantity $1 - \sigma_{ys}/\sigma_0$ where $\sigma_0$ is the maximum uniaxial tensile stress, an estimate of which is the ultimate tensile strength of the material. The value of $M_p$ is presented in Fig. 18 as a function of applied stress ratio $\sigma_g/\sigma_{ys}$ for different values of $m$.

For $a/B$ ratios less than 0.5, the correction for free surfaces in Eq. (59) is higher than that in Eq. (58) by about 6% to 7%, and it appears from the discussion of the subject [30] that the correction for plasticity in Eq. (58) is adequate for moderate values of $\sigma_g/\sigma_{ys}$. Therefore, it seems reasonable to use Eq. (58) to estimate the effect of plasticity on $K_I$ when testing surface-cracked specimens simply because it has been used more often than the approach indicated by Eq. (59).

**Configuration and $K_I$ Calibration of the Double-Edge-Cracked Specimen.** This specimen is shown in Fig. 19. Two calibrations for $K_I$, Eqs. (60) and (61), are shown below;

$$\frac{K_I BW}{P\sqrt{a}} = \left[\frac{W}{a}\left(\tan\frac{\pi a}{W} + 0.1\ \sin\frac{2\pi a}{W}\right)\right]^{1/2} \tag{60}$$

$$\frac{K_I BW}{P\sqrt{a}} = 1.98 + 0.36\left(\frac{2a}{W}\right) - 2.12\left(\frac{2a}{W}\right)^2 + 3.42\left(\frac{2a}{W}\right)^3. \tag{61}$$

Equation (60) is the commonly used closed trigonometric expression [4] and is not considered sufficiently accurate for values of $2a/W$ greater than about 0.4.

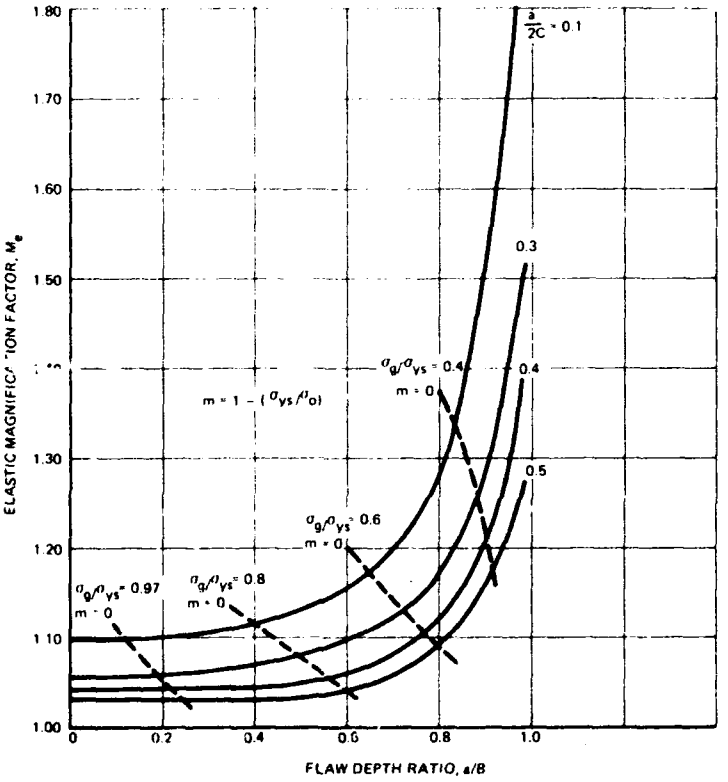


Fig. 17. Elastic stress-intensity magnification factor $M_e$ for surface-flawed tension plate.

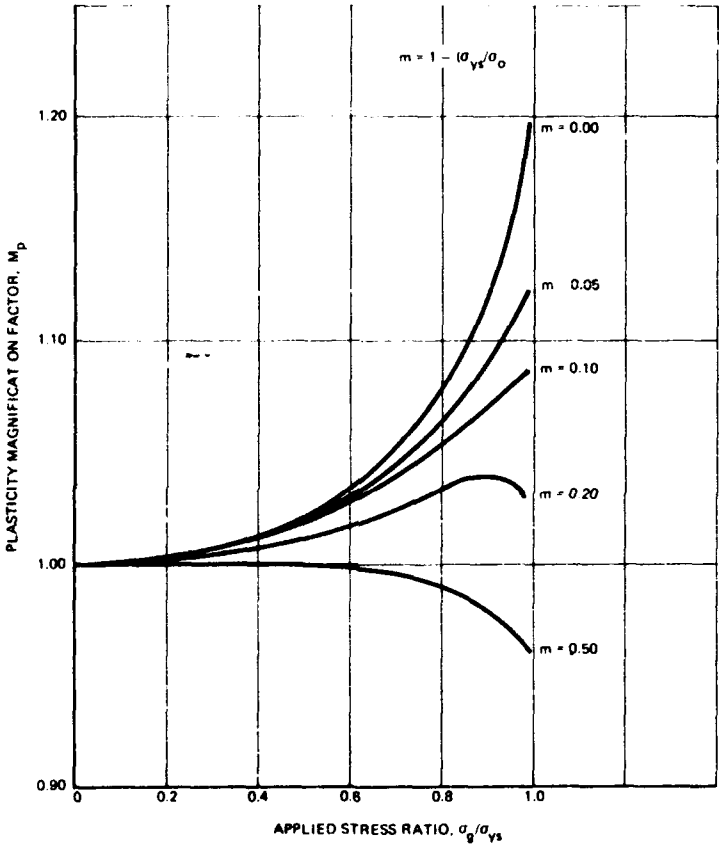


Fig. 18. Plasticity stress-intensity magnification factor $M_p$ for a penny-shaped crack in an infinite solid subjected to uniaxial tension.

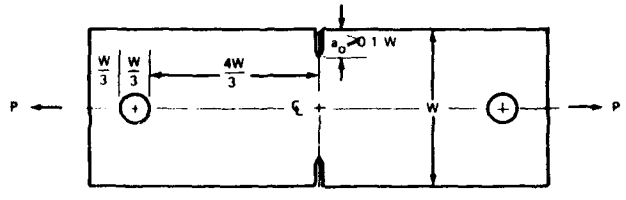


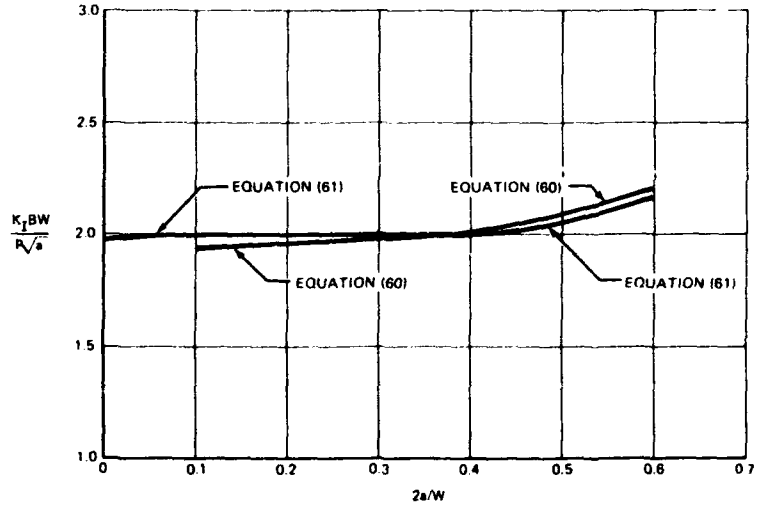


Fig. 19. Configuration and $K_I$ calibration of the remote-loaded, double-edge-cracked plate specimen.

Equation (61) was obtained by complex variable methods [32] and is considered to be accurate to within 1% for $2a/W$ values from 0 to 0.7 [5].

### Circumferentially Cracked Round Bar Specimen

This specimen will probably be used only to evaluate rods or similar products with respect to the initiation value of $K_{Iscc}$. The configuration is shown in Fig. 20. Functions from five references compiled by Bueckner [33] are given in Table 2. His own results are considered to be the most accurate (within 1%) and are recommended for use in Eq. (62);

$$K_I = \frac{4P}{d^2}\sqrt{\pi D^2} \cdot f\left(\frac{d}{D}\right) \tag{62}$$

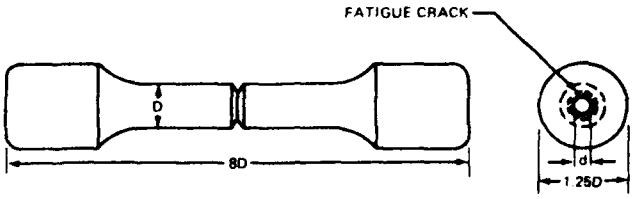


Fig. 20. Configuration and $K_I$ calibration of the circumferentially cracked, round bar specimen.

**Table 2.** Values of $f(d/D)$

| $d/D$ | *Ref. 33* | *Ref. 34* | *Ref. 35* | *Ref. 36* | *Ref. 9* |
|---|---|---|---|---|---|
| 0.5 | 0.240 | 0.239 | 0.230 | 0.224 | 0.227 |
| 0.6 | 0.255 | 0.252 | 0.234 | 0.232 | 0.255 |
| 0.707 | 0.259 | 0.258 | 0.229 | 0.233 | 0.259 |
| 0.8 | 0.251 | 0.250 | 0.217 | 0.224 | 0.251 |
| 0.9 | 0.210 | 0.210 | 0.195 | 0.199 | 0.210 |

$$\frac{K_I D^{3/2}}{P} = 1.72\,\frac{D}{d} - 1.27. \tag{63}$$

Equation (63) is a dimensionless $K_I$ calibration of Eq. (62) and presents coefficients prepared from Ref. 33 as reported in Ref. 5. This form has the advantage of being linear in $D/d$, which simplifies calculations.

### 2.5 Testing Procedure and Data Presentation

Testing methods that use precracked specimens can be conveniently discussed in terms of whether the stress intensity factor $K_I$ increases, decreases, or remains constant with crack extension. In all methods the objective is to establish the threshold stress intensity factor $K_{Iscc}$ for SCC. Evidence has been presented which strongly indicates that $K_{Iscc}$ is a genuine threshold in titanium alloys [37], but at present there is no basis for extending this indication to other alloy systems. In certain aluminum alloys, either residual quenching stresses or stresses generated at the crack tip by the wedging action of corrosion products, or both, have resulted in stress corrosion cracking without an applied stress [38,39]. This behavior has led to the adoption of at least two criteria by which to characterize the stress corrosion threshold.

### $K_{Ii}$ vs Time to Failure

The specimen geometries that are usually employed in tests where $K_I$ increases with crack extension are shown in the overall classification (Fig. 3). To measure resistance to SCC, these specimen configurations are sustain loaded in the presence of the environment by remote tension or bending to selected initial stress intensity $K_{Ii}$ levels below the fracture toughness $K_{Ic}$ of the alloy. The $K_{Ii}$ levels are calculated by substituting the initial crack length measurement, the applied tension load or bending moment, and the pertinent specimen dimensions into the equation that describes the $K_I$ calibration for the specimen. The time to failure of each specimen is then plotted against the corresponding $K_{Ii}$ level. A minimum $K_I$ value is established at which stress corrosion crack growth does not occur after an arbitrarily selected time. This apparent threshold stress intensity level has been designated $K_{Iscc}$.

Shapes of stress corrosion curves plotted in this manner are given schematically in Fig. 21. Curve A is typical for titanium alloys and curve B is typical for steel alloys; however, it should be emphasized that no shape is peculiar to any alloy system. The displacement of curve B toward longer times to failure is specific to the particular alloy/corrodent combination and is thought to indicate different crack-initiation properties. It has been demonstrated that the shape of a stress corrosion curve provides a qualitative indication of the relationship between stress intensity and crack growth rate or crack velocity [40].

The threshold stress intensity level $K_{Iscc}$, like the time-to-failure threshold development on conventional smooth specimens, depends upon the duration of the test. Arbitrary waiting periods have been used to determine whether cracking

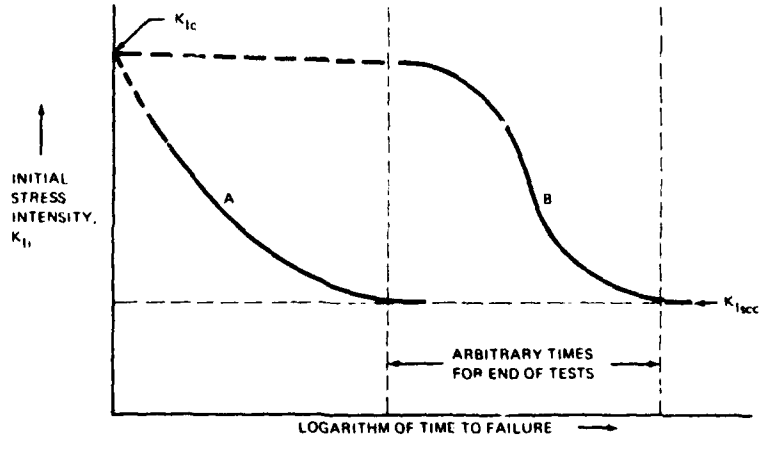


Fig. 21. Schematic representation of stress corrosion data produced by test method based on time to failure.

will occur. In titanium alloys the period would be 6 hr; in low alloy steels, [illegible] hr; and in high alloy steels of the maraging type, 1000 hr. Although aluminum alloys are not usually evaluated by this particular technique they would require a waiting period of about 1000 hr to establish a $K_{Iscc}$ level.* It is recommended that specimens which survive the selected test period should be failed in air and scrutinized for evidence of crack growth that was not visible on the side surfaces of the specimen. Also, the fracture faces of all specimens should be examined so that crack length measurements made on the surface prior to testing can be confirmed.

The crack-initiation testing procedure requires the use of several specimens to [illegible] $K_{Iscc}$. In another version of the same procedure, a single specimen is [illegible] loaded to a $K_I$ level below the anticipated $K_{Iscc}$. After an established [illegible] period the specimen is examined for surface evidence of crack growth. If crack growth has occurred the precrack is resharpened by fatigue and subsequently [illegible] loaded to another $K_I$ level. This procedure is repeated until crack growth is received at a $K_I$ level designated $K_{Iscc}$.

### $K_I$ vs Crack Growth Rate

Constant-deflection, $(W-a)$-indifferent and $(W-a)$-dominated, single-edge cracked plate specimens have been used to measure stress corrosion [illegible] in terms of crack growth rate and crack-arrest criteria. The specimen is fixed in a holding device and the environment applied to the tip of the machined notch. The arms of the specimen are deflected (by turning a bolt, inserting a [illegible] or holding with an elastic proving ring) until a natural crack pops in from the notch. If the specimen has been fatigue precracked, it is deflected, in the presence of the corrodent, to a predetermined $K_{Ii}$ value. Crack opening displacement $v$ is measured along the line of load application and maintained at the same level for the duration of the test. Once the environment is applied to the specimen, the crack length is monitored as a function of time elapsed from pop-in or deflection. The overall result of this procedure is to cause the stress intensity factor to decrease as the crack extends under the influence of the environment. The slope of the crack-length-vs-time curve at any crack length provides crack growth rate. For the $(W-a)$-indifferent specimen, the use of an equation of the type $K_I\sqrt{H/Ev}$ vs $a/H$ converts crack length into stress intensity $K_I$. For the $(W-a)$-dominated specimen, a knowledge of the unique $K_I$ calibration is required to determine the stress intensity level.

The data are plotted as logarithmic crack growth rate or logarithmic crack velocity vs stress intensity factor. Generally, three stages or regions of crack growth rate may be identified in stress corrosion results presented in this manner. They are shown only schematically in Fig. 22 because the actual relationship

*Although these time periods have been used extensively, they are by no means accepted as standards and should not be so regarded. *(Editor)*

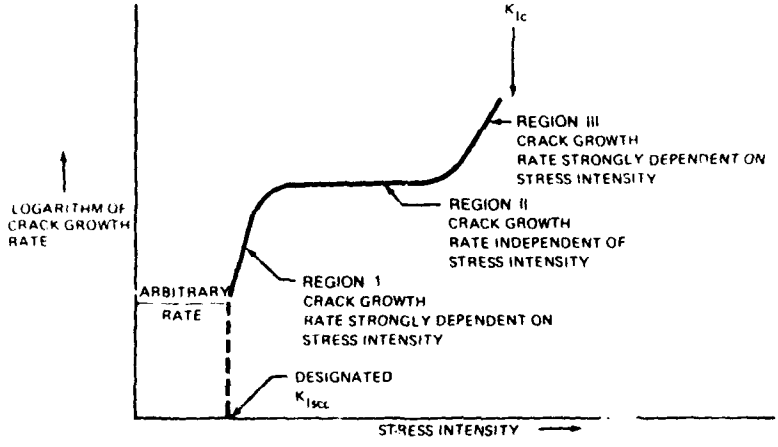


Fig. 22. Schematic representation of stress corrosion data produced by test method based on crack growth rate.

between crack velocity and stress intensity is a function of alloy composition and metallurgical structure and of the chemical and electrochemical characteristics of the environment. The first region occurs at low stress intensities where crack growth rate is strongly stress-intensity dependent and the crack may eventually arrest, thus indicating $K_{Iscc}$. Generally, the crack extends at an extremely slow rate and $K_{Iscc}$ is designated as an arbitrarily selected crack velocity. The second region occurs at intermediate stress intensities where crack growth rate is independent of stress intensity. The third region occurs at stress intensities close to $K_{Ic}$ where the crack growth rate again becomes dependent upon stress intensity.

Variations of this typical stress-intensity-vs-crack-velocity relationship have been reported by a number of investigators. For example, commercial aluminum alloys tested under controlled potential in saturated KI do not exhibit region III behavior and may show two plateaus in the stress-intensity-independent portion (region II) of the curve [41]. Heat-treatment condition also had a strong influence on the slope and position of the region I and II portions of the curve when Ti-8Al-1Mo-1V alloy was tested under 0.6*M* KCl/-500 mV and 10*M* HCl/ open-circuit conditions [42].

The type of specimen and the method of loading employed during a stress corrosion test influences the extent of stress-intensity-vs-crack-velocity data. Crack growth rate and $K_{Iscc}$ data have been taken on single-edge-cracked plate specimens of titanium alloys in which the stress intensity increased with crack extension [43]. Specimens were tested in tension in a universal testing machine at a predetermined crosshead velocity. The crosshead motion was stopped when the crack initiated ($K_{Iscc}$), which allowed the stress corrosion crack growth rate

to be monitored over a longer distance before rapid failure occurred. Only region II and III behavior may be characterized by this tension testing technique. Specimens in which the stress intensity is designed to remain constant during crack extension have been employed to characterize stage I, II, and III behavior of steels [44] and stage I and II behavior of aluminum alloys [41].

Crackline-loaded, single-edge-cracked plate specimens are most efficiently used for testing high strength aluminum alloys in the S-L and S-T orientations, since titanium and steel alloys are usually too tough to pop in mechanically without arm breakoff. Specimens of these materials require precracking by fatigue and may also need side grooving to maintain the crack in plane and/or to avoid crack branching. Crackline-loaded, single-edge-cracked specimens of titanium and steel alloys may be tested to determine $K_{Iscc}$ if they are precracked by fatigue and self-stressed to different applied $K_I$ levels. The specimens that show no crack growth are then deflected below $K_{Iscc}$ and those that do show growth are stressed above $K_{Iscc}$. Cracks in the latter specimens will, of course, arrest at $K_{Iscc}$ if they remain in plane.

Knowing when to terminate the stress corrosion test is a problem when crack-arrest methods are used, since proof is required that the crack is not propagating. When further crack-velocity-vs-stress-intensity data ranging from near $K_{Ic}$ to the arbitrary $K_{Iscc}$ are available for a variety of alloy/corrodent combinations, it may be possible to describe resistance to stress corrosion cracking by referring to features such as the slopes and/or intersections of the different stages. With crack-arrest methods, it is again recommended that specimens should be broken open after testing to observe the fracture characteristics and to check the dimensions and shapes of the precrack and the stress corrosion crack.

## 2.6 Specimen Preparation and Testing

This section is essentially a commentary on the practical aspects of employing precracked specimens for stress corrosion testing. Many recommendations and hints concerning specimen preparation, testing procedure, data reporting, etc., have been made previously [4,5] in conjunction with fracture-toughness testing. Others, however, are the results of experiments conducted specifically to aid in the establishment of realistic guidelines for stress corrosion testing.

### Surface Preparation

The quality of the surface finish on plate specimens is usually governed by the dimensional tolerances required to locate surfaces for positioning the notches and pinholes. Specimens are generally rough sawed from plate, forging, or extrusion stock and milled square with an intermediate mill cutter. The surface quality may be improved at the apex of the machined slot to facilitate observation of both the notch-sharpening operation and crack initiation during actual stress

corrosion testing. Test methods that employ a crack-arrest criterion to establish $K_{Iscc}$ usually require a fine-milled finish or a ground finish on two opposite sides of a specimen so that crack growth can be measured readily. Many investigators hand polish a specimen so that crack length can be monitored visually at several locations along the specimen width.

### Loading Arrangement

Precracked specimens are loaded externally in tension or bending by either constant-load or constant-deflection techniques. Loading arrangements should be designed to conform with the boundary conditions assumed in deriving the $K_I$ calibration, or errors in the determination of $K_I$ will result. The "Proposed Method of Test for Plane Strain Fracture Toughness of Metallic Materials" [6] suggests that (a) bend-test fixtures should be designed to minimize errors which can arise from friction between specimen and supports, (b) the general gripping arrangement for tension testing should be designed to allow rotation as the specimen is loaded, and (c) careful attention should be given to achieving as good alignment as possible. These suggestions should be adopted during stress corrosion testing even though the load (or deflection) is constant rather than increasing until fracture of the specimen.

**Constant Load.** Constant load is usually achieved by deadweight, hydraulic, or mechanical methods that employ lever systems and associated facilities such as tension machines and test rupture racks. The accuracy of the load measurement depends upon the sensitivity of the instrumentation and the accuracy of the calibration for load. The interpretation of stress corrosion results generated on precracked specimens may be severely affected by an external vibration. Corrosion fatigue rather than stress corrosion may cause premature crack initiation when testing techniques that employ a crack-initiation criterion to establish $K_{Iscc}$ are used. If an external vibration exists in the laboratory or at the test site, the experimenter should resort to hydraulic or mechanical rather than deadweight loading. This will eliminate the effect of external vibration.

**Constant Deflection.** Constant-deflection specimens are loaded by deflecting the arms of specimens with a bolt, wedge, pin, or other device. The simplicity of this stressing method allows the specimen to be portable. The accuracy of load measurement depends upon the accuracy with which the specimen compliance depicts the load in terms of deflection and upon the exactness of the measurement of deflection. It is not expected that an external vibration will affect crack velocity when testing techniques that employ a crack-arrest criterion to establish $K_{Iscc}$ are used.

Several techniques have been employed to produce constant deflection in $(W-a)$-indifferent and $(W-a)$-dominated, crackline-loaded, single-edge-cracked plate specimens. A modified version of the original $(W-a)$-dominated fracture specimen [45] has been used for stress corrosion testing of steels [17]. The

loading assembly is shown schematically in Fig. 23a. A drilled and tapped hole in the top arm of the specimen contains a bolt which contacts a pin which is set in a drilled hole located in the bottom arm normal to the bolt and spanning the specimen thickness. Both pin and bolt are machined from high strength steel to prevent plastic flow of each component. After fatigue cracking, the specimen is loaded in a vise with a torque wrench and a NASA-type clip gage. For a loading bolt of reasonably tough steel, this loading operation may require a high torque, so that lubrication of the threads is helpful in preventing shearing of the bolt. When crack growth arrests, the deflection is noted and the specimen is unloaded. It is subsequently reloaded in a tension machine to the deflection at arrest to measure the corresponding load. Alternatively, the load may be calibrated by instrumentation of the bolt or by use of a previous compliance calibration.

Specimens classified as $(W-a)$ indifferent have been loaded in very similar assemblies to measure the crack growth and crack-arrest characteristics of high strength aluminum alloys. In one case [46], the almost circular pin is replaced by a semicircular steel insert and the specimen is stressed by a ball bearing pressed against the steel insert by a setscrew (Fig. 23b). Another method eliminates the steel pin or insert [39] and allows the steel bolt to bear against one face of the machined slot (Fig. 23c). Still another technique [41] employs a drilled and tapped hole which continues completely through the bottom arm of the sample. Bolts are screwed into both arms and upon contact at the center of the machined slot are torqued to provide the necessary deflection (Fig. 23d). These same holes may also be used to grip the specimen during precracking by fatigue loading.

Alternatively, grips have been attached to this specimen and stressing accomplished using a calibrated proving ring [47]. The specimen is loaded to a $K_{Ii}$ level and when the crack propagates, the load imposed by the proving ring relaxes until equilibrium is achieved and the crack arrests. It is claimed that the load is more easily measured to the desired accuracy than is the deflection in bolt-loading arrangement.

Metallic wedges are also employed in place of bolts (Fig. 23e) to stress both standard $(W-a)$-indifferent and $(W-a)$-dominated fracture specimens [42] and specimens that are too thin to accommodate a bolt [48]. The wedge is usually pressed into either the machined slot or a sawcut by using a vise. Plastic deformation of the specimen arms due to wedge loading of thinner samples detracts significantly from the quantitative value of the subsequent data. A small and operationally simple specimen of the decreasing $K_I$ type is currently being used to screen sheet and plate materials for SCC propagation characteristics by crack-arrest methods [49]. The machined slot is spanned at its midpoint by a tapered hole drilled and reamed normal to the anticipated direction of crack propagation to accept a standard tapered pin (Fig. 23f). The load is applied by forcing the tapered pin into the hole. A particular disadvantage of this loading method is that the originally circular reamed hole becomes oval as the tapered pin is forced into it. This results in some uncertainty about the actual points at which the tapered pin applies its load to the specimen.

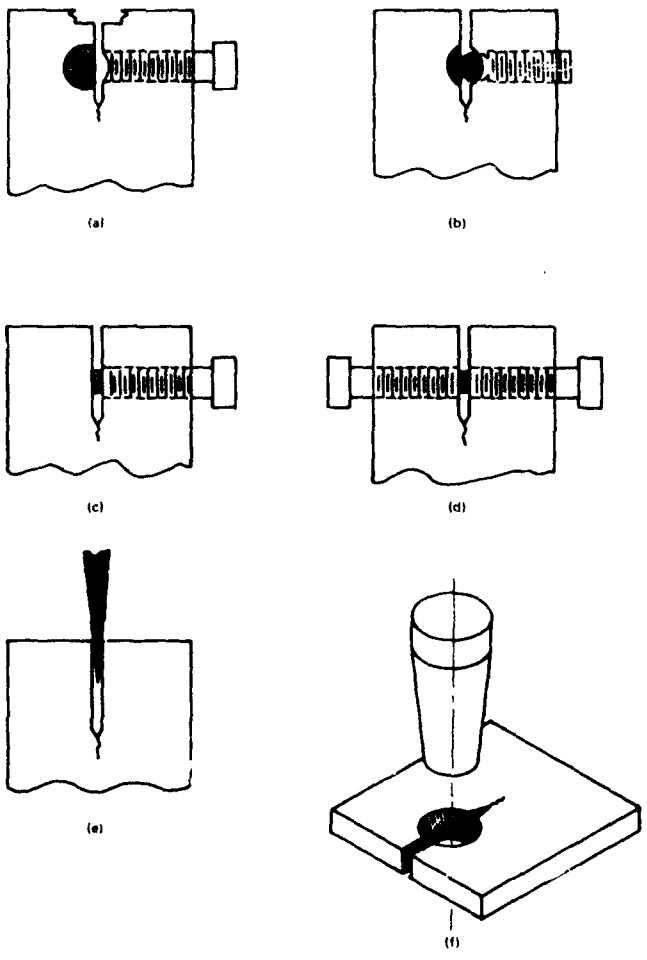


Fig. 23. Constant-deflection loading assemblies.

### Crack Configuration

The width, height (or length), and thickness proportions of each precracked specimen suitable for use in stress corrosion testing, together with the distances between loading supports, are those currently recommended in publications of Committee E-24 on Fracture Testing of Metals of the American Society for Testing and Materials. These primary dimensions are usually expressed in terms of the width $W$ of the specimen. Because testing procedures for SCC are generally based on subcritical rather than unstable crack extension, crack length considerations merit particular discussion. In stress corrosion testing, it is specified that the length of the initial crack-starter notch, that is, the machined slot with a fatigue or mechanical crack at its apex, can be as short as $0.2W$. Both minimum and maximum crack lengths depend upon the limits of accurate $K_I$ calibration with respect to the range of ratios of crack length to specimen width or height.

**Machined Slot.** Several designs of crack-starter notches are available for most plate specimens [6]. The notches that are located centrally with respect to pertinent specimen dimensions usually extend to 20% of the specimen width or, for the case of the crackline-loaded, $(W-a)$-indifferent specimen, to a percentage of the specimen height. The machined slot is used to simulate a crack because it is not practicable to produce plane cracks of sufficient size and accuracy in plate specimens. The compliance of a specimen containing a crack of given length will not be exactly the same as that of a specimen containing a finite-width slot of the same length. To minimize errors arising from this difference, it is recommended that the specimen be made large and the slot width narrow [5]. A slot width of 1/16 in. is suggested because this is the minimum width which is usually obtainable from the milling tools used to prepare the apex of the slot for further fatigue or mechanical extension. For stress corrosion testing of steel [50] and titanium alloys [51] that employed single-edge-cracked plate specimens loaded in bending, machined V-grooves rather than slots have been used extensively. The V-grooves apparently facilitate access of the environment to the crack tip. Special equipment is usually required to prepare the crack-starter notches in circumferentially cracked round-bar and surface-cracked plate specimens.

**Notch Acuity.** The slot should have as sharp a tip radius as possible to minimize either the stress intensity level required to produce a fatigue crack of at least 0.05 in. in a reasonable time or the bending moment required to produce mechanical pop-in to at least the same distance. Machined slots may be sharpened by milling a simple V-notch or chevron notch or by producing a narrower slot with a jeweler's saw. It has been reported that the notch root radius should be $<0.003$ in. [6] and 0.005 in. maximum [4], but when the chevron form of notch is used (Fig. 24), the notch root radius may be 0.01 in. or less [6]. This tolerance may be easily achieved with conventional milling and grinding equipment.

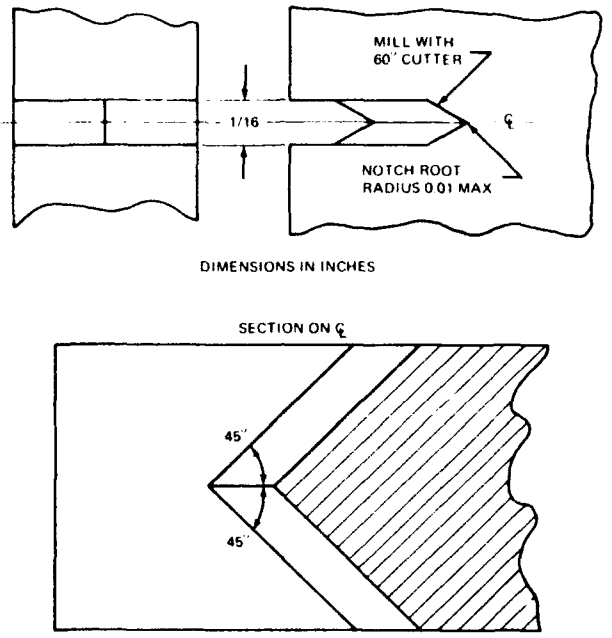


Fig. 24. Chevron notch for edge-cracked plate specimens.

**Fatigue Precracking.** There are few data available to justify recommending a specific procedure for fatigue precracking all types of specimens. The fatigue precrack should be sharp, flat, and normal to the specimen edge. It is desirable to follow the practices of fracture-toughness testing to produce straight cracks. Careful attention should be given to the equipment for fatigue precracking to ensure symmetry of load distribution with respect to the notch. The maximum stress intensity should be carefully controlled during the final stages of fatigue crack extension so that, over the final 2.5% of the overall crack-starter notch, it should be minimal but compatible with achieving at least 0.05-in. growth in a reasonable time. The initial machined notch has been sharpened by fatigue in the presence of a moderately aggressive environment in an effort to reduce the maximum stress intensity factor and the time required to initiate and propagate the precrack [52]. If the fatigue crack departs noticeably from the plane of symmetry of the notch, the greatest angle between the fatigue crack surface and the plane of symmetry should not exceed 10 deg for precise $K_I$ calibration [24]. Properly proportioned side grooves can cause the fatigue precrack to have a straight front rather than lead in the center of the specimen; if the grooves are too deep the crack may lead at the surface [7].

Whether the fatiguing process changes the material near the fatigue crack tip to alter the stress corrosion behavior has been investigated in a titanium alloy [53]. The specimens were fatigue cracked at various $K_I$ levels from about 15% to 85% of $K_{Ic}$, and in all cases similar $K_{Iscc}$ values were obtained. When a $K_{Iscc}$ value is based on the arrest of a propagating crack, fatigue precracking procedures are not as critical as those required for the establishment of $K_I$ vs time-to-failure data. If the crack propagates at the initial $K_I$ level, it soon grows well beyond any fatigue-damaged zone. An objection to fatigue precracking has also been made on the grounds that some local regions of the crack front at the onset of SCC may not be suitably disposed to propagate without either local detouring or mechanical fracturing, either one of which would be expected to require a somewhat higher $K_I$ than would continued propagation [7].

**Mechanical Pop-In.** In stress corrosion test methods that employ constant-deflection specimens, it has been especially convenient to torque the bolt until a short mechanical pop-in occurs. Even though in most instances the geometry of a mechanical crack is more difficult to control than that of a fatigue crack, many experimentalists consider this alternate method of precracking an attractive feature of the overall test procedure. The mechanical pop-in will not only eliminate the costly and time-consuming operation of fatiguing, but in conjunction with the $K_I$ calibration will indicate $K_{Ic}$ at arrest for the material. The mechanical pop-in method should be used only for decreasing $K_I$ tests.

Breakoff of specimen arms has occurred during attempts to sharpen crack-starter notches by mechanical pop-in of $(W-a)$-indifferent specimens. In high strength aluminum alloys, the $K_I$ level required to propagate stress corrosion cracks parallel to the rolling plane is low compared with the fracture toughness normal to this plane, and arm breakoff is not a serious problem. In most high strength titanium and steel alloys this is not true, so the extremely high torque stresses required on the bolt (or deflecting device) cause a high incidence of arm breakoff. It has been suggested [13] that arm breakoff would be minimized if the height of the specimen were increased with respect to the starting crack length.

In an effort to sharpen mechanically the apex of a crack-starter notch in titanium and steel alloys, procedures have been developed to decrease the bending moment required to cause pop-in. This, in turn, should generally reduce the tendency toward arm breakoff. In one method, the material (minus the bolt) is heat treated to a low toughness condition, and the notch is extended mechanically by torquing the bolt. The material is then re-heat treated to the desired condition and the original crack is propagated further by stressing again with the bolt. The second pop-in operation is facilitated by the relatively sharp starter notch produced by the first pop-in when the material was relatively brittle. In a second method, either the entire specimen or just the slotted end (again without the bolt) is cooled in liquid nitrogen (−320°F), and the notch is mechanically extended while the material is in this usually brittle condition. A wedge is generally used with the bolt to stress the specimen during pop-in by alternatively squeezing

the specimen in a vise to force the wedge into the end of the slot and torquing the bolt to maintain the deflection. The chevron form of notch is commonly used and is continually popped in until a relatively straight crack extends at least 0.05 in. beyond the intersection of the chevron with the full specimen thickness. Obviously this procedure is cumbersome enough that it would only be used in the absence of a fatigue loading capability.

**Crack Measurement.** Crack length measurements should be made before and after stress corrosion testing. Measurements made on the specimen surface prior to testing and while monitoring crack velocity often do not accurately represent the true crack length. Observations may also be hampered by corrosion products obscuring the crack tip. Specimens which do not fracture completely during testing are intentionally failed afterwards to allow examination of the morphology of the fatigue or mechanical starter crack. Re-fatigue cracking over a short distance is often employed to delineate the extent or absence of SCC. Crack-arrest-type specimens are commonly broken apart after testing by fracturing at liquid nitrogen temperature.

Several techniques have been recommended to establish the effective crack length and to limit the reporting of data from irregularly shaped crack fronts. For example, in fracture-toughness testing [6] the fatigue precrack is measured from the notched edge of the specimen to the center of the crack front and to midway between the center and the end of the crack front on each side. The average of these three measurements is used to calculate $K_I$. The fracture test is considered invalid if the difference between any two of the crack length measurements exceeds 5% of the average, or if any part of the crack front is closer to the machined notch root than 5% of the average crack length, or if any part of the crack front is less than 0.05 in. in length. Also, the length of the crack on either surface must not be less than 90% of the average crack length. If these rules were applied to a stress corrosion crack, many data would be invalid even though the criteria are less restrictive at longer crack lengths.

The form of the calibration indicates the magnitude of the errors in $K_I$ due to inaccuracies in the measurement of crack length. For example, in the case of crackline-loaded, constant-deflection-type specimens, where measurement of the stress corrosion crack is essential to establish $K_{Iscc}$, errors in $K_I$ may be minimized by maintaining ratios of crack length to specimen height $(a/H) > 3$ during stress corrosion testing. Errors in crack length measurement will result in relatively small errors in $K_I$ because the rate of change of $K_I$ with crack length is minimal in this region of the calibration curve (see Fig. 5).

Crack growth is usually monitored by direct optical observation of the specimen with a relatively low-magnification microscope. In a typical method, the crack is timed as it traverses each equally spaced line of a grid which is lightly scribed or printed along the expected trace of the stress corrosion crack plane. Crack velocity data have been taken on a tension-loaded, single-edge-cracked plate specimen by causing an electrical signal to interrupt the load profile of an X-Y

recorder each time the crack passed scribed lines [54]. The same technique is used to monitor crack velocity in tests performed on crackline-loaded, constant-deflection, single-edge-cracked plate specimens.

If it is not practicable to view the crack growth process directly, an indirect method has to be employed. The types and basic principles of instrumentation available for detecting crack extension by these means have been reviewed for fracture-toughness testing [4,5], and stress corrosion cracking [7]. The methods include monitoring of crack-opening displacement by a clip gage or a linear voltage differential transformer, measurement of electrical resistance of the specimens, and ultrasonic monitoring of crack fronts. In a technique designed specifically for stress corrosion testing, a fine grid of conducting lines is applied to a specimen surface across the anticipated crack path by various vacuum deposition methods [55]. The electrical resistance of the grid is monitored to indicate severing of the individual elements by the advancing crack. Whatever technique is employed, the instrumentation must be resistant to many corrosive environments for long periods of time; in particular, electrical methods must not influence the cracking process.

### Thickness

To regard $K_{Iscc}$ as a basic index of stress corrosion cracking, its value should be independent of specimen design and specimen dimensions, provided certain minimum requirements are fulfilled. These minimum requirements are generally interdependent and can only be established by experiment. The elastic stresses that surround the region of the crack tip are adequately described by the stress intensity factor only when the crack front plastic zone is small compared with other specimen dimensions that characterize the total crack-tip area. Information has been presented which suggests that both crack length and thickness should be greater than some multiple of a characteristic dimension of the plastic zone $(K_{Ic}/\sigma_{ys})^2$ for a valid $K_{Ic}$ test. Pending development of data on a variety of alloys, it has been tentatively recommended that this multiple should not be less than 2.5 [5]. However, it has not been established whether this same rule should be applied during the design of precracked specimens for stress corrosion testing.

The effect of specimen thickness on the stress corrosion characteristics of a titanium alloy [56], a steel [57], and an aluminum alloy [48] has been investigated in an attempt to establish the minimum thickness necessary to obtain a minimum value of $K_{Iscc}$ in terms of some multiple of $(K_{Iscc}/\sigma_{ys})^2$. Single-edge-cracked plate specimens of mill-annealed Ti-6Al-4V alloy (1.5 in. by 7.5 in. by thickness) were prepared by machining 1-in.-thick plate to size. The thicknesses investigated ranged from 0.98 to 0.010 in. Some of the specimens 0.125 in. thick and all of those thicker were tested by four-point bending, whereas some of the specimens 0.125 in. thick and all of those thinner were tested by remote tension. Tests of the 0.125-in.-thick specimens provided a basis for comparison

on bend- and tension-loading modes. To determine the stress corrosion threshold $K_{Iscc}$, at least five specimens for each thickness were tested at different initial stress intensity levels $K_{Ii}$ in 3.5% aqueous sodium chloride solution. No transition was observed in $K_{Iscc}$ values; $K_{Iscc}$ values of about 20 ksi $\sqrt{\text{in.}}$ were obtained for all thicknesses. Good agreement was obtained when the tension test data were compared with the bend test data at a specimen thickness of 0.125 in. A high resistance to SCC in the same environment had been reported earlier for thinner gages of duplex-annealed Ti-8Al-1Mo-1V and mill-annealed Ti-6Al-4V [58]. This investigation used center-cracked specimens loaded in tension to evaluate 0.025- and 0.050-in.-thick alloy sheet and single-edge-cracked specimens stressed in four-point bending to characterize 0.50-in.-thick plate. All specimens were taken from different heats. The observation that SCC of alpha-beta titanium alloys occurs near the (1017) or (1018) planes of the alpha phase suggests that preferred orientation might have a significant effect on stress corrosion behavior and thus influence the interpretation of thickness-effect results.

Specimens of AISI 4340 steel were prepared and tested in the same manner as the mill-annealed Ti-6Al-4V except that loading was accomplished by cantilever rather than four-point bending. In contrast to the results on Ti-6Al-4V, higher stress intensity thresholds were observed for the thinner specimens. The minimum $K_{Iscc}$ was attained when the specimen thickness was $\geqslant 2.5\,(K_{Iscc}/\sigma_{ys})^2$.

In the study of the effect of specimen thickness on the apparent $K_{Iscc}$ and on the $K_I$-vs-crack-growth-rate characteristics of 7079-T651 aluminum-alloy plate [48], constant-deflection, single-edge-cracked specimens of the $(W-a)$-indifferent type in thicknesses ranging from 1.0 in. to 0.050 in. were machined from 1-in.-thick plate. The thicker gages were bolt loaded, while the thinner gages were stressed with an aluminum wedge. No effect of thickness was observed on either $K_{Iscc}$ (defined on the basis of an arbitrary crack growth rate of $10^{-5}$ in./hr) or on $K_{Ic}$ vs crack growth rate where data points for mechanical pop-in ($\approx$20 ksi $\sqrt{\text{in.}}$) and $K_{Iscc}$ ($\approx$4 ksi $\sqrt{\text{in.}}$) correlated well for all thicknesses.

These limited experiments demonstrate that there is no obvious universal, unambiguous value for the thickness dimension in terms of the ratio $(K_{Iscc}/\sigma_{ys})^2$ that would provide a basic index $K_{Iscc}$ for susceptibility to SCC. As in the case of fracture-toughness testing, a reduction in the degree of arbitrariness is only possible when the amount of useful experimental data is increased. In particular, at present it can only be recommended that the dimensions of the plastic zone be kept at a minimum compared with the thickness dimension of the specimen. If the form of the material or the extent of loading facilities dictates the maximum specimen thickness, the resultant $K_{Iscc}$ data should be considered characteristic only of that material and its environment. This result may be satisfactory when specimen thickness and overall configuration resemble service application and experience; however, the translation of the $K_{Iscc}$ value to larger components of different basic geometry and loading detail must await the results of tests on thicker laboratory specimens to determine whether $K_{Iscc}$ is minimum.

The dilemma of estimating specimen thickness requirements and analyzing the corresponding stress corrosion data may be minimized by selecting the proper test specimen. Constant-deflection test specimens that exhibit decreasing $K_I$ with increasing crack length and that rely upon a crack-arrest criterion to establish $K_{Iscc}$ will also show a decrease in relative plastic zone size $(K_I/\sigma_{ys})^2$, as the stress corrosion crack propagates from mechanical pop-in ($K_{Ic}$) to an arrest value at $K_{Iscc}$ ($<K_{Ic}$). If the crack propagates in the corrosive environment at the high $K_I$ level, the resultant $K_{Iscc}$ at complete crack arrest may be regarded as a basic property of the material analogous to $K_{Ic}$. A test technique that relies upon $K_I$ increasing with crack extension usually establishes $K_{Iscc}$ by sustain loading specimens at $K_I$ levels intermediate between $K_{Ic}$ and $K_{Iscc}$ and recording time to failure. Promotion of excessive plasticity at the crack tip at high initial $K_I$ levels may deter the initiation of stress corrosion cracks. This effect may be alleviated by loading the specimen (that is, growing the plastic zone) in the presence of the environment.

**Side Grooving**

Investigators employing crackline-loaded specimens in particular have experienced difficulty in restricting cracking to that single plane which commences at the tip of, and is parallel to the direction of, the machined slot. No severe problems have been observed with 7000-series aluminum alloys to date because their susceptibility to SCC parallel to the rolling direction is much greater than their susceptibility in other directions; the wrought texture also exerts a strong influence to keep the crack in the desired plane. In an attempt to extend the use of crackline-loaded, $(W-a)$-indifferent, single-edge-cracked plate specimens to aluminum alloys with an equiaxed grain structure, side (or face) grooves have been machined along the expected trace of the SCC plane [48]. Semicircular and angular (60-deg) side grooves of depths up to 50% of specimen thickness were machined in 1-in.-thick 7079-T651 plate material (in which cracking out of plane is not a problem) to establish their effect on the relation between $K_I$ and crack growth rate. Although side grooves of either shape had very little effect on this relationship, subsequent limited application of shallow grooves to equiaxed aluminum-alloy specimens was not effective in preventing deviation of the stress corrosion crack from the intended plane. Deeper semicircular or V-grooves might be more effective or the problem might be minimized by increasing or tapering the height of the precracked specimen [13]. Crack growth rate data were obtained on contoured or tapered crackline-loaded, single-edge-cracked plate specimens of three steels [44]. Even with semicircular side grooves of up to 50% of specimen thickness, it was sometimes difficult to maintain the crack in the desired plane of extension. Deviation of stress corrosion cracks has been attributed partly to crack branching [40,44,59,60], which in turn has been associated with the effect of $K_I$ level on crack growth rate. If crack growth rate

increases rapidly with $K_I$, branching is absent; branching can occur when a constant crack growth rate with $K_I$ is indicated.

Shallow side grooves (usually 5% of specimen thickness on both sides) have been employed to suppress the formation of shear lips as well as to guide the crack along a single plane [7,17]. Limiting the size of shear lips facilitates the direct observation of crack length. For aluminum alloys, semicircular grooves are preferred over V-grooves [48] because of difficulty in removing corrosion products from the roots of angular grooves and the tendency for the crack to run into the groove flanks, which makes accurate crack length measurements difficult. Side grooves also minimize crack front bowing during stress corrosion crack growth in aluminum alloys [48]. It has been noticed [61] that the correction factor in $K_I$ for shallow, angular (60-deg) side grooves takes the expected form of $(B/B_n)^n$, where $B$ and $B_n$ are full- and groove-reduced thickness, respectively, and where $1/2 < n < 1$. When the fracture toughness in the groove flank direction relative to the fracture toughness in the forward crack direction is high, $n$ approaches 1/2; when it is low, $n$ increases toward unity. The influence of side grooving on the stress intensity factor is far from established, and correction factors should be treated with caution, especially if deep side grooves are used.

**Environment**

The very nature of the stress corrosion process demands that for meaningful stress corrosion characterization, equal significance should be attached to the metallurgical condition of the alloy, the environment, and stress. Metallurgical effects are described in Chapters 3, 4, and 5, whereas a dissertation on the chemistry of environments is outside the scope of this part. However, attention to elementary environmental considerations directly associated with the testing procedure is necessary to assess unambiguously the importance of quantifying the stress factor.

To date, most investigators have adopted a 3.5% aqueous sodium chloride solution as a "standard" environment, hoping that the resulting order-of-merit ranking will largely hold for other environments. The environment may be applied in a number of different ways to the crack-tip vicinity (similar to smooth-specimen testing), but it has been recommended that the specimen always be loaded in the presence of the environment. In a study of SCC testing techniques [62], aqueous sodium chloride solution was added before and after four-point bending single-edge-cracked plate specimens of a susceptible Ti-8Al-1Mo-1V alloy and a tougher, more resistant Ti-4Al-3Mo-1V alloy. Similar $K_{Iscc}$ values were obtained. A further series of tests on commercially pure titanium, which is very tough but is susceptible to SCC, indicated lower values for $K_{Iscc}$ when the specimens were loaded in the presence of the electrolyte. Recently, a similar trend has been noticed in alpha and alpha-beta commercial titanium alloys [51]. The $K_I$ values of specimens of Ti-6Al-4V alloy approaching $K_{Ic}$ were unaffected

when loaded in air for several hours prior to exposure to halogenated hydrocarbons [63]. Specimens loaded in the presence of the hydrocarbon failed at $K_I$ values close to 50% of $K_{Ic}$.

Vessels for containing the corrodent around each specimen are normally constructed of a suitable inert material. A thick-walled methacrylate container was used in conjunction with a center-cracked plate specimen during stress corrosion studies and acted as an additional buckling restraint [58]. It is essential that metallic containers, loading pins, instrumentation, loading bolts, etc., be insulated from the specimen with an efficient masking compound to eliminate any galvanic and/or crevice corrosion. Stress corrosion cells should be designed large enough to contain instrumentation such as probes and electrodes and also to provide good visibility of crack growth kinetics.

### Recording of Data

A complete account of any type of stress corrosion testing should be reported with care and considerable detail because the results will always reflect the factors that were peculiar to the test. Fracture testing and fracture mechanics analysis are relatively recent developments in materials engineering; consequently, it is necessary to provide the maximum amount of information to the person attempting to use the data. Details of the environment, methods of loading, methods of detecting and measuring crack extension, all dimensions of the specimen, and duration of the test exposure should all be reported. In addition, the orientation of the precrack with respect to the direction of grain flow L, the transverse grain direction T, and the short transverse grain direction S of the specimen may be reported using the method described in Fig. 25.

## 2.7 Discussion of Test Methods

Single-edge-cracked plate specimens, loaded in bending either remotely or at the crackline, are the most widely used in the laboratory to characterize SCC. The constant-deflection version of the crackline-loaded specimen is extremely attractive to the corrosionist and the materials engineer because of its simple design and low cost of preparation. The availability of a compact deflecting device for this specimen offers portability that is very useful when many specimens and environments must be considered. There are also important materials savings when this geometry is compared with other configurations because the $K_{Iscc}$ (and sometimes $K_{Ic}$) and crack growth rate data may be satisfactorily generated on one specimen.

The constant-deflection specimen has been used extensively to date to measure the susceptibility of high strength aluminum alloy plate when the crack plane is parallel to the rolling direction. In other materials, there have been problems in keeping the stress corrosion crack in the required plane, thus limiting the

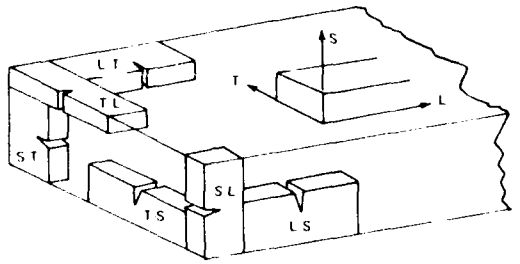


(a) RECTANGULAR SECTION

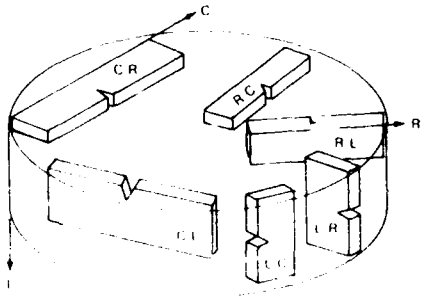


(b) CYLINDRICAL SECTIONS

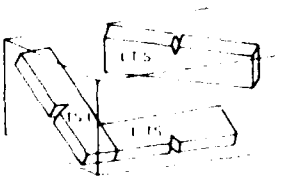


(c) NON-PRIMARY

L DIRECTION OF GRAIN FLOW
T TRANSVERSE GRAIN DIRECTION
S SHORT TRANSVERSE GRAIN DIRECTION
C CHORD OF CYLINDRICAL CROSS SECTION
R RADIUS OF CYLINDRICAL CROSS SECTION

FIRST LETTER: NORMAL TO THE FRACTURE PLANE
SECOND LETTER: DIRECTION OF CRACK PROPAGATION IN FRACTURE PLANE

Fig. 25. Fracture plane identification.

amount of crack growth rate data available when the crack-arrest technique is used. Much of the stress corrosion characterization in alloy systems other than aluminum has employed single-edge-cracked plate specimens in cantilever, three-point, or four-point bending. Other configurations have been used occasionally to simulate the flaw geometry and loading detail found in service. The torsion-loaded, single-edge-cracked specimen is simple and inexpensive and can be used either at constant deflection for experiments with decreasing $K_I$ or at constant load in experiments with constant $K_I$. The former technique shows promise as a method for determining the stress corrosion properties of high strength alloys in sheet form.

Following the report that a fatigue-sharpened precrack was a prerequisite for SCC of titanium alloys at room temperature in aqueous environments [64], several specimen geometries were employed to demonstrate the ability of stress intensity (rather than net-section stress) to describe the contribution of stress in the stress corrosion process. Experiments conducted on a crackline-loaded, center-cracked plate specimen of a titanium alloy showed that the crack velocity in 3.5% aqueous sodium chloride decreased with decreasing stress intensity and eventually stopped [65]. Increasing net-section stresses (with increasing crack length at constant tension load) could not satisfactorily account for either the velocity decrease or the apparent arrest. In a study involving 4340 steel [66] stressed at constant load in 3.5% aqueous sodium chloride, the same $K_{Iscc}$ values were obtained on three different specimen configurations (center- and surface-cracked plate and single-edge-cracked plate in cantilever bending). Net-section stresses were too strongly influenced by geometry to account for initiation of SCC.

Excellent agreement was reported [17] when $K_{Iscc}$ for a 12Ni-5Cr-3Mo maraging steel was measured using single-edge-cracked plate specimens loaded in cantilever bending and in constant deflection. The influence of stress intensity on the propagation rate of stress corrosion cracks and on the apparent $K_{Iscc}$ was determined in high strength aluminum alloys [41]. Of three different types of specimens employed, each exhibited different and characteristic variations of stress intensity with crack length. Excellent agreement of data was accomplished when crack velocity was plotted as a function of stress intensity.

Experiences from tests involving smooth specimens have indicated that a satisfactory test method for SCC should produce data that are reproducible, selective, and also interpretable from fundamental and engineering viewpoints. Data generated at two different laboratories for titanium and aluminum alloys have been compared successfully. Single-edge-cracked plate specimens of Ti-8Al-1Mo-1V alloy were evaluated by cantilever bending at one laboratory and by four-point bending at the other [62]. The $K_{Iscc}$ values obtained were similar. The stress-intensity-vs-crack-growth-rate curves for 7075-T651 and 7079-T651 aluminum alloys were compared at the same two laboratories and showed excellent agreement [39].

The rating of stress corrosion susceptibilities using constant-deflection, single-edge-cracked plate specimens of aluminum alloys agrees with the established trends based on smooth-specimen threshold data [39]. Where some discrepancies occur, service experience with the alloy has borne out the precracked data forecasts [39]. This same specimen has also provided very rapid and discriminating stress corrosion data about developmental high strength aluminum alloys and has aided substantially in the selection of heat-treatment conditions [67,68]. Between the very resistant and extremely susceptible high-strength aluminum alloys, there are about six logarithmic cycles of crack velocity [39]. Furthermore, some alloys can be efficiently rated in terms of crack growth rate after about one week of exposure to the corrodent. Discriminating between highly resistant tempers still poses a problem because of the difficulties associated with identification of extremely slow crack growth rates. Examination of specimens may also be hampered by surface contamination (e.g., general attack on overaged aluminum alloys or rusting of steels).

Precracked specimen techniques have been used extensively to study unambiguously the kinetics of SCC growth. The constant-deflection and constant-$K_I$ single-edge-cracked specimens in particular are well suited to measurement of crack velocity. The constant-deflection specimen has been used to study the influence of corrodent chemistry and electrochemistry on crack velocity in aluminum [41] and titanium alloys [42] and to investigate the solution chemistry within stress corrosion cracks [69]. It is important to note that similar precracked specimens are presently being employed during alloy-development and mechanism studies and during characterization of commercial alloys. The comparison of data will provide a valuable tool to discriminate the competitiveness of experimental alloys with the available commercial alloys. The advantage to the engineer of using fracture mechanics in conducting stress corrosion tests on high strength alloys has been well documented [7,8,70]. Briefly, the method provides characterization under the most severe conditions (i.e., a preexisting flaw), offers translation of laboratory data to larger components, predicts their behavior in service, and prevents a false indication of immunity.

Despite the increasing volume of information concerning the use of precracked specimens during stress corrosion tests, many factors that may contribute to the development of a uniform method of testing remain to be evaluated. Often the magnitude of a particular effect is different for different alloys, making it extremely difficult to formulate standard methods of testing. However, there is sufficient information from which to prepare guidelines for methods of testing with certain precracked specimen geometries. These guidelines, if used in conjunction with a cooperative testing program, will eventually provide the basis for an ASTM-recommended method of test. All methods should be kept up to date and need to be examined periodically to determine whether revisions are desirable as the result of new information.

## 2.8 References


1. F. A. Champion, *Corrosion Testing Procedures*, Wiley, New York, 1952.
2. "Stress Corrosion Testing Methods," in *Stress Corrosion Testing*, ASTM STP 425, Amer. Soc. Testing Mater., Philadelphia, Pa., 1967, p. 3.
3. H. L. Craig, Jr., D. O. Sprowls, and D. E. Piper, "Stress Corrosion Testing," *Handbook on Corrosion Testing* (W. H. Ailor, ed.), Wiley, New York, 1971, p. 231.
4. J. E. Srawley and W. F. Brown, Jr., "Fracture Toughness Test Methods," in *Fracture Toughness Testing and Its Applications*, ASTM STP 381, Amer. Soc. Testing Mater., Philadelphia, Pa., 1965, p. 133.
5. W. F. Brown, Jr., and J. E. Srawley, *Plane Strain Crack Toughness Testing of High Strength Metallic Materials*, ASTM STP 410, Amer. Soc. Testing Mater., Philadelphia, Pa., 1966.
6. "Proposed Method of Test for Plane-Strain Fracture Toughness of Metallic Materials," in *Book of ASTM Standards (Part 31)*, Amer. Soc. Testing Mater., Philadelphia, Pa., May 1969, p. 1099.
7. B. F. Brown, "The Application of Fracture Mechanics to Stress-Corrosion Cracking," *Metallurg. Rev.* **13**, 171 (1968).
8. R. P. Wei, "Application of Fracture Mechanics to Stress-Corrosion Cracking Studies," *Proceedings of International Conference on Fundamental Aspects of Stress Corrosion Cracking* (R. W. Staehle et al., eds.), Nat. Assoc. Corrosion Engrs., Houston, Texas, 1969, p. 104.
9. P. C. Paris and G. C. Sih, "Stress Analysis of Cracks," *Fracture Toughness Testing and Its Applications*, ASTM STP 381, Amer. Soc. Testing Mater., Philadelphia, Pa., 1965, p. 30.
10. H. M. Westergaard, "Bearing Pressures and Cracks," *J. Appl. Mech.* **6** (No. 2), A-49 (1939).
11. G. R. Irwin, "Analysis of Stresses and Strains Near the End of a Crack Traversing a Plate," *J. Appl. Mech.* **24**, 361 (1957).
12. A. S. Kobayashi, D. E. Maiden, B. J. Simon, and S. Iida, "Application of Finite Element Analysis Method to Two-Dimensional Problems in Fracture Mechanics," ASME Publ. 60-WA/PVP-12, Nov. 1969. Presented at 2nd Int. Conf. on Fracture, Brighton, 1969.
13. S. Mostovoy, P. B. Crosley, and E. J. Ripling, "Use of Crackline Loaded Specimens for Measuring Plane Strain Fracture Toughness," *J. Mater.* **2** (No. 3), 661 (1967).
14. C. D. Beachem and B. F. Brown, "A Comparison of Three Precracked Specimens for Evaluating the Stress-Corrosion Susceptibility of Three High-Strength Steels," in *Stress Corrosion Testing*, ASTM STP 425, Amer. Soc. Testing Mater., Philadelphia, Pa., 1967, p. 31.
15. J. E. Srawley and B. Gross, "Stress Intensity Factors for Crackline-Loaded Edge-Crack Specimens," *Mater. Res. Stand.* **7** (No. 4), 155 (Apr. 1967).


16. W. K. Wilson, *Analytic Determination of Stress Intensity Factor for the Manjoine Brittle Fracture Test Specimen*, Westinghouse Research Laboratories Report, Westinghouse Research Laboratories, Churchill Borough, Pa., Aug. 1965.
17. S. R. Novak and S. T. Rolfe, "Modified WOL Specimen for $K_{Iscc}$ Environmental Testing," *J. Mater.* 4 (No. 3), 701 (Sept. 1969).
18. J. E. Srawley, M. H. Jones, and B. Gross, *Experimental Determination of the Dependence of Crack Extension Force on Crack Length for a Single-Edge-Notch Tension Specimen*, TN D-2396, *NASA*, Lewis Research Center, Cleveland, Ohio, Aug. 1964.
19. B. Gross, J. E. Srawley, and W. F. Brown, Jr., *Stress-Intensity Factors for a Single-Edge-Notch Tension Specimen by Boundary Collocation of a Stress Function*, TN D2395, NASA, Lewis Research Center, Cleveland, Ohio, Aug. 1964.
20. B. Gross and J. E. Srawley, *Stress-Intensity Factors for Single-Edge-Notch Specimens in Bending or Combined Bending and Tension by Boundary Collocation of a Stress Function*, TN D-2603, NASA, Lewis Research Center, Cleveland, Ohio, Jan. 1965.
21. B. Gross and J. E. Srawley, *Stress-Intensity Factors for Three-Point Bend Specimens by Boundary Collocation*, TN D-3092, NASA, Lewis Research Center, Cleveland, Ohio, Dec. 1965.
22. J. A. Kies, H. L. Smith, H. E. Romine, and H. Bernstein, "Fracture Testing of Weldments," in *Fracture Toughness Testing and Its Applications*, ASTM STP 381, Amer. Soc. Testing Mater., Philadelphia, Pa., 1965, p. 328.
23. H. F. Bueckner, "Some Stress Singularities and Their Computation by Means of Integral Equations," in *Boundary Problems in Differential Equations*, R. E. Langer (editor), University of Wisconsin Press, Madison, Wis., 1960, p. 215.
24. D. M. Fisher and A. J. Repko, "Note on Inclination of Fatigue Cracks in Plane Strain Fracture Toughness Test Specimens," *Mater. Res. Stand.* 9 (No. 5), 28 (1969).
25. J. E. Srawley and B. Gross, *Stress Intensity Factors for Crackline-Loaded Edge-Crack Specimens*, TN D-3820, NASA, Lewis Research Center, Cleveland, Ohio, Feb. 1967.
26. J. A. Kies and B. J. Clark, "Fracture Propagation Rates and Times to Fail Following Proof Stress in Bulk Glass," *Fracture 1969: Proceedings of the Second International Conference on Fracture, Brighton, April 1969* (P. L. Pratt et al., eds.), pp. 483-491.
27. C. D. Beachem, J. A. Kies, and B. F. Brown, "A Constant K Specimen for Stress-Corrosion Cracking Testing," *Mater. Res. Stand.* 11 (No. 4), 30 (Apr. 1971).
28. H. R. Smith, The Boeing Company, Seattle, Wash., unpublished data.
29. G. R. Irwin, "Plastic Zone Near a Crack and Fracture Toughness," paper presented at 7th Sagamore Ordnance Materials Research Conference.

Published in "Mechanical and Metallurgical Behavior of Sheet Materials," mimeographed by Metallurgy Department, Syracuse University, New York, 1961. University control no. MET-E-661-61/1/F, pp. IV-63 to IV-78.

30. A. S. Kobayashi and W. L. Moss, "Stress Intensity Magnification Factors for Surface-Flawed Tension Plate and Notched Round Tension Bar," *Fracture 1969: Proceedings of the Second International Conference on Fracture, Brighton, April 1969* (P. L. Pratt et al., eds.), pp. 31-45.
31. D. S. Dugdale, "Yielding of Steel Sheets Containing Slits," *J. Mech. Phys. Solids* **8**, 100 (1960).
32. O. L. Bowie, "Rectangular Tensile Sheet With Symmetric Edge Cracks," paper 64-APM-3, ASME, 1964.
33. H. F. Bueckner, *Fracture Toughness Testing and Its Applications*, ASTM STP 381, Amer. Soc. Testing Mater., Philadelphia, Pa., 1965, p. 82.
34. B. M. Wundt, "A Unified Interpretation of Room Temperature Strength of Notch Specimens as Influenced by Size," paper 59-MET9, ASME, 1959.
35. J. D. Lubahn, "Experimental Determination of Energy Release Rate," *Proc. ASTM* **59**, 885 (1959).
36. G. R. Irwin, "Supplement to: Notes for May, 1961 meeting of ASTM Committee for Fracture Testing of High Strength Metallic Materials." Mimeographed. Naval Research Laboratory, Washington, D.C., 1961.
37. B. F. Brown, "On the Existence of a Threshold Stress for Corrosion Cracking in Titanium," *Mater. Res. Stand.* **5**, 786 (1970).
38. M. V. Hyatt, "Effects of Residual Stresses on Stress-Corrosion Crack Growth Rates in Aluminum Alloys," *Corrosion* **26** (No. 11), 547 (Nov. 1970).
39. M. V. Hyatt, "Use of Precracked Specimens in Stress-Corrosion Testing of High-Strength Aluminum Alloys," *Corrosion* **26** (No. 11), 487 (Nov. 1970).
40. C. S. Carter, *Stress Corrosion Crack Branching in High-Strength Steels*, D6-23871, The Boeing Company, Seattle, Wash., Mar. 1969, AD 687725 (to be published in *Engineering Fracture Mechanics*).
41. T. R. Beck, M. J. Blackburn, and M. O. Speidel, *Stress Corrosion Cracking of Titanium Alloys: SCC of Aluminum Alloys, Polarization of Titanium Alloys in HCl and Correlation of Titanium and Aluminum SCC Behavior*, Quarterly Progress Report No. 11, Contract NAS 7-489, The Boeing Company, Seattle, Wash., Mar. 1969.
42. T. R. Beck, M. J. Blackburn, W. H. Smyrl, and M. O. Speidel, *Stress Corrosion Cracking of Titanium Alloys: Electrochemical Kinetics, SCC Studies with Ti:8-1-1, SCC and Polarization Curves in Molten Salts, Liquid Metal Embrittlement, and SCC Studies with other Titanium Alloys*, Quarterly Progress Report No. 14, Contract NAS 7-489, The Boeing Company, Seattle, Wash., Dec. 1969.
43. T. R. Beck and M. J. Blackburn, "Stress Corrosion Cracking of Titanium Alloys," *AIAA J.* **6** (No. 2), 326 (1968).

44. S. Mostovoy, H. R. Smith, R. G. Lingwall, and E. J. Ripling, "A Note on Stress Corrosion Cracking Rates," presented at National Symposium on Fracture Mechanics, Lehigh University, Bethlehem, Pa., August 1969 (to be published in *Eng. Fracture Mech.*).
45. M. J. Manjoine, "Biaxial Brittle Fracture Tests," paper 64-Mat.-3, ASME, May 1964.
46. E. P. Dahlberg, "A Self-Stressed Specimen for Measuring Stress-Corrosion Cracking in Aluminum Alloys," in *Report of NRL Progress*, Naval Research Laboratory, Washington, D.C., Apr. 1968, p. 25.
47. E. P. Dahlberg, "Stress Corrosion-Cracking Test Methods," in *Report of NRL Progress*, Naval Research Laboratory, Washington, D.C., Oct. 1967, p. 41.
48. M. V. Hyatt, *Effects of Specimen Geometry and Grain Structure on Stress-Corrosion Cracking Behavior of Aluminum Alloys*, D6-24470, The Boeing Company, Seattle, Wash., Nov. 1969.
49. E. P. Dahlberg and J. E. Flint, "Compliance Measurements for a Simple (WOL) Stress-Corrosion Cracking Test Specimen," *Report of NRL Progress*, Naval Research Laboratory, Washington, D.C., Oct. 1968, p. 20.
50. C. S. Carter, "The Effect of Silicon on the Stress Corrosion Resistance of Low Alloy High Strength Steels," *Corrosion* **25**, 423 (1969).
51. R. E. Curtis, R. R. Boyer, and J. C. Williams, "Relationship Between Composition, Microstructure, and Stress-Corrosion Cracking (in Salt Solution) in Titanium Alloys," *Quart. Trans. ASME* **62**, 457 (1969).
52. B. F. Brown, "A New Stress-Corrosion Cracking Test for High-Strength Alloys," *Mater. Res. Stand.* **6** (No. 3), 129 (Mar. 1966).
53. *ARPA Coupling Program on Stress-Corrosion Cracking: (Seventh Quarterly Report)*, NRL Memorandum Report 1941, Naval Research Laboratory, Washington, D.C., Oct. 1968, p. 6.
54. T. R. Beck, *Stress Corrosion Cracking of Titanium Alloys: Preliminary Report on Ti-8Al-1Mo-1V Alloy, and Proposed Electrochemical Mechanism*, D1-82-0554, The Boeing Company, Seattle, Wash., July 1965.
55. N. M. Lowry, O. K. Mulkey, J. M. Kuronen, and J. W. Bieber, *A Method of Measuring Crack Propagation Rates in Brittle Materials*, D6-60072, The Boeing Company, Seattle, Wash., May 1967, AD 661814.
56. *ARPA Coupling Program on Stress-Corrosion Cracking: (Eleventh Quarterly Report)*, NRL Memorandum Report 2028, Naval Research Laboratory, Washington, D.C., July 1969, p. 6.
57. *ARPA Coupling Program on Stress-Corrosion Cracking: (Thirteenth Quarterly Report)*, NRL Memorandum Report 2101, Naval Research Laboratory, Washington, D.C., Mar. 1970, p. 8.
58. D. E. Piper, S. H. Smith, and R. V. Carter, "Corrosion Fatigue and Stress-Corrosion Cracking in Aqueous Environments," *Metals Eng. Quart.* **8**, 50 (1968).
59. C. S. Carter, *Observations on the Stress-Corrosion Crack Propagation Characteristics of High-Strength Steels*, D6-25274, The Boeing Company, Seattle, Wash., June 1970.

60. M. O. Speidel, "Effect of Stress and Environment on Velocity and Branching of Subcritical Cracks," presented at AIME Meeting, Las Vegas, May 11-14, 1970.
61. C. N. Freed and J. M. Krafft, "Effect of Side Grooving on Measurements of Plane-Strain Fracture Toughness," *J. Mater.* **1** (No. 4), 770 (Dec. 1966).
62. *ARPA Coupling Program on Stress-Corrosion Cracking: (Second Quarterly Report)*, NRL Memorandum Report 1775, Naval Research Laboratory, Washington, D.C., Apr. 1967, p. 26.
63. L. Raymond and R. J. Usell, "Flaw Growth in Ti-6Al-4V in Freon Environments," *Corrosion* **25** (No. 6), 251 (June 1969).
64. B. F. Brown, "A New Stress Corrosion Cracking Test for High-Strength Alloys," *Mater. Res. Stand.* **6** (No. 3), 129 (1966).
65. H. R. Smith, D. E. Piper, and F. K. Downey, "A Study of Stress-Corrosion Cracking by Wedge-Force Loading," *Eng. Fracture Mech.* **1** (No. 1), 123 (June 1968).
66. B. F. Brown and C. D. Beachem, "A Study of the Stress Factor in Corrosion Cracking by Use of the Precracked Cantilever Beam Specimen," *Corrosion Sci.* **5**, 745 (1965).
67. M. V. Hyatt, "Use of Precracked Specimens in Selecting Heat Treatments for Stress-Corrosion Resistance in High-Strength Aluminum Alloys," *Corrosion* **27** (No. 1), 49 (Jan. 1971).
68. M. V. Hyatt and H. W. Schimmelbusch, *Development of a High-Strength, Stress-Corrosion-Resistant Aluminum Alloy for Use in Thick Sections*, AFML-TR-70-109, Air Force Materials Laboratory, Wright-Patterson Air Force Base, May 1970.
69. E. F. Brown, C. T. Fujii, and E. P. Dahlberg, "Methods for Studying the Solution Chemistry Within Stress Corrosion Cracks," *J. Electrochem. Soc.* **116** (No. 2), 218 (1969).
70. B. F. Brown, *Stress-Corrosion Cracking—a Perspective Review of the Problem*, NRL Report 7130, Naval Research Laboratory, Washington, D.C., June 16, 1970.

# Chapter 3

# HIGH STRENGTH STEELS

**G. Sandoz**
*Naval Research Laboratory*

**CONTENTS**

# 3. HIGH STRENGTH STEELS

## 3.1 Introduction

The steels of interest in this chapter are those within the range of yield strength from about 120 ksi up to the point where the steels become too brittle to be of engineering interest. These are the martensitic steels, precipitation-hardening steels, and the maraging steels. There are stainless grades in each of these three classes. Steels which owe their strengths solely to cold work are excluded. Table 1 shows the typical compositions and useful yield strength ranges of the steels in the general classes which will be considered.

The steels of Table 1 are hardened by the formation of martensite, or by the formation of various precipitates, or by both. The steels of Table 1 are divided into six groups as follows: The low alloy martensitic steels have appreciably less total alloying elements than the high alloy martensitic steels, but even the latter steels do not qualify as being stainless. The martensitic stainless steels have a minimum of 12% Cr. The precipitation-hardening stainless steels have insufficient carbon to produce the desired strength; these steels therefore may contain nickel, molybdenum, copper, aluminum, titanium, columbium, or nitrogen in various amounts and proportions to promote age hardening. The maraging steels contain large amounts of nickel, cobalt, and molybdenum and also contain the precipitation-hardening elements aluminum and titanium. Efforts to combine the toughness of maraging steel with the corrosion resistance of the hardenable stainless steels have been made, giving rise to the maraging stainless steels; Almar 362 in Table 2 is one example.

In addition to the hardening by the formation of martensite, and by precipitates, some of the steels may be further hardened by cold work, and in fact many of the precipitation-hardening stainless steels must either be worked or refrigerated to produce martensite prior to aging.

It is emphasized that the mechanical properties of high strength steels are highly sensitive to processing variables, particularly in the 180- to 210-ksi range of yield strength. For example, there is strong evidence that melting practice is more important than the nominal steel composition in determining fracture toughness [1]. Figure 1 shows that a plot of the fracture toughness parameters $K_{Ic}$ and dynamic tear (DT) energy of several types of steel as a function of yield

**Table 1.** Typical Compositions of High Strength Steels

| Type or Designation | C | Cr | Ni | Mo | Mn | Co | Cu | Al | Ti | Si | V | Other | Range of Nominal Tensile and Yield Strength, ksi | |
|---|---|---|---|---|---|---|---|---|---|---|---|---|---|---|
| | | | | | | | | | | | | | TS | YS |
| **Low-Alloy Martensitic** | | | | | | | | | | | | | | |
| HY-130 | 0.12 | 0.6 | 5.0 | – | 0.9 | – | – | – | – | 0.2 | – | – | 145-155 | 130-145 |
| 4130 | 0.30 | 1.0 | – | 0.2 | 0.5 | – | – | – | – | 0.3 | – | – | 200-300 | 180-250 |
| 4340 | 0.40 | 0.8 | 1.9 | 0.25 | 0.7 | – | – | – | – | 0.6 | – | – | | |
| D6AC | 0.45 | 1.15 | 0.55 | 1.0 | 0.8 | – | – | – | – | 0.25 | 0.05 | – | | |
| H-11 | 0.40 | 5.0 | – | 1.3 | 0.3 | – | – | – | – | 0.90 | 0.50 | – | | |
| **High-Alloy Martensitic** | | | | | | | | | | | | | | |
| HP 9-4-45 | 0.45 | 0.3 | 8.5 | 0.20 | 0.10 | 3.75 | – | – | – | 0.10 | 0.10 | – | 185-250 | 170-220 |
| HP 9-4-25 | 0.25 | 0.50 | 8.5 | 0.50 | 0.10 | 3.75 | – | – | – | 0.10 | 0.10 | – | | |
| HP 9-4-20 | 0.20 | 0.80 | 9.0 | 1.0 | 0.3 | 4.5 | – | – | – | 0.10 | 0.10 | – | | |
| 10Ni-2Cr-1Mo-8Co | 0.11 | 2.20 | 10.0 | 1.0 | 0.06 | 8.0 | – | – | – | 0.1 | – | – | | |
| **Martensitic Stainless** | | | | | | | | | | | | | | |
| 410 | 0.12 | 12.0 | – | – | 0.5 | – | – | – | – | 0.35 | – | – | 120-200 | 100-150 |
| 431 | 0.15 | 16.0 | 2.0 | – | 0.5 | – | – | – | – | 0.35 | 0.25 | – | | |
| 12Mo-V | 0.26 | 12.3 | 0.75 | 1.0 | 0.5 | – | – | – | – | 0.3 | 0.29 | – | 60-220 | 130-210 |
| **Precipitation-Hardening Stainless** | | | | | | | | | | | | | | |
| AM 364 (M)* | 0.011 | 11.1 | 11.2 | – | 0.05 | – | – | 0.61 | 0.22 | 0.05 | – | – | 180-270 | 75-220 |
| Custom 455 (M) | 0.014 | 11.8 | 8.5 | – | 0.03 | – | 2.2 | – | 1.3 | 0.15 | – | 0.26Cb | | |
| PH 13-8-Mo (M) | 0.04 | 13.0 | 8.0 | 2.0 | 0.10 | – | – | 1.0 | – | <0.10 | – | – | | |
| PH 14-8-Mo (SA) | 0.035 | 14.5 | 8.5 | 2.2 | 0.85 | – | – | 1.2 | – | 0.05 | – | – | | |
| PH 15-7-Mo (SA) | 0.07 | 15.0 | 7.0 | 2.2 | 0.60 | – | – | 1.0 | – | 0.30 | – | – | | |
| 15-5-PH (M) | 0.06 | 15.0 | 4.6 | – | 0.25 | – | 3.3 | – | – | 0.40 | – | 0.25Cb | | |
| 17-4-PH (M) | 0.04 | 16.0 | 4.0 | – | 0.25 | – | 3.3 | – | – | 0.30 | – | 0.25Cb | | |
| 17-7-PH (SA) | 0.07 | 17.0 | 7.0 | – | 0.50 | – | – | 1.0 | – | 0.30 | – | – | | |
| AM 350 (SA) | 0.10 | 16.5 | 4.3 | 2.7 | 0.75 | – | – | – | – | 0.30 | – | 0.10N | | |
| AM 355 (SA) | 0.13 | 15.5 | 4.3 | 2.7 | 0.75 | – | – | – | – | 0.30 | – | 0.12N | | |
| AFC 260 (SA) | 0.07 | 15.0 | 1.8 | 4.5 | – | 13.0 | – | – | – | 0.13 | 0.25 | 0.15Cb | | |
| AFC-77 (M) | 0.16 | 14.0 | 0.2 | 5.0 | 0.2 | 13.0 | – | – | – | – | – | – | | |
| **Maraging** | | | | | | | | | | | | | | |
| 12-5-3 | 0.03Max | 5.0 | 12.0 | 3.0 | – | – | – | 0.4 | 0.2 | – | – | – | 175-200 | 160-190 |
| 18Ni-200 | 0.03Max | – | 18.0 | 3.2 | – | 8.0 | – | 0.1 | 0.2 | – | – | – | 215-245 | 200-235 |
| 18Ni-250 | 0.03Max | – | 18.0 | 4.8 | – | 8.0 | – | 0.1 | 0.4 | – | – | – | 245-270 | 230-260 |
| 18Ni-300 | 0.03Max | – | 18.0 | 5.0 | – | 9.0 | – | 0.1 | 0.6 | – | – | – | 275-310 | 260-300 |
| 18Ni-350 | 0.004 | – | 18.5 | 4.6 | – | 11.9 | – | 0.1 | 1.5 | – | – | – | 265-360 | 250-350 |
| **Maraging Stainless** | | | | | | | | | | | | | | |
| Almar 362 | 0.03 | 14.5 | 6.5 | 0.08 | 0.30 | – | 0.1 | 0.6 | 0.80 | 0.2 | – | – | 180-200 | 170-185 |
| Marvac 736 | 0.02 | 10.2 | 9.5 | 2.0 | 0.15 | – | – | 0.30 | 0.25 | 0.15 | – | – | | |

*Semiaustenitic (SA) or martensitic (M)

**Table 2.** Susceptibility to SCC of High Strength Steels in Saline Environments as Measured by Non-Precracked Specimens at 70% of the Yield Stress or Higher

| *Type* | *Yield Strength Range, ksi* | *Environment*[a] | *Susceptibility*[a] *(70-90% Y.S.) (or U-Bend)* | *References* |
|---|---|---|---|---|
| Precipitation-Hardening Stainless | | | | |
| PH-13-8-Mo | 220 | Salt air | Fail | 2 |
| PH-13-8-Mo | 210-217 | 3½% NaCl | OK | 3 |
| PH-14-8-Mo | 220-240 | Salt air | Fail | 2 |
| PH-14-8-Mo | 190-230 | 3½% NaCl | OK | 3 |
| 15-5-PH | 155-175 | 3½% NaCl | OK | 3 |
| PH-15-7-Mo | 200 | *1M* NaCl | Fail | 3,4 |
| 17-4-PH | 140 | 5% NaCl + $H_2S$ | Fail | 5 |
| | 150-210 | Deep sea | OK | 3,6,7 |
| 17-7-PH | 191-220 | 3½% NaCl | Fail | 3,8,9 |
| | 192 | Deep sea | OK | 6,7 |
| AM-350 | 140-210 | 3½% NaCl | Fail | 3,10-12 |
| AM-355 | 170-230 | 3½% NaCl | Fail | 4,10-12 |
| AFC-260 | 205 | 3½% NaCl | Fail | 13 |
| AFC-77 | 190-205 | 3½% NaCl | Fail | 14-16 |
| AFC-77 | 200 | Salt air | Fail | 2 |
| Martensitic Stainless | | | | |
| 410 | 160 | 3½% NaCl | OK | 9 |
| 410 | 125 | 4% HCl + 3% NaCl + As | Fail | 17 |
| 12Mo-V | 260 (UTS) | 3½% NaCl | Fail | 18 |
| 13Cr | 200-220 | 3% NaCl | Fail | 19,20 |
| Martensitic | | | | |
| AISI 4340 | 200-260 | 5% NaCl | Fail | 8,11,21,22 |
| | | 3½% NaCl | Fail | 12,23-25 |
| | | Deep sea | Fail | 6,26-28 |
| | | Salt air | Fail | 7,29 |
| AISI 4340 | 150-190 | Deep sea | OK | 6 |
| AISI 4330 | 220 | 3½% NaCl | Fail | 10,21 |
| AISI 4330M | 217 | 3½% NaCl | Fail | 24 |
| 300M | 210-275 | 3½% NaCl | Fail | 4,10,12,21,23, 29,30 |
| H-11 | 190-250 | 3½% NaCl | Fail | 4,11,12,25,29, 31,32 |
| D6AC | 197-250 | 3½% NaCl | Fail | 4,21,23,29,30 |
| HY130 | 130 | Sea | OK | 33,34 |

[a]Note:
Environmental variables such as alternate immersion, or degree of aeration, and the details of specimen type, geometry, and surface perforation are omitted in order to get an overall view. Specific results may be misleading unless the references are examined in detail.

**Table 2.** Susceptibility to SCC of High Strength Steels in Saline Environments as Measured by Non-Precracked Specimens at 70% of the Yield Stress or Higher–*Continued*

| *Type* | *Yield Strength Range, ksi* | *Environment*[a] | *Susceptibility*[a] *(70-90% Y.S.) (or U-Bend)* | *References* |
|---|---|---|---|---|
| High Alloy Martensitic | | | | |
| HP-9-4-20 | 197 | Sea | Fail | 35,36 |
| HP-9-4-25 | 180 | 3½% NaCl | OK | 18,35,37,38 |
| HP-9-4-30 | 200-240 | 3½% NaCl | OK | 17,39 |
| HP-9-4-40 | 260 | 3½% NaCl | Fail | 31 |
| HP-9-4-45 (Q&T) | 235-260 | 3½% NaCl | Fail | 30,39 |
| HP-9-4-45 (Bainite) | 220-280 | 3½% NaCl | OK | 17,30,39-41 |
| Maraging | | | | |
| 12Ni-5Cr-3Mo | 140-205 | Sea | Fail | 28,42-44 |
| 18Ni | 180-350 | 3½% NaCl | Fail | 11 |
| | 190 | 5% NaCl + $H_2S$ | Fail | 5 |
| | 200 | Sea | OK | 44 |
| | 200-300 | Sea | Fail | 27 |
| | 200-272 | Sea | Fail | 28 |
| | 250 | Salt spray | OK | 45 |
| | 240 | Deep sea | Fail (weld) | 7,26 |
| | 250-255 | 3½% NaCl | OK | 9,30 |
| | 210-286 | Sea | Fail | 43 |
| | 220-250 | 3% NaCl | Fail | 46 |
| | 250-286 | Sea | Fail | 44 |
| | 250-270 | 3½% NaCl | Fail | 47 |
| | 249-354 | Dist $H_2O$ | Fail | 53 |
| | 300 | Water | Fail | 48 |
| | 300 | 5% NaCl | Fail | 25 |
| | 300 | Salt spray | Fail | 45 |
| | 260 | 5% NaCl | Fail | 31 |
| | 260 | 3½% NaCl | Fail | 49 |
| | 280-350 | 3% NaCl | Fail | 50 |
| Maraging Stainless | | | | |
| Almar 362 | 182-227 | 10% NaCl + HAc | Fail | 51 |
| Almar 362 | 115-182 | 10% NaCl + HAc | Fail | 51 |
| Almar 362 | 161 | 3½% NaCl | OK | 3 |

[a]Note:
Environmental variables such as alternate immersion, or degree of aeration, and the details of specimen type, geometry, and surface perforation are omitted in order to get an overall view. Specific results may be misleading unless the references are examined in detail.

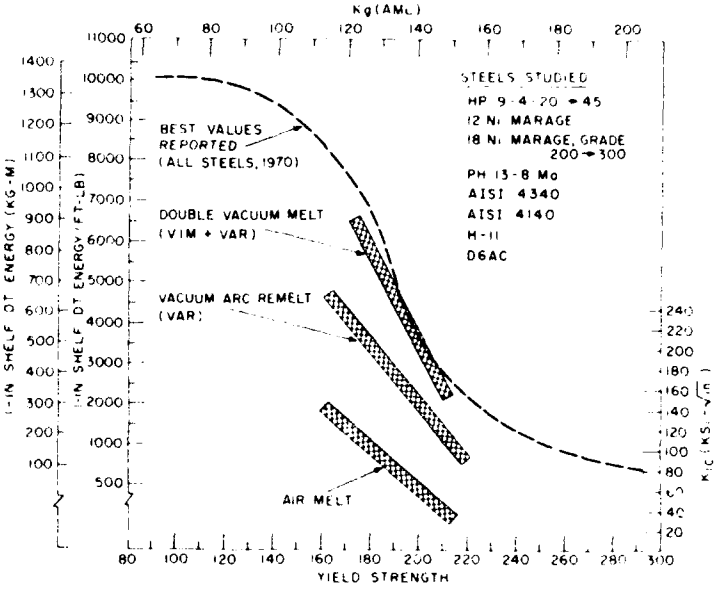


Fig. 1. Effects of melting practice and yield strength on the fracture toughness of some high strength steels [1].

strength produces three distinct ranges of toughness. These three widely separated bands apparently reflect the three types of melting practice indicated in Fig. 1. The gap in toughness between air-melted steels and double vacuum-melted steels (vacuum induction melting (VIM) + vacuum arc remelt (VAR)) is striking. Evidence is presented later that processing practice may also affect SCC characteristics to an important degree.

References 52 through 56 are good summaries of the metallurgy, processing, and properties of high strength steels, and Ref. 57 describes the physical metallurgy of alloy steels in some detail. The welding of high strength steels is summarized in a recent symposium [58].

### 3.2 Test Procedures

In this chapter, data from both smooth and precrack-type specimens will be reviewed and assessed. The stress factor will be treated as simple tensile stress where smooth specimens are involved, and as the appropriate stress intensity factor $K$ for precracked-specimen data. The important $K$ values are designated $K_{Ic}$ and $K_{Iscc}$. Another parameter, $K_{Ix}$, is a first approximation of the fracture toughness parameter $K_{Ic}$ of plates and bars. In the absence of valid $K_{Ic}$ data, $K_{Ix}$ is useful for comparing with $K_{Iscc}$ in order to assess the magnitude of degradation of crack resistance by the action of a corrosive environment.

The parameter $K_{Iscc}$ is the critical stress intensity factor above which crack growth has been observed in a given environment and below which crack growth has not been observed within an arbitrary test time. The minimum test time varies with the steel but is generally 100 hours for low alloy steel and up to 1000 hours for high alloy steels.

### 3.3 SCC Characteristics of Commercial Steels

In Table 2, data from the literature are summarized for smooth specimens of steels stressed at 70% of the yield strength, or higher, in saline environments. The data are not entirely consistent because of the lack of standardization of specimen preparation, variation in the details of test procedure and test environment, and the general lack of reproducibility in smooth specimen tests. Nevertheless, the data show certain general trends. For example, based on time to failure it appears that the susceptibility to SCC increases with increasing yield strength. The literature [12,30,48,59] confirms this trend for a number of steels as illustrated in Figs. 2, 3, and 4. Best performance at moderate strength level is shown by the precipitation-hardening stainless steels (PH 13-8Mo, PH 14-8Mo, 15-5PH) and by the high alloy martensitic steels (HP 9-4-25, HP 9-4-30). A bainitic structure in HP 9-4-45 steel appears superior to a martensitic structure, but this superiority is not observed in the presence of sharp flaws, as will be discussed later.

A summary of available data on the $K_{Iscc}$ values of commercial steel plates in water, salt water, or seawater is given in Figs. 5 through 22. In a few cases, values in salt water containing $H_2S$ and HAc are also presented. When available, the $K_{Iscc}$ values of welds for the steels are also given. The parameters $K_{Ic}$ (□) and $K_{Ix}$ (◇) were plotted for purposes of comparison, when such values could be found. The symbol □ indicates valid $K_{Ic}$ numbers which were claimed by the authors or were implied from the descriptions of the test procedures, and the symbol △ refers to other approximate fracture toughness data. For the values of $K_{Iscc}$ shown, specimen sizes were estimated to provide plane strain at the corresponding values of yield strength (0.2% offset method).

The references cited for the various steels may sometimes reflect a common source of data (either wholly or in part), or are primarily review papers.

No attempt was made to differentiate with regard to plate thickness, crack propagation direction, and heat treatment in plotting the data in Figs. 5 through 22. These variables are treated in later sections. The envelopes drawn around the data points for each steel indicate, therefore, the range of values of fracture toughness and $K_{Iscc}$ that have been observed for each type of steel. The envelopes around the weld data represent the range of values at the weld centerlines. Data on the heat-affected zone (HAZ) of welds are sparse and for the most part judged unreliable.

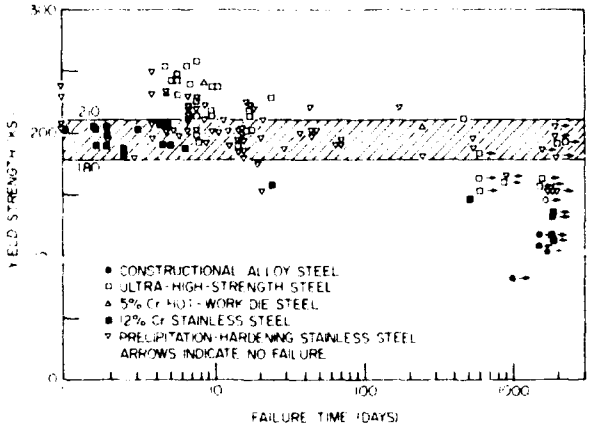


Fig. 2. Stress corrosion behavior of steels exposed to marine atmosphere at 75% of the yield strength (from Ref. 59). From *Proc. 7th World Petroleum Congress*, 1967, Mexico, 1967, p. 203; copyright by Elsevier Publishing Company. Used by permission.

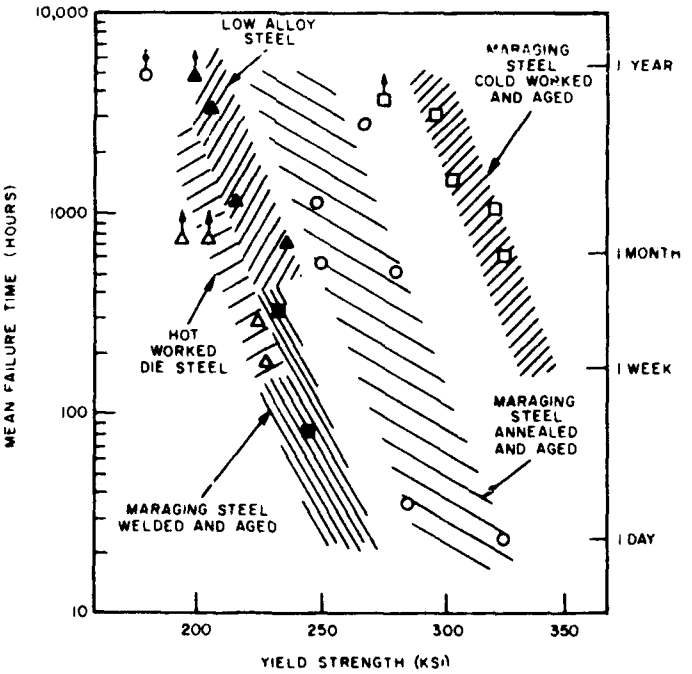


Fig. 3. Results of bent-beam tests in aerated distilled water. These specimens were exposed to the environment at stress of 75% of yield (from Ref. 48). From *Mater. Protect.* 4 (No. 12), 28 (1965); copyright by the National Association of Corrosion Engineers. Used by permission.

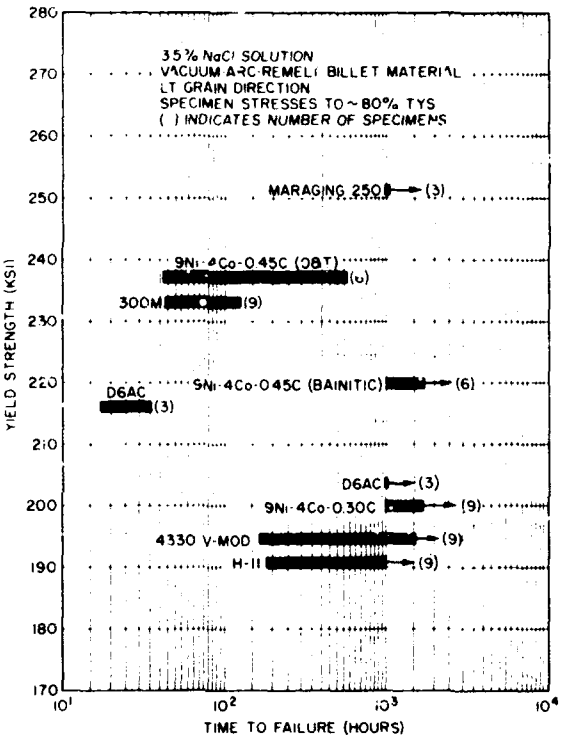


Fig. 4. Alternate immersion stress corrosion data from smooth bend specimens (from Ref. 30).

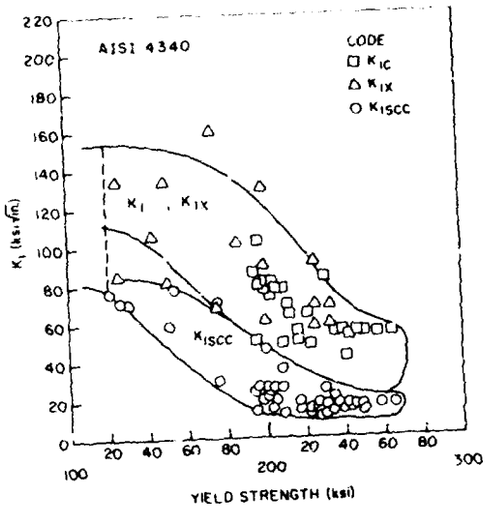


Fig. 5. Stress corrosion resistance and fracture toughness of AISI 4340 steel [23,60-76].

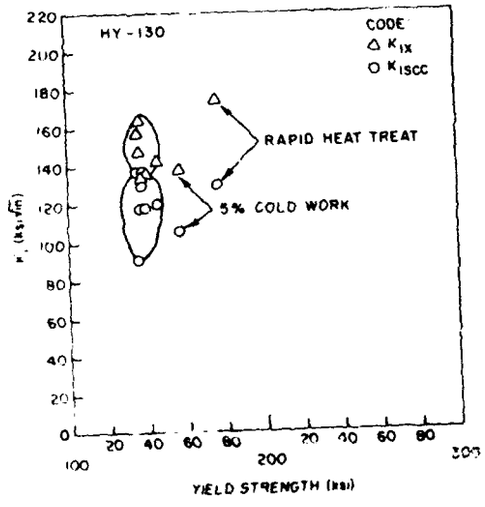


Fig. 6. Stress corrosion resistance and fracture toughness of HY-130 steel [77,77 81].

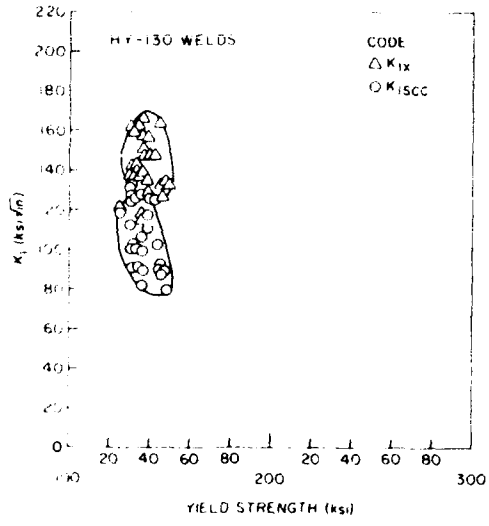


Fig. 7. Stress corrosion resistance and fracture toughness of HY-130 steel weldments [77,78,81-88].

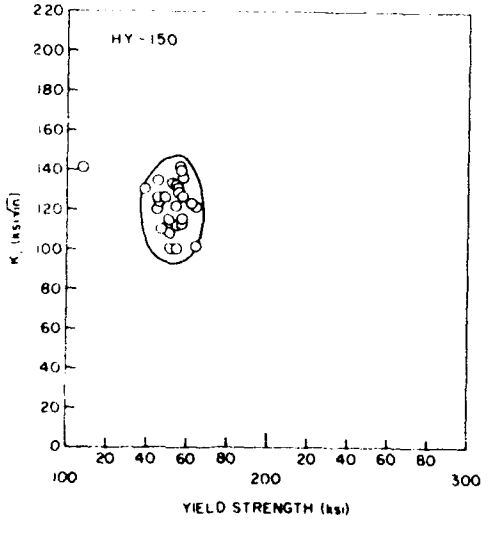


Fig. 8. Stress corrosion resistance and fracture toughness of HY-150 steel [89-91].

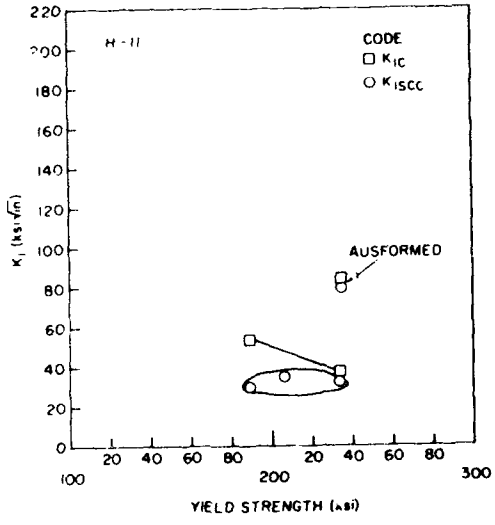


Fig. 9. Stress corrosion resistance and fracture toughness of H-11 steel [23,62,63,92,93].

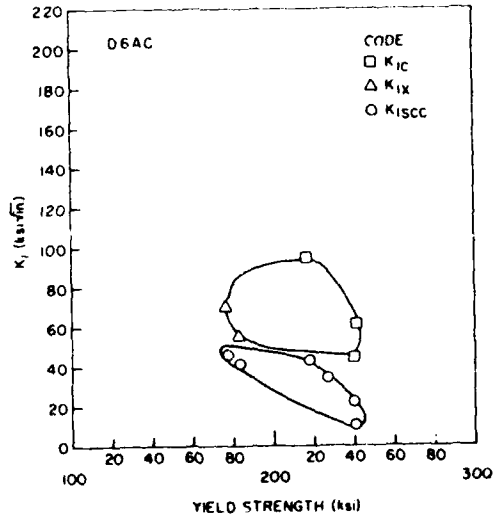


Fig. 10. Stress corrosion resistance and fracture toughness of D6AC steel [60,62,63,68,71,72].

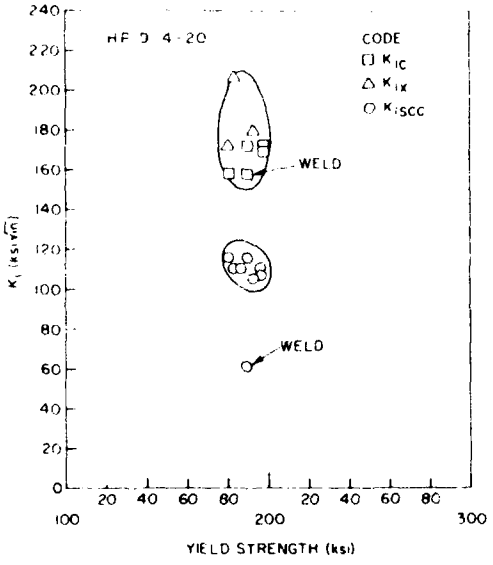


Fig. 11. Stress corrosion resistance and fracture toughness of HP 9-4-20 steel and weldments [35,36,71,72, 87,94-97].

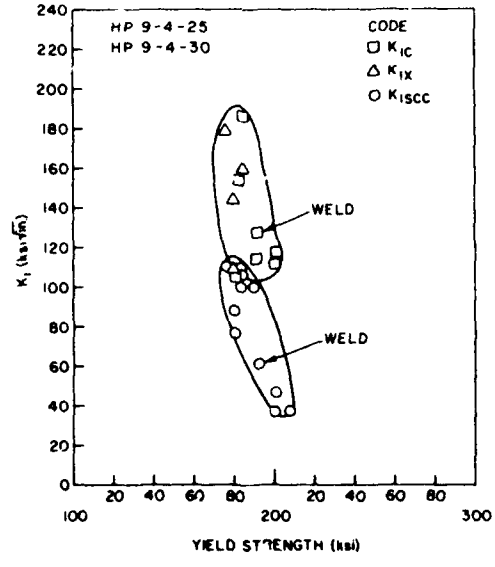


Fig. 12. Stress corrosion resistance and fracture toughness of HP 9-4-25 and PH 9-4-30 steel and weldments [23,35,63,71,75,92,97-100].

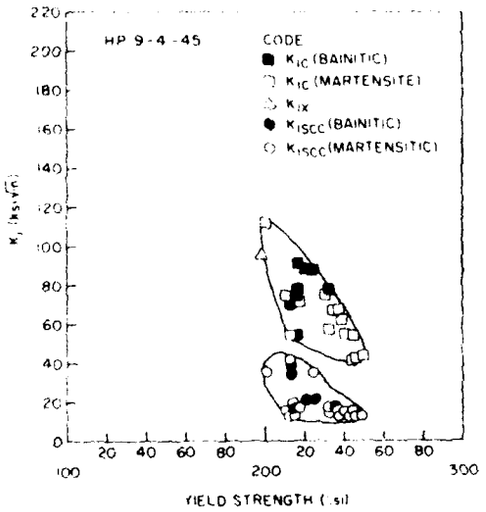


Fig. 13. Stress corrosion resistance and fracture toughness of HP 9-4-45 steel [23,61-63,66,68,72,75,92,96, 101].

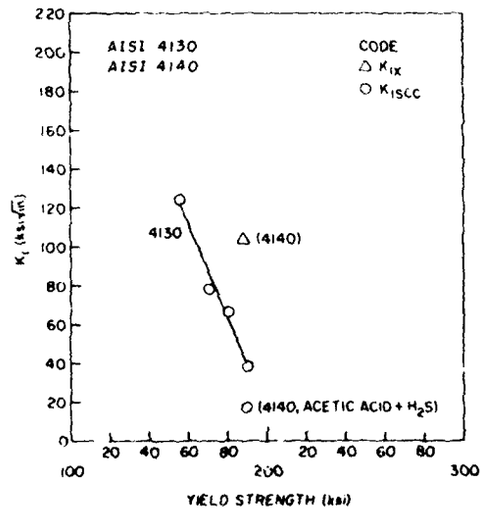


Fig. 14. Stress corrosion resistance and fracture toughness of AISI 4130 and AISI 4140 steel [65,71].

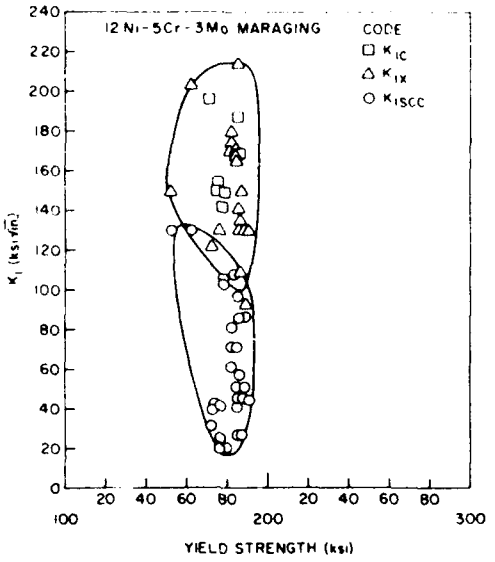


Fig. 15. Stress corrosion resistance and fracture toughness of 12Ni-5Cr-3Mo maraging steel [65,69,71,72,79, 80,87,96,99,102].

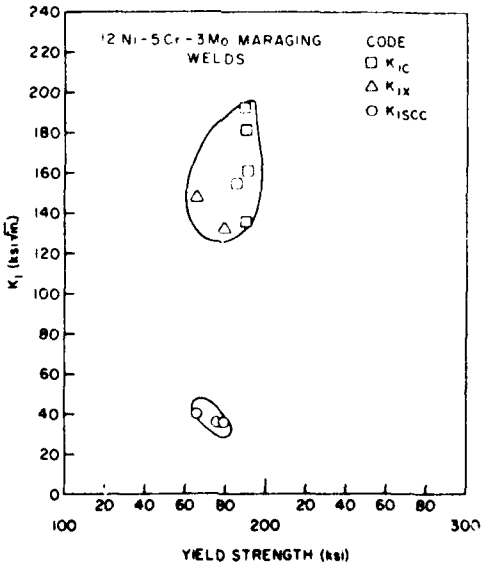


Fig. 16. Stress corrosion resistance and fracture toughness of 12Ni-5Cr-3Mo maraging steel weldments [87,99,103].

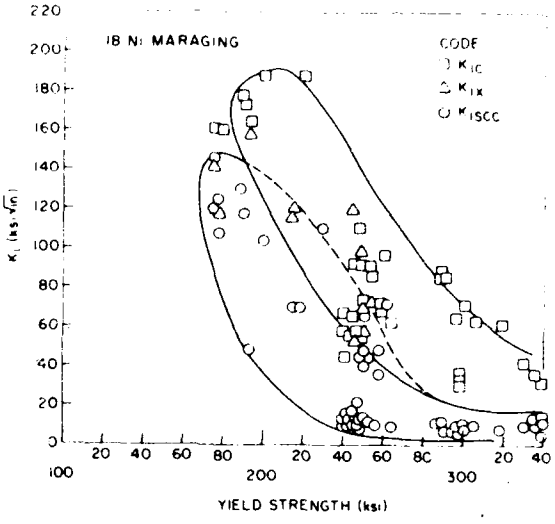


Fig. 17. Stress corrosion resistance and fracture toughness of 18Ni maraging steel [62,66,68,69,71,72,75,80, 81,87,96,100,102,104-115].

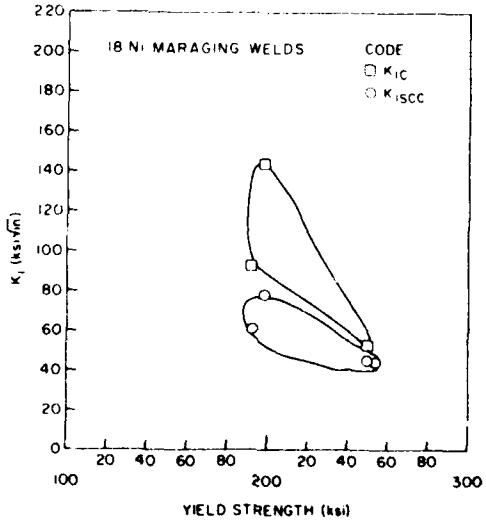


Fig. 18. Stress corrosion resistance and fracture toughness of 18Ni maraging steel weldments [100,102,110, 113].

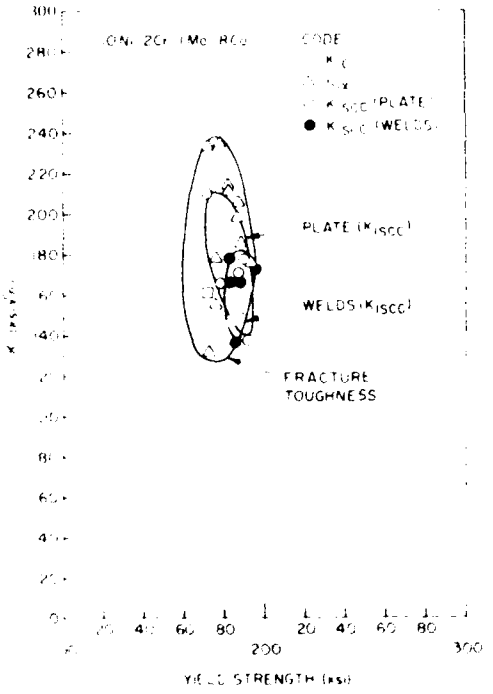


Fig. 19. Stress corrosion resistance and fracture toughness of 10Ni-2Cr-1Mo-8Co steel and weldments [81,87,94,95,99,116-120].

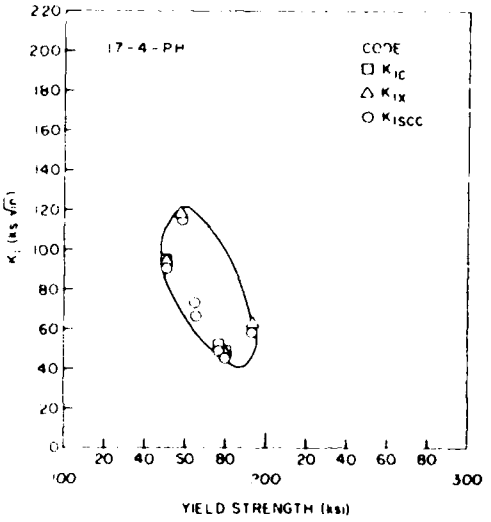


Fig. 20. Stress corrosion resistance and fracture toughness of 17-4-PH steel [100,121].

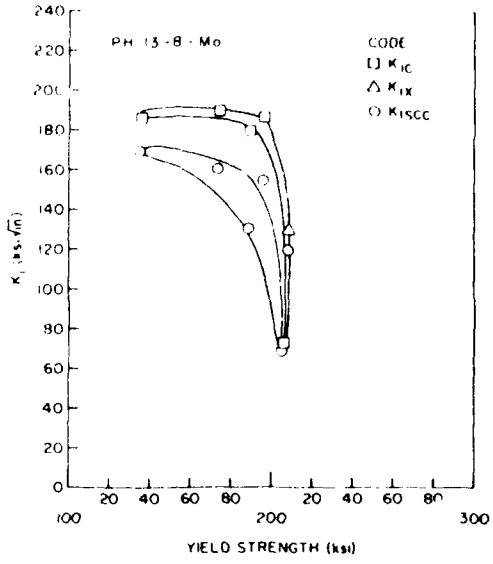


Fig. 21. Stress corrosion resistance and fracture toughness of 13Cr-8Ni-Mo PH steel [71,72,96,121].

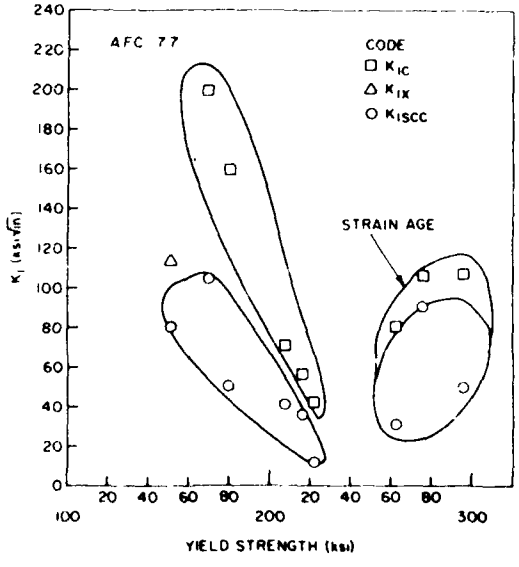


Fig. 22. Stress corrosion resistance and fracture toughness of AFC-77 steel [122,123].

In a few cases in Figs. 5 through 22 the effects of working or heat treatment are indicated when the effects were obvious and significant. The effects of cold work and rapid heat treatment on HY-130 plate are indicated in Fig. 6. The effects of austforming on H-11 are indicated in Fig. 9. The negligible differences between bainitic and martensitic HP 9-4-45 alloys are indicated by the points in Fig. 13. Finally, the effects of strain-aging on AFC-77 are indicated by the separate envelopes in Fig. 22.

A composite of all the envelopes of $K_{Iscc}$ values shown in Figs. 5 through 22 is shown in Fig. 23. A similar plot for welds is shown in Fig. 24.

To compare the characteristics of the various steels, in Figs. 25 through 41 the $K_{Iscc}$ envelopes for individual steels are superimposed in heavy lines over the composite grouping as background. Where weld envelopes or points are available, these are shown on the same graph as the individual steel plates. Thus a steel may be compared readily with its welds, and the $K_{Iscc}$ values of the steel and its welds may be compared readily with another steel and its welds.

The data for the precipitation-hardening stainless steels were generally quite limited. Individual data points of fracture toughness and $K_{Iscc}$ value for several of these steels are plotted in Fig. 40. Values of several other steels for which only a few $K_{Iscc}$ data points could be found are plotted in Fig. 41.

The straight lines in Figs. 23 through 41 show how $K_{Iscc}$ values relate to the maximum depth of long surface flaws which can be tolerated without crack growth. Thus for example a steel with a 200-ksi yield strength and a $K_{Iscc}$ value of 40 ksi $\sqrt{\text{in.}}$ will tolerate a long flaw only 0.01 in. deep when stressed to the yield point (see Fig. 23). However, should it be possible to raise the value of $K_{Iscc}$ to 130 ksi $\sqrt{\text{in.}}$, whether by heat treatment or substituting another steel with a 200-ksi yield strength, then a flaw ten times as deep (0.1 in.) could be tolerated.

The data in Figs. 23 through 41 confirm in general that for any given steel the value of $K_{Iscc}$ decreases with increasing yield strength (see Fig. 25 for AISI 4340, Fig. 31 for HP 9-4-25, Fig. 33 for AISI 4130, Fig. 35 for 18Ni maraging, Fig. 38 for PH 13-8Mo, and Fig. 39 for AFC-77).

Several martensitic steels (H-11 in Fig. 28, D6AC in Fig. 29, HP 9-4-45 in Fig. 32, and 4340V and 300M in Fig. 41) have $K_{Iscc}$ characteristics similar to those for AISI 4340. Other martensitic steels are superior to AISI 4340 at yield strength levels below 200 ksi (HY-130 in Fig. 26, HY-150 in Fig. 27, HP 9-4-20 in Fig. 30, and HP 9-4-25 in Fig. 31). It would appear then that the high alloy martensitic steels in Table 1 are somewhat superior to the low alloy martensitic steels at these strength levels.

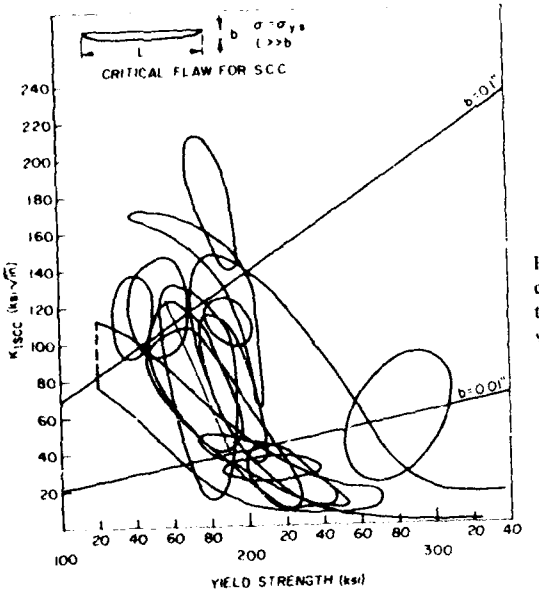


Fig. 23. Composite of the $K_{Iscc}$ envelopes developed in Figs. 5 through 22 for high strength steels.

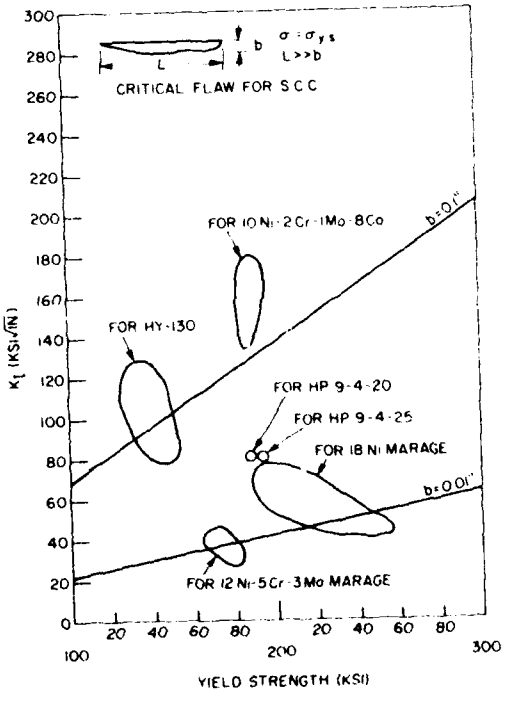


Fig. 24. Composite of the $K_{Iscc}$ envelopes for welds for the steels indicated.

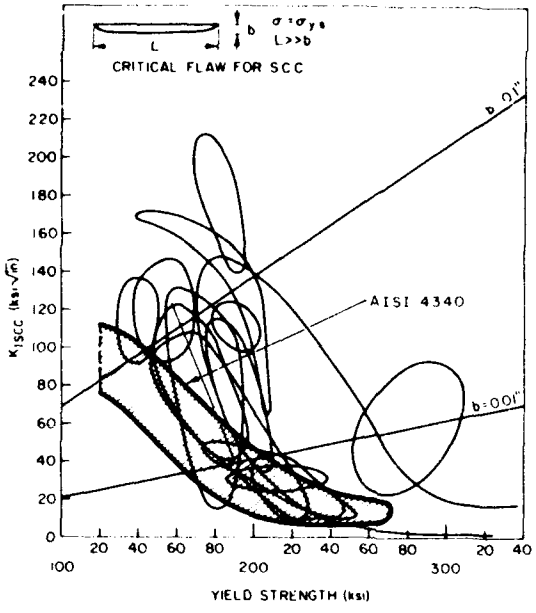


Fig. 25. Envelope of $K_{Iscc}$ values for AISI 4340 steel (heavy lines) compared to composite of $K_{Iscc}$ envelopes for the other steels.

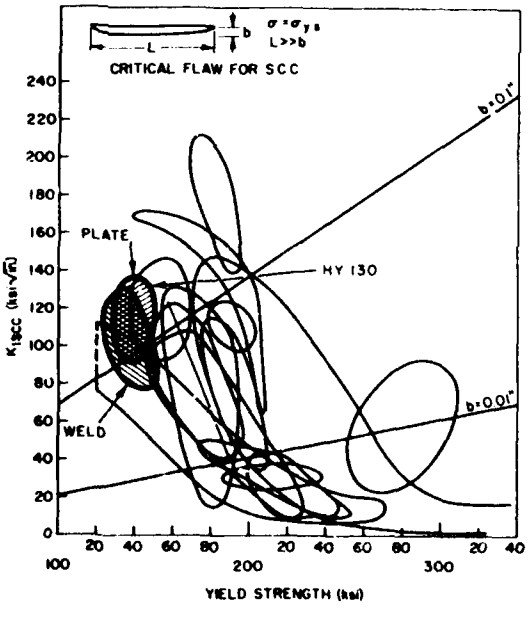


Fig. 26. Envelope of $K_{Iscc}$ values for HY-130 steel and weldments (heavy lines) composite of $K_{Iscc}$ envelopes for the other steels.

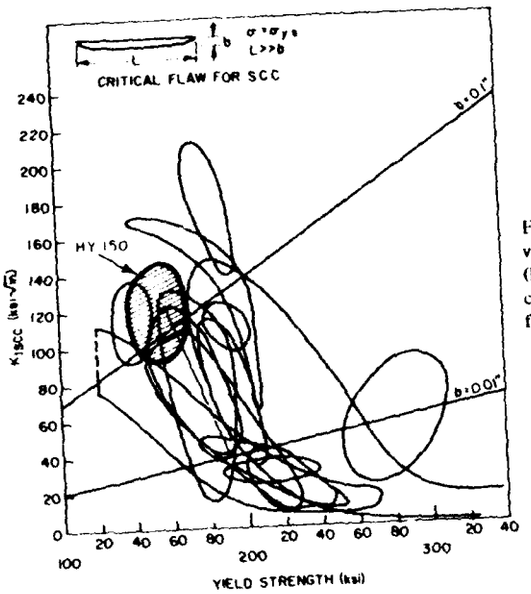


Fig. 27. Envelope of $K_{1scc}$ values for HV-150 steel (heavy lines) compared to composite of $K_{1scc}$ envelopes for the other steels.

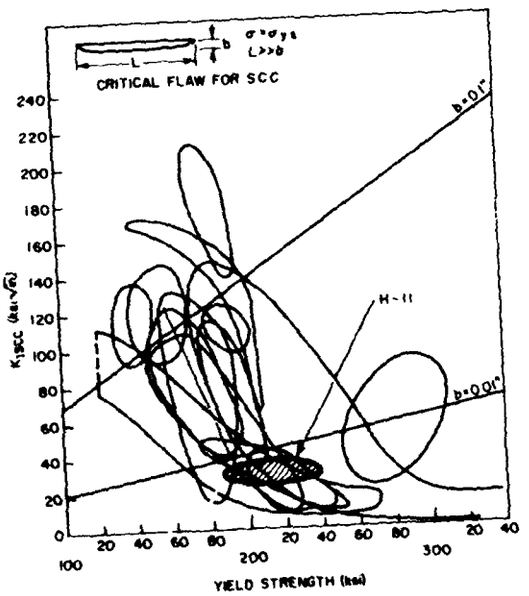


Fig. 28. Envelope of $K_{1scc}$ values for H-11 steel (heavy lines) compared to composite of $K_{1scc}$ envelopes for the other steels.

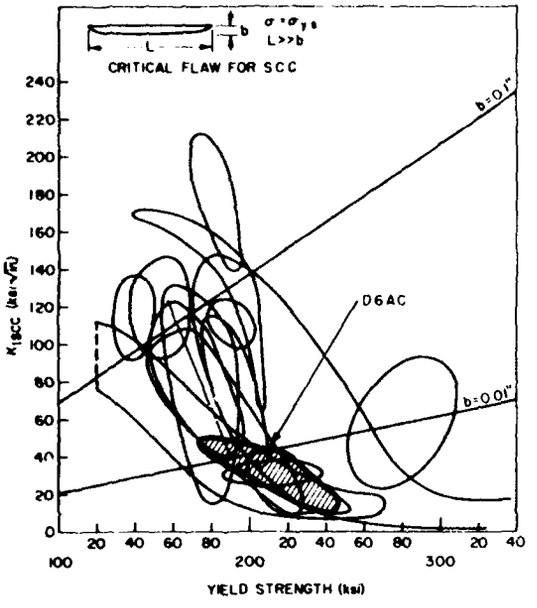


Fig. 29. Envelope of $K_{Iscc}$ values for D6AC steel (heavy lines) compared to composite of $K_{Iscc}$ envelopes for the other steels.

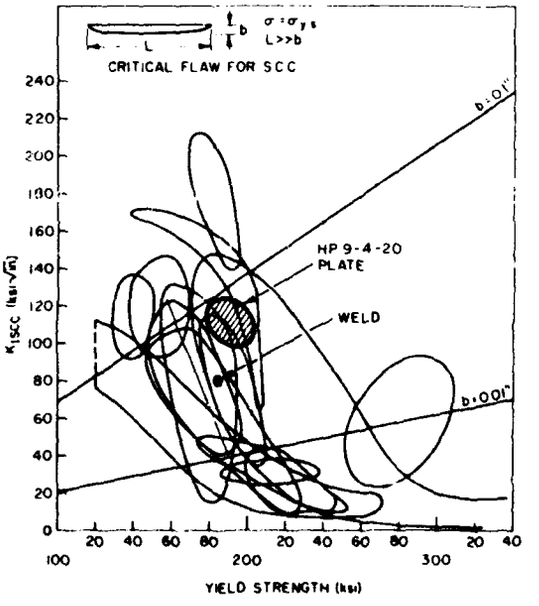


Fig. 30. Envelopes of $K_{Iscc}$ values of HP 9-4-20 steel and welds (heavy lines) compared to composite to $K_{Iscc}$ envelopes for the other steels.

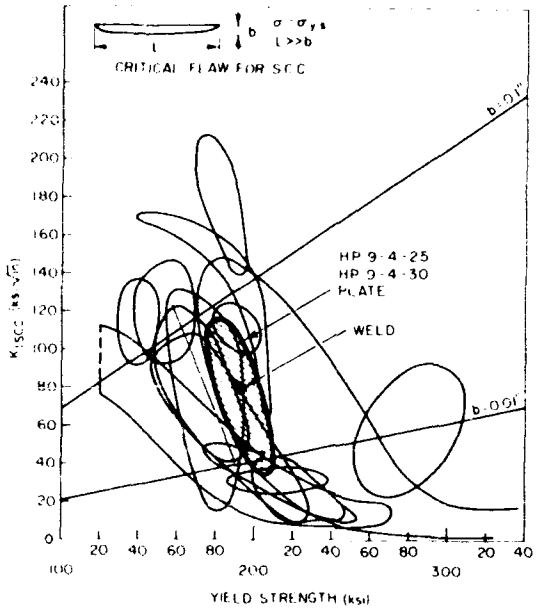


Fig. 31. Envelope of $K_{Iscc}$ values for *HP* 9-4-25 or *HP* 9-4-30 steel and welds compared to composite of $K_{Iscc}$ envelopes for the other steels.

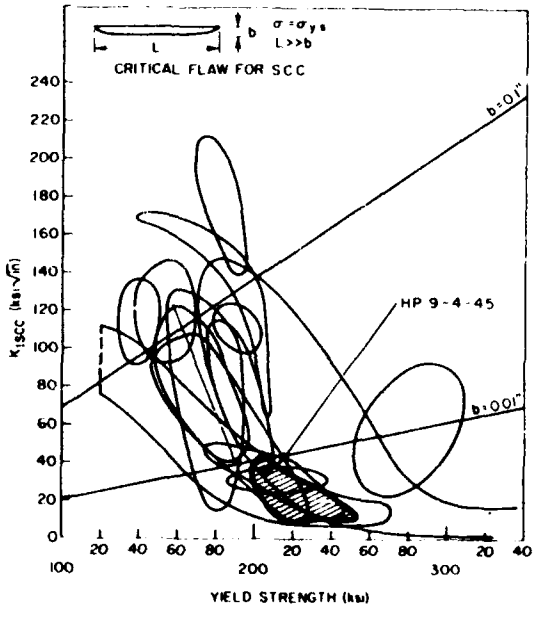


Fig. 32. Envelope of $K_{Iscc}$ values of HP 9-4-45 steel (heavy lines) compared to composite of $K_{Iscc}$ envelopes for the other steels.

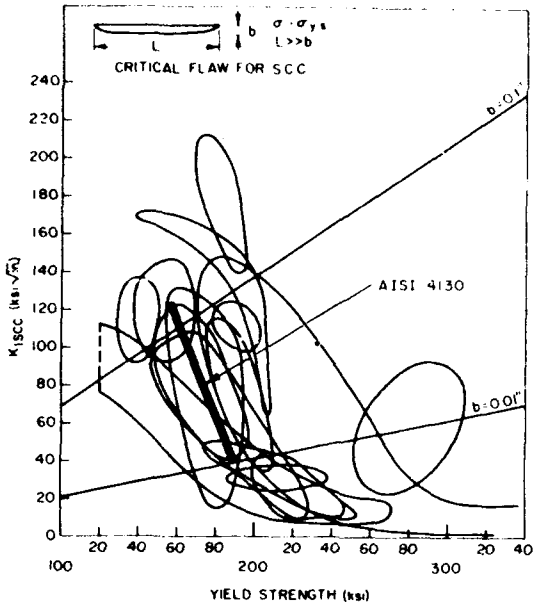


Fig. 33. Envelope of $K_{Iscc}$ values of AISI 4130 steel (heavy lines) compared to composite of $K_{Iscc}$ envelopes for the other steels.

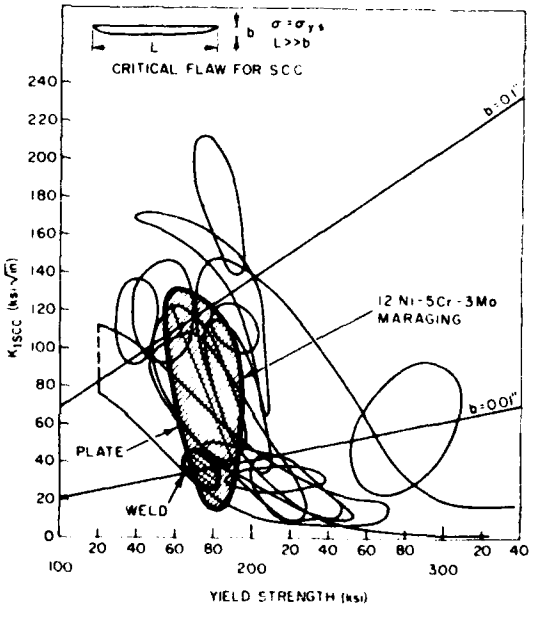


Fig. 34. Envelopes of $K_{Iscc}$ values of 12Ni-5Cr-3Mo maraging steel and welds compared to composite of $K_{Iscc}$ envelopes for the other steels.

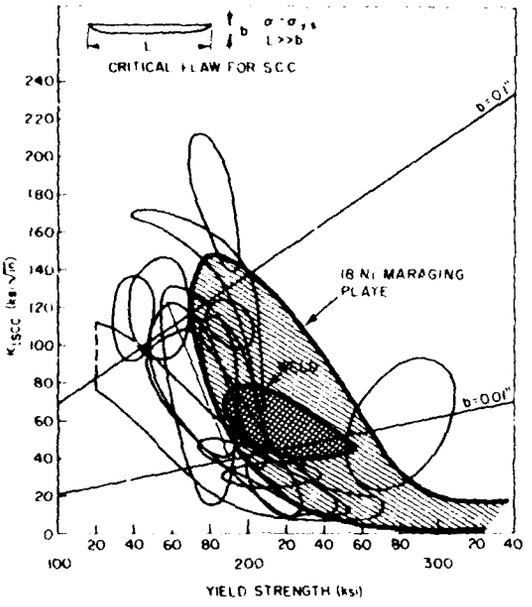


Fig. 35. Envelopes of $K_{Iscc}$ values of 18Ni maraging steel and welds (heavy lines) compared to composite of $K_{Iscc}$ envelopes for the other steels.

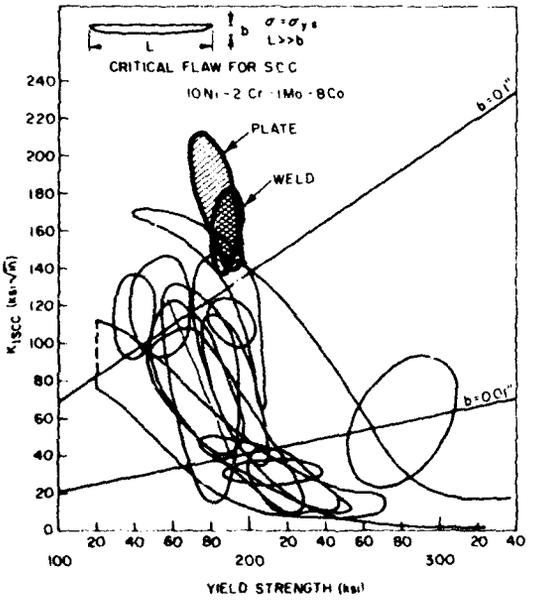


Fig. 36. Envelopes of $K_{Iscc}$ values of 10Ni-2Cr-1Mo-8Co steel and welds (heavy lines) compared to composite of $K_{Iscc}$ envelopes for the other steels.

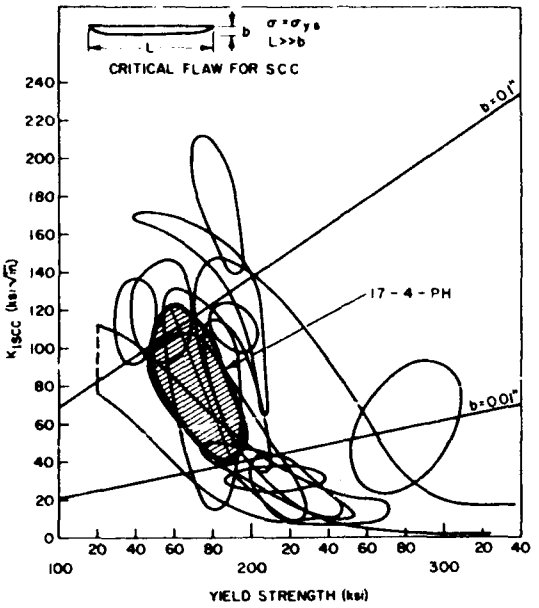


Fig. 37. Envelope of $K_{Iscc}$ values of 17-4-PH steel (heavy lines) compared to composite of $K_{Iscc}$ envelopes for the other steels.

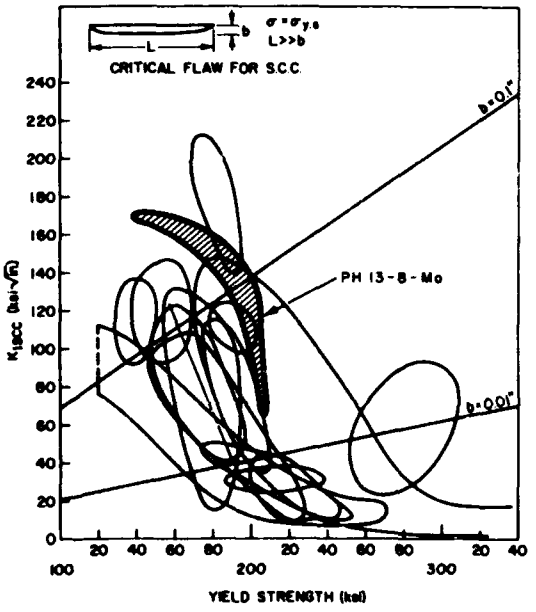


Fig. 38. Envelope of $K_{Iscc}$ values of PH 13Cr-8Ni-Mo steel (heavy lines) compared to composite of $K_{Iscc}$ envelopes for the other steels.

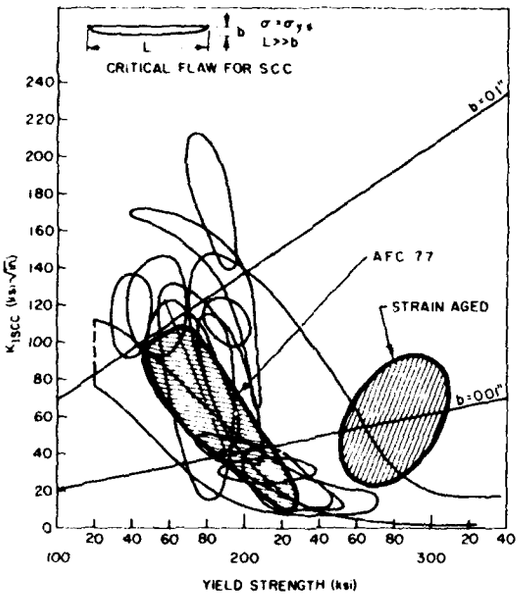


Fig. 39. Envelopes of $K_{1scc}$ values of AFC-77 steel (heavy lines) compared to composite of $K_{1scc}$ envelopes for the other steels.

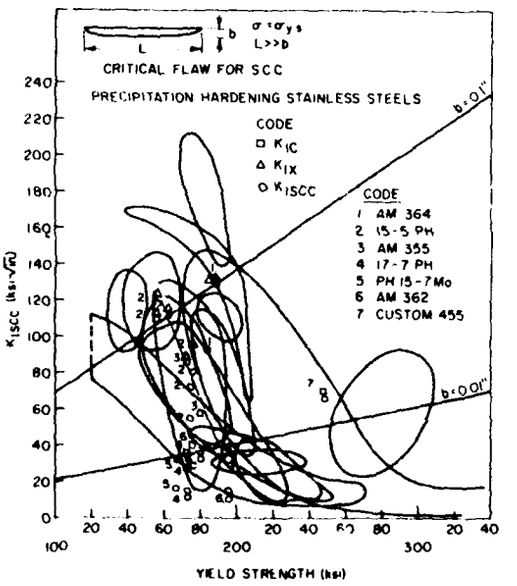


Fig 40. Stress corrosion resistance and fracture toughness of some precipitation-hardening stainless steels. Values are superimposed on $K_{1scc}$ envelopes for other steels.

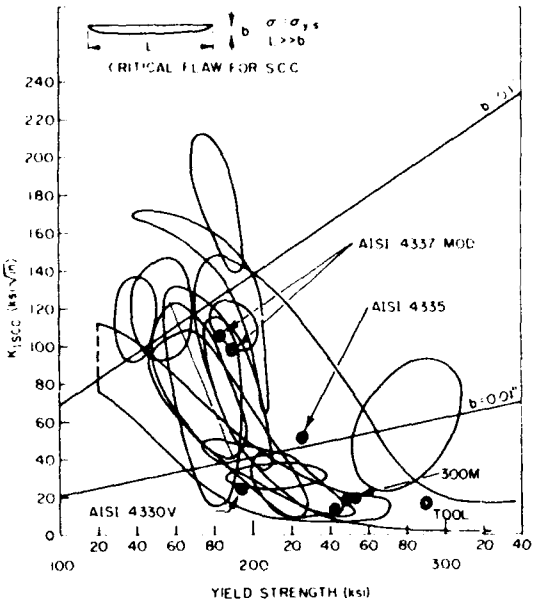


Fig. 41. Single value $K_{Iscc}$ data for a variety of steels, superimposed on a collection of $K_{Iscc}$ envelopes.

The steels with highest $K_{Iscc}$ values appear to be the 10Ni-2Cr-1Mo-8Co steel, the maraging steels, and the precipitation-hardening stainless steels. These are, of course, low carbon highly alloyed steels. Some of them have as yet been produced primarily for experimental purposes using only premium melting stock and premium melt practice. Caution is required in the use of the precipitation-hardening stainless steels for another reason, for it has been shown that the corrodent within crevices (where there is an oxygen deficiency and low pH) may cause crack propagation even when sharp flaws will not propagate under oxidizing conditions [71].

There are sometimes wide ranges of $K_{Iscc}$ values which may be obtained in a given type of steel for a given yield strength. For example, there are wide ranges in $K_{Iscc}$ over a narrow yield strength range for HP 9-4-25 in Fig. 31, 12Ni-5Cr-3Mo maraging steel in Fig. 34, 18Ni maraging steel in Fig. 35, and 17-4PH in Fig. 37. These values reflect all the variables resulting from different melting, processing, heat treating, fabricating, and testing procedures. The fact that the scatter in values among the new alloy steels is so great, compared even to AISI 4340, for which much more data are available, may indicate that these steels are more sensitive to the variables cited. It is obvious from Figs. 23 through 41, certainly, that there is no gain in the use of some of the higher alloy steels unless they are obtained with optimum properties. The poorest quality high alloy steels are no better than the low alloy martensitic steels.

In some cases it appears that the SCC properties of the welds match those of the plate fairly well (at least at the weld centerline). This is seen in Fig. 26 for HY-130, Fig. 31 for HP 9-4-25, and Fig. 36 for 10Ni-2Cr-1Mo-8Co alloy. In other cases the welds compare less favorably to the better values reported for the plate. This is seen in Fig. 30 for HP 9-4-20, Fig. 34 for 12Ni-5Cr-3Mo maraging steel, and to a lesser degree in Fig. 35 for 18Ni maraging steel.

### 3.4 Effect of Composition

Every alloy steel is susceptible to SCC in a specific environment, and it is difficult to generalize on the effects of alloying elements [124]. Still, some data are available to show the effects of individual alloying elements in steels exposed to salt water, and these data will be reviewed here.

One problem with assessing the effects of alloying elements is that these alloying elements may influence the yield strength of the alloy, which in turn is known to influence SCC susceptibility markedly. For example, increasing amounts of titanium have been associated with an increase in SCC susceptibility in maraging steels [124]. But titanium is a hardening element, and any element or process which increases strength would be expected to reduce SCC resistance. The effects of silicon and tempering temperature on the SCC susceptibility of AISI 4340 steel have been treated in a similar manner [125]. Most of the data in Figs. 5 through 41 show general decreases in SCC with increasing yield strength, caused by variations in composition or heat treatment. In this section a review and a comparison of the effects of elements in steels of equal or nearly equal yield strength are made to eliminate the strength variable.

Such studies have been made on quenched-and-tempered steels similar to AISI 4340 in their base composition [126]. The effects of *carbon* are shown in Fig. 42. Obviously at both the 172- and 195-ksi yield strength level, carbon is detrimental to SCC resistance in amounts up to about 0.4 percent. The slightly improved $K_{Iscc}$ at the still higher carbon level (over 0.5 percent) is not yet accounted for.

*Manganese* is also detrimental to SCC resistance in amounts up to 3 percent as shown in Fig. 43. Again, the effects are seen at two yield strength levels. There is no certain explanation for the jog in the curve at the 187-ksi yield strength level [126], if the jog is not an experimental artifact.

*Phosphorus* and *sulfur* in the range of 0.003 to about 0.03 percent have a negligible effect on $K_{Iscc}$, as in Figs. 44 and 45, respectively. Similar results have been found in studies of the effects of phosphorus and sulfur in amounts up to about 0.03% in both bainitic and martensitic HP 9-4-45 steel [127]. [127].

*Chromium* up to about 2%, Fig. 46, also has no effect on $K_{Iscc}$. The same is true of molybdenum in percentages up to about 1% (Fig. 47). Cobalt also has no influence in amounts up to about 3% (Fig. 48).

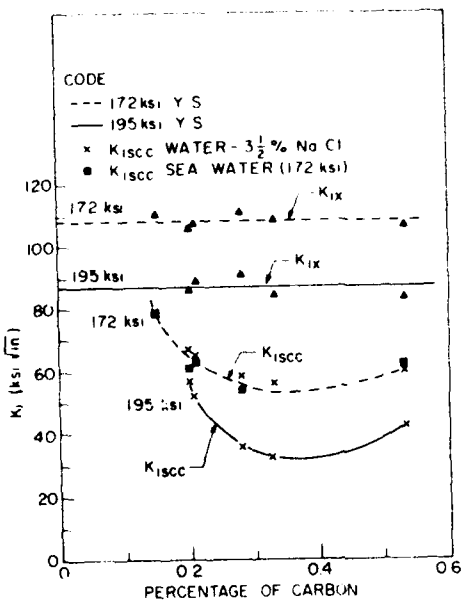


Fig. 42. The effects of carbon on the stress corrosion cracking of AISI 4340-type steels quenched and tempered to either 172- or 195-ksi yield strength.

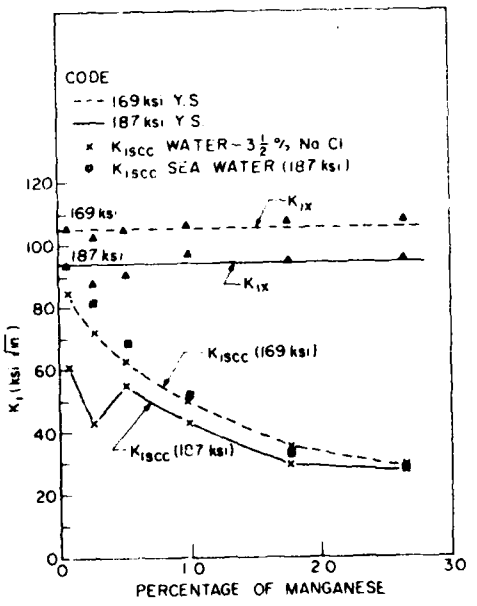


Fig. 43. The effects of manganese on the stress corrosion cracking resistance of AISI 4340-type steels quenched and tempered to 169- and 187-ksi yield strength.

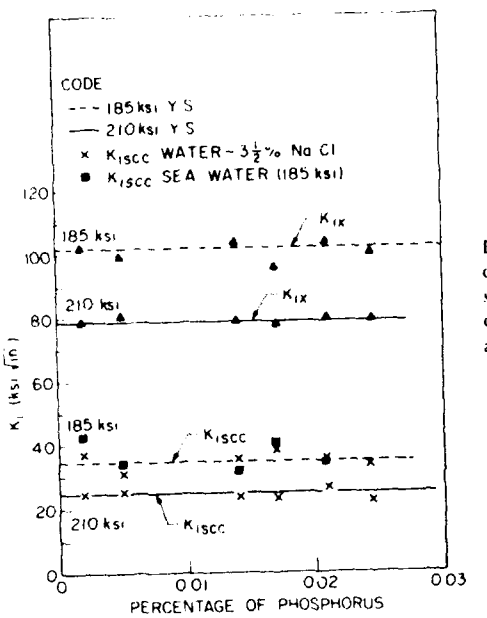


Fig. 44. The effects of phosphorus on the stress corrosion cracking resistance of AISI 4340-type steels quenched and tempered to 185- and 210-ksi yield strength.

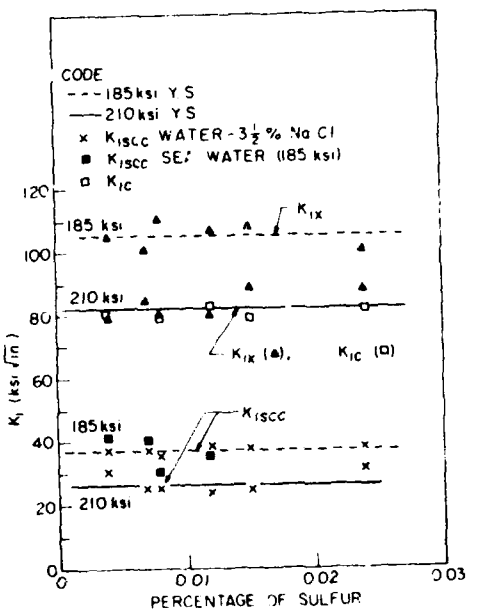


Fig. 45. The effects of sulfur on the stress corrosion cracking resistance of AISI 4340-type steels quenched and tempered to 185- and 210-ksi yield strength.

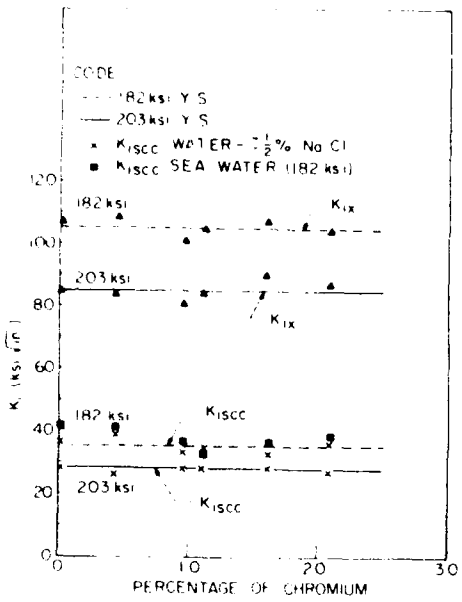


Fig. 46. The effects of chromium on the stress corrosion cracking resistance of AISI 4340-type steels quenched and tempered to 182- and 203-ksi yield strength.

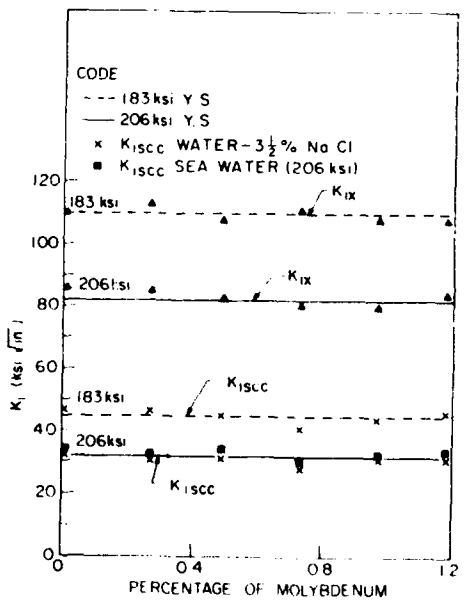


Fig. 47. The effects of molybdenum on the stress corrosion cracking resistance of AISI 4340-type steels quenched and tempered to 183- and 206-ksi yield strength.

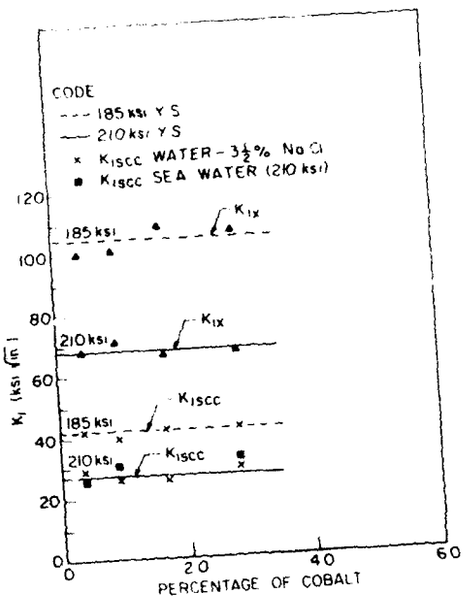


Fig. 48. The effects of cobalt on the stress corrosion cracking resistance of AISI 4340-type steels quenched and tempered to 185- and 210-ksi yield strength.

The effects of *nickel* variation in AISI 4340-type steels on $K_{Iscc}$ have apparently not been studied. However, studies on quenched and tempered pure Fe-C-Ni alloys with nickel in amounts from about 3 to 9% [126], indicate that nickel also has little influence on $K_{Iscc}$, as in Fig. 49. This is also substantiated by the similar $K_{Iscc}$ values recorded for AISI 4340 (nominal nickel content of 1.9%) and HP 9-4-45 (nominal nickel content of 9%) at the same yield strength level (see Figs. 5 and 13).

At least one investigation [67] has demonstrated that the effects of *silicon* variation on AISI 4340 steels are also negligible on $K_{Iscc}$, as in Figs. 50 and 51. Two strength levels were studied, though the yield strength variation within each of two series was considerable. In the 230- to 240-ksi ultimate tensile strength range (Fig. 50), the yield strength varied between 193 and 216 ksi; in the 280- to 300-ksi ultimate tensile strength range (Fig. 51), the yield strength varied between 208 and 241 ksi. In spite of these variations, the effects of up to about 2% silicon on $K_{Iscc}$ could be seen to be essentially negligible. The presence of silicon in amounts over 1.5% does, however, slow crack growth *rate* [67].

Other data confirm that *silicon*, *chromium*, and *molybdenum* have negligible effects on the $K_{Iscc}$ value of AISI 4340-type steels [63,128].

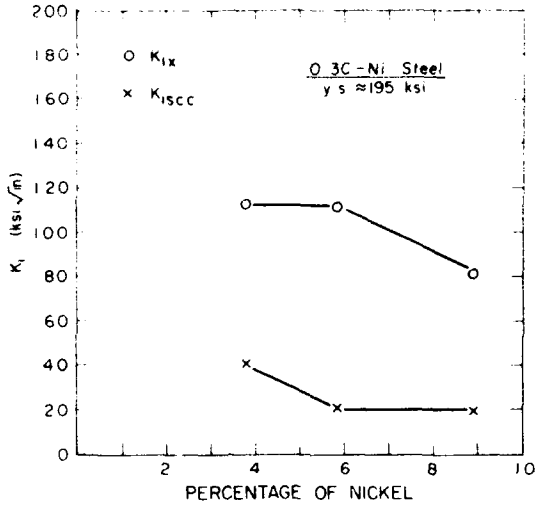


Fig. 49. The effects of nickel on the stress corrosion cracking resistance of 0.3% C steel quenched and tempered to about 195-ksi yield strength.

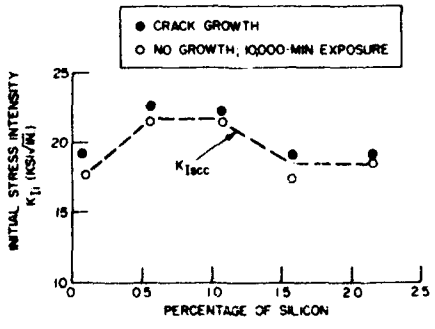


Fig. 50. Effect of silicon on threshold stress intensity $K_{Iscc}$ (193- to 216-ksi yield strength range) (from Ref. 67). From *Corrosion* 25 (No. 10), 423-431 (1965); copyright by the National Association of Corrosion Engineers. Used by permission.

Data on the effects of the variation of the elements nickel, chromium, molybdenum, vanadium, manganese, aluminum, and nitrogen in HY-150 type steels show only chromium to have a greater effect on $K_{Iscc}$ than on $K_{Ic}$ [89-91].

Efforts to enhance the SCC resistance of 18Ni (300 grade) maraging steels by improving the *purity* (controlling sulfur, phosphorus, carbon, silicon, nitrogen, oxygen, chromium, and manganese to low levels) have been unrewarding; $K_{Iscc}$ remains the same as in the less pure commercial alloy [67,107,112,114]. Furthermore, the deliberate addition of impurities (additions of about 0.03S, 0.03P, 0.06C, 0.24Cr, or 0.15Si plus 0.14Mn) beyond normal amounts found in commercial 18Ni-300 maraging steel produces essentially no effect on $K_{Iscc}$

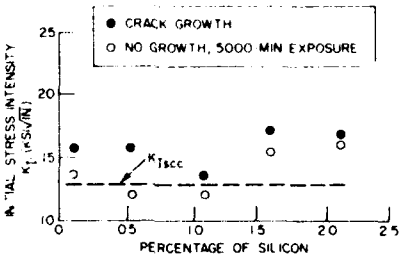


Fig. 51. Effect of silicon on threshold stress intensity $K_{Iscc}$ (202 to 241-ksi yield strength range) (from Ref. 67). From *Corrosion* **25** (No. 10), 423-431 (1965); copyright by the National Associatio.. of Corrosion Engineers. Used by permission.

[112]. Similar studies on the effects of impurities in 18Ni maraging steels of lower yield strength have apparently not been conducted.

In martensitic precipitation-hardening stainless steel it appears that there is some increase in $K_{Iscc}$ value as the nickel content is increased and the chromium content is decreased. From an SCC standpoint, the use of aluminum and perhaps molybdenum as hardeners appears preferable to the use of titanium. Admittedly, however, such composition effects are difficult to interpret by comparing separate studies because of other variations between the steels studied, such as differences in section size and orientation [121].

It seems clear therefore that even substantial variations in the base composition, the presence of impurities, and the presence of alloying elements do not influence $K_{Iscc}$ markedly in most cases. Only carbon and manganese in AISI 4340 steel, and perhaps chromium in HY-150 steel, appear to influence $K_{Iscc}$ values significantly. Control over fluctuations in the base composition, reducing the levels of impurities, or adding alloying elements, therefore, do not appear to promise an easy road to improving the stress corrosion resistance of steels. Nevertheless the relatively favorable stress corrosion properties of the 10Ni-2Mo-1Cr-8Co steel is probably attributable to an unidentified combination of some or all of these factors.

The above discussion concerns only the *threshold* value, $K_{Iscc}$. At stress intensity levels higher than $K_{Iscc}$, composition may influence crack growth *rate* considerably [63,67,112]. The reader is also cautioned again that chromium-bearing steels such as the stainless steels may develop acid conditions within crevices (stagnant conditions) and that $K_{Iscc}$ values are then lowered compared to those in aerated solutions [126,129].

It should be emphasized that studies of the effect of composition on SCC have been conducted varying only one element at a time. It is entirely possible that interaction effects between two or more elements may give rise to SCC effects not disclosed by varying only one element at a time. Indeed, except for the effects of carbon and manganese, only such possible interactions and the effects of melting practice (discussed below) can account for the wide range of SCC behavior shown in Figs. 5 through 22.

### 3.5 Effect of Melting Practice

Evidence was cited earlier that the toughness of steels in the 180- to 200-ksi yield strength range is influenced by melting practice [1,81] (Fig. 1). Similar effects are seen with respect to the threshold value $K_{Iscc}$ for SCC, but the data are limited. As indicated in Fig. 52, AISI 4340 steel which has been vacuum-degassed during melting appears to resist crack propagation in moist air better than air-melted AISI 4340. The silicon-modified 300M steel (VAR) is relatively also resistant to cracking in moist air, as indicated in Table 3. The difference in $K_{Iscc}$ values between the air-melted and vacuum-melted AISI 4340-type steel and vacuum-melted 300M steel was attributed to a lower impurity level, particularly the levels of sulfur and phosphorus [67]. As indicated in the previous section, however, and in Ref. 126, it now appears unlikely that sulfur and phosphorus have much influence on $K_{Iscc}$, at least when varied singly.

Vacuum-induction melting (VIM) of 12Ni-5Cr-3Mo maraging steel apparently improves $K_{Iscc}$ markedly (from 40 to 108 ksi $\sqrt{\text{in.}}$) as shown in Table 3.

With respect to the 18Ni maraging steels it appears that VIM produces a slight increase in the $K_{Iscc}$ values of 18Ni-180 and 18Ni-250 maraging steel, as in Table 3, but the improvement is too small to justify vacuum melting for this purpose only. The previous section included 18Ni-300 grade steel, and no improvement in $K_{Iscc}$ of consequence was obtained by using especially pure raw materials or by VIM + VAR melting practice for steel of this grade and strength level [107,108,112,114].

In one case, vacuum melting appeared to diminish the value of $K_{Iscc}$, as in Table 3 for the 15-5 PH (H-900) alloy. This possibly could reflect a difference in billet size [121].

Only the 12Ni-5Cr-3Mo and 18Ni maraging steels have been made by all three of the processes (air melting, VAR, and VIM + VAR) indicated in Fig. 1. This

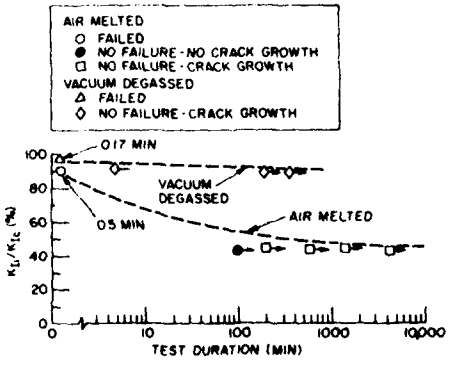


Fig. 52. Commercial alloy 4340 tested in 90% relative humidity air (from Ref. 67). From *Corrosion* **25** (No. 10), 423-431 (1965); copyright by the National Association of Corrosion Engineers. Used by permission.

**Table 3.** Effects of Melting Practice on Susceptibility of SCC*

| Steel | Air Melting | | | | Vacuum Melting | | | | |
|---|---|---|---|---|---|---|---|---|---|
| | Yield Strength, ksi | Stress Intensity | | | Yield Strength, ksi | Stress Intensity | | | |
| | | $K_{Ic}$ | $K_{Ix}$ | $K_{Iscc}$ | | $K_{Ic}$ | $K_{Ix}$ | $K_{Iscc}$ | Process |
| AISI 4340 (moist air) | 212 | 63 | – | 25 | – | – | – | – | – |
| 300M (moist air) | – | – | – | – | 250 | 63.5 | – | ≈60 | CEVR |
| 12Ni-5Cr-3Mo Maraging | 176 | | 130 | 40 | 183 | – | 169 | 108 | VIM |
| 18Ni-180 Maraging | 178 | – | 118 | 108 | 175 | – | 142 | 120 | VIM |
| 18Ni-250 Maraging | 250 | 73 | – | 13 | 247 | 111 | – | 22 | VIM |
| 15-5PH (H900) | 176 | – | ≈97 | 80 | – | – | ≈75 | 56 | Vacuum Melting |
| 15-5-PH (H1000) | 158 | | ≈114 | ≈114 | – | – | ≈120 | ≈120 | Vacuum Melting |

*Ref. 1,67,68,81,102,107,108,121.

spectrum of melting practice may account in part for the large scatter in $K_{Iscc}$ values reported for these steels (see Figs. 15 and 17). The more limited and generally higher range of $K_{Iscc}$ values for 10Ni-2Cr-1Mo-8Co steel (see Fig. 19) may in part reflect the fact that this steel has been produced only by premium melting practice.

The benefits of premium melting practice on $K_{Iscc}$ values seem to be most apparent in the 180- to 210-ksi yield strength range. As the strength increases, the effects of melting practice diminish, and all the steels tend to show low values of fracture toughness and $K_{Iscc}$. Thus the high strength of the 18Ni-300 maraging steel may at this time thwart efforts to raise $K_{Iscc}$ values appreciably by improved melting practice (as above), whereas further efforts to optimize melting practice could possibly improve markedly the lower strength maraging steels.

Different welding processes are analogous to different melting processes, but only data on HY-130/150 appears to offer the basis of any comparison of the relative merits of various welding processes. These data show increasing merit with the SMA, the GMA, and GTA processes, respectively [78,82,83,85,86, 88]. A variety of welding electrodes has been studied but with only modest differences in $K_{Iscc}$ value being observed [85].

### 3.6 Effect of Heat Treatment and Microstructure

The *tempering* and *aging* of steels influence the strength of the steels, so that it is again difficult to isolate the effects of structural changes from purely strength effects. Reviews of the early data, mostly on smooth specimens, show that the general trend is for SCC resistance to increase with higher tempering and aging temperatures [124,125,130]. There are sometimes intermediate tempering or aging temperatures, however, which produce maximum susceptibility [20, 124].

The effects of tempering temperatures on AISI 4340 are obviously related to the resulting yield strength [69,71]. It has been suggested that the improvement with increasing tempering temperature results from progressively less $\epsilon$ carbide and more cementite in the microstructure [125], but this suggestion has not been supported generally [104]. The distribution of carbides is also important [60,131], with a uniform distribution of spheroidal carbide being the best condition. Untempered martensite is highly detrimental to SCC resistance [131].

Since SCC in high strength steels is generally intergranular, it is obvious that the compositional variations and solid state reactions which take place at boundaries may be important. Martensite plate boundaries and transformation twins are known to be favorable nucleation sites for carbide precipitation [63] and hence may also provide preferential and easy paths for crack propagation. The absence of transformation twins has been held as one reason for the superior SCC resistance of the 18Ni maraging and 10Ni-2Cr-1Mo-8Co steels compared to martensitic HP 9-4-45 [92]. Still, the 10Ni-2Cr-1Mo-8Co steel is hypereutectoid, and carbide apparently precipitates during the quench in thick plates, probably at the austenitic grain boundaries [116].

Futhermore, the threshold $K_{Iscc}$ values of the HP 9-4-45 alloy are about the same at the same yield strength level whether the steel is in the *martensitic* or *bainitic* condition [68] (Fig. 13), though only the martensitic structure is twinned. It has been demonstrated, however, that the fracture toughness is superior, and the rate of crack propagation above $K_{Iscc}$ is lower for bainitic HP 9-4-45 compared to martensitic HP 9-4-45. This has been attributed to the absence of both transformation twins and preferential carbide precipitation on platelet boundaries in the bainitic structure [63,132].

A martensitic stainless steel, AFC-77, shows the usual decline in $K_{Iscc}$ value with increasing yield strength [123], as indicated in Fig. 53. In this precipitation-hardening alloy, strength increases with increasing tempering temperature up to about 1000°F. The $K_{Iscc}$ values of the precipitation-hardening stainless steels are quite normally related to the yield strength produced in aging, as in Figs. 38, 39, and 41.

*Overaging* generally produces higher values of $K_{Iscc}$ in both the semi-austenitic and martensitic precipitation-hardening stainless steels [121]. However an additional aging treatment (30 hr at 1000°F) on 12Ni-5Cr-3Mo steel lowers SCC resistance considerably [133], as shown in Fig. 54. It appears that

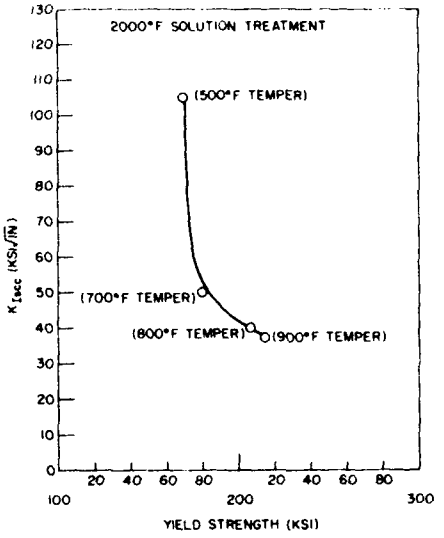


Fig. 53. Effect of yield strength on the $K_{Iscc}$ value of AFC-77 steel (from Ref. 123).

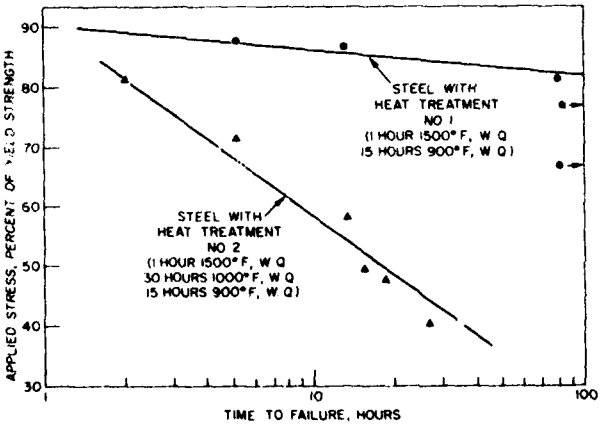


Fig. 54. Stress corrosion behavior of 12Ni-5Cr-3Mo steel in 3% NaCl solution (from Ref. 133). From *Proceedings of Conference on Fundamental Aspects of Stress Corrosion Cracking*, 1969, pp. 411-419; copyright by the National Association of Corrosion Engineers. Used by permission.

the additional aging causes corrosion potential to a region where SCC resistance is low. A change in potential might restore the original SCC resistance value, as implied in Fig. 55.

A variety of annealing and aging treatments in 18Ni-300 maraging steel produces no significant change in $K_{Iscc}$ value provided the same yield strength is reached [111,115]. Again, the *rates* of crack propagation at stress intensity levels higher than $K_{Iscc}$ can vary markedly, generally increasing with lower aging temperatures [115]. Aging at 900°F produces a slight improvement in the $K_{Iscc}$ value of 18Ni-350 maraging steel compared with aging at 800°F [66].

The above seems to show that precipitation and aging reactions influence the threshold $K_{Iscc}$ value primarily by affecting strength. The type, composition, location, and amount of precipitate have a second-order influence on $K_{Iscc}$, but may affect the *rate* of crack propagation above $K_{Iscc}$ considerably.

Although stress corrosion cracks generally progress intergranularly, there are no large effects of *grain size* on $K_{Iscc}$ in AISI 4340 steel, but crack growth *rates* decrease with decreasing grain size [73,134]. An increase in ASTM grain size number from 7 to 12 increased the yield strength from 245 to 265 ksi, but the $K_{Iscc}$ value remained at 14 to 16 ksi $\sqrt{\text{in.}}$

Austenitization treatments on 18Ni-300 grade maraging steel to produce austenitic grain size varying between ASTM No. 9 and No. 0 had little effect on $K_{Iscc}$. However the rate of crack growth decreased with decreasing grain size. All the steels in this study were treated to about the same yield strength [111].

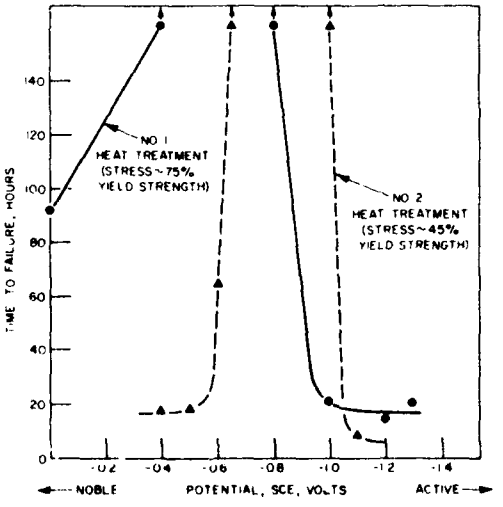


**Fig. 55. Effect of (impressed) potential on time to failure of 12Ni-5Cr-3Mo steel in 3% NaCl solution (applied stress as shown) (from Ref. 133). From *Proceedings of Conference on Fundamental Aspects of Stress Corrosion Cracking*, 1969, pp. 411-419; copyright by the National Association of Corrosion Engineers. Used by permission.**

Decreasing grain size (from 60μm to 2.3μm) in AFC-77 steel by a special thermomechanical treatment is reported to increase the value of $K_{Iscc}$, as shown in Fig. 56. Corresponding increases in yield strength from about 155 to 200 ksi occur with a 500°F temper, and from 175 to 235 ksi with a 1000°F temper. Thus an improvement in both $K_{Iscc}$ and yield strength is achieved. The particular method used to achieve fine grains involves deformation of the steel in the martensitic condition prior to subsequent austenitization treatment.

Retained austenite appears to raise the level of $K_{Iscc}$ in AFC-77 steel [123], as in Fig. 57. The effects appear to override any changes in yield strength.

Reverted austenite in 18Ni-300 grade maraging steel does not appear to influence the $K_{Iscc}$ value greatly [111,115] if the strength is kept constant [111]. The crack growth rate at stress intensities above $K_{Iscc}$ becomes slower with increasing amounts of reverted austenite.

### 3.7 Effect of Deformation

Based on experiments with smooth specimens, *cold work* before aging was concluded to improve the SCC resistance of 18Ni maraging steel [48] (see Fig. 3).

Plastic straining up to 5% in tension apparently reduces the $K_{Iscc}$ value of HY-130 steel only moderately (from 138 to 105 ksi $\sqrt{\text{in.}}$) while increasing the yield strength from 137 to 158 ksi [79]. Plastic straining 12Ni-5Cr-3Mo up to 3% in tension not only increased the yield strength (from 172 to 189 ksi), but

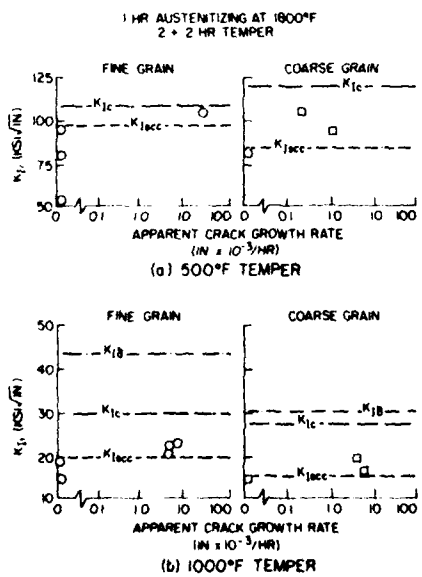


Fig. 56. Effect of grain size on AFC 77 apparent crack growth in 3.5% NaCl solution (from Ref. 122).

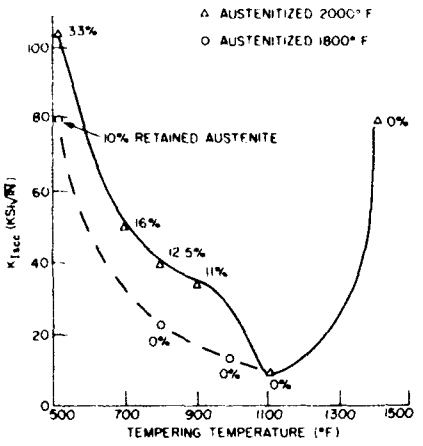


Fig. 57. Variation of $K_{Iscc}$ of AFC-77 steel with tempering temperature as a function of retained austenite content (from Ref. 123).

also appears to have raised the value of $K_{Iscc}$ (from 38 to 50 ksi $\sqrt{\text{in.}}$). These are moderate changes but are not believed to reflect changes in the state of residual stress, which is always a consideration in interpreting the effects of cold work on SCC, particularly in smooth-specimen tests.

*Ausforming* produces considerable improvement in the SCC resistance ($K_{Iscc}$ value) of H-11 steel [93] (Fig. 9). An increase in the $K_{Iscc}$ value of HP 9-4-20 steel (along with an increase in yield strength from 191 to 221 ksi) has also been achieved by ausforming [135]. These rather short-time tests need to be extended, but the results appear to be promising, as in Fig. 58.

Similar improvement in resistance to SCC by ausforming has been shown in smooth-specimen tests of quenched and tempered D6AC steel [136].

One investigation of the effects of *explosion forming* has been conducted on high strength steel, using smooth specimens tested in tension (bending) at 80 percent of the yield strength [137]. Apparently 12Ni-5Cr-3Mo maraging, HP 9-4-25, and 18Ni maraging steels are not much affected by explosion forming. D6AC steel becomes more susceptible after the explosion forming, but data suggest that the effects are not great. A recent review has been published covering the effects of explosive forming on metals, including effects on SCC [138].

The strength of AFC-77 may be increased by a *strain aging* without lowering the threshold $K_{Iscc}$ value [123], as shown in Fig. 59 (see also Fig. 39). In this process the steel is austenitized at 2000°F and tempered at 500°F prior to straining by cold rolling 10 to 20 percent and finally aging at 700°F or 1000°F. The effects of grain size, retained austenite, and strain aging of AFC-77 are compared in Fig. 60.

An illustration of the effect of *rolling direction* in plates of several alloy steels on SCC is given in Table 4 [71,114]. The differences in $K_{Iscc}$ between different heats of the same type of steel obviously are greater than the differences in

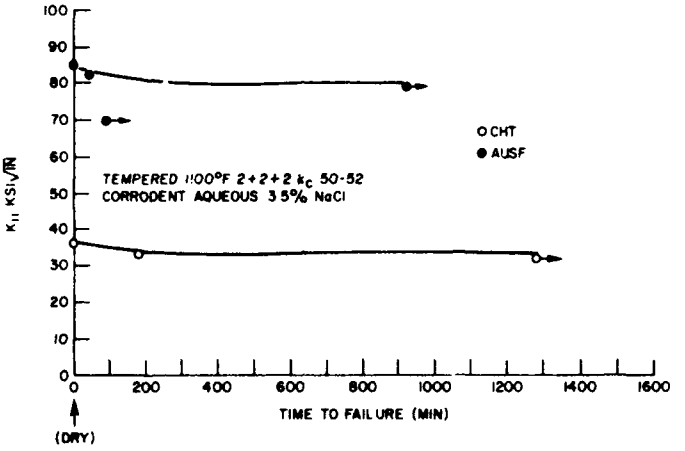


Fig. 58. Precrack cantilever stress corrosion results for ausformed and conventionally heat treated H-11. Corrodent, 3.5% NaCl solution (from Ref. 93). From *Metals Eng. Quart.* 8 (No. 4), 2; copyright 1968 by American Society for Metals. Used by permission.

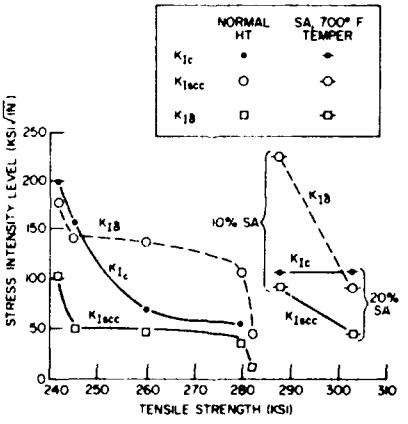


Fig. 59. Variation in $K_{Ic}$, $K_{Iscc}$, and $K_{I\delta}$ of AFC-77 steel as a function of strength for conventionally treated and strain-aged material (from Ref. 123). $K_{I\delta}$ is an estimate of fracture toughness based on the terminal purely mechanical fracture in a stress corrosion test.

$K_{Iscc}$ values caused by a change in the direction of crack propagation with respect to the rolling direction in any one plate.

Studies of HY-130 weldments have shown that the value of $K_{Iscc}$ is not drastically changed whether the notch axis is perpendicular or parallel to the plate surface [84].

It is not concluded here that directionality is of little importance, but the little experience available appears to suggest that this will not be a serious problem area in modern steels.

**Table 4.** Effects of Direction on the Value of $K_{Iscc}$ in Several Steels

| *Steel* | *Stress Intensity, $K_{Iscc}$, ksi $\sqrt{in.}$* | | | |
|---|---|---|---|---|
| | *RT* | *WT* | *WR* | *RW* |
| 9Ni-4Co-0.2C | | 115 | 104 | |
| 18Ni-180 | | 125 | 145 | |
| 12Ni-5Cr-3Mo | - | 19 | 19 | 25 |
| 12Ni-5Cr-3Mo | 70 | 60 | – | |
| 12Ni-5Cr-3Mo | | 105 | 103 | |
| 4340 (200 Yield Strength) | - | - | 11 | 10 |
| 18Ni-300 | - | | 7 | 7 |

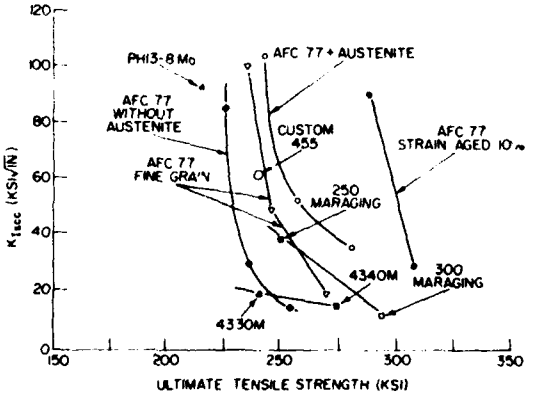


Fig. 60. Effects of grain size, retained austenite, and strain aging on the $K_{Iscc}$ value and strength of AFC-77 steel. Similar data on other steels are included for comparison (from Ref. 138).

### 3.8 Effect of Electrochemical Potential

It has long been considered that electrochemical potential can have an important influence on the susceptibility of steels to SCC. But much of the basis for this belief is work that has been done on smooth specimens, or on precracked specimens with an inadequate test time. Such data reflect initiation time and crack growth rate effects rather than defining clearly a threshold value.

What is essential to know is the effect if any of potential on the $K_{Iscc}$ value of a particular steel. Once these effects are known the effects on crack growth rate may be considered for stress intensities exceeding $K_{Iscc}$.

On AISI 4340 steel, the value of $K_{Iscc}$ is essentially invariant with (impressed) potential over the yield strength range of 125 to 220 ksi (Fig. 61). The *rate* of crack growth at stress intensity levels just above $K_{Iscc}$, however, is highly sensitive to both cathodic and anodic potential, as shown qualitatively in Fig. 62 [140]. This measure of crack growth rate for the AISI 4340 steels reaches a minimum at about -0.8 V (Ag/AgCl). Several other steels (HP 9-4-20, 12Ni-5Cr-3Mo maraging steel, and 17-4 PH) behave similarly with respect to crack growth rate as a function of potential.

A minimum rate of crack growth as a function of potential, similar to that in Fig. 62, has been reported for the following steels: D6AC [63], HP 9-4-45 [61, 63], H-11 [69], HP 9-4-20 (Fig. 63), 12Ni-5Cr-3Mo maraging [65,133], and 18Ni-200 maraging [69,141].

It is rare to find threshold $K$ values as a function of potential, but the data on AISI 4340 (Fig. 61) indicate that the effects of potential are small. There is a lowering of the $K_{Iscc}$ value of HY-130 upon cathodic polarization to -1.2 V [78,80] but to an extent not considered serious [35]. 12Ni-5Cr-3Mo maraging

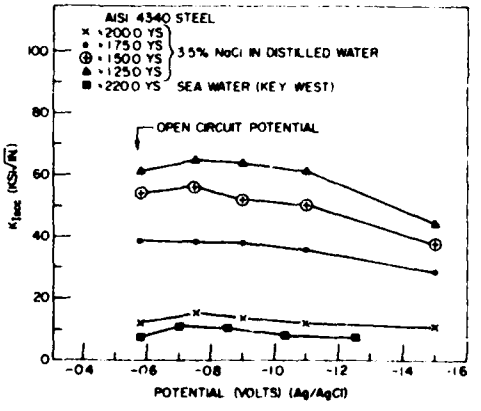


Fig. 61. Effect of (impressed) potential on cracking threshold stress intensity of AISI 4340 steel.

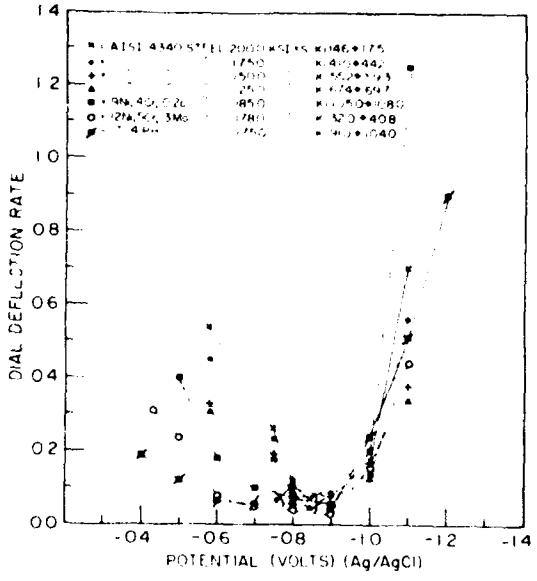


Fig. 62. Effect of (impressed) potential on cracking rates.

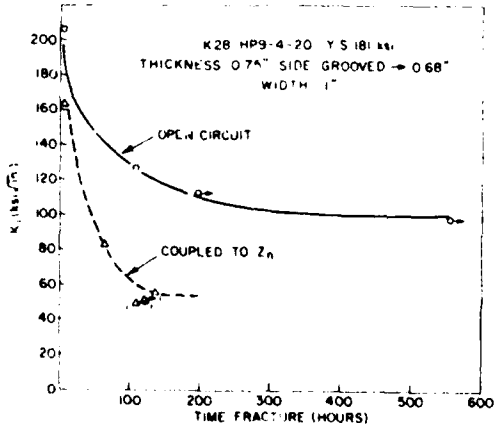


Fig. 63. Effect of coupling HP-9-4-20 steel to zinc on the value of $K_{Iscc}$.

steel is similarly affected by an impressed cathodic potential [80,133]. Data on 18Ni maraging steel are conflicting [69,100,111,141], but the most reliable data indicate that 18Ni-300 grade is insensitive to (impressed) potential insofar as $K_{Iscc}$ is concerned [111]. The data on HP 9-4-25 and 17-4 PH are meager [100] and based on short time tests, but indicate that $K_{Iscc}$ may be lowered by coupling the two steels to zinc. The data of Fig. 63 indicate that the $K_{Iscc}$ value of HP 9-4-20 drops from 100 to at least 60 ksi $\sqrt{\text{in.}}$ upon coupling to zinc. There have been other fragmentary indications that "cathodic protection" reduces the threshold $K$ for a number of precipitation-hardening stainless steels. The 10Ni-2Cr-1Mo-8Co steel definitely appears to show an effect of potential on $K_{Iscc}$ value [118]: Although the $K_{Iscc}$ value of the steel is reported as 160 to 170 ksi $\sqrt{\text{in.}}$, cracks will propagate at a stress intensity as low as 96 ksi $\sqrt{\text{in.}}$ if the steel is polarized to sufficient anodic or cathodic potentials, as shown in Fig. 64. The favorable position of this steel on the $K_{Iscc}$ vs yield strength diagram, Fig. 36, may result in part because of its favorable corrosion potential.

In general it appears that SCC kinetics for all steels are at a minimum at a potential of about -0.6 to about -0.9 V (SCE), but that cathodic polarization does not raise $K_{Iscc}$ and may in fact lower it. Cathodic protection is therefore not an attractive general solution to the SCC problem, but this technique is quite able to prevent corrosion pitting and might therefore be somewhat attractive for preventing the *initiation* of SCC.

### 3.9 Effect of pH

The effects of the pH of the aqueous environment on the SCC susceptibility of *smooth* specimens for normal steels have been reviewed [104,124,133,142,

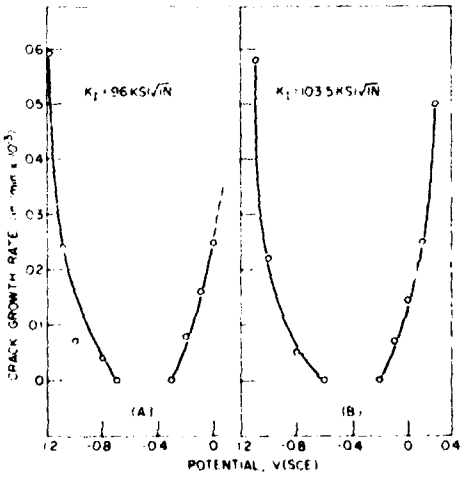


Fig. 64. Crack growth rate as a function of (impressed) potential for 10Ni-2Cr-1Mo-8Co steel in 3.5% NaCl (from Ref. 118).

143]. Generally, highly acid conditions promote cracking, and highly basic conditions reduce or even prevent cracking (by preventing pitting). But over a wide range of intermediate value of pH (about 3 to 10), there is no great change in susceptibility to SCC.

On precracked specimens, a distinction must once again be made between effects on the value of $K_{Iscc}$ and effects on crack growth kinetics. With respect to effects of $K_{Iscc}$, the same general trends appear to obtain as with smooth-specimen data. For example, the variation of the solution pH between 1 and 9 appears to have little effect on the $K_{Iscc}$ value of the martensitic steel En 30 B (4.25Ni:Cr:Mo steel) [144]. At lower values of pH, $K_{Iscc}$ is lowered; at higher values of pH, $K_{Iscc}$ is raised. Changes in pH between 1.7 and 11 have little effect on the $K_{Iscc}$ values of 18Ni-300 maraging steel [111]. However, a pH value of 13.6 stops SCC completely [111].

It appears, therefore, that except with extreme acidic or basic excursions, $K_{Iscc}$ values are not very sensitive to pH. Crack growth rates or time-to-failure values may be influenced, as for example, in the 12Ni-5Cr-3Mo steel [129].

The reason that SCC proceeds over a range of bulk solution pH values appears to be that the solution chemistry within the growing stress corrosion crack is not influenced readily by changes in the pH of the bulk solution. Recent measurements on a variety of steels of the martensitic, maraging, and precipitation-hardening stainless types indicate that near the crack tips of freely corroding specimens the pH value is invariably 3.6 to 3.8 [145-147], and that this is the case over a range of bulk pH values [147]. The pH at the crack tip *is* influenced by applied anodic or cathodic polarization potential [147]; however, there need not be a change in the mechanism of crack growth. This will be discussed further in Section 3.12.

### 3.10 Other Environmental Matters

Environments other than water or salt water can cause stress corrosion in high strength steels, and in fact the identification and study of critical species in different environments is an area which has been neglected [148,149].

Generally, high strength steels are subject to SCC in chloride solutions, marine atmospheres, solutions containing $H_2S$ and acetic acid, and in some cases in solutions containing $SO_4^{=}$, $PO_4^{\equiv}$, or $NO_3^{-}$ ions [29,65,130,142,150-152]. Certain cathodic poisons are known to promote cracking; these are phosphorus, arsenic, antimony, sulfur, selenium, technetium, and ($CN^{-}$) ion [65,104,153]. The poisons are thought to restrict the recombination of atomic hydrogen into molecular form.

Organics and nonelectrolytes can cause SCC in some steels [29,76,150, 154]. Likewise some liquid metals [45,155], but liquid metal embrittlement will not be treated here.

With respect to specific alloys, it appears that the $K_{Iscc}$ value of AISI 4340 steel at the 200-ksi yield strength level is nearly the same whether the environ-

ment be distilled water, 1.5*N* NaCl, or 3*N* NaCl [61]. Similarly, the $K_{Iscc}$ value of AISI 4340 with a 250-ksi yield strength is the same in distilled water as in water with 2 or 4% NaCl [76]. (At 250-ksi yield strength, the value of $K_{Iscc}$ would be quite low and insensitive to a number of variables.) $K_{Iscc}$ values for the SCC of AISI 4340 in flowing seawater are similar to the values obtained using distilled water containing 3.5% NaCl, as in Fig. 65. Small differences between the effects of flowing seawater (worst) and laboratory salt water have been reported for HY-130, 12Ni-5Cr-3Mo maraging, and 18Ni maraging steel [80].

In a solution of 3.5% NaCl and 0.5% HAc saturated with $H_2S$, the $K_{Iscc}$ values of AISI 4340 with 187 to 228-ksi yield strength are low, and fall near the lower bound of the AISI 4340 envelope (see Figs. 5 and 25 and Ref. 65).

AISI 4340 is susceptible to SCC in methanol, with the $K_{Iscc}$ values intermediate between $K_{Ix}$ and $K_{iscc}$ in 3.5% NaCl solution, as in Fig. 66. Similar

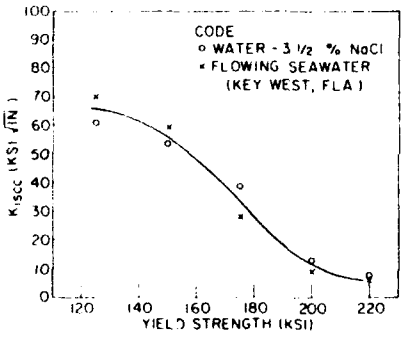


Fig. 65. Effects of quiescent distilled water containing 3½% NaCl and flowing seawater on the threshold stress intensity parameter for stress corrosion cracking of AISI 4340 steel in the 125-ksi to 220-ksi range of yield strength [156].

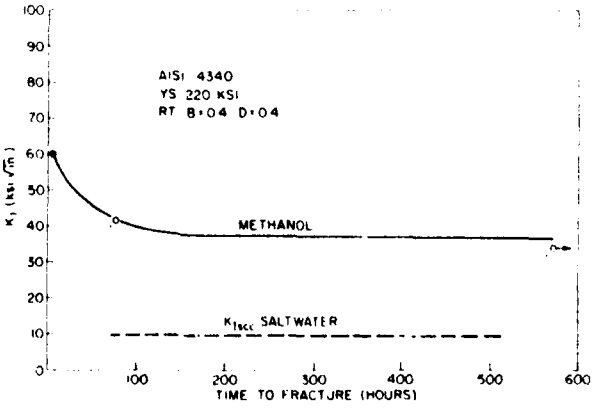


Fig. 66. Comparison of the values of $K_{Iscc}$ in methanol and in salt water for AISI 4340 steel.

effects on $K_{Iscc}$ have been observed with butyl alcohol and acetone [76]. In another investigation utilizing notched tensile specimens, AISI 4340 was observed to be susceptible to SCC in $CCl_4$ [157].

AISI 4140 at the 187-ksi yield strength level is susceptible to SCC in a solution of 3.5% NaCl and 0.5% HAc saturated with $H_2S$, with a $K_{Iscc}$ value somewhat lower than the $K_{Iscc}$ values of AISI 4130 in salt water [65] (see Fig. 14), though it is not known whether the difference is due to the steels or to the environment. The 12Ni-5Cr-3Mo maraging steel at 187-ksi yield strength is susceptible in this acid chloride-sulfide environment, the value of $K_{Iscc}$ falling within the lower region of the envelope in Fig. 15.

There is no change in the $K_{Iscc}$ value for martensitic HP 9-4-45 steel as the environment is changed from distilled water to 1.5*N* NaCl or to 3*N* NaCl [61].

With 18Ni-300 maraging steel, the value of $K_{Iscc}$ is the same in distilled water, 3% NaCl, and 1*N* $H_2SO_4$ [111].

It seems therefore that large changes in the acidity, salt concentration, etc., of aqueous environments do not change $K_{Iscc}$ very much. Introduction of the "poison" $H_2S$ appears to lower $K_{Iscc}$ to the lowest values reported for a particular type of steel in salt water.

The data showing that high strength steel may be susceptible to SCC in organics and nonelectrolytes is not greatly surprising because similar effects have been observed with titanium alloys [158] and with aluminum alloys [159]. Such data are often held in question because of the suspicion that minor amounts of impurities may be responsible.

### 3.11 Mitigation of SCC

Inhibitors in aqueous solution are of two types: (a) those that function by forming a solid film (oxidizing or precipitation inhibitors) and (b) those that function by forming an adsorbed layer. Examples of the solid-film type are nitrites, silicates, phosphates, and chromates. The adsorbed-film types are generally organic nitrogen and sulfur compounds. Sometimes inhibitors are incorporated into layers (coatings) which also form a barrier to the environment.

On nonprecracked specimens the solid film inhibitors appear to be more effective than the adsorbed layer organic type inhibitors with respect to stress corrosion. For example, the addition of $NaNO_3$, $Na_2CrO_4$, $Na_2SiO_3$, or thiourea to distilled water extends the time to fracture of U-bend AISI 4340 specimens treated to 230-ksi yield strength. Thus the standard inhibitors used to mitigate the corrosion of steels tend to prevent stress corrosion of smooth specimens. The concentration of inhibitor needed to inhibit stress corrosion is, however, greater than that required to control general corrosion. The effectiveness of these inhibitors is enhanced if the environment is alkaline (pH 10 to 12). However, there is no simple correlation of inhibitor effectiveness with pH of the bulk

solution [160]. Caution is needed in using inhibitors as above, for certain critical conditions may promote stress corrosion, e.g., a critical concentration or pH level [133].

The data on the effectiveness of inhibitors on precracked specimens are limited. The addition of 0.25% $Na_2CrO_4$ to a distilled water environment extends the failure time of AISI 4340 considerably, probably by stabilizing the surface oxide film. However, the same concentration of $Na_2CrO_4$ in 1.5*N* and 3*N* NaCl solutions has no effect on the same steel. Apparently, the $K_{Iscc}$ value is not influenced greatly either [61].

The addition of 1.75% $Na_2CrO_4$ to 3.5% NaCl solution has little influence on the $K_{Iscc}$ value of 18Ni-200 and 18Ni-250 maraging steel [110]. Similarly, the addition of 1.5% $Na_2CrO_4$ does not affect $K_{Iscc}$ values in 18Ni-300 maraging steel [111].

The conclusion reached on the basis of this limited data is that there is no evidence that inhibitors influence $K_{Iscc}$ values on high strength steels. There is some evidence that the usual corrosion inhibitors may be beneficial in avoiding SCC when sharp cracks are not present, but higher concentrations are needed. The fundamental problem with inhibiting stress corrosion crack *propagation* is that the crack tip region is acidic, and inhibitors are incompletely effective in acid solutions, particularly if chloride is also present.

Obviously an inert coating is one way to prevent SCC, and such coatings work provided no flaws penetrate to the metal either in application or during service. Other coatings provide cathodic protection or contain inhibitors as a second-line defense in case the coating is breached. When flaws do appear, there is danger that cracking may be enhanced through hydrogen embrittlement (cathodic charging). The considerations which specify a desirable coating and the experience which has been accumulated on specific coatings for smooth specimens has been reviewed adequately elsewhere [74,124,141,142,150,161].

With respect to precracked specimens, there is almost no experience with the efficacy of coatings. There are no effects on the $K_{Iscc}$ value of 18Ni maraging steel when 12-5-3 maraging steel, a Ni-Cu alloy, or carbon steel, is used as cladding, provided the precrack penetrates the clad. The data are considered only qualitative because the stress intensity factor could not be determined with the thick coatings which produce what could be considered a laminated plate. It would be expected that coatings such as zinc on the precipitation-hardening stainless steels (and other steels sensitive to cathodic charging) would lower $K_{Iscc}$ at a local flaw in the coating. (See Fig. 62.)

In the absence of a coating involving another material, a "coating" of worked metal in compression, such as that produced by shot peening, could be effective. In fact, the surface condition produced by a number of finishing treatments can be very important on smooth specimens [150,162]. If large flaws are present, such surface effects will diminish. Thus the effects of coatings, inhibitors, and surface treatments would be expected to vary with the number and depth of flaws which may exist.

### 3.12 Mechanisms

The theories of SCC have been widely reviewed in recent years [148,151, 152,162-172]. It seems that the detailed mechanisms which have been proposed for the great number of metal-corrodent systems can be grouped into two general categories: dissolution models and mechanical models. There are two types of dissolution model: (a) the film rupture model and (b) the mechano-chemical model. There are also two types of mechanical model: (c) the adsorption model and (d) the brittle film model. Thus there are basically four (a, b, c, and d) different categories of SCC models. The models have been discussed thoroughly, and it will suffice here merely to indicate briefly the basic features, which are as follows:

1. Film rupture model. Plastic deformation at the crack tip ruptures a passive film intermittently. This enables localized anodic dissolution to take place. The crack walls remain passive and are cathodes.
2. Mechano-chemical model. Deforming *film-free* metal at the crack tip is anodic to the nondeforming metal at the crack walls, and the process of deforming opposes stifling of the process by polarization.
3. Adsorption model. The adsorption of specific species at the crack tip reduces the energy required to form new surfaces. The specific species must therefore adsorb and react with the strained metal bond at the crack tip and reduce the fracture strength.
4. Brittle-film model. Exposure to the environment causes the metal to form an embrittled surface layer which fractures under tensile stress. Crack propagation may be intermittent.

The development of techniques for the measurement of pH and electrode potential at the tips of propagating stress corrosion cracks [145-147], together with the use of the Pourbaix diagram, seems to clarify the meaning of many of the observations on the SCC behavior of steels. For example, the minimum in crack growth rate as a function of decreasing potential (e.g., Fig. 62) has often been cited as evidence of a change in cracking mechanism from one of anodic dissolution to one of hydrogen embrittlement [104,153]. By measuring *both* crack tip and potential, however, it has been found that the crack-tip conditions in a propagating crack are always favorable for the reduction of hydrogen, and that therefore only the hydrogen embrittlement mechanism is required (Fig. 67).

The minimum in the rate curve appears to occur at the transition from the region of corrosion to the region of immunity, indicated in Fig. 68. On this basis the minimum can be regarded as the consequence of moving the anodic reaction from within the crack to outside the crack [140]. The application of cathodic protection may at first stifle the anodic reaction and reduce the amount of hydrogen discharged, but as cathodic hydrogen evolution increases the crack growth rate may increase as a result of increased hydrogen charging.

Hydrogen may be absorbed by AISI 4340 and HP 9-4-45 under *anodic* polarization [174], and therefore a single hydrogen cracking mechanism may apply across the board of the polarization potential.

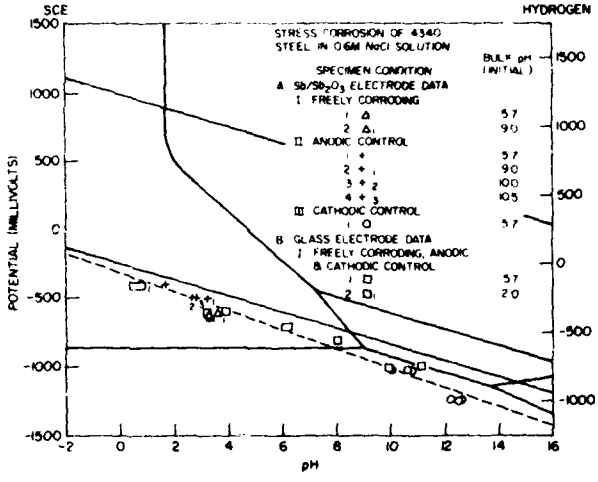


Fig. 67. Effects of anodic and cathodic (impressed) potential on the pH at the tip of propagating stress corrosion cracks in AISI 4340 steel. Obviously water may be reduced to release hydrogen at the crack tip in every case.

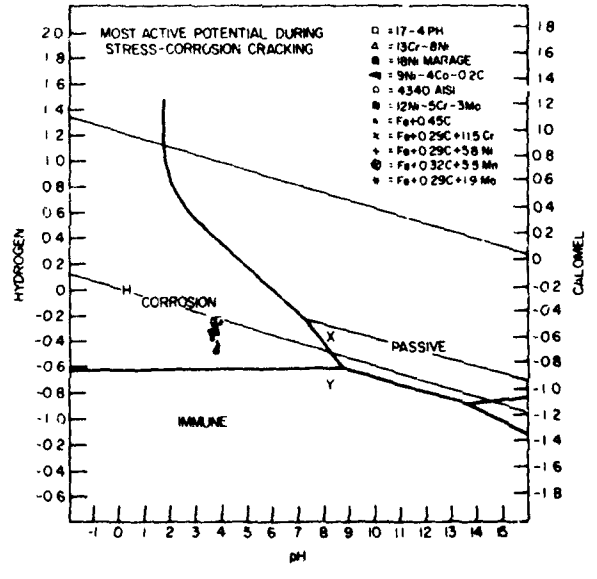


Fig. 68. Values of potential and pH at the crack tips of several steels during stress corrosion crack propagation.

When pits or a precrack are essential to the initiation of stress corrosion cracks, it may be because of the need to provide a local environment where the acidification may take place by hydrolysis [147,175,176]. Once crack growth begins, the crack itself provides the necessary localized environment.

The hydrogen embrittlement mechanism is also consistent with the observation that slow crack growth can take place in hydrogen-containing steels in the absence of a corrodent.

The activation energies for crack growth are similar whether hydrogen is supplied externally or from a stress corrosion process [105,177,178]. The fractographic fracture surfaces are similar [179]. Thin-film microscopy [180] indicates that the structure of AISI 4340 tempered at 400°F resembles the structure of the as-quenched martensitic defect state upon cathodic charging, whereas the same steel tempered at 1300°F does not. (This agrees with observations that the steel is susceptible to SCC when tempered at 400°F, but not susceptible at 1300°F.) The formation of films (presumably oxides) impedes crack initiation, but not crack growth [181]. All the foregoing are in accord with a model for SCC involving hydrogen embrittlement.

## 3.13 References


1. P. P. Puzak and E. A. Lange, *Fracture Toughness Characteristics of the New Weldable Steels of 180- to 210-Ksi Yield Strengths*, NRL Report 6951, Naval Research Laboratory, Washington, D.C., Sept. 18, 1969.
2. A. F. Hoenie and D. B. Roach, *New Developments in High Strength Stainless Steels*, DMIC Report 223, Battelle Mem. Inst., Jan. 3, 1966, AD 481725.
3. T. S. Humphries and E. E. Nelson, *Stress Corrosion Cracking Evaluation of Several Precipitation Hardening Stainless Steels*, NASA TM-X-53910, Sept. 12, 1969.
4. C. J. Owen, *Stress Corrosion of High Strength Steels and Alloys: Artificial Environment*, Mellon Institute Final Report, July 1960-June 30, 1962 Research Project No. 389-2, Contract DA36-034-ORD-3277RD.
5. C. M. Hudgins, R. L. McGlasson, P. Mehdizadeh, and W. M. Rosborough, "Hydrogen Sulfide Cracking of Carbon and Alloy Steels," *Corrosion* 22, 238 (Aug. 1966).
6. F. M. Reinhart, *Corrosion of Materials in Hydrospace*, Naval Facilities Engineering Command, Technical Report R504, Dec. 1966, AD 644473.
7. J. J. DeLuccia, "Evaluation of Metals in Deep Ocean Environments," *Mater. Protect.* 5, 49 (Aug. 1966).
8. S. J. Ketcham, *Chemical Milling of Alloy Steels*, Report No. NAEC-AML-2418, Mar. 9, 1966, Naval Air Engineering Center, Aeronautical Materials Laboratory, Wep Task RRMA 02 01/200 1/F020-01-01, AD 631952.
9. S. J. Ketcham, *Chemical Material Influence on Stress-Corrosion Behavior of High Strength Materials*, Naval Air Engineering Center, Aeronautical

Materials Laboratory, NAEC-AML-2174, Apr. 7, 1965, Wep Task RRMA 05 010/200 1/R007 08 01.

10. G. A. Dreyer, *Investigation of Susceptibility of High Strength Martensitic Steel Alloys to Stress Corrosion*, Technical Documentary Report No. ASD-TDR-62-876, Sept. 1962. Project No. 7381, Task No. 738103, prepared under Contract No. AF 33(616)-7859 by The Boeing Company, Seattle, Wash., AD 603219.
11. A. Gallaccio and M. A. Peleasky, "Stress-Corrosion of High Strength Steel Alloys Environmental Factors," in *Stress-Corrosion Testing*, ASTM STP 425, Amer. Soc. Testing Mater., Philadelphia, Pa., 1967, p. 99, AD 681293.
12. R. A. Davis, G. A. Dreyer, and W. C. Gallaugher, "Stress-Corrosion Cracking Study of Several High Strength Steels," *Corrosion* **20**, 93t (Mar. 1964).
13. W. S. Hyler and O. Deel, *Mechanical Property Data–AFC-260 Stainless Steel (Aged Sheet)*, Battelle Mem. Inst., Contract F33615-67-C-1292 Mar. 1968, AD 834919.
14. W. S. Hyler, and L. Beall, *Mechanical Property Data–AFC-77 Sheet (1100°F Temper)*, AF 33(615)-2494, prepared by Battelle Mem. Inst., Oct. 1966, AD 803545.
15. W. S. Hyler and L. Beall, *Mechanical Property Data–AF-77 Steel (700°F Temper)*, AF 33(615)-2494, prepared by Battelle Mem. Inst. Oct. 1966, AD 803544.
16. O. L. Deel and W. S. Hyler, *Engineering Data on Newly Developed Structural Materials*, Technical Report AFML-TR-67-418, prepared by Battelle Memorial Institute, Apr. 1968, Contract AF 33(615)-2494, AD 834938.
17. J. H. Hoke, *The Stress-Corrosion Susceptibility of High Strength Steels*, Pennsylvania State University Report NYO-3257-1 to U.S. Atomic Energy Commission, Contract No. AT(30-1)3257, June 1965, N66-30970.
18. H. J. Bhatt and E. H. Phelps, "Effect of Solution pH on the Mechanism of Stress-Corrosion Cracking of a Martensitic Stainless Steel," *Corrosion* **17** (No. 9), 430t (Sept. 1961).
19. J. E. Truman, R. Perry, and G. N. Chapman, "Stress-Corrosion Cracking of Martensitic Stainless Steels," *J. Iron Steel Inst.* **202**, 745 (Sept. 1964).
20. R. Perry, *Stress Corrosion Resistance of High-Tensile Stainless Steels*, Spec. Report 86, The Iron and Steel Institute, London, 1964, p. 227.
21. G. A. Dreyer and W. C. Gallaugher, *Investigation of the Effects of Stress-Corrosion on High Strength Steel Alloys*, Technical Documentary Report No. ML-TDR-64-3, Feb. 1964, prepared under Contract No. AF 33(657)-8705 by the Boeing Company, Project No. 7381, Task No. 738103, AD 605672.
22. E. H. Phelps and A. W. Loginow, "Stress Corrosion of Steels for Aircraft and Missiles," *Corrosion* **16**, 325t (Feb. 1960).

23. J. L. Guthrie, *High Strength Steel Evaluation for Supersonic Aircraft*, Boeing Document D6A10093-2, Mar. 1967, Phase II-C Report FA-SS-66-5, The Boeing Company, Seattle, Wash., AD 818490.
24. R. A. Davis, "Stress-Corrosion Cracking Investigation of Two Low Alloy, High Strength Steels," *Corrosion* **19** (No. 2), 45t (Feb. 1963).
25. J. F. Hildebrand, "Stress-Corrosion Cracking of High Strength Nickel Alloys for Aircraft Applications," *Mater. Protect.* **3** (No. 9), 36 (1964).
26. J. J. DeLuccia, *Metallic Corrosion in the Deep-Ocean Environment, Six Months at 2540 Feet*, Report No. NADC-MA-6868, Naval Air Development Center, Johnsville, Pa., Jan. 10, 1969. Air Task A32-523 001/2021 R007-01-01, Work Unit D -Work Element 2, AD 848907.
27. S. W. Dean and H. R. Copson, "Stress Corrosion Behavior of Maraging Nickel Steels in Natural Environments," *Corrosion* **21**, 95 (Mar. 1965).
28. W. W. Kirk, R. A. Covert, and T. P. May, "Corrosion Behavior of High-Strength Steels in Marine Environments," *Metals Eng. Quart.* **8** (No. 4), 31 (Nov. 1968).
29. E. A. Steigerwald, "Engineering Aspects of Stress Corrosion Failure in Martensitic Steels," AGARD, Stress Corrosion Cracking in Aircraft Structural Materials, Conference at Turin, Italy, April 18-19, 1967.
30. D. F. Bulloch, T. W. Eichenberger, and J. L. Guthrie, "Evaluation of the Mechanical Properties of 9Ni-4Co Steel Forgings," AFML-TR-68-57 and Boeing Document D6-19769-3, The Boeing Company, Seattle, Wash., Mar. 1968, AD 833650.
31. R. L. Jones and F. C. Nordquist, *An Evaluation of High Strength Steel Forgings*, Technical Documentary Report No. RTD-TDR-63-4050, by General Dynamics, Fort Worth, Texas, May 1964, under Air Force Contract No. AF 33(600)-41891, AD 601446.
32. P. C. Hughes, "Delayed Fracture of a 5% Cr Tool Steel," *J. Iron Steel Inst.* **204** (Pt.1), 385 (1966).
33. F. Ginsberg and I. L. Stern, "Stress Corrosion Characteristics of HY-130 Butt Weldments," U.S. Naval Applied Sciences Laboratory Technical Memo 56, SF 020-01-01 Task 0722, Feb. 1967, AD 809399L.
34. A. W. Loginow, *Corrosion and Stress-Corrosion of HY-130 (T) Steel and HY-80 Steel in Marine Environments*, Project N. 39.001-100(2), U.S. Steel Corp., Applied Sciences Laboratory, July 15, 1967, AD 817366.
35. G. A. Wacker, *The Effects of Marine Environment in High-Strength Steels*, Report 2840, Naval Research and Development Center, Annapolis, Md., Feb. 1969, AD 848165.
36. A. H. Rosenstein, M. R. Gross, W. G. Schreitz, and G. A. Wacker, *Metallurgical Investigations of 9Ni-4Co-0.20C Steel*, Report 2678, Naval Research and Development Center, Annapolis, Md., July 1968, AD 837086.
37. L. G. Beall and W. S. Hyler, *Mechanical Property Evaluation of Newly Developed Structural Materials*, Technical Report AFML-TR-66-155, Battelle Mem. Inst., Apr. 1966, AD 485824.

38. W. S. Hyler and L. Beall, *Mechanical Property Data HP 9Ni-4Co-25C Steel Tempered Plate* AF 33(615)-2494, Battelle Mem. Inst., Oct. 1966, AD 803546.
39. R. V. Turley, C. H. Avery, and M. Sinclaire, *The Effect of Processing Variables in Stress-Corrosion Cracking of 9Ni-4Co Steel Alloy*, AFML-TR-66-388, Douglas Aircraft Company, Dec. 1966, Contract AF 33(615)-2849, AD 810834.
40. W. S. Hyler and L. Beall, *Mechanical Property Data HP 9Ni-4Co-45C Steel*, Contract AF 33(615)-2494, Battelle Mem. Inst. Columbus, O., Oct. 1966, AD 803547.
41. W. H. Hyler and L. Beall, *Mechanical Property Data HP 9Ni-4Co-45C Steel* Contract AF 33(615)-2494, Battelle Mem. Inst. Columbus, Ohio, June 1967, AD 821651.
42. A. W. Loginow, *Stress-Corrosion Behavior of 12 Percent Nickel Maraging Steels*, U.S. Steel, Dec. 31, 1964, Project No. 40.001-100(3), Nobs-88540 SS 050-000, Task 1567 S-23309, AD 616982.
43. G. A. Wacker, *Stress-Corrosion Cracking Studies of 10-, 12-, and 18-Percent Ni Maraging Steel Alloys in Seawater*, MEL Report No. 73/66, Naval Marine Engineering Laboratory, Annapolis, Md., Mar. 1966, AD 809021.
44. G. A. Wacker, *Effects of Marine Environment on High Strength Steels*, ASTM STP 445, 1969, p. 68.
45. A. F. Hoenie, J. A. Lumm, R. J. Shelton, and R. A. Wallace, *Determination of Mechanical Projecting Design Values for 18 Ni Co Mo 250 and 300 Grade Maraging Steels*, Technical Report AFML-TR-65-197, North American Aviation, Inc., July 1965, AD 470742.
46. J. E. Truman and R. Perry, "The Resistance to Stress-Corrosion Cracking of Maraging and Other High Strength Steels," *Iron Steel*, 37 (No. 13), 574 (Dec. 1964).
47. E. Trabocco, *Evaluation of 18Ni-Co-Mo Maraging Steel*, Report No. NAEC-AML-2102, Naval Air Engineering Center, Aeronautical Materials Laboratory, Jan. 12, 1965, RRMA 02 018/200 1/R007 05 01, AD 456201.
48. R. B. Setterlund, "Stress-Corrosion Cracking of Maraging Steel," *Mater. Protect.*, 4 (No. 12), 27-29 (1965).
49. R. B. Setterlund, *Investigation of Stress-Corrosion Cracking of High-Strength Steels*, Aerojet-General Corp. report for May 1964, contract DA-04-495-ORD-3069, AD 602023.
50. W. S. Crownover and J. W. Wright, *Stress-Corrosion Susceptibility of 18-Percent Ni Maraging Steels at High Strength Levels*, Report No. RK-TR-66-11, July 1966, U.S. Army Missile Command, Redstone Arsenal, Arsenal, Ala., AD 800104.
51. P. Kalofonos, "Stress Corrosion Cracking in Almar 362 Mar-Aging Stainless Steel," M.S. Thesis, Georgia Institute of Technology, 1968.

52. A. M. Hall, "The Status of Ultrahigh Strength Steels Today," *Metal Progr.* 88 (No. 2), 178 (Aug. 1965).
53. A. M. Hall, "Fabricating the Ultrahigh Strength Steels," *Metal Progr.* 92, 91 (Sept. 1965).
54. A. M. Hall and C. J. Slunder, *The Metallurgy, Behavior and Application of the 18-Percent Nickel Maraging Steels (A Survey)*, NASA SP-5051, 1968.
55. A. M. Hall, "Bringing the Ultrahigh Strength Steels Up to Date," *Metal Progr.* **96** (No. 2), 103 (Aug. 1969).
56. *Metallurgical Developments in High-Alloy Steels*, Special Report 86, The Iron and Steel Institute, London, 1964.
57. J. Nutting, "The Physical Metallurgy of Alloy Steels," *J. Iron Steel Inst.* **207**, 872 (June 1969).
58. Symposium papers, entire issue of *Metals Eng. Quart.* **9** (No. 1) (Feb. 1969).
59. E. H. Phelps, "Stress-Corrosion Behavior of High Yield-Strength Steels," vol. 9, Proceedings Seventh World Petroleum Congress, Mexico, 1967, Elsevier Publishing Co. Ltd., pp. 201, 261, 262.
60. J. H. Mulherin, "Stress-Corrosion Susceptibility of High-Strength Steel in Relation to Fracture Toughness," *Trans. ASME J. Basic Eng.* 88, Series D, 777 (Dec. 1966).
61. W. D. Benjamin and E. A. Steigerwald, *Stress-Corrosion Cracking Mechanisms in Martensitic High Strength Steels*, Tech. Report AFML-TR-67-98, Air Force Materials Laboratory, Apr. 1967, AD 813716.
62. W. D. Benjamin, *Stress-Corrosion Cracking Mechanisms in Martensitic High Strength Steels*, 7th Quarterly Progress Report, Contract AF 33(615)-3651, TRW Equipment Laboratories, Inc., Report No. ER-6877-7, Jan. 15, 1968.
63. W. D. Benjamin and E. A. Steigerwald, *Environmentally Induced Delayed Fractures in Martensitic High-Strength Steels*, Technical Report AFML-TR-68-80, Air Force Materials Laboratory, Apr. 1968, AD 832650.
64. V. J. Colangelo and M. S. Ferguson, "The Role of the Strain Hardening Exponent in Stress-Corrosion Cracking of a High Strength Steel," *Corrosion* **25** (No. 12), 509 (Dec. 1969).
65. E. Snape, "Stress-Induced Failue of High-Strength Steels in Environments Containing Hydrogen Sulphide," *Br. Corrosion J.* **4** (No. 5), 253 (Sept. 1969).
66. C. S. Carter, "The Effect of Heat Treatment on the Fracture Toughness and Subcritical Crack Growth Characteristics of a 350-Grade Maraging Steel," Boeing Document D6-22978, June 1969; *Met. Trans.* **1** (No. 6), 1551 (June 1970).
67. C. S. Carter, "The Effect of Silicon on the Stress-Corrosion Resistance of Low Alloy High Strength Steels," *Corrosion* **25** (No. 10), 423 (Oct. 1969).
68. A. R. Fletcher, "Evaluation of $K_{Iscc}$ Stress Corrosion Susceptibility for Thick Sections of Several High Strength High Strength Steels," *Navy Mater. Bull.* **II** (No. 3), 3 (Oct. 1968).

69. M. H. Peterson, B. F. Brown, R. L. Newbegin, and R. E. Groover, "Stress Corrosion Cracking of High Strength Steels and Titanium Alloys in Chloride Solutions at Ambient Temperature," *Corrosion* **23** (No. 5), 142 (May 1967).
70. B. F. Brown, "A New Stress-Corrosion Cracking Test Procedure for High-Strength Alloys," *Mater. Res. Stand.* **6** (No. 6), 129 (1966).
71. G. Sandoz, "The Resistance of Some High Strength Steels to Slow Crack Growth in Salt Water," presented at ASTM Fall Meeting in Atlanta, Sept. 1968. To be published.
72. R. W. Judy and R. J. Goode, "Procedures for Stress-Corrosion Cracking Characterization and Interpretation to Failure-Safe Design for High-Strength Steels," presented at NACE Conference, Philadelphia, Pa., Mar. 2-6, 1970.
73. R. P. M. Procter and H. W. Paxton, "The Effect of Prior-Austenite Grain-Size on the Stress-Corrosion Susceptibility of AISI 4340 Steel," *ASM Trans. Quart.* **62** (No. 4), 989 (Dec. 1969).
74. C. D. Beachem and B. F. Brown, "A Comparison of Three Precracked Specimens for Evaluating the Susceptibility of High-Strength Steel to Stress Corrosion Cracking," *Stress Corrosion Testing*, ASTM STP 425, Amer. Soc. Testing Mater., Philadelphia, Pa., 1967, p. 31.
75. C. S. Carter, "Stress Corrosion Crack Branching in High-Strength Steels," Boeing Document D6-23871, The Boeing Company, Seattle, Wash., Mar. 1969.
76. N. Taniguchi and A. R. Troiano, "Stress Corrosion Cracking of 4340 Steel in Different Environments," *Trans. Iron Steel Inst. Japan*, **9** (No. 4), 306 (1969).
77. A. H. Rosenstein and M. R. Gross, *Properties of HY-130, 5Ni-Cr-Mo-V Steel: A Summary Report*, Report 2448, Naval Ships Research and Development Center, Annapolis, Md., Sept. 1967, AD 821456.
78. L. P. Connor, L. F. Porter, and S. T. Rolfe, *Third Progress Report: Extended Investigation of HY 130/150 Weldments*, U.S. Steel Corp., Monroeville, Pa., Jan 1, 1968, AD 825331.
79. S. R. Novak, *Effect of Plastic Strain on the $K_{Iscc}$ of HY-80, HY-130(T), and 12Ni-5Cr-3Mo Steels*, U.S. Steel Corp., Monroeville, Pa., Jan. 1, 1968, AD 825336L.
80. H. P. Leckie and A. W. Loginow, "Stress Corrosion Behavior of High Strength Steels," *Corrosion* **24** (No. 9), 291 (Sept. 1968).
81. J. H. Gross, "The New Development of Steel Weldments," 1968 Adams Lecture, *Welding J.* **47**, 241s (June 1968).
82. L. P. Connor, L. F. Porter, and S. T. Rolfe, *Second Progress Report Extended Investigation of HY-130/150 Weldments*, U.S. Steel Corp., Monroeville, Pa., Aug. 1, 1967.
83. J. H. Smith and S. T. Rolfe, *Effects of Welding Position and Process on the $K_{Iscc}$ of HY-130(T) Weld Metals*, U.S. Steel Corp., Monroeville, Pa., Jan. 1, 1968, AD 825330.

84. J. H. Smith and S. T. Rolfe, *Effect of Notch Orientation on $K_{Iscc}$ of Weld Metal*, U.S. Steel Corp., Monroeville, Pa., Dec. 29, 1967, AD 825328.
85. S. R. Novak and S. T. Rolfe, *Fatigue-Cracked Cantilever Beam Stress-Corrosion Tests of HY-80 and 5Ni-Cr-Mo-V Weldments*, U.S. Steel Corp., Monroeville, Pa., Jan 1, 1966, AD 482783.
86. J. H. Smith and S. T. Rolfe, *$K_{Iscc}$ Behavior of Weld Metals Used in Fabrication of an HY-130(T) Steel Structure*, U.S. Steel Corp., Monroeville, Pa., Jan. 1, 1968, AD 854657L.
87. G. M. Sinclair and S. T. Rolfe, *Analytical Procedure for Relating Subcritical Crack Growth to Inspection Requirements*, U.S. Steel Corp., Monroeville, Pa., Jan. 2, 1969, AD 846116L.
88. H. E. Romine and H. L. Smith, "$K_{Iscc}$ Stress-Corrosion Tests of HY-140 Welds for DSRV 2," NRL Memo Report 1923, Naval Research Laboratory, Washington, D.C., Sept. 1968.
89. L. P. Connor, L. F. Porter, and S. T. Rolfe, *Fourth Progress Report: Extended Investigation of HY 130/150 Weldments*, U.S. Steel Corp., Monroeville, Pa., July 1, 1968, AD 835687.
90. L. P. Connor, L. F. Porter, and S. T. Rolfe, *Fifth Progress Report: Extended Investigation of HY 130/150 Weldments*, U.S. Steel Corp., Monroeville, Pa., Jan. 2, 1969, AD 846122.
91. J. H. Smith and S. T. Rolfe, *Effect of Composition on the $K_{Iscc}$ of Experimental HY-150 Steels*, U.S. Steel Corp., Monroeville, Pa., Dec. 20, 1968, AD 846121.
92. C. S. Carter, "Crack Extension in Several High-Strength Steels Loaded in 3.5% Sodium Chloride Solution," Boeing Document D6-19770, The Boeing Company, Seattle, Wash., Nov. 1967, AD 685377.
93. C. N. Ahlquist, "The Influence of Ausforming on the Stress-Corrosion Susceptibility of Some High Strength Steels," *Metals Eng. Quart.* 8 (No. 4), 52 (Nov. 1968).
94. D. S. Dabkowski, P. J. Konkol, S. R. Novak, and L. F. Porter, *Evaluation of the HP 9-4-20 Steel Weldment System*, U.S. Steel Corp., Monroeville, Pa., Jan. 2, 1969, AD 846119L.
95. L. P. Connor, L. F. Porter, and S. T. Rolfe, *Fifth Progress Report: Development of an HY 180/210 Weldment*, U.S. Steel Corp., Monroeville, Pa., Jan. 2, 1969, AD 846120.
96. B. F. Brown, "Interpreting Laboratory Stress-Corrosion Cracking Data in Materials Selection," Paper 69-MET-10, ASME Metals Engineering Division and Pressure Vessels and Piping Division Conference, Washinton, D.C., Mar. 31-Apr. 2, 1969.
97. W. G. Clark and F. T. Wessel, "Influence of a Synthetic Seawater Environment on the Fracture Behavior of HP 9-4-25 and HP 9-4-20 Alloy Steels," *Symposium on Materials Performance and the Deep Sea*, ASTM STP 445, Amer. Soc. Testing Mater., Philadelphia, Pa., 1969, p. 93.

98. R. D. Large, S. A. Kulin, and B. S. Lement, *Slow Crack Growth in Gun Tubes*, final report, Contract No. PA-30-144-AMC-1639(W), to Watervliet Arsenal, Materials Research and Development ManLabs, Inc., Aug. 1967, AD 682712.
99. S. R. Novak and S. T. Rolfe, *$K_{Iscc}$ Tests of HY 180/210 Steels and Weldments*, U.S. Steel Corp., Monroeville, Pa., Aug. 1, 1967.
100. G. J. Biefer and J. G. Garrison, "Stress-Corrosion Cracking Tests on Some High-Strength Steels Using the U.S.N. Cantilever Method," Internal Report PM-R-67-8, Physical Metallurgy Division, Dept. of Energy, Mines and Resources, Mines Branch, Ottawa, Canada, Mar. 14, 1967.
101. R. T. Ault, Republic Steel Corp., private communication.
102. S. R. Novak and S. T. Rolfe, *$K_{Ic}$ Stress-Corrosion Tests of 12Ni-5Cr-3Mo and 18Ni-8Co-3Mo Maraging Steels and Weldments*, U.S. Steel Corp., Monroeville, Pa., Jan. 1, 1966, AD 482761L.
103. F. R. Stonesifer and H. L. Smith, *Characterization of TIG Welds in 12-5-3 Maraging Steel Plate with Application of a New Scaling Method for $K_{Ic}$ Plasticity Corrections*, NRL Report 7053, Naval Research Laboratory, Washington, D.C., Apr. 16, 1970.
104. E. H. Phelps, "A Review of the Stress Corrosion Behavior of Steels with High Yield Strength," *Proceedings of Conference on Fundamental Aspects of Stress Corrosion Cracking*, Nat. Assoc. Corrosion Eng., Houston, Texas, 1969, p. 398.
105. E. A. Steigerwald and G. L. Hanna, "Initiation of Slow Crack Propagation in High-Strength Materials," *Proc. ASTM*, **62**, 885-905 (1962).
106. C. S. Carter, "The Tensile, Fracture Toughness, and Stress Corrosion Properties of Vacuum Melted (300) Maraging Steel," Boeing Document D6-23888, Apr. 1969.
107. C. S. Carter, "Evaluation of High Purity 18Ni (300) Maraging Steel Forgings–First Technical Management Report," Boeing Document D6-24393-1, Contract F33615-69-C-1620, Aug. 1969.
108. C. S. Carter, "Evaluation of High Purity 18Ni (300) Maraging Steel Forgings–Third Technical Management Report," Boeing Document D6-24393-3, Contract F33615-69-C1620, Feb. 1970.
109. F. R. Stonesifer, H. L. Smith, and H. E. Romine, "Evaluation of Three Materials as Candidates for Lift-Pad Studs in an Ocean Environment," NRL Memo Report 2068, Naval Research Laboratory, Washington, D.C., Nov. 1969.
110. C. D. Beachem and T. C. Lupton, "The Effects of Three Aqueous Environments on High Stress Low-Cycle Fatigue of 18% Nickel Maraging Steels," NRL Memo Report 1685, Naval Research Laboratory, Washington, D.C., Feb. 1966.
111. A. J. Stavros and H. W. Paxton, "Stress-Corrosion Cracking Behavior of an 18% Ni Maraging Steel," *Met. Trans.* 1, 3049 (1970).

112. R. P. M. Proctor and H. W. Paxton, "The Effect of Trace Impurities on the Stress-Corrosion Cracking Susceptibility and Fracture Toughness of 18 Ni (300 Grade) Maraging Steel," Carnegie-Mellon University (to be published).
113. G. Sandoz and R. L. Newbegin, "Stress-Corrosion Cracking Resistance of an 18Ni 200 Grade Maraging Steel Base Plate and Weld," NRL Memo Report 1772, Naval Research Laboratory, Washington, D.C., Mar. 1967.
114. C. S. Carter, *Evaluation of a High-Purity 18% Ni (300) Maraging Steel Forging*, Technical Report AFML-TR-70-139, The Boeing Company, June 1970.
115. C. S. Carter D. E. Austin, and J. C. McMillan, "Fracture Toughness and Stress-Corrosion Characteristics of a High Strength Maraging Steel," Boeing Document D6-25459, Aug. 1970.
116. L. P. Connor, L. F. Porter, and S. T. Rolfe, *Fourth Progress Report: Development of an HY 180/210 Weldment*, U.S. Steel Corp., Monroeville, Pa., July 1, 1968, AD 835686.
117. L. P. Connor, L. F. Porter, and S. T. Rolfe, *Extended Investigation of HY 130/150 Weldments*, Progress Report No. 3, Contract NObs-9435, U.S. Steel Corp., Monroeville, Pa., Jan. 1968, AD 825331L.
118. J. A. Davis and W. D. Henry, *The Influence of Applied Potential on Crack Growth Rates of 10Ni-2Cr-1Mo-8Co Steel in 3.5 percent Sodium Chloride*, U.S. Steel Corp., Monroeville, Pa., Jan. 26, 1970.
119. F. R. Stonesifer and H. L. Smith, "Properties of Hot Pressed 10Ni-Cr-Mo-Co Steel," NRL Memo Report 2065, Naval Research Laboratory, Washington, D.C., Nov. 1969.
120. P. W. Holsberg, *Corrosion Studies of 10Ni-2Cr-1Mo-8Co Steels*, Report 8-438, Naval Ship Research and Development Center, Annapolis, Md., Mar. 1970, AD 867332.
121. C. S. Carter, D. G. Farwick, A. M. Ross, and J. M. Uchida, "Stress Corrosion Properties of High-Strength Precipitation-Hardening Stainless Steels in 3.5% Aqueous Sodium Chloride Solution," Boeing Document D6-25219, The Boeing Company, Seattle, Wash., Feb. 1970.
122. D. Webster, "The Use of Deformation Voids to Refine The Austenitic Grain Size and Improve the Mechanical Properties of AFC 77," Boeing Document D6-23870, The Boeing Company, Seattle, Wash., Feb. 1969, AD 687724.
123. D. Webster, "The Stress Corrosion Resistance and Fatigue Crack Growth Rate of a High Strength Martensitic Stainless Steel, AFC 77," Boeing Document D6-23973, The Boeing Co., Seattle, Wash., June 1969, AD 695794.
124. J. W. Kennedy and J. A. Whittaker, "Stress-Corrosion Cracking of High-Strength Steels," *Corrosion Sci.* 8 (No. 6), 359 (June 1968).

125. N. A. Tiner and C. B. Gilpin, "Microprocesses in Stress Corrosion of Martensitic Steels," *Corrosion* 22, 271 (Oct. 1966).
126. G. Sandoz, "The Effects of Alloying Elements on the Susceptibility to Stress-Corrosion Cracking of Martensitic Steels in Salt Water," *Met. Trans.* 2, 1055 (1971).
127. R. T. Ault, *Development of An Improved Ultra High Strength Steel for Forged Aircraft Components*, Republic Steel Report TR-12000-2, Project 12000, Nov. 1969, Second Quart. Progress Report, 1 Aug-31 Oct 1969 for Air Force Materials Laboratory, Wright Patterson AFB, Ohio.
128. R. T. Ault, Republic Steel Corp. private communication.
129. M. H. Peterson, T. J. Lennox, and R. E. Groover, "A Study of Crevice Corrosion in Type 304 Stainless Steel," *Mater. Protect.* 9 (No. 1), 23 (1970).
130. C. J. Slunder and W. K. Boyd, "Environmental and Metallurgical Factors of Stress-Corrosion Cracking in High Strength Steels," DMIC Report 151, Defense Metals Information Center, Battelle Mem. Inst., Apr. 14, 1961.
131. E. Snape, "The Role of Composition and Microstructure in Sulfide Cracking of Steel," *Corrosion* 24 (No. 9), 261 (Sept. 1968).
132. B. Wilde, U.S. Steel Corp., private communication.
133. H. P. Leckie, "Effects of Environments on Stress Induced Failure of High Strength Maraging Steels," *Proceedings of Conference on Fundamental Aspects of Stress Corrosion Cracking*, NACE, Houston, Texas, 1969, p. 411.
134. D. Webster, "Effect of Grain Refinement on the Microstructure and Properties of 4340 M Steel," Boeing Document D6-25220, The Boeing Company, Seattle, Wash., Apr. 1970.
135. D. Kalish and S. A. Kulin, *Coupling of Ultrahigh Strength and Fracture Toughness in Steels by Means of Thermomechanical Processes*, Technical Report AFML-TR-68-96, Air Force Materials Laboratory, Wright-Patterson AFB, Ohio, Mar. 1968.
136. R. T. Ault, K. O. McDowell, P. L. Hendricks, and T. M. F. Ronald, "Increased Reliability of a High-Strength Steel Through Thermal-Mechanical Treatments," *ASM Trans. Quart.* 60 (No. 1), 79-87 (Mar. 1967).
137. K. R. Agricola and J. T. Snyder, "Stress Corrosion of Explosively Deformed High-Strength Alloys," *Metals Eng. Quart.* 7 (No. 3), 59 (1967).
138. P. N. Orava and H. E. Otto, "The Effect of High Energy Rate Forming on the Terminal Characteristics of Metal A Review," *J. Metals* 22, 17 (Feb. 1970).
139. D. Webster, "Stainless Steel can be Strong and Tough," Boeing Document D6-24379, The Boeing Company, Seattle, Wash.
140. B. F. Brown, "The Role of the Occluded Corrosion Cell in Stress-Corrosion Cracking of High Strength Steels," *Rapports Techniques*, 112, RT170, 1-3 (Jan. 1970).

141. G. J. Biefer, "Environmental Cracking Susceptibility of High Strength Steels," *Mater. Protect.* 7, 23 (Nov. 1968).
142. H. L. Logan, "The Stress-Corrosion Cracking of Metals," *Metals Eng. Quart.* 5 (No. 2), 32 (May 1965).
143. W. A. Van Der Sluys, "Mechanisms of Environment Induced Subcritical Flaw Growth in AISI 4340 Steel," *Eng. Fracture Mech.* 1, 447 (1969).
144. A. H. Priest, "Stress Corrosion Testing of High Strength Steels Using Precracked Specimens," *Metals Mater.* 3, 175 (May 1969).
145. G. Sandoz, C. T. Fujii, and B. F. Brown, "Solution Chemistry Within Stress-Corrosion Cracks in Alloy Steels," *Corrosion Sci.* 10, 839-845, (1970).
146. B. F. Brown, C. T. Fujii, and E. P. Dahlberg, "Methods for Studying the Solution Chemistry Within Stress Corrosion Cracks," *J. Electrochem. Soc.* 116 (No. 2), 218 (Feb. 1969).
147. J. A. Smith, M. H. Peterson, and B. F. Brown, "Electrochemical Conditions at the Tip of an Advancing Stress-Corrosion Crack in AISI 4340 Steel," *Corrosion* 26 (No. 12), 539 (Dec. 1970).
148. E. N. Pugh and A. R. C. Westwood, "Critical Species in Stress Corrosion Phenomena," *Stress Corrosion Testing*, ASTM STP-425, Amer. Soc. Testing Mater., Philadelphia, Pa., 1967, p. 228.
149. A. Gallaccio and M. A. Pelensky, "Stress Corrosion of High Strength Steel Alloys–Environmental Factors," *Stress Corrosion Testing*, ASTM STP-425, Amer. Soc. Testing Mater., Philadelphia, Pa., 1967, p. 99.
150. H. J. Logan, *The Stress Corrosion of Metals*, John Wiley, New York, 1966.
151. M. E. Holmberg and T. V. Bruno, "Metallurgy and the Corrosion Engineer: What He Should Know," *Mater. Protect.* 5 (No. 5), 8 (1966).
152. E. E. Denhard, "Stress-Corrosion Cracking of High Strength Stainless Steels," AGARD Conference Proceedings No. 18, 24th Meeting, Turin, Italy, Apr. 17-20, 1967.
153. E. E. Fletcher, W. E. Berry, and A. R. Elsea, "Stress-Corrosion Cracking and Hydrogen-Stress Cracking of High Strength Steel," DMIC Report 232, Battelle Mem. Inst., July 29, 1966.
154. H. H. Uhlig, "An Evaluation of Stress-Corrosion Cracking Mechanisms," *Proceedings of Conference on Fundamental Aspects of Stress Corrosion Cracking*, Nat. Assoc. Corrosion Eng., Houston, Texas, 1969, p. 86.
155. W. Rostocker, J. M. McCaughey, and H. Markus, *Embrittlement by Liquid Metals*, Reinhold, New York, 1960.
156. G. Sandoz and R. L. Newbegin, "A Comparison of Laboratory Salt Water and Flowing Natural Seawater as an Environment for Tests of Stress-Corrosion Cracking Susceptibility," *Report of NRL Progress*, Naval Research Laboratory, Washington, D.C., May 1969, p. 29.
157. G. L. Hanna and E. A. Steigerwald, *Influence of Environment on Crack Propagation and Delayed Failures in High-Strength Steels*, Technical Document Report No. RTD-TDR-63-4225, Contract AF 33(657)-7512, by Thompson Ramo Wooldridge, Inc., Jan. 1964, AD 433286.

158. G. Sandoz, "Subcritical Crack Propagation in Ti-8Al-1Mo-1V Alloy in Organic Environments, Salt Water, and Inert Environments," *Proceedings of Conference on Fundamental Aspects of Stress Corrosion Cracking*, (R. W. Staehle et al., eds.), Nat. Assoc. Corrosion Eng., Houston, Texas, 1969, p. 684.
159. R. P. M. Proctor and H. W. Paxton, "Stress-Corrosion of the Aluminum Alloy 7075-T651 in Organic Liquids," ASTM *J. Mater.* **4**, 729 (1969).
160. C. R. Singleterry and H. R. Baker, Naval Research Laboratory, Washington, D.C., private communications.
161. S. Goldberg, *Corrosion Protection of High Strength Steels*, DMIC Report 210, Battelle Mem. Inst., Oct. 26, 1964.
162. H. W. Paxton and R. P. M. Proctor, "The Effects of Machining and Grinding on the Stress-Corrosion Cracking Susceptibility of Metals and Alloys," TP EM68-520, Amer. Soc. Tool Mfg. Eng., Jan. 1968.
163. W. L. Williams, "Stress-Corrosion Cracking: A Review of Current Status," *Corrosion* **17** (No. 7), 92 (July 1961).
164. B. F. Brown, *Stress-Corrosion Cracking and Related Phenomena in High-Strength Steels: A Review of the Problem, with an Annotated Bibliography*, NRL Report 6041, Naval Research Laboratory, Washington, D.C., Nov. 6, 1963.
165. R. W. Staehle, "Montage of Processes Operating During Stress Corrosion Cracking," *Corrosion*, **23** (No. 7), 202 (July 1967).
166. M. C. Huffstutler, "Fundamental Considerations of Stress Corrosion," *Corrosion*, **19** (No. 12), 423t (Dec. 1963).
167. T. P. Hoar, "Stress-Corrosion Cracking," *Corrosion* **19** (No. 10), 331t (Oct. 1963).
168. J. F. Bates and A. W. Loginow, "Principles of Stress-Corrosion Cracking as Related to Steels," *Corrosion* **20** (No. 1), 189t (1964).
169. H. J. Leidheiser, "Corrosion," *Chem. Eng. News*, Apr. 5, 1965, p. 78.
170. T. P. Hoar, "Stress-Corrosion Cracking," Symposium on the Coupling of Basic and Applied Research, Nat. Assoc. Corrosion Eng., Houston, Texas, 1969, p. 53.
171. J. E. Truman, R. Perry, and G. D. Peaker, "The Nature of Stress-Corrosion Crack Initiation with Martensitic Stainless Steels," *Br. Corrosion J.* **1**, 360 (Nov. 1966).
172. E. N. Pugh, J. A. S. Green, and A. J. Sedriks, *Current Understanding of Stress Corrosion Phenomena*, Technical Report 69-3, Research Institute for Advanced Studies, Martin Marietta Corp., Mar. 1969.
173. R. W. Staehle, "Comments on the History, Engineering and Science of Stress Corrosion Cracking," *Proceedings of Conference on Fundamental Aspects of Stress Corrosion Cracking*, NACE, Houston, Texas, 1969, p. 3.
174. C. F. Barth, E. A. Steigerwald, and A. R. Troiano, "Hydrogen Permeability and Delayed Failure of Polarized Martensitic Steels," *Corrosion* **25** (No. 9), 353 (Sept. 1969).

175. J. C. Scully, "Fracture Mechanics and Stress Corrosion," *Metals Mater.* 3 (No. 5), 174 (May 1969).
176. J. C. Scully, "The Mechanical Parameters of Stress-Corrosion Cracking," *Corrosion Sci.* 8 (No. 10), 759 (Oct. 1968).
177. W. A. Van Der Sluys, *Environmental Cracking in AISI 4340 Steel*, T&AM Report 312, final report, Contract ARO-D-31-124-G872, Dept. of Theoretical and Applied Mechanics, University of Illinois, 1967.
178. H. H. Johnson, "On Hydrogen Brittleness in High Strength Steels," *Proceedings of Conference on Fundamental Aspects of Stress Corrosion Cracking*, (R. W. Staehle et al., eds.), Nat. Assoc. Corrosion Eng., Houston, Texas, 1969, p. 439.
179. W. W. Gerberich and C. E. Hartbower, "Monitoring Crack Growth of Hydrogen Embrittlement and Stress-Corrosion Cracking by Acoustic Emission," *Proceedings of Conference on Fundamental Aspects of Stress Corrosion Cracking* (R. W. Staehle et al., eds.) Nat. Assoc. Corrosion Eng., Houston, Texas, 1969, p. 420.
180. D. A. Vaughn and D. I. Phalen, "Reactions Contributing to the Formation of Susceptible Paths for Stress-Corrosion Cracking," *Stress Corrosion Testing*, ASTM STP-425, Amer. Soc. Testing Mater., Philadelphia, Pa., 1967, p. 209.
181. W. D. Benjamin and E. A. Steigerwald, "An Incubation Time for the Initiation of Stress-Corrosion Cracking in Precracked 4340 Steel," *Trans. ASM* **60**, 547 (1967).

# Chapter 4

# HIGH STRENGTH ALUMINUM ALLOYS

**M. V. Hyatt and M. O. Speidel**
*The Boeing Company*

**CONTENTS**





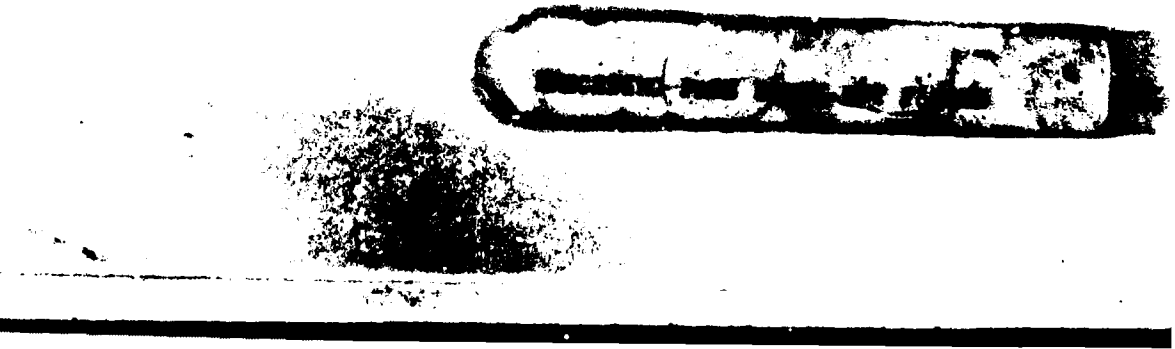

# 4. HIGH STRENGTH ALUMINUM ALLOYS

## 4.1 Introduction

This chapter is a state-of-the-art review of the engineering aspects of stress corrosion cracking of high strength aluminum alloys. It is primarily written for the practicing engineer, and contains published and unpublished information available up through May 1970. An attempt is made to achieve a balance between the newer experimental results obtained using the linear elastic fracture mechanics approach and the results of the traditional smooth specimen time-to-failure tests. The mechanical, environmental, and metallurgical parameters which influence stress-corrosion crack growth are reported in detail, and are discussed in terms of the available quantitative stress corrosion theories.

Special sections are devoted to modern alloy development and prevention of stress corrosion failures in aerospace and other structures. The somewhat related topics of exfoliation and intergranular corrosion are treated briefly.

High strength aluminum alloys are of considerable importance in our technologically advanced society. Perhaps the best-known applications are for rockets, spacecraft, aircraft and hydrospace vehicles. Table 1 lists the chemical compositions for the commonly used high strength aluminum-base alloys. Mechanical properties of the alloys are listed in Table 2. (Data in Tables 1 and 2 were obtained from Refs. 1 through 48.) The highest strength aluminum alloys are those based on the Al-Cu-Mg (2000 series) and Al-Zn-Mg-Cu (7000 series) alloy systems. Since these alloys are the most widely used for today's high performance structures, this chapter will concentrate on them.

In their service environment, many of the high strength aluminum alloys can, under specific conditions, fail at stresses far below the yield strength due to SCC. The large potential losses in load-carrying capability due to SCC can be appreciated by noting the low SCC threshold stresses in many of the alloys in Table 2. Since such cracking often occurs below gross yielding, it is appropriate to use linear elastic fracture mechanics analysis.

The main purpose of this chapter is to present and review the engineering aspects of the wealth of knowledge accumulated to date about stress corrosion cracking of high strength aluminum alloys. The fracture mechanics approach has, in the past few years, allowed us to design quantitative stress corrosion tests [50, 51] and to compare environmental and metallurgical effects on a quantitative basis, as will be shown in the following sections. Before such modern testing techniques had been developed, the conventional and more qualitative time-to-



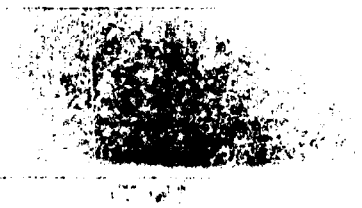

failure (TTF) tests had been used [52] for almost half a century to assess the susceptibility to stress corrosion of high strength aluminum alloys. Smooth specimens are also used to determine a threshold stress ($\sigma_{scc}$) below which stress corrosion cracking is not observed within a given time (Ref. 42). Using this technique, metallurgists have been remarkably successful in developing aluminum alloys that combine high strength and resistance to SCC, and a number of reviews have been published that adequately cover what smooth specimen testing has contributed to our understanding of SCC high strength aluminum alloys [53-55]. Today, however, quantitative SCC data are equally needed for alloy development, fundamental studies of SCC, and advanced design. Already, quantitative SCC data based on fracture mechanics analysis are used for the design of pressure vessels in the aerospace industry, and efforts are under way to introduce the same concepts to other designs as well.

In the following sections, the authors will describe the conditions under which SCC failures can occur. It is the authors' hope that metallurgists and engineers can use the information presented here to further develop and safely use the high strength aluminum alloys.

## 4.2 Mechanical Aspects (Effects of Stress)

Techniques for stress corrosion testing are discussed in Chapter 2 of this monograph. In the present chapter, we will discuss only those aspects of stress corrosion testing that are peculiar to the high-strength commercial aluminum alloys by virtue of the pronounced effect of grain shape and orientation on the stress-corrosion performance of these alloys.

### Grain Shape and Orientation

Since SCC in aluminum alloys is almost always intergranular, the stress corrosion performance of these alloys is strongly related to the local grain shape and orientation with respect to the applied stresses. The grain orientations in the standard wrought forms are indicated schematically in Fig. 1. For hand and die forgings, grain shape and orientation can vary widely throughout the part, and cross sectioning is required to determine local grain shape and orientation. Grain flow in a typical die forging is illustrated in Fig. 2, which shows a cross section perpendicular to the parting plane.

Because it is important to relate stressing direction and grain flow directions in aluminum alloys, two systems have been devised to relate these two parameters. In one system, used primarily for testing smooth specimens, the three stressing directions are designated simply by denoting whether the stress is parallel to the longitudinal (L), long transverse (LT), transverse (T), or short transverse (ST) directions as defined in Fig. 3.

**Table 1.** Chemical Composition Limits of Commercial Aluminum Alloys

| *Alloy* | *Zinc*[a] | *Magnesium* | *Copper* | *Iron* | *Silicon* | *Manganese* | *Chromium* | *Titanium* | *Others* | |
|---|---|---|---|---|---|---|---|---|---|---|
| | | | | | | | | | *Each* | *Total* |
| 2014 | 0.25 | 0.20-0.8 | 3.9-5.0 | 0.7 | 0.50-1.2 | 0.40-1.2 | 0.10 | 0.15 | 0.05 | 0.15 |
| X2020 | 0.25 | 0.03 | 4.0-5.0 | 0.4 | 0.40 | 0.30-0.8 | – | 0.10 | 0.05[b] | 0.15 |
| 2021 | 0.10 | 0.02 | 5.8-6.8 | 0.3 | 0.20 | 0.20-0.40 | – | 0.20-0.10 | 0.05[c] | 0.15 |
| 2024 | 0.25 | 1.2-1.8 | 3.8-4.9 | 0.50 | 0.50 | 0.30-0.9 | 0.10 | – | 0.05 | 0.15 |
| 2124 | 0.25 | 1.2-1.8 | 3.8-4.9 | 0.30 | 0.20 | 0.30-0.9 | 0.10 | – | 0.05 | 0.15 |
| 2219 | 0.10 | 0.02 | 5.8-6.8 | 0.30 | 0.20 | 0.20-0.40 | – | 0.02-0.10 | 0.05[d] | 0.15 |
| 2618 | – | 1.3-1.8 | 1.9-2.7 | 0.9-1.3 | 0.25 | – | – | 0.04-0.10 | 0.05[e] | 0.15 |
| 5052 | 0.10 | 2.2-2.8 | 0.10 | 0.45 Fe + Si | | 0.10 | 0.15-0.35 | – | 0.05 | 0.15 |
| 5083 | 0.25 | 4.0-4.9 | 0.10 | 0.40 | 0.40 | 0.30-1.0 | 0.05-0.25 | 0.15 | 0.05 | 0.15 |
| 5086 | 0.25 | 3.5-4.5 | 0.10 | 0.50 | 0.40 | 0.20-0.7 | 0.05-0.25 | 0.15 | 0.05 | 0.15 |
| X5090 | 0.20 | 6.0-8.0 | 0.25 | 0.50 | 0.50 | 0.35 | 0.05-0.30 | 0.15 | 0.05[f] | 0.15 |
| 5454 | 0.25 | 2.4-3.0 | 0.10 | 0.40 Fe + Si | | 0.50-1.0 | 0.05-0.20 | .20 | 0.05 | 0.15 |
| 5456 | 0.25 | 4.7-5.5 | 0.10 | 0.40 Fe + Si | | 0.50-1.0 | 0.05-0.20 | 0.20 | 0.05 | 0.15 |
| 6061 | 0.25 | 0.8-1.2 | 0.15-0.40 | 0.7 | 0.40-0.8 | 0.15 | 0.04-0.35 | 0.15 | 0.05 | 0.15 |
| 6066 | 0.25 | 0.8-1.4 | 0.7-1.2 | 0.50 | 0.9-1.8 | 0.6-1.1 | 0.40 | 0.20 | 0.05 | 0.15 |
| 6070 | 0.25 | 0.50-1.2 | 0.15-0.40 | 0.50 | 1.0-1.7 | 0.40-1.0 | 0.10 | 0.15 | 0.05 | 0.15 |
| 6151 | 0.25 | 0.45-0.8 | 0.35 | 1.0 | 0.6-1.2 | 0.20 | 0.15-0.35 | 0.15 | 0.05 | 0.15 |
| 7001 | 6.8-8.0 | 2.6-3.4 | 1.6-2.6 | 0.40 | 0.35 | 0.20 | 0.18-0.35 | 0.20 | 0.05 | 0.15 |
| 7005 | 4.0-5.0 | 1.0-1.8 | 0.10 | 0.40 | 0.35 | 0.20-0.70 | 0.06-0.20 | 0.01-0.06 | 0.05[g] | 0.15 |
| X7007 | 6.0-7.0 | 1.4-2.2 | 0.25 | 0.40 Fe + Si | | 0.40 | 0.05-0.25 | 0.01-0.06 | 0.05[h] | 0.15 |
| 7039 | 3.5-4.5 | 2.3-3.3 | 0.10 | 0.40 | 0.30 | 0.10-0.40 | 0.15-0.25 | 0.10 | 0.05 | 0.15 |
| 7049 | 7.2-8.2 | 2.0-2.9 | 1.2-1.9 | 0.35 | 0.25 | 0.20 | 0.10-0.22 | 0.10 | 0.05 | 0.15 |
| X7050 | 5.7-6.7 | 1.9-2.6 | 2.0-2.8 | 0.15 | 0.12 | 0.10 | 0.04 | 0.06 | 0.04[q] | 0.10 |
| 7075 | 5.1-6.1 | 2.1-2.9 | 1.2-2.0 | 0.50 | 0.40 | 0.30 | 0.18-0.35 | 0.20 | 0.05 | 0.15 |
| 7076 | 7.0-8.0 | 1.2-2.0 | 0.3-1.0 | 0.60 | 0.40 | 0.30-0.80 | – | 0.20 | 0.05 | 0.15 |
| AZ74 | 5.5-6.5 | 2.1-2.5 | 0.7-1.0 | 0.50 | 0.40 | 0.10 | 0.15-0.25 | 0.10 | 0.05[i] | 0.15 |
| 7079 | 3.8-4.8 | 2.9-3.7 | 0.40-0.8 | 0.40 | 0.30 | 0.10-0.30 | 0.10-0.25 | 0.10 | 0.05 | 0.15 |

| | | | | | | | | | | |
|---|---|---|---|---|---|---|---|---|---|---|
| X7080 | 5.0-7.0 | 1.5-3.0 | 0.50-1.50 | 0.40 | 0.30 | 0.10-0.70 | 0.25 | 0.20 | 0.05 | 0.15 |
| 7175 | 5.1-6.1 | 2.1-2.9 | 1.2-2.0 | 0.20 | 0.15 | 0.10 | 0.18-0.30 | 0.10 | 0.05 | 0.15 |
| 7178 | 6.3-7.3 | 2.4-3.1 | 1.6-2.4 | 0.50 | 0.40 | 0.30 | 0.18-0.35 | 0.20 | 0.05 | 0.15 |
| X7475 | 5.2-6.2 | 1.9-2.6 | 1.2-1.9 | 0.12 | 0.10 | 0.06 | 0.18-0.25 | 0.06 | 0.05 | 0.15 |
| Cladding alloys | | | | | | | | | | |
| 1230[j] | 0.10 | – | 0.10 | 0.7 Fe + Si | | 0.05 | – | – | 0.05 | – |
| 6003[k] | 0.20 | 0.8-1.5 | 0.10 | 0.6 | 0.35 1.0 | 0.08 | 0.35 | 0.10 | 0.05 | 0.15 |
| 7008[l] | 4.4-5.5 | 0.7-1.4 | 0.05 | 0.10 | 0.10 | 0.05 | 0.12-0.25 | 0.05 | 0.05 | 0.10 |
| 7011[m] | 4.0-5.5 | 1.0-1.6 | 0.05 | 0.20 | 0.15 | 0.10-0.30 | 0.05-0.20 | 0.05 | 0.05 | 0.15 |
| 7072[n] | 0.8-1.3 | 0.10 | 0.10 | 0.7 Fe + Si | | 0.10 | – | – | 0.05 | 0.15 |
| Welding wires | | | | | | | | | | |
| 2319 | 0.10 | 0.02 | 5.8-6.8 | 0.30 | 0.20 | 0.20-0.40 | – | 0.10-0.20 | 0.05[o] | 0.15 |
| 4043 | 0.10 | 0.05 | 0.30 | 0.8 | 4.5-6.0 | 0.05 | – | 0.20 | 0.05[p] | 0.15 |
| 4145 | 0.20 | 0.15 | 3.3-4.7 | 0.8 | 9.3-10.7 | 0.15 | 0.15 | – | 0.05 | 0.15 |
| 5039 | 2.4-3.2 | 3.3-4.3 | 0.03 | 0.40 | 0.10 | 0.30-0.50 | 0.10-0.20 | 0.10 | 0.05[p] | 0.10 |

[a]Composition in weight percent maximum unless shown as a range.
[b]X2020 contains cadmium 0.10-0.35, lithium 0.90-1.7.
[c]2021 contains zirconium 0.10-0.25, vanadium 0.05-0.15, cadmium 0.05-0.20, tin 0.03-0.08.
[d]2219 contains zirconium 0.10-0.25, vanadium 0.05-0.15.
[e]2618 contains nickel 0.9-1.2.
[f]X5090 contains beryllium 0.001-0.02, boron 0.001-0.050.
[g]7005 contains zirconium 0.06-0.20.
[h]X7007 contains zirconium 0.05-0.25.
[i]AZ74 contains silver 0.3-0.5.
[j]Cladding on alclad 2024.
[k]Cladding on alclad 2014.
[l]High-strength cladding for 7075 and 7178.
[m]High-strength cladding for 7075, 7079, and 7178.
[n]Cladding on alclad 2219, 6061, 7075, 7079 and 7178.
[o]2319 contains zirconium 0.10-0.25, vanadium 0.05-0.15, beryllium 0.0008 maximum.
[p]4043 and 5039 beryllium content for welding electrodes will be 0.008 maximum.
[q]X7050 contains zirconium 0.08-0.15.

**Table 2.** Mechanical, Fracture, and Stress Corrosion Properties for Plates of Several Aluminum Alloys

| Alloy and Temper | Thickness (in.) | Axis[b] of Test Spec | Minimum Tensile Strength | | Min Elong (% in 2 in or 4D) | Range in Plane-Strain Fracture Toughness $K_{Ic}$ | | | Estimated Stress Corrosion Threshold Stress | | |
|---|---|---|---|---|---|---|---|---|---|---|---|
| | | | Ultimate, ksi | 0.2% Yield, ksi | | Long, ksi $\sqrt{in}$ | Long Trans, ksi $\sqrt{in}$ | Short Trans, ksi $\sqrt{in}$ | Long ksi | Long Trans ksi | Short Trans ksi |
| **Plates** | | | | | | | | | | | |
| 2014-T451 | 0.500-1.000 | LT | 58 | 36 | 14 | ≈40 | ≈38 | 17-25 | | | |
| 2014-T651 | 0.500-1.000 | LT | 67 | 59 | 6 | 21-28 | 19-27 | 16-19 | 45 | 30 | 8 |
| X2020-T651 | 1.275 | LT | 75 | 70 | 1.5 | 18-23 | 15-21 | | >57 | >56 | 34 |
| 2021-T81 | 0.500-1.000 | LT | ≈67 | ≈59 | 3 | 26-37 | 21-34 | | >48 | >46 | 35 |
| 2024-T351 | 0.500-1.000 | LT | 63 | 42 | 8 | ≈45 | ≈40 | 20-26 | 35 | 20 | <8 |
| 2024-T62 | 0.500-3.000 | LT | 63 | 50 | 5 | 27 | 26 | | >50 | >50 | 43 |
| 2024-T851 | 0.500-1.000 | LT | 66 | 58 | 5 | 20-32 | 20-32 | 16-24 | >50 | >50 | 40 |
| 2024-T86 | 0.500 | LT | 70 | 64 | 4 | 22 | 21 | | | | |
| 2124-T851[d] | 1.001-1.449 | LT | 66 | 57 | 5 | 28 | 24 | 23 | >50 | >50 | 30 |
| 2219-T351 | 0.250-2.000 | LT | 46 | 28 | 10 | >40 | >40 | | | | |
| 2219-T37 | 0.040-2.000 | LT | 49 | 37 | 6 | ≈40 | ≈34 | 33 | | | <10 |
| 2219-T62 | 0.250-1.000 | LT | 54 | 36 | 8 | 50 | 36 | | >34 | | >32 |
| 2219-T87 | 0.250-1.000 | LT | 64 | 51 | 7 | 26-29 | 24-28 | 26-30 | >44 | | >41 |
| RR 58 | 0.250 | LT | ≈56 | ≈45 | ≈6 | 27-34 | 26 | | >44 | | >40 |
| 5083-H112 | 0.250-1.500 | L | 40 | 18 | 12 | ≈40 | ≈38 | | | | |
| 5083-H321 | 0.188-1.500 | L | 44 | 31 | 12 | ≈45 | ≈45 | | >25 | | >25 |
| 5456-H112 | 0.250-1.500 | L | 42 | 19 | 12 | ≈38 | ≈36 | | | | |
| 5456-H321 | 0.625-1.250 | L | 46 | 33 | 12 | ≈45 | ≈45 | 30-33 | | | |
| 6061-T651 | 0.500-1.000 | LT | 42 | 35 | 9 | ≈50 | ≈50 | 32-35 | >38 | | >36 |
| 7001-T75 | 1.275 | LT | 77 | 66 | 4 | 19-26 | 17-23 | | >56 | | 25 |
| 7005-T6351 | 0.250-3.000 | LT | 47 | 38 | 7 | ≈50 | | | ≈29 | ≈29 | <20 |
| X7007-T6 | | | | | | 44 | 37 | | | | |
| 7039-T6151 | 0.250-2.000 | LT | 55 | 45 | 10 | 48 | 40 | 25-35 | | | <5 |
| 7039-T63 | | | | | | 44-45 | 36-37 | 20-25 | >42 | 35 | <8 |
| 7039-T64 | up to 1.500 | LT | 60 | 51 | 9 | >40 | ≈40 | 30-34 | | | <5 |
| X7050-T7E54 | 2.5 | LT | | | | | | 18-19 | | | |
| 7075-T651 | 0.500-1.000 | LT | 78 | 68 | 7 | 25-33 | 19-31 | 15-20 | 50 | 45 | <8 |
| 7075-T7651 | 0.500-1.000 | LT | 71 | 60 | 6 | 31 | 23-26 | 22 | >49 | >49 | 25 |
| 7075-T7351 | 0.250-1.000 | LT | 69 | 57 | 7 | 30-41 | 24-35 | 19-21 | >50 | >48 | >43 |
| X7475-T7351 | 2.6 | LT | ≈59 | ≈49 | | 52 | | 35 | >50 | >48 | >43 |
| 7079-T651 | 0.250-1.000 | LT | 74 | 65 | 8 | 25-34 | 22-28 | 15-18 | >55 | 40 | <8 |
| 7178-T651 | 0.500-1.000 | LT | 84 | 73 | 6 | 21-27 | 18-23 | 14-21 | 55 | 38 | <8 |
| 7178-T7651 | 0.500-1.000 | LT | 73 | 62 | 6 | 26-30 | 21-28 | 17-19 | >52 | >52 | 25 |

**Table 2.** Mechanical, Fracture, and Stress Corrosion Properties for Plates of Several Aluminum Alloys—*Continued*

| *Alloy and Temper* | *Heat Treat Thickness (in.* | *Product Form*[a] | *Grain Dir*[b] | *Minimum Tensile Strength* | | *Min Elong. in* | *Ranges in Plane Strain Fracture Toughness $K_{Ic}$* | | | *Estimated Short Trans. Stress Corrosion Threshold Stress* |
|---|---|---|---|---|---|---|---|---|---|---|
| | | | | *Ultimate, ksi* | *0.2% Yield, ksi* | *2 in. or 4D) %* | *Long., ksi $\sqrt{in}$* | *Long Trans., ksi $\sqrt{in}$* | *Short Trans., ksi $\sqrt{in}$* | *ksi*[c] |
| Forgings | | | | | | | | | | |
| 2014-T4 | 0.0-4.000 | D.F. | L | 55 | 30 | 11 | | | | ? |
| 2014-T6 | 0.0-1.000 | D.F. | L | 65 | 56 | 6 | 25-31 | 18-23 | 15-19 | 7-10 |
| | 0.0-1.000 | D.F. | T | 64 | 55 | 3 | | | | |
| | 1.001-2.000 | D.F. | L | 65 | 56 | 6 | | | | |
| | 1.001-2.000 | D.F. | T | 64 | 55 | 3 | | | | |
| | 2.001-3.000 | D.F. | L | 65 | 55 | 6 | | | | |
| | 2.001-3.000 | D.F. | T | 63 | 54 | 2 | | | | |
| | 3.001-4.000 | D.F. | L | 63 | 55 | 6 | | | | |
| | 3.001-4.000 | D.F. | T | 63 | 54 | 2 | | | | |
| | 4.001-5.000 | H.F. | L | 62 | 54 | 7 | | | | |
| | 5.001-6.000 | H.F. | L | 61 | 53 | 7 | | | | |
| | 7.001-8.000 | H.F. | L | 59 | 51 | 6 | | | | |
| | 7.001-8.000 | H.F. | LT | 59 | 51 | 2 | | | | |
| 2124-T852 | 0.0-4.000 | D.F. | L | 63 | 56 | 12 | 26 | 18 | 16 | ≈15 |
| | 0.0-4.000 | D.F. | T | 59 | 52 | 3 | | | | |
| | 0.0-4.000 | H.F. | L | 63 | 56 | 8 | | | | |
| | 4.000-5.000 | H.F. | L | 61 | 55 | 8 | | | | |
| | 5.000-6.000 | H.F. | L | 59 | 54 | 8 | | | | |
| 2219-T6 | 4.0 max | D.F. | L | 58 | 38 | 8 | ≈36 | ≈34 | | >32 |
| | 4.0 max | D.F. | T | 56 | 36 | 4 | | | | |
| 2219-T852 | 4.0 max | H.F. | L | 62 | 50 | 6 | | | | >38 |
| 2618-T6 | 4.0 max | D.F. | L | 58 | 45 | 4 | | | | >40 |
| | 4.0 max | D.F. | T | 55 | 42 | 4 | | | | |
| 5083-H112 | 4.0 max | D.F. | L | 40 | 18 | 16 | | | | |
| | 4.0 max | D.F. | T | 39 | 16 | 14 | | | | |
| 5456-H112 | 4.0 max | D.F. | L | 44 | 20 | 16 | | | | |
| 6061-T6 | 4.0 max | D.F. | L | 38 | 35 | 7 | | | | >36 |
| | 4.0 max | D.F. | T | 38 | 35 | 5 | | | | |
| 6061-T652 | 8.0 max | H.F. | L | 37 | 34 | 8 | | | | >36 |
| 6066-T6 | 4.0 max | D.F. | L | 50 | 45 | 8 | | | | >26 |
| 6151-T6 | 4.0 max | D.F. | L | 44 | 37 | 10 | | ≈33 | | |
| | 4.0 max | D.F. | T | 44 | 37 | 6 | | | | |
| 7039-T64 | 0.0-4.000 | D.F. | L | 57 | 48 | 8 | | | | <10 |
| | 0.0-4.000 | D.F. | T | 54 | 45 | 4 | | | | |
| 7049-T73 | 0.0-1.000 | D.F. | L | 72 | 62 | 7 | 32-34 | | 18-29 | 45 |
| | 0.0-1.000 | D.F. | T | 71 | 61 | 3 | | | | |
| | 1.001-2.000 | D.F. | L | 72 | 62 | 7 | | | | |
| | 1.001-2.000 | D.F. | T | 70 | 60 | 3 | | | | |
| | 2.001-3.000 | D.F. | L | 71 | 61 | 7 | | | | |
| | 2.001-3.000 | D.F. | T | 70 | 60 | 3 | | | | |
| | 3.001-4.000 | D.F. | L | 71 | 61 | 7 | | | | |
| | 3.001-4.000 | D.F. | T | 70 | 60 | 2 | | | | |
| | 4.001-5.000 | D.F. | L | 70 | 60 | 7 | | | | |
| | 4.001-5.000 | D.F. | T | 68 | 58 | 2 | | | | |
| | 4.001-5.000 | H.F. | L | 67 | 56 | 7 | | | | |

**Table 2.** Mechanical, Fracture, and Stress Corrosion Properties for Plates of Several Aluminum Alloys *Continued*

| Alloy and Temper | Heat Treat Thickness (in.) | Product Form[a] | Grain Dir.[b] | Minimum Tensile Strength | | Min Elong. (in 2 in. or 4D) % | Range in Plane Strain Fracture Toughness $K_{Ic}$ | | | Estimated Short Trans. Stress Corrosion Threshold Stress (ksi)[d] |
|---|---|---|---|---|---|---|---|---|---|---|
| | | | | Ultimate ksi | 0.2% Yield, ksi | | Long., ksi$\sqrt{in.}$ | Long Trans., ksi$\sqrt{in.}$ | Short Trans., ksi$\sqrt{in.}$ | |
| Forgings | | | | | | | | | | |
| 7075-T6 | 0.01-1.000 | D | L | 75 | 64 | 7 | 22-36 | 21-33 | 17-20 | ≤8-14 |
| | 0.01-1.000 | D | T | 71 | 61 | 3 | | | | |
| | 1.001-2.000 | D | L | 74 | 63 | 7 | | | | |
| | 1.001-2.000 | D | T | 71 | 61 | 3 | | | | |
| | 2.001-3.000 | D | L | 74 | 63 | 7 | | | | |
| | 2.001-3.000 | D | T | 70 | 60 | 3 | | | | |
| | 3.001-4.000 | D | L | 73 | 62 | 7 | | | | |
| | 3.001-4.000 | D | T | 70 | 60 | 2 | | | | |
| | 4.001-5.000 | H | L | 69 | 58 | 7 | | | | |
| | 5.001-6.000 | H | L | 68 | 56 | 6 | | | | |
| 7075-T73 | 3.0 max | D | L | 66 | 56 | 7 | 27-35 | 21-26 | 19-25 | ≤43 |
| | 3.0 max | D | T | 62 | 53 | 3 | | | | |
| | 3.001-4.000 | D | L | 64 | 55 | 7 | | | | |
| | 3.001-4.000 | D | T | 61 | 52 | 2 | | | | |
| | 4.001-5.000 | D | L | 62 | 53 | 7 | | | | |
| | 4.001-5.000 | D | T | 61 | 51 | 2 | | | | |
| | 4.001-5.000 | H | L | 62 | 53 | 7 | | | | |
| | 5.001-6.000 | D | L | 61 | 51 | 6 | | | | |
| | 5.001-6.000 | D | T | 58 | 50 | 2 | | | | |
| | 5.001-6.000 | H | L | 61 | 51 | 6 | | | | |
| 7076-T61 | 4.0 max | D | L | 70 | 60 | 9 | | | | ≈7 |
| AZ74-61 | 2.0 max | D | L | ≈71 | ≈61 | ≈4 | | | | ≈45 |
| | 2.0 max | D | T | ≈69 | ≈59 | ≈3 | | | | |
| | 4.0 max | H | L | ≈69 | ≈58 | ≈9 | | | | |
| 7079-T6 | 0.01-1.000 | D | L | 72 | 62 | 7 | 25-30 | 23-35 | 18-25 | ≤8-6 |
| | 0.01-1.000 | D | T | 71 | 61 | 5 | | | | |
| | 1.001-2.000 | D | L | 72 | 62 | 7 | | | | |
| | 1.001-2.000 | D | T | 70 | 60 | 5 | | | | |
| | 2.001-3.000 | D | L | 71 | 61 | 7 | | | | |
| | 2.001-3.000 | D | T | 70 | 60 | 4 | | | | |
| | 3.001-4.000 | D | L | 71 | 61 | 7 | | | | |
| | 3.001-4.000 | D | T | 70 | 60 | 4 | | | | |
| | 4.001-5.000 | D | L | 70 | 60 | 7 | | | | |
| | 4.001-5.000 | D | T | 68 | 58 | 3 | | | | |
| | 4.001-5.000 | H | L | 70 | 60 | 9 | | | | |
| | 5.001-6.000 | H | L | 70 | 59 | 7 | | | | |
| | 5.001-6.000 | H | T | 68 | 58 | 3 | | | | |
| | 5.001-6.000 | H | L | 69 | 59 | 7 | | | | |
| | 7.001-8.000 | H | L | 67 | 57 | 9 | | | | |
| | 7.001-8.000 | H | LT | 66 | 53 | 4 | | | | |
| X7080-T7 | 6.0 max | D | L | 65 | 57 | 6 | 32-39 | 20-29 | 20-26 | ≥5-15 |
| | 6.0 max | D | T | 63 | 56 | 3 | | | | |
| | 6.0 max | H | L | 65 | 55 | 10 | | | | |
| 7175-T66 | 3.0 max | D | L | 86 | 76 | 7 | 26-33 | 24 | 17-26 | ≤8 |
| | 3.0 max | D | T | 77 | 66 | 4 | | | | |

**Table 2.** Mechanical, Fracture, and Stress Corrosion Properties for Plates of Several Aluminum Alloys—*Continued*

| Alloy and Temper | Heat Treat Thickness (in.) | Product Form[a] | Grain Dir[b] | Minimum Tensile Strength | | Min Elong (% in 2 in. or 4D) | Range in Plane-Strain Fracture Toughness $K_{Ic}$ | | | Estimated Short Trans Stress Corrosion Threshold Stress (ksi)[d] |
|---|---|---|---|---|---|---|---|---|---|---|
| | | | | Ultimate, ksi | 0.2% Yield, ksi | | Long., ksi $\sqrt{in}$ | Long. Trans., ksi $\sqrt{in}$ | Short Trans., ksi $\sqrt{in}$ | |
| Forgings *Continued* | | | | | | | | | | |
| 7175-T736[c] | 0.0-3.000 | D.F. | L | 76 | 66 | 7 | 32-36 | 32 | 23-33 | 35 |
| | 0.0-3.000 | D.F. | T | 71 | 62 | 4 | | | | |
| | 0.0-3.000 | H.F. | L | 73 | 63 | 9 | | | | |
| | 3.001-4.000 | D.F. | L | 73 | 63 | 7 | | | | |
| | 3.001-4.000 | D.F. | T | 70 | 60 | 4 | | | | |
| | 3.001-4.000 | H.F. | L | 71 | 61 | 9 | | | | |
| | 4.001-5.000 | D.F. | L | 70 | 61 | 7 | | | | |
| | 4.001-5.000 | D.F. | T | 68 | 58 | 4 | | | | |
| | 4.001-5.000 | H.F. | L | 68 | 57 | 8 | | | | |
| | 5.001-6.000 | D.F. | L | 68 | 58 | 7 | | | | |
| | 5.001-6.000 | D.F. | T | 65 | 55 | 4 | | | | |
| | 5.001-6.000 | H.F. | L | 65 | 54 | 8 | | | | |
| 7175-T7365[c] | 0.0-3.000 | D.F. | L | 73 | 63 | 7 | | | | 35 |
| | 0.0-3.000 | D.F. | T | 68 | 55 | 4 | | | | |
| | 0.0-3.000 | H.F. | L | 71 | 61 | 9 | | | | |
| | 5.001-6.000 | D.F. | L | 65 | 55 | 7 | | | | |
| | 5.001-6.000 | D.F. | T | 62 | 49 | 4 | | | | |
| | 5.001-6.000 | H.F. | L | 63 | 51 | 8 | | | | |

[a] Formerly designated Alcoa 417 Process 2024.
[b] LT = Long transverse
L = Longitudinal
T = Transverse
[c] D.F. = Die forged
H.F. = Hand forged
[d] When two numbers are shown, the first is the threshold stress in 3.5% NaCl alternate immersion and the second is the threshold in an inland industrial environment
[e] Tentative minimum mechanical properties applicable to parts with a maximum cross sectional area of approximately 100 in.$^2$

Another system has been devised that is particularly useful for precracked specimens. This system specifies both the cracking plane and crack propagation direction. It uses three letters (L,T,W) to indicate the three mutually perpendicular directions: L for the longitudinal direction, T for the thickness direction, and W for the width direction. The crack plane is identified by the direction normal to the crack. The crack propagation direction is identified by one of the three directions, L, T, or W. Figure 3 illustrates the various possible double cantilever beam (DCB) specimen orientations in plate material. Using this system, cracks propagating in the parting plane of die forgings would correspond to TL and TW cracks in plate.

## The Sources of Stress

Tensile stresses are always necessary for SCC to occur. Service stress corrosion failures in susceptible aluminum alloys usually result from sustained, uninten-

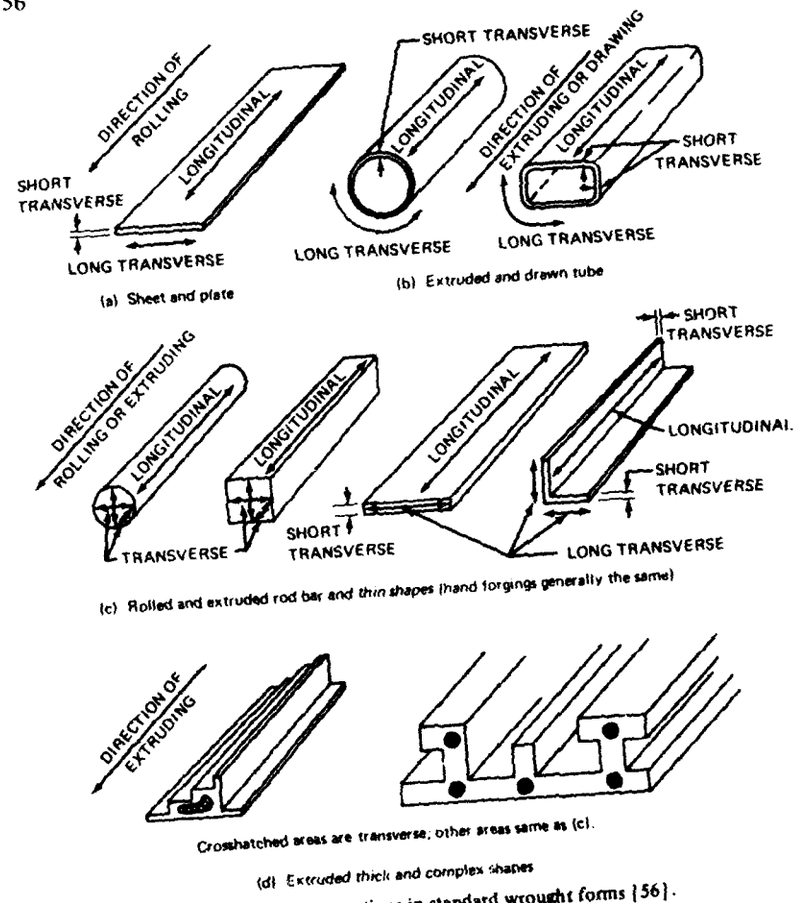


Fig. 1. Grain orientations in standard wrought forms [56].

tionally induced stresses or residual short transverse or transverse tension stresses acting at the surface. A typical source of an unintentionally induced stress resulting from assembly is illustrated in Fig. 4. Residual stresses usually result from quenching after solution heat treatment. Examples showing the magnitude and sense of such stresses are shown in Fig. 5. The problems usually arise when machining operations expose the *material under* high residual tension stresses. In some parts of complicated geometry, cooling rates may vary from area to area during quenching due to variations in section size or formation of steam pockets. This can lead to surface residual tension stresses even without subsequent machining operations. Since design loads are seldom of the sustained type, they

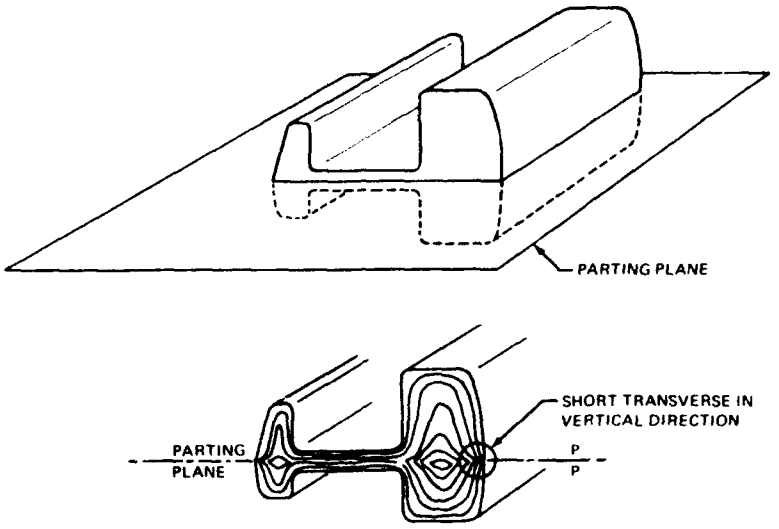


Fig. 2. Schematic representation of the grain flow in a section of a typical die forging.

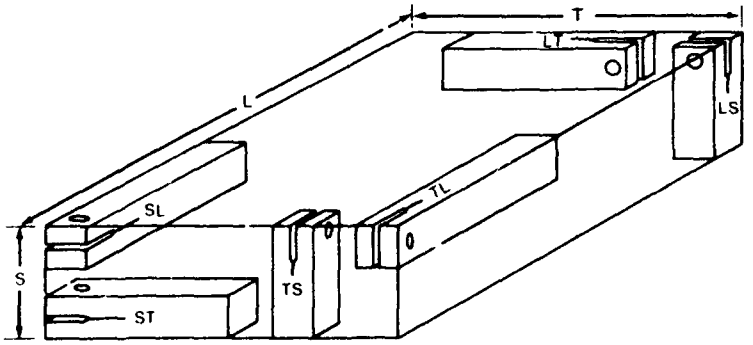


T Long Transverse
L Longitudinal (Rolling or extrusion) direction
S Thickness
First letter Normal to the fracture plane
Second letter *Direction of propagation in fracture plane*

Fig. 3. Some possible double-cantilever-beam (DCB) specimen orientations in plate material.

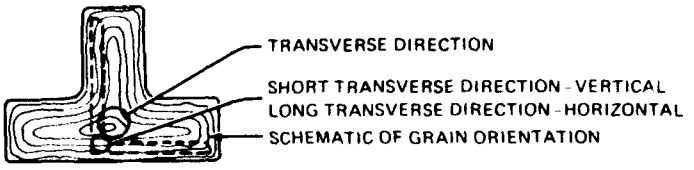


Location of machined angle with respect to transverse grain flow in thick tee

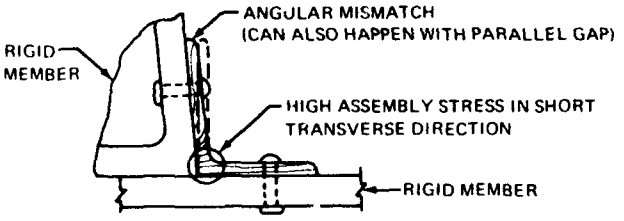


Fig. 4. Illustration of one way in which locked-in short transverse assembly stresses can result [56].

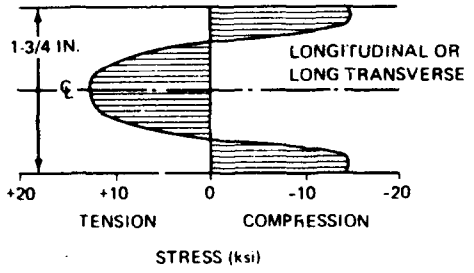


Fig. 5. Typical residual stress pattern in 7075-T6 plate given a cold-water quench and not stress relieved [56].

are not usually the cause of SCC. There are exceptions to this rule, however, and SCC often occurs in hydraulic parts or pressure vessels where pressurization may last for long periods of time. Other exceptions are interference fitted bushings and fasteners.

Although it is probably less common, it is worth noting that once a stress corrosion crack has initiated, the formation of voluminous corrosion products within the crack itself can help in maintaining high stresses at the crack tip. This phenomenon has been observed in several high strength aluminum alloys [46, 48,49].

Two other forms of corrosion in high strength aluminum alloys, namely intergranular and exfoliation, are related to SCC inasmuch as the attack

also occurs along grain boundaries. Applied stresses are not necessary for these forms of corrosion. It is significant that some alloys not susceptible to SCC may suffer intergranular corrosion or exfoliation corrosion.

### Smooth-Specimen Test Techniques

Traditionally, SCC data for aluminum alloys have been obtained by exposing smooth, stressed specimens to a corrosive environment [57]. Time to failure (TTF) is then plotted as a function of the applied gross section stress as illustrated in Fig. 6. Note that there appears to be a stress below which no stress corrosion failures occur. This estimated threshold stress $\sigma_{scc}$ depends on the particular alloy, temper, grain direction, environment, and testing time; it is referred to as the smooth-specimen stress-corrosion threshold stress. Most of the available threshold stresses are listed in Table 2. Determination of the threshold stress is not a simple matter and usually requires exposure of a number of specimens stressed to each of several stress levels. The most widely used testing procedure involves alternate immersion in an aqueous 3.5% NaCl solution. Specimens are immersed 10 min followed by a 50-min drying period in air. Test times range from 30 to 180 days in aggressive environments like the ones used in the alternate-immersion test. In less aggressive environments such as industrial atmospheres, testing times of not less than three years are required.

Failure is usually defined as either actual fracture of the specimen or the visual appearance of the first crack at some nominal magnification. It is often necessary to conduct metallographic examination on specimens at the conclusion of testing to verify test results, since failure can result from deep pitting or general corrosion rather than SCC. In addition, while some specimens may not appear to have failed by the previously defined failure criterion, sharp, intergranular stress corrosion cracks may be found during the metallographic examination, thus indicating failure. The important influence of grain shape and orientation with respect to the stressing direction on the SCC threshold of smooth specimens is illustrated in Figs. 7 and 8.

Note in Fig. 7 that both the threshold stress and TTF decrease as the stressing direction is changed from the longitudinal to the short transverse direction. There are two reasons for this behavior. First, the stress corrosion cracking path is shortest for short transverse stresses, as illustrated in Fig. 9. Second, in the short transverse direction the tensile stresses are more nearly perpendicular to the grain boundaries, and it has been shown that susceptibility to SCC is a function of the resolved stress component acting normal to the grain boundaries [58,59]. Despite the lower threshold stress in the short transverse direction, it is important to note that even in longitudinal SCC specimens, cracks can initiate easily on boundaries that are perpendicular to the applied stress [60]. However, for cracks of this orientation there is no available continuous intergranular path perpendicular to the stressing direction. Therefore, these cracks have great difficulty propagating by stress corrosion. Nevertheless, such shallow stress corrosion

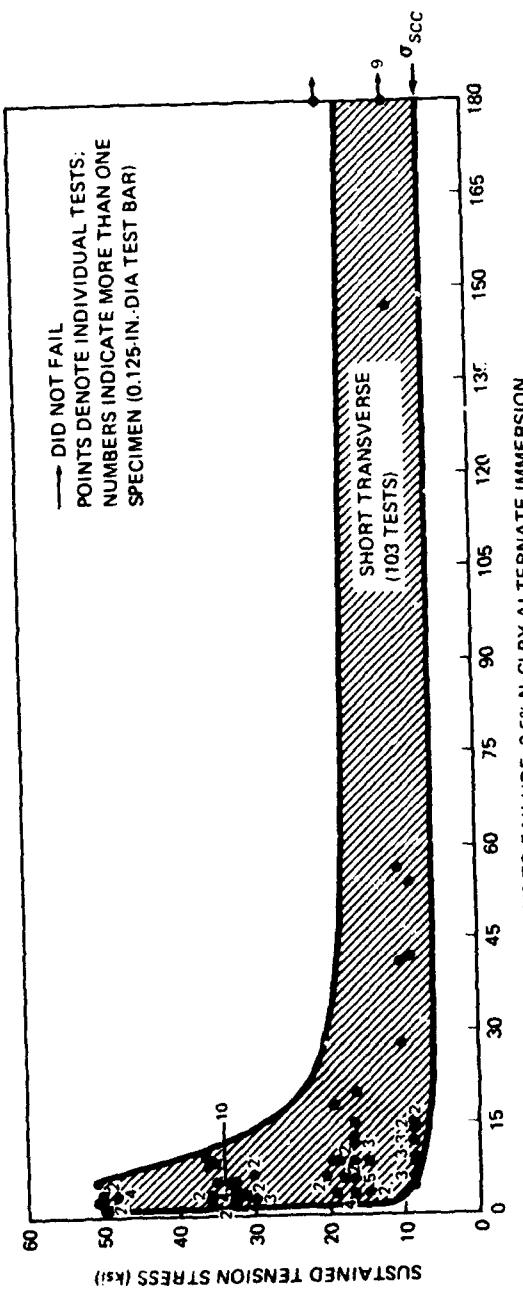


Fig. 6. Smooth-specimen stress corrosion data for 0.25- to 3-in.-thick 7075-T6 plate illustrating the time-to-failure (TTF) method of obtaining threshold stresses. For the short transverse direction, the threshold stress of 7075-T6 obtained using this technique is about 7 ksi [42].

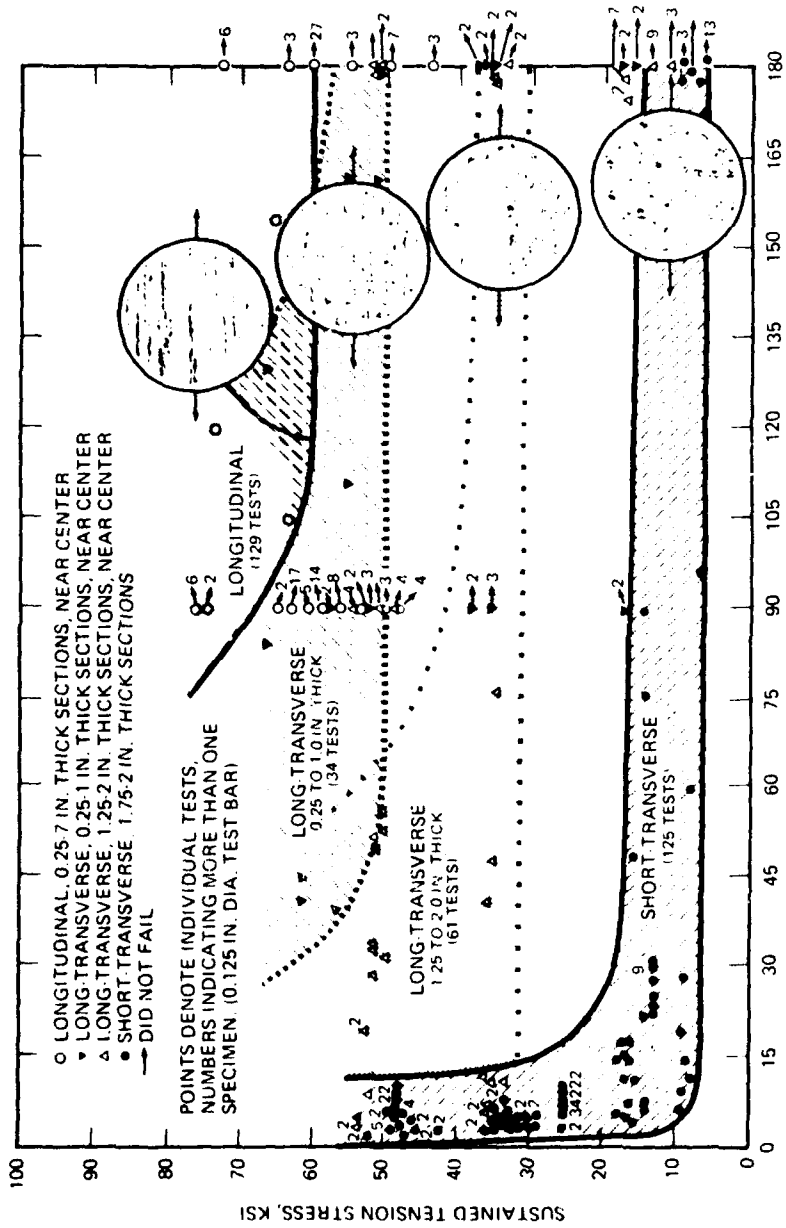


FIG. 7. Smooth-specimen stress-corrosion data for 7075-T6 extruded sections illustrating the effect of grain geometry on TTF data [42]. From *Metal Prog.* **81** (No. 4), Fig. 6, p. 84, copyright 1962 by The American Society for Metals. Used by permission.

cracks only one or two grains deep could be responsible for initiating fatigue cracks in longitudinally stressed members.

The limitations of TTF data from smooth specimens have been discussed in Chapters 1 and 2 of this monograph.

### Precracked-Specimen Test Techniques

There are several methods of obtaining stress corrosion data from aluminum alloys using precracked specimens. One involves testing a series of fatigue-precracked specimens using constant loads to achieve a series of plane-strain stress intensity $K_I$ levels below the plane-strain fracture toughness $K_{Ic}$. If the cracks propagate by stress corrosion, the $K_I$ level increases until $K_{Ic}$ is reached and failure occurs. By plotting the time to failure against the initial, applied stress intensity, an apparent threshold can be determined, which is denoted $K_{Iscc}$. This test method is illustrated in Fig. 10.

This method overcomes some of the objections against smooth-specimen TTF testing listed in the preceding section, since with the test results it is possible to

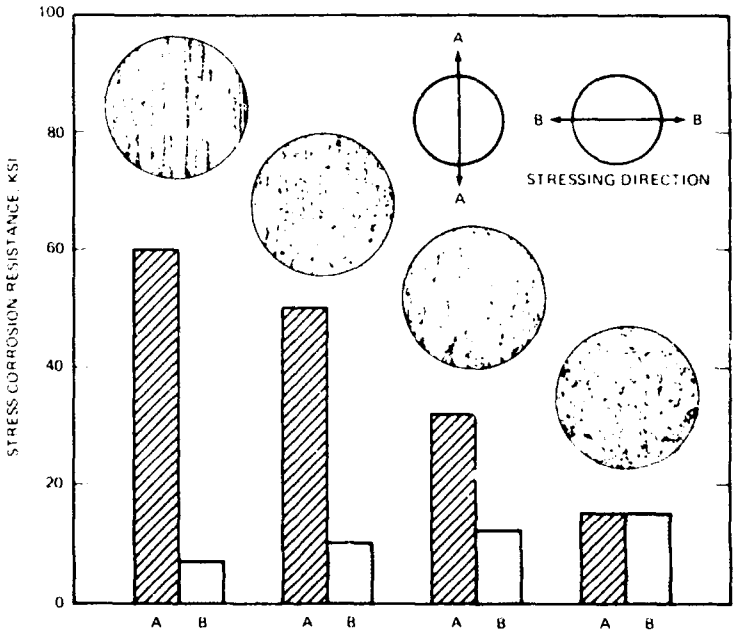


Fig. 8. Effect of grain geometry and stressing direction on resistance to stress corrosion cracking (SCC) for 7075-T6 extrusions. This same trend is applicable to other manufactured forms of 7075-T6 and also to other high-strength aluminum alloys in a susceptible temper [55]. From *Proceedings of Conference on Fundamental Aspects of Stress Corrosion Cracking*, 1969, p. 468, Fig. 3; copyright by the National Association of Corrosion Engineers. Used by permission.

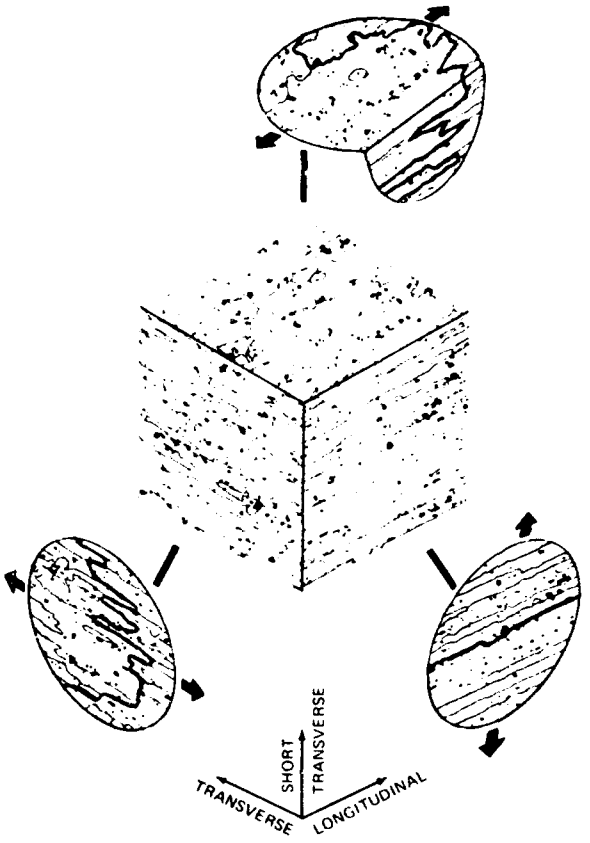


Fig. 9. Effect of stressing direction on the intergranular stress-corrosion crack path in a susceptible high-strength aluminum alloy.

predict whether cracks in flawed structures can propagate by SCC. Since stress corrosion crack growth rates in aluminum alloys can be extremely slow, failure times can be extremely long; if impatient investigators select too short testing times, erroneously high $K_{Iscc}$ values can result. Threshold $K_I$ levels can be estimated by mechanically fracturing precracked specimens after they have been exposed at a series of $K_I$ levels for a sufficiently long time. Subsequent examination of the fractured specimens allows the determination of the $K_I$ levels above which growth is observed and below which no growth is observed. For any of these tests, either the bent-beam, single-edge-notch, or surface-flaw type of specimen can be used, although it is usually difficult if not impossible to test the

short transverse direction using such specimens, unless very thick material is available or extension arms can be fitted.

The above described methods have been used in recent years by a number of investigators to overcome some of the disadvantages associated with smooth-specimen TTF testing [35,36,61-64]. In addition to the establishment of a $K_{Iscc}$ using this technique, some of the first crack velocity measurements have been made from additional fractographic observations. A more convenient and accurate technique for measuring crack growth rates as a function of the applied crack-tip stress intensity is outlined in Chapter 2.

### Crack Velocity as a Function of Stress Intensity

Obviously the knowledge of the stress corrosion crack velocity as a function of the crack-tip stress intensity would constitute more complete and detailed information than either TTF or $K_{Iscc}$. The double cantilever beam (DCB) specimen provides the most economical and convenient method for measuring such crack velocities at known stress intensity levels. The DCB specimen is also called the single-edge-cracked-specimen. Its stress intensity calibration is described in Chapter 2 of this monograph.

The DCB specimen is ideally suited to testing the critical short transverse direction of high strength aluminum alloy materials because the intergranular nature of SCC in these alloys prevents the stress corrosion cracks from running out of the center plane.

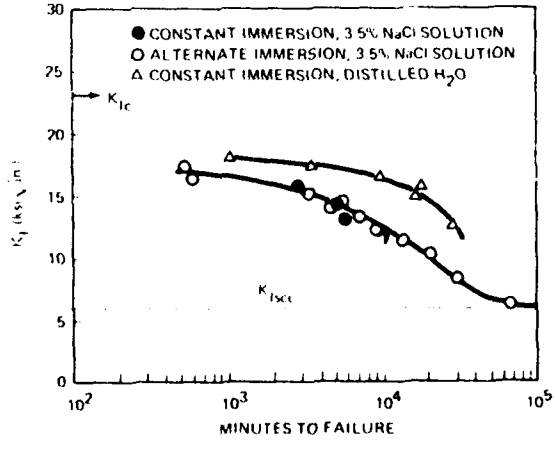


Fig. 10. Precracked-specimen stress corrosion data for short transverse 7075-T651 plate illustrating the TTF method of obtaining $K_{Iscc}$. Using this technique, a $K_{Iscc}$ of about 6 ksi $\sqrt{in.}$ is obtained [61]. From *Symposium on Stress Corrosion Testing*, Atlantic City, 1966, p. 24, Fig. 1; copyright by the American Society for Testing and Materials. Used by permission.

Most of the quantitative stress corrosion data presented in the following sections were obtained using DCB specimens of the TL (short transverse) orientation. A typical result is given in Fig. 11, which shows the velocity of the tip of a stress corrosion crack in the alloy 7075-T651 as a function of the applied crack-tip stress intensity [46]. This is one of the key figures of this chapter and the reader should carefully examine it before going on. It summarizes much of the progress that has recently been made with the new and quantitative stress corrosion tests. Note that at low stress intensities the crack-tip velocity is strongly stress dependent. This part of the crack velocity vs stress intensity curve (V-$K$ curve) is labeled region I. At higher stress intensities, the crack-tip velocity is almost independent of stress. This plateau of the V-K curve is labeled region II. It is important to note that the slope in region I when measured on a single specimen has always been found to be finite, at least down to very low velocities ($10^{-8}$ to $10^{-9}$ cm/sec). This means that at the present time no true lower limit of stress intensity $K_{Iscc}$ has been observed below which stress corrosion cracks do not propagate in aluminum alloys. Therefore, the assumption of a $K_{Iscc}$ value for aluminum alloys based on data shown in Figs. 10 and 11 is incorrect.

For the alloy 7075-T651, stress-corrosion crack velocities are identical for specimens completely immersed in saturated NaCl solution and for specimens alternately immersed in 3.5% NaCl solution. Thus, the data presented in Fig. 11 have been obtained for the same alloy, crack orientation, and environment as the data in Fig. 6 (smooth-specimen TTF) and in Fig. 10 (precracked specimen TTF, $K_{Iscc}$). These three figures, therefore, represent a fair comparison of the results obtained with the three different SCC testing methods for high strength aluminum alloys.

## Relationship Between Data from Smooth and Precracked Specimens

Since the precracked-specimen approach is fairly new in stress corrosion testing of aluminum alloys, it seems appropriate to discuss briefly some of the suggested relationships between stress corrosion results from smooth and precracked specimens of high strength aluminum alloys.

One suggested means for merging the two types of data [65] is illustrated in Fig. 12. In this figure, both the SCC threshold stress for smooth specimens and the threshold stress intensity $K_{Iscc}$ for precracked specimens are plotted vs flaw depth. ($K_{Iscc}$ is used here for illustrative purposes only, since a true threshold apparently does not exist for most aluminum alloys.) The generalized equation $K = \sigma\sqrt{\pi a}$, relating stress intensity $K_I$, stress $\sigma$, and flaw size $2a$, has been used to construct the $K_{Iscc}$ lines in Fig. 12. There are two implications from this type of plot. First, to avoid SCC, 7075-T6510 should not be stressed at levels above the smooth-specimen threshold stress (7 ksi), regardless of the flaw size in the material. Second, when relatively large flaws are present, 7075-T6510 should not be stressed at levels above those defined by the threshold stress-intensity $K_{Iscc}$.

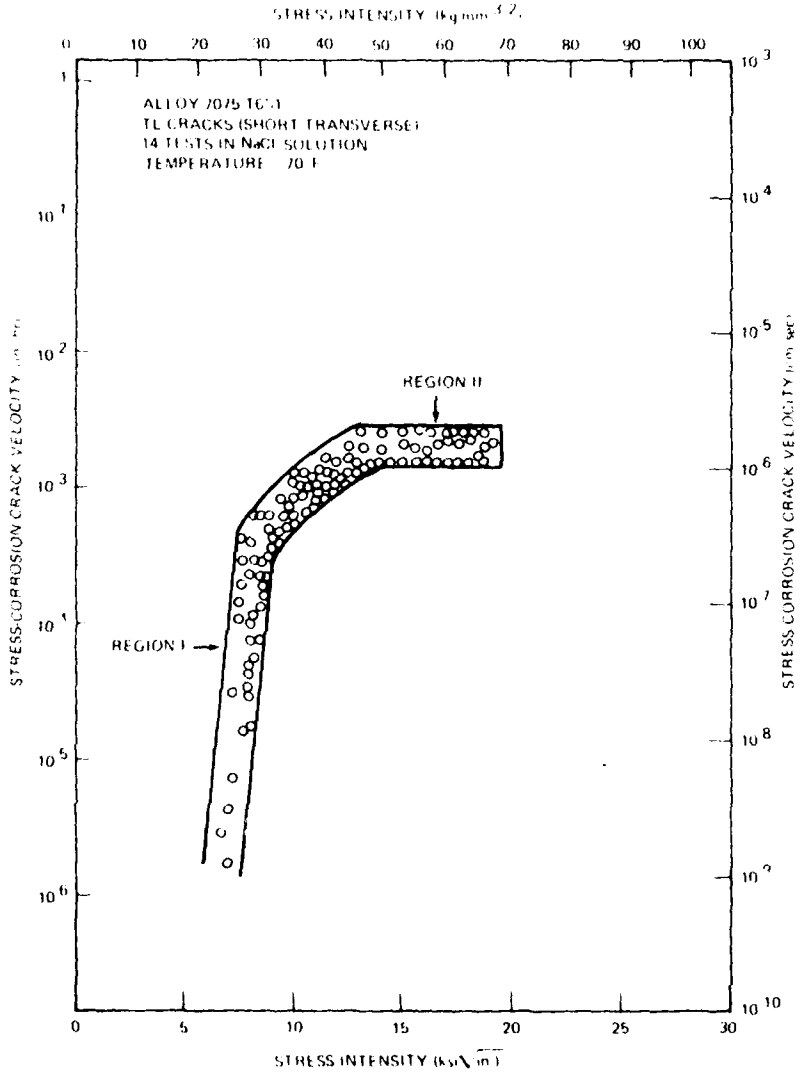


Fig. 11. Typical V-K curves for 7075-T651 obtained using TR DCB stress corrosion specimens. Regions I (stress-intensity dependent) and II (stress-intensity independent) are clearly evident, as is the finite slope of the curve in region I. The $K_{Iscc}$ value for 7075-T651 from these tests is just less than 7 ksi $\sqrt{in.}$ [45].

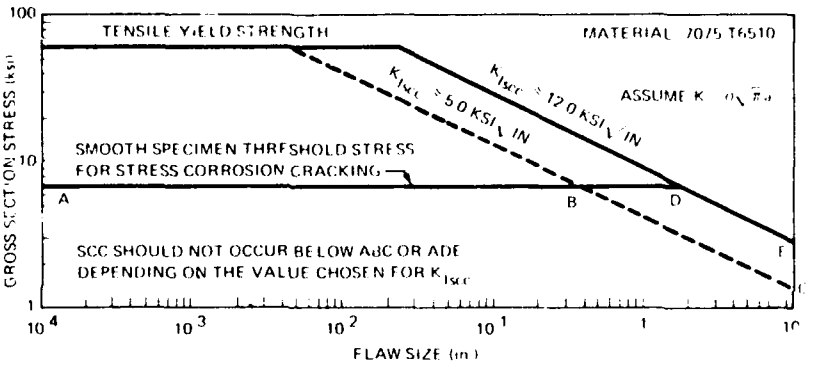


Fig. 12. Suggested method for combining stress corrosion data on smooth and precracked specimens for predicting when SCC will occur [65].

The approximate $K_{Iscc}$ value for 7075-T6510 from Ref. 65 used to construct Fig. 12 is much higher than would be expected from the data for 7075-T651 in Figs. 10 and 11. Therefore, we have added a second $K_{Iscc}$ line based on a value of 5 ksi $\sqrt{\text{in.}}$ to show the effect of a lower $K_{Iscc}$ value on this type of plot.

While not particularly useful for design purposes, this type of plot does illustrate the fact that susceptible aluminum alloys are subject to failure at stress *intensity* levels below the *apparent* $K_{Iscc}$, provided the stress level is above the smooth-specimen threshold stress. This fact in itself shows that the $K_{Iscc}$ data used in Fig. 12 are not the lower limit of stress intensity below which SCC cannot occur. The reasons for this are threefold. First, as pointed out in the preceding section, even at low stress intensities and extremely low growth rates, a threshold stress intensity for aluminum alloys has not yet been observed. This is different from the observed behavior of magnesium alloys, titanium alloys, and steels in neutral aqueous halide solutions, where apparently a true $K_{Iscc}$ exists. Second, the reason that SCC is observed below the extended $K_{Iscc}$ line in specimens with very small flaws or no apparent initial flaws (Fig. 12) is that other forms of corrosion can occur. These could be either pitting or intergranular corrosion, both of which can provide stress raisers that could increase the effective stress intensity to levels where the growth rate is sufficiently high to cause eventual failure. (*Note that pitting or intergranular corrosion may also* cause changes in the local solution chemistry and thus influence stress-corrosion crack growth.) Stress corrosion failures in alloy 7039-T6 have occurred at extremely low stress levels, i.e., at stress levels below the 7-ksi level typical of that observed for other susceptible 7000-series alloys [66]. It is significant in this context that SCC cracks in 7039-T6 have been observed to initiate at pits resulting from corrosion in laboratory air of $Mg_2Si$ particles along grain boundaries [60]. A number of other factors could also provide effective stress intensities higher than those calculated. These include local plastic deformation,

cracked intermetallic particles, and residual stresses. Third, the assumption $K_I = \sigma\sqrt{\pi a}$ in Fig. 12 is an oversimplification. It would be more appropriate to adjust $K_I$ values with a correction factor that takes into account the depth of the flaw with respect to the specimen size. For the relatively small specimens generally used in stress corrosion testing, this factor is not insignificant and could increase appreciably the actual crack-tip stress intensities over those shown in Fig. 12 for the flaw depth listed there.

## Experimental Difficulties in Testing Precracked Specimens

Experience gained with many hundreds of tests to date has shown that there are a number of experimental problems that must be overcome if accurate V-K curves are to be obtained. These problems are discussed below.

**Residual Stresses.** When SCC specimens are machined from heat-treated, quenched, and aged material that has not been stretched or compressively stress relieved after quenching, residual stresses can cause large errors in $K_I$ levels calculated using the $K_I$ calibration equation [61]. Error is introduced by the bowing apart of the DCB specimen arms due to the residual compressive stresses on the surface of the specimen.

Similar problems are encountered if DCB specimens are machined from hand or die forgings containing quenched-in residual stresses; the $K_I$ levels calculated for such specimens based on the $K_I$ calibration of the DCB specimen are not valid. In this connection, the effect of residual stresses on the behavior of DCB specimens has clearly demonstrated the important role that quenched-in residual stresses can play in the propagation of stress corrosion cracks in actual parts. Thus, in many cases it may be extremely dangerous to predict growth rates in an actual part based on a $K_I$ level calculated from assumed loads and crack geometry. Local geometry changes in the part may keep the $K_I$ level much higher than that calculated.

The majority of the quantitative stress corrosion data reported in this paper for the high strength aluminum alloys was obtained from plate material that was stretcher straightened to remove residual stresses. This is indicated in the temper designation, TX51, for stretcher-straightened material.

**Corrosion-Product Wedging.** The buildup of corrosion products in the crack of a DCB specimen can cause stresses at the crack tip. These stresses can reach an intensity higher than the crack-tip stress intensity applied by external loading. This has been observed in both 2000- and 7000-series alloys [46,48,65]. Thus, $K_I$ values calculated from the $K_I$ calibration of the DCB specimen can be in error. In extreme cases, the corrosion-product-wedging action can be so severe that the loading bolts are lifted free, with the entire stress being supplied by the corrosion products [46,65].

There are two ways to determine that corrosion-product wedging has not introduced errors into the measured V-K curves. First, the DCB specimen can be unloaded after the test and the deflection at the load line can be remeasured and

compared to the deflection at the beginning of the test. If the two are nearly equal, no substantial amount of corrosion products has accumulated in the crack. Second, when at low applied crack-tip stress intensities the crack growth rate becomes immeasurably small, one can conclude that corrosion-product wedging is insignificant.

**Specimen Orientation and Grain Flow.** Grain flow in forgings varies with location in the part. Because stress corrosion cracks are intergranular in high strength aluminum alloys, they follow the grain flow. Therefore, care must be taken to ensure that DCB specimens are machined from forgings in such a way that they are loaded normal to the grain flow. If they are not loaded in this manner, growth rates several orders of magnitude slower than those in the short transverse direction can result.

**Crack Branching.** Generally, stress corrosion cracks in commercial high strength aluminum alloys in the TL and TW directions do not branch. The same is true in forgings if cracks grow along a direction of pronounced grain flow. If, however, an equiaxed grain structure exists, macroscopic crack branching is possible under certain conditions [68].

- The V-K curve must show a $K_I$-independent region (e.g., region II in Fig. 11).
- The crack-tip stress intensity at the point of branching must be at least 1.4 times the stress intensity at which region II begins.

Note that these conditions are necessary but not sufficient for branching.

**Delamination.** When specimens with precracks in LT and WT orientations are SCC tested, delamination (grain-boundary separation along TL and TW planes) can occur. This can effectively blunt the crack, thus invalidating the calculated stress intensity [62].

**Short Testing Times.** Stress corrosion crack growth rates observed in aluminum alloys can be extremely slow ($10^{-5}$ in./hr or less). Therefore, long testing times may be required to accurately determine the lower end of the V-K curve. Long testing times can be a problem, either because data are required immediately or because testing facilities cannot be tied up for long periods of time. Moreover, it has often not been realized that instead of a $K_{Iscc}$, region I of the V-K curve must be determined; i.e., cracks often do not stop even though they may slow down considerably. For these reasons, short test runout times can lead to erroneously high $K_{Iscc}$ values. Too short testing times could cause significant problems when it becomes necessary to ensure integrity in aluminum alloy pressure vessels for use in deep-space probes (3-year mission to Mars and back, for example).

**Relating Laboratory Data to Crack Growth in Service.** Under service conditions, the environment as well as the stress level varies with time. Therefore, laboratory data should be supplemented with tests conducted in actual and simulated service environments.

### Advantages of Precracked Specimens for SCC Testing

The use of precracked DCB specimens for stress corrosion testing of aluminum alloys has several advantages.

- Measurement can be made of the stress-corrosion crack-tip velocity as a function of the crack-tip stress intensity. Thus, while smooth-specimen data cannot be used to evaluate failure times of flawed structures or to prescribe loads below which unintentionally flawed structures will not fail in a given time, precracked specimen data can be used for these purposes. It is not intended that precracked specimens should replace all smooth specimens for stress corrosion testing of aluminum alloys. Rather, such precracked-specimen data are a valuable addition to the smooth-specimen threshold data in the same way that fatigue crack growth data are a valuable addition to the standard S-N fatigue curves for different alloys [65]. And, like fatigue-crack growth data, actual stress corrosion crack growth data can be useful for setting inspection intervals and for monitoring some structures. In addition, V-K data can be used to establish loads which ensure that structures containing possible undetectable flaws will operate safely in corrosive environments during their design lifetimes. Specific examples where precracked-specimen data have actually been used are given in the next section.
- The use of DCB specimens can eliminate scatter due to the initiation of stress corrosion cracks in smooth specimens, raising hopes for the first time that reproducible test results can be obtained in different laboratories.
- The DCB specimen can be used equally well for fundamental studies, alloy development, and design, making communications between these various disciplines much easier.
- The simple design, low cost, portability, and self-stressing capability of the bolt-loaded DCB specimen, and the ease with which data are generated from this specimen, are the keys to its eventual widespread use.
- When testing smooth tension specimens for SCC, it is good testing practice to expose unstressed specimens simultaneously with stressed specimens, since stressed specimens could fail simply by cross-section reduction due to intergranular, pitting, or general corrosion. Such a double check is not needed with DCB specimens because all possible effects of corrosion can be studied on the unstressed part of the same specimen after the test. Thus, when the DCB specimen is broken open after a SCC test, the crack face will show not only the depth of the SCC crack but also the depth of pits and intergranular corrosion in the unstressed part of the specimen.

### Some Advantages of Smooth-SCC Specimens

Smooth-specimen stress corrosion tests measure a sequence of phenomena in one test, i.e., initiation and propagation of cracks, and this can be an advantage for practical applications. In cases where crack initiation takes up a major part of the time to failure, smooth specimens are useful to simulate service behavior of a

flawless structure. In addition, a wealth of smooth-specimen data has been generated over the past several decades for most of the high strength aluminum alloys currently in use. This makes the use of smooth-specimen test techniques attractive in alloy development since the new alloy can be compared directly with the well-known alloys already in service. However, alloys can be rated equally well using crack growth rate data at known $K_I$ levels, and it is thought that such test techniques will eventually be preferred over the smooth-specimen test technique for many applications.

### Some Specific Applications of Precracked-Specimen Data

The use of threshold stress intensity data in actual design is probably best illustrated in the case of pressure vessels for the U.S. space program [35,36,62, 63]. In such cases, the relationship between fracture toughness $K_{Ic}$, threshold stress intensity level $K_{Iscc}$, applied stress intensity level $K_{Ii}$, operating stress $\sigma_{op}$, and proof test pressure ($\sigma_{op}$ × proof test factor $\alpha$) are illustrated in Fig. 13.

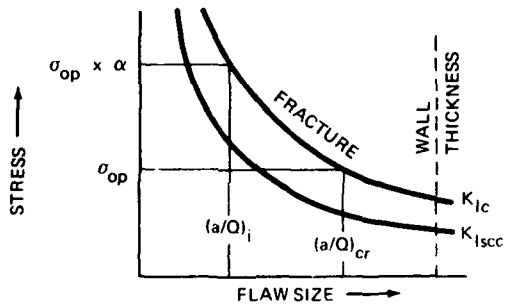


Fig. 13. Use of $K_{Ic}$ and $K_{Iscc}$ criteria in pressure-vessel and critical-burst design [36].

In this particular instance, vessels successfully passing a proof test at the $\sigma_{op}$ × $\alpha$ stress level are presumed to have defects not larger than $(a/Q)_i$ (Fig. 13). Any preexisting defects larger than $(a/Q)_i$ would cause bursting since the intersection of the $\sigma_{op}$ × $\alpha$ horizontal line with the vertical projection of a flaw larger than $(a/Q)_i$ would fall to the right of the $K_{Ic}$ curve or into the fracture region.

At the operating stress level $\sigma_{op}$, a preexisting flaw as large as $(a/Q)_i$ would remain stationary under sustained load because the resultant $K_{Ii}$ is smaller than the $K_{Iscc}$, as seen from the fact that the intersection of the $\sigma_{op}$ and $(a/Q)_i$ lines falls to the left of the intersection between the $K_{Iscc}$ curve and the $\sigma_{op}$ line. If the vessel were subjected to cyclic loading at $\sigma_{op}$, the initial flaw $(a/Q)_i$ would grow in size by fatigue until it reached the $(a/Q)_{cr}$ size, at which point bursting would occur.

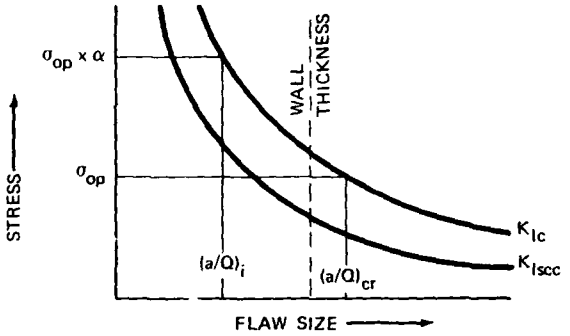


Fig. 14. Use of $K_{Ic}$ and $K_{Iscc}$ criteria in pressure-vessel and leak-before-burst design [36].

In a thinner walled pressure vessel, the critical flaw size $(a/Q)_{cr}$ may be larger than the wall thickness (Fig. 14). In this case, the vessel would be safe to operate at $\sigma_{op}$ sustained load just as in the previous case; again, the maximum initial flaw size $(a/Q)_i$ that could remain after proof test is smaller than what would be required to generate $K_{Ii}$ above the $K_{Iscc}$ level. If this vessel were subjected to cyclic loading, the flaw would again grow in size, but the pressure vessel would leak and depressurize rather than burst because the wall thickness is less than the critical flaw size $(a/Q)_{cr}$. In both cases a relatively short fatigue-crack extension could increase the crack-tip stress intensity above $K_{Iscc}$, resulting in failure by SCC even without further cycling. If the V-K curve for the material environment combination were known, it would be possible to predict quantitatively the remaining lifetime of the pressure vessel.

V-K curves have actually been used in setting inspection intervals for structural parts known or suspected to contain flaws. In one case [69] serious stress corrosion problems arose in a large machined 7075-T6 forging used to transmit loads from the wing to the fuselage of a fighter aircraft. An attempt was made to determine inspection intervals such that the largest undetectable flaw could not grow to a critical size between inspections. To set a realistic inspection interval, the small amount of stress corrosion crack growth rate data for 7075-T6 available at the time [61] was examined. An equation for the growth rate ($da/dt$) as a function of $K$ was determined, and the time necessary for growth from initial to critical flaw size for given load conditions was determined by integrating the expression between the appropriate limits. This work was carried a step further [69] by incorporating into the crack growth equation a term accounting for simple intergranular corrosion, which, in the assumed model, precedes the rapid stress-accelerated corrosion stage. Further modifications to the formula incorporated the smooth-specimen stress-corrosion threshold stress and an initiation term.

This early work illustrated the need for more stress corrosion crack growth rate data as a function of stress intensity in several commonly encountered environments. It also illustrated the need for more data on the rates of intergranular attack since this mode of corrosion may precede the stress-accelerated form of cracking. Data of the type reported in Fig. 11 should be useful in this regard and should make analysis of the type just described both more quantitative and more accurate.

### 4.3 Effects of Environment

The environment has a most important effect on the nucleation and growth of subcritical cracks in high strength aluminum alloys. Actually measured crack velocities in a single alloy may range over more than nine orders of magnitude, depending solely on the environment that fills the crack [47]. One should, however, keep in mind that stress corrosion cracks are influenced not only by the environment but also by the microstructure of the alloy and by the crack-tip stress intensity.

#### Gaseous Environments

*Gaseous environments are among the most important ones to consider, since* obviously the use of high strength aluminum alloys in air is widespread.

**Hydrogen Gas.** Aluminum alloys do not appear to be embrittled to any appreciable extent by high-purity hydrogen gas at ambient temperature [70]. Tensile strength and ductility of alloys 6061-T6 and 7075-T73 are not substantially reduced when the test environment is changed from helium to hydrogen of 10,000-psi pressure, and the same is true for notched specimens of these alloys [71]. No loss in mechanical properties and no change in fracture behavior is observed when alloy 7039-T61 is tested in hydrogen up to 10,000 psi [72].

The effect of high-pressure, high-purity hydrogen gas on subcritical crack growth of aluminum alloy 2219-T6 was studied with surface-flawed, part-through-crack specimens [35], as outlined earlier in this chapter. The results of such tests are shown in Fig. 15. These results indicate that the threshold stress intensity factor ($K_{TH}$) for this alloy exposed to hydrogen gas at 5,200 psi was about 28 ksi $\sqrt{\text{in.}}$ for specimens from 0.75- and 1.00-in.-thick plates. Corresponding data for weld metal in welded specimens indicated that the threshold stress intensity was about 26 ksi $\sqrt{in.}$ for the hydrogen environment. Since these tests proved that base metal and weldments of 2219-T6E46 aluminum alloy retain their load-carrying capability in pressurized hydrogen gas at stress intensities of more than 80% of their respective fracture toughness values, the alloy was recommended for pressure vessels containing hydrogen gas [35].

Four of the most widely used high-strength aluminum alloys showed no crack growth when precracked, stressed to near $K_{Ic}$, and exposed to dry hydrogen for 47 days [46].

**Other Gases.** Stress corrosion cracking of high strength aluminum alloys in argon, nitrogen, oxygen, air, and hydrogen is generally characterized by the following rules [47]:

- Stress corrosion cracks do not initiate or propagate in dry gases.
- In humid gases, stress corrosion cracks initiate immediately from precracks stressed to near $K_{Ic}$.
- In gases of 100% relative humidity, crack growth occurs with a velocity of about $10^{-3}$ in/hr. in the stress-independent region II of the V-K curve of several commercial high strength aluminum alloys.
- The stress-dependent crack velocity in region I of the V-K curve is strongly influenced by the metallurgical parameters, with alloy 7079-T651 being the most susceptible, followed by 7039-T61, 7178-T651, and 7075-T651.

It has also been observed that the stress-independent stress corrosion crack velocity of alloy 7075-T651 is linearly dependent on the water vapor concentration in the air [47].

## Outdoor Exposure

Stress corrosion cracks in specimens exposed outdoors can be alternately filled with gases and liquids due to rainy and dry periods. V-K curves have been determined for all major high strength aluminum alloys [46,48,73]. Generally,

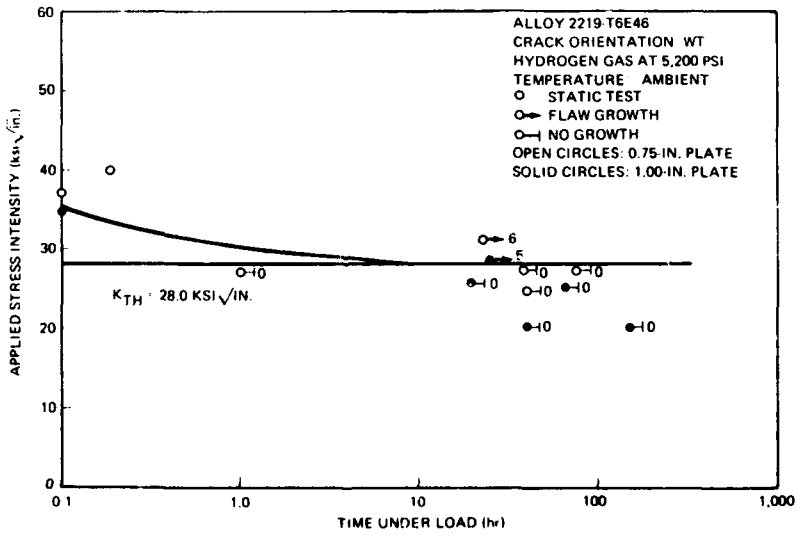


Fig. 15. Sustained-load flaw growth in pure hydrogen gas [35]. The numbers next to the points indicate the extent of crack growth in thousandths of an inch.

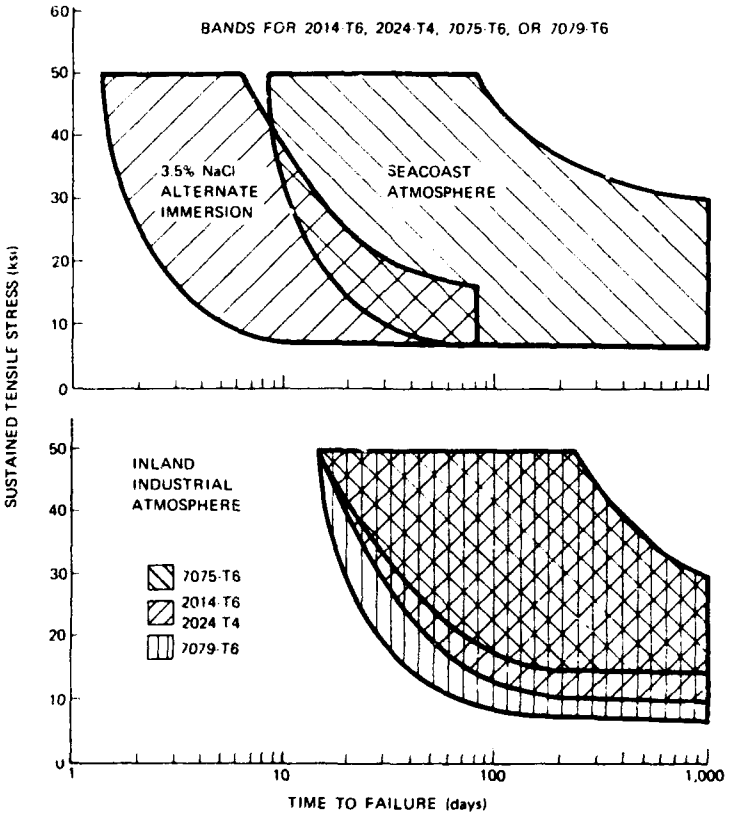


Fig. 16. Time to failure by stress corrosion of smooth specimens stressed in the short transverse direction and exposed to three different environments [42]. From *Metal Prog.* 81 (No. 4), Fig. 8, p. 85; copyright 1962 by the American Society for Metals. Used by permission.

the shape of V-K curves resembles the one in Fig. 11 and in most cases, the rules mentioned in the previous section apply.

Smooth SCC test specimens of many high strength aluminum alloys have been exposed in the stressed condition to both seacoast and inland atmospheres. Typical results are shown in Fig. 16 [42]. Note that in the seacoast atmosphere, all alloys listed seem to have the same smooth-specimen threshold stress of 7 ksi. However, in the inland industrial atmosphere, alloy 7079-T6 cracks not only fastest but also at the lowest stress levels. This is consistent with the results for precracked specimens [73] as well as with the service behavior of the alloy. A different kind of comparison of the SCC resistance of high strength aluminum alloys in various atmospheres is shown in Fig. 17; the probability of failure of smooth SCC tests specimens is compared for four different alloys in three different environments. Note the significant high percentage of failure of alloy

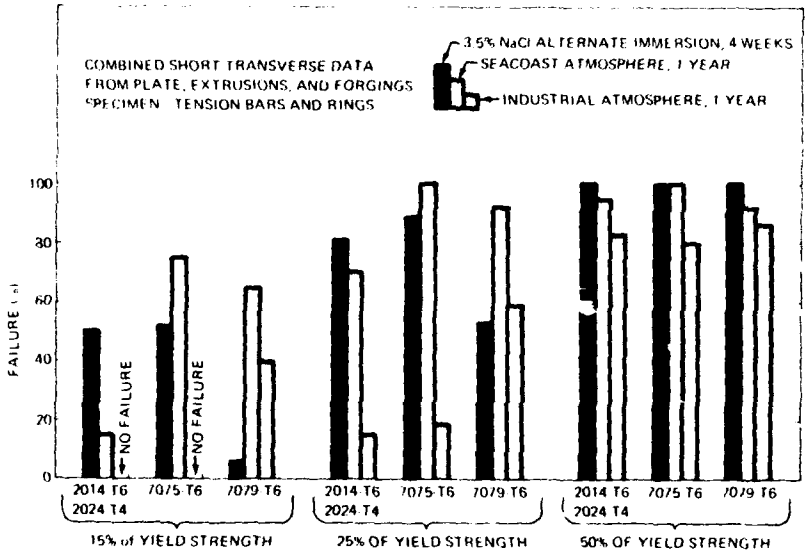


Fig. 17. Comparison of the probability of failure of smooth stress-corrosion-cracked specimens in several environments [42]. From *Metal Prog.* 81 (No. 4), p. 80, Fig. 4; copyright 1962 by American Society for Metals. Used by permission.

7079-T6 specimens in an industrial atmosphere when stressed to only 15% of their yield strength. If more attention is given to such data the incidence of SCC service failures in future designs can be greatly reduced. Unfortunately, the smooth-specimen threshold stress level from 3.5% NaCl alternate-immersion tests cannot always be relied upon to assess the SCC susceptibility of high strength aluminum alloys, and the results of such tests do not indicate any difference between many alloys when tested in the critical short transverse direction (see Table 2). Here is a clearcut case where the method of determining V-K curves using precracked specimens is not only cheaper and faster than other methods, but it also shows quantitatively just how much more susceptible than other alloys 7079-T6 really is as will be seen later in this chapter.

### Aqueous Solutions

Distilled water and most aqueous solutions can cause SCC of susceptible high strength aluminum alloys. For most alloys (e.g., alloy 7075-T651) the crack velocity is about the same in distilled water as in moist air. The few cations tested to date in aqueous solutions (i.e., $Li^+$, $Na^+$, $K^+$, $Rb^+$, $Cs^+$, $Ca^{++}$, $Al^{+++}$, $NH_4^+$) do not appear to have any specific effect on the growth of stress corrosion cracks, except that they influence the solubility product and thus can govern the concentration of specific anions. Among the anions tested so far,

only chloride, bromide, and iodide have been observed to accelerate the growth of stress corrosion cracks above and beyond the velocity measured in water. It has been shown that the stress-corrosion crack velocity in region II of the V-K curve of alloy 7079-T651 depends linearly on the halide ion concentration when concentrations of $2 \times 10^{-2}$ moles/liter are exceeded [46,73].

Time-to-failure tests can be used in some cases as a first approximation to indicate whether an environment will cause rapid failure of a part under stress. A summary of such TTF test results is given in Table 3 [60,74]. Note in Table 3 that for alloy 7075-T651, the shortest failure times are always measured in solutions containing chloride.

### Effect of Electrochemical Potential

The effect of an applied electrochemical potential on stress corrosion crack growth in high strength aluminum alloys has been studied in detail [46,73]. Some of the results can be summarized as follows:

- In *strongly acidic* aqueous halide solutions the stress corrosion crack velocity in region II of the V-K curve is *in*dependent of the applied electrochemical potential; i.e., cathodic protection against stress corrosion cracking in such solutions is impossible.
- In neutral aqueous halide solutions, there exists a potential range within which the crack velocity depends exponentially on the applied electrochemical potential, and can be markedly reduced by negative potentials. Thus, cathodic protection appears possible. The potential dependence of the crack velocity is further influenced by the halide ion concentration of the solution and the metallurgical parameters of the alloy.
- At very noble applied anodic potentials, the crack velocity is independent of potential, even in concentrated neutral aqueous halide solutions.

### Effect of pH

Qualitative studies of pH on stress corrosion cracking of high strength aluminum alloys abound. There is general agreement that the occurrence of SCC in chloride solutions is markedly reduced as the solution is made increasingly alkaline [55]. Sometimes it is possible to prevent SCC of aluminum alloys by restricting their application to an environment with a pH larger than a fixed minimum [75]. Acidifying the solution usually reduces the time to failure. Typical results for smooth specimens are shown in Fig. 18.

Quantitative studies of the crack growth rate as a function of stress intensity and pH in aqueous halide solutions [46,73] can be summarized as follows:

- Region II crack velocity is almost *in*dependent of pH between pH 1 and pH 11.
- Region I of the V-K curve is displaced to lower stress intensities when the pH is reduced to values smaller than 3.

## Table 3. Time to Failure by SCC of Aluminum Alloys in Various Aqueous Environments*

| Concentration | Solution | Nominal pH | Adjusted with | Median Failure Time, days[a] | | | | |
|---|---|---|---|---|---|---|---|---|
| | | | | 7075-T651 | 2219-T87 | 7039-T63 | 7075-T7351 | 2219-T87 |
| **Halide Ions** | | | | | | | | |
| 1 N | NaCl | 2 | HCl | 3 | 19 | No test | 18 NS | 54 NS |
| 1 N | NaCl | 7 | NaOH | 42 | 28 | 14 | | |
| 1 N | NaBr | 2 | HBr | 10 | | No test | | 99 NS |
| 1 N | NaBr | 7 | NaOH | >60 | | 9 | | |
| 1 N | NaI | 2 | HI | 12 | No test | No test | | 32 NS |
| 1 N | NaI | 7 | HI | | | 10 | | |
| 1 N | $KFH_2$ | 2 | | 34 | | No test | | |
| 1 N | NaF | 7 | HF | | | 19 | | |
| **Complex Anions** | | | | | | | | |
| 1 N | $NaNO_3$ | 2 | $HNO_3$ | | | No test | | |
| 1 N | $NaNO_3$ | 7 | NaOH | | | 60 | | |
| 1 N | $NaNO_3$ | 9 | NaOH | | | No test | No test | No test |
| 1 N | $Na_2CrO_4$ | 2 | $CrO_3$ | | | No test | | |
| 1 N | $Na_2CrO_4$ | 7 | $CrO_3$ | | | 60 | | |
| 1 N | $Na_2CrO_4$ | 9 | NaOH | 25 | | No test | No test | No test |
| 1 N | $Na_2SO_4$ | 2 | $H_2SO_4$ | 40 B | | No test | | |
| 1 N | $Na_2SO_4$ | 7 | NaOH | | | No test | | |
| 1 N | $Na_2SO_4$ | 9 | NaOH | | | No test | No test | No test |
| 0.5 N | $Na_2SO_4$ + 0.5 N $NaNO_3$ | 2 | $H_2SO_4$ | 56 Q | | No test | | |
| 0.5 N | $Na_2SO_4$ + 0.5 N $NaNO_3$ | 7 | NaOH | | | No test | No test | No test |
| 0.5 N | $Na_2SO_4$ + 0.5 N $Na_2CrO_4$ | 2 | $H_2SO_4$ | | >60 | No test | | |
| 0.5 N | $Na_2SO_4$ + 0.5 N $Na_2CrO_4$ | 7 | $H_2SO_4$ | | | No test | No test | No test |
| 1 N | $NaHCO_3$ | 9 | | | | No test | No test | No test |
| 1 N | $NaHSO_4$ | 1 | | 17 Q | | No test | 54 NS | |
| 1 N | $Na_2HPO_4$ | 9 | | | | No test | No test | No test |
| 1 N | $NaH_2PO_4$ | 4 | | | | No test | | |
| 1 N | $NaH_2PO_4$ | 4 | $H_2SO_4$ | | | No test | No test | No test |
| 1 N | $NaC_2H_3O_2$ | 4 | $CH_3COOH$ | 6 B | | No test | No test | No test |
| **Sodium Chloride + Oxidizing Acids** | | | | | | | | |
| 1 N | NaCl | 2 | $HNO_3$ | 1 | 7 | No test | 7 NS | 7 NS |
| 1 N | NaCl | 2 | $H_3PO_4$ | 1 | 8 | No test | No test | No test |
| 1 N | NaCl | 2 | $H_2SO_4$ | 1 | 8 | No test | 7 NS | 7 NS |
| 1 N | NaCl | 2 | $CrO_3$ | 60 | >60 | No test | 42 NS | 21 NS |
| 4 N | NaCl + 0.5 $KNO_3$ | 0.4 | $HNO_3$ | 1 | 1 | No test | 19 NS | 25 NS |
| **Sodium Chloride + Complex Anion** | | | | | | | | |
| 0.5 N | NaCl + 0.5 N $NaNO_3$ | 2 | $HNO_3$ | 8 | | No test | | |
| 0.5 N | NaCl + 0.5 N $NaNO_3$ | 7 | NaOH | 60 | | No test | | |
| 0.5 N | NaCl + 0.5 N $Na_2SO_4$ | 2 | $H_2SO_4$ | 2 Q | No test | No test | 4 NS | 5 NS |
| 0.5 N | NaCl + 0.5 N $Na_2SO_4$ | 7 | NaOH | 21 Q | 6 | No test | >60 NS | >60 NS |
| 0.5 N | NaCl + 0.5 N $Na_2CrO_4$ | 2 | HCl | 10 B | 1 | No test | 52 NS | 22 NS |
| 0.5 N | NaCl + 0.5 N $Na_2CrO_4$ | 7 | HCl | 26 | 33 | No test | | |
| **Ammonium Salts** | | | | | | | | |
| 1 N | $NH_4Cl$ | 7 | $NH_4OH$ | 15 | 24 | No test | 52 NS | |
| 1 N | $NH_4NO_3$ | 7 | $NH_4OH$ | | | No test | No test | No test |
| 1 N | $(NH_4)_2SO_4$ | 7 | $NH_4OH$ | | | No test | No test | No test |
| 1 N | $(NH_4)_2CrO_4$ | 7 | $CrO_3$ | | | No test | No test | No test |
| **Miscellaneous** | | | | | | | | |
| 1 N | NaCl + 10 ml 30% $H_2O_2$ | 5.8 | | 4 | 3 | No test | 27 NS | 6 NS |
| 1 N | NaCl + 1 N $AlCl_3$ | 2 | HCl | 4 | 16 | No test | 10 NS | 4 NS |
| 1 N | $Na_2SO_4$ + 10 ml 30% $H_2O_2$ | 5.8 | | 15 | >60 | No test | 31 NS | |
| 1 N | $Na_2SO_4$ + 1 N $Al_2(SO_4)_3$ | 2 | $H_2SO_4$ | >60 Q | | No test | | |

* Short transverse tensile specimens were stressed to 75% of their yield strength and exposed by continuous immersion at 80° to 85°F. Tests were terminated at the end of 60 days. Therefore, absence of failure does not necessarily indicate immunity to stress corrosion cracking particularly in the less corrosive solutions. Median failure times shown are for three specimens.

No failures after 60 days of testing.

B Borderline susceptibility to SCC.

Q SCC questionable because of high strength losses in unstressed and corroded specimens.

NS Failures not due to SCC.

[a] From Ref. 74.

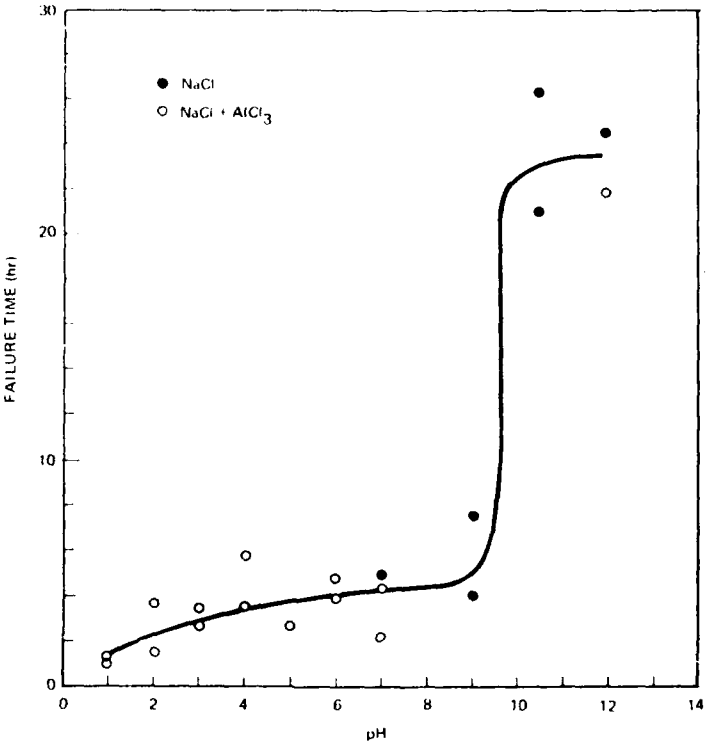


Fig. 18. Effect of pH on time to failure by SCC of aluminum alloy 7075-T6 [76].

• Region I of the V-K curve is not affected by variations of pH between 3.5 and 11.

The latter result may be related to the observation that the solution chemistry within a narrow crevice can be very different from the chemistry of the bulk solution [77]. Consider an aluminum alloy in a neutral 0.5 *M* NaCl solution. If the metal contains a crack filled with the solution, aluminum chloride is formed in the crack. The aluminum chloride can hydrolyze and acidify the medium. Theoretical calculations predict a pH of 3.5 in the crack under such conditions. Direct measurements of electrolyte from a narrow crevice yielded pH values of 3.2 to 3.4 [77].

### Effect of Temperature

For many years it has been known that higher temperatures can cause a decrease of the time to failure by stress corrosion of susceptible aluminum

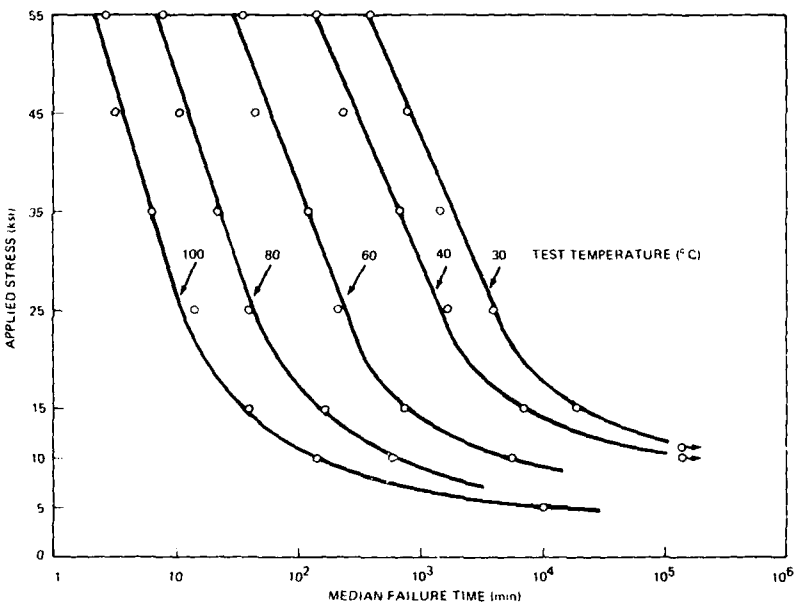


Fig. 19. Effect of stress and temperature on time to failure by SCC of alloy 7039-T64 [78]. From *Symposium on Stress Corrosion Testing*, Atlantic City, 1966, STP 425; copyright by the American Society for Testing and Materials. Used by permission.

alloys. Typical data are shown in Fig. 19. Extensive measurements of the effect of temperature on stress-corrosion crack velocity [46,73] can be summarized as follows:

- Stress-corrosion crack velocity in region I of the V-K curve of high strength aluminum alloys in concentrated aqueous halide solutions depends strongly on temperature with an apparent activation energy of 27 kcal/mole.
- Stress-corrosion crack velocity in region II of the V-K curve is not so strongly influenced by the temperature. A typical measured apparent activation energy is 4 kcal/mole.

### Effect of Solution Viscosity

The effect of the viscosity of a 2-*M* aqueous KI solution on the velocity of stress corrosion cracks in alloy 7079-T651 has recently been measured [46,73]. It appears that viscosity affects only the plateau of the V-K curve, and that region I crack growth is not influenced. Experimentally, a linear functional relationship has been found between the stress-independent crack velocity and the reciprocal solution viscosity.

### $HNO_3$ and Inhibited Red Fuming Nitric Acid

The few experimental data available on the effect of concentrated nitric acid (70.9%) on the growth of SCC cracks in alloy 7079-To51 indicate that the crack velocity is equal to or close to that measured in distilled water [46]. Smooth specimens of a number of high strength aluminum alloys were tested in hot (165° F) inhibited red fuming nitric acid (IRFNA) [79]. The results are illustrated in Fig. 20. Note that the highly stressed 7075-T7351 specimens that were resistant in 3.5% NaCl failed in the hot IRFNA, as did 7075-T651. Alloys 6061-T6, 2024-T851, and 2219-T87 apparently are resistant to SCC in IRFNA.

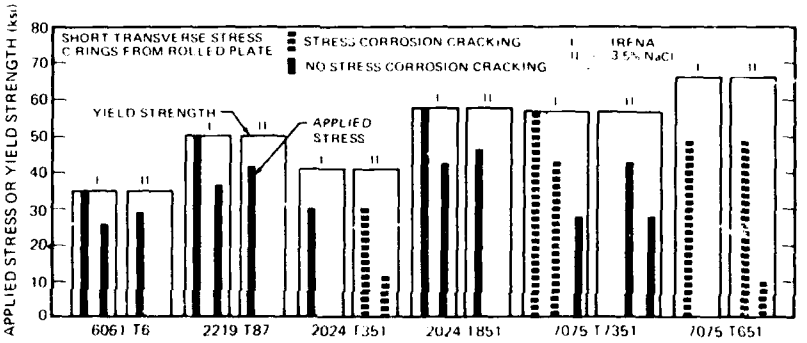


Fig. 20. Comparison of smooth-specimen resistance to SCC of various alloys in inhibited red fuming nitric acid at 165°F and in 3.5% NaCl alternate immersion [79]. From *Proceedings of Conference on Fundamental Aspects of Stress Corrosion Cracking*, 1969, p. 24, Fig. 1; copyright by the National Association of Corrosion Engineers. Used by permission.

### Nitrogen Tetroxide

Nitrogen tetroxide has been considered as an oxidizer in liquid fuel rocket propellants. However, certain high strength aluminum alloys are susceptible to environment-induced subcritical crack growth in $N_2O_4$ [36]. The effect of applied stress intensity on growth of surface flaws in alloy 2021 exposed to $N_2O_4$ is shown in Fig. 21 [36]. An apparent threshold is designated $K_{TH}$. The numbers next to the data points indicate the extent of crack growth in thousandths of an inch. It is apparent that subcritical crack growth occurs at stress intensities much lower than $K_{Ic}$. The fact that the threshold stress intensity $K_{TH}$ is only 10.0 ksi $\sqrt{\text{in.}}$ for alloy 2021-T81 is quite likely to create functional problems if the alloy is used to make pressurized $N_2O_4$ storage vessels.

### Organic Liquids

Stress corrosion cracking of high strength aluminum alloys in oil has been observed for some time, but only recently has the growth of stress corrosion

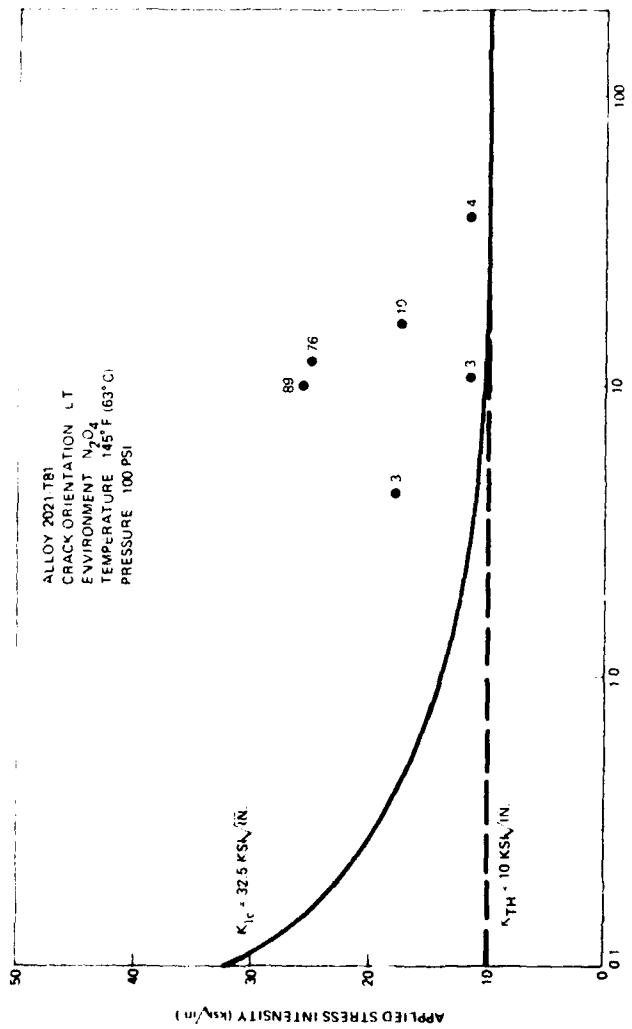


Fig. 21. Subcritical crack growth of an aluminum alloy in $N_2O_4$ [36]. The numbers next to the points indicate the extent of crack growth in thousandths of an inch.

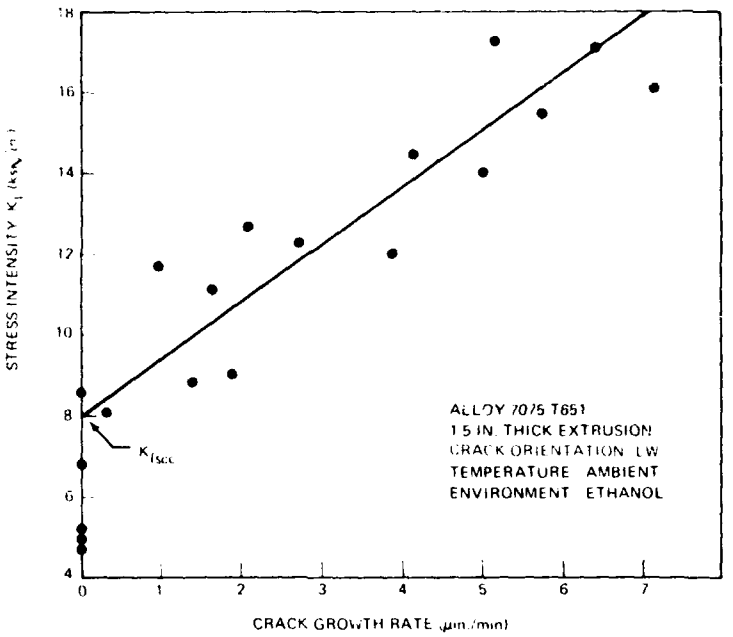


Fig. 22. Effect of stress intensity on stress-corrosion-crack growth rate of a high-strength aluminum alloy immersed in ethanol [80]. From *J. Mater.* **4** (No. 3), p. 747, Fig. 12; copyright 1969 by the American Society for Testing and Materials. Used by permission.

cracks been quantitatively studied as a function of crack-tip stress intensity in various organic liquids [46,80,81]. One of the first published results is shown in Fig. 22, where the crack growth rate of alloy 7075-T651 in ethanol is plotted as a function of the plane-strain crack-tip stress intensity. A linear relationship between crack velocity and stress intensity was reported for alloy 7075-T651 in both ethanol and carbon tetrachloride. From the intersection of the straight line with the stress axis, $K_{Iscc}$ was estimated to be 7 to 9 ksi $\sqrt{in.}$ in ethanol and 10 to 12 ksi $\sqrt{in.}$ in carbon tetrachloride [80]. It was thought that crack propagation was not due to traces of water in the organic liquids [80,81]. Note that these results were generated with cracks in the WL orientation and that the cracking mode was observed to be mixed transgranular and intergranular [81].

The velocities of stress corrosion cracks in the TL direction in alloy 7075-T651 immersed in flight fuel, engine oil, and two hydraulic fluids have recently been measured and were found to be very similar to the crack velocities in many other commercially available organic liquids and also similar to the stress-corrosion crack velocity in moist air of about 30% relative humidity [73].

### Liquid Metals

All high strength aluminum alloys are susceptible to intergranular liquid-metal embrittlement (LME). The following liquid metals have been found to embrittle aluminum alloys: Hg, Ga, Na, In, Sn, and Zn [82]. The effect of liquid mercury on subcritical crack growth of high strength aluminum alloys at room temperature has been intensively investigated. In contrast to the historical TTF test, the fracture mechanics approach allows quantitative measurement of crack-tip velocity as a function of crack-tip stress intensity. At high subcritical stress intensities, the LME crack growth rate in most high strength aluminum alloys is typically about $10^4$ in./hr. [73]. At very low stress intensities, the crack velocity is so strongly stress dependent that it is almost meaningful to speak of a threshold stress intensity $K_{I_{LME}}$ below which crack growth is not measureable. Typical $K_{I_{LME}}$ values of high strength aluminum alloys in mercury at ambient temperature scatter around 1 ksi $\sqrt{\text{in.}}$ [73].

## 4.4 Metallurgical Aspects and Alloy Development

### Aluminum-Magnesium Alloys (5000 Series)

Wrought, strain-hardened Al-Mg alloys are used because they combine corrosion resistance with good formability, weldability, and medium strength. Alloy compositions for several common 5000-series alloys are listed in Table 1. Mechanical, fracture, and corrosion properties are listed in Table 2.

**Temper Designations.** Commercial Al-Mg Alloys are strengthened primarily by strain hardening. A brief description of the symbols used to indicate the amount of strain hardening is given below.

Strain-hardened commercial alloys are identified by the letter H in their temper designation. The first digit following the H indicates whether the material has been strain hardened only (H1), strain hardened and then partially annealed (H2), or strain hardened and then stabilized (H3). The digit following H1, H2, or H3 indicates the final degree of strain hardening. These digits range from 0 (annealed) to 8 (full work-hardened, or about 75% reduction of area). The third digit, when used, indicates a variation of the two-digit H temper. For example, H323, H343, H116, and H117 apply to products specially fabricated to have acceptable resistance to SCC or exfoliation resistance. For more detailed information about temper designations, see Ref. 2.

**Microstructure and SCC.** Rapid cooling of Al-Mg alloys can result in a supersaturated solid solution. However, no appreciable precipitation hardening is observed with these alloys because the precipitation reaction is sluggish at room temperature. It is accelerated by deformation (cold work), by exposure to elevated temperatures, and by higher magnesium content. Each of these factors

plays an important role in determining the susceptibility to SCC of Al-Mg alloys. The effect of each of these variables on the susceptibility to SCC of Al-Mg alloys is illustrated in Figs. 23 through 26.

It has been thought that preferential precipitation along the grain boundary in the form of a continuous film causes susceptibility to SCC in 5000-series alloys. Consequently, two ways have been proposed to produce SCC-resistant microstructures: Keep the grain boundaries free of a continuous film of precipitates, or stimulate precipitation throughout the grains. The first approach is successful if the magnesium content of the alloys is limited to about 3%. In alloys of higher magnesium content, however, a network of continuous grain-boundary precipitates can develop during precipitation at ambient temperatures. To simulate long-time atmospheric temperature aging, a sensitizing treatment consisting of heating at 212°F for 7 days is often used. At ambient temperatures, it is not known how fast continuous networks will develop, but the probable time is from several years to as long as 50 years. However, under equal metallurgical and exposure conditions, it will take much longer to develop a network in an alloy with a low magnesium content (i.e., 5086 with 4.0% Mg) than in an alloy with a high magnesium content (i.e., 5456 with 5.1% Mg). To avoid SCC and especially exfoliation corrosion, this factor should be given

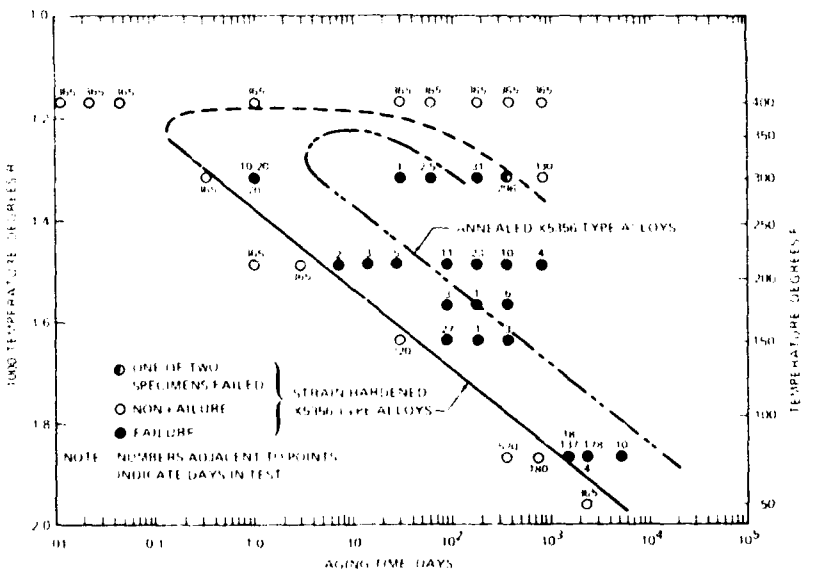


Fig. 23. Effects of time and temperature on sensitization to SCC in an Al-5.15%Mg-0.03% Cu-0.22%Fe-0.11%Si-0.11%Mn-0.10%Cr-0.10%Ti alloy. Data were obtained on simple beam specimens loaded to 75% of yield strength and exposed to the 3.5% NaCl alternate-immersion test [83]. From *Corrosion* **15**, p. 58t, Fig. 9; copyright 1959 by the National Association of Corrosion Engineers. Used by permission.

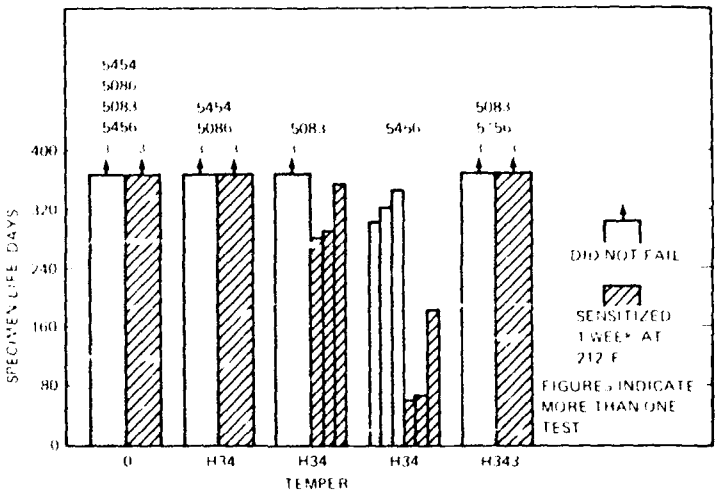


Fig. 24. Stress corrosion resistance of stressed preformed specimens of several alloys of Al-Mg-Mn alloy sheet (0.064 in.) exposed to 3.5% NaCl solution by alternate immersion. In the O temper, alloys with Mg content up to 5.5% (5456) exhibit an excellent resistance to SCC. Strain-hardened and stabilized tempers such as H34 have a low resistance when Mg content is in the 4.0 to 5.5% range, as in alloys 5083 and 5456. Special tempers such as H343 have been developed to provide a high resistance to SCC for the latter alloys [55].

serious consideration, and it should lead to a choice of 5086 over 5456 unless the extra strength of 5456 is needed [84]. (See also Fig. 24.)

Another method of achieving a SCC-resistant microstructure in Al-Mg alloys containing 4% to 8% magnesium has been described as follows [85]. After homogenizing in the $\alpha$ solid-solution region (800 to 1050°F), the alloys are hot rolled and annealed between 600 and 800°F to remove the effects of work hardening. After cooling, the supersaturated solid solution is cold worked at temperatures below 500°F, with a reduction in cross section of at least 20%. This cold-worked material is then subjected to thermal treatment to produce the extensive general precipitation of the $\beta$ phase required to improve resistance to SCC. This treatment consists of heating to a temperature between 400 to 525°F for a period of from 2 to 24 hr. Then, to achieve the desired strength, the material is cold worked, with a reduction in cross section of between 10 and 80%.

These and other treatments provide tempers with increased stress corrosion resistance. Examples are the H321, H323, H343, H116, and H117 tempers for Al-5%Mg alloys 5083 and 5456 [1,75,84,86,87].

**SCC and Exfoliation Corrosion in Commercial Al-Mg Alloys.** The authors are not aware of any service stress corrosion problems with Al-Mg alloys containing less than 3.5% magnesium. SCC in Al-5%Mg alloy rivets has occurred, however.

after exposure of the material to tropical temperatures [88]. The failures occurred at the junction of the shank and head, where the rivet had been severely cold worked during driving.

The stress corrosion crack growth in alloy 5456 in the more resistant H321 temper is very slow, but nevertheless the alloy is not immune to SCC [73]. This alloy is also susceptible to exfoliation and intergranular corrosion, as the Navy has experienced in a number of marine vessels where pitting, exfoliation, and intergranular corrosion occurred in the bilges and decks. The alloy 5086-H32 can also be susceptible to these forms of attack although its lower magnesium content makes it much less of a problem. To eliminate these problems with the H321 temper, two new tempers, designated H116 and H117 are recommended. These tempers apparently eliminate the continuous grain-boundary film of $Mg_5Al_8$. All production lots are examined metallographically and compared with standard photomicrographs to verify that each lot has a microstructure that is predominately free of a continuous grain-boundary network of Al-Mg precipitate [84].

In addition to metallographic examination techniques, accelerated-corrosion tests for determining susceptibility to exfoliation corrosion in 5000-series alloys

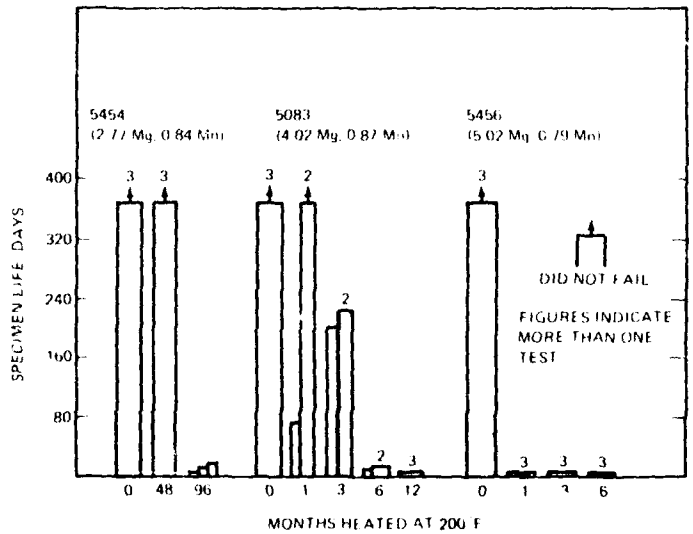


Fig. 25. Effect of heating on resistance to SCC of stressed, preformed specimens of Al-Mg-Mn alloy sheet (0.064 in.) exposed to 3.5% NaCl solution by alternate immersion. Strip specimens of O temper sheet were plastically deformed at room temperature prior to the 200°F exposure. Only the lower-magnesium-content alloy 5454 maintained a high resistance to SCC after prolonged heating at 200°F [55]. From *Proceedings of Conference on Fundamental Aspects of Stress Corrosion Cracking*, 1969, p. 476, Fig. 10; copyright by the National Association of Corrosion Engineers. Used by permission.

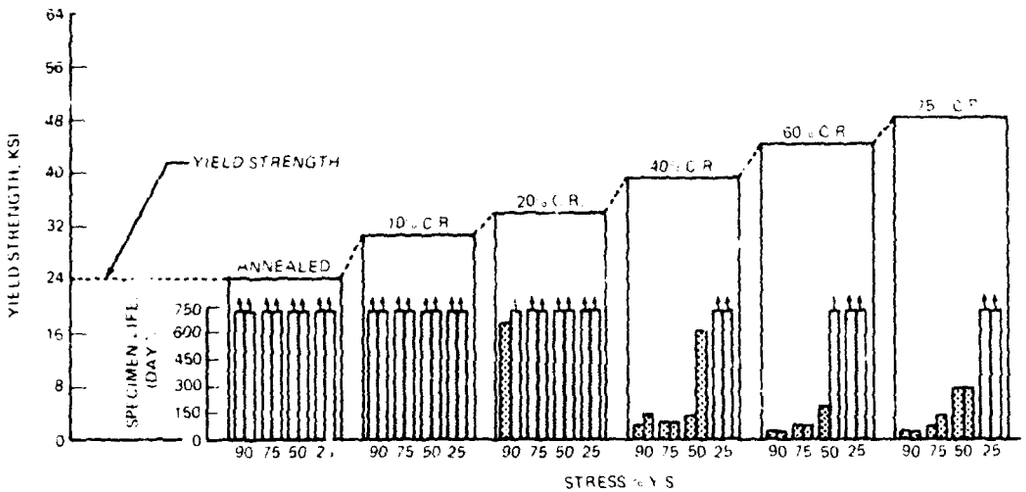


Fig. 26. Effect of cold reduction on yield strength and stress corrosion resistance of Al-5.1% Mg-0.1% Mn-0.1% Cr-0.09% Cu alloy sheet (0.064 in.) exposed 1 week at 212°F. Sheet specimens were stressed by bending in constant deformation fixtures and exposed to 3.5% NaCl solution by alternate immersion. Bar graphs represent lives of individual specimens [55]. From *Proceedings of Conference on Fundamental Aspects of Stress Corrosion Cracking*, 1969, p. 476, Fig. 9; copyright by the National Association of Corrosion Engineers. Used by permission.

have recently been developed [89-91]. One method, designated the seawater acetic acid test (SWAAT), involves a week-long exposure in an acidified salt fog at 120°F. The test cycle involves 30 min of continuous spraying followed by 90 min with the spray off [90]. This test has recently been adopted upon recommendation of the Aluminum Association as a method of predicting exfoliation corrosion resistance in the Al-Mg alloys for boat and ship hull construction [90, 92].

Another accelerated test for exfoliation and intergranular corrosion susceptibility under consideration for incorporation in future specifications involves total immersion of the alloy for 24 hr in a solution of 1 *M* ammonium chloride, 0.25 *M* ammonium nitrate, 0.01 *M* ammonium tartrate, and 3g/liter hydrogen peroxide maintained at 150°F [91]. This test, designated the ASSET immersion test, is somewhat simpler to perform than the SWAAT test and requires a considerably shorter test period. Materials showing exfoliation or intergranular attack in either of these tests are considered unacceptable for boat or ship hull construction [90,92].

**5000-Series Alloy Development.** X5090 is a recently developed Al-7%Mg strain-hardened and stabilized alloy. The composition limits for this alloy are shown in Table 1. As noted earlier, cold-rolled and stabilized tempers of Al-Mg alloys with magnesium contents above 5% usually are extremely susceptible to SCC. This problem apparently has been overcome with the X5090 alloy, which was developed specifically to provide an alloy with the improved strength afforded by a magnesium content greater than 5% and a high resistance to SCC in the temper rolled and stabilized conditions. Processing techniques for this alloy are still proprietary, and the only known difference between X5090 and other Al-$Mg$ alloys besides its higher magnesium content is the addition of small amounts of beryllium and boron (Table 1).

The corrosion and stress corrosion resistance of X5090 are being determined using two techniques. One method involves exposing preformed long transverse U-bend specimens to a marine atmosphere. To date, specimens of X5090 in about the H34 temper have been exposed more than 5 years in this atmosphere without failure. Other specimens in the H36 and H38 temper have been exposed for nearly 3 years without failure [93].

During the development of X5090, an accelerated laboratory test for stress corrosion susceptibility was also developed. In this test, long transverse tension specimens are deadweight loaded to 80% of their 0.2% yield stress and exposed to an aqueous 7%NaCl + 0.006 *M* $NaHCO_3$ solution. During testing, an external anodic current is applied. An empirical correlation between the life of the specimen in the anodic tensile stress corrosion test and the life of U-bend specimens exposed to the marine atmosphere has been observed and is shown in Fig. 27. On the basis of this correlation, it has been concluded that material with an anodic tensile life greater than 13 to 15 hr will not fail when exposed to the marine atmosphere, and therefore it has excellent, practical stress corrosion

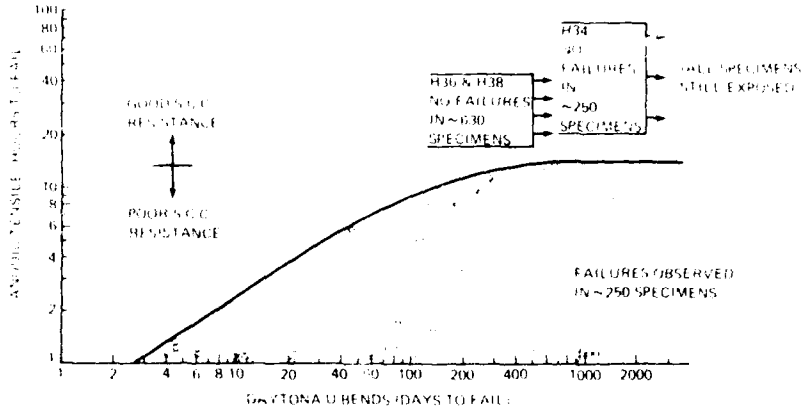


Fig. 27. Accelerated anodic tensile life vs marine-atmosphere exposure life of U-bend specimens of alloy X5090 [93]. From *Corrosion Performance of MRL-A8*, Report MRL-70-PR-17, Feb. 19, 1970; copyright by the Olin Metals Research Laboratories. Used by permission.

resistance [93]. The X5090 alloy in the H38 temper typically has an anodic tensile life of 20 to 25 hr, while less strain-hardened tempers show correspondingly longer lives. In actual practice, production lots of X5090 are evaluated using the anodic tensile test [93].

In addition to excellent stress corrosion resistance, X5090 apparently also possesses excellent resistance to general and localized corrosion, including pitting and exfoliation. Five-year test results from a 20-year test program being conducted in a marine atmosphere have been reported [93]. These results indicate that X5090 exhibits pitting resistance equal or superior to that of 5086-0 and 5086-H34, which are known to possess excellent resistance to pitting corrosion. Whereas bare 2024-T3 and 7075-T6 test panels have shown typical exfoliation corrosion, X5090 has been found to be essentially resistant to marine atmospheric exfoliation corrosion after 5 years' exposure.

To more fully characterize X5090, test data in several other areas are required. These include

- Low-temperature mechanical and fracture properties
- Corrosion characteristics in industrial atmospheres
- Corrosion characteristics after various exposure times at several elevated temperatures that may be encountered in service or during assembly (adhesive bonding cycles)
- Fatigue-crack growth rate properties in various environments
- Fatigue tests of built-up structural panels to determine whether the smooth fatigue properties adequately reflect actual performance in structural applications

### Aluminum-Magnesium-Silicon Alloys (6000 Series)

Alloys of the 6000 series are used in applications requiring intermediate strength and a high resistance to corrosion and SCC. Alloy compositions for several common 6000-series alloys are listed in Table 1. Mechanical, fracture, and corrosion properties are listed in Table 2.

Commercial alloys based on the ternary system Al-Mg-Si (6000 series) are strengthened by precipitation hardening.

Although the Al-Mg-Si alloys are highly resistant to corrosion and to SCC [55,94], certain abnormal thermal treatments can make these alloys susceptible to SCC in the naturally aged T4 condition. This occurs when a high solution-heat-treating temperature is used, followed by a slow quench [55,95]. Even in this condition, SCC on transverse 6061-T4 specimens has occurred only on highly stressed, plastically deformed (preformed) specimens and not on tensile-type specimens stressed to 75% of the yield strength. Aging the slowly quenched 6061-T4 material to the T6 temper eliminates the SCC tendency [55].

### Aluminum-Copper-Magnesium Alloys (2000 Series)

Al-Cu-Mg alloys were the first heat-treatable, high strength aluminum alloys and today they are still among the most popular and useful. Chemical compositions for the most widely used commercial 2000-series alloys are listed in Table 1. Mechanical, fracture, and corrosion properties are given in Table 2.

Al-Cu and Al-Cu-Mg alloys derive their high strength from precipitation hardening. This is achieved by solution heat treatment, followed by rapid cooling and either natural aging at room temperature (T4 temper) or artificial aging at intermediate temperatures (T6 temper). Cold working after the quench further increases strength, resulting in the T3 temper and when artificially aged, the T8 temper.

**Susceptibility to SCC.** In the naturally aged T3 and T4 tempers, 2000-series alloys such as 2024, 2014, and 2219 are highly susceptible to SCC in the short transverse direction (Table 2). Even in the artificially aged T6 temper, 2014 is susceptible. Examples for in-service SCC of these alloys attesting to this susceptibility can be found in recent literature [54,96]. For example, SCC of machined 2024-T4 parts has occurred fairly recently on the Saturn V Apollo moon rocket.

Typical V-K curves for these three alloys are shown in Fig. 28. Cracking in both regions I and II (defined earlier) is apparent. Similar V-K curves for the naturally aged 2024 and 2219 alloys and the artificially aged 2014-T6 alloy agree well with the fact that all these alloys have similar low stress corrosion resistance based on TTF data (Table 2 and Fig. 16). In addition, the survival rate data in Fig. 17 show that 2014-T6 and 2024-T4 have similar low resistance when stressed in the short transverse direction.

Data for alloy RR 58 (2618) are shown in Fig. 29. The high apparent $K_{Iscc}$ value is in line with the high smooth-specimen threshold stress reported for this

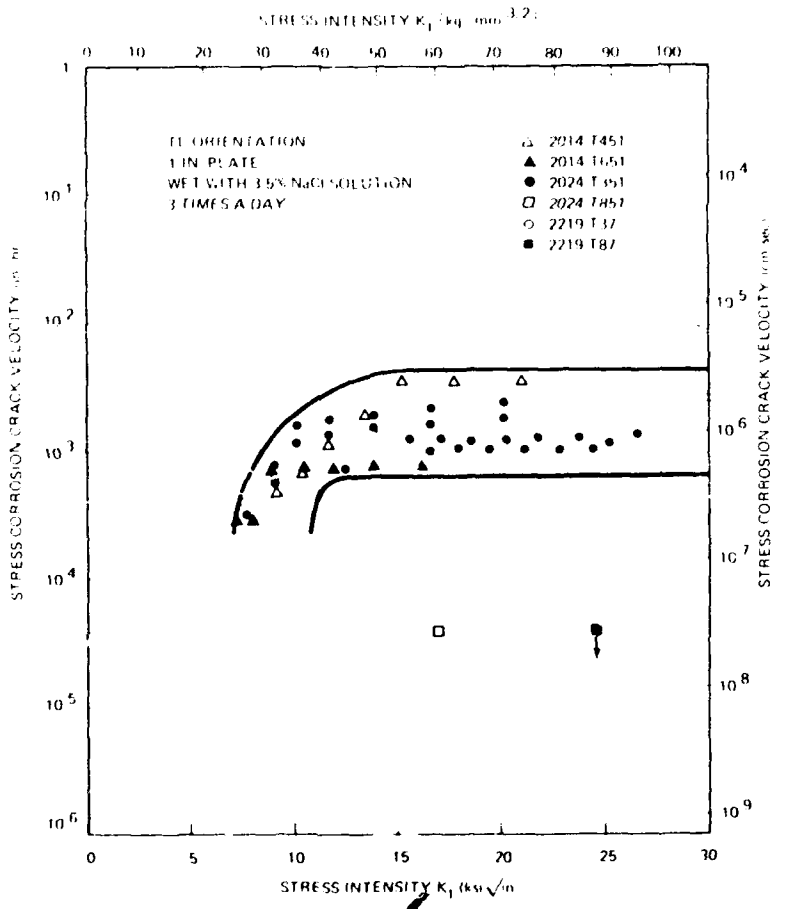


Fig. 28. Typical V-K curves for some 2000-series alloys obtained using TR DCB stress corrosion specimens.

alloy (Table 2). The fact that the maximum growth rates reported for RR.58 (Fig. 29) are nearly an order of magnitude greater than those of the susceptible alloys 2024-T3, 2014-T6, and 2219-T37 (Fig. 28) is somewhat surprising.

**Effects of Quench Rate.** The effect of quench rate on susceptibility to stress corrosion and intergranular corrosion is illustrated in Fig. 30. Note that at quench rates faster than a certain limit (which depends on alloy composition) no susceptibility to SCC is found. At slower quench rates, SCC and intercrystalline corrosion may occur. It appears that Al-Cu and Al-Cu-Mg alloys can indeed be susceptible to SCC even if they are not susceptible to intergranular corrosion in a $NaCl$-$H_2O_2$ solution.

The significant effects of quench rate on susceptibility to intergranular attack (as well as SCC and exfoliation corrosion) in 2024-T3 and T4 products mean that in thickness ranges where quench rates cannot be kept above about 1000°F/sec, severe intergranular corrosion problems may occur in service. Thus, it is recommended that 2024 products thicker than about 0.25 in. should be used only in the artificially aged tempers (T6X and T8X) [99] unless adequate surface protection can be provided.

**Effects of Artificial Aging.** During artificial aging of alloys like 2024, susceptibility to corrosion and stress corrosion initially increases, reaches a maximum,

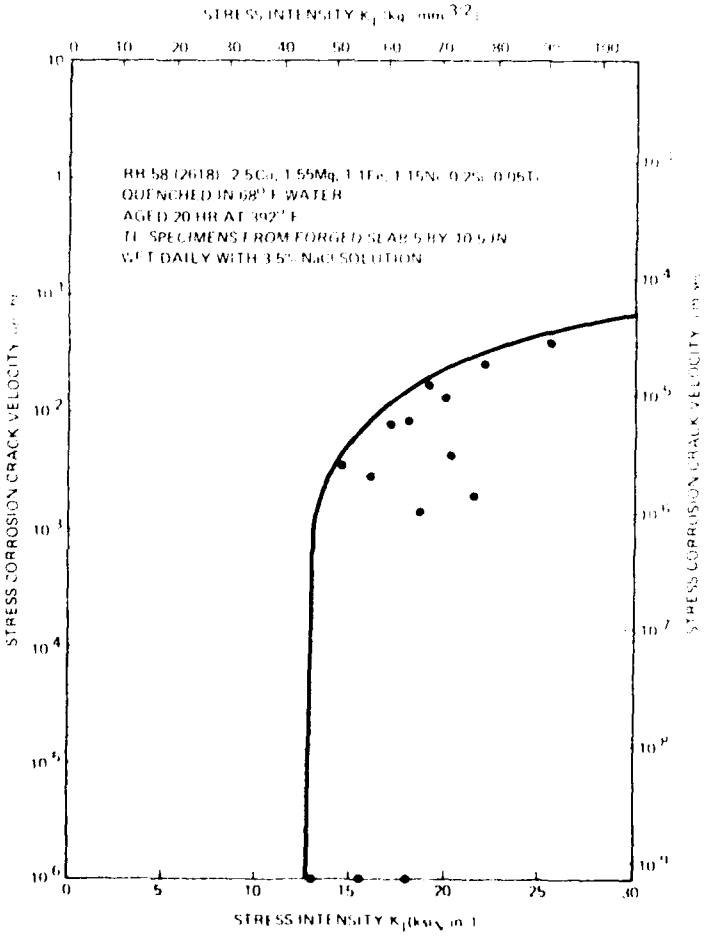


Fig. 29. V-K data for alloy RR 58 (2618-T6) [97]

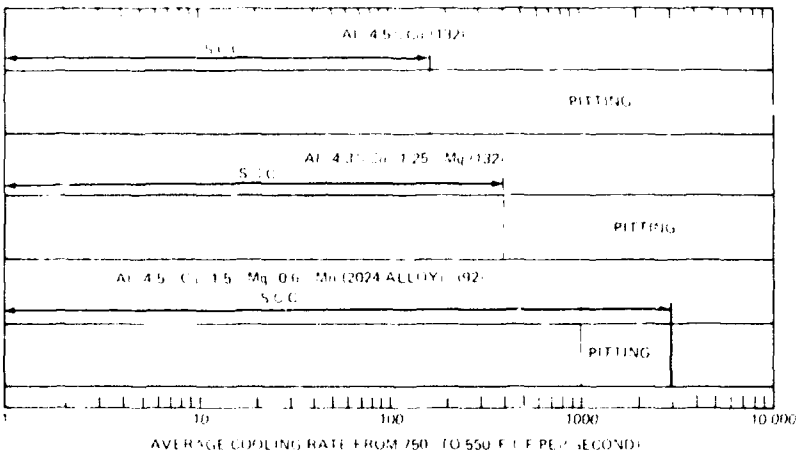


Fig. 30. Effect of quenching rate on susceptibility to intergranular corrosion and SCC for some 2000-series alloys [55,79,98]. From *Proceedings of Conference on Fundamental Aspects of Stress Corrosion Cracking*, 1969, p. 484, Fig. 23; copyright by the National Association of Corrosion Engineers. Used by permission.

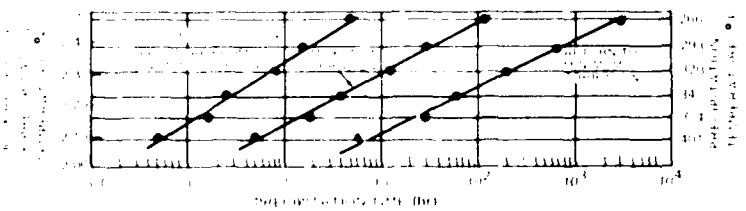

Fig. 31. Effect of temperature on the time required for sensitization to stress corrosion of 0.057-in.-thick 2024-T3 sheet [100].

and then decreases. The higher the temperature, the shorter the time required for sensitization. Figure 31 summarizes data obtain over a range of temperatures [100]. These data are of interest since it is often necessary to subject 2024-T3 to medium temperatures (around 250°F) during curing of certain adhesively bonded structures. In addition, temperatures around 250°F are near the skin stagnation temperature of aircraft operating at Mach 2. At 266°F the alloy becomes susceptible to intergranular attack after only about 5 hr of exposure. Thus, if temperatures of 266°F were to be encountered during 2024-T3 processing, strict controls on allowable exposure times would have to be made to ensure against sensitization to intergranular attack.

**Determining Susceptibility to Intergranular Attack and SCC Resistance.** An electrochemical test has recently been developed for predicting the stress corro-

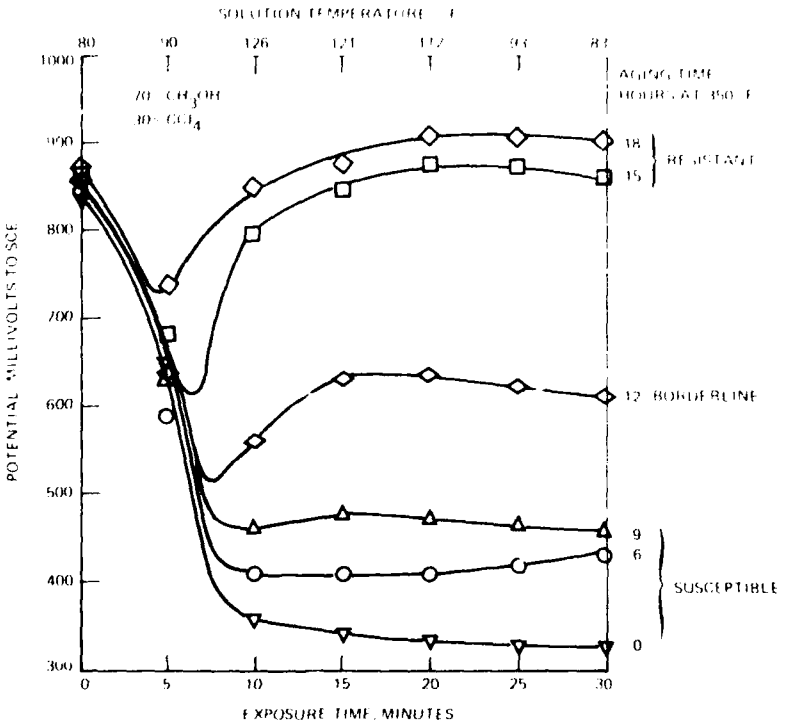


Fig. 32. Time-potential curves in $CH_3OH$-$CCl_4$ solution for 2219-T351 plate aged for various periods at 350°F up to the T851 temper (18 hr at 350°F) [101]. From *Corrosion* **25**, p. 202, Fig. 4; copyright 1969 by the National Association of Corrosion Engineers. Used by permission.

sion performance of 2219 alloy products in the T851 and T87 tempers [101]. The test offers an attractive possibility of evaluating the performance of 2219 products quickly as an alternate or supplement to the conventional 30-day alternate-immersion test in 3.5% sodium chloride solution. The test can be completed in less than 1 hr and requires only a simple measurement of solution potential of an unstressed specimen in a mixture of absolute methyl alcohol and carbon tetrachloride. Typical potential vs time data for 2219 specimens in the T351 to T851 temper range aged for various periods at 350°F are shown in Fig. 32. Note the large difference in potential (over 200 mV) that this test provides between borderline and resistant material after potentials have stabilized.

Recently, a rapid test method for determining the resistance to exfoliation corrosion was developed by ASTM Task Group G01.05.02-T.G.8. This test method is applicable to Al-Cu (2000-series) and Al-Zn-Mg-Cu (7000-series) alloys. The test, designated EXCO test, specifies total immersion of freshly etched specimens in a solution of the following composition:

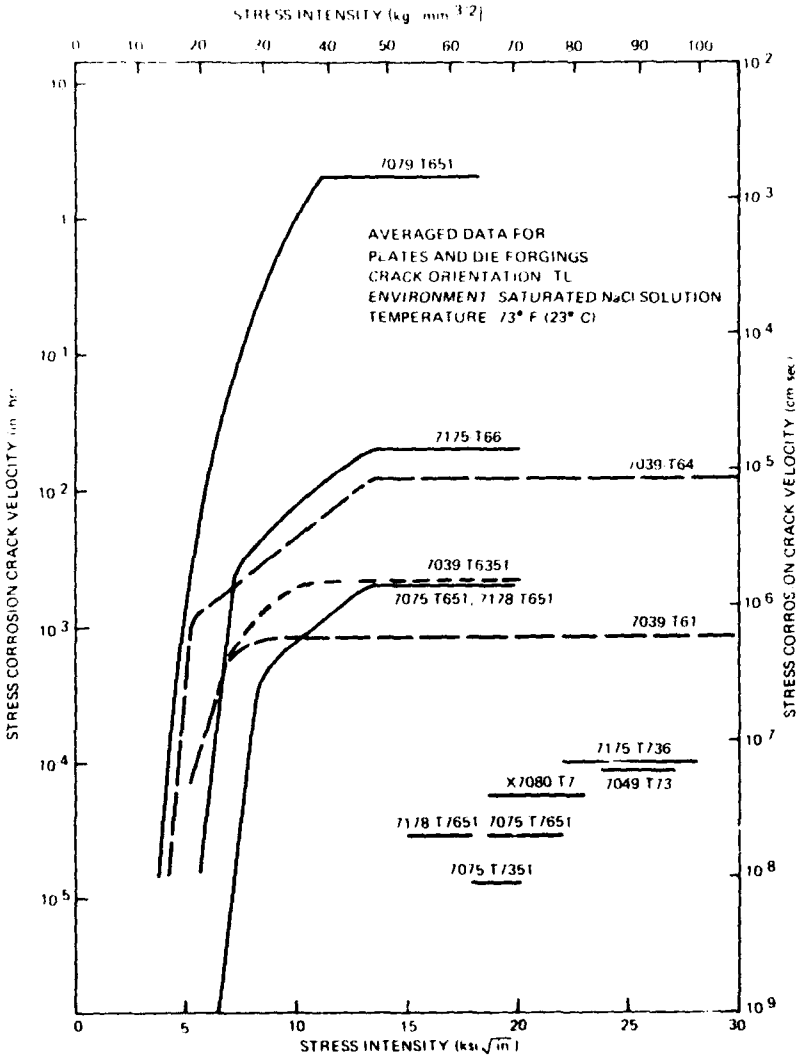


Fig. 33. Effect of stress intensity on stress corrosion crack velocity for several high-strength aluminum alloys immersed in saturated aqueous NaCl solutions.

4.0*N* NaCl + 0.5*N* $KNO_3$ + 0.1*N* $HNO_3$.

Testing times required are 48 hr for 7000-series alloys and 96 hr for 2000-series alloys. Specimens having a high resistance to exfoliation should show no visible blistering or delamination after this test.

### Aluminum-Zinc-Magnesium and Aluminum-Zinc-Magnesium-Copper Alloys (7000 Series)

The precipitation-hardened 7000-series alloys are used in applications requiring the highest strengths. Composition limits for this series of alloys are shown in Table 1. Mechanical, fracture, and corrosion properties are listed in Table 2.

**Susceptibility to SCC.** The stress corrosion properties of most of the 7000-series alloys in the short transverse directon are now quantitatively known. Figure 33 shows stress-corrosion crack velocity as a function of crack-tip stress intensity for these alloys. These data, together with the stress corrosion properties given in Table 2, can be used to quantitatively rate the stress corrosion performance of the various 7000-series alloys.

Note the inferior stress corrosion resistance of the low-copper-content alloys 7079-T651 and 7039-T61 and T64. Note also that alloy 7079-T651 shows by far the highest stress corrosion crack velocity of the commercial 7000-series alloys at all stress intensities. This is consistent with the fact that the majority of service SCC failures have occurred with this alloy. Such large differences in performance between the various 7000-series alloys in the T6 temper are not reflected in the SCC threshold data from smooth-specimen TTF tests. The poor service performance of 7079-T6 could, however, be anticipated from the survival data shown earlier in Fig. 17. These low survival rates [42] and, more important, the newer quantitative stress corrosion results (Fig. 33) and actual service experience itself, dictate that alloy 7079-T6 be eliminated from future use where there is any possibility of sustained applied or residual tensile stresses in the short transverse direction. Other alloys with good strength in thick sections and better stress corrosion resistance should be used in its place. Such alloys are now available or under development, as outlined below.

**Effects of Quenching Rate.** The rate of cooling from the solution treatment temperature through a critical temperature range (750 to 550°F), has a pronounced effect on both the resistance to corrosion and the characteristics of the corrosive attack for copper-bearing 7000-series alloys like 7075-T6. The effect of quenching rate on the mechanical properties and type and extent of corrosion in long transverse 7075-T6 sheet specimens is shown in Fig. 34. Rapid cooling produced immunity to intergranular corrosion and to SCC; cooling rates greater than about 200°F/sec also produced maximum tensile properties. Decreasing the cooling rate to about 40°F/sec results in the formation of coarse precipitates of

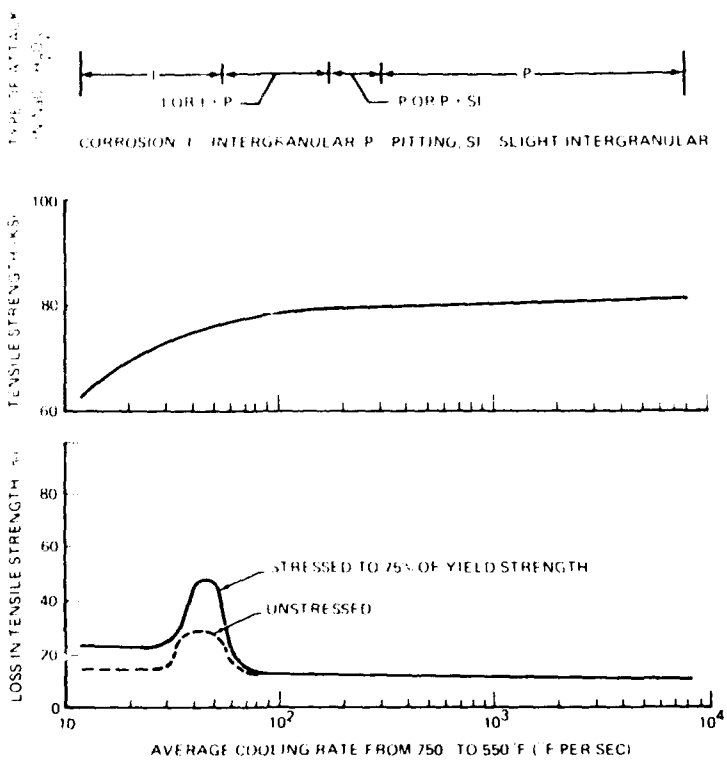


Fig. 34. Effects of quenching rate on tensile properties and corrosion resistance of 7075-T6 sheet. Stressed and unstressed specimens were exposed to alternate immersion in 3.5% NaCl solution for 12 weeks before testing [102].

$\eta'$ or $\eta$ phase in the matrix and in the grain boundaries resulting in a marked reduction in strength and a high degree of susceptibility to intergranular attack and SCC [55]. Further decreases in cooling rate nearly eliminate susceptibility to SCC but result in drastic strength losses.

It should be noted that the beneficial effects of high quenching rates mentioned above for 7075-T6 sheet are relatively insignificant for plate and other products thick enough to permit stressing in the short transverse direction relative to the grains. Thus, even drastically quenched (>1000°F/sec) short transverse specimens of 7075-T6 machined from 2-in.-thick plate stress corrosion crack in sodium chloride solution at stresses as low as 11 ksi even though they are not susceptible to intergranular attack in the absence of applied stress [55]. In fact, it has been found that such specimens are not appreciably more resistant than similar specimens quenched at rates slow enough that they are susceptible to intergranular attack in the absence of stress [55].

For copper-free 7000-series alloys, the behavior is generally opposite to that just described and resistance to SCC in sodium chloride solutions is favored by a low cooling rate, as by cooling in air [103,104].

**Effects of Overaging.** As shown in the preceding section, all high strength 7000-series alloys are susceptible to SCC when aged to peak hardness (T6 temper) and stressed in the short transverse direction. Furthermore, composition changes cannot increase appreciably the stress corrosion resistance in the short transverse direction. As in the case of the 2000-series alloys, the only effective means of improving short transverse SCC resistance in 7000-series alloys is by artificial aging at fairly high temperatures (325° to 350°F). The relationship generally found between precipitation hardening and resistance to SCC is illustrated in Fig. 35. Note that during aging, the minimum resistance to SCC is reached before peak hardness is achieved. Overaging beyond peak hardness improves resistance to SCC.

Over the past few years, a number of commercial overaging heat treatments have been developed for several high strength 7000-series alloys [10,14,106, 107]. The T76 tempers for 7075 and 7178 were developed primarily to improve resistance to exfoliation corrosion. A new and rapid method for testing resistance to exfoliation corrosion for these alloys (EXCO test) has been described earlier. In addition, exfoliation and stress corrosion resistance of 7178-776 and 7075-T76 have been estimated based on the measurement of solution potentials in methyl alcohol-carbon tetrachloride solutions [108]. The test procedures and solutions are similar to those discussed earlier for 2219; again the test requires less than an hour. Test results are shown in Figs. 36 and 37. Note that alloys

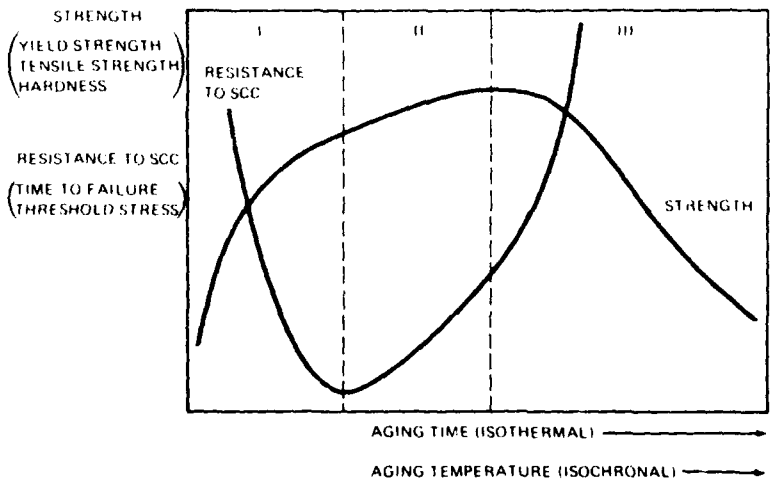


**Fig. 35. Relationship between strength and stress corrosion resistance during aging of high-strength, 7000-series alloys [105].**

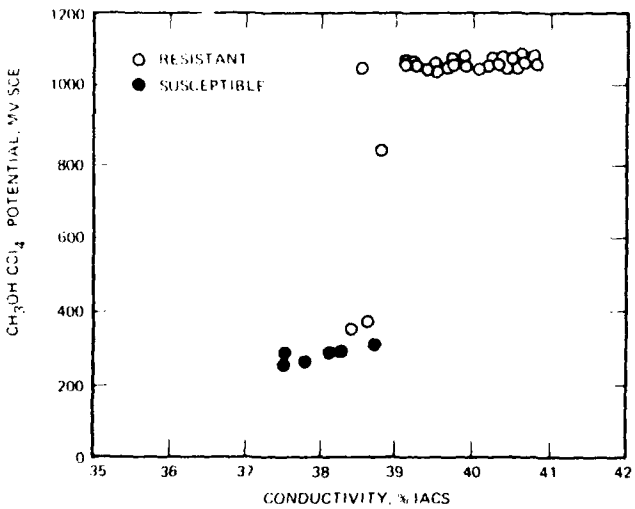


Fig. 36. Comparison of the ability of electrical conductivity and $CH_3OH$-$CCl_4$ potential to distinguish between the exfoliation-resistant and susceptible conditions of 36 production lots of 7178-T76 sheet [108]. From *Corrosion* **26**, p. 116, Fig. 11; copyright 1970 by the National Association of Corrosion Engineers. *Used by permission.*

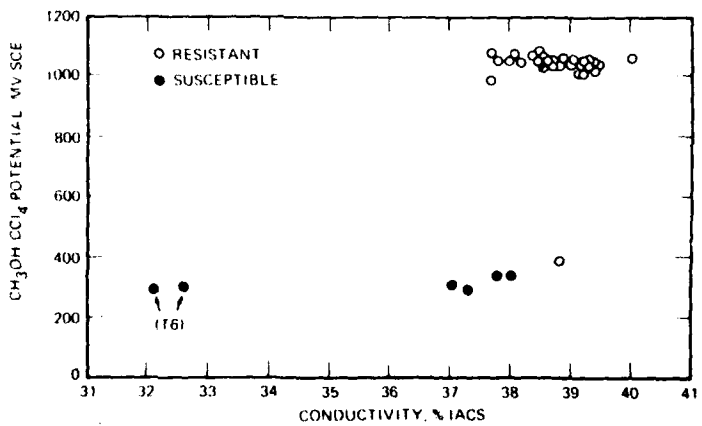


Fig. 37. Comparison of the ability of electrical conductivity and $CH_3OH$-$CCl_4$ potential to distinguish between the exfoliation-resistant and susceptible conditions of 31 production lots of 7075-T76 sheet and plate and four experimentally aged lots of 0.6-in. 7075-T76 plate [108]. From *Corrosion* **25**, p. 116, Fig. 12; copyright 1970 by the National Association of Corrosion Engineers. Used by permission.

exhibiting MeOH/$CCl_4$ potentials less than about −400 mV vs SCE are always found to be exfoliation resistant, while electrical conductivity values greater than 38% IACS do not always ensure that the product is resistant. It is not yet known whether this test can be applied to extrusions and other products.

The T73 heat treatment for 7075 provides a high degree of stress corrosion resistance, regardless of minor deviations in the heat-treatment practice. A drawback of the T73 temper, however, is the loss of strength of about 14% compared to the T6 temper.

Verification of the T73 temper for 7075 is usually accomplished using hardness and electrical conductivity data [109]. The methyl alcohol-carbon tetrachloride solution potential test is also being evaluated as a method for verifying the T73 temper for 7075 [108]. Through careful control of heat-treating variables and other processes, a T736 temper for alloys 7175 and 7075 has been developed that provides strengths equivalent to those of 7075-T6 and stress corrosion resistance intermediate between that of the T76 and T73 tempers [7, 14,10]. Other partially overaged alloy-temper combinations providing improved exfoliation and stress corrosion resistance are 7001-T75 and X7475-T761. Specific properties for these alloys and tempers can be found in Table 2 and Fig. 33.

It should be noted that for alloys with low copper content, such as 7039 and 7007, overaging treatments are not nearly so effective as they are for other 7000-series alloys. Alloys with low copper content can be artificially aged to have a high resistance to SCC in the longitudinal and long transverse directions, but they are still highly susceptible in the short transverse direction [55].

Other overaged intermediate-copper-content alloys such as X7080-T7 have presented additional problems in that the threshold stresses developed after lengthy exposures to industrial environments (3 years or more) are lower than those determined from the standard 3.5% NaCl alternate-immersion test. Thus, this boiling-water-quenchable, thick-section-forging alloy initially showed an adequate threshold stress in alternate-immersion tests of 25 ksi which later had to be lowered to 15 ksi based on industrial environment tests [110]. Since these data were published, X7080-T7 has essentially been removed from the list of candidate thick-section, high strength, SCC resistant alloys.

Improved resistance to SCC through overaging is accompanied by a loss in strength. It has been the goal of several recent research projects to achieve a high degree of stress corrosion resistance without incurring significant strength losses. One technique aimed at achieving this goal has been through the addition of small amounts of silver to these alloys.

**Silver Additions.** The effects of silver have been extensively investigated because it was reported that silver additions increased the maximum strength attainable by Al-Zn-Mg-Cu alloys that were aged above 250°F [111-120] and because silver reportedly increased the lifetime of smooth specimens tested in accelerated stress corrosion tests [121,122]. Others [123] also reported that silver-bearing alloys aged above 300°F had higher resistance to short transverse

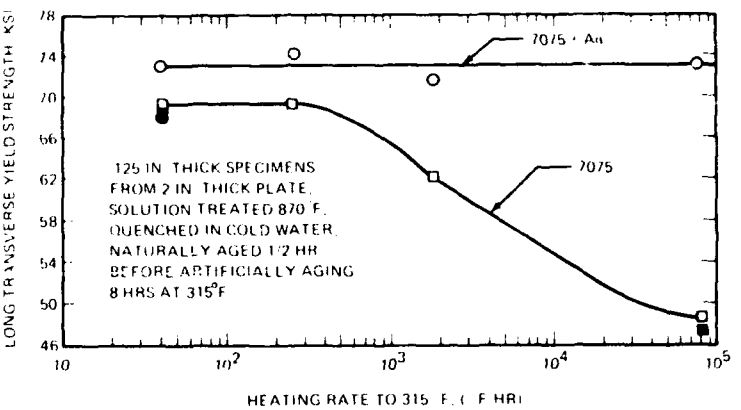


Fig. 38. Effect of rate of heating to the artificial aging temperature on the yield strength of 7075 and 7075 + 0.3% Ag [110].

SCC than similar silver-free material aged below 300°F. As a result of this work, at least one 7075-type alloy containing silver is available commercially (the German alloy AZ74.61). Other alloys containing silver are currently under development [124].

However, many of the workers investigating silver additions have found no significant increases in strength or stress corrosion resistance in overaged alloys due to the presence of this element [55,110,125,126]. Much of this confusion regarding the effect of silver additions on strength was eliminated when it was pointed out that the higher temperature overaging treatments performed in much of the earlier work were carried out using thin products or small pieces that were heated rapidly to the aging temperature in either oil or salt baths [110]. It has since been clearly demonstrated [110] that under these conditions, silver-bearing alloys do indeed maintain higher strengths than silver-free alloys (Fig. 38). However, virtually the same strengthening effect can be achieved in silver-free alloys by exposing them for appropriate times near 200°F so that GP zones can grow to sizes that will not revert (redissolve) during subsequent aging at higher temperatures. The necessary exposure time near 200°F is short enough in 7075-type alloys that it can be attained during normal production heating rates to the artificial aging temperature [110].

In addition to the dependence on the rate of heating to the aging temperature, the effect of silver additions on strength depends on the quenching rate [110,127,128]. Specifically, silver additions increase quench sensitivity of 7075-type alloys containing either chromium or manganese. On the other hand, silver additions to chromium- and manganese-free 7075-type alloys containing zirconium can improve strength slightly, even at fairly slow quench rates (2° F/sec). However, high strength alone is not sufficient and to achieve adequate

stress corrosion resistance in silver-free or silver-bearing 7075-type alloys containing chromium, manganese, or zirconium, overaging is required. Thus, again, aging temperature and not chemical composition is the most important factor governing short transverse SCC resistance in these alloys [110]. If they are aged for sufficient times at 325°F, high SCC resistance can be achieved. The length of time at 325°F depends on alloy composition. Chromium-bearing 7075-type alloys develop a high resistance to SCC after relatively short exposure periods at 325°F, whereas chromium-free 7075-type alloys containing either manganese or zirconium require longer aging times. In spite of the slower aging rate of chromium-free alloys containing manganese and/or zirconium, the strengths of 7075-type alloys with the various additions are comparable, after the alloys are aged to have good resistance to SCC. It was concluded that silver-bearing 7075-type alloys could not be aged to a higher strength than 7075-T73 and yet maintain equal resistance to SCC [110]. Thus several investigators have recommended that development work on silver-bearing Al-Zn-Mg-Cu alloys be discontinued [110,125]. No further alloy development work has been carried out in the United States, although silver-bearing alloys are still being investigated in Great Britain [124] and Australia [129]. It seems worthwhile, however, to determine if silver-bearing alloys can be made resistant to exfoliation corrosion with less overaging and therefore higher strength than silver-free alloys.

**New Alloy Development.** With the introduction of the overaged T73 temper for 7075, many of the stress corrosion problems in the 7075 alloy exposed to the more common environments were eliminated. Although the overaged 7075-T73 offers significant stress corrosion resistance, the lower strength accompanying overaging can result in weight penalties in certain high-performance structures. This weight penalty is particularly severe in thick-section applications because in addition to strength losses resulting from overaging (about 14%), the chromium in 7075 imparts a high degree of quenching sensitivity to the alloy. Thus, strength drops off rapidly with decreasing quenching rate (increasing thickness). Efforts have continued toward developing alloys with good stress corrosion resistance and even higher strengths.

A recent advance toward this goal has been the introduction of 7175-T736 and 7075-T736 alloys for die forgings. The 7175 alloys is essentially a cleaned-up version of 7075, containing lower concentrations of the tramp elements iron and silicon and therefore providing significant increases in fracture toughness. The mechanical processing and aging parameters used in achieving the T736 tempers are proprietary, but these alloy/temper combinations provide the highest strength consistent with adequate stress corrosion resistance of any die-forging alloy available today, at least up to thicknesses of 3 in. (Table 2). These alloy/temper combinations are not available in other wrought-product forms and are not available for die forgings thicker than 3 in.

The chromium content in the 7175 and 7075 alloys and the high attendant quenching sensitivity as well as the special processing required in achieving the T736 properties, will limit 7175-T736 and 7075-T736 to section thicknesses of

about 3 in. Thus there is still a need for a good thick-section alloy with high strength, high resistance to SCC, and good fracture toughness. It is with this aim that most of the current aluminum alloy development in this country has been carried out.

One thick-section-forging alloy introduced several years ago was X7080-T7. This alloy was for use in parts up to 6 to 8 in. thick. One attractive feature of X7080-T7 is that it is boiling-water quenchable. This quenching technique is desirable because it minimizes residual quenching stresses and distortion problems during subsequent machining operations. The boiling-water quench was made possible by the low degree of quenching sensitivity in X7080-T7 achieved by virtue of its low copper content and the replacement of chromium with manganese. As mentioned earlier, this alloy also showed adequate stress corrosion resistance when tested by 3.5% NaCl alternate immersion, having a short transverse threshold stress of 25 ksi. However, subsequent testing in outdoor industrial environments showed that stress corrosion failures in short transverse specimens occurred at stresses as low as 15 ksi [110]. This discrepancy between 3.5% NaCl alternate-immersion and industrial environment test results has been a common problem in other low-copper-content alloys such as 7079-T6 (Fig. 17). In any case, since the industrial environment results for X7080-T7 were published, much less interest has been shown in this alloy for thick-section-forging applications, especially in view of the good results currently being obtained on several experimental thick-section alloys.

A promising stress-corrosion-resistant material available in thicknesses up to 5 in. is the recently introduced 7049-T73 alloy. This chromium-bearing alloy contains about the same zinc content as 7001 and about the same magnesium and copper content as 7075. The heat treatment for this alloy is proprietary, but the alloy possesses strength properties essentially equivalent to those of 7079-T6 in thicknesses up to 5 in. (Table 2). In addition, 7049-T73 shows excellent stress corrosion resistance with a smooth stress corrosion threshold stress of about 45 ksi (Table 2). Thus 7049-T73 provides mechanical properties comparable to those of 7079-T6 and stress corrosion resistance comparable to that of 7075-T73. In addition, this alloy does not require special processing; therefore, existing dies for die forgings can be used if changes from a susceptible material such as 7079-T6 or 7075-T6 to the more stress-corrosion-resistant 7049-T73 material are desired.

Despite the existence of 7175-T736, 7075-T736, and 7049-T73, work aimed at developing an improved high strength, stress-corrosion-resistant alloy for use in very thick sections has been under way for the past few years [130-149]. To minimize quenching sensitivity, each of the alloys developed as a result of these programs has had reduced concentrations of chromium with zirconium instead being used as the primary recrystallization retardent. Recommended composition limits for alloys developed during these studies are listed in Table 4.

**Comparison of Various Thick-Section Alloys with Commercially Available Alloys.** Figure 39 compares the strengths of the various thick-section alloys with

**Table 4.** Recommended Chemical Composition Limits of Some Thick-Section Experimental Alloys

| *Element* | *Alloy*[a] | | |
|---|---|---|---|
| | *Boeing Alloy 21* | *Reynolds Alloy 2* | *Alcoa MA-15*[b] |
| Zinc | 5.9-6.9 | 6.4-7.1 | 5.7-6.7 |
| Magnesium | 2.2-2.9 | 2.2-2.8 | 1.9-2.6 |
| Copper | 0.7-1.5 | 1.1-1.4 | 2.0-2.8 |
| Zirconium | 0.10-0.25 | 0.08-0.18 | 0.08-0.14 |
| Iron | 0.20 | 0.12 | 0.15 |
| Silicon | 0.20 | 0.10 | 0.12 |
| Chromium | 0.05 | 0.03 | 0.04 |
| Manganese | 0.05-0.15 | 0.10 | 0.10 |
| Titanium | 0.10 | 0.05 | 0.06 |
| Others | | | |
| Each | 0.05 | 0.05 | 0.04 |
| Total | 0.15 | 0.15 | 0.10 |

[a]Composition in weight percent maximum unless shown as a range.
[b]MA-15 was recently registered with the Aluminum Association as X7050 (see Table 1).

the commercially available forging alloys. To construct Fig. 39, the typical yield strengths of Reynolds alloy 2 plate, Alcoa MA15 plate, and Boeing alloy 21 die forgings were compared with typical properties for die forgings of the commercially available materials. The typical yield strengths for all the commercially available die forgings were obtained by adding 6 ksi to the minimum-allowable-strength properties for each thickness (typical properties are commonly 6 ksi above minimums for the high-strength aluminum alloys). This strength value was then plotted at a cooling rate determined by the thickness and quenching water temperature commonly used to quench each alloy. In all cases for the die forgings, cooling rates were determined assuming cylindrically shaped forgings. Arrows indicating different quenching rates for various forging diameters and quenching water temperatures are shown in Fig. 39 to better illustrate the relationship between thickness and cooling rate. For this plot, the following quenching water temperatures were used for the forging alloys: 70°F for 7175-T66, 7175-T736, 7079-T6, and Boeing alloy 21; 140°F for 7075-T6, 7075-T73, 7049-T73, and 2014-T6; and 212°F for X7080-T7.

To compare the commercial and experimental alloys, their relative resistance to SCC should be known. Stress corrosion properties for the various alloys are shown in Table 5.

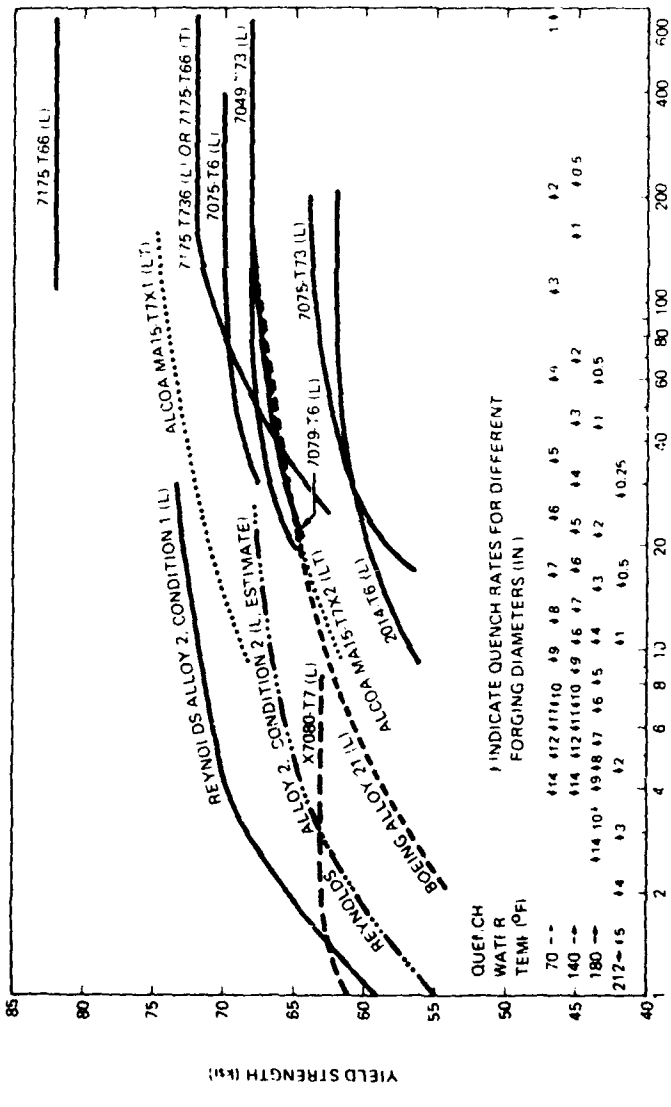


Fig. 39. Effect of quench rate (thickness and quench-water temperature) on the mechanical properties of several experimental alloys and commercial alloys 7175-T66, 7175-T736, 7075-T6, 7049-T73, 7079-T6, 7075-T73, and 2014-T6. Commercial-alloy properties are for die forgings. Experimental-alloy properties are for plate or die forgings. Grain directions are as indicated (L = longitudinal plate, LT = long transverse plate, T = transverse forging).

**Table 5.** Aging Treatments and Stress Corrosion Resistance of Experimental- and Commercial-Alloy Forgings

| *Alloy* | *Aging Treatment* | *Short Transverse SCC Threshold Stress (ksi)* | |
|---|---|---|---|
| | | *3.5% NaCl Alternate Immersion* | *Industrial Atmosphere* |
| Reynolds alloy 2 | | | |
| Condition 1 | 24 hr 250°F + 18 hr 325°F | ≈25 | ? |
| Condition 2 | 24 hr 250°F + 24 hr 325°F | ? | ? |
| MA15-T7X1 | 4 hr 250°F + 9 hr 325-335°F | ≈25 | ? |
| MA15-T7X2 | 4 hr 250°F + 24 hr 325-335°F | ≈45 | ? |
| Boeing alloy 21 | 24 hr 250°F + 35 hr 325°F | ≈35 | ? |
| 7175-T736 | Proprietary { 24 hr 250°F + | ≈35 | ≈35 |
| 7049-T73 | 48 hr R.T. + { 14 hr 320°F | 45 | 45 |
| 7075-T73 | 24 hr 250°F + 27 hr 325°F | 45 | 45 |
| X7080-T7 | Proprietary | 25 | 15 |
| 7175-T66 | Proprietary | 7 | ? |
| 7075-T6 | 24 hr 250°F | 7 | 14 |
| 7079-T6 | 48 hr 240°F | 7 | 6 |
| 2014-T6 | 18 hr 320°F | 7 | 10 |

The combined data of Table 5 and Fig. 39 point out the excellent properties of 7175-T736 for thinner sections and 7049-T73 for thicker sections, especially to those familiar with the numerous in-service stress corrosion problems of 7075-T6, 2014-T6, and particularly 7079-T6 forgings. Not until fracture toughness and stress corrosion testing of all experimental alloys are complete and the minimum allowable properties have been established will it be possible to judge whether these alloys offer real advantages over 7175-T736 and 7049-T73 in section thicknesses up to 5 in. It appears, however, that for thicknesses greater than 5 in. a new alloy may be available soon that is superior to anything now available.

It should be added here that current work on chromium-free 7000-series alloys is also being carried out in Europe. In Italy, work on two promising Zr + Mn alloys (Zergal-3 and Zergal-4) is being conducted [126]. Zergal-3 is being tested in the form of sheet, extrusions, and forgings while Zergal-4 is being developed specifically for forgings [126]. In England, a chromium-free Ag+Zr-bearing alloy is being investigated [124]. The chemical compositions of these three alloys are compared with Alcoa's MA15, Reynold's alloy 2, and Boeing's alloy 21 in Table 6. With the exception of the high copper content in MA15 and

**Table 6.** Chemical Composition of Some Experimental European and American Alloys

| *Element* | *Alloy* | | | | | |
|---|---|---|---|---|---|---|
| | *Zergal-3* | *Zergal-4* | *British Alloy* | *Alcoa MA-15* | *Reynolds Alloy 2* | *Boeing Alloy 21* |
| Zinc | 6.0 | 6.0 | 6.1 | 6.0 | 6.58 | 6.40 |
| Magnesium | 2.5 | 2.3 | 2.8 | 2.15 | 2.39 | 2.55 |
| Copper | 1.5 | 0.8 | 1.0 | 2.50 | 1.22 | 1.10 |
| Chromium | 0.05 max | 0.05 max | | | <0.01 | <0.01 |
| Manganese | 0.20 | 0.20 | | | <0.01 | 0.10 |
| Zirconium | 0.18 | 0.18 | 0.13 | 0.11 | 0.11 | 0.13 |
| Silver | | | 0.30 | | | |
| Titanium | 0.06 | 0.06 | | 0.04 max | 0.03 | 0.02 |
| Iron | 0.25 max | 0.25 max | 0.17 | 0.12 max | 0.07 | 0.13 |
| Silicon | 0.20 max | 0.20 max | 0.07 | 0.10 max | 0.05 | 0.06 |

the silver addition in the British alloy, the chemical compositions of these alloys are very similar.

Although strength data as a function of thickness and quenching rate were not available for Zergal-3 and Zergal-4, one strength data point for 2.75-in.-thick plate of the British alloy was available [151]. This information indicates that the silver-bearing British alloys have strength properties very similar to those of other silver-free experimental alloys being developed in the United States.

Recent aluminum alloy development studies have used, with two exceptions [125,130], stress corrosion tests with smooth specimens only. The measurement of stress corrosion crack velocity as a function of crack-tip stress intensity could, however, be a more useful approach for reasons discussed earlier in this chapter.

**Thermomechanical Processing.** It is well known that for some aluminum alloys, such as the Al-Cu-Mg type, plastic deformation at room temperature after quenching and before aging can increase strength properties after normal aging treatments. However, for Al-Zn-Mg-Cu alloys such as 7075-T6, room-temperature deformations of 0 to 20% after quenching and prior to aging have resulted in properties after aging that are not much different from those of material directly aged after quenching.

On the other hand, work on an Al-Zn-Mg-Cu alloy has shown that if it is hot deformed (20% at 248°F) before the normal aging treatment at 248°F, strength can be increased without noticeable decreases in ductility [152]. This work has prompted others [153] to employ multistage aging cycles in combination with plastic deformation after the first stages of aging at low temperatures and before

a subsequent higher temperature aging (Fig. 40). Using this technique, the strength of Al-5%Zn-1%Mg and Al-4%Zn-2.7%Mg (+ Cr, Mn, Zr) alloys was increased significantly with little decrease in ductility. Based on these results, it was suggested that it may be possible to decrease magnesium content in an Al-Zn-Mg-Cu alloy to increase stress corrosion resistance and at the same time use thermomechanical treatments of the type shown in Fig. 40 to maintain high strength levels. The prospects are intriguing, and some work is being carried out in this direction [153]. To date, however, we are aware of no real breakthrough in this area.

In another program, thermomechanical treatments of 3- to 4-in.-thick 7075 blocks involving a two-step overaging/press forging operation are claimed to result in improved strength and stress corrosion resistance [154]. However, close examination of the data reveals that stress corrosion specimens machined from the thermomechanically processed blocks were not really short transverse speci-

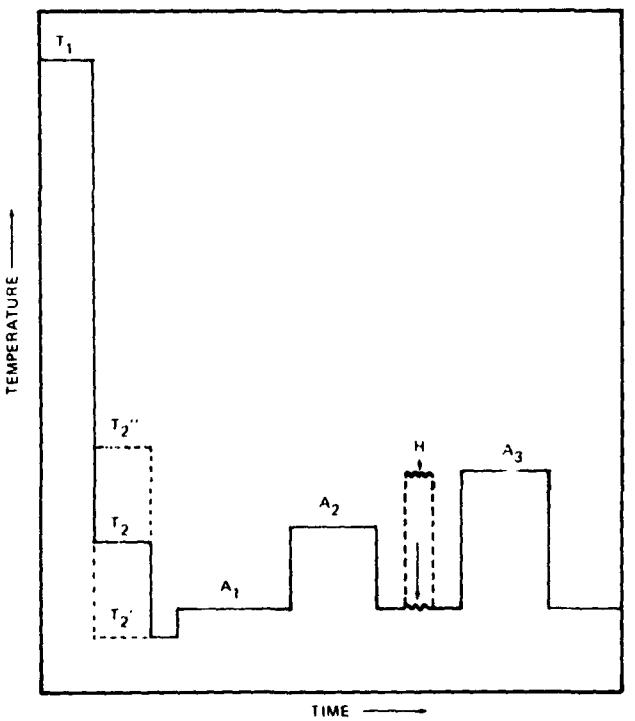


Fig. 40. Thermomechanical treatment scheme for Al-Zn-Mg alloys. $T_1$ = solution treatment temperature; $T_2'$ - $T_2''$ = temperature range of quenching medium; $A_1$ = first stage of aging; $A_2$ = second stage of aging; H = plastic deformation; $A_3$ = third stage of aging [153].

mens, as they were in the control blocks, due to changes in grain shape and orientation resulting from the press forging operation. Thus, any conclusions concerning improvements in inherent stress corrosion resistance of the press-forged blocks are questionable.

**New Fabrication Techniques.** It is often stated that if end-grain exposure can be avoided, even quite susceptible alloys can be used without undue concern for SCC problems. Unfortunately, it is almost impossible except in the simplest of configurations to produce a forging without any end grain. Furthermore, subsequent machining of the forging generally exposes even more end grain. In an attempt to resolve this problem, a recent study was conducted to minimize end-grain exposure in 7079-T6 in cylindrical landing gear forgings [155]. A hollow barrel section was extruded forward or backward such that there was some circumferential grain flow in the barrel wall. Forgings thus produced were significantly more resistant to SCC than the parts produced by the conventional forge, regular cog, and upset cog methods.

However, use of some of the newer high strength, corrosion-resistant alloys or, in the near future, use of some of the thick-section alloys currently under development, will lessen the need for such novel forging techniques, even though such techniques may still be desirable to optimize the grain-flow pattern in some parts.

**New Sheet Alloys.** Before leaving the subject of new developments, a few words should be said about new developments for sheet applications. The improved exfoliation-corrosion resistance of 7075-T76 and 7178-T76 sheet, plate, and extrusions has already been mentioned; in areas where other protective measures have proved inadequate, these T76-temper products can offer improved performance. More recently, new high strength cladding materials 7011 [156-159] and 7008 [4] have been developed for the high strength 7000-series alloys. The new clad alloys protect the copper-bearing 7000-series electrochemically; in the heat-treated condition, they develop nearly the same mechanical properties as the core alloy, in contrast to the normal 7072 alclad alloy (which does not respond to heat treatment) for these 7000-series materials. This difference results from the increased zinc and magnesium contents in the new clad alloys with 7011 and 7008 are 2 to 4 ksi higher than those for the regular 7072 alclad materials and only 2 to 3 ksi below those for bare material. Of course, as sheet thickness increases, the difference in strength between bare and clad material decreases. Fatigue strengths of materials clad with 7011 and 7008 are also significantly higher than for materials clad with the lower strength 7072 alloy.

Another new development is the introduction of X7475 alloy sheet in both the high-strength T61 temper and the exfoliation-resistant T761 temper [160]. This alloy is also available with or without the high strength 7008 cladding. The X7475 alloy is a cleaned-up version of 7075, which has excellent fracture-toughness properties comparable to those of 2024-T3, and strength in the T61 and T761 tempers that is only 2 to 4 ksi below that for the 7075 alloy in the T6

and T76 tempers. X7475-T6 is also nearly identical in strength to 7079-T6 and has a fracture toughness about 20% greater than that for 7079-T6. The high toughness of X7475 results from the reduced iron and silicon contents, which in turn eliminate most of the iron- and silicon-bearing intermetallic particles present in normal material. More effective homogenization and dissolution of copper-bearing intermetallics during processing are probably also partly responsible for the significantly increased toughness.

### Weldable Alloys

For many welding applications, such as for large storage tanks, structural marine applications, or cryogenic applications, the 5000-series non-heat-treatable alloys such as 5456, 5083, 5086, 5454, and 5052 are often used. Alloys 2014 (Al-Cu-Mg) and 2219 (Al-Cu) have a higher strength-to-density ratio and are therefore often used for aerospace applications. Of the weldable 7000-series alloys, 7039 and 7005 may be considered for structural applications.

In an attempt to provide even higher strength weldable aluminum alloys with good cryogenic toughness, two additional alloys—2021 and X7007—have been introduced [161]. The longitudinal and short transverse stress corrosion resistance of 2021 and X7007 in the unwelded condition is compared with the stress corrosion resistance of unwelded 2014, 7039, 7005, 6061, and 2219 in Fig. 41. With the exception of the copper-free alloys (7005, 7039, X7007), the data in Fig. 41 were obtained from specimens removed from plate and exposed to a 3.5% NaCl solution by alternate immersion. For the copper-free types, the

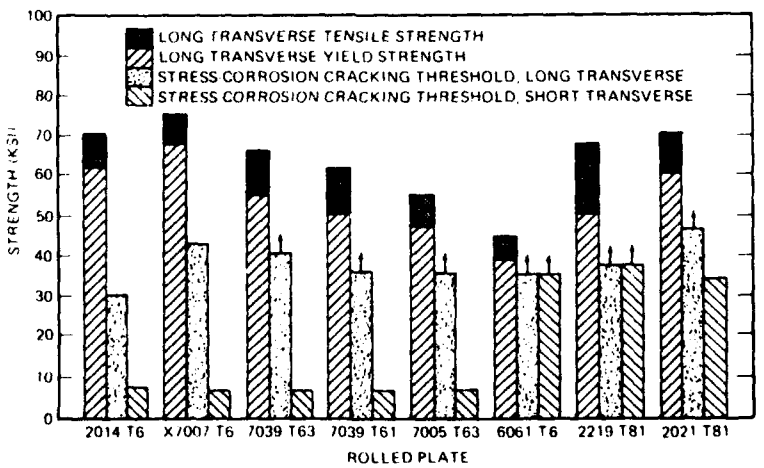


**Fig. 41. Stress corrosion resistance of several weldable high-strength aluminum alloys. Arrows indicate that the specimen did not fail at the highest stress at which it was tested [161]. From *Metal Prog.* 95 (No. 5), p. 72, Fig. 5; copyright 1969 by the American Society for Metals. Used by permission.**

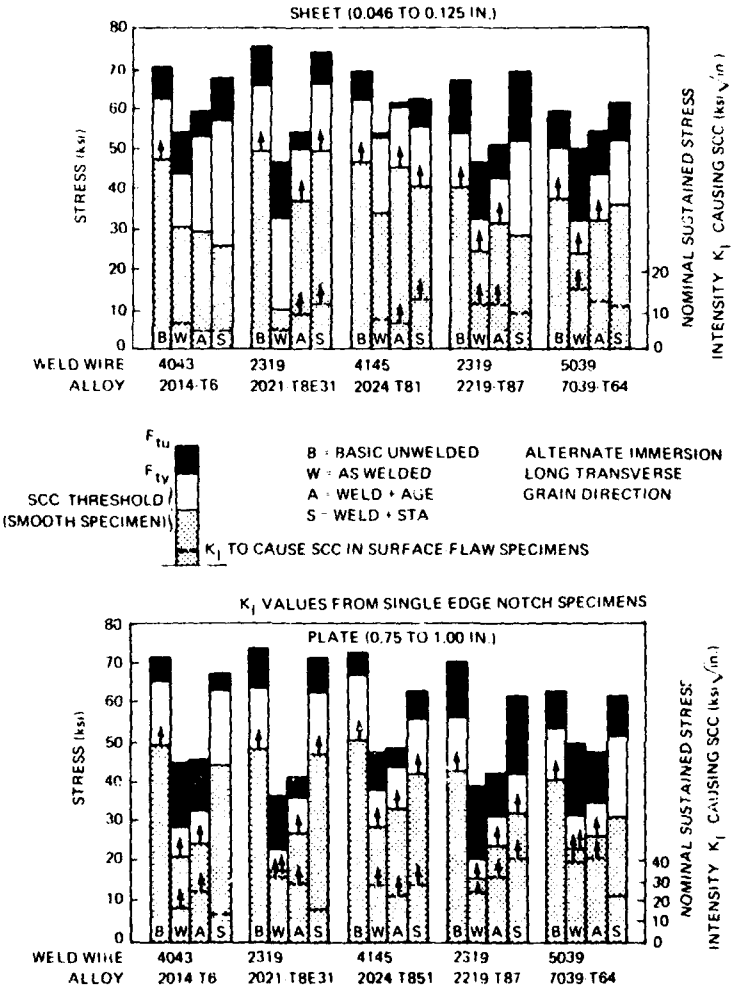


Fig. 42. Mechanical properties and stress corrosion resistance of sheet and plate weldments of several high-strength aluminum alloys [162].

threshold values for SCC are based on exposure to an inland industrial atmosphere that, as previously discussed, provides more reliable information than the alternate-immersion test. Except for 6061-T6, 2219-T81, and 2021-T81, the short transverse stress corrosion resistance of the alloys shown in Fig. 41 is quite low (7 to 16 ksi).

In the as-welded condition, the stress corrosion resistance of many of these alloys is reduced. Stress corrosion cracks usually develop at the edge of the weld bead if smooth specimens are tested. The reduction of stress corrosion resistance due to welding is illustrated in Fig. 42. Aging or resolution treatment and aging after welding often improves resistance to SCC (Fig. 42).

It can be seen from the data in Figs. 41 and 42 that alloys 2021 and X7007 possess attractive strength properties although the short transverse stress-corrosion resistance of X7007-T6 is quite low. It has been reported that toughness values of repaired welds are much lower for 2021 than for 2219. Since more often than not repair welding is required, this parameter could be of the utmost importance, and a choice between alloys 2021, 2219, or 2104 may well hinge on this factor.

### 4.5 Discussion

A satisfactory theory of SCC in high strength aluminum alloys would have to predict quantitatively and explain from first principles the experimental results presented in the previous sections. Such a theory is not yet available. There are many reasons for the lack of a complete quantitative theoretical treatment of SCC. Three are mentioned below.

First, quantitative experimental SCC data have only recently become available. Some of the data are presented here for the first time.

Second, theoretical treatments of SCC attempt to understand the basic mechanisms in atomic dimensions near the crack tip. On this scale, however, observations near the crack tip are extremely difficult, if not impossible. Therefore, the basic assumptions of most theories cannot be verified directly.

Third, the complexity of the subject requires that theoretical treatments take into account mechanical, chemical, and metallurgical aspects. These three aspects are interrelated, as evident from the previous sections of this monograph. Therefore, significant progress toward understanding SCC is likely to come only from research teams that combine the results of fracture mechanics, chemistry (especially electrochemistry), and metallurgy. Tradition and lack of funds do not favor the formation of such research teams.

The following short discussion is broken down into three parts, depending on whether the predominating aspect is mechanical, chemical, or metallurgical. The discussion reflects the fact that we are still far from a quantitative theory that integrates all three aspects. A more detailed discussion of the mechanisms of SCC of aluminum alloys has recently been given elsewhere [46,73].

### Effect of Stress on Crack Velocity

The crack velocity vs stress intensity curves shown in Figs. 11 and 33 demonstrate the effect of crack-tip stress intensity on stress corrosion crack velocity. It is evident that these V-K curves consist of a stress-dependent part (labeled region I) and a stress-independent part (labeled region II or plateau). In many cases, a transition region between the two parts of the V-K curve is also observed. In this section we present some models that have been proposed to explain the effect of stress on the stress corrosion crack velocity, and which are therefore applicable to region I of the V-K curve.

**Stress-Activated Dissolution.** It has been shown that a blunt crack in a dissolving solid under stress can sharpen if the dissolution rate is stress dependent [163,164]. If both the stress and the stress dependence of the dissolution rate are high enough, this could lead to failure by SCC. Based on these ideas, the stress corrosion crack velocity can be expected to depend on the crack-tip stress intensity in the following way [163]:

$$V = V_0 \exp(-Q + bK_I)/RT,$$

where

$V$ = crack velocity
$Q$ = apparent activation energy; $Q = E + V_M \gamma/\rho$
$E$ = stress-free activation energy
$V_M$ = molar volume
$\gamma$ = fracture surface energy
$\rho$ = radius of the crack-tip curvature
$b$ = $2U\sqrt{\pi\rho}$
$U$ = activation volume
$K_I$ = plane-strain stress intensity.

Thus, this model predicts correctly the experimentally observed functional relationship between crack velocity and applied crack-tip stress intensity.

**Stress-Assisted Diffusion of Damaging Species.** Liu [166] has analyzed the elastic interaction between a solute atom and the stress field in a solid ahead of the crack tip. He shows that the solute atom concentration increases rapidly toward the crack tip if the solute atom is interstitial or if it relaxes the crack-tip stress field. Assuming that the solute atoms might embrittle the material and also assuming that the crack growth rate is controlled by the reaction rate within a material whose structure is characterized by a length $r_0$, he can write the crack growth rate as

$$V = V_0 C_0 \exp\left(\frac{-\Delta H}{kT}\right) \exp\left(\frac{MK}{kT\sqrt{r_0}}\right),$$

where

$C_0$ = volume concentration of solutes
$H$ = activation energy
$M$ = a parameter which describes the elastic interaction between the solute atom and the stress field
$K$ = stress intensity
$k$ = Boltzmann constant
$T$ = absolute temperature.

This model, too, predicts correctly the experimentally observed functional relationship between crack-tip velocity and crack-tip stress intensity.

**Effects of Environment**

The effect of environment on the propagation of stress corrosion cracks is most conveniently studied (and most accurately measured) in the stress-independent plateau region of the crack velocity vs stress intensity curves. For any given alloy this permits a separation of the environmental effects from the mechanical and metallurgical parameters. Moreover, experimental results have shown that in many (but not all) cases, region II is the only part of the V-K curve that is affected by the environment. Therefore, this discussion is concerned primarily with the effects of environment on the plateau velocity in region II of the V-K curve.

**Influence of Water Vapor on Crack Propagation in Gaseous Atmospheres.** In Section 4.3, it was pointed out that dry gases such as argon, hydrogen, oxygen, nitrogen, and air do not support measurable stress corrosion crack growth. It is the water vapor content of the gases that makes stress corrosion cracks grow. Region I of the V-K curves seems little affected by the water vapor content of the gases, but the plateau depends linearly on the water vapor pressure. This can be rationalized in the following way.

Starting at the lower end of the V-K curve (see Fig. 33, for example), crack velocity increases with increasing stress intensity. In region I, the crack velocity could be limited by the kinetics of the tip reactions as outlined earlier. As the crack velocity increases, it might eventually reach a limit set by the rate at which the damaging species arrives at the crack tip. The rate-limiting step could be either the diffusion of water vapor through the gas that fills the crack or the diffusion of water through an oxide layer covering the crack tip. In either case, we would expect the crack velocity to be strongly dependent on the water vapor concentration in the bulk atmosphere but nearly independent of the applied crack-tip stress intensity. This is indeed what is observed for the plateau velocity.

**SCC in Aqueous Solutions.** A change of the environment from gases with 100% relative humidity to immersion in liquid distilled water does not change the V-K curves of high strength aluminum alloys very much. The only exception is alloy 7079, where such a change of environment increases the plateau velocity

by a modest factor of three [73]. The similar growth rates in liquid water and gases saturated with water vapor indicate that in neither environment is the crack growth limited by the rate that water arrives in the crack-tip zone. There must be a slower rate-controlling step yet to be identified. Diffusion through an oxide layer at the crack tip is one of the possible rate-controlling steps.

**Stress-Corrosion Crack Velocity Limited by Mass-Transport Kinetics.** The mass-transport-kinetics (MTK) model was first developed for SCC of titanium alloys in aqueous chloride, bromide, and iodide solutions [167] and later extended to aluminum alloys [168,169]. It indicates that the stress corrosion crack velocity in region II of the V-K curve is limited by the kinetics of halide-ion transport to the crack tip.

The MTK model is in good agreement with a number of experimental observations on stress corrosion crack growth in region II of the V-K curve.

*Halide-Ion Concentration.* The theory predicts that the crack velocity should be proportional to the halide-ion concentration. This agrees well with the experimental observations reported in Refs. 47, 73, and 168.

*Temperature.* The temperature dependence of stress corrosion crack growth in region II, according to the MTK model, would be determined mainly by the temperature dependence of the diffusivity of the halide ions. The activation energy of approximately 4 kcal/mole measured for region II is well within the range predictable for the activation of a process limited by ionic mass transport [170].

*Ionic Species.* To explain the fact that chloride, bromide, and iodide accelerate SCC in aluminum alloys is outside the scope of the MTK model. However, since the crack becomes acidic as indicated earlier, hydrogen ions and $Al^{+++}$ ions displace other cations within the crack so that the velocity is independent of the cations, as reported above.

### Metallurgical Aspects

In this section, we would have liked to present those theories that predict quantitatively the stress corrosion performance of high strength aluminum alloys, based solely on the microstructure and composition of the alloy. There is no such theory; indeed, there is not even a single successful attempt to relate the stress corrosion V-K curve and the microstructure of aluminum alloys on a quantitative basis. This is all the more deplorable since hundreds of papers have been written on the relationship between microstructure and SCC of aluminum alloys. Even the single most important metallurgical treatment to improve stress corrosion resistance–the overaging of precipitation-hardened alloys–has not yet been analyzed quantitatively.

Qualitative hypotheses of the relationship between microstructure and stress corrosion resistance are still highly controversial. They have been reviewed adequately [171], allowing the present section to be brief. Progress in understanding the metallurgical aspects of SCC of high strength aluminum alloys will come when

- Hypotheses and the tests they are supposed to explain are made quantitative.
- Assumptions upon which the hypotheses are based can be checked independently.

**Precipitation Hardening.** According to the experimental data reported in the last section (Proper Storage), the effect of precipitation hardening on resistance to SCC seems to follow these rules:

- The initial stages of precipitation hardening decrease the resistance to SCC [105].
- Precipitation hardening beyond peak hardness (overaging) can increase the resistance to SCC [105].

Figure 35 illustrates these observations. Since precipitation hardening is of the utmost importance for high strength aluminum alloys, studies on the effect of metallurgical parameters on SCC have often attempted to explain these two rules. The following hypotheses are among those discussed presently.

**Precipitate-Free Zones.** It is well established that preferential precipitation during aging of Al-Zn-Mg alloys can lead to the formation of a precipitate-free zone (PFZ) at grain boundaries [172]. Wide PFZ's are easily observed in ternary alloys. In commercial high strength aluminum alloys, PFZ's are much smaller and often are not observed at all. Therefore, most studies on the relationship between PFZ width and stress corrosion resistance have concentrated on high-purity ternary Al-Zn-Mg alloys of academic interest. Three schools of thought have developed, each contradicting the other:

- Reducing the PFZ width will *increase* resistance to SCC [173].
- Reducing the PFZ width will *decrease* resistance to SCC [174].
- PFZ width is of minor or no importance to SCC resistance [105,175].

Those who believe that PFZ's are important in the resistance to SCC assume this is so because preferential deformation in the PFZ leads to preferential dissolution and thus to intercrystalline SCC [174,176].

At this time, neither the PFZ hypothesis nor the experiments supporting or contradicting it are on a quantitative basis.*

**Interaction of Dislocations with Precipitates and SCC.** This hypothesis proposes that the effect of precipitation hardening on the resistance to SCC is due to the interaction of dislocations with those precipitates that cause the hardening [105,177-180]. High strength aluminum alloys exhibit characteristic dislocation arrangements after deformation. In material of low resistance to SCC, straight, narrow bands of high-dislocation density extend across the grains. The dislocations in the bands are piled up against the grain boundaries. In materials aged to a reduced susceptibility, the slip bands contain dislocations of irregular curvature and many dislocation loops. It is thought that different dislocation-particle interactions cause the differences in slip mode, and it is concluded that

*The evidence appears to indicate that although changing the width of the PFZ affects SCC behavior, the concomitant changes in the nature of precipitate affects SCC behavior more. (*Editor.*)

resistance to SCC in high strength aluminum alloys is reduced by precipitates that are sheared by plastic deformation. Particles bypassed by moving dislocations are thought to result in improved stress corrosion resistance. According to the dislocation-particle interaction hypothesis, overaging reduces stress corrosion susceptibility because the volume fraction of particles that can be sheared decreases [105].

The hypothesis that dislocation-particle interaction affects the resistance to SCC in high-strength aluminum alloys predicts specifically that

- Matrix precipitates (i.e., GP zones), and not grain-boundary precipitates or the PFZ, control resistance to SCC.
- Susceptibility to SCC in aqueous chloride solution increases with the volume fraction of the GP zones [103].

Results of recent experimental investigations are in full agreement with these predictions [175,181,182].

The dislocation-particle-interaction hypothesis is at present transformed into a quantitative SCC theory [46,182]. Until a quantitative comparison of theory and experiment is presented, the assumptions and predictions remain open to questioning as do the other hypotheses mentioned.

**SCC Due to an Anodic Path Along Grain Boundaries.** Nearly three decades ago, a "generalized theory of stress corrosion cracking" was given [183] that describes the mechanism of SCC of aluminum alloys as follows: Corrosion occurs along localized paths, producing fissures; components of tensile stress normal to the path then create a stress concentration at the base of the localized fissures. In aluminum alloys, such preexistent anodic paths are thought to be due to the difference in electrochemical potentials between grain-boundary precipitates or grain-boundary margins and the grain interior [55]. The role of stress in stress corrosion crack growth is thought to be the opening of the fissures, thus exposing fresh unprotected metal to corrosion attack. It is assumed that in this way, corrosion along the grain boundary is accelerated because freshly exposed metal is more anodic. This theory is still widely accepted, especially in the aluminum industry, because it is consistent with many experimental observations concerning the effect of heat treatment on resistance to SCC. The anodic-path hypothesis has the merit of being among the first to attempt a correlation between microstructure and stress corrosion experience. This hypothesis has been used to explain the superior stress corrosion resistance of the overaged alloy 7075 in the T73 temper compared to the T6 temper [60].

### 4.6 Preventing SCC Failures in Aerospace and Other Structures

Attempts to eliminate SCC problems with high strength aluminum alloys have not been completely successful. For example, numerous stress corrosion failures have occurred in the Saturn V launch vehicle, primarily on parts made from 7075-T6, 7079-T6, and 2024-T4 [184]. Nor has the Apollo lunar landing module been free from SCC [185,186]. While these particular problems have

been alleviated by switching to stress-corrosion-resistant alloys and tempers or by changing processing procedures to minimize residual and fit-up stresses, etc., questions may still be asked: Why? Why so many? Why so many in this late stage of our technological advancement?

Some have suggested that the overriding fact about SCC is a lack of awareness of existing data [187]. Hopefully, this trend will be reversed as builders of aerospace and hydrospace equipment place more emphasis on materials selection. To help achieve this goal, this chapter has attempted to put into perspective the mechanical and stress corrosion properties of the more common alloys: the newly introduced alloys such as 7175-T736, 7049-T73, and X7475; and some of the development alloys yet to be offered commercially. In this manner, those involved in recommending materials to the designer can be made more aware of the changes coming to the aluminum-alloy-development area. Thus they can be better prepared to make materials recommendations in the coming years.

## Materials Selection

**High Strength Alloys for Hand- and Die-Forging Use.** While it is sometimes possible to locate the parting plane of die forgings in an area that will minimize short transverse stresses, it is often difficult or impossible in complex forgings to predict the exact nature of the grain flow at each specific area. Thus, end grains may be exposed after machining, especially on heavily machined parts. For this reason and because of the possible presence of residual surface tensile stresses acting normal to local grain flow and the presence, unintentional though it may be, of fit-up or assembly stresses, alloy 7079-T6 should not be used where stress corrosion problems must be avoided. This same recommendation also applies to hand forgings. The low survival rates of 7079-T6 industrial-atmosphere stress corrosion specimens stressed to only 15% of the yield strength (Fig. 17), the rapid stress corrosion crack growth rates possible in 7079-T6 (Fig. 33), and actual service experience dictate that this recommendation be made. The recommendation should be even more emphatic in view of the recent development of stress-corrosion-resistant alloys such as 7049-T73, 7175-T736, and 7075-T736, which have strength properties equal to or greater than those for the 7079-T6 alloy (Table 2). Alloy 7075-T73, despite its slightly lower strength properties, can also be justified as a replacement for 7079-T6.

This single recommendation to avoid use of 7079-T6 could save millions of dollars yearly by minimizing downtime necessary to replace cracked parts. The increased reliability and reduced maintenance costs should also be obvious.

While 7075-T6 forgings have shown better service performance than 7079-T6, they too are highly susceptible under short transverse stresses; it is recommended that for most applications 7075-T73, 7175-T736, 7049-T73, or 7075-T736 be considered as replacements for 7075-T6.

For the 2000-series alloys, the artificially aged T6 and T8 tempers provide a higher degree of resistance to SCC than the naturally aged T3 and T4 tempers.

Note, however, that alloy 2014 even in the artificially aged T6 temper is highly susceptible to SCC in the short transverse direction. In certain applications where parts may be fatigue critical, 2014-T6 forgings are often used successfully despite this short-transverse stress corrosion susceptibility.

For lower strength applications, 6061-T6 has excellent resistance to SCC.

**Alloys for Sheet and Plate Applications.** Material selections for sheet and plate applications are often dictated by such factors as fatigue life and fracture toughness rather than stress- or exfoliation-corrosion resistance. However, if service performance has shown that protective measures against exfoliation corrosion of the 7000-series alloys have been inadequate, the newer T76 tempers for 7178 and 7075 and the T761 temper for the newer X7475 alloy can be used. For applications where regular alclad 7000-series alloys have been used, strength and possibly fatigue-life improvements can be obtained by use of the higher strength 7011 and X7008 clad materials. In addition, significant gains in fracture toughness can be achieved by use of bare or X7008 alclad X7475 alloy.

In fatigue critical applications or where high toughness is required, 2000-series alloys such as 2024-T3 and 2014-T3 are often used. For most applications, these alloys are used in the alclad condition to protect against general and exfoliation corrosion. It should be recalled that the resistance to stress corrosion and exfoliation corrosion of 2024-T3 decreases rapidly during the first stages of any reheating (Fig. 35) until a minimum resistance is obtained. Additional heating then increases the resistance. Thus, care must be exercised to ensure that exposure times to elevated temperatures during service or fabrication are below those levels that would sensitize the 2024-T3 to intergranular attack. Too slow a cooling rate during quenching can also sensitize 2024-T3 material to exfoliation and SCC (Fig. 30). Since cooling rates are a direct function of thickness, it is recommended that 2024 products thicker than about 0.25 in. should be used only in the artificially aged tempers (T6X, T8X) [85], unless of course protective measures have proven to be adequate in protecting against exfoliation and stress corrosion in parts fabricated from thicker sections.

For marine applications, alloys such as 5052, 5454, 5086, 5083, and 5456 are used. Low-magnesium-content alloys such as 5454 (2.75% Mg) can be used where service temperatures may be expected to exceed 150°F [77]. Since extended heating of wrought Al-Mg alloys with magnesium content in excess of about 3% results in susceptibility to SCC (Figs. 23-25), special sheet tempers designated H343 and H323 were developed to provide good resistance to SCC at ambient temperatures of about 150°F or below for alloys such as 5456 (5.25% Mg) and 5083 (4.45% Mg) [188]. The even newer 116 and 117 tempers for 5186 and 5456 alloys should be considered if service conditions indicate that the H321, H323, and H343 tempers may not provide adequate resistance.

**Alloys for High Strength Extrusion Applications.** The same general comments made for sheet and plate apply to extrusions. Exfoliation-resistant T76 tempers are also available for 7075 and 7178 extrusions, and these alloy temper combinations have the additional benefit of improved SCC resistance. Probably the

most common problem results when thick extrusions are heavily machined, thus exposing essentially transverse grain structure. This problem can be particularly acute if interference-fit fasteners or stresses from assembly mismatch or joggling are present in the region of transverse-grain structure.

One potential method of minimizing the amount of machining for certain applications is the use of stepped extrusions. Use of these products can provide for thick sections only in the area where it is needed.

This resume of some of the recommended uses of aluminum alloys, especially some of the newer ones, has purposely been brief, and anyone involved in aluminum-alloy selection should consult the various alloy producers.

### Proper Design, Fabrication, Assembly, and Finishing Practice

Extensive coverage of the many facets of design, fabrication, and assembly practices that must be closely controlled to avoid SCC problems in high-strength aluminum alloys is beyond the scope of this monograph. If stress-corrosion-resistant tempers cannot be used, certain precautions should be taken to avoid service failures due to SCC. Some of the more common rules are discussed below [189].

- Avoid where possible the machining of thin sections from thick sections since the grain structure in the machined part may be adversely oriented with respect to locked-in assembly or quenching stresses (see Fig. 4).
- When deep hole or pocket machining in thick non-stress-relieved material is required, rough machine as extensively and as close to finish dimensions as practicable prior to heat treatment. Even if final machining removes the residual surface compressive layer, the removal of less material after heat treatment exposes lower internal tensile stresses.
- Avoid deep blind bores since an inadequate quenching in such areas can lead to high inside-diameter surface tensile stresses.
- In hand forgings, rings, and many die forgings, minimize residual quenching stresses by using stress-relieved (T652) material, especially when a part is to be machined all over. In die forgings that are not machined all over, caution is required because the T652 compressive treatment tends to produce residual tension stresses of a few thousand psi on the surface of the part.
- Bending, joggling, roll forming, and twisting can result in residual surface tension stresses that, if combined with adverse grain structure, can lead to stress corrosion problems. Perform these operations on susceptible material when it is in the freshly quenched (W) temper or possibly hot. Hot forming of certain 5000-series alloys in the annealed condition is recommended to minimize the effect of cold work as well as to lower the residual stresses.
- Swaging and shape drawing at room temperature are capable of inducing residual surface tensile stresses in the transverse direction on the formed parts. If feasible with susceptible heat-treatable alloys, form the parts in the O-temper and then heat treat. Alloys 2020, 2024, and 2219 may be swaged in the

solution-heat-treated condition and then aged to minimize SCC; however, this procedure is not recommended for 2014 and the 7000-series alloys aged to the T6 temper.

- Interference-fit bushings and pins can cause stress corrosion. This problem is particularly severe where holes to be bushed are located on the parting plane of die forgings, and this practice should be avoided. Minimize stresses by controlling the interference fit that is permitted. When tolerances required are too tight, make the bushing very thin in comparison to the wall around it so that a larger part of the necessary deformation takes place in the bushing.
- Eliminate moisture traps. This also applies to faying surfaces, particularly if one of the materials is an absorbent. If one of the materials is a dissimilar metal, galvanic corrosion may occur and accelerate any possible SCC hazard that already exists.
- Use shims to compensate for assembly mismatch.

### Surface Treatments

The safest way to prevent SCC service failures with high strength aluminum alloys is to use SCC-resistant alloys and tempers. Where this approach is not possible because of other requirements of the material, adequate protective measures must be taken if alloys and tempers that are susceptible to SCC are used. Such protective measures include treatments of the metal surface, notably shot peening and coating. Obviously, evaluation of the effectiveness of surface treatments as SCC preventives can be made with smooth specimens only; this is one situation where precracked specimens are of no use. However, this situation will be reversed if and when self-healing coatings and inhibitors are studied.

**Shot Peening.** One of the most effective SCC preventives for high strength aluminum alloys is surface working by shot peening, particularly when used in combination with protective coatings. This procedure can be used as a "fix" in troubleshooting or can be incorporated into the original design of a vehicle [190].

Shot peening differs from most protective measures because it changes the surface of the metal instead of merely coating it. Hammering of the shot plastically deforms the surface metal and obliterates the grain structure, resulting in a thin surface layer of metal being placed in compression. Shot peening is effective, therefore, only if

- All exposed surfaces are thoroughly worked (saturated) to an adequate intensity.
- The resultant compressively stressed layer is not penetrated by either mechanical damage or corrosion.

Usually the cold-worked layer is thick enough to tolerate minor surface scratches. The layer can be penetrated readily, however, by the pitting attack that occurs on high-copper-content aluminum alloys in corrosive environments. Thus, it could be expected that the effectiveness of peening would be related not

only to the adequacy of peening, but also to the environment and the resistance to corrosion of the given alloy in that environment. Therefore, shot peening is of no appreciable benefit to stressed specimens of 2014-T651 (low resistance to corrosion) in the 3.5% NaCl alternate-immersion test where pitting rapidly penetrates the cold-worked layer. However, peening considerably extends the time to failure of stressed specimens of 7079-T651 (comparatively high resistance to pitting). A 4-year exposure to a seacoast environment, which is considerably less corrosive than the alternate-immersion environment, showed that peening does improve the performance of 2014-T651 and can prevent failure of 7079-T651. In the even less corrosive industrial inland environment, stressed specimens of both alloys can survive for several years without failure. These effects are illustrated in Fig. 43. Short transverse 7075-T6 tensile specimens stressed to 75% of their yield strength and exposed to the mildly corrosive industrial environment at New Kensington fail in less than 6 months, whereas shot-peened specimens last longer than 17 years [191].

The reason shot peening can delay or prevent SCC is twofold. First, cold working of the surface develops high compressive surface stresses in a layer several hundredths of an inch deep. Second, the plastic deformation of the surface layer distorts and bends the grain boundaries, thereby impeding the

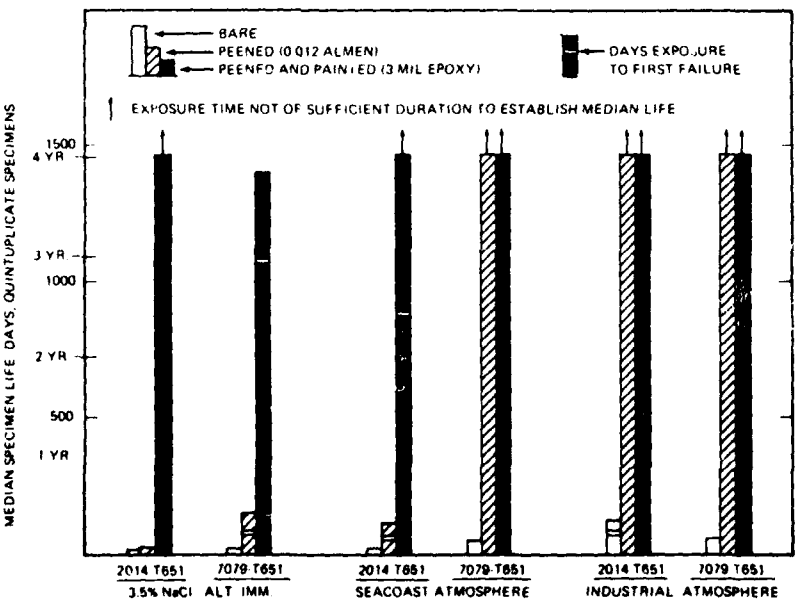


**Fig. 43. Comparison of the effect of alloy and environment on the protection against SCC afforded by peening and peening plus painting on specimens stressed in the short transverse direction to 75% of their yield strength [193].**

initiation of intergranular corrosion and intergranular stress corrosion cracks [191,192]. If pitting corrosion penetrates the cold-worked surface layer, the beneficial effect of shot peening is lost.

The necessity of achieving thorough saturation of the cold-worked surface cannot be emphasized too strongly. Instances where peening was not effective in service applications have often been attributed to critical areas not being worked or worked only superficially.

**Painting and Coating.** Paint systems, in general, are effective measures against surface corrosion. However, a significant disadvantage of paint systems in protecting against SCC is that they provide only a barrier layer to exclude the environment. Paint coatings lose much of their effectiveness if mechanical damage occurs (Fig. 44). In this regard, an inadvertent holiday in the coating or a slight scratch may be all that is required to destroy its protective ability. In service applications, the stress contributing to SCC may be introduced after protective coatings have been applied. Although organic films have excellent flexibility, microcrazing can occur if the metal is deformed appreciably. It is prudent whenever practicable, and particularly when severe attack is expected,

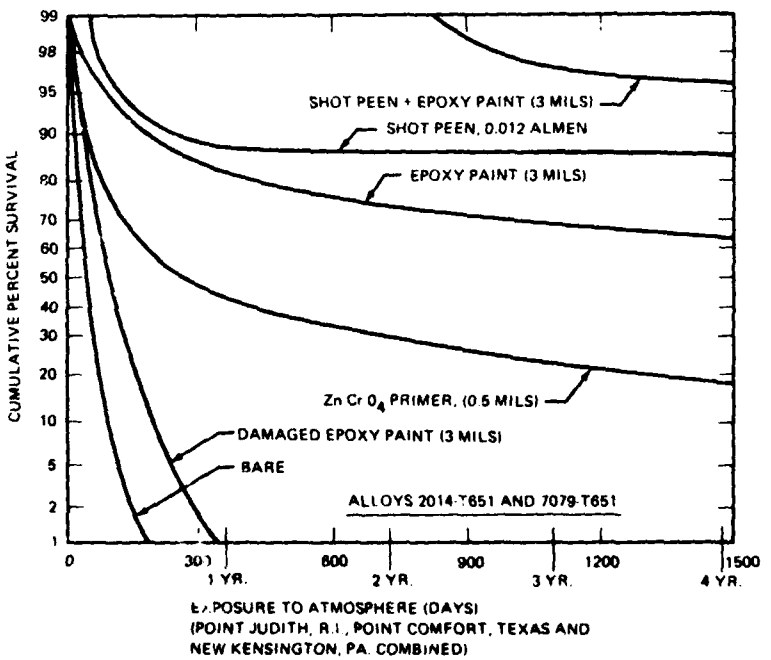


**Fig. 44. Relative protection against SCC of various protective systems on 2014-T651 and 7079-T651 short transverse specimens stressed to 75% of their yield strength [191, 193].**

to provide paint protection to shot-peened parts to prevent rapid penetration of the cold-worked surface layer. The excellent protection afforded by the combination of peening and painting is illustrated in Fig. 44.

**Galvanic Protection.** Since it is impossible to maintain the integrity of coatings in service, sacrificial aluminum anodes or protective claddings are sometimes used to supplement the primary protection provided by the coating. For example, the deep-diving submersible Aluminaut uses aluminum alloy anodes to supplement the protection of the pressure hull offered by several layers of polyurethane coating [75].

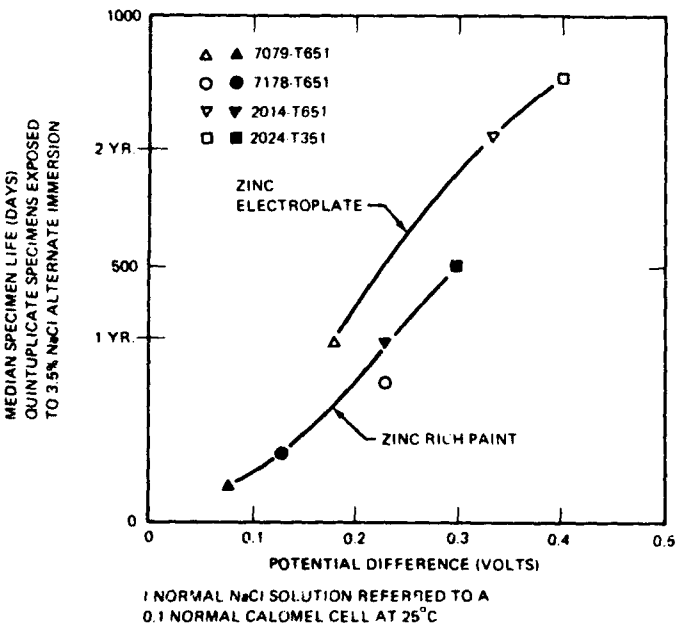


**Fig. 45. Effect of increasing potential difference between the substrate metal and the galvanic coating on the degree of protection against SCC of short transverse specimens stressed to 75% of the yield strength [193].**

To be highly effective, galvanic coatings must be sufficiently anodic to provide adequate electrochemical protection. The effect of this increasing anodic relationship on the degree of protection for a zinc electroplate and zinc-rich paint on four aluminum alloys is shown in Fig. 45. However, standard solution potential measurements provide only a limited basis for predicting the feasibility of electrochemically protecting any given alloy by a galvanic coating. The actual degree of electrochemical protection depends on both the electrolyte to which the system is exposed and the cathodic area exposed.

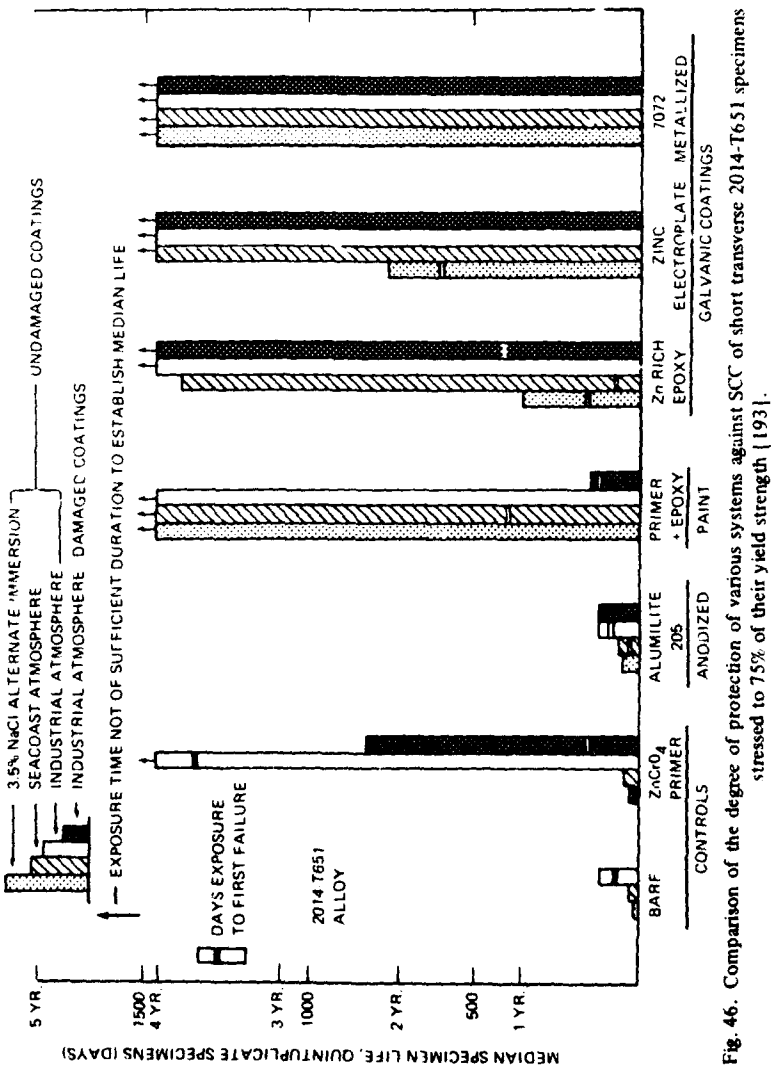


Fig. 46. Comparison of the degree of protection of various systems against SCC of short transverse 2014-T651 specimens stressed to 75% of their yield strength [193].

The effectiveness of the various galvanic coatings on 2014-T651 and 7079-T651 is compared with some other protective treatments in Figs. 46 and 47. Specimens metallized with the 7072 alloy performed quite well, although some failures did occur in some metallized 7079-T651 specimens. The poorer performance of the metallized 7079-T651 specimens has been rationalized on the basis of the smaller difference in solution potential between the 7079-T651 and the 7072 alloy (Table 7).

**Table 7.** Solution Potentials of Some Commercial Aluminum Alloys

| *Alloy and Temper* | *Solution Potential (mV)* |
|---|---|
| 2024-T351 | -700 |
| 2014-T651 | -790 |
| 7178-T651 | -830 |
| 7079-T651 | -865 |
| 7072 | -940 |

Data from Ref. 248 (unpublished data).

Average steady value in NaCl-$H_2O_2$ solution, referred to 0.1*N* calomel cell at 25°C.

Pure aluminum coatings, deposited by such methods as ion vapor deposition or vacuum deposition, also provide good protection to 7075-T6 aluminum if the coating is around 1 mil thick and if the coating is protected against pitting attack by a supplementary chromate treatment.

Magnesium pigment added to a proprietary, air-curing, inorganic binder has also proved to be effective in minimizing SCC of 7075-T6 [194]. Magnesium pigment added to an epoxy primer has also given good results [195].

While galvanic coatings have the important advantage over other protective measures in that the degree of protection is less affected by mechanical damage or holidays in the coating, there is a limit to the size of the void that can be electrochemically protected. It has been shown that a void as narrow as 0.0625 in. can seriously impair the effectiveness of a 7072 metallized coating [194]. Some of the drawbacks of 7072 metallized coatings are that they have a rough finish; they are difficult to apply to close tolerances; they sometimes spall when formed, drilled, or countersunk; and they can bridge base metal cracks and thus interfere with crack or defect inspection. Also, their porous nature precludes die-penetrant inspection.

Zinc-plated specimens do not perform as well as metallized specimens in the alternate-immersion environment due to the relatively rapid consumption of the

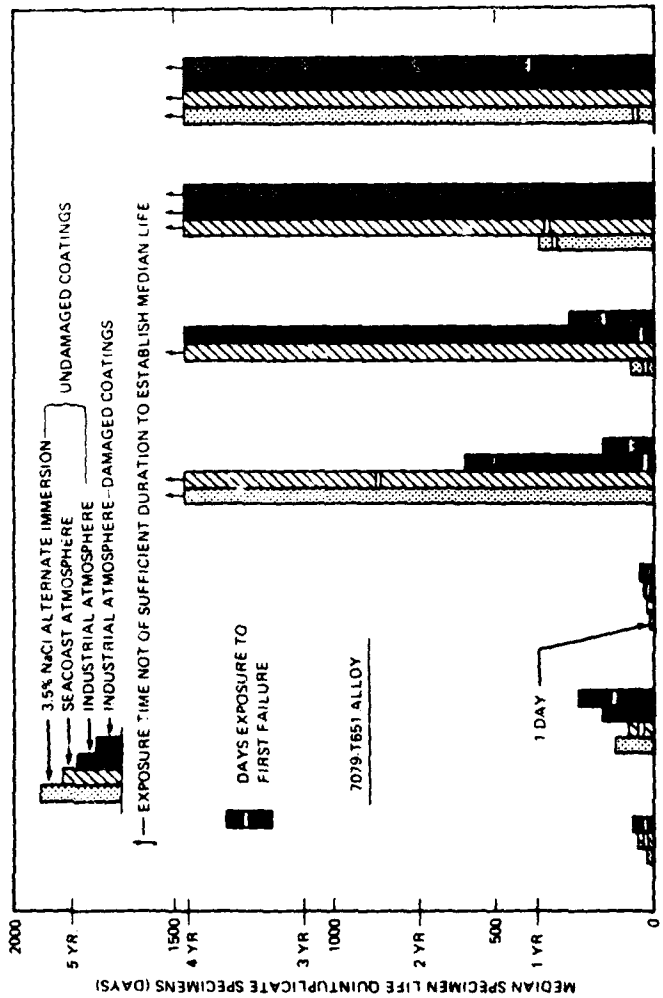


Fig. 47. Comparison of the degree of protection of various systems against SCC of short transverse 7079-T651 specimens stressed to 75% of their yield strength [193].

zinc (Figs. 46 and 47). In atmospheric tests, overall performance of the zinc-plated specimens is more favorable, with failures confined to 7079-T651. The effectiveness of zinc electroplate can be improved through use of paint topcoats to reduce rapid consumption of the zinc [194]. While zinc-electroplate coatings are smooth and relatively nonporous, zinc imparts a greater weight penalty than aluminum metallized coatings.

Zinc-rich epoxy paint systems can be applied with normal paint procedures. Because the zinc must be in intimate contact with the substrate metal to provide electrochemical protection, the chromate conversion coating and primer pretreatments cannot be used; thus, adhesion is less for the zinc paint systems than for the other epoxy systems. Zinc-rich paint systems provide appreciable protection, however, except in the severe alternate-immersion environment and when intentionally damaged (Fig. 46 and 47).

While some of these shot-peening and coating treatments can do an effective job of delaying SCC, none is a substitute for the selection of a stress-corrosion-resistant alloy. A possible sequence of events leading to failure of a fully protected part is as follows: Mechanical damage can cause the loss of the protection afforded by the anodized layer, the primer, and the topcoat, thus allowing the environment to reach the shot-peened layer. Under suitable conditions pitting corrosion can then penetrate the shot-peened layer, leading to SCC if the material is susceptible and if tensile stresses are present. It should be noted that future aerospace specifications may require that critical forgings be subjected to a 2000-hr alternate-immersion test in their bare, final-machined condition to locate potential problem areas. While it may be sufficient to ensure that such located problem areas are adequately peened and painted, the best way to ensure passing such a test is to use SCC-resistant materials.

**Protective Treatments for Preventing Exfoliation and Faying-Surface Corrosion.** Exfoliation corrosion usually starts at fastener holes because the holes are drilled after the protective anodizing and conversion coatings are applied. Under service conditions, electrolytes are present in the form of rain condensation, paint strippers, brighteners, seawater, etc. Corrosion usually originates in the countersink areas because that is where initial penetration by the electrolyte occurs. Exfoliation and general corrosion also often start at faying surfaces where electrolytes penetrate the space between riveted, bonded, or bolted overlapping panels. This type of corrosion can be particularly severe if absorbent materials are located between the faying surfaces. Severe corrosion of this type can cause a loss of structural strength.

Typical methods of combating exfoliation corrosion involve wet installation of rivets treated with polysulfide sealing compound or zinc chromate primer. However, recent tests [197] on 7075-T6 and 7178-T6 have indicated that neither of these materials provides complete protection against exfoliation corrosion because moisture from sustained high-humidity test conditions eventually penetrated to the inside surface of fastener holes, where corrosion occurred. The

moisture was not merely seeping between the sealants and the sides of the fastener holes but was permeating the sealants.

This weakness of the elastomers can be eliminated by incorporating a water-soluble chromate inhibitor into the elastomer [197]. This inhibitor dissolves in any moisture penetrating the sealant/metal interface and converts it into a protective solution. The validity of this concept has been proven by simulated service tests, and field tests and inhibitive sealants are now being used on a number of commercial and military aircraft [197]. Inhibitive compounds are now being produced for brush application, for spraying, for fillet work, and for faying surfaces. A special formulation with aluminum pigment is available for use as a topcoating. It should be kept in mind that presently used inhibitors inhibit general corrosion but do not inhibit the growth of stress corrosion cracks.

By reducing the viscosity of the inhibitive sealants, a successful coating system has also developed from these materials; it is now being used on aircraft surfaces, in the rework and refinishing of dry bays, and in the internal spaces of aircraft wings that are not filled with fuel [197]. Depletion of the soluble chromate ions from the elastomer coating is prevented by overcoating with an aluminized elastomeric antileaching topcoat.

### Proper Storage

Stress corrosion cracks in susceptible high strength aluminum alloys such as 7079-T6 and 7075-T6 are often found in parts that have been sitting on the shelf awaiting installation. Residual surface tensile stresses exposed by machining or resulting from straightening or forming operations, combined with a transverse grain structure and the water vapor normally present in the air, are all that are required.

Besides in-service cracking, many parts fail in structures even before the structure has performed its intended mission. For example, some swaged 7075-T6 support struts for the lunar module were found to contain stress corrosion cracks. Such problems are of great importance, especially since storage times may greatly exceed original plans due to funding cutbacks, etc. In this regard, recently measured quantitative crack velocity data may be useful [73]. These data suggest that if relative humidities in storage areas are maintained below about 2%, stress corrosion cracks could not grow faster than about $10^{-8}$ cm/sec, even if cracklike flaws were already present and loaded to high $K_I$ levels.*

*Further practical guidance in the avoidance of SCC in aerospace structures is given in Military Specification MIL F-7179D (3 March 1969) on finishings and coatings and in "General Specifications for Design and Construction of Aircraft Weapon Systems SD-24J, Vol I: Fixed Wing Aircraft," 10 October 1966. *(Editor)*

**ACKNOWLEDGMENTS**

The authors would like to thank their colleagues Dr. T. R. Beck, D. M. J. Blackburn, and Dr. W. H. Smyrl for many helpful discussions. Managerial support by Dr. D. E. Piper and Dr. H. Brunner is gratefully acknowledged. Mr. C. Bilbao provided valuable experimental assistance.

### 4.7 References

1. *Registration Record of Aluminum Association Alloy Designations and Chemical Composition Limits for Wrought Aluminum Alloys*, The Aluminum Association.
2. *Aluminum Standards and Data*, 2nd ed., The Aluminum Association, December 1969.
3. *Alcoa Aluminum Handbook*, Aluminum Company of America, 1967.
4. P. J. Wright, Aluminum Company of America, private communication.
5. R. A. Schultz, "Alcoa Aluminum Alloy 2021," *Alcoa Green Letter*, Aluminum Company of America, Apr. 1968 (not released for publication).
6. *Hiduminium Technical Data*, High Duty Alloys Ltd., Slough, Bucks, England.
7. F. C. Maciejewski, Harvey Aluminum, Inc., private communication, July 17, 1970.
8. *Aluminum 7076*, published by Engineering Alloy Digest, Inc., Upper Montclair, N.J., Filing Code: Al-143 Aluminum Alloy, Feb. 1965.
9. *Aluminum Alloy Armor Plate, Heat Treatable, Weldable*, Military Specification MIL-A-46063B, Feb. 15, 1965.
10. *Aluminum Alloy Die Forgings and Hand Forgings, 7.7 Zn-2.5 Mg-1.5 Cu-0.15 Cr (7049-T73)*, Proposed Aerospace Material Specification AMS 41 DM, SAE, Nov. 25, 1969.
11. R. A. Schultz, "Alcoa Alloys 7075-T76 and 7178-T76," *Alcoa Green Letter*, Aluminum Company of America, Apr. 1970.
12. R. A. Schultz, "Alcoa Alloy 7075-T73," *Alcoa Green Letter*, Aluminum Company of America, June 1969 (not released for publication).
13. *Alcoa Alloy X7080 Preliminary Technical Information*, Aluminum Company of America, Sept. 1965 (not released for publication).
14. *Facts About a New Alcoa Alloy (7175-T66 and 7175-T736), Technical Information on Premium Strength Forgings*, Aluminum Company of America, May 1, 1968.
15. J. A. Dickson, "Alcoa 467 Process X7475 Alloy," *Alcoa Green Letter*, Aluminum Company of America, May 1970 (not released for publication).
16. *Semi-Finished Products in Aluminum, Magnesium, Titanium*, Otto Fuchs Metallwerke Meinerzhagen/Westfalen, Aug. 1963.
17. *Aluminum Alloy Forgings*, Federal Specification QQ-A-367g, June 30, 1966.

18. *Aluminum Alloy Armor, Forged*, Military Specification MIL-A-45225C(MR), Jan. 19, 1970.
19. B. W. Lifka and J. G. Kaufman, *Fracture Toughness, Fatigue Crack Propagation and Corrosion Characteristics of Aluminum Alloy Plates for Wing Skins*, Quarterly Report 4, March 3 to June 3, 1964, Contract AF33(657)-11155, Aluminum Company of America, June 15, 1964.
20. J. G. Kaufman and M. Holt, *Fracture Characteristics of Aluminum Alloys*, Technical Paper 18, Alcoa Research Laboratories, Aluminum Company of America, 1965.
21. J. G. Kaufman, G. E. Nordmark, and B. W. Lifka, *Fracture Toughness Characteristics of 7075-T651, 7075-T7351 and 7079-T651 Aluminum Alloys*, Technical Report AFML-TR-65-170, Wright-Patterson AFB, Ohio, May 1965.
22. G. E. Nordmark, B. W. Lifka, and J. G. Kaufman, *Fracture Toughness, Fatigue Crack Propagation and Corrosion Characteristics of Aluminum Alloy Plates for Wing Skins*, Yearly Summary Technical Report, June 3, 1964, to June 3, 1965, Contract AF33(615)-2012, Aluminum Company of America, June 15, 1965.
23. G. E. Nordmark, B. W. Lifka, and J. G. Kaufman, *Fracture Toughness, Fatigue Crack Propagation and Corrosion Characteristics of Aluminum Alloy Plates for Wing Skins*, Quarterly Report, June 3 to Sept. 3, 1965, Contract AF33(615)-2012, Aluminum Company of America, Sept. 15, 1965.
24. C. M. Carman, D. F. Armiento, and H. Markus, *Plane-Strain Fracture Toughness of High-Strength Aluminum Alloys*, Report A65-16, United States Army, Frankford Arsenal, Philadelphia, Pa., Dec. 1965.
25. G. E. Nordmark, B. W. Lifka, and J. G. Kaufman, *Fracture Toughness, Fatigue Crack Propagation and Corrosion Characteristics of Aluminum Alloy Plates for Wing Skins*, Quarterly Report, Sept. 3 to Dec. 3, 1965, Contract AF33(615)-2012, Aluminum Company of America, Dec. 15, 1965.
26. *Alcoa Research Laboratories 1966 Research Review*, Application Engineering Division, Aluminum Company of America, New Kensington, Pa. (not released for publication).
27. J. G. Kaufman, G. E. Nordmark, and B. W. Lifka, *Fracture Toughness, Fatigue and Corrosion Characteristics of 2020-T651, 2024-T851, 2219-T851, and 7001-T75 Aluminum Alloys*, Technical Report AFML-TR-66-291, Wright-Patterson AFB, Ohio, Sept. 1966.
28. G. J. Petrak, *Evaluation of the Plane Strain Fracture Properties of an X7080-T7 Aluminum Alloy Forging*, Report MAA 67-7, Contract F33615-67-C-1262, University of Dayton Research, Feb. 1967.
29. S. O. Davis et al., *Effect of Specimen Type and Crack Orientation on Fracture Toughness*, Technical Report AFML-TR-67-32, Materials Information Research, Wright-Patterson AFB, Ohio, Mar. 1967.

30. *Mechanical Property Data, 7039 Aluminum, Plate (T651 Condition)*, prepared by Battelle Memorial Institute, Columbus Laboratories, Columbus, Ohio, under Contract AF33(615)-2494, and issued by Air Force Materials Laboratory, Research and Technology Division, Air Force Systems Command, Wright-Patterson AFB, Ohio, Mar. 1967.
31. H. J. Oberson, *Metallurgical Evaluation of X7080-T7 Aluminum Forging Alloy*, Document T6-5258, The Boeing Company, Dec. 8, 1967.
32. J. W. Coursen, *Mechanical Properties and Fracture Characteristics of Some 7075-T651, T7351, and T7651 and 7178-T651 and T7651 Plate*, Report 9-68-4, Aluminum Company of America, New Kensington, Pa., Jan. 23, 1968 (not released for publication).
33. R. V. Turley, *Evaluation of Aluminum Alloy X7080-T7 Hand Forging*, Engineering Technical Report ETR-DAC-67295, Materials Research and Process Engineering, Douglas Aircraft Division, Oct. 23, 1968.
34. R. L. Moore, G. E. Nordmark, and B. W. Lifka, *Stress-Corrosion and Corrosion Fatigue Susceptibility of High-Strength Alloys*, 6th Quarterly Report, Contract AF33(615)-67-C-1922, Aluminum Company of America, Oct. 31 to Dec. 31, 1968.
35. P. M. Lorenz, *Effect of Pressurized Hydrogen Upon Inconel 718 and 2219 Aluminum*, Jet Propulsion Laboratory Contract P.O. EG 479375 and University of California Contract P.O. G 845350, Document D2-114417-1, The Boeing Company, Seattle, Wash., Feb. 1969.
36. P. M. Lorenz, *Compatibility of Tankage Materials With Liquid Propellants*, Technical Report AFML-TR-69-99, Wright-Patterson AFB, Ohio, May 1969.
37. J. Trizil, *Investigation of the 7039 Aluminum Alloy*, Document T2-114449-1, The Boeing Company, Seattle, Wash., July 1969.
38. J. G. Kaufman, P. F. Schilling, and F. G. Nelson, "Fracture Toughness of Aluminum Alloys," *Metals Eng. Quart.* 9, 39 (Aug. 1969).
39. J. G. Kaufman, P. E. Schilling, G. E. Nordmark, B. W. Lifka, and J. W. Coursen, *Fracture Toughness, Fatigue and Corrosion Characteristics of X7080-T7E41 and 7178-T651 Plate and 7075-T6510, 7075-T73510, X7080-T7E42, and 7178-T6510 Extruded Shapes*, Technical Report AFML-TR-69-255, Wright-Patternson AFB, Ohio, Nov. 1969.
40. F. R. Schwartzberg, R. D. Keys, and T. F. Kiefer, "Fracture Behavior of Two New High-Strength Aluminum Alloys," *Metals Eng. Quart.* 9, 53 (Nov. 1969).
41. *7049-T73–Kaiser Aluminum's New Aluminum Alloy for Forgings*, Kaiser Aluminum, Jan. 1970.
42. D. O. Sprowls and R. H. Brown, *Resistance of Wrought High-Strength Aluminum Alloys to Stress Corrosion*, Technical Paper 17, Aluminum Company of America, New Kensington, Pa., 1962.

43. D. O. Sprowls and R. H. Brown, "What Every Engineer Should Know About Stress Corrosion of Aluminum," *Metals Prog.* **81** (No. 4), 79, (1962).
44. D. O. Sprowls and R. H. Brown, "What Every Engineer Should Know About Stress Corrosion of Aluminum," *Metals Prog.* **81** (No. 5), 77, (1962).
45. R. H. Brown, D. O. Sprowls, and M. B. Shumaker, "Influence of Stress and Environment on the Stress-Corrosion Cracking of High Strength Aluminum Alloys," *Engineering Practice to Avoid Stress Corrosion Cracking*, AGARD Conference Proceedings 53, NATO, Feb. 1970.
46. M. O. Speidel, The Boeing Company, Seattle, Wash., unpublished data.
47. M. O. Speidel, "Current Understanding of Stress Corrosion Crack Growth in Aluminum Alloys," in *The Theory of Stress Corrosion Cracking in Alloys*, Proceedings of a Research Evaluation Conference, Portugal, published 1971 by NATO Scientific Affairs Division, Brussels.
48. M. V. Hyatt The Boeing Company, Seattle, Wash., unpublished data.
49. J. A. Dickson, "Aluminum Alloy 2124," *Alcoa Green Letter*, Aluminum Company of America, September 1970 (not released for publication).
50. S. M. Wiederhorn, "Moisture Assisted Crack Growth in Ceramics," *Int. J. Fracture Mech.* **4** (No. 2), 171 (June 1968).
51. S. R. Novak and S. T. Rolfe, "Modified WOL Specimen for $K_{Iscc}$ Environmental Testing," *J. Mater.* **4** (No. 3), 701 (1969).
52. W. Rosenhain and S. L. Archbutt, "On the Inter-Crystalline Fracture of Metals Under Prolonged Applications of Stress (Preliminary Paper)," *Proc. Roy. Soc. London* **96A**, 55 (1919).
53. W. Rosenkranz, *Forschungsber. Wirts. Verkehrsmin. Nordrhein-Westfalen* **158**, 1956.
54. F. H. Haynie and W. K. Boyd, *Stress-Corrosion Cracking of Aluminum Alloys*, DMIC Report 228, Battelle Mem. Inst., July 1966.
55. D. O. Sprowls and R. H. Brown, "Stress Corrosion Mechanisms for Aluminum Alloys," *Proc. Conf. on Fundamental Aspects of Stress Corrosion Cracking*, NACE, Houston, Texas, 1969, p. 466.
56. E. H. Spuhler and C. L. Burton, "Avoiding Stress-Corrosion Cracking in High Strength Aluminum Alloy Structures," *Alcoa Green Letter*, Aluminum Company of America, Aug. 1, 1962, revised Apr. 1970 (not released for publication).
57. *Stress Corrosion Testing Methods*, ASTM STP 425, Amer. Soc. Testing Mater., Philadelphia, Pa., 1967, p. 3.
58. J. S. Prestley, Jr., *Effect of Stress Orientation on Resistance to Stress-Corrosion Cracking of Wrought Aluminum Products*, MRD 35-901-3-T, Reynolds Metal Company, Feb. 19, 1965.
59. F. H. Haynie, D. A. Vaughan, D. I. Phalen, W. K. Boyd, and P. D. Frost, *A Fundamental Investigation of the Nature of Stress-Corrosion Cracking in*

*Aluminum Alloys*, Technical Report AFML-TR-66-267, Wright-Patterson AFB, Ohio, June 1966, p. 67.

60. M. S. Hunter and W. G. Fricke, Jr., *Study of Crack Initiation Phenomena Associated With Stress Corrosion of Aluminum Alloys*, Final Summary Report, NASA Contract NAS 8-20396, Aluminum Company of America, New Kensington, Pa., Oct. 6, 1969.
61. J. H. Mulherin, *Influence of Environment on Crack Propagation Characteristics of High Strength Aluminum Alloys*, ASTM STP 425, Amer. Soc. Testing Mater., Philadelphia, Pa., 1967, p. 66.
62. C. F. Tiffany, P. M. Lorenz, and R. C. Shah, *Extended Loading of Cryogenic Tanks*, NASA Contract NAS 3-6290, The Boeing Company, Seattle, Wash., 1966.
63. L. R. Hall and C. F. Tiffany, *Fracture and Flaw Growth Investigation for 2014-T6 Aluminum Weldments Used in Saturn II $LH_2$ Tanks*, NASA Contract NAS 8-5608, The Boeing Company, Seattle, Wash., Nov. 15, 1967.
64. T. G. Gooch, D. McKeown, and D. Willingham, "Stress Corrosion of Welded Materials: Evaluation and Control," *Metal Const. Br. Welding J.* **1**, 469 (Oct. 1969).
65. J. G. Kaufman, P. E. Schilling, G. E. Nordmark, B. W. Lifka, and J. W. Coursen, *Fracture Toughness, Fatigue, and Corrosion Characteristics of X7080-T7E41, and 7178-T651 Plate and 7075-T6510, 7075-T73510, X7080-T7E42, and 7178-T6510 Extruded Shapes*, Technical Report AFML-TR-69-255, Air Force Materials Laboratory, Wright-Patterson AFB, Ohio, Nov. 1969.
66. Lee Craig, Reynolds Metal Company, private communication, July 15, 1970.
67. M. V. Hyatt, *Effects of Residual Stresses on Stress-Corrosion Crack Growth Rates in Aluminum Alloys*, Document D6-24469, The Boeing Company, Seattle, Wash., Nov. 1969, also, *Corrosion* **26** (No. 12), 547 (1970).
68. M. O. Speidel, "Effect of Stress and Environment on Velocity and Branching of Subcritical Cracks," paper presented at AIME Spring Meeting, Las Vegas, Nev., May 1970.
69. T. A. Renshaw, "New Approaches to the Analysis of Stress Corrosion Data," in Technical Report AFML-TR-67-329, *Proceedings of the Air Force Materials Laboratory Fiftieth Anniversary Technical Conference on Corrosion of Military and Aerospace Equipment*, Denver, Colo., Nov. 1967.
70. J. E. Campbell, *Effects of Hydrogen Gas on Metals at Ambient Temperature*, DMIC Report S-31, Battelle Mem. Inst., April 1970.
71. R. J. Walter and W. T. Chandler, *Effects of High-Pressure Hydrogen on Metals at Ambient Temperature*, Reports of NASA Contract NAS 8-19, 1969.

72. R. M. Vennett and G. S. Ansell, "A Study of Gaseous Hydrogen Damage in Certain FCC Metals," *Trans. ASM*, 62, 1007 (1969).
73. M. V. Hyatt and M. O. Speidel, *Stress-Corrosion Cracking of High Strength Aluminum Alloys*, Document D6-24840, The Boeing Company, Seattle, Wash., 1971.
74. M. S. Hunter, *Study of Crack Initiation Phenomena Associated With Stress Corrosion of Aluminum Alloys*, One-Year Summary Report, NASA Contract NAS 8-20396, Aluminum Company of America, New Kensington, Pa., 1967.
75. H. L. Craig, Jr., and F. E. Loftin, "Preventing Stress Corrosion Failures in Susceptible Alloys" (to be published in *Corrosion*).
76. J. McHardy and E. H. Hollingsworth, *Investigation of the Mechanism of Stress Corrosion of Aluminum Alloys*, Final Report, U.S. Navy, Bureau of Naval Weapons Contract NOw 65-0327f, Aluminum Company of America, New Kensington, Pa., 1966.
77. I. L. Rosenfeld and I. K. Marshakov, "Mechanism of Corrosion of Metals in Narrow Cracks and Crevices," *Zh. Fiz. Khim.* 31, 2328 (1957).
78. W. F. Helfrich, "Influence of Stress and Temperature on Short Transverse Stress Corrosion Cracking of an Al-4.2Zn-2.5Mg Alloy," ASTM STP 425, Amer. Soc. Testing Mater., Philadelphia, Pa., 1967.
79. B. W. Lifka, unpublished work at Alcoa Research Laboratories, reported by D. O. Sprowls and R. H. Brown, *Proceedings of Conference on Fundamental Aspects of Stress Corrosion Cracking*, NACE, Houston, Texas, 1969, p. 466.
80. R. P. M. Procter and H. W. Paxton, "Stress Corrosion of the Aluminum Alloy 7075-T651 in Organic Liquids," *ASTM J. Mater.* 4, 729 (1969).
81. H. W. Paxton and R. P. M. Procter, "The Stress Corrosion Cracking of 7075-T6 Aluminum Alloy in Organic Liquids," *Proceedings of Conference on Fundamental Aspects of Stress Corrosion Cracking*, NACE, Houston, Texas, 1969, p. 509.
82. W. Rostoker, J. M. McCaughey, and H. Markus, *Embrittlement by Liquid Metals*, Reinhold Publishing Co., New York, 1960.
83. E. H. Dix, Jr., W. A. Anderson, and M. B. Shumaker, "Influence of Service Temperature on the Resistance of Wrought Aluminum-Magnesium Alloys to Corrosion," *Corrosion* 15 (No. 2) (Feb. 1959).
84. C. L. Brooks, "Aluminum-Magnesium Alloys 5086 and 5456-H116" *Nav. Eng. J.* 82 (No. 4), 29 (Aug. 1970).
85. W. A. Anderson, *Treatment of Aluminum-Magnesium Alloys*, U.S. Patent 3,232,796, Feb. 1, 1966.
86. E. H. Dix, Jr., W. A. Anderson, and M. B. Shumaker, *Development of Wrought Aluminum-Magnesium Alloys*, Technical Paper 14; Alcoa Research Laboratories, Aluminum Company of America, 1958.
87. C. L. Wood, Jr., "Selecting Wrought Aluminum Alloys for Marine Use," *Alcoa Green Letter*, Aluminum Company of America, June 1969.

88. P. Brenner and G. J. Metcalfe, "The Effect of Cold Work on the Microstructure and Corrosion-Resistance of Aluminum-5% Magnesium Alloys Containing 0-1% Zinc," *J. Inst. Metals* **81**, 261 (1952).
89. H. B. Romans, "An Accelerated Laboratory Test to Determine the Exfoliation Corrosion Resistance of Aluminum Alloys," *Mater. Res. Stand.* **9**, 31 (Nov. 1969).
90. D. O. Sprowls, T. J. Summerson, H. B. Romans, and S. J. Sansonetti, *The Aluminum Association Tentative Exfoliation Test for Al-Mg Alloys for Boat and Ship Hull Construction*, The Aluminum Association, 1970.
91. *The Aluminum Association ASSET Immersion Test for Aluminum Alloys 5086 and 5456 Plate, Sheet, and Extrusions, for Seawater Applications*, The Aluminum Association (to be published).
92. *Aluminum Alloy 5456 Plate and Sheet for Seawater Applications*, Federal Specification QQ-A-00250/20, Dec. 31, 1968.
93. J. A. Ford and M. J. Pryor, *Corrosion Performance of MRL-A8*, Report MRL-70-PR-11, Project 0335, Olin Metals Research Laboratories, New Haven, Conn., Feb. 19, 1970.
94. R. Chadwick, N. B. Muir, and H. B. Granger, "The Effect of Iron, Manganese and Chromium on the Properties in Sheet Form of Aluminum Alloys Containing 0.7% Mg and 1.0% Si," *J. Inst. Metals* **82**, 75 (1953-54).
95. E. H. Dix, Jr., R. H. Brown, and W. W. Binger, *ASM Metals Handbook*, 8th ed. Vol. 1, p. 916.
96. J. G. Williamson, "Stress Corrosion: Saturn V Fights Back," *Mater. Eng.* **67**, 35 (June 1968).
97. D. C. Baxter, High Duty Alloys Ltd., Slough, Bucks. England, private communication, June 1970.
98. S. J. Ketcham, "Polarization and Stress-Corrosion Studies of an Al-Cu-Mg Alloy," *Corrosion Sci.* **7** (No. 6), 305 (1967).
99. J. A. Nock, Jr., "Properties of Commercial Wrought Alloys," *Aluminum*, Vol. 1: Properties, Physical Metallurgy, and Phase Diagrams (K. R. Van Horn, ed.), American Society for Metals, 1967, pp. 303-336.
100. W. D. Robertson, "Correlation of Mechanical Properties and Corrosion Resistance of 24S-Type Aluminum Alloys as Affected by High Temperature Precipitation," *Trans. Amer. Inst. Mining Metal. Eng.*, Institute of Metals Division, **166**, 216 1946.
101. R. L. Horst, Jr., E. H. Hollingsworth, and W. King, "A New Solution Potential Measurement for Predicting Stress-Corrosion Performance of 2219 Aluminum Alloy Products," *Corrosion* **25** (No. 5), 199 (May 1969).
102. H. Y. Hunsicker, "The Metallurgy of Heat Treatment," *Aluminum*, Vol. 1: Properties, Physical Metallurgy, and Phase Diagrams (K. R. Van Horn, ed.) American Society for Metals, 1967, pp. 109-162.
103. M. B. Shumaker and W. B. Vernam, unpublished work at Alcoa Research Laboratories (1962) reported by D. O. Sprowls and R. H. Brown,

*Proceedings of Conference on Fundamental Aspects of Stress Corrosion Cracking*, NACE, Houston, Texas, 1969, p. 466.

104. W. D. Vernan and W. A. Anderson, *Thermal Treatment of Aluminum Base Alloy Products*, U.S. Patent 3,171,760, Mar. 2, 1965.
105. M. O. Speidel, "Interaction of Dislocations With Precipitates in High Strength Aluminum Alloys and Susceptibility to Stress Corrosion Cracking," *Proceedings of Conference on Fundamental Aspects of Stress Corrosion Cracking*, NACE, Houston, Texas, 1969, p. 561.
106. D. O. Sprowls and J. A. Nock, Jr., *Thermal Treatment of Aluminum Base Alloy Article*, U.S. Patent 3,198,676, Aug. 3, 1965.
107. J. A. Vaccari, "New Wrought Aluminum Alloys Fight Corrosion," *Mater. Eng.* **71**, 22 (June 1970).
108. R. L. Horst, Jr., and B. W. Lifka, "Prediction of Exfoliation and Stress Corrosion Performance of 7178-T76 and 7075-T76 Aluminum Alloy Sheet and Plate," *Corrosion* **26** (No. 3), 111 (Mar. 1970).
109. *Heat Treatment, Aluminum Alloys*, Military Specification MIL-H-6088D, Dec. 23, 1968.
110. J. T. Staley, *Investigation to Improve the Stress-Corrosion Resistance of Aluminum Alloys Through Alloy Additions and Specialized Heat Treatment*, Final Report, Naval Air Systems Command Contract N00019-68-C-0146, Feb. 28, 1969.
111. E. DiRusso, *Further Investigations on Wrought Complex Al-Zn-Mg-Cu Alloys*, Final Status Report, Contract DA-91-591-EUC 3425, European Research Office, July 26, 1965.
112. I. J. Polmear, "A Trace-Element Effect in Alloys Based on the Al-Zn-Mg System," *Nature* **186**, 303-304 (Apr. 23, 1960).
113. I. J. Polmear, "The Aging Characteristics of Complex Al-Zn-Mg Alloys: Distinctive Effects of Copper and Silver on the Aging Mechanism," *J. Inst. Metals* **89**, 51-59 (1960-1961).
114. I. J. Polmear, "The Properties of Commercial Al-Zn-Mg Alloys: Practical Implications of Trace Additions of Silver," *J. Inst. Metals* **89**, 193-202 (1960-1961).
115. I. J. Polmear, "Studies on High Strength Aluminum Alloy in Australia," *Metal Prog.* **81**, 82 (Jan. 1962).
116. J. T. Vietz, K. R. Sargent, and I. J. Polmear, "The Influence of Small Additions of Silver on the Aging of Aluminum Alloys: Further Observations of Al-Zn-Mg Alloys," *J. Inst. Metals* **92**, 327 (1963-1964).
117. I. J. Polmear, "Tensile Properties of Modified Aluminum-Zinc-Magnesium Alloys Containing Silver," *J. Inst. Metals* **94**, 36-37 (1966).
118. E. DiRusso, *Structural and Mechanical Properties and Stress-Corrosion Resistance of Wrought Complex Alloys of the Al-Zn-Mg-Cu System With Defined Amounts of Chromium, Zirconium, and Silver*, U.S. Army Contract DA-91-591-EUC 2464, Report 13.719/6407.069, Instituto Sperimentale Dei Metalli Leggeri, July 21, 1964.

119. E. DiRusso, "Experimental Investigation on Complex Al-Zn-Mg-Cu Alloys With Controlled Amounts of Chromium, Zirconium, and Silver," *Aluminio* **33**, 505-519 (Oct. 1964).
120. E. DiRusso, "Resistance to Stress-Corrosion and Structural Characteristics of Al-Zn-Mg-Cu Alloys With Controlled Amounts of Chromium, Zirconium, and Silver," *Aluminio, Neuva Metallurgia*, **XXXIV**, 331 (July 1965).
121. W. Rosenkranz (assignor to Otto Fuchs Metallwerke), *Al-Mg-Zn Alloy Having High Stress-Corrosion Resistance*, U.S. Patent 2,823,994, Feb. 18, 1958.
122. W. Rosenkranz, "Development of a High Strength, Stress-Corrosion Resistant Alloy of the Al-Zn-Mg Type; Part II: The Effect of the Chemical Composition on the Artificial Aging and Stress-Corrosion of High Strength Al-Zn-Mg-Cu Alloys," *Aluminum* **39**, 741-752 (Dec. 1963).
123. R. W. Elkington and A. N. Turner, "The Effect of Silver on the Stress-Corrosion Resistance of High Strength Al-Zn-Mg-Cu Alloys," *J. Inst. Metals* **95**, 294-298 (1967).
124. A. J. Kennedy, "The Prospects for Materials," *Aeron. J. Roy. Aeron. Soc.* **73** (No. 697), 1 (Jan. 1969).
125. J. C. McMillan and M. V. Hyatt, *Development of High-Strength Aluminum Alloys With Improved Stress-Corrosion Resistance*, Technical Report AFML-TR-68-148, Air Force Materials Laboratory, Wright-Patterson AFB, Ohio, June 1968.
126. E. DiRusso, Instituto Sperimentale Dei Metalli Leggeri, private communication.
127. J. C. McMillan and M. V. Hyatt, *Development of High-Strength Aluminum Alloys With Improved Stress-Corrosion Resistance*, Technical Report AFML-TR-67-180, Air Force Materials Laboratory, Wright-Patterson AFB, Ohio, June 1967.
128. H. Brooks, "Stress Corrosion Cracking of Aluminum Alloys—A Review of U.K. Service Experience and Current Research," Technical Report AFML-TR-67-329, *Proceedings of the Air Force Materials Laboratory Fiftieth Anniversary Technical Conference on Corrosion of Military and Aerospace Equipment*, Denver, Colo., Nov. 1967, p. 133.
129. G. Blankenburgs, Aeronautical Research Laboratories, Fishermans Bend, Australia, private communication, Nov. 18, 1969.
130. M. V. Hyatt and H. W. Schimmelbusch, *Development of a High-Strength Stress Corrosion Resistant Aluminum Alloy for Use in Thick Sections*, Technical Report AFML-TR-70-109, Air Force Materials Laboratory, Wright-Patterson AFB, Ohio, May 1970.
131. D. S. Thompson and S. A. Levy, *High Strength Aluminum Alloy Development*, First Quarterly Progress Report, Contract F33-615-69-C-1643, Sept. 1969.
132. J. T. Staley, *Investigation to Develop a High Strength, Stress-Corrosion Resistant Aluminum Aircraft Alloy*, Bimonthly Progress Letter, Dec. 15,

1968 to Feb. 14, 1969, Naval Air Systems Command Contract N00019-69-C-0292, Mar. 4, 1969.

133. J. T. Staley, *Investigation to Develop a High Strength, Stress-Corrosion Resistant Aluminum Aircraft Alloy*, Bimonthly Progress Letter, Feb. 15 to Apr. 14, 1969, Naval Air Systems Command Contract N00019-69-C-0292, Apr. 30, 1969.
134. J. T. Staley, *Investigation to Develop a High Strength, Stress-Corrosion Resistant Aluminum Aircraft Alloy*, Bimonthly Progress Letter, Apr. 15 to June 14, 1969, Naval Air Systems Command Contract N00019-69-C-0292, June 27, 1969.
135. J. T. Staley, *Investigation to Develop a High Strength, Stress-Corrosion Resistant Aluminum Aircraft Alloy*, Final Report, Naval Air Systems Command Contract N00019-69-C-0292, Jan. 20, 1970.
136. J. T. Staley, *Development of a High Strength, Stress-Corrosion Resistant Naval Aircraft Aluminum Alloy*, Bimonthly Progress Letter, Dec. 15, 1969 to Feb. 14, 1970, Naval Air Systems Command Contract N00019-70-C-0118, Mar. 3, 1970.
137. J. T. Staley, *Development of a High Strength, Stress-Corrosion Resistant Naval Aircraft Aluminum Alloy*, Bimonthly Progress Letter, Feb. 15 to Apr. 15, 1970, Contract N00019-70-C-0118, Aluminum Company of America, Apr. 27, 1970.
138. J. T. Staley, *Development of a High Strength, Stress-Corrosion Resistant Naval Aircraft Aluminum Alloy*, Bimonthly Progress Letter, Apr. 16, 1970 to June 15, 1970, Contract N00019-70-C-0118, Aluminum Company of America, June 24, 1970.
139. J. T. Staley, *Investigation to Develop a High Strength Stress-Corrosion Resistant Naval Aircraft Aluminum Alloy*, Final Report, Contract N00019-70-C-0118, Aluminum Company of America, Nov. 20, 1970.
140. J. T. Staley, *Exploratory Development of High-Strength Stress-Corrosion Resistant Aluminum Alloys Usable in Thick Section Applications*, First Quarterly Report, Contract F33615-69-C-1644, Aluminum Company of America, Sept. 22, 1969.
141. J. T. Staley, *Exploratory Development of High-Strength Stress-Corrosion Resistant Aluminum Alloys Usable in Thick Section Applications*, Second Quarterly Report, Contract F33615-69-C-1644, Aluminum Company of America, Dec. 10, 1969.
142. J. T. Staley, *Exploratory Development of High-Strength Stress-Corrosion Resistant Aluminum Alloys Usable in Thick Section Applications*, Monthly Report, Dec. 1 to Dec. 31, 1969, Contract F33615-69-C-1644, Aluminum Company of America, Jan. 12, 1970.
143. J. T. Staley, *Exploratory Development of High-Strength Stress-Corrosion Resistant Aluminum Alloys Usable in Thick Section Applications*, Third Quarterly Report, Contract F33615-69-C-1644, Aluminum Company of America, Mar. 31, 1970.

144. J. T. Staley, *Exploratory Development of High-Strength Stress-Corrosion Resistant Aluminum Alloys Usable in Thick Section Applications*, Fourth Quarterly Report, Contract F33615-69-C-1644, Aluminum Company of America, June 12, 1970.
145. J. T. Staley and H. Y. Hunsicker, *Exploratory Development of High-Strength Stress-Corrosion Resistant Aluminum Alloys for Use in Thick Section Applications*, Technical Report AFML-TR-70-256, Aluminum Company of America, Nov. 1970.
146. J. T. Staley, *Development of a High Strength Stress-Corrosion Resistant Aluminum Aircraft Alloy*, Bimonthly Progress Letter, Sept. 16, 1970 to Nov. 15, 1970, Contract N00019-71-C-0131, Aluminum Company of America, Dec. 10, 1970.
147. J. T. Staley, *Development of a High Strength Stress-Corrosion Resistant Aluminum Aircraft Alloy*, Bimonthly Progress Letter, Nov. 16, 1970 to Jan. 15, 1971, Contract N00019-71-C-0131, Aluminum Company of America, Jan. 22, 1971.
148. D. S. Thompson and S. A. Levy, *High Strength Aluminum Alloy Development*, Second Quarterly Progress Report, Contract F33615-69-C-1643, Reynolds Metals Co., Richmond, Va., Dec. 1969.
149. D. S. Thompson and S. A. Levy, *High Strength Aluminum Alloy Development*, Third Quarterly Progress Report, Contract F33615-69-C-1643, Reynolds Metals Co., Richmond, Va., Mar. 1970.
150. D. S. Thompson and S. A. Levy, *High Strength Aluminum Alloy Development*, Technical Report AFML-TR-70-171, Air Force Materials Laboratory, Aug. 1970.
151. J. T. Staley, Aluminum Company of America, private communication.
152. V. A. Pavlov, I. Y. U. Filippov, and S. A. Frisen, "Strengthening of the AV and V95 Type Al Alloys by Thermo-Mechanical Treatment," *Fiz. Metal. I Metalloved.* **20**, 770-774 (Nov. 1965).
153. M. Conserva, E. DiRusso, and F. Gatto, "A New Thermomechanical Treatment for Al-Zn-Mg Type Alloys," *Memos and Reports, ISML*, Series 27, No. 415, 1968.
154. A. J. Jacobs, *Optimizing the Combination of Strength and Stress-Corrosion Resistance of 7075 Aluminum by Thermal-Mechanical Treatments*, Final Report, Contract N00019-69-C-0339, North American-Rockwell Corp., Canoga Park, Calif., Mar. 1970.
155. C. A. Morris and A. G. Cerrone, *Establish Manufacturing Methods for Closed Die Aluminum Forgings With Improved Stress-Corrosion Resistance*, Technical Report AFML-TR-69-264, Air Force Materials Laboratory, Wright-Patterson AFB, Ohio, Sept. 1969.
156. *Reynolds X7011 Alclad 7075, 7079 and 7178 Sheet and Plate*, Reynolds Metal Company, Jan. 1968 (not released for publication).
157. *Aluminum Alloy 7075, Alclad 7011, Plate and Sheet*, Federal Specification QQ-A-00250/26 (ASG), 10 Nov. 1969.

158. *Aluminum Alloy 7079, Alclad 7011, Plate and Sheet*, Federal Specification QQ-A-00250/27 (ASG), 10 Nov. 1969.
159. *Aluminum Alloy 7178, Alclad 7011, Plate and Sheet*, Federal Specification QQ-A-00250/28 (ASG), 10 Nov. 1969.
160. J. A. Dickson, "Alcoa 467 Process X7475 Alloy," *Alcoa Green Letter*, May 1970 (not released for publication).
161. L. W. Mayer, "What Four New Aluminum Alloys Have to Offer," *Metal Prog.* **95**, 68 (May 1969).
162. R. V. Turley, E. Dash, and C. H. Avery, *Stress Corrosion Susceptibility of Welded Aluminum Alloys*, Technical Report AFML-TR-67-291, Air Force Materials Laboratory, Wright-Patterson AFB, Ohio, Aug. 1967.
163. R. J. Charles and W. B. Hillig, "The Kinetics of Glass Failure by Stress Corrosion," *Proceedings of Symposium on Mechanical Strength of Glass and Ways of Improving It*, Forence, Italy, Sept. 1961.
164. W. B. Hillig and R. J. Charles, "Surfaces, Stress-Dependent Surface Reactions, and Strength," *High-Strength Materials*, (V. V. Zackay, ed.) New York, John Wiley & Sons, Inc., 1965, p. 682.
165. S. M. Wiederhorn and L. H. Bolz, "Stress Corrosion and the Static Fatigue of Glass," *J. Amer. Ceram. Soc.* **53**, 543 (1970).
166. H. W. Liu, "Stress Induced Diffusion and Stress Corrosion Cracking," *Trans. ASME, J. Basic Eng.* **92** (Ser. D), 633 (1970).
167. T. R. Beck and E. A. Grens, II, "An Electrochemical Mass Transport-Kinetic Model for Stress Corrosion Cracking of Titanium," *J. Electrochem. Soc.* **116** (No. 2), 177 (Feb. 1969).
168. T. R. Beck, M. J. Blackburn, and M. O. Speidel, *Stress Corrosion Cracking of Titanium Alloys: SCC of Aluminum Alloys, Polarization of Titanium Alloys in HCl and Correlation of Titanium and Aluminum SCC Behavior*, Quarterly Progress Report 11, Contract NAS 7-489, The Boeing Company, Seattle, Wash., Mar. 1969.
169. T. R. Beck, M. J. Blackburn, and M. O. Speidel, *Effect of Solution Viscosity on SCC Velocity* (to be published).
170. S. Glasstone, K. Laidler, and H. Eyring, *Theory of Rate Processes*, McGraw-Hill Book Company, New York, 1941.
171. R. W. Staehle, A. J. Forty, and D. van Rooyen eds., *Proceedings of Conference on Fundamental Aspects of Stress Corrosion Cracking*, NACE, Houston, Texas, 1969.
172. E. A. Starke, "The Causes and Effects of Denuded or Precipitate-Free Zones at Grain Boundaries in Aluminum-Base Alloys," *J. Metals* **22**, 54 (1970).
173. I. J. Polmear, "The Properties of Commercial Al-Zn-Mg Alloys," *J. Australian Inst. Metals* **89**, 193 (1960).
174. A. J. Sedriks, P. W. Slattery, and E. N. Pugh, "Precipitate-Free Zones and Stress Corrosion Cracking in a Ternary Al-Zn-Mg Alloy," *Trans. ASM* **62**, 238 (1969).

175. A. J. DeArdo, Ph.D. Thesis, Carnegie-Mellon University, 1969.
176. G. Thomas and J. Nutting, "Aging Characteristics of Aluminum Alloys," *J. Inst. Metals*, **88** (Part 2), 81-90 (Oct. 1959).
177. E. Hornbogen, *Z. Metallk.* **58**, 31 (1967).
178. M. O. Speidel, "Coherent Particles and Stress Corrosion Cracking of High Strength Aluminum Alloys," Technical Report AFML-TR-67-329, *Proceedings of the Air Force Materials Laboratory Fiftieth Anniversary Technical Conference on Corrosion of Military and Aerospace Equipment*, Denver, Colo., Nov. 1967, p. 1915.
179. H. A. Holl, "Deformation Substructure and Susceptibility to Intergranular SCC in an Aluminum Alloy," *Corrosion* **23**, 173 (1967).
180. M. O. Speidel, "Interaction of Dislocations With Coherent Particles and Stress Corrosion Cracking of High-Strength Aluminum Alloys," *Phys. Stat. Sol.* **22**, 71 (1967).
181. A J. DeArdo and R. D. Townsend, "The Effect of Microstructure on the Stress Corrosion Susceptibility of an Al-Zn-Mg Alloy" (to be published).
182. W. J. Kovacs and J. R. Low, "Intergranular Fracture in an Al-15 wt% Zn Alloy" (to be published).
183. E. H. Dix, Jr., "Aluminum Zinc Magnesium Alloys, Their Development and Commercial Application," *Trans. ASM*, **42**, 1057 (1950).
184. Report on MRL-A8 (X5090), New Haven, Conn., Olin Metals Research Laboratories, Dec. 17, 1969 (not released for publication).
185. *Aviation Week and Space Technology*, Jan. 27, 1967, p. 13.
186. E. P. Dahlberg, *Analysis of Cracking in Swaged 7075-T6 Aluminum Alloy Tubing*, NRL Memorandum Report 1894, Naval Research Laboratory, Washington, D.C., June 1968.
187. N. B. Schwartz and N. B. Wakefield, "Stress Corrosion Can Be Controlled," *The Iron Age*, Nov. 28, 1968, p. 71.
188. H. C. Rutemiller and D. O. Sprowls, "Susceptibility of Aluminum Alloys to Stress Corrosion," *Mater. Protect.* **2** (No.6), 62 (June 1963).
189. H. W. Zoeller and B. Cohen, "Shot Peening for Resistance to Stress Corrosion Cracking," *Metals Eng. Quart.*, **66-20** (No. 1), 16 (Feb. 1966).
190. B. W. Lifka and D. O. Sprowls, "Protective Treatments for the Prevention of Stress-Corrosion Cracking of High Strength Aluminum Alloys," paper presented at the Northeast Regional Conference of the National Association of Corrosion Engineers, New York, Oct. 1968.
191. F. C. Ruach, F. W. Luciw, and M. A. Murray, *Passivation of Metal Aircraft Surfaces*, Naval Air Systems Command Contract N00019-67-C-0499, Final Report, July 1968.
192. H. Borchers and E. Tenckhoff, "The Influence of Surface Condition on the Stress Corrosion of Al-Mg-Zn Casting Alloys," *Z. Metallk.* **59**, 58 (1968)
193. B. W. Lifka and D. O. Sprowls, "Shot Peening–A Stress Corrosion Cracking Preventative for High Strength Aluminum Alloys," paper

presented at the 26th Annual Conference of the National Association of Corrosion Engineers, Philadelphia, Pa., Mar. 1970 (to be published in *Corrosion*).

194. S. R. Brown and S. J. Ketcham, *Evaluation of Sermatel 385 Coating for Protection of Aluminum Alloys Against Stress Corrosion Cracking*, Report No. NADC-MA-6930, Naval Air Development Center, Oct. 24, 1969.
195. S. J. Ketcham, Naval Air Development Center, private communication.
196. R. N. Hooker and J. L. Waisman, "Control of Stress-Corrosion Cracking in Airframe Components," *Corrosion* **10**, 325 (1954).
197. R. N. Miller, "Inhibitive Sealing Compounds and Coating Systems Solve Aircraft Corrosion Problems," *SAMPE J.* **6**, 54 (Apr.-May 1970).

# Chapter 5

# TITANIUM ALLOYS

**M. J. Blackburn, W. H. Smyrl, and J. A. Feeney**
*The Boeing Company*

**CONTENTS**

# 5. TITANIUM ALLOYS

## 5.1 Introduction

Titanium and its alloys are relatively young structural materials which have been in use for the past two decades, a considerably shorter time than many of the high strength steels and aluminum alloys. Thus the amount of data presented in this chapter, although superficially large, is certainly not as detailed and reproducible as that for, say, aluminum alloys presented in Chapter 4. Another way in which the data for aluminum alloys differ is that the scatter of results for titanium alloys is quite large due to the many variables that may operate within one alloy. For example, the SCC results for the aluminum alloy 7075-T6 tend to be reproducible from lot to lot while for Ti-6Al-4V the results obtained depend on factors such as microstructure, oxygen content, texture, etc. which are not specified or controlled in many cases.

The bulk of titanium alloy production is used by the aerospace industries with the predominant applications in gas turbine engines. There has been an increasing amount of titanium used in the primary structure of airplanes and rockets. Titanium alloys have an excellent record in service and in fact it is difficult, with a few rather dramatic exceptions, to base any of the sections in this chapter on service experience. In general we shall have to project laboratory test results to *potential* service situations. This is not a particularly desirable method as it has been shown in the case of hot salt stress corrosion cracking, such an extrapolation can be misleading.

The chronological development of SCC problems in titanium alloys, based on limited service and extensive laboratory experience, is briefly as follows. In 1953 it was discovered that SCC occurred in titanium and its alloys [1] in red fuming nitric acid, which was circumvented by modifying the composition of the acid. Research in the mid-1950's demonstrated that SCC could occur at elevated temperatures in the presence of chloride salts; even though many laboratory failures were produced, service failures have not been reported. However, problems were encountered in turbines attributed to the presence of other metals in the structure, notably cadmium [1,2] and silver. In the early 1960's titanium alloys began to find increasing applications in air frames and space vehicles and some material-environmental incompatibilities became evident. The most dramatic were failures of Apollo tanks containing nitrogen tetroxide or methanol

[3,4] which were fortunately discovered during proof testing. It should be noted that the nitrogen tetroxide problem was eliminated very quickly by modification of the composition of the environment. In 1964 it was shown that some titanium alloys, although showing excellent corrosion resistance in seawater, could exhibit severe and very rapid cracking if a sharp flaw was present in the material [5].

In this chapter we attempt to summarize the state of knowledge of SCC of titanium alloys with emphasis on the engineering aspects of the problem. However, the reader may consider that in fact the emphasis is placed on the metallurgical part of the problem which essentially indicates that to use a material well one must be fully familiar with it. Sections 5.2 and 5.3 therefore give a general introduction to the physical metallurgy and chemical behavior of titanium alloys. Section 5.4 describes the external parameters which influence SCC with emphasis on the use of fracture mechanics methods to delineate the influence of stress on such factors. Thus where possible a threshold stress intensity ($K_{Iscc}$) is used to define the lower limit of cracking although we shall also comment on the velocity of cracking. Section 5.5 describes some of the morphological features of crack surfaces produced during the propagation of stress corrosion cracks. Finally in Section 5.6 a summary of additional practical aspects of SCC is given and possible methods of minimizing or eliminating SCC hazards are outlined.

No comprehensive review of the SCC behavior of titanium has been published since 1966 [6], although several conferences [7-12] have been devoted at least in part to the phenomenon.

## 5.2 Physical Metallurgy of Titanium Alloys

The aim of this section is to outline briefly the physical metallurgy of titanium and its alloys with emphasis on the phase transformations and their influence on mechanical properties encountered in commercial alloys. Such a description is important as only by understanding these factors can the patterns of stress corrosion behavior of alloys, especially in aqueous solutions, be discerned. For a more detailed account of the physical metallurgy of these materials, the reader is referred to two more extensive reviews [13,14].

### Allotrophy of Titanium

Titanium exists in two allotropic forms at ambient pressures. At low temperatures the metal has a hexagonal crystal structure, the $\alpha$ phase, while at temperatures above 880°C (1650°F) the metal has a body centered cubic (bcc) structure, the $\beta$ phase.

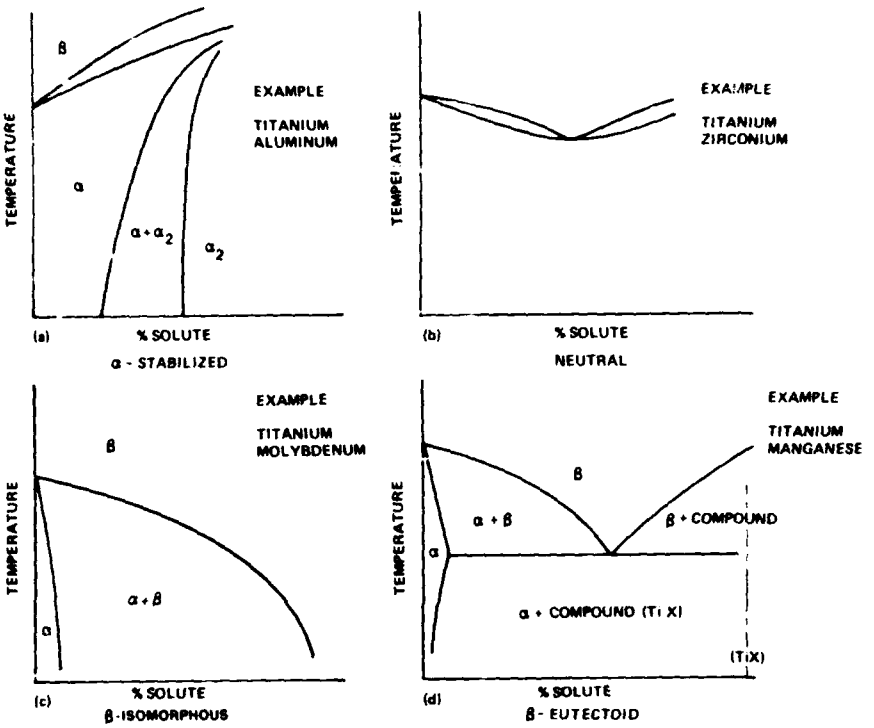


Fig. 1. Typical phase diagrams of titanium alloy systems.

## Phase Transformations

**Alloy Chemistry.** The classification of binary (and more complex) titanium alloy systems is based on the allotropic modification of the metal stabilized by the added solute element. The most important types of (substitutional) phase diagrams are shown in Fig. 1. Elements such as aluminum stabilize the $\alpha$ phase as shown in Fig. 1a and therefore are known as $\alpha$-stabilizing elements; usually in such systems an ordered phase based on the composition $Ti_3X$ (e.g. $Ti_3Al$, $Ti_3Sn$, etc.) occurs. Elements such as zirconium have little influence on the allotropic transformation (Fig. 1b), and are known as neutral additions. Most transition elements when added to titanium stabilize the $\beta$ phase (and are thus $\beta$ stabilizers), although two types of diagrams are developed. Elements such as molybdenum produce fully stable $\beta$ phases if present in sufficient amounts; such a $\beta$-stabilized or $\beta$-isomorphous system is shown in Fig. 1c. Other transition elements such as manganese, although tending to stabilize the $\beta$ phase, exhibit a eutectoid transformation at lower temperatures; such a $\beta$-eutectoid system is

shown in Fig. 1d. The rate of the eutectoid reaction varies considerably from system to system; it occurs rapidly and cannot be suppressed by rapid cooling in the titanium-gold system, but is extremely sluggish in other systems such as titanium-manganese.

Although the above brief description of alloying characteristics describes in general terms the phases that may be present in titanium alloys, it neglects such factors as the kinetics and mode of phase formation (phase transformations), the distribution of phases (microstructure), and the possible presence of metastable phases. Such factors are described in the following sections, where the most important phase transformations for *commercial* titanium alloys are discussed.

**Phase Transformations.** The solid state phase transformations which occur in titanium alloys may be divided into two general types. One type occurs by the cooperative movement of atoms, without diffusion, and the reactions are known as martensitic or shear transformations. The second type occurs by diffusional processes, and the reactions are known as nucleation-and-growth transformations.

*Martensitic Transformations.* Such reactions occur in pure titanium and some alloys if they are cooled very rapidly (quenched) from temperatures in the $\beta$ phase field. In pure titanium the product phase or martensite $\alpha'$ has a hexagonal structure and a rather irregular morphology (often termed a "massive-martensite") as shown in Fig. 2a. The $\alpha$-stabilized and neutral systems exhibit the same hexagonal martensitic crystal structure, but the morphology of the $\alpha'$ (martensite) phase may be more acicular. Martensitic transformations in $\beta$-stabilized or $\beta$-eutectoid systems tend to be somewhat more complicated, and we shall use the titanium-molybdenum system to illustrate the types of transformations that may occur. The temperature and compositional regions of phases produced in titanium molybdenum alloys on quenching from the $\beta$-phase field are shown in Fig. 3 with the exception of $\omega$-phase formation. Alloys containing solute element contents up to $C_1$ transform to hexagonal ($\alpha'$) martensite on quenching. Alloys with solute contents between $C_1$ and $C_2$ transform to a martensite with an orthorhombic crystal structure ($\alpha''$). Both phases have acicular microstructures such as illustrated for orthorhombic martensite in Fig. 2b.

In alloys with compositions up to $C_3$, the $\beta$ phase is completely retained on quenching; however, diffusionless reactions may be induced by plastic deformation. In Ti-Mo alloys, the shear products have been shown to consist of a mixture of orthorhombic martensite and complex twinning. This latter deformation mode tends to predominate as the alloy composition approaches $C_3$. Between $C_3$ and $C_4$, the metastable $\beta$ phase which is retained in quenching deforms by slip alone. This schematic does not show the transition between these transformation products, e.g., mixture of athermal and deformation-induced orthorhombic martensite. However, since the slope of $M_S$ vs composition is very steep in alloys such as Ti-Mo, these transition regions may be extremely narrow.

Orthorhombic martensites and such twinning processes do not occur in all titanium alloys which contain $\beta$-stabilizing elements; however, such transformations may be more widespread than has been recognized to date.

(a) Commercial-purity titanium quenched from above the $\beta$-transus hexagonal martensite ($\alpha'$) with a "massive" morphology (×200)

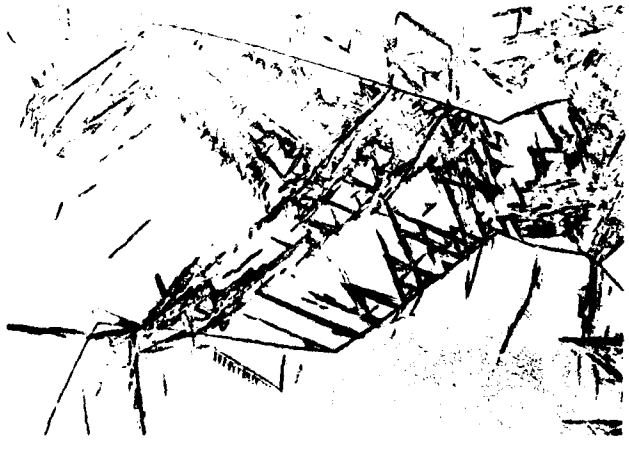

(b) Ti-8Mo-6Zr-4Sn quenched from above the $\beta$-transus orthorhombic martensite ($\alpha''$), with an acicular morphology and retained $\beta$ phase (×200)

Fig. 2. Martensitic phases in titanium alloys.

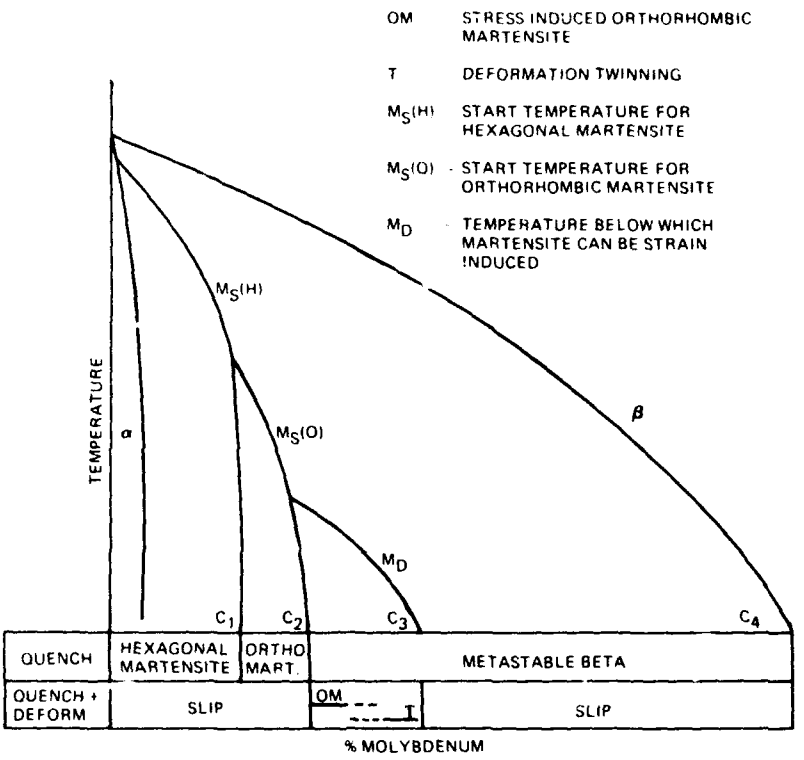


Fig. 3. Summary of diffusionless transformations and deformation modes occurring in Ti-Mo base alloys.

*Diffusional Transformations.* The most common reaction of this type in titanium alloys is the formation of the $\alpha$ phase or $\alpha+\beta$ dispersion. This latter form of phase mixture may occur by several reaction paths. The $\alpha$ phase may be precipitated from the $\beta$ phase by cooling to temperatures at which the $\alpha$ phase is stable. In $\alpha$-stabilized or neutral systems the transformation goes to completion and a Widmanstätten $\alpha$ structure is produced. Systems which contain $\beta$-stabilizing (or $\beta$-eutectoid) elements produce Widmanstätten $\alpha+\beta$ structures on slow cooling. Figure 4a illustrates such a structure in an alloy in which the $\alpha$ phase is the dominant constituent; such acicular microstructures are sometimes known as "basket-weave" structures. In alloys which contain more stabilizing element the $\beta$ phase predominates and is obviously the matrix phase as shown in Fig. 4b.

More controlled and higher strength $\alpha+\beta$ dispersions can be produced by quenching and tempering. Thus depending on the composition of the alloy either a martensitic structure or a retained $\beta$ phase may be utilized as a basis for

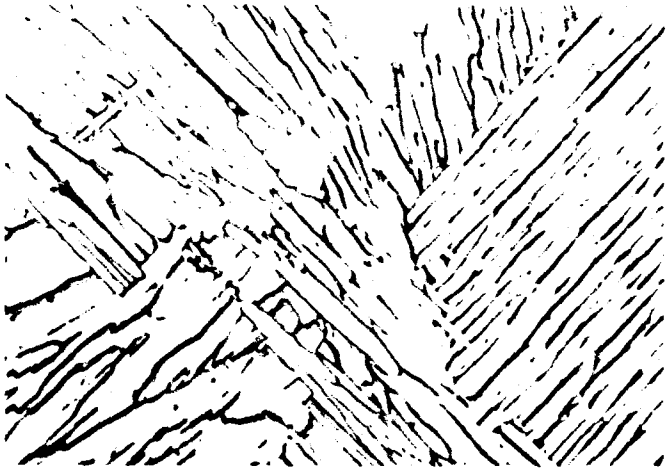

(a) Ti-6Al-4V slowly cooled from above the $\beta$ transus ($\times 500$) *(courtesy of* W. F. Spurr)

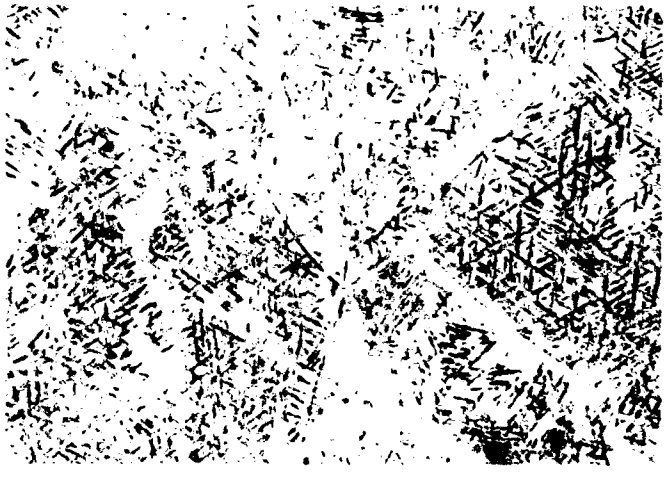

(b) Ti-11.5Mo-6Zr-4.5Sn cooled to 1150°F and held for 16 hr ($\times 500$)

Fig. 4. Widmanstätten $\alpha+\beta$ structures in titanium alloys.

subsequent development of an $\alpha+\beta$ mixture by tempering. In some alloys, problems are encountered in thick section as decomposition to $\alpha+\beta$ structures occurs in the center of the section during quenching. The ability of a titanium alloy to produce a satisfactory structure on quenching is referred to as its hardenability. We shall note in later sections the hardenability characteristics of several alloys.

*Tempering of Martensites.* It is obvious that pure titanium martensites or similar phases formed in α-stabilized or neutral systems will not precipitate a second phase on tempering. Hexagonal martensites, $\alpha'$, which are formed in alloys containing β-phase stabilizer elements, precipitate the $\beta$ phase when tempered at intermediate temperatures. The volume fraction and size of the precipitated $\beta$ phase depends on the temperature and time of the tempering treatment. (The volume fraction of this phase is controlled by the tempering temperature; the size of the precipitate by both tempering temperature and time.) Orthorhombic martensites [15] temper by precipitation of the $\alpha$ phase, and the orthorhombic matrix transforms to the $\beta$ phase at some stage of the tempering process. The exact details of this reaction have not been widely studied.

*Tempering of Metastable β Phases.* Such phases decompose by complex reactions which may involve metastable phases. For β-isomorphous systems, e.g., Ti-Mo, these reactions may be written as

$$\beta_m \rightarrow \beta+\omega \rightarrow \beta+\omega+\alpha \rightarrow \beta+\alpha \tag{1}$$

$$\beta_m \rightarrow \beta_1+\beta_2 \rightarrow \beta_1+\beta_2+\alpha \rightarrow \beta+\alpha. \tag{2}$$

In β-eutectoid systems, the equilibrium phase structure consists of α + compound, and the precipitation sequence may be written as follows:

$$\beta_m \rightarrow \beta+\omega \rightarrow \beta+\omega+\alpha \rightarrow \beta+\alpha \rightarrow \beta+\alpha+\mathrm{TiX} \rightarrow \alpha+\mathrm{TiX} \tag{3}$$

$$\beta_m \rightarrow \beta_1+\beta_2 \rightarrow \beta_1+\beta_2+\alpha \rightarrow \beta+\alpha \rightarrow \beta+\alpha+\mathrm{TiX} \rightarrow \alpha+\mathrm{TiX}. \tag{4}$$

The exact sequence in any alloy depends upon its composition and the specific aging treatment. The approximate temperature and compositional ranges for the formation of the metastable $\omega$, $\beta_1$ and $\beta_2$ phases are shown for a β-stabilized system in Fig. 5 [15].

The formation of the $\omega$ phase in titanium alloys has recently been reviewed [16], and will only be described briefly here. The $\omega$ phase (athermal $\omega$ phase) may form on quenching in dilute alloys as shown in Fig. 5. This athermal $\omega$ phase grows on aging and the phase forms in more concentrated alloys if aged at intermediate temperatures. The $\omega$ phase forms as small coherent particles (not resolvable by optical techniques) shown in Fig. 6a, and in dilute alloys constitutes a large volume fraction of the microstructure.

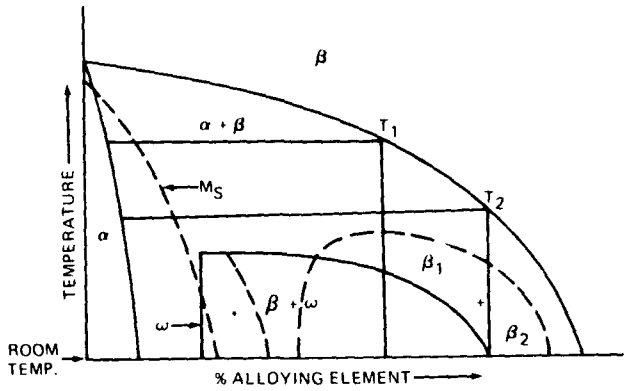


Fig. 5. Summary of transformations that may occur in β-isomorphous systems. Note differences in β-phase composition produced by aging at temperatures $T_1$ and $T_2$ in the α+β phase field [15]. *Composition regions for athermal ω formation.

Separation of a metastable β phase into two bcc phases $\beta_1+\beta_2$ occurs in more concentrated alloys as shown in Fig. 5. Again the particle size of the precipitated phase is small, and electron microscopy techniques are required for its resolution, as shown in Fig. 5b.

The α phase can be produced from both the β+ω and $\beta_1+\beta_2$ phase structures after further aging, and such starting structures result in very fine α-plate sizes. If an alloy is aged at temperatures above the stability field of β+ω or $\beta_1+\beta_2$ structures, the α phase is precipitated directly. The exact details of the dispersion depend on the tempering time and temperature, lower aging temperatures resulting in higher volume fractions of the α phase. One final point may be made concerning the thermal stability of β+α structures, which can be seen from Fig. 5. Dispersions of β+α produced at high aging temperatures may not be stable when exposed to lower temperatures, such as those encountered during service. Thus if a material aged at temperature $T_1$ were subsequently exposed to lower temperatures, the ω phase could form in the β phase. Likewise the β phase formed at the aging temperature $T_2$ could decompose into the $\beta_1+\beta_2$ structure. Such reactions can lead to changes both in mechanical properties and in the dimensions of parts, a process known as *thermal instability*. (This term is also applied to the formation of $\alpha_2$ in α alloys at intermediate temperatures.)

In β-eutectoid systems the equilibrium structure consists of a dispersion of an intermetallic compound in the α phase. Although such structures are not common in commercial alloys at this time, such phase mixtures are utilized in the Ti-2.5Cu alloy where the phase is formed from a supersaturated α phase. The intermetallic phase $TiCr_2$ is also formed in the Ti-11Cr-13V-3Al alloy after prolonged aging.


(a) Bright field electron micrograph of the $\omega$ phase formed in Ti-11.6Mo

(b) Bright field electron micrograph of $\beta_1+\beta_2$ phases in Ti-13V-11Cr-3Al

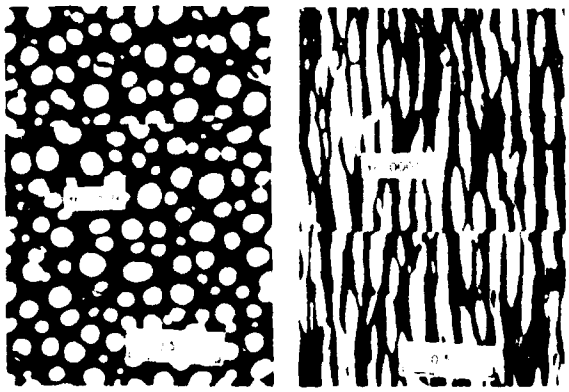

(c) Dark field electron micrograph of $\alpha$-phase $Ti_3Al$ in a Ti-9Al alloy

Fig. 6. Some microscopic phases that may form in titanium alloys.

As noted in the section on alloy chemistry, an ordered phase can form in most α-stabilized systems if a sufficient amount of solute element is present. A two-phase region lies between the disordered solid solution α and the ordered phase $\alpha_2$. The titanium-aluminum system is the most important with regard to commercial alloys; in this system the ordered phase is based on the composition $Ti_3Al$ and has an ordered hexagonal structure ($DO_{19}$) closely related to the α-phase titanium structure. The ordered phase $Ti_3Sn$ has the same structure and is completely miscible with $Ti_3Al$. As the $\alpha \rightarrow \alpha+\alpha_2$ phase line has a convex shape in the titanium-aluminum system, it is possible to retain a disordered α phase by quenching from temperatures above this phase boundary. (This is not true in very concentrated alloys, >12%Al,* but such alloys are too brittle to be of commercial importance.) Subsequent aging within the $\alpha+\alpha_2$ phase field causes precipitation of the ordered phase, which of course may also be accomplished by slow cooling through this phase field. In alloys of 6 to 8% Al the $\alpha_2$-phase particles are too small to be resolved by optical microscopy; typically the phase exists as ellipsoids up to about 1000Å in diameter (Fig. 6c). The phase forms quite rapidly at temperatures between 500°C (930°F) and 650°C (1200°F) but forms only very slowly at temperatures <450°C (840°F).

The range of stability of the phase in titanium-aluminum alloys is extended by additions of oxygen and tin, which are common elements in commercial alloys.

### Microstructure and Mechanical Properties

In the above sections the phase transformations of titanium alloys have been described, using relatively simple systems as the illustrative examples. This section will also concentrate on similar simple systems before discussing the more complex commercial alloys.

*Alpha-Phase Systems.* Pure titanium is soft and ductile. The flow strength of high-purity titanium is about 15 ksi, with elongation of about 50%. However, titanium has a hexagonal crystal structure, and anisotropy of properties is observed; for example, Young's modulus varies between $12 \times 10^6$ psi in the basal plane to $20 \times 10^6$ ksi normal to this plane. All elements present in solid solutions of α-titanium increase the flow strength and reduce ductility, the most important ones being oxygen, aluminum, and tin.

Oxygen produces large increases in the yield strength of titanium, strength levels in excess of 100 ksi being produced by the addition of 0.5% oxygen. However, the ductility and fracture toughness fall with increasing oxygen content, which places a practical limit on oxygen additions of about 0.4%. It should be noted that some oxygen is present in all commercial titanium alloys and is always a factor in determining the mechanical properties.

*All alloy compositions in the text are expressed as weight percent.

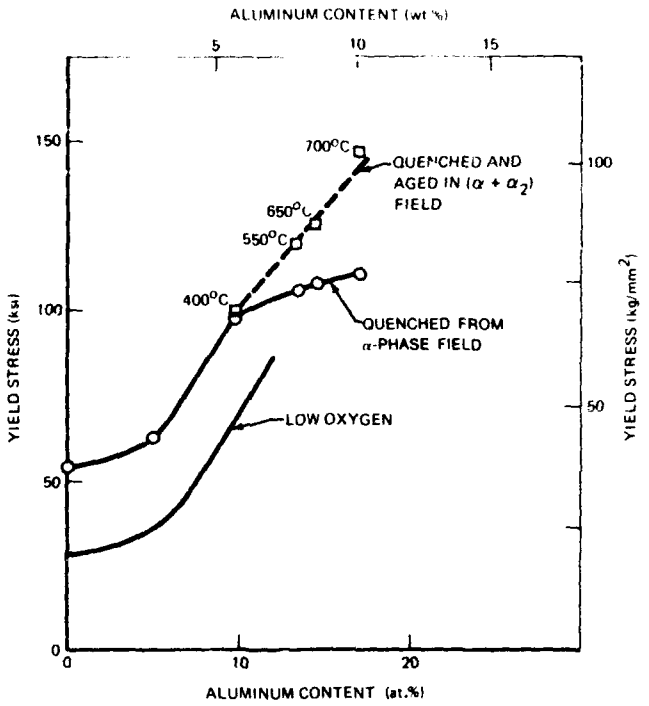


Fig. 7. Variation of yield stress of Ti-Al alloys containing up to 17 at.% aluminum. Note that the precipitation of the $\alpha_2$ phase produces increases in strength and that the strength level is dependent on oxygen content [17]. From *Trans. ASM* 62 (No. 2), p. 399, Fig. 1; copyright 1969 by the American Society for Metals. Used by permission.

Aluminum additions to titanium increase both modulus and strength and decrease density. Such an attractive combination of properties causes aluminum to be a common constituent of commercial alloys. The increase in yield strength produced by aluminum is shown in Fig. 7, from which the following points may be made. Rapid solid solution strengthening occurs up to 5%, and further increases in strength may be accomplished in alloys containing ≥6% Al by precipitation of the $\alpha_2$ phase. The influence of oxygen appears to be additive to that of aluminum as may also be seen from Fig. 7. However, there is a practical limit to aluminum additions, as alloys containing approximately 11% aluminum exhibit virtually no ductility and very low toughness even in the absence of $\alpha_2$-precipitates. The limit is lowered to about 8% aluminum if the $\alpha_2$-phase is precipitated during the heat treatment procedure. High aluminum contents have an even greater adverse influence on the stress corrosion properties of alloys, as will be demonstrated in the section on metallurgical variables, and thus there has been a tendency in recent alloy development work to reduce the aluminum content of alloys to less than 6%.

*Beta-Phase Systems.* The variety of phase structures that may be produced in these systems is reflected in the wide range of mechanical properties that may be produced. In order to provide a generalized description, we shall utilize the titanium-molybdenum system as an illustration. The variation in mechanical properties with molybdenum content is shown in Fig. 8. For material quenched from the $\beta$-phase field, the following points may be made:

- The hexagonal martensite is relatively soft—typical of the substitutional martensites in most titanium alloys. However, the ductility of such structures tends to be low.
- A minimum in yield strength occurs near the boundary between the orthorhombic martensite and the retained $\beta$ phase. This low strength is coupled with large ductility which is typical of titanium alloys that undergo stress-induced transformations.
- The retained $\beta$ phases which contain high molybdenum contents exhibit intermediate strengths and ductility.

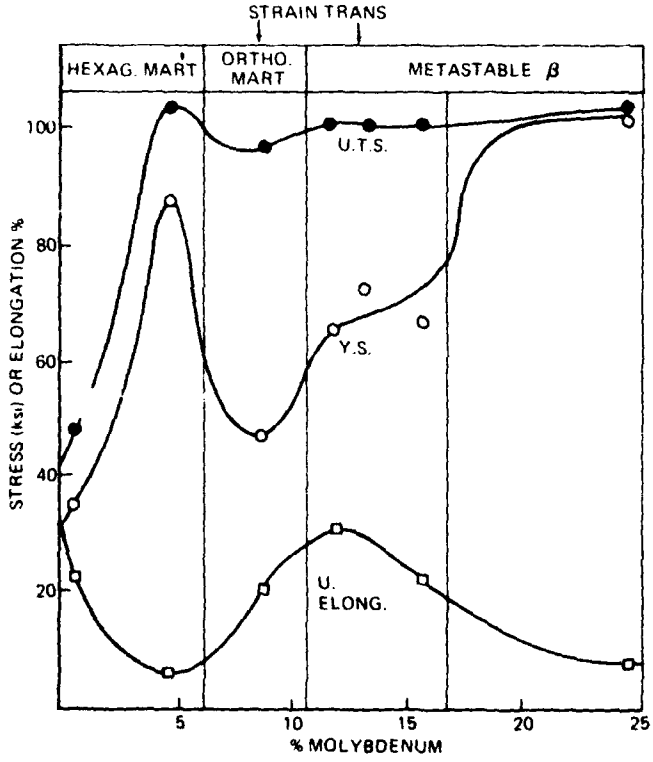


Fig. 8. Variation of mechanical properties and phase structure of $\beta$ quenched Ti-Mo alloys [13].

The above behavior is similar in many other binary alloy systems, although it should be noted that orthorhombic martensite and stress-induced transformations do not occur in all systems.

All of the structures in Fig. 8 can be tempered to produce $\alpha+\beta$ dispersions, or such dispersion may be generated directly by suitable treatments. The mechanical properties of such mixtures depend on the volume fraction, mean free path, and particle size of the precipitate. In general, the small particle sizes and high volume fractions of precipitate result in high yield strengths, although there is little quantitative understanding of the strengthening process. To give one example, Figs. 9a and b illustrate the $\alpha$-particle sizes in a Ti-8Mn alloy aged at 400°C (750°F) and 700°C (1300°F); the yield strengths of these structures are 200 and 90 ksi, respectively. Coupled with increases in strength in these $\alpha+\beta$ dispersions are the usual decreases in ductility parameters and fracture toughness. However, although this is a general correlation, one additional factor must be noted. It was observed in the early stages of titanium alloy development that acicular $\alpha+\beta$ microstructures developed from martensitic starting structures exhibited lower values of tensile elongation compared to an equiaxed $\alpha+\beta$ dispersion; thus such structures tended to be avoided in practice. Subsequently it was shown that in certain alloys acicular structures have superior fracture toughness properties compared to equiaxed structures, and this observation has led to the development of $\beta$-processing techniques discussed in more detail on pp. 321 and 322. The maximum strength level achievable in titanium alloys (>240 ksi) occurs in alloys treated to produce fine $\beta+\alpha$ structures, although the usual complex compositions of the alloys coupled with additions of $\beta$-eutectoid elements makes structural analysis difficult.

Finally, in this section we shall discuss briefly the influence of the $\omega$ phase and intermetallic compounds ($\beta$-eutectoid type) on mechanical properties. The $\omega$ phase can be formed quite easily in many experimental and commercial alloys, although it is not utilized in alloys as a strengthening agent. This phase produces large increases in strength and modulus, but these potential benefits are more than offset by decreases in ductility and toughness. The degree of strengthening is again related to the particle size and volume fraction of the precipitate, yield strengths in excess of 220 ksi being achievable. When the $\omega$ phase is present after quenching from the $\beta$-phase field, its influence depends on the solute atoms present. For example, in titanium-molybdenum alloys which undergo a strain-induced transformation the phase produces little strengthening, while in quenched titanium-manganese alloys the phase results in intermediate strength levels and low ductilities. In all systems aging to produce the $\omega$ phase causes the strength to increase; it appears from limited data that fracture toughness decreases with aging but tends to remain constant after a certain $\omega$-phase particle size is reached. The chief concern with the $\omega$ phase in practice is its development during service or processing exposure at intermediate temperatures in alloys containing the $\beta$ phase. If this occurs then the changes in properties (both mechanical and dimensional) lead to poor material performance. The $\omega$

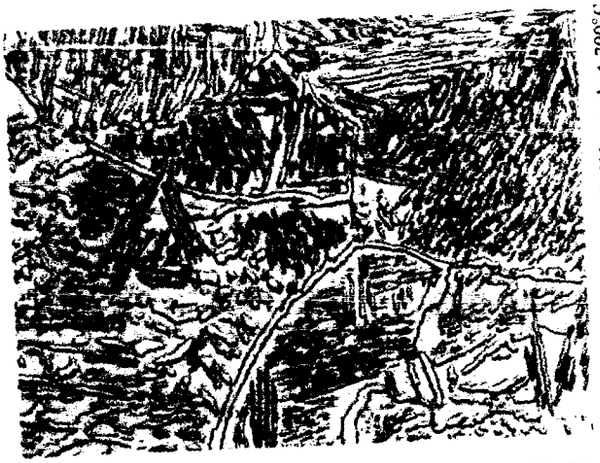

(b) Optical micrograph of Ti-8Mn aged at 700°C (×200)

(a) Dark field electron micrograph of Ti-8Mn aged at 400°C (×150,000)

Fig. 9. The range in α-phase particle size obtainable in β-α titanium alloys.

phase is not developed intentionally as a strengthening agent in titanium alloys at this time; however, some experimental work has demonstrated that $\alpha+\beta$ aging followed by low-temperature aging to develop the $\omega$ phase (see Fig. 5) can result in useful increases in strength coupled with appreciable ductility. It remains to be demonstrated that these treatments produce superior properties to the conventional $\beta+\alpha$ dispersions.

A few alloys utilize intermetallic particles formed in eutectoid systems as a basis for strengthening: Several high-temperature alloys contain silicon which results in the formation of silicides; these particles probably produce some strengthening but also serve to prevent grain growth at service temperature. The Ti-2.5Cu alloy is an example of one which utilizes compound formation as a strengthening precipitate, although the strength level at room temperature is not much higher than that of interstitially hardened commercial-grade titanium. In this alloy and in Ti-13V-11Cr-3Al, compound formations can tend to embrittlement if large amounts of the intermetallic phase are formed at the grain boundaries of the alloys.

**Commercial Titanium Alloys**

The above sections serve as a background to discuss the behaviour and properties of commercial titanium alloys – such an introduction is necessary, as many titanium alloys contain both $\alpha$- and $\beta$-stabilizing elements. Thus, the transformational characteristics and mechanical properties exhibit a combination of the above effects. We shall use as a basic classification of titanium alloys two characteristics – the equilibrium phase structure present at room temperature and the product phases formed on quenching from the $\beta$-phase field.

The starting point is (commercially) pure titanium, an $\alpha$-phase alloy. From this is derived a series of *$\alpha$-phase alloys*, the commercial grades of titanium which are essentially titanium oxygen alloys, and the solid solution type alloys containing aluminum, tin and zirconium, e.g., Ti-5Al-2.5Sn and Ti-5Al-5Zr-5Sn.

It has been noted that the maximum practical aluminum content that can be tolerated in titanium is about 8% Al. (The current commercial limit is about 6%.) The alloy Ti-8Al-1Mo-1V contains both $\alpha$ and $\beta$ phases, although the former predominates. As the amount of $\beta$-stabilizing elements is increased and the aluminum content is decreased, the proportion of $\beta$ phase present in the structure increases. Thus a series of $\alpha+\beta$ *type* of titanium alloys may be cited, e.g., Ti-8Al-1V-1Mo, Ti-6Al-4V, and Ti-4Al-3Mo-1V, in which the $\alpha$ phase predominates but decreases in volume fraction progressively through the series. These alloys form hexagonal martensites on quenching from the $\beta$-phase field, although a small amount of retained $\beta$ phase may also be present in Ti-4Al-3Mo-1V. A final factor of importance in both the $\alpha+\beta$ and $\beta+\alpha$ alloys is that in complex alloys solute elements tend to partition themselves between the two phases. Thus $\alpha$-phase stabilizing elements concentrate in the $\alpha$ phase and likewise $\beta$-phase stabilizing elements tend to segregate to the $\beta$ phase. This can render a

phase susceptible to stress corrosion cracking even though the overall alloy composition appears to be outside the susceptible range.

No fully stable $\beta$-phase alloy is produced commercially, but several alloys contain sufficient $\beta$-stabilizer or eutectoid elements to retain a metastable phase on quenching from the $\beta$-phase field; for example, Ti-13V-11Cr-3Al, Ti-8Mo-8V-3Al-2Fe, or Ti-11.5Mo-6Zr-4.5Sn (note, however, that these alloys contain the $\alpha$ stabilizers aluminum or tin). In such alloys, the $\beta$ phase predominates and is the matrix phase—thus we designate them $\beta+\alpha$ *alloys*.

A rather indistinct boundary exists between the $\beta+\alpha$ and $\alpha+\beta$ alloys perhaps best exemplified by the alloy Ti-6Al-2Sn-4Zr-6Mo, which contains large amounts of both $\alpha$- and $\beta$-stabilizing elements. In this alloy the quench product is orthorhombic martensite, and subsequent tempering produces a $\beta+\alpha$ type of structure.

This alloy classification is summarized in Table 1. A more complete description of the phase structure and properties of some commercial titanium alloys is given on pp. 309-333. In the following section, these properties are summarized and an account given of conventional heat-treatment procedures.

**Table 1**. Titanium Alloy Classification

| ALLOY TYPE[a] | α PHASE | | α + β ⟶ β + α | β PHASE |
|---|---|---|---|---|
| EXAMPLES | PURE Ti COM. GRADES CP 35A 50A 70A | Ti-5Al-2.5Sn<br>Ti-5Al-5Zr-5Sn | Ti-8Al-1Mo-1V<br>Ti-6Al-4V<br>Ti-4Al-3Mo-1V<br>Ti-6Al-4Zr-2Sn-6Mo<br>Ti-13V-11Cr-3Al<br>Ti-8Mo-8V-3Al-2Fe<br>Ti-11.6Mo-6Zr-4.5Sn | NONE |
| STRUCTURE ON QUENCH FROM β FIELD | MARTENSITE HEXAGONAL | | MARTENSITE ORTHORHOMBIC | RETAINED β PHASE |

[a]Note that the boundary between $\alpha+\beta$ and $\beta+\alpha$ alloys is not well defined.

In Table 2 typical room-temperature mechanical properties are shown for several commercial alloys in different heat-treatment conditions. It should be emphasized that this table is not intended for the purpose of rating alloys, since the properties shown are not minimum design-allowable values. With the exception of density, any one property possibly could be improved by slight compositional or heat-treatment variations.

Reference is made in Table 2 and also in the section on metallurgical variables to standard heat treatments given to titanium alloys, which are denoted mill annealed (MA), duplex annealed (DA), solution treated and aged (STA), etc. Schematical representations (Figs. 10 through 15) and brief descriptions of such heat-treatment procedures are given in the following sections.

**Table 2.** Some Typical Physical and Mechanical Properties of Commercial Titanium Alloys

| *Alloy* | *Thickness* | *Heat Treatment* | *UTS, ksi* | *TYS, ksi* | *El %* | $K_{1c}$ or $K_c$, $ksi\sqrt{in.}$ | $^*K_{Iscc}$ or $K_{scc}$, $ksi\sqrt{in.}$ | *E, psi* | *ρ lb/cu in* |
|---|---|---|---|---|---|---|---|---|---|
| α Alloys | | | | | | | | | |
| Ti-70A | 0.50 | αA-AC | 102 | 83 | 25 | 123 | 33 | $16.9 \times 10^6$ | 0.163 |
| | 0.50 | αA-WQ | 106 | 85 | 22 | 128 | 34 | 17.0 | 0.163 |
| | 0.50 | STA | 103 | 82 | 25 | 113 | 39 | 17.0 | 0.163 |
| | 0.50 | βA-WQ | 101 | 76 | 23 | 105 | 70 | 16.4 | 0.163 |
| | 0.50 | β-STA | 102 | 77 | 22 | 96 | 48 | 16.7 | 0.163 |
| Ti-5Al-2.5Sn | 0.50 | αA-AC | 134 | 126 | 19 | 88 | 30 | 19.6 | 0.162 |
| | 0.50 | αA-WQ | 135 | 124 | 17 | 103 | 27 | 18.3 | 0.162 |
| | 0.5 | STA | 139 | 129 | 19 | 83 | 23 | 18.3 | 0.162 |
| | 0.5 | βA-WQ | 140 | 126 | 14 | 119 | 37 | 16.8 | 0.162 |
| Ti-5Al-5Zr-5Sn | 0.5 | αA-AC | 128 | 116 | 17 | 83 | 50 | 17.2 | 0.162 |
| | 0.5 | αA-WQ | 127 | 110 | 17 | 101 | 67 | 17.0 | 0.162 |
| | 0.5 | STA | 128 | 119 | 17 | 83 | 34 | 17.5 | 0.162 |
| α+β Alloys | | | | | | | | | |
| Ti-8Al-1Mo-1V | 0.050 | MA | 155 | 145 | 10 | 75 | 30 | $18.5 \times 10^6$ | 0.158 |
| | 0.050 | DA | 145 | 135 | 12 | 160 | 50 | 18.0 | 0.158 |
| | 0.5 | MA | 155 | 145 | 10 | 48 | 20 | 18.5 | 0.158 |
| | 0.5 | DA | 145 | 135 | 12 | 100 | 32 | 18.0 | 0.158 |
| Ti-6Al-4V | 0.060 | MA | 144 | 137 | 15 | 150 | 110 | 16.0 | 0.160 |
| | 0.060 | DA | 140 | 133 | 18 | 150 | 110 | 16.0 | 0.160 |
| | 0.060 | STA | 167 | 160 | 13 | 95 | 65 | 16.5 | 0.160 |
| | 0.060 | β-STA | 165 | 155 | 7 | 95 | 65 | 16.5 | 0.160 |
| | 0.5 | MA | 144 | 137 | 15 | 60 | 35 | 16.0 | 0.160 |
| | 0.5 | DA | 140 | 133 | 18 | 70 | 52 | 16.0 | 0.160 |
| | 0.5 | STA | 167 | 160 | 13 | 47 | 25 | 16.5 | 0.160 |
| | 0.5 | β-STA | 165 | 155 | 7 | 70 | 45 | 16.5 | 0.160 |
| Ti-4Al-3Mo-1V | 0.050 | MA | 135 | 125 | 14 | 170 | 130 | 16.0 | 0.163 |
| | 0.050 | DA | 135 | 125 | 12 | 190 | 145 | 16.0 | 0.163 |
| | 0.050 | β-STA | 155 | 140 | 7 | 120 | 100 | 16.5 | 0.163 |
| | 0.050 | MA | 135 | 125 | 14 | 115 | 105 | 16.0 | 0.163 |
| | 0.50 | DA | 135 | 125 | 12 | 125 | 120 | 16.0 | 0.163 |
| | 0.50 | β-STA | 155 | 140 | 7 | 95 | 70 | 16.5 | 0.163 |
| Ti-5Al-6V-2Sn | 0.50 | MA | 165 | 157 | 14.5 | 60 | 20 | 16.0 | 0.164 |
| | 0.50 | DA | 160 | 146 | 12 | 80 | 25 | 15.5 | 0.164 |
| | 0.50 | STA | 180 | 170 | 6 | 45 | 30 | 16.5 | 0.164 |
| | 0.50 | β-STA | 165 | 152 | 9 | 70 | 45 | 16.0 | 0.164 |
| Ti-7Al-4Mo | 0.50 | MA | 157 | 144 | 9 | 73 | 31 | 17.0 | 0.162 |
| | 0.50 | STA | 191 | 167 | 1.5 | 36 | 26 | 17.0 | 0.162 |
| IMI 680 | 0.50 | βF+DA | 190 | 166 | 7 | 44 | 28 | 15.5 | 0.175 |
| IMI 700 | 0.50 | DA | 200 | 180 | 7 | 20 | 10 | 16.5 | 0.164 |
| | 0.50 | STA | 185 | 165 | 8 | 20 | 10 | 16.5 | 0.164 |

**Table 2.** Some Typical Physical and Mechanical Properties of Commercial Titanium Alloys–*Continued*

| *Alloy* | *Thickness* | *Heat Treatment* | *UTS, ksi* | *TYS, ksi* | *El %* | $K_{1c}$ or $K_c$, ksi $\sqrt{in.}$ | $^*K_{Iscc}$ or $K_{scc}$, ksi $\sqrt{in.}$ | *E, psi* | *ρ lb/cu in.* |
|---|---|---|---|---|---|---|---|---|---|
| Ti-6Al-2Sn-4Zr-2Mo | 0.50 | STA | 173 | 152 | 10 | 53 | 27 | 16.0 | 0.164 |
| Ti-6Al-2Sn-4Zr-6Mo | 0.50 | MA | 177 | 160 | 14 | 55 | 2[illegible] | 17.0 | 0.169 |
| | 0.50 | DA | 185 | 150 | 8 | 80 | 45 | 17.0 | 0.169 |
| β+α Alloys | | | | | | | | | |
| Ti-13V-11Cr-3Al | 0.50 | β-ST | 125 | 120 | 10 | >100 | 35 | $14.5 \times 10^6$ | 0.176 |
| | 0.50 | β-STA | 170 | 160 | 4 | 70 | 30 | 15.5 | 0.176 |
| Ti-11.5Mo-6Zr-4.5Sn | 0.50 | β-ST | 115 | 80 | 28 | – | – | 14.5 | 0.184 |
| | 0.50 | β-STA | 185 | 170 | 9 | 65 | 25 | 15.5 | 0.[illegible]34 |
| Ti-8Mo-8V-3Al-2Fe | 0.50 | β-ST | 121 | 119 | 28 | – | – | 14.5 | 0.175 |
| | 0.50 | β-STA | 187 | 181 | 5 | 50 | 31 | 15.5 | 0.175 |
| Ti-3Al-8V-6Cr-4Mo-4Zr | 0.50 | β-ST | 126 | 120 | 20 | – | – | 15.0 | 0.174 |
| | 0.50 | β-STA | 205 | 193 | 6.5 | 50 | 37 | 16.0 | 0.174 |

*3.5% salt water

**Heat Treatment of Commercial Alloys.*** Various classes of commercial alloys may be given any of the following heat treatments either by the metal producer or by the fabricator.

*(α+β) Alloys.* Mill annealing for α+β alloys consists of (a) forming to size, (b) heating to 1350°F (730°C) and soaking 4 hr, and (c) furnace cooling to room temperature. This treatment is often specified for Ti-6Al-4V; the mill annealing treatment for other α+β alloys may differ. Mill annealing generally produces a fine-grained equiaxed α+β microstructure (see Fig. 10). The volume fraction of the β phase depends on the composition of the alloy and the annealing temperature. In alloys containing high percentages of Al and Sn, furnace cooling causes the precipitation of $\alpha_2$ in the α phase; $\alpha_2$ is usually not resolvable under the optical microscope.

Duplex annealed alloys are (a) formed to size, (b) heated to 1750°F (955°C) and soaked 10 min, (c) air cooled to room temperature, (d) heated to 1250°F (675°C) and soaked 4 hr, and (e) air cooled to room temperature.

There are apparently several other duplex-annealing treatments in use at the present time. The duplex anneal for Ti-8Al-1Mo-1V consists of reheating mill-annealed material to 1450°F and then either air cooling or water quenching it; under the optical microscope little difference can be discerned between MA and DA microstructures.

*Throughout this chapter, the sequence of α+β denotes a predominantly α structure, and, conversely, β+α denotes a predominantly β structure.

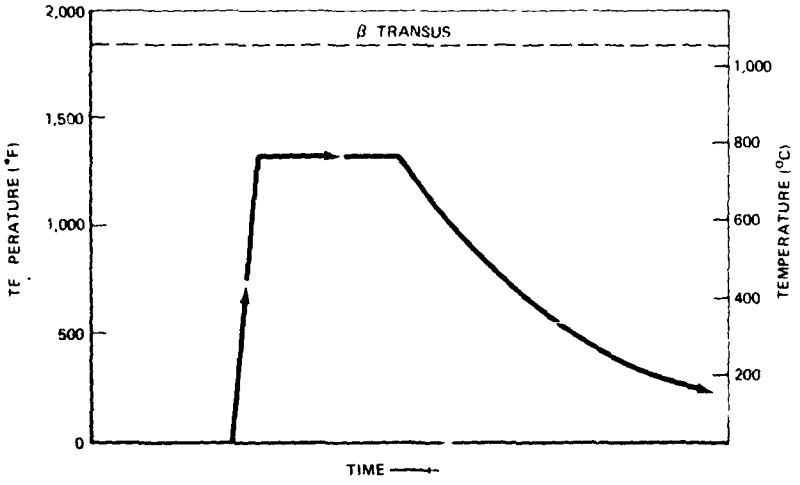


(a) Schematic representation

(b) Optical microstructure (courtesy of R. E. Curtis)

Fig. 10 Mill anneal for Ti-6Al-4V.

In alloys such as Ti-6Al-4V and Ti-4Al-3Mo-1V the duplex annealing treatment is similar to that shown in Fig. 11. During the first annealing treatment the $\beta$ phase partially decomposes, forming fine plates of $\alpha$ phase. In the second, low-temperature anneal, the volume fraction of the $\beta$ phase decreases but is more enriched in $\beta$-stabilizing elements (such as V and Mo).

Solution treated and aged (STA or $\alpha+\beta$ STA) alloys are (a) formed to size, (b) heated to 1750°F (955°C) and soaked 10 min, (c) water quenched, (d) heated to 1000°F (540°C) or 1250°F (675°C) and aged 4 hr, and (e) air cooled to room temperature.

It can be seen from Figs. 11 and 12 that the temperature and time cycles for these two treatments are similar. The basic difference is that the material is water quenched after the first high-temperature anneal and thus the $\beta$ phase does not decompose by diffusional processes but transforms to martensite. On subsequent aging at temperatures between 1000°F (540°C) to 1250°F (675°C), the martensite decomposes to form fine $(\alpha+\beta)$-phase dispersions while the primary phase is relatively unaffected.

Beta-solution treated and aged ($\beta$-STA) alloys are (a) formed to size at temperatures above the $\beta$ transus or heated to 2000°F (1095°C) and soaked 1 hr., (b) water quenched, (c) heated to 1000°F (540°C) or 1250°F (675°C) and aged 4 hr, and (d) air cooled to room temperature.

Normal $\beta$-STA treatments consist of solution treating (as shown in Fig. 13) at a temperature above the $\beta$ transus followed by water quenching to form a fully martensitic structure. On subsequent low-temperature aging (tempering), fine $(\alpha+\beta)$-phase structures are produced. A second $\alpha+\beta$ solution treatment is often used after the first $\beta$ treatment; if this is employed, material may be air cooled from the $\beta$-phase field. It is also possible to incorporate $\beta$ processing into this heat-treatment schedule. Material is worked to the desired shape at a temperature above the $\beta$ transus. Working may then be followed by a water quench and a low-temperature temper, as for $\beta$-STA. Alternatively, the material can be air cooled from the finishing temperature, which results in a coarse Widmanstätten $(\alpha+\beta)$-phase structure.

*Beta and $\beta+\alpha$ Alloys.* These alloys may be either solution treated ($\beta$ ST) or solution treated and aged (STA). Metastable $\beta$-phase alloys are solution treated above the $\beta$ transus (Fig. 14) and then either air cooled or water quenched. The microstructure consists of equiaxed grains of $\beta$ phase.

Solution treated and aged ($\beta$-STA) alloys, after solution treatment, are generally aged at temperatures within the $(\beta+\alpha)$-phase field (see Fig. 14).

At the lower aging temperatures, the microstructure consists of fine Widmanstätten plates of $\alpha$ phase (composition X) in a $\beta$-phase matrix (composition Y). The $\omega$ phase might form on cooling from the aging temperature and cause embrittlement.

The more conventional heat treatment for commercial metastable $\beta$-phase alloys is to both solution treat and age below the transus temperature. Such a

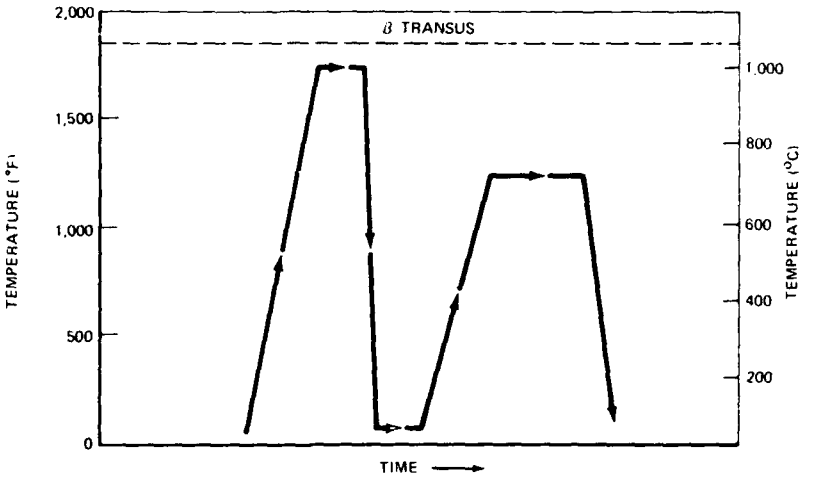


(a) Schematic representation

(b) Optical microstructure (courtesy of R. R. Boyer)

Fig. 11. Duplex anneal for Ti-6Al-4V.

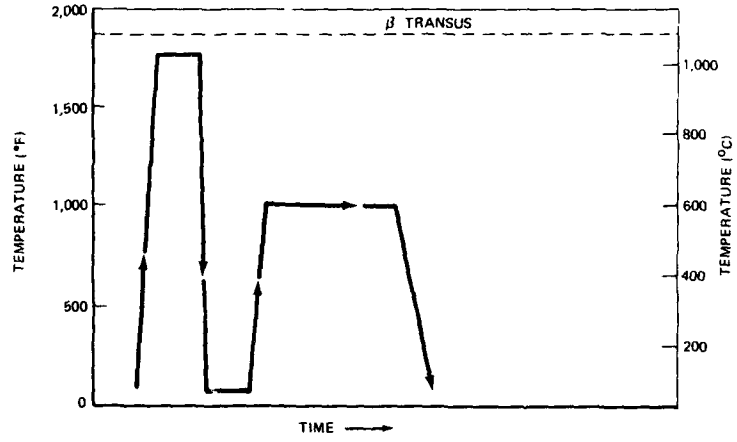


(a) Schematic representation

(b) Optical microstructure (courtesy of R. R. Boyer)

Fig. 12. STA heat treatment for Ti-6Al-4V.

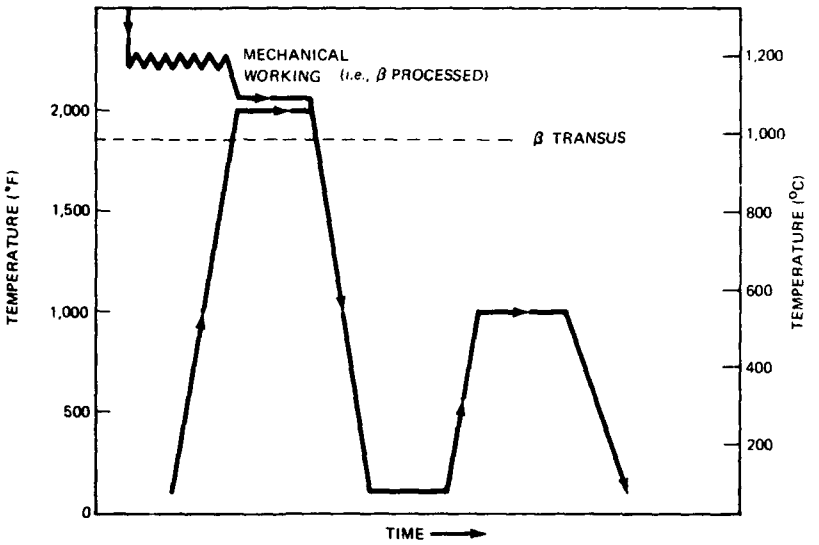


(a) Schematic representation. Note that the β-processing procedure is also indicated.

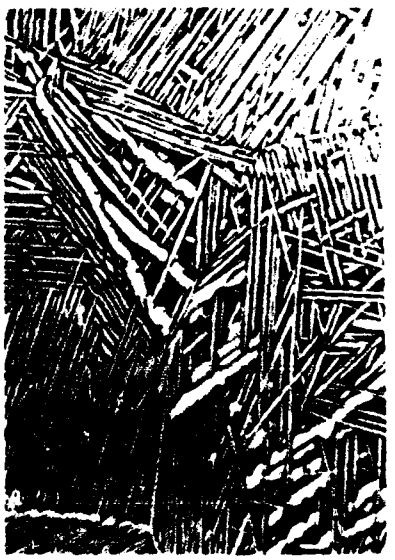

(b) Optical microstructure (courtesy of R. E. Curtis)

Fig. 13. β–STA heat treatment for Ti-6Al-4V.

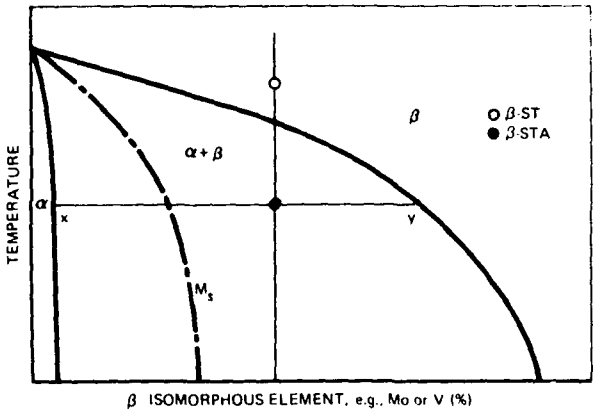


Fig. 14. Schematic representation of β-ST heat treatments for metastable β-phase alloys.

heat treatment produces higher yield strength but somewhat lower toughness than β-STA material.

*Alpha-Phase Alloys. Alpha annealing* in the α-phase field (Fig. 15) (αA-AC, αA-WQ, STA) produces an equiaxed grain structure irrespective of cooling rate. Little microstructural or property variations, however, can be achieved by changing the heat treatment of α-phase alloys. Small amounts of residual impurities, such as iron, can stabilize up to 5% β phase, and transformation in this phase can influence mechanical and stress corrosion properties. For example, decomposition to (β+ω)-phase structures can lower stress corrosion resistance.

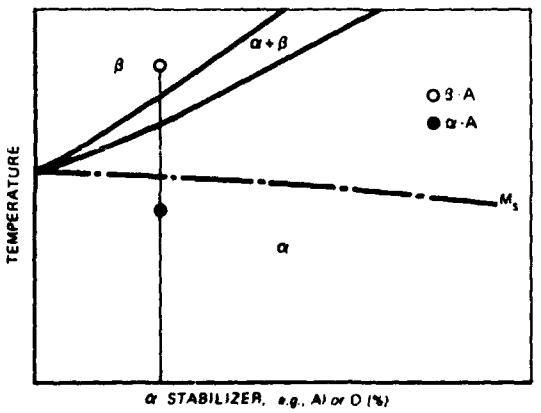


Fig. 15. Schematic of β annealing and α annealing in α alloys.

In alloys such as Ti-5Al-5Zr-5Sn and Ti-5Al-2.5Sn, the $\alpha$ phase may also decompose during slow cooling or low-temperature aging to form $\alpha+\alpha_2$ structures. Neither $(\beta+\omega)$- nor $(\alpha+\alpha_2)$-phase structures can be resolved under the optical microscope.

*Beta annealing* ($\beta$ A-WQ, $\beta$-STA) is done by solution treating alloys in the $\beta$-phase field (Fig. 15) and then water quenching, producing a microstructure of 100% massive martensite. When such structures are aged (tempered) at low and intermediate temperatures, recovery and recrystallization occur. In some alloys, the $\alpha_2$ phase may form during tempering.

*Step cooling* (SC) is a heat treatment in which alloys are cooled from the annealing temperature to some intermediate temperature, at which they are held for some time before being cooled to room temperature. This is not a commercial heat treatment but has been used to induce SCC susceptibility for experimental purposes.

## Interstitial Elements in Titanium Alloys

In the previous sections, the phase transformations and mechanical properties were described for titanium alloys containing substitutional elements. However, the smaller elements dissolve interstitially in titanium alloys, the most important being oxygen and hydrogen. Boron is usually considered an undesirable element especially in $(\beta+\alpha)$-type alloys as it causes large reductions in toughness.

**Oxygen.** The oxygen element is present in all commercial alloys; the various grades of commercially pure titanium are based essentially on the Ti-O system. The Ti-O phase diagram is complex, but the element is not present in sufficient quantities in commercial titanium alloys to form any of the superlattices or compounds that occur at higher oxygen levels. Oxygen may influence phase transformations; for example, being a potent $\alpha$ stabilizer, it raises the $\beta$ transus of alloys. Further it influences the transformation kinetics and extends the stability field of the $\alpha_2$ phase in Ti-Al alloys. The element produces considerable solid solution strengthening as described above and concurrently reduces ductility and fracture toughness. This behavior is accentuated at low temperatures, which has led to the development of extra-low-interstitial (ELI) grades of titanium alloys for cryogenic and other applications.

Contamination of titanium alloys by oxygen can occur at elevated temperatures ($\geq$1200°F) where the rate of scale formation is rapid. Further, the oxide is soluble in the metal, and thus there is often no clear-cut metal-oxide interface as occurs in, for example, aluminum alloys. Thus the surface layers of a titanium part may be high in oxygen and exhibit different properties than the interior of the material.

**Hydrogen.** The titanium-hydrogen system is of the $\beta$-eutectoid type, and at low temperatures titanium hydride ($TiH_2$) is precipitated. The solubility of hydrogen in titanium at room temperature is very low, and hydrogen in solid solution precipitates as the hydride. (Note that the hydrogen solubility limit

may be reduced by plastic deformation of the alloy.) In β-phase alloys, the solubility is higher yet, and very large hydrogen levels are required for hydride formation.

Although hydrogen does not influence the flow strength of alloys appreciably, it degrades fracture toughness. This degradation is known as hydrogen embrittlement. Two forms of embrittlement occur in titanium alloys [18]:

- Fast-strain-rate hydrogen embrittlement (FSRHE) is most often observed in α-phase alloys during impact testing at low temperatures. This form of embrittlement may occur in (α+β)- and (β+α)-phase alloys; however, much higher hydrogen concentrations are normally required.
- Slow-strain-rate hydrogen embrittlement (SSRHE) is most often observed in (α+β)-phase alloys but may also occur in other alloy types. Such embrittlement is observed only at very low applied strain rates or under static loading, and this characteristic forms the basis for the distinction between the two phenomena.

The latter form of embrittlement occurs by the nucleation and growth of cracks and is a time-dependent process. Little further work on SSRHE has been performed (at least on useful commercial alloys) since a review [18] was published in 1962. Hydrogen contamination of α+β alloys does not influence $K_{Iscc}$ [19,20].*

### 5.3 Corrosion of Titanium and Its Alloys

The purpose of this section is to describe briefly the corrosion properties of titanium alloys in common environments and under conditions which limit their usefulness. The section specifically excludes stress corrosion, which is reserved for section 5.4. Several reviews cover the general chemistry of titanium and the corrosion properties of the material in detail [21-25].

#### General Behavior

Titanium is a highly reactive metal which forms compounds with oxygen, nitrogen, the halogens, carbon, boron, etc. The reactions are in several cases explosive, e.g., titanium with dry chlorine, and in all cases liberate a considerable quantity of heat. This general reactivity of titanium is modified at low temperatures by the presence of a tenacious, protective oxide film. In fact the corrosion properties essentially reflect the conditions under which this film is removed or becomes nonprotective. The oxide film can also be ruptured by mechanical methods, e.g., stresses (above the yield stress) or abrasion, and in such cases the ease and rate of oxide formation or rehealing of the film determine the corrosion properties.

*Dissolved hydrogen can cause slow cracking under sustained stress in the absence of a reactive environment [20]. This phenomenon may be of practical importance. (*Editor.*)

### Gases

Titanium forms a multiplicity of oxide phases with oxygen, e.g., $Ti_2O$, TiO, $Ti_2O_3$, and $TiO_2$; many of these phases are structural modifications of other oxides. In most cases at least the outer layer of an oxide film has the composition and structure of rutile, $TiO_2$. Under certain temperature and pressure conditions titanium can react explosively with pure oxygen. The reaction with air, which is usually less violent, is of importance in determining the formation and breakdown of the protective surface film. At elevated temperatures the surface film on titanium may have the composition $TiO_2$, but the oxygen level varies continuously into the metallic substrate. The contaminated layer can be quite thick (1 to 10 mils), and as this layer is brittle it may crack under load. Further, if the contamination is not removed before a subsequent heating cycle, the oxygen penetrates deeper into the material on reheating. This form of contamination is a problem at temperatures above 1200°F, and significant scaling may occur above 1400°F. The depth of penetration by oxygen (for a constant time and temperature) increases with the solute content in an alloy, the degree of contamination being approximately proportional to the total solute content.

Reaction with nitrogen takes similar form as that with oxygen, although the nitride is less stable than the oxide.

Hydrogen is absorbed almost reversibly above approximately 600°F up to the composition $TiH_2$. Reaction also occurs with hydrogen gas at room temperature to produce the hydride, although the oxide film must be perforated for this reaction to occur. In hydrogen, as in several other gases such as chlorine and sulphur dioxide, reaction is suppressed by the presence of moisture, which maintains the integrity of the oxide film.

### Aqueous Solutions

The corrosion behavior of titanium and its alloys in aqueous solutions is determined by the pH, electrochemical potential, and the ionic species present, among other factors. This corrosion behavior is summarized in Fig. 16, which shows the stable titanium species and corrosion behavior (passive, active, and pitting) in various regimes of potential and pH. The information such as that of Fig. 16 may also be plotted according to the convention of Pourbaix, as shown in Fig. 17 [26].

Titanium and its alloys do not undergo either general corrosion or pitting in neutral or nearly neutral solutions, even those containing chloride, at room temperature unless the potential is moved artificially in the positive direction, as shown in Fig. 16. If the temperature is raised to 270°F, however (the exact temperature depends upon the concentration of chloride and the composition of the alloy), titanium and its alloys are susceptible to crevice corrosion.

In acidic solutions, the corrosion behavior of titanium and its alloys depends on the nature and strength of the acid as well as on temperature. Titanium is

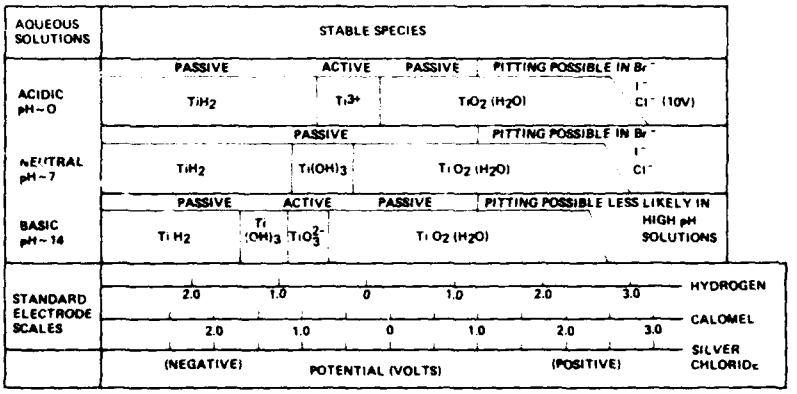


Fig. 16. A summary of the stable species and corrosion behavior of titanium in aqueous solutions. Note the dependence on potential and pH. The calomel scale for the saturated reference electrode and the silver chloride electrode refers to a 3.5% sodium chloride solution.

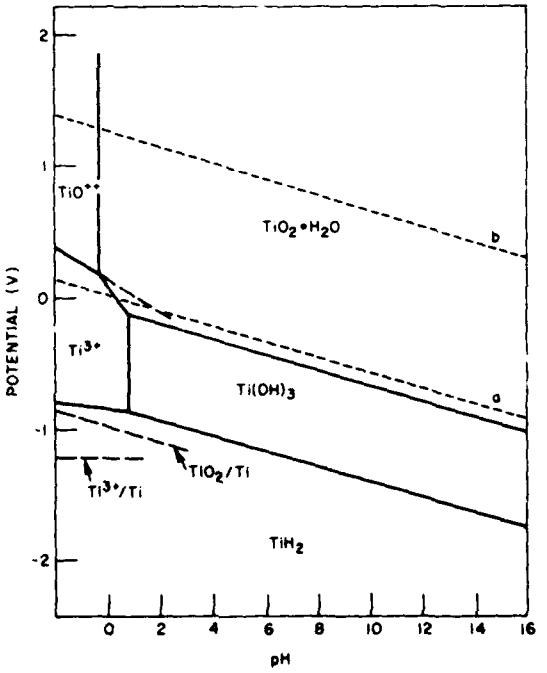


Fig. 17. Potential-pH equilibrium diagram for titanium in aqueous solutions [26].

incompatible with anhydrous red fuming nitric acid and may react explosively. As shown in Figs. 16 and 17, titanium is soluble in acid solutions, forming $Ti^{3+}$ ions which thereby leave the surface of the metal unprotected and reactive, a matter which may be of importance in SCC.

Hydrogen can be absorbed by titanium and its alloys from acidic aqueous solutions, e.g., HCl, $H_2SO_4$, and HF. Such absorption at room temperature does not lead usually to embrittlement of the bulk titanium, as the hydride is restricted to the surface layers. At 200 to 400°F, however, hydrogen pickup and embrittlement have been observed in nonoxidizing conditions. Hydrogen pickup is promoted by surface contamination by iron.

## 5.4 Stress Corrosion Cracking Behavior

### Introduction

The SCC test methods utilized for titanium alloys depend quite strongly on the environment to be evaluated; for example, smooth specimens are the predominant type used in hot salt SCC studies, while precracked specimens are utilized extensively in aqueous SCC evaluations. Test methods that employ such prescribed specimens are described in detail in Chapter 2. Note that such techniques avoid the problem of crack nucleation, a factor that may merit reconsideration in certain applications as titanium becomes more widely used. In the following sections we shall comment on the test techniques and crack nucleation problems in the various environments discussed. In the presentation of data, emphasis will be placed on the threshold stress-intensity value for the onset of cracking $K_{Iscc}$ (where this parameter is real). The velocity of cracking is important in the SCC problem; therefore, we shall describe the cracking rates observed in the various environments and how these rates are changed by the external conditions. The general methods of representing SCC data are shown in Fig. 18, for both smooth specimens (Fig. 18a), and precracked specimens (Fig. 18b, c, and d).

In general there are two methods of presenting results from precracked specimens. First, the initial stress intensity factor $K_I$ is plotted vs time to failure in a specific environment. This plot is used to define a threshold stress intensity $K_{Iscc}$ for those systems for which a true threshold appears to exist. Second, crack velocity V is plotted against stress intensity $K$, which can also define $K_{Iscc}$; that is the value of $K$ at which the crack velocity goes to zero. From these different types of data, there are two ways of describing or defining susceptibility: first, the absolute value of $K_{Iscc}$ and the ratio of $K_{Iscc}/K_{Ic}$,* and second,

*Although this ratio has been widely used, it has no merit over reporting absolute values, and it has the disadvantage of incorporating the considerable errors which may easily occur in the $K_{Ic}$ determination, especially in titanium alloys. (*Editor*)

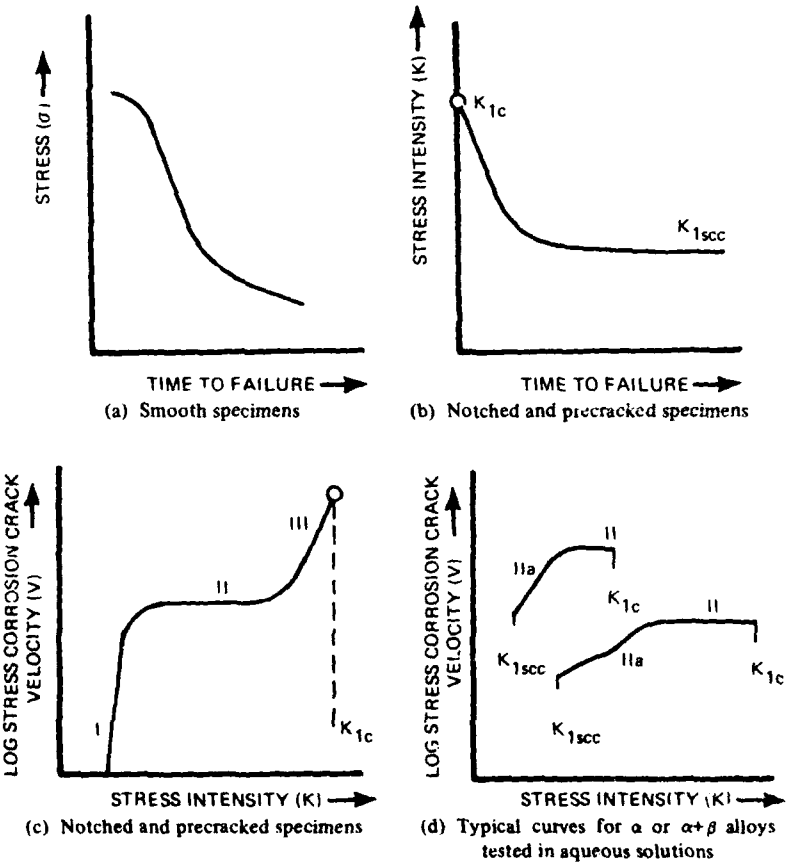


(a) Smooth specimens

(b) Notched and precracked specimens

(c) Notched and precracked specimens

(d) Typical curves for α or α+β alloys tested in aqueous solutions

Fig. 18. Methods of presenting SCC data for various specimens.

the velocity of cracking at various stress intensity levels. The velocity vs stress intensity approach was first used for analyzing subcritical crack growth in glass [27], steel [28], and brass [29], and was subsequently extended to titanium alloys [30,31]. Generally, three stages may be exhibited in a $V$ vs $K$ plot (Fig. 18c); regions I and III are strongly stress intensity dependent, whereas region II is virtually independent of $K$; i.e., a plateau velocity exists. (Typical $V$-$K$ curves for titanium alloys observed in aqueous solutions are shown in Fig. 18d.)

In the following sections we attempt to separate the many variables influencing SCC into three main groups. These are mechanical effects, environmental effects, and metallurgical effects. Some difficulties arise with such a division since most of the variables are interrelated. Therefore, before this division is made, we will list the environments in which SCC of titanium alloys has been observed. These are aqueous solutions, organic liquids, hot salt, nitrogen tetroxide ($N_2O_4$), red fuming nitric acid (RFNA), molten salts, liquid metals, and gases. A discussion of SCC in these environments is given under "Environmental Variables." We also classify the titanium alloys that are susceptible to SCC into three basic types:

- $\alpha$ alloys, including $\alpha+\beta$ alloys, in which only the $\alpha$ phase is susceptible to transgranular SCC (in aqueous solutions).
- $\beta$ alloys, including $\beta+\alpha$ alloys, in which only the $\beta$ phase is susceptible to transgranular SCC (in aqueous solutions).
- Alloys of the $\beta+\alpha$ type which are subject to intergranular SCC (in aqueous solutions).

In the following discussion of SCC of titanium alloys we will use specific examples of alloys and heat treatments that best illustrate the phenomenon under consideration. The "model systems" we have chosen are shown in Table 3. Relative terms such as "very susceptible to SCC" are used in the text. For example, a "very susceptible" alloy in aqueous solution would exhibit SCC in distilled water, a low $K_{Iscc}$ in salt water, and cracking rates of about $10^{-2}$ cm/sec.

**Table 3.** Phase Susceptibility of Selected Titanium Alloys

| *α-Phase Susceptible Alloys* | | *β-Phase Susceptible Alloys* | |
|---|---|---|---|
| *α Phase* | *α+β Phase* | *β+α Phase* | *β Phase* |
| Ti-Al | Ti-8Al-8Mo-1V | Ti-8Mn<br>Transgranular | Ti-13V-11Cr-3Al |
| Ti-5Al-2.5Sn | Ti-6Al-4V | Ti-11.5Mo-6Zr-4.5Sn (Beta III)<br>Intergranular | |
| Ti-5Al-5Zr-5Sn | | | |

## Mechanical Variables

**Stress Concentrations.** Most $\alpha$ alloys when tested as smooth specimens in neutral aqueous solutions do not exhibit SCC, and the initial discovery of SCC in precracked samples of Ti-7Al-2Nb-1Ta tested in seawater came as a surprise both to the users of titanium and to the scientific community. Indeed, one major aerospace company reevaluated its alloy selection for a supersonic aircraft on the basis of the results of this type of test. It had been thought prior to the results on precracked specimens that $\alpha$ titanium alloys were immune to both general corrosion and SCC in such environments, although susceptibility of Ti-13V-11Cr-3Al had been observed earlier [32].

The presence of a notch is often stated to be a requirement for SCC in aqueous solutions [33]. This is not a necessary requirement for all alloys in aqueous solutions and is certainly not a necessary condition for all environments. Thus, titanium alloys that are susceptible to SCC can be divided into two general types.

- Those which experience SCC in any solution even without a stress concentration. These are mostly $\beta$ alloys such as Ti-13V-11Cr-3Al and Ti-8Mn. However, this classification also includes some $\alpha$ and $\alpha+\beta$ alloys which can be very susceptible to SCC, e.g., Ti-8Al-1Mo-1V.
- Those which will not experience SCC in certain environments without notches or cracks.

Figure 19 is an attempt to show schematically where a stress concentration (a notch or notch plus precrack) would be required.

- Type 1 Behavior: Specimens require a fatigue crack to indicate susceptibility to SCC; e.g., duplex-annealed Ti-6Al-4V in neutral aqueous solutions.
- Type 2 Behavior: Specimens may have a fatigue crack or a machined notch to indicate susceptibility to SCC; e.g., mill-annealed Ti-8Al-1Mo-1V in neutral aqueous solutions.
- Type 3 Behavior: Susceptibility to SCC is apparent on testing smooth specimens; e.g., Ti-8Al-1Mo-1V, Ti-8Mn, and Ti-13V-11Cr-3Al in neutral aqueous solutions.

**Thickness Effect.** Soon after the discovery of SCC in aqueous solutions, it was found that the level of susceptibility in $\alpha$ and $\alpha+\beta$ alloys was dependent upon specimen thickness [34]. Typical results are shown for Ti-6Al-4V and Ti-8Al-1Mo-1V in Fig. 20a, where it is apparent that susceptibility decreases with decreasing specimen thickness. Thus, it can be concluded that there is a critical specimen thickness, $t_{crit}$, where SCC does not occur, as shown schematically in Fig. 20b. The value of $t_{crit}$, can be different for each alloy and in fact may not be exhibited if the alloy is very susceptible. For example, Ti-6Al-4V with a very low $K_{Iscc}$ in thick sections (0.5 in.) exhibited the same value in thin sections (0.01 in.) (see p. 300). Furthermore, for an alloy that exhibits a

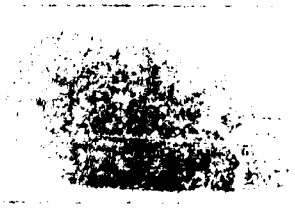

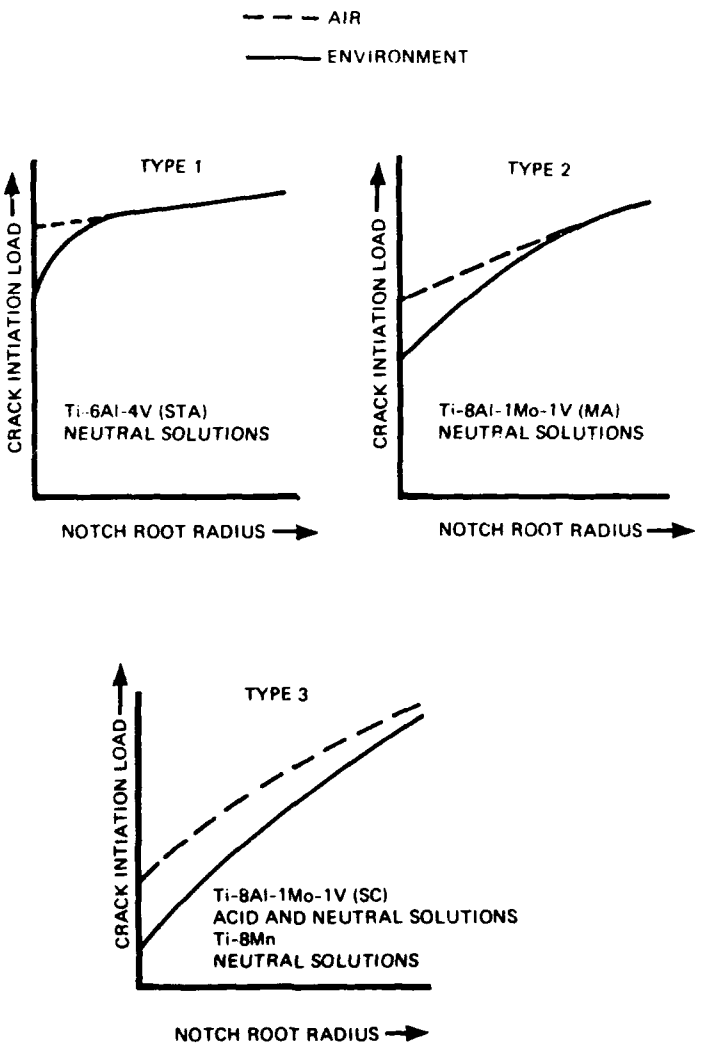


Fig. 19. Schematic of the effect of notch acuity on fracture load in air and in aqueous solutions.

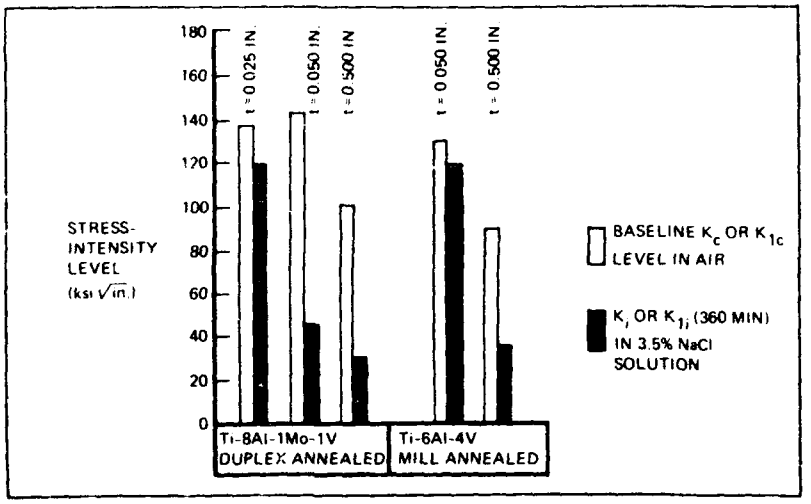


(a) Effect of specimen thickness on the fracture toughness of Ti-8Al-1Mo-1V (DA) and Ti-6Al-4V (MA) tested in air and in 3.5% NaCl [34]

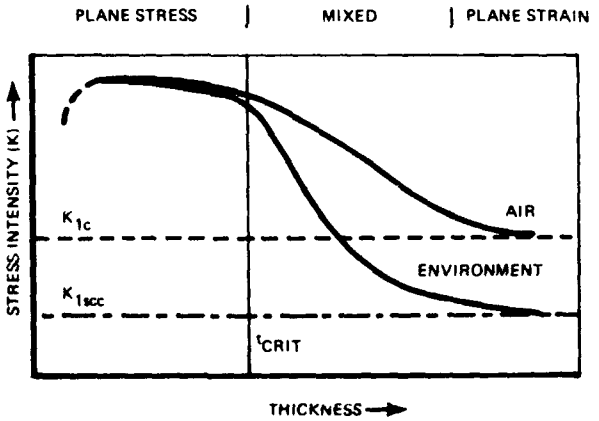


(b) Schematic of the variation of fracture toughness with specimen thickness ($t_{crit}$ is the specimen thickness below which SCC does not occur)

Fig. 20. Specimen thickness effects.

thickness effect, the value of $t_{crit}$ may be changed by (a) preferred orientation, (b) loading rate of the test, and (c) heat treatment.

**Specimen Orientation.** It will be shown in the sections on metallurgical variables and stress corrosion fracture that many titanium alloys fail by a cleavage-like process in many environments. As such processes occur on specific planes, it is obvious that the average orientation of these planes with respect to the tensile axis will influence the measured degree of susceptibility. Such a preferred orientation effect is most pronounced in the $\alpha$ and $\alpha+\beta$ alloys for which the cleavage plane is about 15° from the basal plane [35]. In $\beta$ alloys the cleavage plane is [100], and thus the anisotropy of properties is normally less pronounced.

After certain mechanical and thermal treatment procedures, $\alpha+\beta$ alloys in sheet or plate form exhibit a pronounced texture of the $\alpha$ phase in which the basal planes (0001) are aligned parallel to the rolling direction and normal to the top and bottom surfaces of the sheet or plate. The influence of specimen orientation on the SCC susceptibility of a highly textured Ti-8Al-1Mo-1V plate is shown in Fig. 21 [36]. It can be seen that specimens selected so that the general cracking plane is parallel to the basal planes exhibit the most susceptibility (curve C in Fig. 21), while specimens that have the general cracking plane aligned normal to the basal planes exhibit much higher $K_{Iscc}$ levels. In highly susceptible $\alpha+\beta$ alloys the influence of texture becomes less pronounced and SCC occurs irrespective of specimen orientation [37].

The presence of a strongly preferred orientation in titanium alloys is also important in stress corrosion testing. For example, when using the DCB specimen, advantage may be taken of the preferred orientation to restrict the propagating subcritical crack to the general cracking plane, as in Fig. 22a. In contrast, if preferred orientation is not considered when selecting a specimen orientation, the crack may deviate immediately from the general cracking plane and break the arm off the DCB specimen, as in Fig. 22b.

The thickness effect described in the previous section may also result from the relationship between specimen orientation and texture in the $\alpha$ phase. It has been proposed that effective local plane strain conditions can still be obtained in very thin sheet if the specimens are selected so that the individual $\alpha$ grains, in highly textured sheet, are unfavorably oriented for slip. Such a situation was considered to result in sufficient constraint to cause inhibition of plane stress conditions [38].

Some titanium alloys, tested in certain environments, exhibit an intergranular fracture mode. With such alloy-environment combinations, unless there is a strongly preferred grain direction such as the short transverse direction in aluminum alloys, no anisotropy of SCC results of the type discussed above would be expected in an equiaxed structure.

**Strain Rate Effects.** Loading procedure may influence markedly the results from stress corrosion tests of precracked specimens [39-44]; for example, it has been reported that $K_{Iscc}$ in the alloy Ti-6Al-4V could be increased 30% by decreasing the rate of loading. This effect of loading rate is strongly dependent on

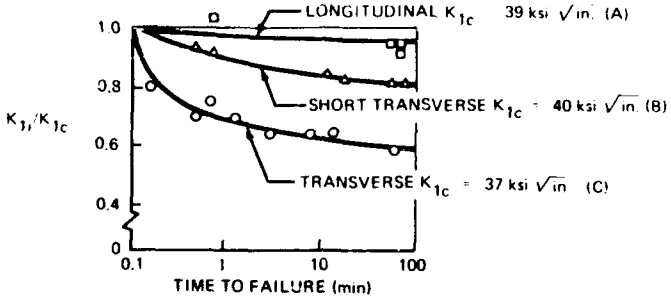


(a) Stress corrosion susceptibility as a function of specimen orientation in Ti-8Al-1Mo-1V 0.5-in. annealed plate (three-point-loaded notched bend specimens) [36]

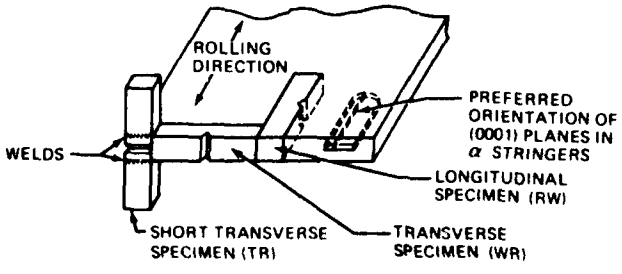


(b) Orientation of specimens in Ti-8Al-1Mo-1V 0.5-in. plate [36]

Fig. 21. Specimen orientation effects.

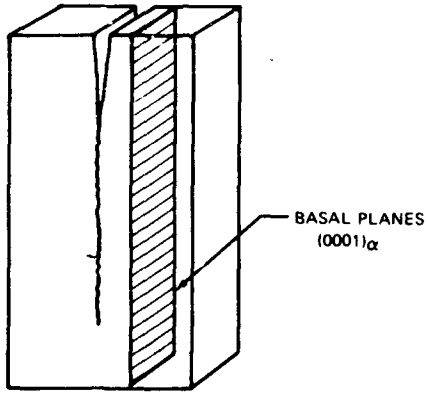


(a) (0001) planes parallel to general cracking plane

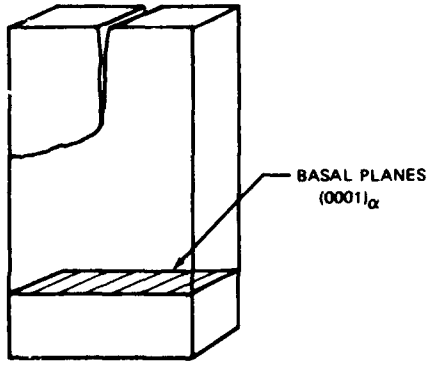


(b) (0001) planes normal to general cracking plane

Fig. 22. Influence of texture on crack propagation in DCB specimens of $\alpha$ or $\alpha+\beta$ alloys. From *Met. Trans.* **245**, p. 1257, Fig. 8; copyright 1969 by the American Society for Metals. Used by permission.

alloy composition [41]. For example, the effect appears to be quite pronounced in Ti-11.5Mo-6Zr-4.5Sn [45], but is less marked in Ti-8Al-1Mo-1V.

A different aspect of test procedures has been evaluated in a number of $\alpha$ and $\alpha+\beta$ specimens that were either (a) loaded in air prior to adding the 3.5% NaCl solution, or (b) loaded in the 3.5% NaCl solution [39]. It was found that in alloys showing intermediate susceptibility, e.g., Ti-6Al-4V and Ti-70A, higher $K_{Iscc}$ values were obtained by test procedure (a). In alloys which exhibit either a very low or very high degree of susceptibility, little or no difference in $K_{Iscc}$ was observed between the two test procedures. This type of behavior is represented schematically in Fig. 23.

**Preloading Effects.** Two aspects of preloading will be considered; first, the influence of local load application, and second, overall prior deformation of material.

The influence of either fatigue loading on the nucleation of cracks or a prior monotonic overload on an existing crack is of importance in testing, design analysis, and life prediction. It has been shown that the fatigue precracking stress-intensity level ($K_{max}$) has little influence on the subsequently measured $K_{Iscc}$ value of this level is low (about 20 ksi $\sqrt{\text{in.}}$). The more important case where $K_{Iscc}$ is relatively high (60 to 80 ksi $\sqrt{\text{in.}}$) has not been investigated at this time. Monotonic preloading to a level $K_I$ which is greater than $K_{Iscc}$ also has little influence on the $K_{Iscc}$ determined if $K_{Iscc}$ is low. It has been shown, however, in material with a higher $K_{Iscc}$ level that the measured value is raised by preloading above $K_{Iscc}$, often approaching the preload level.

The influence of prior cold work of titanium alloys on subsequent SCC behaviors has not been widely studied, as most titanium alloy mill products are

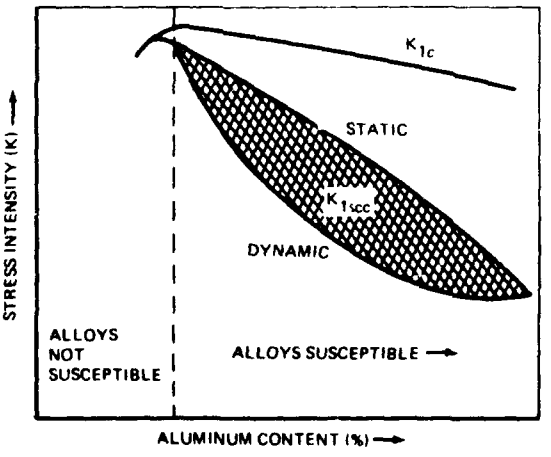


Fig. 23. Schematic of the influence of aluminum content and type of loading on the measured $K_{Iscc}$ value [39,40].

delivered in the annealed or STA condition. The limited data on the influence of cold work on SCC is presented in the section on metallurgical variables. For $\alpha$ alloys such as Ti-70A, $K_{Ic}$ is lowered by cold work, and $K_{Iscc}$ is first lowered and then raised by successively greater amounts of cold work. Data on other $\alpha$ and one $\alpha+\beta$ alloy indicate that cold work slightly increases the $K_{Iscc}$ level [39].

**Summary.** It should be emphasized that many of the above observations on mechanical effects are applicable only to neutral aqueous solutions. In other environments, such as those which cause region I crack growth behavior, the mechanical effects described above may have only a minor influence. Furthermore, the above discussion on mechanical effects is concerned primarily with changes in $K_{Iscc}$ values. Virtually no data are available on the influence of these factors on crack propagation kinetics. It is probable that preferred orientation will modify crack growth behavior.

## Environmental Variables

In this section the many environments that have been shown to cause SCC of titanium alloys will be considered separately. Within each subsection an attempt is made to isolate the individual factors that operate in a specific environment.

**SCC in Aqueous Solutions.** Some titanium alloys in certain heat-treatment conditions are susceptible to SCC in distilled water. Examples are Ti-8Al-1Mo-1V (SC), Ti-5Al-2.5Sn, and Ti-11.5Mo-6Zr-4.5Sn (STA). The SCC information generated in distilled water gives a basis for comparing the effects of concentration and specificity of ions in solution.

Titanium alloys do not exhibit region I type crack growth kinetics in neutral aqueous solutions. Tests have been performed over sufficient time periods to allow detection of crack growth rates of $10^{-7}$ cm/sec, but no such cracking was observed. The slowest crack velocity which has been detected is $10^{-6}$ cm/sec, but in general the cutoff crack velocity is about $10^{-3}$ cm/sec. Thus it is concluded that in neutral aqueous solutions a threshold ($K_{Iscc}$) exists below which cracks will not propagate.

*Effect of Ion Additions.* The halide anions $Cl^-$, $Br^-$ and $I^-$ are the only ions that have been shown to either (a) accelerate cracking in alloys susceptible to SCC in distilled water or (b) induce susceptibility in alloys immune to SCC in distilled water. The additions of other anions produce neither of the above effects and may in some cases inhibit SCC [43,46]. Examples of such neutral or inhibiting ions are $NO_3^-$, $SO_4^{2-}$, $OH^-$, $CrO_4^{2-}$, and $PO_4^{3-}$. The ability of these ions to inhibit SCC depends on the alloy and its heat treatment (see Effect of Concentration, below).

The influence of cation type in $Cl^-$, $Br^-$, and $I^-$ solutions can be divided on the basis of their position with respect to titanium in the electromotive series. Cations less noble than titanium, e.g., Na, K, Li, etc., have no influence on SCC behavior. Cations more noble than titanium may influence SCC behavior. For example, the $K_{Iscc}$ in Ti-8Al-1Mo-1V may be raised by $CuCl_2$ additions [47];

however, this effect is strongly dependent upon heat treatment in this alloy [48].

*Effect of Concentration.* Increasing the concentration of $Cl^-$, $Br^-$, or $I^-$ usually increases the velocity of cracking. The influence of concentration on $K_{Iscc}$ is more complex since it is dependent upon the alloy and its heat treatment. In general $K_{Iscc}$ is lowered by increasing $Cl^-$ concentration, although the decrease is small in very susceptible alloys.

In concentrated solutions the velocity of cracking varies as $C^{1/4}$ to $C^{1/2}$ [44, 49], and this exponent is independent of alloy type, heat treatment, and fracture mode. The position and extent of this relationship, however, are dependent on such variables, and in less concentrated solutions the relationship between crack velocity and concentration is more complicated. Figure 24a summarizes schematically the velocity dependence in aqueous halide solutions. Highly susceptible material (curve A) shows a velocity plateau. Material with intermediate susceptibility (curve B) exhibits downward deviations of velocity at very low ion concentrations; material with relatively low susceptibility (curve C) is immune in distilled water and therefore a discontinuity is observed in the concentration dependence. This behavior is also reflected in the variation of $K_{Iscc}$ with concentration, as shown schematically in Fig. 24b.

The addition of anions other than $Cl^-$, $Br^-$, and $I^-$ to distilled water tends to reduce susceptibility to SCC. The extent of such reduction is again dependent on the susceptibility of the material in distilled water. Considering the same example as that used in Figs. 24a and b, the effect of other ion additions on crack velocity is shown schematically in Fig. 25. Thus, in highly susceptible alloys (curve A), very high anion concentrations are necessary to reduce the velocity of cracking. In contrast, in materials that exhibit intermediate susceptibility in distilled water, SCC can be prevented by relatively small additions of these other anions (curve B).

*Effect of Potential.* In this section, only neutral, high-conductivity aqueous solutions containing $Cl^-$, $Br^-$, or $I^-$ ions will be treated. The effects of potential must be considered in practice as titanium alloys are often coupled to other metals when incorporated into a structure.

The variation of cracking behavior in three solutions with potential for duplex-annealed Ti-8Al-1Mo-1V is shown in Fig. 26 [43,50]. The following points are apparent in this figure and are in general true for all susceptible alloys studied to date:

- The crack-initiation load reaches a minimum at about -500 mV (SCE) in $Cl^-$-containing solutions.
- The open-circuit potential of titanium alloys in 3.5% NaCl and seawater (about -800 mV SCE) is slightly more negative than the initiation load minimum (-500 mV).
- A region of cathodic protection may exist at potentials more negative than -1000 mV. It should be noted that *complete* cathodic protection appears to be achievable only in alloys which are immune in distilled water.

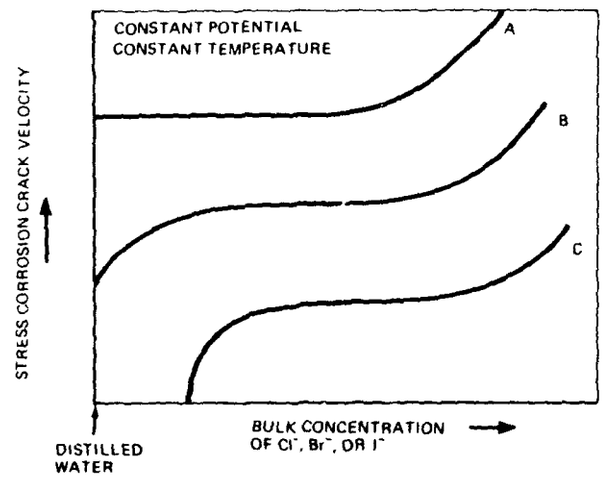


(a) On crack velocity

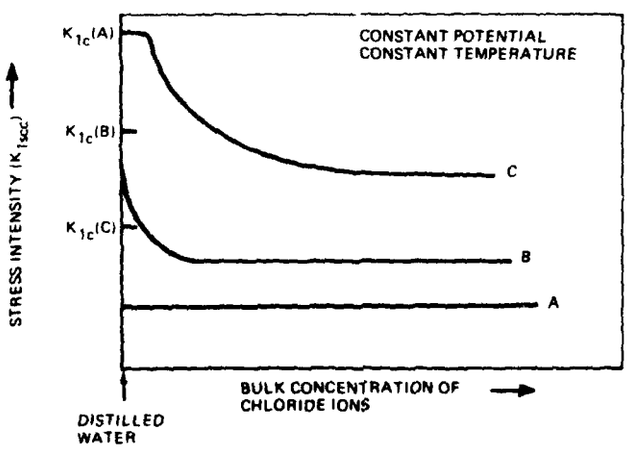


(b) On $K_{Iscc}$

Fig. 24. Schematic of the influence of halide ion concentration and metallurgical factors.

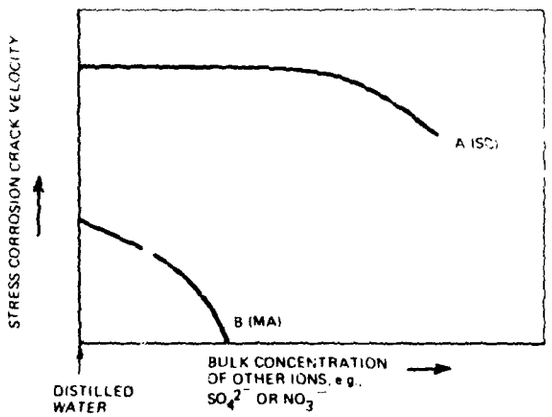


Fig. 25. Schematic of the influence of other ions and metallurgical factors on crack velocity.

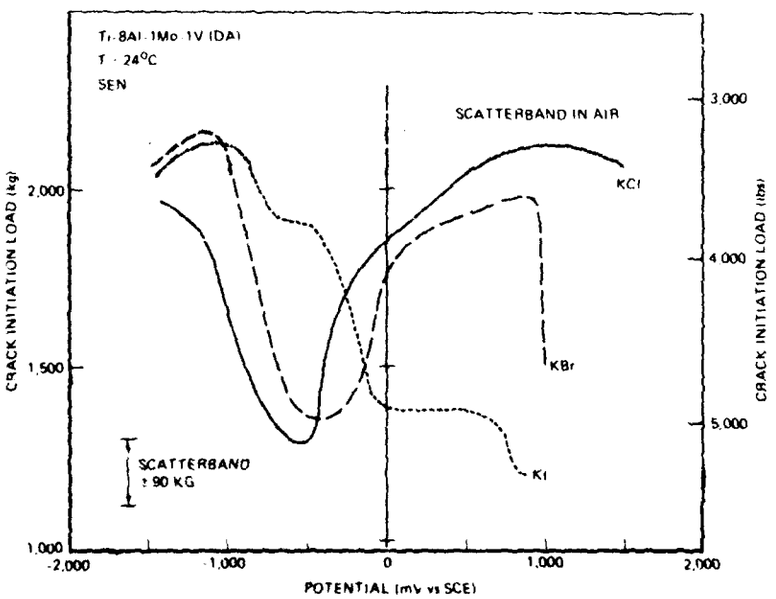


Fig. 26. Variation of crack-initiation load with potential in 0.6 *M* halide solutions for Ti-8Al-1Mo-1V [50].

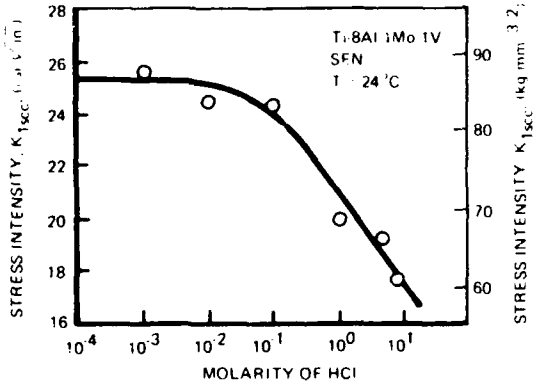


Fig. 27. Variation of $K_{Iscc}$ with molarity of HCl for Ti-8Al-1Mo-1V [30].

• A region of anodic protection may exist with $Br^-$ and $Cl^-$ solutions, especially the latter, but not with $I^-$ solutions.

There is an approximately linear relationship between potential and average crack velocity ($\bar{V}$) for solutions containing $Cl^-$, $I^-$, and $Br^-$ ions [48, 49].

*Effect of pH.* In contrast to neutral aqueous solutions, titanium alloys exhibit both region I and region II types of crack growth in concentrated (>7 *M*) halogen acid solutions. Thus in these solutions it may not be possible to define a $K_{Iscc}$ value. The acidity of the solution influences the $K_{Iscc}$ value, as can be seen in Fig. 27, which shows that the value is reduced [30] at molarities above about $10^{-1}$. This is approximately the acidity reported at the tips of growing stress corrosion cracks where the bulk corrodent is neutral sodium chloride.

In highly acidic solutions, region II crack propagation velocity is virtually independent of potential [40], and no cathodic protection is possible in such solutions [44].

Little work has been performed to determine effect of alkaline solutions on either crack initiation or crack propagation. Some studies have indicated beneficial effects of increasing alkalinity [43]; others have failed to find such effects [51].

*Effect of Temperature.* The critical stress intensity for crack initiation ($K_{Iscc}$) in Ti-8Al-1Mo-1V in neutral 3.5% NaCl does not vary with temperature [52]. (In less susceptible alloys $K_{Iscc}$ might be lowered by increasing the temperature but this does not seem to have been studied.) The *velocity* of cracking in 3.5% NaCl is strongly temperature dependent. An Arrhenius plot of the limiting crack velocity of (equivalent to either region II or IIa velocity) indicates an activation energy value of Q = 5.6 kcal/mole [53].

**SCC in Organic Liquids.** The failures of the Ti-6Al-4V Apollo pressure vessels during proof testing with dry, reagent-grade methanol stimulated intensive research in the late 1960's to investigate SCC of titanium in organic liquids. Much

of the background information and major findings of this research effort has been summarized [54]. Another review summarizes the more recent work on the subject [55].

In the following sections, the organic solvents are grouped as alcohols, halogenated hydrocarbons, and miscellaneous solutions.

*Alcohols.* Two types of SCC behavior in methanolic solutions have been distinguished on the basis of failure mode [56,57]:

- Intergranular failure, which occurs in pure titanium and all alloys. Such cracking requires the presence of halogen, e.g., 0.3 ppm $Cl^-$.
- Transgranular failure, which usually occurs in alloys also susceptible to aqueous SCC.

This classification will serve as a basis for discussing the variables which influence SCC in methanolic solutions.

1. Intergranular Failure Mode. The first observation of intergranular attack in titanium alloys was made using methanol plus bromine solutions [58]. Subsequently it was demonstrated that methanolic solutions containing HCl or $H_2SO_4$ cause SCC in both titanium and zirconium [59,60]. Recent work has indicated that several factors influence intergranular failure, and a separation of these factors is attempted below.

The time to failure of *smooth* specimens of commercially pure titanium (Ti-35A) can vary considerably with the impurity content of methanolic solutions [61]. Cracking occurs in this material only when the concentration exceeds $10^{-6}$ *N* HCl. The water content of methanolic solutions influences time to failure in this and other materials. (See also Ref. 60).

A potential more negative than −250 mV (Ag/AgCl) prevents cracking of CP titanium in neutral methanolic solutions [62].

2. Transgranular Failure Mode. Alloys such as Ti-8Al-1Mo-1V exhibit a transition from intergranular cracking in region I to transgranular cracking in region II in many environments. In addition to the complex cracking behavior exhibited by the alloy Ti-8Al-1Mo-1V, the alloy Ti-11.5Mo-6Zr-4.5Sn fails by intergranular cracking in region II in neutral aqueous solutions and also in methanol-KI solutions [63]. Thus, it is perhaps useful to classify the cracking behavior of alloys on the basis of the stress dependence of cracking rate.

Little work has been performed on the influence of the degree of methanol purity on region II type growth. However, it has been established that the inhibiting effect of water additions on SCC *initiation* will not be observed if the alloy is susceptible to SCC in distilled water.

In general, additions of Cl, Br, and I increase the rate of region II cracking, again independent of the form in which they are added. Other additions, such as $NO_3^-$ and $SO_4^{2-}$, appear to prevent cracking [50]. However, insufficient work has been performed to demonstrate the extent or generality of these effects.

Several workers have demonstrated that cracking can be prevented in neutral methanolic solutions by applied potentials of −1000 to −1500 mV (SCE). The

velocity of region II cracking is accelerated by anodic potentials, and the range of $K$ over which rapid cracking occurs is extended by such potentials.

It is generally agreed that increasing the temperature of methanolic solutions also increases the velocity of cracking, an activation energy of about 5 kcals/mole having been measured [64].

No investigations have been performed on pure titanium in anhydrous alcohols. However, cracking occurs in smooth specimens of Ti-8Al-1Mo-1V and Ti-6Al-4V in anhydrous ethanol [65,66]. Cracking in ethylene glycol was also observed in the Ti-8Al-1Mo-1V alloy, but not in the Ti-6Al-4V alloy [66].

The SCC behavior of Ti-8Al-1Mo-1V in a number of alcohols is summarized in Fig. 28. It can be seen that the methanol and ethylene glycol produce very low values of $K_{Iscc}$. Increasing the chain length of the alcohols to four carbon atoms increases $K_{Iscc}$ to $\approx 40$ ksi $\sqrt{\text{in.}}$, above which $K_{Iscc}$ remains constant. In addition, it was shown that $K_{Iscc}$ was not sensitive to the type (primary, secondary, etc.) of alcohol [67].

*Halogenated Hydrocarbons.* SCC testing in halogenated hydrocarbons appears to have been conducted only on alloys. Cracking has been detected in carbon tetrachloride, methylene chloride, methylene iodide, trichlorethylene, trichlorofluoromethane, trichlorotrifluoroethane, and octafluorocyclobutane. There is no evidence in the literature that pure titanium is susceptible to SCC in any of these

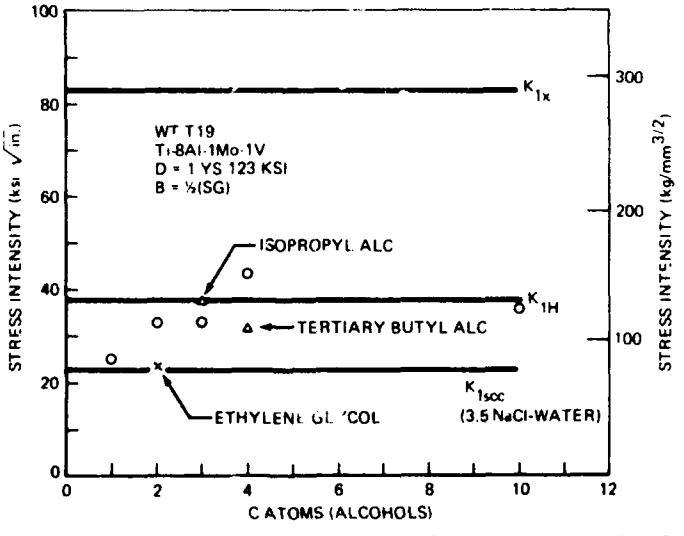


Fig. 28. Apparent threshold stress intensity ($K_{Iscc}$ in 360 min) for Ti-8Al-1Mo-1V tested in alcohols with increasing number of carbon atoms. ($K_{IH}$ refers to a threshold for slow crack growth in an inert environment, perhaps caused by internal hydrogen) [67]. From *Proceedings of Conference on Fundamental Aspects of Stress Corrosion Cracking*, 1969, p. 687, Fig. 1; copyright by the National Association of Corrosion Engineers. Used by permission.

organic liquids. Further, in some cases a notch or precrack is required for SCC to occur.

*Carbon Tetrachloride ($CCl_4$).* The first reports of cracking on $CCl_4$ noted that Ti-8Al-1Mo-1V exhibited a cracking behavior similar to that observed in 3.5% NaCl solution [50,68]. Subsequently, *V-K* relationships were established for Ti-8Al-1Mo-1V [64]. These results showed that (a) the region II cracking rate in pure $CCl_4$ is almost two orders of magnitude faster than in pure methanol and almost an order of magnitude faster than in distilled water; and (b) the apparent region I type growth does not continue below $10^{-6}$ cm/sec and thus a $K_{Iscc}$ can be defined for Ti-8Al-1Mo-1V in this environment. It should be noted that the $K_{Iscc}$ value of this alloy in $CCl_4$ is similar to the value observed in 3.5% NaCl solution.

*Freons.* Freon is a DuPont registered trade name for fluorinated hydrocarbons. The common varieties are Freon TF ($C_2Cl_3F_3$). Freon MF ($CCl_3F$), and Freon C318 ($C_4F_8$). Most investigations on these solvents have been concerned with determining $K_{Iscc}$ thresholds. Table 4 summarizes the results of several investigators. From this table of approximate values, it is obvious that rather variable behavior has been observed, which in some cases may be due to the short testing times. In general, alloys appear to be less susceptible in the TF grade of freon.

Additions of chlorine do not reduce $K_{Iscc}$ values for Ti-6Al-4V from those obtained in pure grades of freon.

From the kinetics of subcritical crack growth of Ti-6Al-4V in Freon TF, an apparent region I is observed, and therefore very slow crack growth may occur below $K$ values normally listed as threshold levels [72].

**Table 4.** Variation of $K_{Iscc}$ in Several Grades of Freons

| *Grade* | *Alloy* | *Heat Treatment* | $K_{Ic}$, ksi $\sqrt{in.}$ | $K_{Iscc}$, ksi $\sqrt{in.}$ | *Ref.* |
|---|---|---|---|---|---|
| TF | Ti-6Al-4V | STA | 50 | 50 | 69 |
| TF | Ti-6Al-4V | STA | 40 | 33 | 70 |
| TF | Ti-6Al-4V | MA | 59 | 52 | 69 |
| TF | Ti-5Al-2.5Sn | MA | 67 | 30 | 69 |
| TF | Ti-8Al-1Mo-1V | STA | 80 | 44 | 69 |
| TF | Ti-8Al-1Mo-1V | MA | 30 | <23 | 69 |
| MF | Ti-6Al-4V | STA | 40 | 23 | 71 |
| MF | Ti-6Al-4V | MA | 59 | <25 | 69 |
| MF | Ti-5Al-2.5Sn | MA | 67 | 23 | 69 |
| MF | Ti-8Al-1Mo-1V | MA | 30 | 23 | 69 |
| C318 | Ti-5Al-2.5Sn | MA | 67 | <49 | 69 |

*Other Halogenated Organics.* Ti-8Al-1Mo-1V heat treated to a rather low toughness level exhibited a small degree of susceptibility ($K_{Iscc}/K_{Ic}$ = 25/40 = 0.63) when tested in trichlorethylene [69].

Two alloys, Ti-8Al-1Mo-1V and Ti-5Al-2.5Sn, have been shown to exhibit a small degree of SCC susceptibility in inhibited trichlorethylene. However, Ti-5Al-2.5Sn showed a larger degree of susceptibility ($K_{Iscc}/K_{Ic}$ = 28/70 = 0.4) in the uninhibited solvent [69].

Cracking of Ti-8Al-1Mo-1V has also been observed in methylene chloride and in methylene iodide [50].

*Miscellaneous Solutions.* $K_{Iscc}$ values have been reported for Ti-8Al-1Mo-1V and Ti-6Al-4V in various other organic solvents. Examples are shown for Ti-6Al-4V in Table 5 below [71].

**Table 5.** The Variation of $K_{Iscc}$ of Ti-6Al-4V Tested in Two Solvents

| *Environment* | *Heat Treatment* | $K_{Ic}$, *ksi* $\sqrt{in.}$ | $K_{Iscc}$, *ksi* $\sqrt{in.}$ | *Temperature* (°F) |
|---|---|---|---|---|
| Monomethylhydrazine | STA | 40 | 33 | 80 |
| Monomethylhydrazine | STA | 40 | 30 | 105 |
| Aerozene 50 | STA | 40 | 34 | 70 |
| Aerozene 50 | STA | 40 | 32 | 85 |

The SCC behavior of Ti-8Al-1Mo-1V in a series of alkanes is shown in Fig. 29. It can be seen that $K_{Iscc}$ is independent of both the chain length of the alkane and its state (i.e., whether gas or liquid).

**SCC in Hot Salts.** In the late 1950's considerable consternation was caused by the premature failure of a titanium alloy during creep testing. This failure was traced to cracking caused by small amounts of NaCl originating from fingerprints on the specimen. Many laboratory investigations were conducted after this observation, and it has been clearly demonstrated that SCC can occur in many titanium alloys stressed in contact with certain salts at elevated temperatures. It should be noted, however, that no service failures attributed to hot salt SCC have been reported.

The most comprehensive data compilation on hot salt SCC can be found in a review [6] and a symposium [7]. Some of the salient points from these and other sources are listed below.

1. Various test techniques have been used to evaluate susceptibility of titanium alloys to hot salt cracking. The most common are the following:

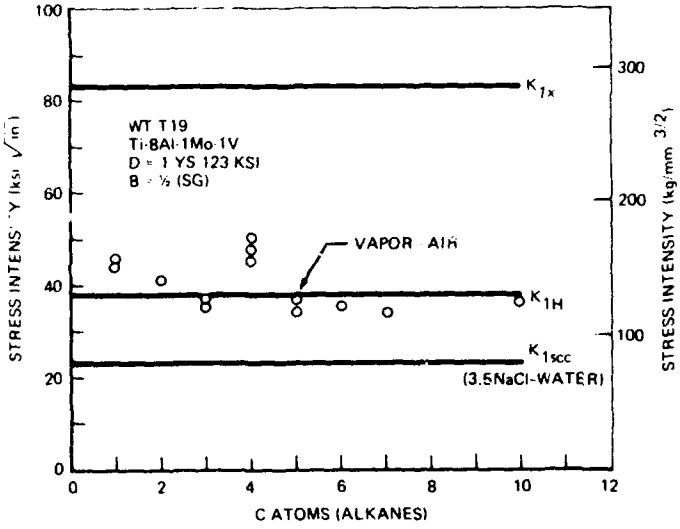


Fig. 29. Apparent threshold stress intensity ($K_{Iscc}$ in 360 min) for Ti-8Al-1Mo-1V tested in normal alkanes with increasing number of carbon atoms [67]. From *Proceedings of Conference on Fundamental Aspects of Stress Corrosion Cracking*, 1969, p. 686, Fig. 6; copyright by the National Association of Corrosion Engineers. Used by permission.

a. Evaluation of tensile properties at elevated temperatures and at room temperature after exposure. Apparently the presence of a precrack does not influence hot salt cracking.

b. Evaluation of bend properties in which there are two general types. First, self-stressed specimens are heated to the required temperature, exposed for various times, then cooled and tested in compression at room temperature. Second, sheet specimens are externally loaded at the exposure temperature and the following properties determined:

- Time for first visual observation of cracking and/or time to failure.
- Properties of specimens machined from the exposed sheet and tested at room temperature.

It should be noted that exposed specimens may be completely or partially coated with salt, and that another test variable is the method of applying the salt coating. The reader is referred to Ref. 7 for typical examples. It is not surprising from the variability of test techniques, the method of application of salt coatings, and the possible differences in exposure conditions, that a large degree of scatter is observed in the results.

2. $Cl^-$, $Br^-$, and $I^-$ salts have been shown to cause hot salt cracking [73], while $F^-$ salts [75] and hydroxides do not. The severity of attack has been correlated with the cation type of $Cl^-$ salts, as follows: $MgCl_2$ (least severe), $<SrCl_2 <CsCl <CaCl_2 <KCl <BaCl_2 <NaCl <LiCl$ (most severe) [75].

3. The role of water in hot salt cracking is not well established. Most workers have concluded that water is essential for cracking to occur [33,76,77]. Some

results indicate that water accelerates cracking but may not be essential to the overall degradation of properties [75]. There is also evidence that excess water can retard cracking [76].

4. The effect of oxygen on hot salt cracking is even less well established than that of water. Most workers have studied the effect of oxygen pressure by reducing the overall pressure of the system. It has been shown that reducing the pressure to 10 microns eliminated cracking in Ti-5Al-2.5Sn [33], and a similar reduction in susceptibility under reduced pressure has been observed in Ti-8Al-1Mo-1V [78]. It is possible, however, that such reductions in overall pressure lower both the moisture and oxygen content of the system, and thus the results could be regarded as ambiguous.

5. In general, increases of both stress and temperature increase hot salt cracking. The kinetics of hot salt cracking have not been established due to experimental difficulties.

Several workers have reported that titanium alloys suffer a degradation of room-temperature mechanical properties after high-temperature exposure in NaCl. Despite a lack of evidence of cracking in Ti-8Mn during high-temperature exposure, tensile specimens cracked on subsequent straining at room temperature [79]. Smooth tensile specimens of Ti-8Al-1Mo-1V exposed to hot salt conditions (100 hr at 850°F at $\sigma$ = 50 ksi) were tested at room temperature. There was a dramatic reduction in percent elongation if the specimens were tested at slow strain rates as shown in Fig. 30a but the effect occurs only below approximately 200°F (Fig. 30b).

6. Unalloyed titanium is not susceptible to hot salt stress corrosion cracking, but all alloys exhibit some degree of susceptibility. A rating of alloy susceptibility has been made [81]. The highly susceptible alloys are Ti-5Al-2.5Sn, Ti-7Al-12Zr, Ti-5Al-5Sn-5Zr, Ti-8Al-1Mo-1V, and Ti-8Mn. The intermediately susceptible alloys are Ti-5Al-5Sn-5Zr-1Mo-1V, Ti-6Al-4V, Ti-6Al-6V-2Sn, Ti-5Al-2.75Cr-1.25Fe, and Ti-3Al-13V-11Cr. The most resistant alloys are Ti-4Al-3Mo-1V, Ti-2.25Al-1Mo-11Sn-5Zr-0.25Si, and Ti-2Al-4Mo-4Zr. Not all workers may agree with this classification. It has also been reported recently that some of the $\beta$ alloys, such as Ti-11.5Mo-6Zr-4.5Sn and Ti-8Mo-8V-3Mo-2Fe, are relatively resistant to hot salt SCC [82].

Surface treatments that inhibit hot salt cracking are described in section 5.6.

**SCC in Nitrogen Tetroxide.** Nitrogen tetroxide ($N_2O_4$) is an oxidizer used with hydrazine rocket fuels in space and missile applications. Early studies of the behavior of titanium and its alloys in $N_2O_4$ indicated that no corrosion problems were to be expected. In 1964, however, a Ti-6Al-4V pressure vessel containing a high-purity grade of $N_2O_4$ failed during proof testing [3]. This unexpected failure once again stimulated a number of research projects. The results of these early studies are summarized in Ref. 83, and the major conclusion was that cracking occurred in red $N_2O_4$ but not in green $N_2O_4$. Typical compositions of these two varieties are shown in Table 6 [84].

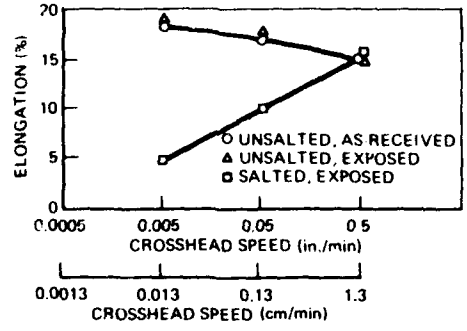


(a) Crosshead speed at 22°C

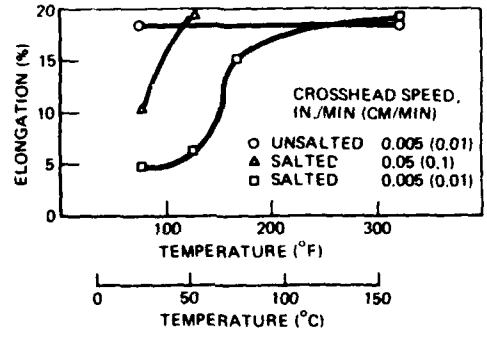


(b) Test temperature at various crosshead speeds

Fig. 30. Variation of tensile ductility of Ti-8Al-1Mo-1V alloy specimens after exposure at 800°F for 100 hr at 50,000 psi in NaCl [80]. From *Corrosion* 25, p. 339, Fig. 5, and p. 340, Fig. 7; copyright 1969 by the National Association of Corrosion Engineers. Used by permission.

**Table 6.** Typical Composition of Two Grades of Nitrogen Tetroxide

| *Component* | *Red $N_2O_4$, %* | *Green $N_2O_4$, %* |
|---|---|---|
| $N_2O_4$ | 99.99 | 99.26 |
| NO (Lab. A) | – | 0.81-0.86 |
| NO (Lab. B) | – | 0.72 |
| $H_2O$ | 0.05 | 0.05 |
| Cl as NOCl | 0.001 | 0.001 |
| $CO_2$ | 0.028 | 0.045 |
| Oxygen | 0.006 | 0.002 |
| Particulates (mg/liter) | 2.3 | 3.1 |

The essential difference is that no nitric oxide (NO) is present in red $N_2O_4$. Furthermore, it contains a higher free oxygen content.

Early work established that the incidence of SCC was increased when higher purity (red) $N_2O_4$ was substituted for the lower purity (green) $N_2O_4$. Thus, susceptibility can be eliminated in red $N_2O_4$ by the addition of NO or $H_2O$. The latter addition essentially increases the amount of NO and eliminates free oxygen. Green $N_2O_4$ will promote cracking if pressurized with oxygen; such pressurization essentially converts green $N_2O_4$ to red $N_2O_4$. The addition of NOCl to green $N_2O_4$ does not cause cracking of titanium alloys.

Only a limited amount of work has been performed on the influence of temperature on cracking in $N_2O_4$. Such evidence as is available shows that the time to failure of smooth specimens [85] and the $K_{Iscc}$ [86] decrease with increasing temperature.

**SCC in Red Fuming Nitric Acid.** In the early 1950's it was found that titanium and its alloys underwent a pyrophoric reaction in red fuming nitric acid (RFNA). The SCC studies in this medium up to 1957 are summarized in Ref. 1. As little work appears to have been conducted after this period, only a brief synopsis of the important features of the phenomenon will be given.

Commercially pure (CP) titanium and all alloys tested to date crack in RFNA containing 20% $NO_2$. Reducing the $NO_2$ content to none eliminates the susceptibility of CP titanium, but not that of the alloys Ti-8Mn and Ti-6Al-4V. The addition of 2% water eliminates susceptibility in all alloys. The military specification for RFNA is 82 to 85% $HNO_3$, 14% $NO_2$, and 2.5% $H_2O$.

Most kinetic studies in RFNA have been concerned with general corrosion rather than stress corrosion. Thus, there is only a small amount of data on the rates of cracking in this environment. Furthermore, there are apparently no quantitative data on the influence of stress, although the observations of cracking near sheared edges of sheet materials indicate an effect.

**SCC in Molten Salts.** Molten salts are used or may be used in heat-treating baths, fast breeder reactors, descaling baths, and battery research. Thus, if titanium is under consideration for use in or treatment in such environments, a knowledge of its SCC behavior is essential. From a more fundamental standpoint, studies of SCC in molten salts may bridge the gap between hot salt cracking and aqueous SCC.

Ti-8Al-1Mo-1V is apparently the only alloy to have been tested in molten salts. In a LiCl + KCl eutectic mixture, smooth tensile specimens loaded to a stress level of 10 ksi failed in about 1 hr. However, if specimens were made cathodic, then the failure time doubled [75].

Subsequently it has been shown that both region I and region II behavior are exhibited by Ti-8Al-1Mo-1V tested in molten LiCl-KCl eutectic at 375°C (706°F). The $K_{Iscc}$ value (if such a threshold exists in this environment) is <9 ksi $\sqrt{in.}$ under these conditions [87].

Cracking has also been shown to occur in two other molten inorganic salts. No cracking of Ti-8Al-1Mo-1V has been observed in pure molten nitrates, but

additions of $Cl^-$, $Br^-$, and $I^-$ caused cracking. In contrast, additions of $F^-$, which can only be added in small concentrations, did not cause cracking. Limited work on molten hydroxides containing $Cl^-$ or $I^-$ has shown that crack propagation can occur in Ti-8Al-1Mo-1V. The rate of cracking, however, is considerably slower than in nitrate salts containing equivalent concentrations of halide ions [87].

**Cracking by Liquid and Solid Metals.** Titanium and its alloys can be cracked by several liquid metals. The first liquid metal cracking problem in service was the reported cracking of Ti-4Al-4Mn compressor disks in the XJS4 engine [2]. Such cracking originated from cadmium-plated bolts attached to the component.

The general-corrosion and stress-corrosion behavior of titanium alloys in liquid metals was summarized in Ref. 83. At that time it had been demonstrated that cracking could be induced by silver braze alloys and mercury. Certain other liquid metals also degraded the properties of titanium, including cesium and gallium. However, in many cases such problems arise from general corrosion rather than stress corrosion.

The metals that are known to cause cracking in titanium and its alloys are discussed below.

*Cadmium.* The titanium alloys known to be susceptible to cracking in liquid cadmium are Ti-4Al-4Mn, Ti-8Mn, Ti-13V-11Cr-3Al, and Ti-50A.

Cadmium-plated, smooth tensile specimens suffered dramatic reductions in percent elongation and some reduction in ultimate tensile strength in the temperature range 620° to 750°F [88]. It was postulated that the critical stage was the penetration of the titanium oxide by the liquid cadmium. Tests were conducted on smooth tensile specimens of Ti-50A in liquid cadmium, and the variations of the strain at fracture with temperature and strain rate were measured [89]. A strain-rate-dependent brittleness occurs similar to that found in other systems [90].

Cracking has been observed in Ti-8Al-1Mo-1V and Ti-6Al-4V in the temperature range 100° to 600°F and therefore has been designated solid cadmium embrittlement [91]. Necessary conditions for failure were considered to be intimate contact of the cadmium with the base metal and an applied tensile stress. It was also proposed that the titanium alloy must plastically deform, although this condition has not yet been conclusively demonstrated.

*Mercury.* The following titanium alloys are known to be cracked by liquid mercury [92,93]: Ti-75A, Ti-13V-11Cr-3Al, Ti-6Al-4V, Ti-8Al-1Mo-1V, and Ti-8Mn. Most of the published information on this subject is based on observations of crack initiation on bend specimens. In recent work *V-K* relationships were established for Ti-8Al-1Mo-1V. Both regions I and II may be exhibited, and the range of velocity is extremely large, the region II plateau velocity of the step-cooled (SC) condition being greater than 10 cm/sec [64]. The threshold levels were $\leq$ 10 ksi $\sqrt{\text{in.}}$ and dependent upon heat treatment condition.

*Silver.* As with cadmium embrittlement of titanium alloys, problems with silver-plated components were first encountered in a compressor stage of a jet

engine and arose from a silver-plated steel bolt in contact with a Ti-7Al-4Mo compressor disk. The failure of the disk was attributed to the formation of AgCl and its interaction with the titanium. In later experiments, it was shown that AgCl is a more aggressive stress corrosion agent than pure silver or, in fact, NaCl. Pure silver and silver braze alloys cause cracking of titanium alloys such as Ti-8Al-1Mo-1V, Ti-7Al-4Mo, and Ti-5Al-2.5Sn. The test temperatures above which cracking by silver has been observed were 343°C (650°F) for the silver braze alloy and 469°C (875°F) for pure silver. Since both these temperatures are well below the melting points of both the materials, these observations are thought to be additional examples of solid metal embrittlement [94,95].

*Zinc.* Limited data indicate that titanium alloys can be cracked by solid zinc under the same conditions as those found for solid cadmium cracking [38].

**SCC in Gaseous Environments.** A number of technologically important elements and compounds in gaseous or vapor form have been found to give rise to SCC in titanium alloys, as summarized below.

*Chlorine Gas.* Ti-8Al-1Mo-1V will crack in moist chlorine at 288°C (550°F) [96], and cracking can occur in many binary titanium alloys exposed to moist chlorine at 427°C (800°F) [97].

*Hydrogen Chloride Gas.* The time for crack initiation in U-bend specimens of Ti-8Al-1Mo-1V in HCl gas decreased with increasing test temperature for a constant pressure of HCl gas of one atmosphere. Additions of about 5 to 6 mole % water to the system increased the time for crack initiation by a factor of approximately two. Cracks formed in HCl are similar to those which occur in hot salt [98].

*Hydrogen.* One of the first titanium hardware problems involving hydrogen was the failure of titanium fittings in a liquid hydrogen storage tank. Failure was attributed to the reaction between titanium and hydrogen gas formed during temperature cycling. It was proposed that the fittings perforated by the formation and subsequent spalling of titanium hydrides [99]. The reaction between hydrogen and titanium metal and some alloys was strongly dependent upon the purity of the hydrogen and the nature of the metal or alloy surface [100]. Other factors that influenced hydrogen pickup were hydrogen pressure, time, temperature, and alloy composition. Microstructural analysis showed that hydrogen pickup was relatively uniform, i.e., layers of hydride were formed at the surface and penetrated inward. One Ti-6Al-4V specimen showed extensive pitting after exposure to hydrogen only when stressed. The stress in this one example acted to assist the spalling of the hydride layers, thus allowing further reaction.

More recently, the reaction of gaseous hydrogen with a series of metals and alloys, including titanium, has been studied [101]. Most of the data from these studies were unpublished, but the following is a summary of the most pertinent results [102-104]:

- Hydrogen gas can cause slow crack growth in titanium alloys, e.g., CP titanium, Ti-6Al-4V, and Ti-5Al-2.5Sn.
- The fracture surfaces show many similarities to aqueous SCC failures.

- No hydride has been detected on the fracture surfaces. (There is, however, some controversy on this point.)
- The maximum degrading influence of hydrogen is observed at 0°C (32°F) in Ti-6Al-4V, and its influence decreases as the temperature is either raised or lowered.
- The maximum degrading influence of hydrogen occurred in materials with an acicular structure.
- Velocity of cracking $\leq 10^{-3}$ cm/sec has been observed.

From these results there appear to be some similarities between SCC in liquids and in hydrogen gas. However, some of the compositional and microstructural effects appear to be different; therefore, any direct comparisons must await the publication of the details of these studies.

*Methanol Vapor.* Methanol vapor has been reported to promote SCC in Ti-8Al-1Mo-1V [105]. Embrittlement occurred in both pure titanium and Ti-5Al-2.5Sn in the presence of methanol vapor without an applied stress. No cracks were observed during or after exposure, and the embrittlement was detected on later tensile testing. Fracture in embrittled regions of specimens was intergranular. The embrittlement could be removed by vacuum annealing [106].

In comparing the behavior of U-bend specimens of pure titanium and Ti-8Al-1Mo-1V in methanol liquid and methanol vapor, it was found that methanol vapor was the more aggressive environment, the time to failure in methanol vapor was inversely proportional to the volume of the closed system, and the susceptibility to methanol vapor was inhibited by ammonia or water.

*Humid Air (>50% RH).* Crack propagation has been observed in laboratory air, in very susceptible alloys, but there have been no systematic investigations in which crack growth rate has been measured in air of varying humidity.

**Metallurgical Variables**

In the previous section it was shown that cracking can occur in titanium alloys exposed to a wide variety of environments. The essential question for the user of titanium alloys is what can be done about a potential SCC problem. In some systems the problem can be controlled by relatively simple environmental modification (e.g., $N_2O_4$), or exclusion of the environment (e.g., cadmium, mercury). However, in other environments, which include the most important case of aqueous solutions, control is preferably exercised by metallurgical methods. Therefore in this section we shall concentrate on the behavior of titanium alloys in aqueous solutions, specifically in seawater or solutions with an equivalent chloride concentration.

The section is divided into three parts. The first part describes in general terms the factors which have been shown to influence the SCC susceptibility of titanium alloys. The second part then takes the more important commercial alloys and gives a more detailed description of their SCC behavior. (One problem inherent in such an analysis is the very large degree of scatter in results observed

in one material. In order to reduce such scatter to a reasonable level, a detailed knowledge of the factors which influence susceptibility within a given alloy is required. Armed with such knowledge, it should be possible to eliminate or minimize SCC susceptibility by tight control of composition, melting, processing, fabrication, and assembly.) The final section deals with some trends in alloy development and indicates the authors' thoughts on how titanium alloys might be further improved.

**Generalized Description**

*Alpha Alloys.* The critical factor in determining susceptibility of an $\alpha$ alloy to aqueous SCC is the composition of this phase. Second-order parameters include phase structure, texture, and grain size. The most important elements that induce SCC susceptibility of the $\alpha$ phase are aluminum and oxygen. Other elements, such as tin, have an additive effect to these elements but are not usually present in sufficient quantity in commercial alloys to exert a separate influence.

It has been established that a critical aluminum content (about 5%) must be exceeded for SCC to occur in aqueous solutions [30,107]. This critical composition is approximately the same for the transition from intergranular to transgranular cracking in methanolic solutions [44,57,108]. The influence of aluminum content on $K_{Iscc}$ is shown in Fig. 31. At the higher aluminum contents $\alpha_2$ ($Ti_3Al$) can precipitate during low-temperature aging, which both lowers $K_{Iscc}$ and increases the velocity of cracking. There is limited information on the influence of volume fraction and particle size of the $\alpha_2$ phase on SCC susceptibility. From the few results available, it can be concluded that the lower the aging temperature (which increases the volume fraction of $\alpha_2$) the lower the $K_{Iscc}$ and the higher the velocity of SCC. Recovery of stress corrosion properties occurs at aging times approaching 500 hr at 650°C (1200°F) in a Ti-7Al alloy [109].

Studies of the SCC behavior of binary Ti-O alloys have shown that susceptibility occurred at oxygen contents between 0.2 and 0.4% [110]. Similar results have been obtained on various grades of CP titanium, for example Ti-50A (0.12, $O_2$) exhibits a $K_{Ic}$ and $K_{Iscc}$ of approximately 60 ksi $\sqrt{in.}$, whereas Ti-70A (0.38, $O_2$) with a $K_{Ic}$ of 100 ksi $\sqrt{in.}$ can have a $K_{Iscc}$ as low as 30 ksi $\sqrt{in.}$ [39].

It has been reported that aluminum and oxygen have additive effects on susceptibility to SCC, although this conclusion was based on results from ($\alpha+\beta$)-phase alloys [110].

The effect of oxygen level and aging on SCC kinetics in Ti-Al-O ternary alloys is shown in Fig. 32 [111]. In as-quenched specimens the 0.05% oxygen alloy was immune to SCC in 0.6 *M* KCl. Increasing the oxygen content to 0.15% induced susceptibility, which was accentuated by further increasing the oxygen level to 0.3%. Aging in the ($\alpha+\alpha_2$)-phase field caused the 0.05% oxygen alloy to become susceptible and promoted SCC in the higher oxygen alloys. These results

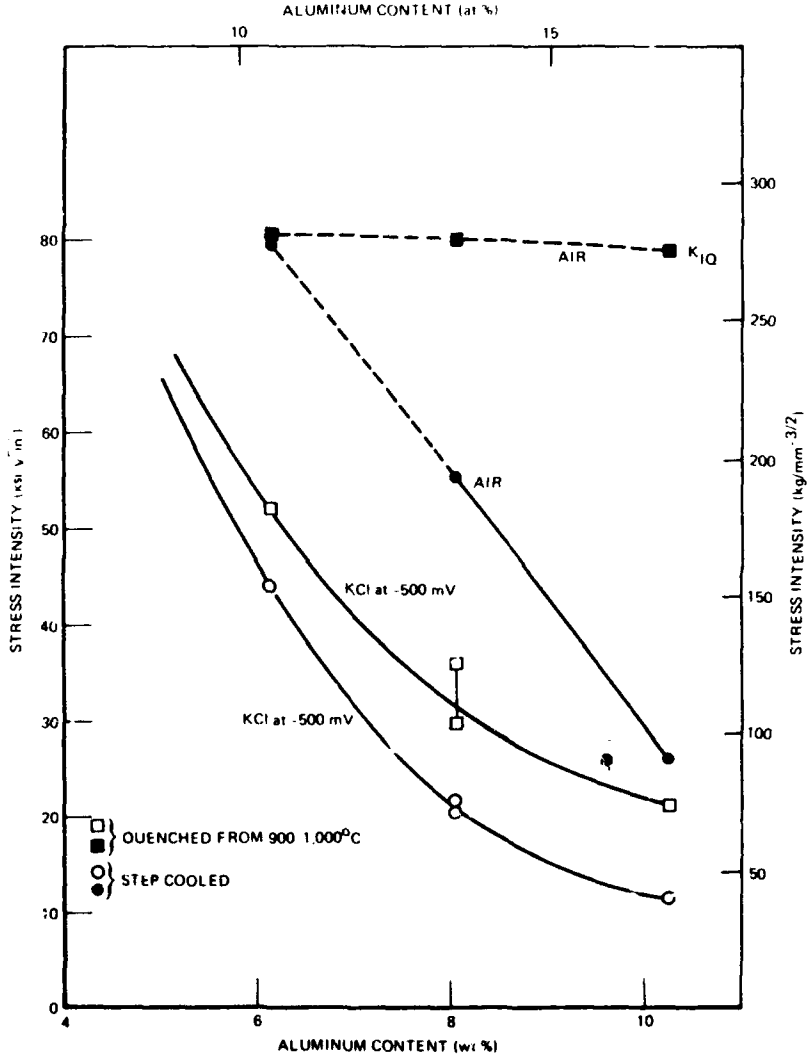


Fig. 31. Variation of $K_{Ic}$ and $K_{Iscc}$ with aluminum content and heat treatment in binary titanium-aluminum alloy [30]. From *Proceedings of Conference on Fundamental Aspects of Stress Corrosion Cracking*, 1969, p. 630, Fig. 20a; copyright by the National Association of Corrosion Engineers. Used by permission.

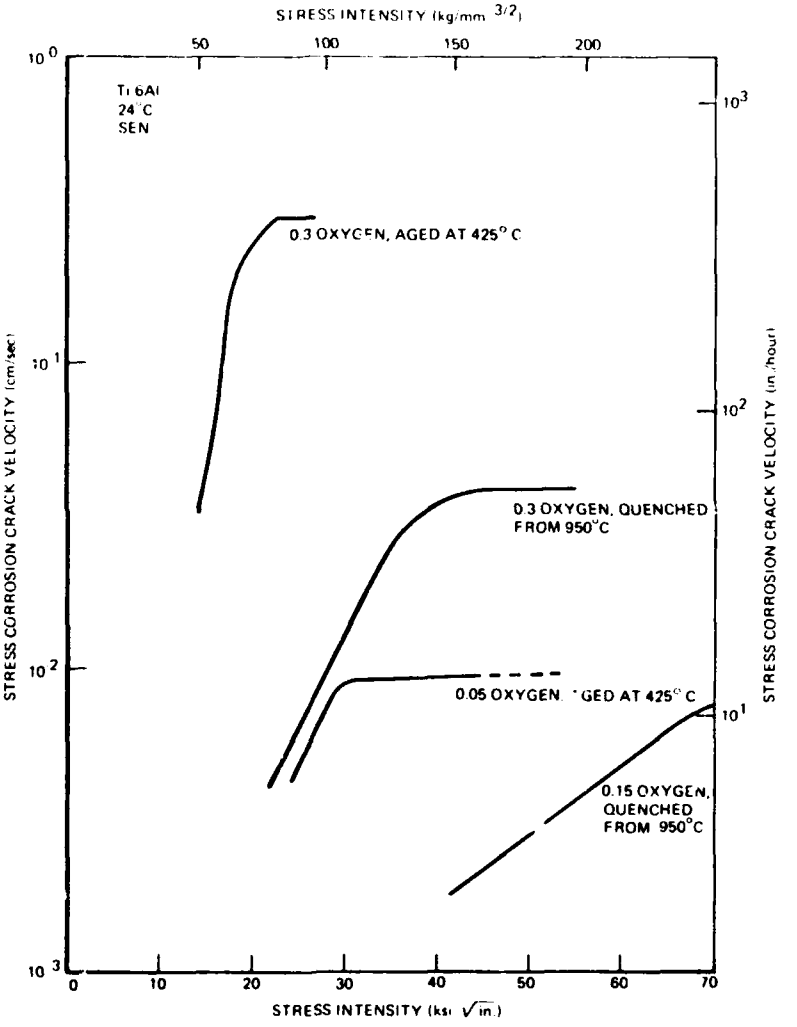


Fig. 32. Influence of oxygen and heat treatment on crack velocity $V$ vs stress intensity $K$ relationships for Ti-6Al binary alloys tested in 0.6 $M$ KCl [111].

support the conclusion that aluminum and oxygen additions are additive in increasing susceptibility.

Increasing the tin content of α alloys generally decreases the resistance to SCC. This may be deduced from the behavior of Ti-5Al-2.5Sn and Ti-5Al-5Zr-5Sn with respect to binary Ti-5Al alloys.

There is little information in the literature on the effect of other elements on α-phase susceptibility. However, the following qualitative statements can be made. Zirconium possibly reduces susceptibility to SCC, as is evident by comparing the results of Ref. 39 for Ti-5Al-2.5Sn and Ti-5Al-5Zr-5Sn. The only report on the influence of silicon is for a proprietary alloy (Ti-4Al-4Mo-2Sn-0.25Si), in which susceptibility has been attributed to the presence of intermetallic compounds containing silicon [39].

The martensites in α alloys are susceptible to SCC (Fig. 33), although the $K_{Iscc}$ value may be slightly higher than that for equiaxed structures.

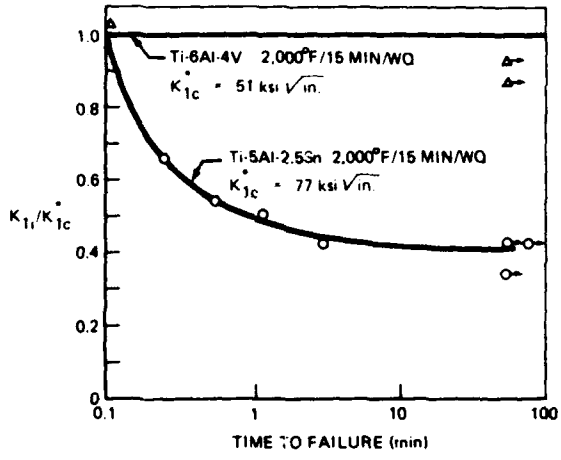


Fig. 33. Variation of applied stress intensity $K_{1i}$ to critical stress intensity $K_{1c}$ ratio with time to failure for martensitic structures in Ti-6Al-4V and Ti-5Al-2.5Sn tested in 3.5% NaCl [30].

Both grain size and texture are known to influence $K_{Iscc}$ in α alloys, but there are no comprehensive studies of these factors. A few examples are noted in the following sections on specific commercial alloys.

*α + β Alloys.* In most alloys that belong to this group and exhibit SCC in aqueous solution, only the α phase is susceptible. The critical parameters for such α phases are the same as those listed above; thus the susceptibility is determined by the aluminum, oxygen, and tin contents. An example is shown in Fig. 34 in which the increasing susceptibility in the alloy series Ti-4Al-3Mo-1V,

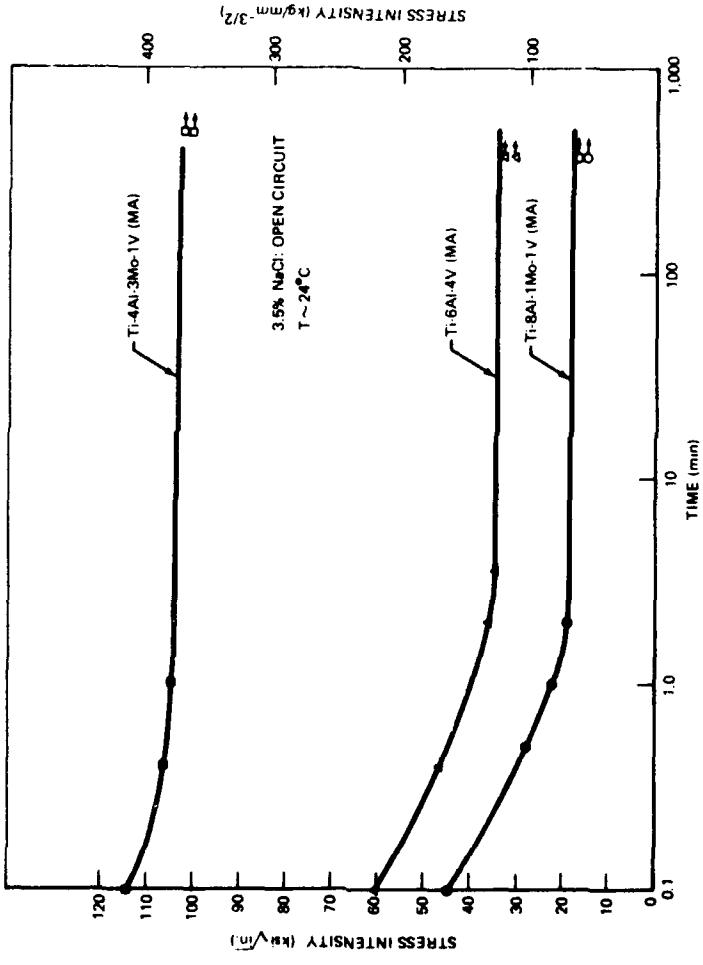


Fig. 34. Variation of time to failure with stress intensity $K$ for three mill-annealed commercial $\alpha+\beta$ alloys tested in 3.5% NaCl [112,113]. From *Trans. ASM* 61 (No. 2), p. 286, Fig. 6; copyright 1968 by the American Society for Metals. Used by permission.

Ti-6Al-4V, and Ti-8Al-1Mo-1V is evident. In alloys of this type the alloying elements are partitioned between the $\alpha$ and $\beta$ phases, and the aluminum content of the $\alpha$ phase may be considerably higher than the average composition; for example, the $\alpha$ phase contains >5% Al in mill-annealed Ti-4Al-3Al-1Mo. The influence of texture of the $\alpha$ phase on SCC susceptibility has been described in the section on specimen orientation and illustrated for the alloy Ti-8Al-1Mo-1V in Fig. 21. Grain size in equiaxed $\alpha+\beta$ structures is not a large factor in determining susceptibility, as it cannot be varied (independently) over large ranges.

The major difference in the behavior of $\alpha+\beta$ alloys and comparable $\alpha$ alloys is in the behavior of the martensitic and tempered martensitic (or acicular) structures. Martensitic structures produced by quenching from above the $\beta$ transus are virtually immune to SCC, as illustrated for Ti-6Al-4V in Fig. 33. Tempering the martensite to produce acicular $\alpha+\beta$ dispersions (which may also be produced by slower cooling rates from the $\beta$-phase field) results in material susceptible to SCC. However, such microstructures exhibit higher fracture toughness and $K_{Iscc}$ levels, as illustrated for Ti-6Al-4V in Fig. 35. This effect is utilized in $\beta$-processing techniques used for several $\alpha+\beta$ alloys, but such processing is not effective in

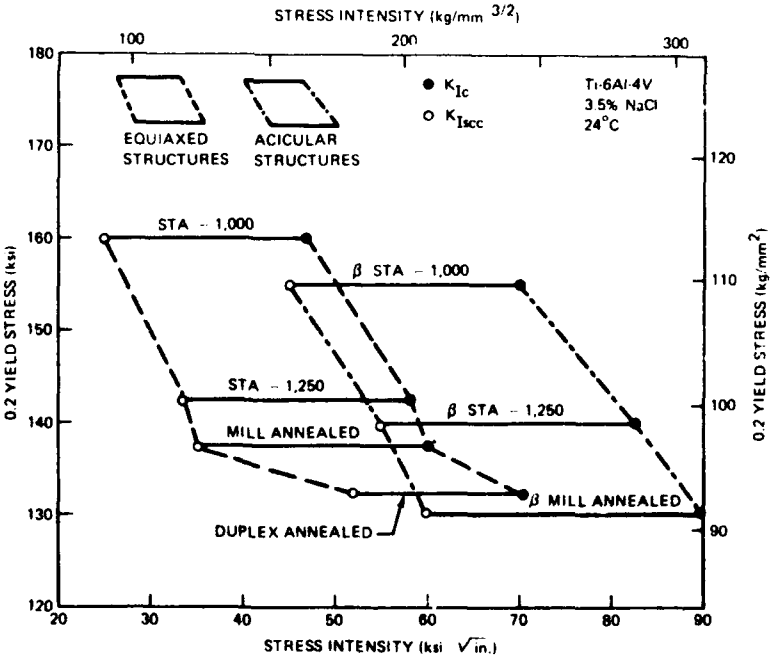


Fig. 35. Relationship between yield stress, fracture toughness $K_{Ic}$, and stress corrosion threshold $K_{Iscc}$ for several phase structures and morphologies in Ti-6Al-4V tested in 3.5% NaCl [113].

all alloys. Materials with limited susceptibility in the equiaxed (e.g., mill-annealed) condition such as Ti-4Al-3Mo-1V exhibit improvements only at the highest strength levels [39]. In alloys with a high degree of susceptibility, for example, those having high aluminum or oxygen contents such as Ti-8Al-1Mo-1V, the inherent susceptibility of the alloy overrides the potential benefits of the acicular structures

*$\beta + \alpha$ Alloys.* Two types of susceptibility to SCC can occur in $\beta+\alpha$ alloys, and in fact both types may occur in the same alloy in different heat treatment conditions.

*Intergranular* cracking occurs in $\beta+\alpha$ alloys for which the dominant variable is microstructure. The critical structure is an equiaxed $\beta$ phase containing a fine Widmanstätten dispersion of the $\alpha$ phase. As this form of SCC was recognized relatively recently, the following generalizations are based on limited data.

The volume fraction of the $\alpha$ phase and the details of the dispersion (e.g., $\alpha$-plate size) influence susceptibility. Thus, for the alloy Ti-11.5Mo-6Zr-4.5Sn, the $K_{Iscc}$ levels fall as the aging temperature is reduced; for example $K_{Iscc}$ was 24 ksi $\sqrt{\text{in.}}$ after aging at 900°F and was more than 60 ksi $\sqrt{\text{in.}}$ after aging at 1150°F. The influence of solution treatment temperature (and also $\beta$ phase grain size) has not been studied in detail. It has been shown, however, that heat treatment above and below the $\beta$ transus has little influence on $K_{Iscc}$ in equiaxed $\beta$ structures. Intergranular failure has been detected in a wide variety of alloys (Ti-8Mn, Ti-11.6Mo, Ti-11.5Mo-6Zr-4.5Sn, Ti-8Mo-8V-3Al-2Fe, and Ti-3Al-8V-6Cr-4Mo-4Zr), which indicates that the effect is relatively general, and no clear-cut compositional influence is evident. However, preliminary work has shown that for the same strength level $K_{Iscc}$ increases slightly in the series Ti-11.5Mo-6Zr-4.5Sn, Ti-8Mo-8V-3Al-2Fe, and Ti-3Al-8V-6Cr-4Mo-4Zr, which may offer a suggestion of some compositional dependence. Finally, let us note that in some alloys, e.g., Ti-8Mn [64] and Ti-6Al-2Sn-4Zr-6Mo [114], both intergranular and transgranular SCC have been observed after specific heat treatments. Both intergranular and transgranular SCC have not been observed in a given alloy after a single heat treatment. Heat treatments leading to intergranular separation of the $\beta$ phase are shown in Table 7.

**Table 7.** Alloys and Heat Treatments Resulting in Intergranular Separation of the $\beta$-Phase Matrix

| *Alloy* | *Aging Temperature* |
|---|---|
| Ti-11.5Mo-6Zr-4.5Sn | 482°C-650°C (900°F to 1200°F) |
| Ti-8Mo-8V-3Al-2Fe | 454°C-538°C (850°F to 1000°F) |
| Ti-11.6Mo | 500°C (932°F) |
| Ti-8Mn | 400°C (752°F) |
| Ti-13V-11Cr-3Al | 590°C (1094°F) |

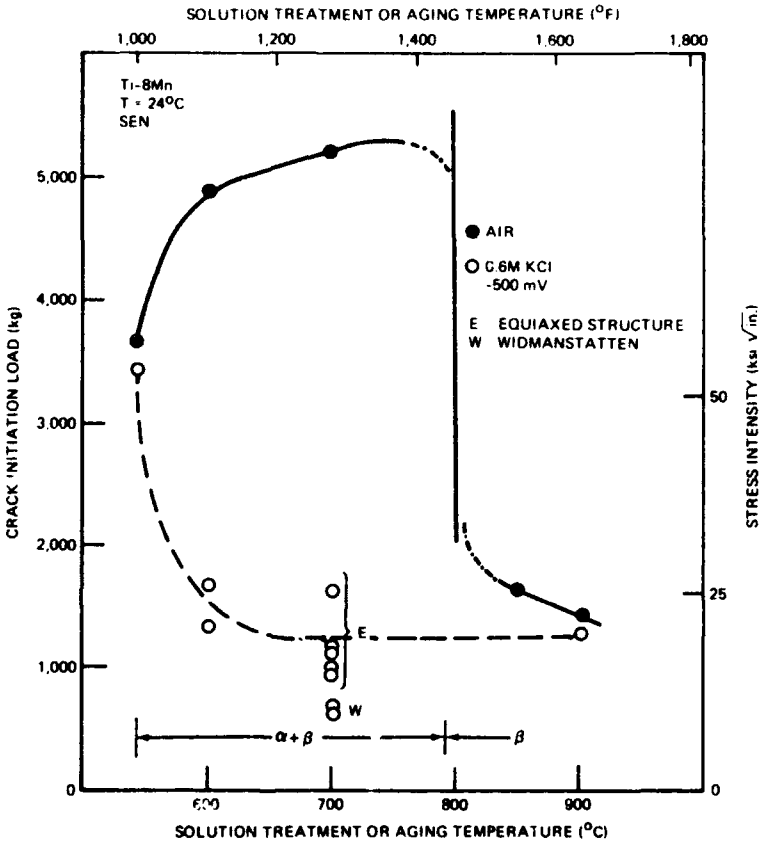


Fig. 36. Variation of crack-initiation load $K_{Iscc}$ with solution-treatment or aging temperature in Ti-8Mn. Specimens were water quenched from the solution-treatment or aging temperature and the resulting phase structures are indicated [115].

*Transgranular* cracking occurs in a limited number of $\beta$+$\alpha$ alloys in which the $\beta$ phase is susceptible and the $\alpha$ phase is immune. Such cracking can also occur in metastable $\beta$ retained after cooling from temperatures above the $\beta$ transus. The dominant variable for this form of SCC is the composition of the $\beta$ phase, although there are considerably fewer data for such systems than for the $\alpha$ alloys. Manganese content is important, the critical level being about 10%. This figure was deduced from the high susceptibility of a (quenched) Ti-16Mn alloy and from aging studies of a Ti-8Mn alloy which is immune in the quenched condition [40,115]. Figure 36 illustrates the latter point and shows that the Ti-8Mn alloy becomes susceptible when aged in the ($\beta$+$\alpha$)-phase field which results in enrichment of the $\beta$ phase in manganese. Results for a lower tempera-

ture aging treatment are shown in Fig. 37, from which it can be seen that the $\beta+\omega$ structure is immune to SCC, which is true for all alloys containing such dispersions investigated to date. The Ti-8Mn alloy does exhibit some susceptibility when a $\beta+\alpha$ structure is generated; however, in this case the failure is intergranular. It has been concluded that some $\beta$-stabilizing elements do not promote SCC susceptibility. This has been shown directly for Ti-Mo alloys in which the metastable $\beta$ phase in Ti-12Mo and Ti-18Mo is immune to SCC [40, 114]. Work on commercial and experimental $\alpha+\beta$ alloys indicates that vanadium, tantalum, and niobium do not produce susceptible $\beta$ phases.

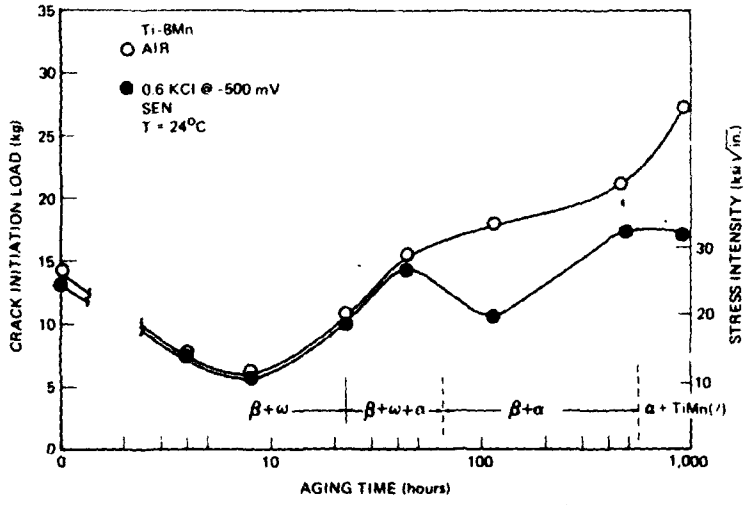


Fig. 37. Variation of crack-initiation load for specimens for Ti-8Mn quenched from 900°C and aged at 400°C, tested in air and 0.6 *M* KCl at -500 mV. The phase structure of the alloy is also indicated [115].

**Commercial Alloys.** This section describes the general characteristics, critical parameters, and reported properties for some of the more important titanium alloys. (Some high temperature alloys utilized in gas turbine applications are not included.) The alloy Ti-6Al-4V is described in some detail with the object of providing a relatively complete description of its SCC properties—and to account for the wide ranges of values encountered in the literature.

Such detailed descriptions cannot be attempted for all alloys due to lack of data. In presenting property data for such alloys, we have usually selected one set of self-consistent results which indicate essential features of alloy behavior. Most of the data reported are for intermediate material thicknesses ($\leq$ 0.5 in.). This is perhaps unfortunate, as it means that several of the $K_{Ic}$ values are invalid in that the thickness criterion is not met (see Chapter 2). The values employed by an engineer must be dictated by the thickness of material to be used. It should also be noted that other properties may be influenced by variation of ma-

terial thickness; for example, the homogeneity, preferred orientation, and grain shape are controlled by the reduction of an ingot to the finished product size. In reality even more information is required for a complete evaluation of an alloy than that given below. For example complete chemical, mechanical, dimensional, directional, microstructural and environmental details are required together with specific features of the test techniques used.

*Alpha-Phase Alloys.* Of the commercial-purity grades of titanium, the low interstitial grades Ti-35A and Ti-50A are not susceptible to aqueous SCC; thus this discussion will concentrate on Ti-70A. This alloy contains up to 0.4% oxygen, which determines SCC susceptibility. The alloy contains up to 0.5% iron, which may stabilize up to about 4% $\beta$ phase.

In the absence of iron the alloy Ti-70A should not show a marked heat treatment response, as it is essentially a simple Ti-O alloy. However the presence of iron in the alloy results in the $\beta$ phase being present after low temperature treatments. Further the $\beta$ composition may be adjusted by solution temperature to a state where the $\omega$ phase may form on cooling or low temperature aging. The $\beta$ transus (0.4% oxygen) is about 1740°F, and the product of quenching from the $\beta$ field is hexagonal martensite $\alpha'$. The $\omega$ phase may be formed on slow cooling from the $\beta$-transus temperature to 1200°F. The volume fraction of the $\omega$ phase decreases on raising the solution treatment temperature, but the tendency to form the $\omega$ phase increases as the phase contains less iron. The influence of texture, grain size, composition, and thickness on properties has not been studied.

*Tests of Ti-70A.* Composition: 0.38O, 0.007N, 0.03C, 0.007H, and 0.38Fe. Specimens: notch bend fatigue precracked, fracture, WR orientation. SCC tests in 3.5% NaCl. Results are shown in Tables 8a and b, the latter showing the effect of hot and cold working [39].

Two grades of Ti-5Al-2.5Sn are produced, an ELI grade (0.12 maximum oxygen and low iron) and a standard grade (0.2 oxygen, 0.5 iron, 0.3 manganese). The alloy has good weldability and can be utilized over a relatively wide range of temperatures, from cryogenic (ELI-grade) to gas turbine temperatures. The composition ranges of the two grades are shown below. The higher oxygen content of the standard grade makes it more susceptible to SCC.

| | *Standard Grade* | *ELI Grade* |
|---|---|---|
| Al | 4.0-6.0 | 4.7-5.6 |
| Sn | 2.0-3.0 | 2.0-3.0 |
| Fe | 0.50 | 0.1-0.2 |
| Mn | 0.30 | – |
| O | 0.20 | 0.12 |
| C | 0.15 | 0.08 |
| N | 0.07 | 0.05 |

**Table 8a.** Influence of Heat Treatment on Properties of Ti-70A

| *Heat Treatment*[a] | *Phase Structure* | *Yield Stress, ksi* | *Thickness, in.* | $K_{Ic}$ *or* $K_Q$, *ksi* $\sqrt{in.}$ | $K_{Iscc}$, *ksi* $\sqrt{in.}$ | *Remarks* |
|---|---|---|---|---|---|---|
| 1350°F (½ hr) AC | Equiaxed $\alpha+(\beta+\omega)$ | 84.3 | 0.48 | 114 | 54 | Increasing volume fraction of $\omega$ phase reduces $K_{Iscc}$. |
| 1400°F (½ hr) AC | Equiaxed $\alpha+(\beta+\omega)$ | 83.6 | 0.48 | 121 | 38 | |
| 1500°F (½ hr) AC | Equiaxed $\alpha+(\beta+\omega)$ | 83.2 | 0.48 | 123 | 33 | |
| 1700°F (½ hr) WQ | $\alpha'$ (martensitic) | 76.5 | 0.48 | 105 | 70 | Martensite susceptible—but not as susceptible as equiaxed structures. |

[a] AC = Air cooled.
WQ = Water quenched.

**Table 8b.** Properties of Ti-70A After Hot and Cold Working

| *Heat Treatment*[a] | *Phase Structure* | *Yield Stress, ksi* | *Thickness, in.* | $K_{1c}$ *or* $K_Q$, *ksi* $\sqrt{in.}$ | $K_{1scc}$, *ksi* $\sqrt{in.}$ | *Working Treatment* | *Remarks* |
|---|---|---|---|---|---|---|---|
| 1750°F (½ hr) WQ + 1050°F (½ hr) AC | α+β | 77.2 | 0.3 | 96 | 48 | 0% Cold Work | Note reduction in $K_{1c}$ and no improvement in $K_{1scc}$ with hot or cold working. |
| | | 115.2 | 0.3 | 82 | 33 | 30% Cold Work | |
| | | 121.4 | 0.2 | 45 | 40 | 60% Cold Work | |
| Working Temp. 1100°F | Equiaxed α+β | 94.4 | 0.3 | 115 | 34 | 30% Hot Work | |
| Working Temp. 1500°F | Equiaxed α+β | 87.6 | 0.3 | 104 | 35 | 50% Hot Work | |
| Working Temp. 1700°F | Acicular α+β | 86.9 | 0.3 | 93 | 54 | 30% Hot Work | |

[a]WQ = Water quenched.
AC = Air cooled.

Theoretically Ti-5Al-2.5Sn is an $\alpha$ alloy. However, the iron and manganese content causes up to about 5% $\beta$ phase in the structure of the standard grade. The alloy is not considered heat treatable, although some modification of properties can be accomplished (see Table 9). The $\beta$ transus is about 1925°F. The product of quenching from the $\beta$ field is hexagonal martensite. The alloy contains sufficient aluminum and tin to form the $\alpha$ phase at temperatures below approximately 1120°F. (Note that this temperature will depend on exact composition.) This phase has a strong influence on both $K_{Ic}$ and $K_{Iscc}$. The $\omega$ phase can form in the $\beta$ phase; the transformational behavior is similar to that of Ti-70A. Increasing grain size reduced $K_{Iscc}$ (see Table 9). Little information on the influence of texture of thicknesss has been generated for the alloy.

*Tests of Ti-5Al-2.5Sn.* Composition: 5.6Al, 2.6Sn, 0.39Fe, 0.16O, 0.007H (standard grade). Specimen: notch bend, fatigue precracked, fracture WR orientation. SCC tests in 3.5% NaCl. Results are shown in Table 9 [39]. Composition: 5.1Al, 2.5Sn, 0.19Fe, 0.007N, 0.094O (ELI grade). Specimen: DCB fracture WR orientation. SCC tests in 3.5% NaCl. Results are shown in Table 9 [116].

The $\alpha$ alloy Ti-5Al-5Zr-5Sn is somewhat similar to the Ti-5Al-2.5Sn (ELI grade), exhibiting good weldability and elevated temperature properties. The $\beta$ transus is about 1820°F. The product of quenching from the $\beta$ field is hexagonal martensite. The $\alpha$ phase contains sufficient aluminum and tin to precipitate the $\alpha_2$ phase (phase boundary position unknown but probably about 1050°F). There is evidence that increasing grain size reduces $K_{Iscc}$ and that hexagonal martensite is equivalent to a large grain size. There is limited evidence that plate does not show such extreme texture as some other $\alpha$- and $(\alpha+\beta)$-type alloys.

*Tests of Ti-5Al-5Zr-5Sn.* Composition: 5.3Al, 5.1Sn, 5.3Zr, 0.05 Fe, 0.006N, 0.1O. Specimen: notch bend, fatigue precracked, fracture WR orientation. SCC tests in 3.5% NaCl. Results are shown in Table 10 [39].

*$\alpha+\beta$ Alloys.* In this section we shall present data on several alloys but concentrate on the alloy Ti-6Al-4V, the most important commercial titanium alloy. The variety of phase structures and heat treatments possible on $\alpha+\beta$ alloys is much greater than the $\alpha$ alloys, and only the most important treatments and structures will be described.

The super $\alpha$ alloy Ti-8Al-1Mo-1V exhibits good combinations of strength, modulus, weldability, and density. However, the extreme stress corrosion susceptibility in aqueous solutions has rendered it virtually obsolete. Although probably more work has been performed on this alloy than all other titanium alloys, we shall only briefly describe its characteristics here.

The $\beta$ transus is about 1930°F. The product of quenching from the $\beta$ field is hexagonal martensite; possibly orthorhombic martensite may be produced from the $\beta$ phase by quenching in the range of 1560 to 1650°F. Composition of the $\alpha$ phase is such that $\alpha_2$ may form readily at temperatures below 1250°F. This phase has a very large influence on the $K_{Ic}$ and $K_{Iscc}$ value. Utilization of quenched and tempered structures offers some improvement over annealed structures. This alloy often exhibits extreme transverse preferred orientation.

**Table 9.** Properties of Ti-5Al-2.5Sn

| *Heat Treatment*[a] | *Phase Structure* | *Yield Stress, ksi* | *Thickness in.* | $K_{Ic}$ or $K_Q$ *ksi* $\sqrt{in.}$ | $K_{Iscc}$ *ksi* $\sqrt{in.}$ | *Remarks* |
|---|---|---|---|---|---|---|
| | | | Standard Grade | | | |
| 1400°F (2 hr) AC | Equiaxed α+β (diff ω) | 129.2 | 0.48 | 72 | 26 | |
| 1650°F (1 hr) WQ | Equiaxed α+β (diff ω) | 124.2 | 0.48 | 103 | 27 | |
| 1650°F (1 hr) AC | Equiaxed α+β (diff ω) | 126.5 | 0.48 | 88 | 30 | Increase in grain size products–slight decrease in $K_{Iscc}$. |
| 1650°F (100 hr) AC | Equiaxed α+β (diff ω) | 125.1 | 0.48 | 92 | 27 | |
| As-recd + 1000°F (8 hr) + 932°F (120 hr) | $\alpha(+\alpha_2)+\beta$ | 130.5 | 0.48 | 46 | 21 | $\alpha_2$ precipitation decreases $K_{Iscc}$ although the air-cooled material could contain diffuse $\alpha_2$. |
| 2000°F (½ hr) WQ | $\alpha'$ (martensite) | 126.6 | 0.48 | 119 | 37 | $\alpha'$–martensite susceptible but not as susceptible as equiaxed structures. |
| | | | ELI Grade | | | |
| Mill annealed | $\alpha(+$ diff $\alpha_2)$ | 120 | 0.375 | 98 | 41 | Note higher $K_{Iscc}$ value than standard grade. |

[a] AC = Air-cooled.
WQ = Water-quenched.

**Table 10.** Selected Properties of Ti-5Al-5Zr-5Sn

| *Heat Treatment*[a] | *Phase Structure* | *Yield Stress, ksi* | *Thickness, in.* | $K_{Ic}$ *or* $K_Q$, *ksi* $\sqrt{in.}$ | $K_{Iscc}$, *ksi* $\sqrt{in.}$ | *Remarks* |
|---|---|---|---|---|---|---|
| 1650°F (½ hr) WQ | α | 109.7 | 0.48 | 101 | 67 | Reduced $K_{Iscc}$ due to $\alpha_2$–precipitation. |
| 1650°F (½ hr) AC | $\alpha+\alpha_2$ | 116.5 | 0.48 | 83 | 50 | |
| 1650°F (½ hr) AC + 1100°F (8 hr) + 992°F (120 hr) | $\alpha+\alpha_2$ | 120.5 | 0.48 | 54 | 28 | |
| 1850°F (½ hr) WQ | α′ (martensite) | 114.1 | 0.48 | 102 | 55 | Martensitic α′ structure susceptible and exhibits lower $K_{Iscc}$ than some equiaxed structures. |

[a]WQ = Water-quenched.
AC = Air-cooled.

*Some (proprietary) processes were developed in the mid 1960's to produce more random textures but appeared to produce limited improvements.*

*Tests on Ti-8Al-1Mo-1V.* Composition: 7.9Al, 1.1V, 0.95Mo, 0.100. Specimen: DCB, fracture WR orientation. SCC tests in 3.5% NaCl. Results are shown in Table 11 [64].

The most important and widely used titanium alloy is Ti-6Al-4V. Several grades are produced including ELI and standard grades; in many thick-section products the oxygen level may be increased (to about 0.2%) in order to attain specific strength goals. The yield strength in the alloy can be varied between (approximately) 100 and 170 ksi by controlled heat treatments, and it exhibits relatively good elevated temperature properties. Although in certain heat treatments the alloy can be cold formed, hot or creep forming is often utilized to produce the required shapes. The alloy exhibits good hardenability and welding characteristics.

The $\beta$ transus is about 1820°F, and the product of quenching from the $\beta$ field is hexagonal martensite ($\alpha'$). As the solution treatment temperature is reduced below the $\beta$ transus the primary $\alpha$ phase is retained on quenching. However, the $\beta$ phase will transform to martensite at temperatures as low as 1550°F. A second form of martensite (possibly orthorhombic) may form between 1550 and 1600°F. The $\beta$ phase is retained on quenching from 1500°F but undergoes a stress-induced transformation at room temperature resulting in good formability properties.

Aging treatments are based on tempering of martensitic-type structures. Either super- or subtransus treatments are used, although it is usual to use a second, subtransus, treatment after a supertransus treatment. The selection of the solution treatment and aging temperature and time depends upon the specific strength requirement. Aging at low temperatures (about 1000°F) results in the highest strength levels; lower strength and higher toughness may be produced by aging at 1150 to 1350°F. If the material is subsequently exposed at lower temperatures, 300 to 900°F, further precipitation of the $\alpha$ phase may occur within the $\beta$ phase. The $\omega$ phase does not form in this alloy. If the alloy has high aluminum and oxygen, the $\alpha_2$ phase may form in the $\alpha$ phase.

Figure 38 is a compilation of $K_{Ic}$, $K_{Iscc}$, and yield-strength data for the alloy Ti-6Al-4V in the form of plate, extrusions, and forgings 0.5 to 1.5 in. thick. This figure, if nothing more, illustrates the rather extreme variation of properties that may be exhibited by one material. If the use of this or any other alloy is contemplated in a situation where SCC may be a problem then the internal variables which influence the $K_{Iscc}$ value must be known and controlled. A separation of these variables is attempted in the following paragraphs. To isolate one variable means that all others must be held constant, and unfortunately this is not always possible.

The critical compositional factors of the alloy are the oxygen and aluminum contents. Figures 39a and b illustrate the effect of oxygen level on $K_{Ic}$ and (optimum) $K_{Iscc}$ after two heat treatments—which means of course different

**Table 11.** Selected Properties of Ti-8Al-1Mo-1V

| *Heat Treatment*[a] | *Phase Structure* | *Yield Stress, ksi* | *Thickness, in.* | $K_{Ic}$ *or* $K_Q$, *ksi* $\sqrt{in.}$ | $K_{Iscc}$, *ksi* $\sqrt{in.}$ | *Remarks* |
|---|---|---|---|---|---|---|
| 1500°F (1 hr) WQ | Equiaxed $\alpha+\beta$ | 122 | 0.5 | >100 | 42 | Decreasing $K_{Iscc}$ due to $\alpha_2$ formation. |
| 1500°F (1 hr) FC | Equiaxed $\alpha (+\alpha_2) + \beta$ | 128 | 0.5 | 69 | 28 | |
| 1500°F (1 hr) + 1100°F (24 hr) + 930°F (24 hr) AC | Equiaxed $\alpha (+\alpha_2) + \beta$ | 135 | 0.5 | 39 | 20 | |
| 2000°F (½ hr) WQ | $\alpha'$ (martensite) | 126 | 0.5 | >100 | >100 | Martensitic structure immune, but tempered structure shows susceptibility. |
| 2000°F (½ hr) WQ +1450°F (8 hr) AC | Acicular $\alpha+\beta$ | 130 | 0.5 | 68 | 48 | |

[a] WQ = Water-quenched.
FC = Furnace-cooled.
AC = Air-cooled.

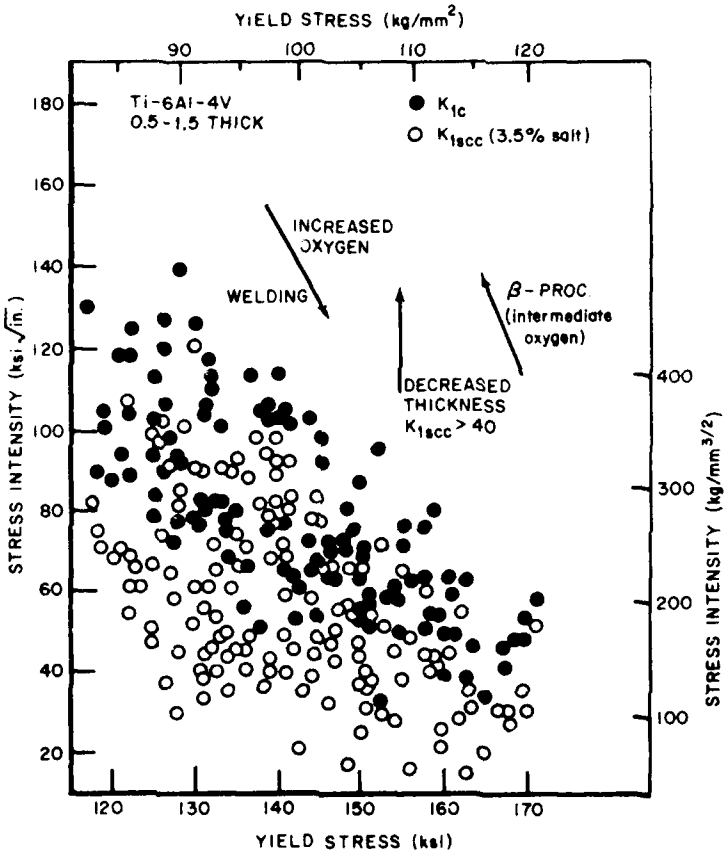


Fig. 38. The variation of $K_{Ic}$ and $K_{Iscc}$ with yield strength for the alloy Ti-6Al-4V.

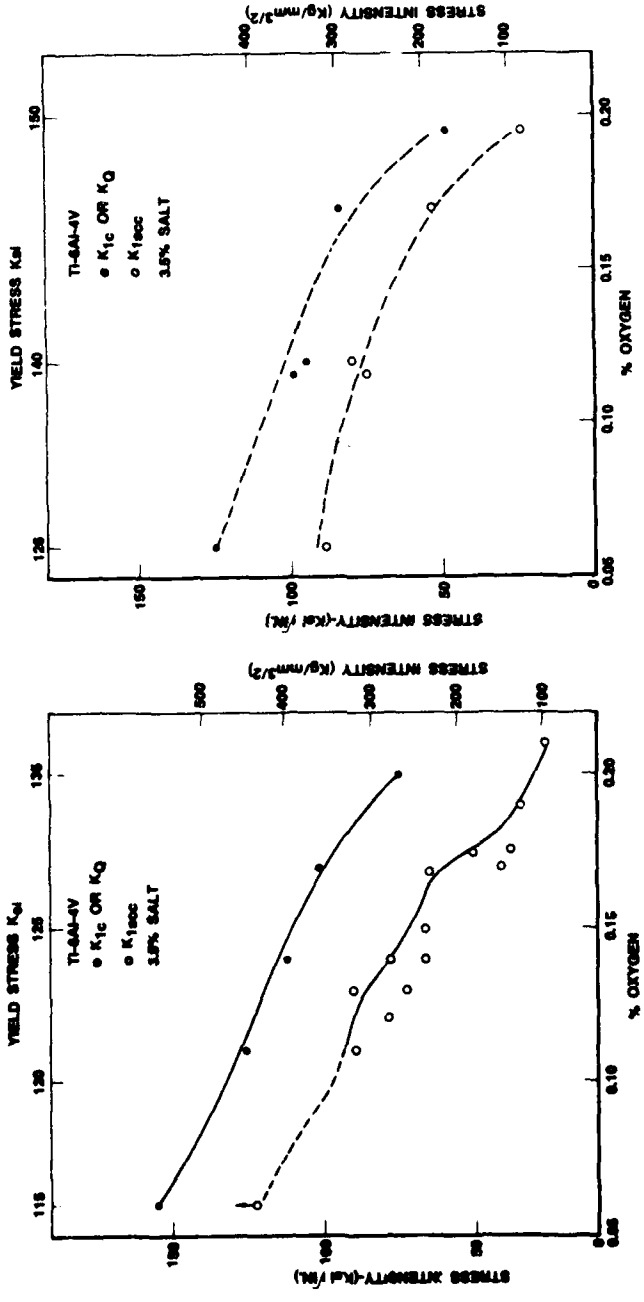


(a) Optimum properties for β-ST + MA treatment

(b) Optimum properties for β-STA material (1950°F AC + 1725°F WQ + 1200°F WQ + 1200°F (4 hr) AC)

Fig. 39. Variation of $K_{Ic}$ (or $K_Q$) and $K_{Iscc}$ with oxygen content in Ti-6Al-4V (RW orientation, 3.5% NaCl) [63,117,118].

strength levels. High aluminum contents also lead to a reduction in $K_{Iscc}$. The $\beta$-stabilizing elements vanadium and iron are beneficial; increasing the amount of these elements increases $K_{Iscc}$.

As noted in the section on thickness effects, the thickness of $\alpha+\beta$ alloys appears to influence the $K_{Iscc}$ value. Such an influence is inferred from the comparison of (as received) plate and sheet material. In one series of experiments it has been demonstrated that if the $K_{Iscc}$ value is low in plate material, then no increase occurs as the thickness of the plate is reduced, as shown in Table 12. It would be of interest to measure the $K_{Iscc}$ variation with thickness in material with an intermediate $K_{Iscc}$ value (about 50 to 60 ksi $\sqrt{\text{in.}}$) in thick sections. At this time it appears probable that the superior properties of thin sheet Ti-6Al-4V may be attributed in part to the lower oxygen content and more random texture of sheet material.

**Table 12.** Effect of Thickness of Mill-Annealed Ti-6Al-4V[a] on $K_{Iscc}$ and $K_{Ic}$[b]

| *Thickness, in.* | $K_{Ic}$, *ksi* $\sqrt{in.}$ | $K_{Iscc}$, *ksi* $\sqrt{in.}$ |
|---|---|---|
| 0.98 | 57.9 | 21 |
| 0.70 | 60.0 | 19 |
| 0.50 | 61.3 | 21 |
| 0.25 | 90.0 | 17 |
| 0.125[c] | 93.2 | 22 |
| 0.125[c] | – | 22 |
| 0.050 | – | 19 |

[a] Mechanical properties:
UTS = 155.6 ksi
YS = 147.9 ksi
Elong. = 13%
RA = 34.5%

[b] From Ref. 119.

[c] Single-edge, notched, tension specimens; the remainder were precracked bend specimens. WR orientation.

As the $\alpha$ phase is the constituent susceptible to SCC in Ti-6Al-4V, it is obvious that the preferred orientation or texture of the material with respect to the loading direction will exert an influence on the SCC susceptibility. The important question is what governs the development of texture in this material, and unfortunately no really comprehensive answer can be given. It appears that such factors as the processing temperature, the reduction accomplished during working, and the finishing temperature all influence texture. The following statements are based on results for Ti-8Al-1Mo-1V [38] and observations on Ti-6Al-4V [117, 118] which are summarized in Fig. 40.

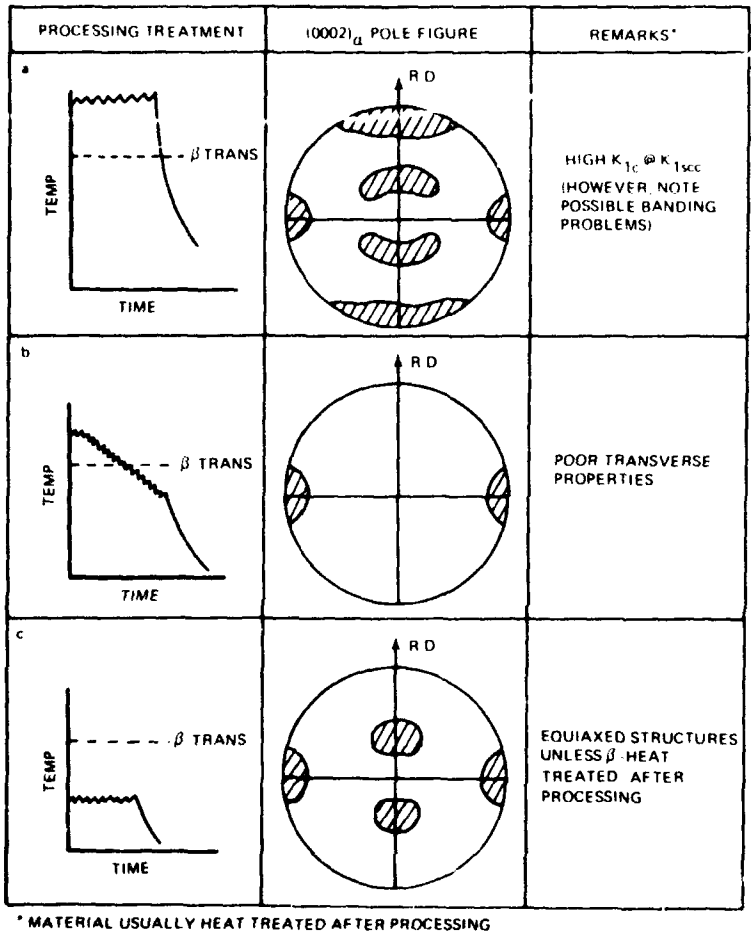


Fig. 40. Schematic of the influence of processing on texture and SCC properties.

- Processing in the β-phase field *often* leads to the development of the α-phase texture shown in Fig. 40a. Such a texture leads to relatively isotropic properties and relatively high values of $K_{Iscc}$.
- Processing through the α+β transus *often* leads to the development of the texture shown in Fig. 40b, which leads to poor transverse SCC values (and very anisotropic mechanical properties).
- Processing at lower temperatures (1500 to 1700°F) *often* leads to the development of crystallographic texture shown in Fig. 40c, which is typical of some sheet material. However, such processing results in an equiaxed structure

(grain morphology) unless a $\beta$-solution treatment is used subsequently; thus, the toughness properties and SCC resistance of the material processed at the low temperature are usually lower than $\beta$-processed material.

- There is evidence that $\beta$-heat treatment modifies the preferred orientation developed during prior processing, tending to produce a more random crystallographic texture.

Data on other product forms are less complete. From limited data it seems possible that extrusions and forgings may exhibit somewhat more isotropic properties and higher $K_{Iscc}$ values.

Most Ti-6Al-4V is relatively homogeneous on a macroscopic scale; however, regions of gross $\alpha$-phase segregation have been observed (e.g., Ref. 120). Such $\alpha$-phase regions persist at most scales of structural examination and are often called $\alpha$-stringer structures or banded structures. In annealed material the banded or $\alpha$-stringer structures have not been shown to have a marked influence on SCC properties. It has been suggested that residual stresses present in such regions may lower $K_{Iscc}$.

At the microstructural level several factors have been shown to influence SCC properties. The general superiority of acicular microstructures over equiaxed microstructures has been described above, although it must be reiterated that this effect is most pronounced in alloys with intermediate 0.1 to 0.15 oxygen contents. The exact details of the acicular microstructure are important, as follows:

1. The prior $\beta$-grain size should be as small as possible; i.e., tight control of the solution treatment and of hot working schedule must be exercised.
2. The $\alpha$-plate or grain size should be small. This is related to the $\beta$-grain size and subsequent aging treatments.
3. The precipitated $\beta$ phase should be distributed as a continuous film around the $\alpha$-phase grains.
4. In high aluminum- and oxygen-containing alloys, heat treatment which forms the $\alpha_2$ phase should be avoided [38,117].

As may be seen from Fig. 38, there is in general an inverse relationship between strength and both toughness ($K_{Ic}$) and SCC resistance ($K_{Iscc}$). Thus for the best combination of SCC properties at a given strength level, the composition, texture, and microstructure have to be optimized. The exact selection is also dictated by other property requirements. For example $\beta$-processed material exhibits inferior formability characteristics and often lower strength levels than ($\alpha$+$\beta$)-processed material.

Material that has been $\beta$ processed to produce an acicular structure is often solution treated again in the $\alpha$+$\beta$ region and water quenched. The cooling rate from the first $\beta$-processing treatment influences subsequent fracture toughness properties—air cooling producing higher values than water quenching. The following are illustrative examples for Ti-6Al-4V containing intermediate oxygen levels after heat treatment designed for specific applications.

For structural applications requiring high toughness and intermediate strength [19]:

| Heat Treatment | UTS | YS | $K_{Ic}$ | $K_{Iscc}$ |
|---|---|---|---|---|
| 1900°F 30 min AC+ 1725°F 30 min WQ+ 1250°F 4 hr AC | 158 | 142 | 86 | 58 |

For structural applications requiring high strength in compression:

| Heat Treatment | UTS | YS | $K_{Ic}$ | $K_{Iscc}$ |
|---|---|---|---|---|
| 1900°F 30 min AC+ 1725°F 30 min WQ+ 1000°F 4 hr AC | 180 | 160 | 65 | 49 |

For sheet material requiring good toughness and high formability:

| Heat Treatment | UTS | YS | $K_{Ic}$ | $K_{Iscc}$ |
|---|---|---|---|---|
| 1725°F 30 min AC+ 1250°F AC | 150 | 143 | 70 | 53 |

A comprehensive analysis of data from a large number of plates of Ti-6Al-4V has resulted in the development of an empirical equation for the prediction of $K_{Iscc}$ [117,118]. This was derived from a regression analysis of data after the delineation of critical factors and takes the form:

$$K_{Iscc} = 40.5 - 262\,O_2 - 9.2Al + 38.9V + 2.11(MR),$$

where the compositions are in weight % and the microstructural rating (MR) varies between 0 (poor) and 20 (excellent). The latter factor includes the factors listed above—$\beta$-grain size, $\alpha$-plate size, and $\beta$-phase distribution—but is a somewhat subjective parameter. The equation is derived for one heat treatment, $\beta$-processed + mill anneal, and thus further work is required to extend it to all strength levels. Further modifications to include the influence of texture, phase formation, and the presence of iron are also required. The standard deviation of predicted values from observed values was approximately 10 ksi $\sqrt{\text{in.}}$

The variation of $K_{Iscc}$ in the alloy Ti-6Al-4V in 3.5% NaCl solutions is relatively well understood and thus by careful control of processing and manufacturing techniques, the material can be used in salt water. All the above factors

**Table 13.** Properties of Ti-6Al-6V-2Sn (Fe+Cu)

| *Heat Treatment*[a] | *Phase Structure* | *Yield Stress, ksi* | *Thickness, in.* | $K_{Ic}$ *or* $K_Q$, *ksi* $\sqrt{in.}$ | $K_{Iscc}$, *ksi* $\sqrt{in.}$ | *Remarks* |
|---|---|---|---|---|---|---|
| 1800°F (½ hr) AC + 1625°F (1 hr) WQ + 1200°F (4 hr) AC | Acicular α+β | 152 | 0.48 | 72 | 45 | Note higher $K_{Ic}$ and $K_{Iscc}$ of acicular structures. |
| 1300°F (2 hr) AC | Equiaxed α+β | 150 | 0.48 | 59 | 37 | |

[a] AC = Air-cooled.
WQ = Water-quenched.

are interrelated to some extent, and thus all factors must be recognized and controlled.

The alloy Ti-6Al-6V-2Sn is similar to Ti-6Al-4V but can be heat treated to higher strength levels and exhibits good hardenability. The alloy contains iron (0.35 to 1.0%) and copper (0.35 to 1.0%). The oxygen level is controlled to between 0.12 and 0.2%.

The $\beta$ transus is about 1725°F, and the quench product is hexagonal martensite; the $\beta$ phase is retained on quenching from about 1550°F. For the highest strength levels an ($\alpha$+$\beta$)-ST (1650°F) treatment is employed followed by water quenching and aging at 1000 to 1100°F. The strength of mill-annealed material is greater than that of Ti-6Al-4V. The aluminum content of the $\alpha$ phase may permit the formation of the $\alpha_2$ phase.

*Tests on Ti-6Al-6V-2Sn.* Composition: 5.6Al, 5.6V, 2.1Sn, 0.8Fe, 0.75Cu, 0.150O. Specimen: notch bend, fatigue precracked, fracture WR orientation. SCC tests in 3.5% NaCl. Results are shown in Table 13 [39].

The versatile alloy Ti-4Al-3Mo-1V can be heat treated to a wide range of strength levels but does not exhibit good hardenability in thick sections. The alloy is quite resistant to aqueous SCC at all strength levels. Little is known of the influence of composition on SCC. Oxygen levels are not called out in specifications. The $\beta$ transus of the alloy is about 1750°F; the quench product is hexagonal martensite with some retained $\beta$. The $\beta$ phase is retained on quenching from about 1550°F. Aging the martensite structures result in $\alpha$+$\beta$ dispersions. The composition of the retained $\beta$-phase is such that it can be aged (below about 750°F) to precipitate the $\omega$ phase. Conventional heat treatments utilize annealing (producing equiaxed $\alpha$+$\beta$ structures): $\alpha$+$\beta$ STA treatments at 1650-1725°F WQ with subsequent aging at 110-1200°F (producing equiaxed $\alpha$ martensite, tempered to $\alpha$+$\beta$); or $\beta$-ST treatments at about 1800°F and tempering (producing acicular $\alpha$+$\beta$).

*Tests on Ti-4Al-3Mo-1V.* Composition: 4.5Al, 3.3Mo, 1.0V, 0.110O. Specimen: notch bend, fatigue precracked, fracture WR orientation. SCC tests in 3.5% NaCl. Results are shown in Table 14 [19].

Ti-6Al-2Sn-4Zr-6Mo is also related to Ti-6Al-4V, but the more complex composition is reflected in the wider variety of phase structures and properties that can be produced. Little information is available on the influence of minor compositional changes in SCC susceptibility.

It is difficult to give a concise account of the transformation and resulting properties that can be produced in this alloy. The following is a brief description of the major points. The $\beta$ transus is about 1800°F, and the product of quenching from the $\beta$ field is orthorhombic martensite. Tempering of this structure results in fine $\alpha$-phase precipitates. The limit of stability of the $\beta$ phase is unknown, although the $\beta$ phase retained on quenching from about 1550°F will undergo a stress-induced transformation. The retained $\beta$ phase can be strengthened by aging it at lower temperatures to precipitate the $\alpha$ phase. As the $\alpha$ phase contains high aluminum and tin concentration, the $\alpha_2$ phase can form at low

**Table 14.** Properties of Ti-4Al-3Mo-1V

| *Heat Treatment*[a] | *Phase Structure* | *Yield Stress, ksi* | *Thickness, in.* | $K_{Ic}$ *or* $K_Q$, *ksi* $\sqrt{in.}$ | $K_{Iscc}$, *ksi* $\sqrt{in.}$ | *Remarks* |
|---|---|---|---|---|---|---|
| 1250°F (8 hr) AC | Equiaxed α+β | 125 | 0.48 | 115 | 102 | Note that β processing does not lead to much improvement of $K_{Ic}$ and $K_{Iscc}$ at the same strength level. |
| 1725°F (1 hr) WQ +1150°F (8 hr) AC | Equiaxed α + acicular β+α | 158 | 0.48 | 72 | 60 | |
| 1875°F (1 hr) AC +1725°F (1 hr) WQ +1150°F (8 hr) AC | Acicular α+β | 138 | 0.48 | 97 | 78 | |
| 1640°F (1 hr) WQ +1175°F (8 hr) AC | Equiaxed α + acicular β+α | 137 | 0.48 | 103 | 84 | |
| 1800°F (1 hr) AC +1640°F (1 hr) WQ +1175°F (8 hr) | Acicular α+β | 128 | 0.48 | 101 | 98 | |

[a] AC = Air-cooled.
WQ = Water-quenched.

temperature aging. Thus the material can be utilized in a mill-annealed type structure in which the behavior is analogous to Ti-6Al-4V or a quenched and tempered condition in which behavior resembles that of Ti-11.5Mo-6Zr-4.5Sn.

*Tests on Ti-6Al-2Sn-4Zr-6Mo.* Composition: 5.9Al, 6.0Mo, 4.0Zr, 1.9Sn, 0.09O. Specimen: tapered DCB, fracture WR orientation. SCC tests in 3.5% NaCl. Results are shown in Table 15 [114].

*β+α Alloys.* As noted above, two SCC separation modes have been detected in such alloys. Thus the first part of this section will be concerned with the intergranular failure mode with emphasis on the alloy Ti-11.5Sn-6Zr-4.5Sn for which most data are available. The second section will discuss briefly an alloy in which transgranular separation of the β phase occurs.

Ti-11.5Mo-6Zr-4.5Sn exhibits a range of attractive mechanical properties. In the quenched condition the material undergoes a stress-induced transformation resulting in excellent formability. Quenching and tempering treatments can be employed to produce yield strengths >180 ksi, and the alloy exhibits good hardenability. There is no evidence that variations of chemistry within specification influence SCC properties. (Inadvertent boron contamination may result in general embrittlement.)

The β transus is about 1400°F but is raised by increasing the oxygen content. The product of quenching β is retained β, which is immune to SCC. Either β or β+α (1350°F) solution treatments can be used. The (β+α)-ST can be heat treated to higher strength levels. The aging temperatures employed range from 900 to 1160°F (8 hr at 900°F is conventional), to produce β+α dispersion. Aging of β-ST material at temperatures ≥800°F results in ω-phase precipitation. Equiaxed β structure containing the α phase are susceptible to SCC, while β+ω structures are immune.

There is limited evidence that $K_{Iscc}$ depends on sheet thickness. For example β quenched specimens aged for 8 hr at 900°F exhibit $K_{Iscc}$ values of 40 ksi $\sqrt{\text{in.}}$ in 0.08 in. sheet and 24 ksi $\sqrt{\text{in.}}$ in 0.5 in. plate.

*Tests on Ti-11.5Mo-6Zr-4.5Sn.* Composition: 10.7Mo, 4.12Zr, 4.6Sn, 0.03Fe, 0.13O. Specimen: DCB or notch bend, fracture WR orientation. SCC tests in 3.5% NaCl. Results are shown in Table 16 [63,121].

It should be noted from Table 16 that the equiaxed structures are susceptible to SCC. Two methods of eliminating such susceptibility have been suggested. First, the critical microstructure feature has been proposed to be the formation of a continuous film of α phase at the β-grain boundaries. Thus it is possible that by selecting, for example, double aging treatments, this film could be eliminated along with SCC susceptibility. The authors are unaware of any direct demonstration of the effectiveness of such methods. Second, as the critical structure occurs at the grain boundaries, modification of grain shape could eliminate SCC susceptibility in some directions. By employing hot working processes below the β transus, such microstructural modifications can be accomplished, and the resulting grain shapes are not dissimilar from those produced in aluminum alloys (Chapter 3). From Table 16 it can be seen that such operations eliminate SCC

**Table 15.** Properties of Ti-6Al-4Zr-2Sn-6Mo

| *Heat Treatment*[a] | *Phase Structure* | *Yield Stress, ksi* | *Thickness, in.* | $K_{1c}$ *or* $K_Q$, ksi $\sqrt{in.}$ | $K_{Iscc}$, ksi $\sqrt{in.}$ | *Remarks* |
|---|---|---|---|---|---|---|
| As received (mill anneal) | Equiaxed $\alpha+\beta$ | 140 | 0.3 | 52 | 26 | Note decrease in $K_{Iscc}$ due to $\alpha_2$ precipitation. |
| As received +step cooled | Equiaxed $\alpha+\alpha_2+\beta$ | 145 | 0.3 | 55 | 20 | |
| 1550°F WQ | Equiaxed $\alpha+\beta$ | 45 | 0.3 | 45 | 38 | Very low yield strength due to stress induced transformation. |
| 1550°F WQ +1100°F (24 hr) | Equiaxed $\alpha$ + acicular $\beta+\alpha$ | 135 | 0.3 | 35 | 16 | |
| 1830°F WQ | Orthorhombic martensite | 125 | 0.3 | 95 | >90 | Orthorhombic martensite immune to SCC. |
| 1830°F WQ +1100°F (24 hr) | Equiaxed $\beta$ + Widm $\alpha$ | 170 | 0.3 | 81 | 45 | *Intergranular* failure. |
| 1830°F AC | Equiaxed $\beta$ + Widm $\alpha$ | 75 | 0.3 | 98 | >90 | |

[a] WQ = Water-cooled.
AC = Air-cooled.

**Table 16.** Properties of Ti-11.5Mo-6Zr-4.5Sn

| *Heat Treatment*[a] | *Phase Structure* | *Yield Stress, ksi* | *Thickness, in.* | $K_{Ic}$ *or* $K_Q$, *ksi* $\sqrt{in.}$ | $K_{Iscc}$, *ksi* $\sqrt{in.}$ | *Remarks* |
|---|---|---|---|---|---|---|
| 1600°F (½ hr) WQ +900°F (8 hr) | Equiaxed β+α precipitates | 166 | 0.5 | 50 | 26 | Susceptible to SCC. |
| 1600°F (½ hr) WQ +900°F (100 hr) | Equiaxed β+α precipitates | 151 | 0.5 | 65 | 24 | |
| 1500°F (½ hr) WQ +1150°F (100 hr) | Equiaxed β+α precipitates | 146 | 0.5 | >100 | 70 | |
| 1500°F (½ hr) WQ +700°F (100 hr) | Equiaxed β+ω | 215 | 0.5 | 21 | >20 | Immune to SCC. |
| 1350°F (1 hr) WQ +900°F (8 hr) AC | Equiaxed β + two sizes of α precipitate | 172 | 0.5 | 50 | 26 | Susceptible to SCC. |
| Hot worked +1375°F (1 hr) WQ +900°F (8 hr) | Unrecrystallized β+α precipitates | 168 | 0.5 | 51 | >50 | Immune to SCC. |

[a] AC = Air-cooled.
WQ = Water-quenched.

susceptibility at least in the WR direction. The susceptibility in the short transverse direction has not been determined at this time. (It is possible that this method also eliminates grain boundary films of the $\alpha$ phase, but this possibility has not been investigated.)

The alloy Ti-8Mo-8V-3Al-2Fe is similar to Ti-11.5Mo-6Zr-4.5Sn, although the higher $\beta$-stabilizer content leads to some modification of the phase tranformations. The alloy exhibits excellent hardenability and can be heat treated to high strength levels.

The $\beta$ transus is about 1350°F. The $\beta$ phase is retained on water quenching or air cooling. The $\beta$ phase does not undergo a stress-induced transformation at room temperature. Aging of the retained $\beta$-phase is usually performed at temperatures from 900 to 1100°F, in which range the $\alpha$ phase is precipitated. Aging at temperatures below about 650°F results in a phase separation, $\beta \rightarrow \beta_1+\beta_2$, causing considerable strengthening. This structure, as with $\beta+\omega$ mixtures, appears immune to SCC. The authors are unaware of any compositional or processing data which have been related to SCC susceptibility. It is probable that the hot working techniques described for Ti-11.5Mo-6Zr-4.5Sn would also be effective for this alloy.

*Tests on Ti-8Mo-8V-3Al-2Fe.* Composition: 7.8Mo, 8.1V, 2.9Al, 2.0Fe, 0.09O. Specimen: DCB, fracture WR orientation. SCC tests in 3.5% NaCl. Results are shown in Table 17 [63].

Ti-8V-6Cr-4Mo-4Zr-3Al is similar to the alloy just described. It has excellent hardenability and can be heat treated to very high strength levels (>220 ksi yield).

The $\beta$ transus is about 1340°F. The $\beta$ phase is retained on water quenching or on relatively slow cooling. The alloy is hardened by precipitation of the $\alpha$ phase at temperatures from 900 to 1100°F. Precipitation at lower temperatures has not been studied in detail, although it is possible that a phase separation, $\beta \rightarrow \beta_1+\beta_2$, occurs. The SCC fractures are intergranular after low temperature aging but may be transgranular in material aged at higher temperatures, possibly due to the chromium content of the alloy.

*Tests on Ti-8V-6Cr-4Mo-4Zr-3Al.* Composition: 3.4Al, 8.2V, 5.8Cr, 3.9Zr, 4.0Mo, 0.09O. Specimen: notch bend, fracture WR orientation. SCC tests in 3.5% NaCl. Results are shown in Table 18 [122].

Ti-13V-11Cr-3Al is nearest to a stable $\beta$-phase alloy that is produced commercially. In the all $\beta$-phase condition it is very formable but can be strengthened to high strength levels by aging. Cold work plus aging treatments can develop strengths as high as 230 ksi. The $\beta$ transus is about 1240°F (0.05% O) but can be higher (up to 1300°F) with high oxygen contents. The $\beta$ phase is retained on cooling to room temperature even at relatively slow rates. The yield strength of the $\beta$ phase can be increased from 130 to 180 ksi by cold working.

Aging at temperatures between 800 and 1000°F results in $\alpha$-phase precipitation. Prolonged aging ($\geq$100 hr at 1000°F) can cause the formation of $TiCr_2$

**Table 17.** Properties of Ti-8Mo-8V-3Al-2Fe

| *Heat Treatment*[a] | *Phase Structure* | *Yield Stress, ksi* | *Thickness, in.* | $K_{Ic}$ *or* $K_Q$, *ksi* $\sqrt{in.}$ | $K_{Iscc}$, *ksi* $\sqrt{in.}$ | *Remarks* |
|---|---|---|---|---|---|---|
| 1500°F (½ hr) WQ +1000°F (32 hr) | Equiaxed β+α precipitates | 150 | 0.5 | 61 | 38 | Equiaxed β+α structures susceptible to SCC |
| 1500°F (½ hr) WQ +850°F (16 hr) | Equiaxed β+α precipitates | 178 | 0.5 | 45 | 28 | |
| 1500°F (½ hr) WQ +700°F (250 hr) | Equiaxed $\beta_1+\beta_2$ structure | 205 | 0.5 | 20 | 20 | Structure immune to SCC |

[a] AC = Air-cooled.
WQ = Water-quenched.

**Table 18.** Properties of Ti-3Al-8V-6Cr-4Mo-4Zr

| *Heat Treatment*[a] | *Phase Structure* | *Yield Stress, ksi* | *Thickness, in.* | $K_{Ic}$ *or* $K_Q$, *ksi* $\sqrt{in.}$ | $K_{Iscc}$, *ksi* $\sqrt{in.}$ | *Remarks* |
|---|---|---|---|---|---|---|
| 1500°F (1 hr) AC +950°F (8 hr) AC | Equiaxed $\beta+\alpha$ precipitates | 192 | 0.5 | 50 | 34 | Intergranular SCC. Note that $K_{Iscc}$ does not follow $K_{Ic}$ variations. |
| 1500°F (1 hr) AC +1050°F (8 hr) AC | Equiaxed $\beta+\alpha$ precipitates | 164 | 0.5 | 63 | 29 | |
| 1500°F (1 hr) AC +1150°F (8 hr) AC | Equiaxed $\beta+\alpha$ precipitates | 148 | 0.5 | 74 | 28 | Transgranular SCC. |

[a] AC = Air-cooled.
WQ = Water-quenched.

which reduces the toughness of the alloy to rather low levels. Aging at temperatures below about 600°F causes a phase separation within the $\beta$ phase ($\beta \rightarrow \beta_1+\beta_2$).

The $\beta$ phase is susceptible to SCC, and thus the grain size of the phase could be expected to influence $K_{Iscc}$. Limited evidence indicates that the larger the grain size the lower the $K_{Iscc}$ value. The influence of cold work on $K_{Iscc}$ does not appear to have been studied.

*Tests on Ti-13V-11Cr-3Al.* Composition: 3.3Al, 13.2V, 10.3Cr, 0.10O. Specimen: notch bend or single-edge-notched, fatigue precracked, fracture WR orientation. SCC tests in 3.5% NaCl. Results are shown in Table 19 [31,63].

Considerably more data are available than those listed above both for some of the alloys listed and for other experimental and commercial alloys. We have tried to demonstrate the critical parameters which are involved in determining the SCC behavior of titanium alloys in salt water. The points covered should be applicable to other alloys of the same type. Less is known of the influence of metallurgical parameters on SCC in other environments, but from an engineering point of view, metallurgical methods of avoiding the problem are of less interest. One possible exception is the (potential) hot salt problem in which at least some of the metallurgical factors are similar to those found in aqueous solutions, but a detailed analysis is not possible at this time.

**Metallurgical Methods of Improving SCC Properties**

*Compositional and Microstructural Methods.* An example of an alloy development program undertaken with the object of producing material with adequate strength coupled with good SCC resistance has been performed within The Boeing Company [123]. The essential concepts of the program were as follows. It had been shown at its inception that titanium alloys could not tolerate high aluminum contents, and therefore this alloy element was held below 5%. Further, molybdenum and vanadium were known to be beneficial elements, and these were added. Additions of $\beta$-eutectoid elements were made to provide additional strengthening and also to study their influence on SCC susceptibility. The results obtained on the most successful alloys developed are shown in Fig. 41, which demonstrates that considerable improvements were achieved. However, the reader who has followed the discussions on metallurgical variables to this point will no doubt see that there are some additional subtleties which must be considered.

*Other microstructural and compositional modifications* that could be anticipated to improve SCC properties are based on the observation that transgranular SCC occurs in alloys in which slip is concentrated in narrow bands—so-called planar slip. If deformation could be made to occur in a turbulent manner (multiple cross-slip), it is possible that SCC resistance would be improved. The essential difficulty is to provide hard stable particles, which usually cause such a modification of slip morphology in a titanium-rich matrix. Some progress on a fundamental level has been made—for example, additions of the (expensive)

**Table 19.** Properties of Ti-13V-11Cr-3Al

| *Heat Treatment*[a] | *Phase Structure* | *Yield Stress,, ksi* | *Thickness, in.* | $K_{Ic}$ *or* $K_Q$, *ksi* $\sqrt{in.}$ | $K_{Iscc}$, *ksi* $\sqrt{in.}$ | *Remarks* |
|---|---|---|---|---|---|---|
| 1575°F (1 hr) WQ | Equiaxed β | 128 | 0.125 | 89 | 26 | Quenched condition very susceptible subsequent aging to precipitate α lowers $K_{Ic}$ and raises (slightly) $K_{Iscc}$. |
| 1450°F (¼ hr) AC | Equiaxed β+α precipitates | 138 | 0.125 | 78 | 39 | |
| 1450°F (¼ hr) WQ +875°F (½ hr) AC | Equiaxed β+α precipitates | 146 | 0.125 | 54 | 40 | |
| 1700°F (½ hr) WQ +1100°F (16 hr) | Equiaxed β+α precipitates | 153 | 0.20 | 65 | 32 | |
| 1700°F (½ hr) WQ +1100°F (250 hr) | Equiaxed β+α and $TiCr_2$ precipitates | – | 0.20 | 27 | 23 | –Precipitation of $TiCr_2$ embrittles alloy and produces little SCC susceptibility. |

[a] AC = Air-cooled.
WQ = Water-quenched.

element gallium to Ti-Al alloys can result in the formation of $Ti_2Ga$ particles which improve at least the ductility properties, although other properties have not been studied. Perhaps systems based on carbides, borides, and rare-earth elements may prove a more practical method of achieving the desired dispersions.

*More Macroscopic Methods.* It has been shown that thermomechanical processing of at least one $\beta+\alpha$ alloy can result in improved SCC properties. Such processing no doubt could be applied to similar alloys with the object of providing high-strength material coupled with adequate toughness and SCC resistance. However, such processing may result in the same condition as that found

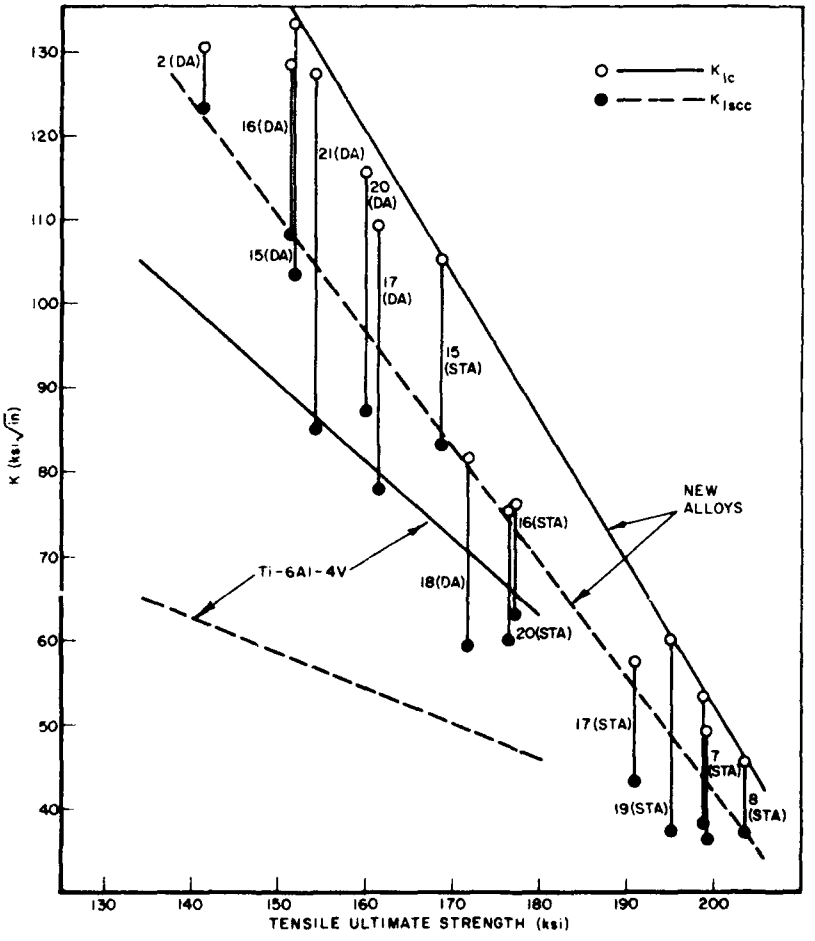


Fig. 41. Strength, toughness, and stress corrosion resistance of some experimental Boeing-developed alloys (0.5 in. thick, WR orientation, 3.5% NaCl) [123].

in wrought aluminum products, i.e. susceptibility to SCC only in the short transverse direction. It is possible that hot working could also be useful in $\alpha+\beta$ alloys, although this does not appear to have been studied directly. Most alloys of this type are given further heat treatments after working which essentially remove the structure caused by hot work.

The development of composite materials has been a very active field in recent years, no doubt due to the availability of boron, carbon, and other fibers. Problems are encountered with such fibers in titanium alloy matrices due to their extreme reactivity. Recently methods and alloys have been developed which reduce the extent of fiber-matrix reaction. However, such materials have not reached the stage of development where the SCC properties are of concern. Likewise, directional composites produced by controlled solidification processes (such as Ti-Si alloys) are in the early development stages.

One other macroscopic method of producing composite structures in titanium alloys is by the utilization of diffusion bonding techniques. Such methods are eminently suitable for titanium alloys, as these alloys can be readily joined by diffusion bonding. Development work on armor plate is in progress utilizing very high strength alloys (such as $\beta+\omega$ structures) bonded with high toughness material. This approach could conceivably be extended to composite or sandwich materials which would couple high strength with SCC immunity.

## 5.5 Stress Corrosion Fracture

This section describes the characteristic fracture features observed in titanium alloys that have failed under SCC conditions. Such a description may prove useful in diagnostic analyses of the fracture of titanium alloys both under laboratory and service conditions. It should be noted that fracture surfaces from service failures may be complex due to such factors as discontinuous failure due to variable applied loads and the superposition of variables other separation modes by corrosion, fatigue, etc. "Brittle-failure" of titanium alloys can occur by mechanisms other than SCC, such as the pickup of hydrogen at elevated temperatures and the resultant hydrogen embrittlement at lower temperatures. Titanium alloys (incorrectly selected) may exhibit cleavage failure at cryogenic temperatures. These failure modes are not described in the following paragraphs.

### Topology of Fracture

Nearly all stress corrosion failures exhibit macroscopically flat fracture faces. However, if cracking is transgranular, the inclination of the crack plane to the principal stress axis depends upon the degree of preferred orientation. Crack branching may also modify the direction of cracking.

Thin titanium alloy specimens often tend to exhibit a mixture of ductile tearing and environmentally assisted crack growth. Such areas might be separable

into shear lips at the specimen surface and a flat central portion. When these conditions prevail, velocity measurements tend to be unreproducible.

In previous sections the *V-K* relationships have been separated into the different regions I, II, and III. In these regions a wide variety of fracture topologies may be exhibited, depending on alloy composition, microstructural factors, environment, and stress level. In Fig. 42 an attempt is made to relate the fracture topologies resulting from environmentally assisted crack growth in titanium alloys to a "generalized" *V-K* plot. Thus, in most cases crack growth occurs in region I by intergranular separation (A), in region II by transgranular cleavage (C), and in the supercritical region ($K_{Ic}$) by microvoid coalescence (E) Therefore, there are two transition regions:

- Between regions I and II, mixed intergranular and transgranular fracture is observed (B).
- Between Region II and unstable (fast) fracture, mixed transgranular cleavage and dimpled fracture is observed (D).

There are some exceptions to this generalized description of fracture, and thus Fig. 42 must be regarded as an oversimplification. These exceptions for different environments are discussed below.

**Fracture in Aqueous Solutions.** In most titanium alloys, SCC in neutral aqueous solutions occurs by transgranular cleavage. Examples of such failures are shown for an α alloy (Ti-10Al) and β alloy (Ti-16Mn) in Figs. 42 (C) and 43, respectively. In two-phase α+β or β+α structures, the fracture topology may be modified, especially if one phase is immune to SCC, as is often the case in commercial alloys. These modifications to the fracture surfaces are shown in Figs. 44a and b for Ti-6Al-4V and Ti-8Mn, respectively. The immune phases normally fail in a ductile manner, and there is evidence that they can act as crack-arrest sites. As mentioned earlier, transgranular cleavage cracking of titanium alloys occurs on or near specific crystallographic planes. Figure 45 summarizes cleavage-plane determinations for α alloys in aqueous and other solutions. It is clear that the cleavage plane of the α phase is 14 to 16 deg from the basal plane, although there is some scatter in the actual indices of the plane. Less work has been performed on establishing the cleavage plane for β alloys. SCC occurs on the $\{100\}$ planes in Ti-13V-11Cr-3Al [36]. The crack topologies in the Ti-Mn alloys also appear consistent with this fracture plane.

The occurrence of only transgranular cleavage during the SCC of all the α alloys, as well as several of the β alloys in neutral aqueous solutions, is consistent with the "generalized" cracking behavior shown in Fig. 42. However, in certain heat-treatment conditions, some of the β alloys fail by intergranular separation of the type shown in Fig. 46. A fine Widmanstätten α-phase precipitate in β-phase matrix appears to be a requirement for such cracking. Such failures have been observed in the alloys and heat treatments of Table 7 [45,63].

It must be noted that the ranges for aging temperatures may be more extensive than those listed above.

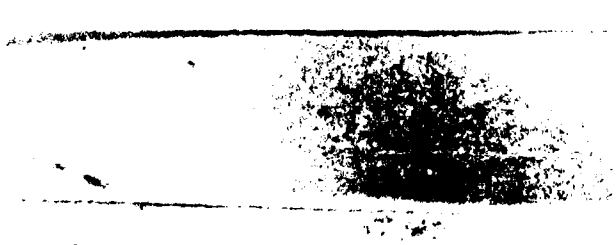

No region I behavior is observed for these alloys in neutral aqueous solutions. In contrast, region I crack growth does occur in concentrated acidic solutions. In such solutions, however, it has not been demonstrated that cracking is intergranular [40].

A final point concerning aqueous solutions is that the extent of the transition region D (in Fig. 42) appears to be dependent upon the halide-ion concentration; the higher the concentration, the narrower the transition region.

**Fracture in Methanolic Solutions.** Two types of fracture behavior are exhibited by titanium alloys in methanolic solutions; both are dependent on the stress (or $K$) level and the alloy composition. The first type is observed in alloys

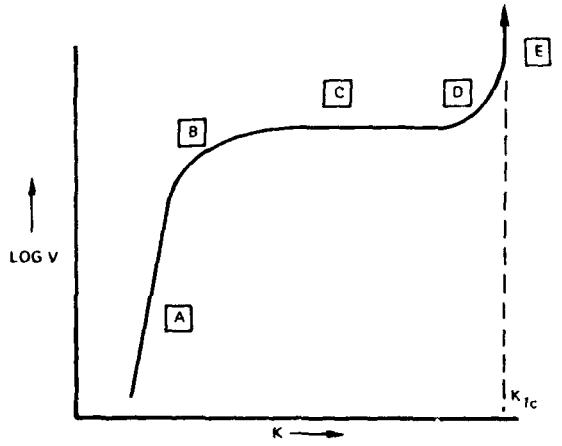


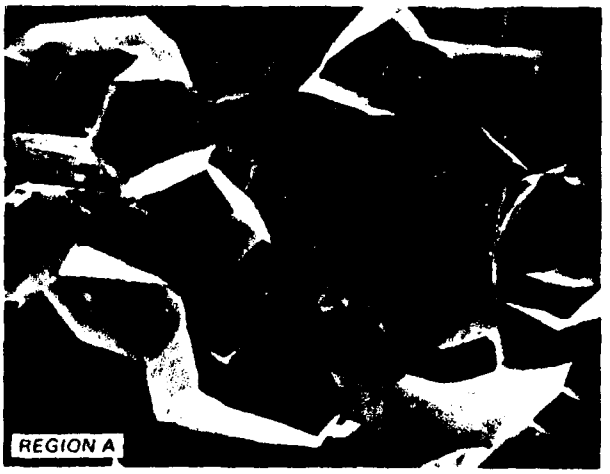

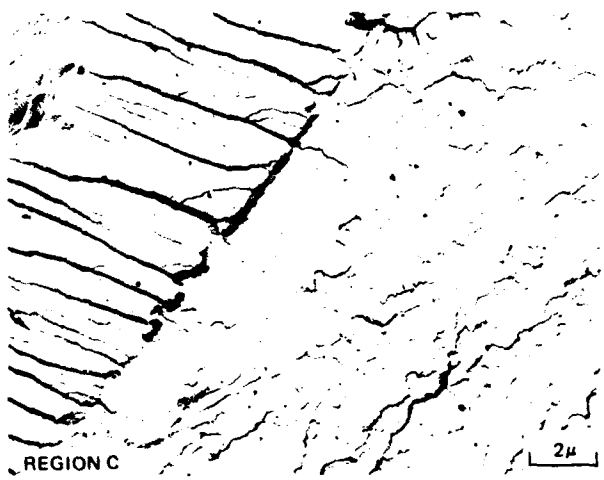


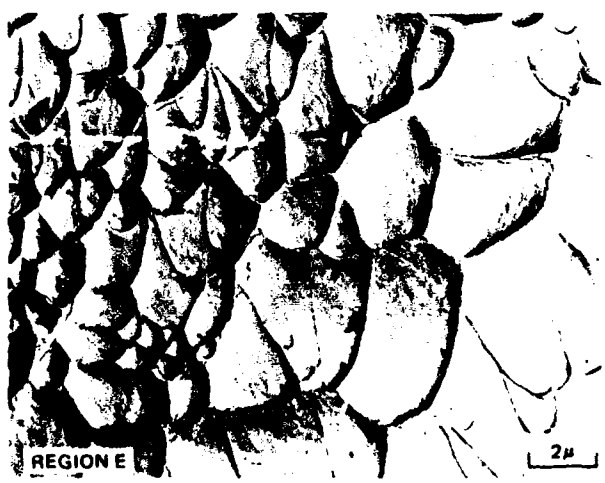


Fig. 42. Schematic of fracture topology observed in the various regions of the SCC velocity vs stress intensity curve. Region A. Intergranular separation typical of region I crack growth. Example: Scanning electron micrograph of Ti-4Al tested in methanol (×500) [34]. Region C. Transgranular cleavage failure typical of region II type growth. Example: Ti-8Al tested in 3.5% NaCl (courtesy of R. R. Boyer). Region E. Dimpled failure typical of supercritical crack growth. Example: Ti-11.5Mo-6Zr-4.5Sn [45]. Regions B and D are transition regions.

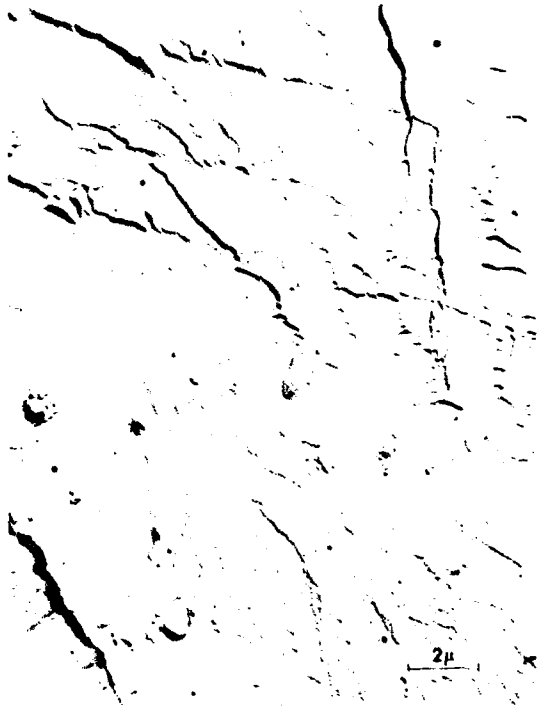


Fig. 43. Stress corrosion failure observed in region II type crack growth for Ti-16Mn alloy tested in 0.6 *M* KCl [40].

(a) Ti-6Al-4V showing cleavage of the α phase [126]

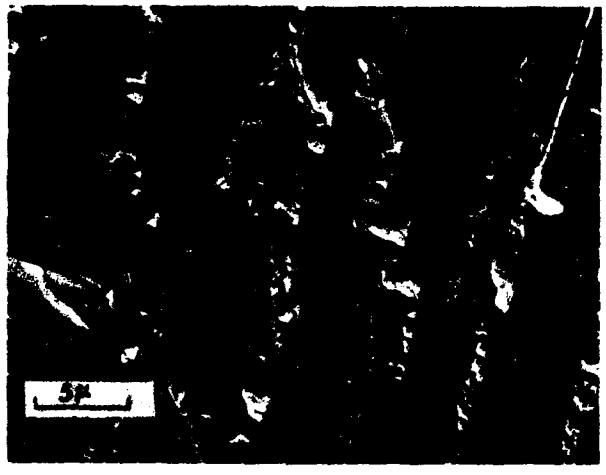


(b) Ti-8Mn showing cleavage of the $\beta$ phase [127]

Fig. 44. Stress corrosion fractures in two-phase alloys in which one phase is immune.

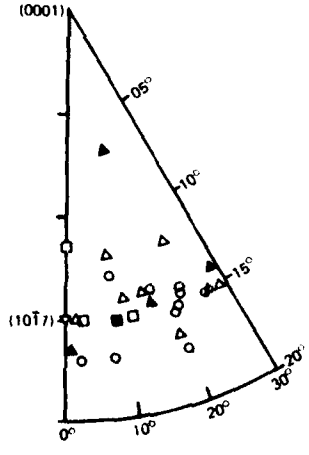


- Ti-7-2-1 (WATER)
- Ti-8Al (AIR AND SALT SOLUTION)
- Ti-8-1-1 (METHANE, CARBON TETRACHLORIDE)
- Ti-8-1-1 (HEXANE)
- Ti-5-2-5 (SALT SOLUTION)
- Ti-0.35% O (SALT SOLUTION)

Fig. 45. Central portion of unit stereographic triangle of the HCP projection showing the experimentally determined positions of the transgranular cleavage plane. The left side is $(11\bar{2}0)$ zone, the right side is the $(10\bar{1}0)$ zone [125].

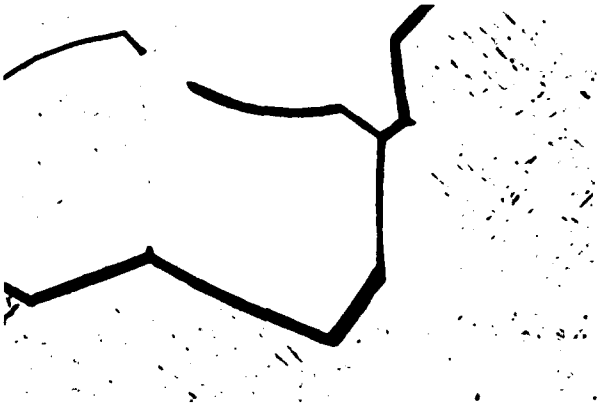

Fig. 46. Intergranular SCC of Ti-11.5Mo-6Zr-4.5Sn aged 100 hr at 900°F and tested in 0.6 + *K*Cl (×200) (region II type growth) [45].

not susceptible to SCC in aqueous solutions (e.g., Ti-50A); such alloys show intergranular separation in the methanolic solutions, and cracking may occur in the absence of stress [55,57,60,108]. The application of stress accelerates cracking, but the intergranular failure mode is unchanged and remains independent of stress level. A typical example is shown in the scanning electron micrograph in Fig. 47. Such behavior is considered (by the authors) to correlate with region I.

The second type of fracture behavior, region II growth, is generally observed in alloys that are susceptible to SCC in aqueous solutions (e.g., in alloys containing 5% or more aluminum. In such alloys both intergranular and transgranular fracture are observed in methanolic solutions [55,57,108]. The general appearance of the transgranular, cleavagelike failure and the habit of the

Fig. 47. Intergranular separation of Ti-8Al tested in methanol (×425).

cleavage plane [125] are essentially the same as those observed in aqueous solutions. Region I type growth occurs by intergranular separation [64] and is thus consistent with the "generalized" behavior shown in Fig. 42. Although both intergranular and transgranular cracking have been observed by several workers on smooth specimens of titanium alloys, it is only recently that the dependence of cracking mode on stress intensity has been established [64]. The cleavage plane in the $\alpha$ phase is the same as that observed in aqueous solutions [128, 129].

There are three possible exceptions to the "generalized" behavior shown in Fig. 42, all of which occur in $\beta$ alloys. The fracture mode in Ti-16V and Ti-20Mo has been reported to change from transgranular cleavage to intergranular separation if the grain size is decreased from 100 to 50 $\mu$m or if the coarse-grained material is deformed [62]. In addition, intergranular separation observed in fine ($\beta$+$\alpha$)-phase structures in some metastable $\beta$ alloys tested in aqueous solutions also occurs during region II crack growth in methanolic solutions (Fig. 49, Ref. 63). It has been reported that Ti-11.5Mo-6Zr-4.5Zn (Beta III) fails transgranularly at low stress intensities in methanolic solutions [92].

**Fracture in Other Organic Liquids.** The fracture topology and cleavage plane of Ti-8Al-1Mo-1V in a number of organic liquids have been found to be similar to those observed in aqueous and methanolic solutions [67].

One possible deviation from the "generalized" behavior shown in Fig. 42 is that, on testing Ti-8Al-1Mo-1V in carbon tetrachloride, no intergranular failure is observed in region I [64]. Furthermore, the transgranular failure in $CCl_4$ is characterized by very flat and featureless cleavage facets [130].

Again the cleavage plane in the $\alpha$ phase is the same as in aqueous and methanolic solutions [125]. There is a scarcity of data on the fracture behavior of $\beta$ alloys in organic liquids.

**Fracture in Nitrogen Tetroxide.** The fracture of Ti-5Al-2.5Sn in $N_2O_4$ occurs by both transgranular and intergranular separation modes [106]. The transgranular mode has the typical cleavagelike appearance. A more detailed study on the nature of cracking in $N_2O_4$ has been performed [52] where a series of alloys, mostly of the $\alpha$ and $\alpha$+$\beta$ types, was investigated. While cracking in Ti-4Al was entirely intergranular, cracking in Ti-8Al occurred by both intergranular separation and a transgranular cleavage mode. Additions of $\beta$-stabilizing elements such as vanadium to either Ti-4Al or Ti-8Al produced more transgranular cleavagelike failures. Furthermore, there was some evidence that the mode of cracking in the Ti-4Al-4V alloy was dependent on stress intensity; at low $K$ levels intergranular failure was observed, and at high $K$ levels transgranular failure occurred. These observations are therefore consistent with the "generalized" fracture behavior shown in Fig. 42. It must be emphasized, however, that the $V$-$K$ relationships are not known for $N_2O_4$ environments.

**Fracture in Red Fuming Nitric Acid.** There are very few data on the fracture topology behavior of titanium alloys in RFNA. Some limited work performed on Ti-8Mn indicates that cracking is predominately intergranular [1].

**Fracture in Hot Salts.** The details of fracture path analysis after hot salt testing are not as well established as those for other environments due to the corrosive nature of hot salts. The crack path depends upon the alloy composition. For example, in Ti-4Al-3Mo-1V cracking was shown to be predominantly intergranular, while in Ti-5Al-2.5Sn both intergranular and transgranular cracking were observed. It has been shown that cracking in Ti-8Al-1Mo-1V and Ti-6Al-4V is predominantly intergranular [76,131-134]. There is no information on the influence of stress, if any, on the fracture behavior of titanium alloys in hot salt environments. The fracture path appears to be dependent upon heat treatment in $\alpha$ alloys. For example, in material solution treated above the $\beta$ transus, cracking is predominantly transgranular, while in material treated below the transus, fracture is predominantly intergranular.

Cracking of a series of $\alpha$ and $\alpha+\beta$ alloys is predominantly intergranular when tested in magnesium chloride at 154°C [135].

**Fracture in Molten Salts.** Ti-8Al-1Mo-1V is the only alloy that has been tested in molten salts, and in this alloy cracking occurs by a transgranular cleavage mode in region II [64]. The cleavage plane has not been determined accurately, but preferred orientation effects indicate that it is the same as that observed in aqueous solutions and organic liquids. At this time, the fracture mode in region I has not been determined.

**Fracture in Liquid Metals.** There is only a limited amount of data on the fracture mode of titanium alloys in liquid metals. The fracture of Ti-8Al-1Mo-1V in mercury conforms with the generalized behavior illustrated in Fig. 42. Thus, region II crack growth occurs by transgranular cleavage; at low $K$ levels (in region I) cracking is predominantly intergranular [64].

All other observations of liquid-metal-induced cracking have been obtained from tests in which $V$-$K$ conditions were not well defined. For example, it has been shown that both Ti-50A [89] and Ti-13V-11Cr-3Al [48] fail by intergranular separation in liquid cadmium. Ti-8Al-1Mo-1V and Ti-6Al-4V fail by a mixture of transgranular and intergranular cracking after embrittlement by solid cadmium [91].

In contrast to its behavior in liquid cadmium, Ti-31V-11Cr-3Al fails by a predominantly transgranular mode in liquid zinc [48].

## Crack Branching

**General Behavior.** Crack branching (or bifurcation) was first recognized during studies of the propagation of unstable (fast fracture) cracks in glass and plastic materials [136]. A similar phenomenon also occurs during subcritical crack growth and has recently been systematically investigated in a variety of materials [137]. Two types of branching are distinguished:

1. Microbranching, in which the crack front splits into several local cracks with separation distances of the order of a grain diameter.

2. Macrobranching, in which the crack separates into two or more macroscopic components that tend to diverge. Rules proposed for macrobranching are

a. The existence of a region II behavior.

b. A stress intensity $K_B \geq 1.4\ K_p$, where $K_B$ is the stress intensity for macrobranching and $K_p$ is the stress intensity for the initiation of plateau behavior (Fig. 48).

c. The existence of a relatively isotropic microstructure or SCC susceptibility.

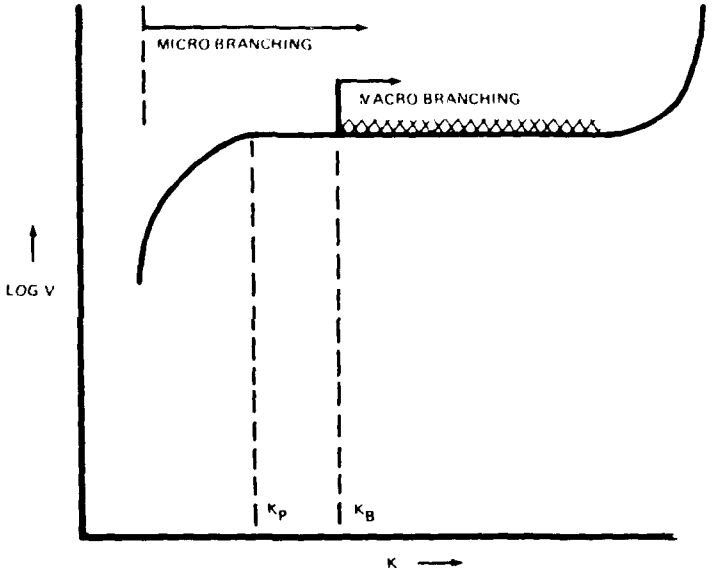


Fig. 48. Schematic of the dependence of micro and macro crack branching on the $K$ level. $K_p$ is the onset of region II plateau behavior. $K_B$ is approximately 1.5 times $K_p$ at the onset of macrobranching [137].

There appears to be no detailed analyses for microbranching behavior, although it is a common occurrence in SCC, especially in region IIa type growth (Region IIa is shown in Fig. 18.)

Crack branching modifies and complicates the determination of $K$ values, and its occurrence can lead to incorrect determinations of $K_{Iscc}$ [137].

**Branching in Titanium Alloys.** An example of crack branching in Ti-11.5Mo-6Zr 4.5Sn is shown in Fig. 49. This micrograph was taken from a SEN specimen tested in 0.6 *M* LiCl in methanol under increasing stress intensity. It can be seen that cracking can be divided into three regions: region X, in which the crack is relatively straight but with a few microbranches; region Y, in which profuse microbranching occurs; and region Z, where the crack divides macroscopically


X: Region with some microbranching
Y: Profuse microbranching
Z: Macrobranching with some associated microbranching

Fig. 49. Morphology of cracking in Ti-11.5Mo-6Zr-4.5Sn aged 100 hr at 900°F and tested in 0.6 *M* LiCl in methanol at −500 mV [63].

into two components. Since cracking is intergranular and the grain structure is equiaxed, this is an example of propagation in an isotropic material.

Branching also occurs in $\beta$ alloys that fail by transgranular cracking, as the three $\{100\}$ type cleavage planes are sufficient to allow relatively isotropic behavior. An example for Ti-8Mn is shown in Fig. 50. In $\alpha$ alloys, however, transgranular cleavage occurs on planes near $\{0001\}$ and thus the situation is more complicated. Macroscopic crack branches with large angular separations are therefore impossible, especially in materials with a high degree of preferred orientation. However, macrobranching has been observed in some $\alpha$ alloys; an example is shown for Ti-7Al-1.5Mo-0.5V in Fig. 51. In such alloys the angle between the crack branches is controlled by the relationship of specimen orientation to the preferred orientation. Finally, it should be noted that microbranching is very prevalent in many $\alpha$ alloys, possibly because of the extensive region IIa behavior.

### 5.6 Additional Factors and Prevention of SCC

This section examines briefly the use and service experience gained with titanium alloys over the past decades and the influence of manufacturing processes on SCC.

#### Service Experience

Titanium alloys are used in diverse fields ranging from outer space to the circus ring. The bulk of material used at this time is in gas turbine engines in which the use of alloys is limited by high temperature mechanical properties rather than by SCC resistance. It is possible that if the operating temperatures are increased, hot salt SCC problems may be encountered. In this and other applications which for high strength titanium alloys are almost entirely restricted to aerospace usage, titanium has been remarkably free from SCC problems. Some examples (and possible examples) are listed below:

- Turbines. Problems with cadmium-plated parts (liquid- or solid-metal cracking). Also problems with silver-plated parts (due to hot salt SCC by AgCl).
- Rocket Pressure Vessels, etc. Apollo tank failures in $N_2O_4$ and methanol. Minuteman II rocket cases; these failures may not be assigned to SCC with certainty.
- Airplanes. No failures have been reported that were caused by SCC, although such failures were encountered in initial SST hardware constructed of Ti-8Al-1Mo-1V.
- Marine. One case of SCC failure of a propeller casting has been reported, initiated by high cycle corrosion fatigue.

The reasons for the excellent service record of titanium alloys (when compared with high strength aluminum alloys and steels) can be attributed to several factors including:

Fig. 50. Macrobranching in Ti-8Mn (MA) tested in 0.6 *M* KCl at 500 mV [48].

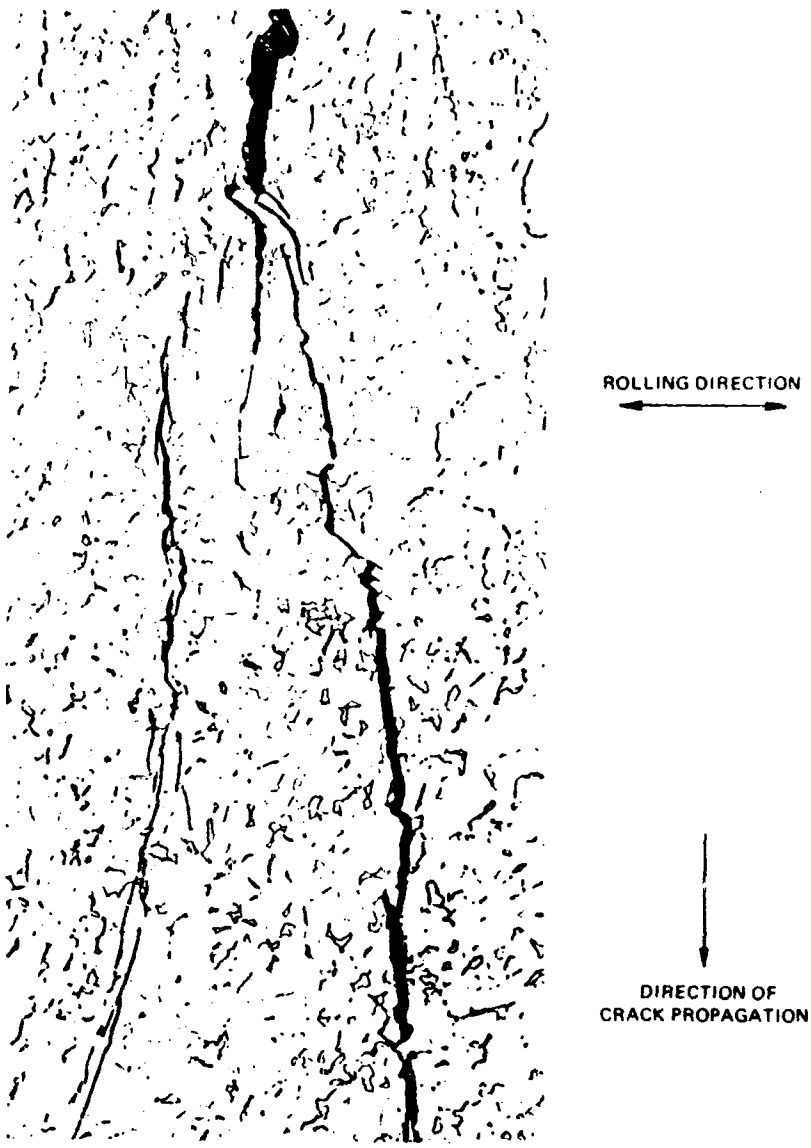


Fig. 51. Macro- and microbranching in Ti-7Al-1.5Mo-0.5V tested in 3.5% NaCl (open circuit) [34].

- Less titanium is used (cost is a factor).
- Where it is used the stresses are usually relatively low.
- Humid air and water are much less aggressive environments toward titanium alloys than salt water; this is not true for high strength steels and aluminum alloys.
- Corrosion pits, which often act as SCC crack nucleation sites in structures, do not form in titanium alloys at room temperature.
- Titanium alloys exhibit good fatigue-crack nucleation and crack-growth (at low $K$ levels) properties.
- Most titanium alloys have relatively high $K_{Iscc}$ levels, and no (slow) region I type crack growth is expected in neutral aqueous environments.

To take some extreme examples, and assuming long time exposures (i.e., the kinetics of crack growth are not important), we can compare the high-susceptibility materials 4340 steel (280 ksi), 7079 T651 aluminum alloy, and Ti-8Al-1Mo-1V MA titanium alloy. As a basis of comparison the ratio (yield strength/density) $K_{Iscc}$ is used from which the following rating results: Aluminum 3500, steel 9300, titanium 17,500, which demonstrates perhaps the merit of a high and real $K_{Iscc}$ value. (However if a cost factor were also included the titanium alloy would rate last.) The comparison of more resistant alloys is difficult, as the kinetics of crack growth are a much more important factor in determining the life time of a structure.

The following sections attempt to provide the engineer with additional information on factors which may influence the service performance of titanium alloys. It should be pointed out that the accurate characterization of the mechanical and chemical environments experienced by a structure is an essential prerequisite to an entirely rigorous approach to material selection from laboratory data, and such characterization is almost never available. Further, the points made can only be regarded as indications of potential problems as they are not based on service experience.

## Residual Stresses

In addition to any externally applied stresses, other stresses can be present in structural parts due to forming and shaping, heat treatment and manufacturing processes. The origin of such stresses and stress-relieving procedures are summarized in Ref. 138. Probably the most important influence of residual stresses in titanium alloys is the loss of properties under a reversed stress (the Bauschinger effect, which is quite large in titanium alloys). However, residual stresses could influence SCC behavior in two ways. First, it has been shown that compressive surface stresses (produced by peening) can be beneficial in reducing hot salt SCC [92]. Second, residual tension stresses could lead to unanticipated SCC problems, as local stresses may be amplified to values well above design stresses.

### Crack Nucleation

All structures are designed to operate under elastic loads, and thus in many titanium alloys some form of stress concentration is required for the nucleation of a stress corrosion crack in aqueous environments. Such concentrations may be produced in several ways as discussed below.

1. Material imperfections. No manufacturing process is perfect and most structural materials contain imperfections which may be potential cracks—the larger the structure the more likely that imperfections are present.

2. Design and mechanical damage. Many structures contain holes, reentrant angles, etc., and such regions may act as potential crack-nucleation sites. Furthermore, poor machining techniques and accidental damage could lead to long shallow surface flaws; it should be noted that such flaws are both common and potentially very damaging.

3. Fatigue cracks can be formed if a structure is subject to cyclic stressing. These cracks usually nucleate at the sites listed in 1 and 2. The growth of fatigue cracks in a corrosive environment is a complex process and lies outside the field of this monograph. It is obvious that such cracks could act as very effective SCC nucleation sites.

4. Corrosion. The general corrosion resistance of titanium alloys is excellent in many environments (p. 273). However, titanium alloys can undergo crevice and pitting corrosion. Crevice corrosion occurs at elevated temperatures in the presence of $Cl^-$, $Br^-$, or $I^-$ ions, and the concentration of these ions and the crevice geometry also influence the rate of attack.

### Joining

In most structures of titanium alloys the material will be joined to other parts of the structure. Some factors relevant to SCC in such assembled structures are listed below:

1. Welding. Most $\alpha$ and $\alpha+\beta$ titanium alloys can be welded successfully. $\beta+\alpha$ alloys present welding problems, but technology in this field is improving and some $\beta$ alloys are considered weldable. For example, a German space vehicle contains a welded hemisphere of Ti-13V-11Cr-3Al. Electron beam, tungsten inert gas (GTA or TIG) and metal inert gas (GMA or MIG) methods are the most widely used welding processes. As the risk of contamination is high, welding is normally carried out in either argon or vacuum. Porosity and contamination by oxygen and hydrogen are potential problems that could influence subsequent SCC behavior, but these may be avoided by careful welding procedures. It has been shown that very high residual stresses are present after welding; for example, longitudinal stresses of >60 ksi have been measured in Ti-6Al-4V at the weld centerline [139]. Most welded structures are given postweld heat-treatment cycles, the exact details of which depend upon the alloy. Heating to 1000 to 1600°F for 15 to 60 min is the most common practice. Finally, it should be

noted that the weld metal and the heat-affected zone will have different microstructures from the base metal, and these microstructures will be further modified by a postweld heat treatment. Heat treatment should be designed to circumvent undesirable phase structures; for example, slow cooling of Ti-5Al-2.5Sn may result in the precipitation of the $\alpha_2$ phase and thus increase SCC susceptibility.

Examples of the influence of welding on SCC resistance are shown in Fig. 52. It can be seen that in most cases weld metal has slightly lower toughness properties with respect to the base metal and that properties are restored after subsequent heat treatment. The extent of the property changes is dependent on the alloy and possibly on the method of welding [140].

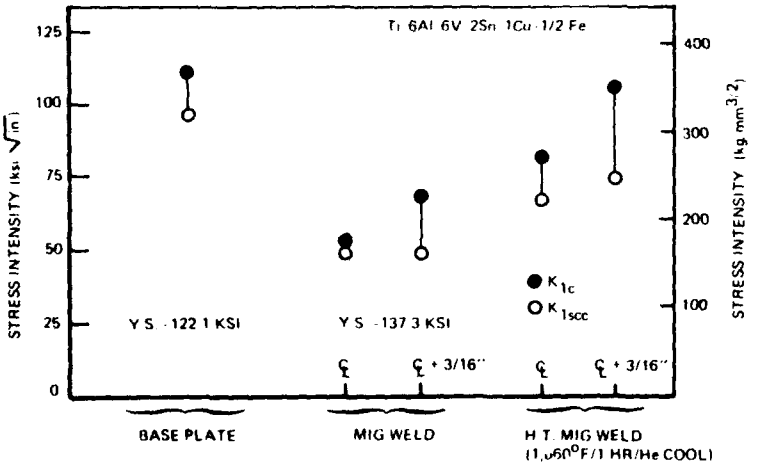


Fig. 52. Environmental cracking characteristics of a MIG weldment of the titanium alloy Ti-6Al-6V-2Sn-1Cu-0.5Fe [140].

2. Brazing. Titanium alloys can be successfully brazed with a wide variety of braze alloys, e.g., Ti-Cu-Ni, Ti-Zr-Be, Al, etc. There appear to have been no reports on the subsequent SCC behavior of brazed structures. The problems encountered with silver braze alloys in turbines [90] may serve to illustrate the problems that can arise from other metals in titanium structure.

3. Mechanical joints. Titanium fasteners have been used relatively widely in airplane and aerospace applications. For example, as early as 1953 the B-52 bomber utilized a large number of titanium fasteners. The most common fastener alloys are commercial purity titanium and Ti-6Al-4V although some of the new $\beta+\alpha$ phase alloys such as Ti-11.6Mo-5Zr-4.5Sn are being considered for this application due to their superior driveability. Titanium fasteners have performed well in service, and no failures attributable to SCC have been reported.

## ACKNOWLEDGMENTS

The authors thank the many people at Boeing who assisted in the preparation of this manuscript, in particular R. Boyer, W. F. Spurr, F. Parkinson, P. Finden, and L. Hall for valuable discussions especially on the properties of commercial alloys; Mary Myer for typographical assistance; and J. Messeth for graphics support. Drs. Blackburn and Smyrl gratefully acknowledge the financial assistance of NASA for grant No. 7-489 and Dr. Feeney the financial support under ARPA, Order 878.

## 5.7 References

1. D. W. Stough, F. W. Fink, and R. S. Peoples, *The Stress Corrosion and Pyrophoric Behavior of Titanium and Titanium Alloys*, TML Report 84, Battelle Mem. Inst., Columbus, Ohio, Sept. 15, 1957.
2. *Examination of Cracks in Titanium-Alloy Compressor Disc, Westinghouse Electric Corporation, Aviation Gas Turbine Division, Caused by Molten Cadmium*, TML Memorandum Report, Battelle Mem. Inst., Columbus, Ohio Feb. 8, 1956.
3. R. E. Johnson, G. K. Kappelt, and L. J. Korb, "A Case History of Titanium Stress Corrosion in Nitrogen Tetroxide," NASA-TM-X-59615, NASA, Houston, Texas, 1966.
4. W. E. Berry, E. L. White, and J. J. English, *Review of Recent Developments, Corrosion and Compatibility*, DMIC Report, Battelle Mem. Inst., Columbus, Ohio, Nov. 1966.
5. B. F. Brown et al., *Marine Corrosion Studies (Third Interim Report of Progress)*, NRL Memorandum Report 1634, July 1965.
6. J. D. Jackson and W. K. Boyd, *The Stress Corrosion and Accelerated Crack Propagation Behavior of Titanium and Titanium Alloys*, DMIC Technical Note, Battelle Mem. Inst., Feb. 1, 1966.
7. *Stress Corrosion Cracking of Titanium*, ASTM STP 397, Amer. Soc. Testing Mater., Philadelphia, Pa., 1966.
8. *Applications Related Phenomena in Titanium Alloys*, ASTM STP 432, Amer. Soc. Testing Mater., Philadelphia, Pa., 1968.
9. R. W. Staehle, A. J. Forty, and D. van Rooyen (eds.), *Proceedings of Conference on Fundamental Aspects of Stress Corrosion Cracking*, National Assoc. Corrosion Eng., Houston, Texas, 1969.
10. R. I. Jaffee and N. E. Promisel (eds.), *The Science, Technology, and Application of Titanium*, Pergamon Press, New York, 1970.
11. J. C. Scully (ed.), *The Theory of Stress Corrosion Cracking in Alloys*, Proceedings of Research Evaluation Conference, Portugal, published in 1971 by NATO Scientific Affairs Division, Brussels.

12. R. F. Hochman and J. C. Scully (eds.), *Stress Corrosion Mechanisms in Titanium Alloys*, Proceedings of a conference sponsored by the National Association of Corrosion Engineers, Atlanta, Ga., 1971, to be published.
13. R. E. Jaffee, "The Physical Metallurgy of Titanium Alloys," *Prog. Metal Phys.* 7, 65 (1958).
14. M. K. McQuillan, "Phase Transformations in Titanium and Its Alloys," *Met. Rev.* 8 (No. 29), 41 (1963).
15. J. C. Williams, B. S. Hickman, and D. H. Leslie, "The Effect of Ternary Additions on the Decomposition of Metastable Beta-phase Titanium Alloys," *Met. Trans.* 2, 477 (1971).
16. B. S. Hickman, "The Formation of Omega Phase in Titanium and Zirconium: A Review," *J. Mater. Sci.* 4, 554 (1969).
17. M. J. Blackburn and J. C. Williams, "Strength, Deformation Modes and Fracture in Titanium-Aluminum Alloys," *Trans. Amer. Soc. Metals* 62, 398 (1969).
18. D. N. Williams, "The Hydrogen Embrittlement of Titanium Alloys," *J. Inst. Metals* 91, 147 (1962).
19. W. F. Spurr, "Titanium Development Program," Boeing Document No. D6A-10065-1, Boeing Co., Seattle, Wash., Mar. 1966.
20. G. Sandoz and R. L. Newbegin, "Effects of Hydrogen Content and Environment and Subcritical Crack Growth in Ti-7Al-2Cb-1Ta and Ti-6Al-4V Alloys," *Report of NRL Progress*, Nov. 1968, p. 31-32.
21. R. J. Hawes Clark, *The Chemistry of Titanium and Vanadium*, Elsevier, Amsterdam, 1968.
22. J. Barksdale, *Titanium*, Ronald Press, New York, 1966.
23. N. D. Tomashov and R. M. Al'tovskii, "Corrosion and Protection of Titanium," Mashgiz., Moscow, 1963 (in Russian).
24. D. Schlain, "Corrosion Properties of Titanium and its Alloys," U.S. Bureau of Mines Bulletin 619 (1964).
25. F. W. Fink and W. K. Boyd, *The Corrosion of Metals in Marine Environments*, DMIC Report No. 245, Battelle Mem. Inst., 1970.
26. T. R. Beck, (after M. Pourbaix), "State of the Art of Stress Corrosion Cracking of Titanium Alloys", Boeing Document No. DI 82-1054, The Boeing Company, Seattle, Wash., 1971.
27. S. Wiederhorn, "Effects of Environment on the Fracture of Glass," *Environment-Sensitive Mechanical Behavior* (A. R. C. Westwood and N. S. Stoloff, eds.), Gordon & Breach, New York, 1966.
28. H. H. Johnson and A. M. Willner, "The Moisture and Stable Crack Growth in a High Strength Steel," *Appl. Mater. Res.* 4 (No. 1), 34 (Jan. 1965).
29. A. J. McEvily and A. P. Bond, "On the Initiation and Growth of Stress Corrosion Cracking in Tarnished Brass," *J. Electrochem. Soc.* 112, 131 (1965).
30. M. J. Blackburn and J. C. Williams, "Metallurgical Aspects of the Stress Corrosion Cracking of Titanium Alloys", *Proceedings of Conference on*

*Fundamental Aspects of Stress Corrosion Cracking* (R. W. Staehle et al., eds.), National Assoc. Corrosion Eng., Houston, Texas, 1969, p. 620.

31. H. R. Smith, F. K. Downey, and D. E. Piper, "A Study of Stress-Corrosion Cracking by Wedge-Force Loading," *Eng. Fracture Mech.* 1, 123 (June 1968).
32. F. A. Crossley, C. J. Reicher, and C. R. Simcoe, *The Determination of the Effects of Elevated Temperature on the Stress-Corrosion Behavior of Structural Materials*, Technical Report 69-191, Wright Air Development Division, Wright-Patterson AFB, May 1960.
33. A. J. Hatch, H. W. Rosenberg, and E. F. Erbin, "Effects of Environment on Cracking in Titanium Alloys," *Stress Corrosion Cracking of Titanium*, ASTM STP 397, Amer. Soc. Testing Mater., Philadelphia, Pa., 1968, p. 122.
34. D. E. Piper, S. H. Smith, and R. V. Carter, "Corrosion Fatigue and Stress-Corrosion Cracking in Aqueous Environments," *Metals Eng. Quart.* 8 (No. 3), 50 (1968).
35. D. A. Meyn, "A Study of the Crystallographic Orientation of Cleavage Facets Produced by Stress-Corrosion Cracking of Ti-7Al-2Nb-1Ta in Water," *Report of NRL Progress*, Aug. 1965, p. 21-23.
36. D. N. Fager and W. F. Spurr, "Some Characteristics of Aqueous Stress Corrosion in Titanium Alloys," *Trans. Amer. Soc. Metals* **61**, 283 (1968).
37. M. J. Harrigan, A. W. Sommer, and G. A. Alers, "The Effect of Textures on Mechanical Behavior of Alpha + Beta Titanium Alloys," paper presented at AIME Spring Meeting, Las Vegas, May 1970.
38. D. N. Fager, The Boeing Company, private communication.
39. R. E. Curtis, R. R. Boyer, and J. C. Williams, "Relationship Between Composition, Microstructure, and Stress-Corrosion Cracking (in Salt Solution) in Titanium Alloys," *Trans. ASM* **62**, 457 (1969).
40. T. R. Beck, M. J. Blackburn, and M. O. Speidel, "Stress-Corrosion Cracking of Titanium Alloys: SCC of Aluminum Alloys, Polarization of Titanium Alloys in HCl and Correlation of Titanium and Aluminum SCC Behavior," Contract NAS 7-489, Quarterly Progress Report 11, The Boeing Company, Seattle, Wash., Mar. 1969.
41. *A Study of the Stress-Corrosion Cracking of Titanium Alloys in Sea Water with Emphasis on the Ti-6Al-4V and Ti-8Al-1Mo-1V Alloys*, Research Report No. R471, Proj. No. 93002, Reactive Metals, Inc., Niles, Ohio, Oct. 18, 1965.
42. D. N. Williams, R. A. Wood, E. L. White, W. K. Boyd, and H. R. Ogden, *Studies of the Mechanism of Crack Propagation in Salt Water Environments of Candidate Supersonic Transport Titanium Alloy Materials*, Final Report SST-66-1, FAA Contract FA-SS-66-1, Battelle Mem. Inst., Columbus, Ohio, Jan. 1966.
43. T. R. Beck, "Stress-Corrosion Cracking of Titanium Alloys, Preliminary Report on Ti-8Al-1Mo-1V Alloy and Proposed Electrochemical Mecha-

nism," Boeing Document No. DI-82-0554, The Boeing Company, Seattle, July 1965.
44. D. T. Powell and J. C. Scully, "Stress-Corrosion Cracking of Alpha Titanium Alloys at Room Temperature," *Corrosion* **24** (No. 6), 151 (1968).
45. J. Feeney and M. J. Blackburn, "The Effect of Microstructure on the Strength, Toughness and Stress-Corrosion Cracking Susceptibility of the Metastable Beta Titanium Alloy Ti-11.5Mo-6Zr-4.5Sn," *Met. Trans.* **1**, 3309 (1970).
46. N. G. Feige and T. Murphy, "Fracture Behavior of Titanium Alloys in Aqueous Environments," *Metals Eng. Quart.* **7** (No. 1), 53 (1967).
47. B. F. Brown, Naval Research Laboratory, private communication.
48. M. J. Blackburn, The Boeing Company, unpublished work.
49. T. R. Beck, "Stress-Corrosion Cracking of Titanium Alloys: II. An Electrochemical Mechanism," *J. Electrochem. Soc.* **115**, 890 (1968).
50. T. R. Beck and M. J. Blackburn, "Stress Corrosion Cracking of Titanium Alloys," *AIAA J.* **6** (No. 2), 326 (1968).
51. D. A. Litvin and B. Hill, "Effect of pH on Sea-Water Stress-Corrosion Cracking of Ti-7Al-2Cb-1Ta," *Corrosion* **26** (No. 3), 89 (1970).
52. J. D. Boyd, P. J. Moreland, W. K. Boyd, R. A. Wood, D. N. Williams, and R. I. Jaffee, *The Effect of Composition on the Mechanism of Stress-Corrosion Cracking of Titanium Alloys in $N_2O_4$, and Aqueous and Hot-Salt Environments*, NASA-CR-1525, Contract NASr-100(09), Battelle Mem. Inst., Columbus, Ohio, Aug. 29, 1969.
53. J. D. Boyd, "Kinetics of Subcritical Cracking of Ti-8Al-1Mo-1V in Aqueous Environments," paper presented at AIME Spring Meeting, Las Vegas, May 1970.
54. "Accelerated Crack Propagation of Titanium by Methanol, Halogenated Hydrocarbons, and Other Solutions," DMIC Memorandum 228, Battelle Mem. Inst., Columbus, Ohio, Mar. 6, 1967.
55. A. J. Sedriks and J. A. S. Green, *Stress-Corrosion Cracking of Titanium Alloys in Organic Liquids*, RIAS Technical Report 69-11, Martin-Marietta Corp., Baltimore, Md., 1969, to be published in AIChE Journal.
56. G. Sanderson, D. T. Powell, and J. C. Scully, "Metallographic Studies of the Stress Corrosion Cracking of Titanium Alloys in Aqueous Chloride Solutions," *Proceedings of Conference on Fundamental Aspects of Stress Corrosion Cracking* (R. W. Staehle et al., eds.), National Assoc. of Corrosion Eng., Houston, Texas, 1969, pp. 638-649.
57. A. J. Sedriks, J. A. S. Green, and P. W. Slattery, "Stress-Corrosion Cracking and Corrosion Behavior of Ti and Ti-Al Alloys in Methanol Iodine Solutions," *Corrosion* **24** (No. 6), 172 (1968).
58. N. D. Tomashov, R. M. Al'tovskii, and V. B. Vladimirov, "Study of the Corrosion of Titanium and Its Alloys in Methyl Alcohol Solutions of Bromine," Transl. FTD-TT 63-672/1 + 2, Translation Division, Foreign

Technology Division, Wright-Patterson AFB, Ohio, from *Korroz. Zashch. Konst. Metal. Mater.*, Moscow, USSR, 221-233a (1961).

59. S. Segawa, K. Mori, A. Takamura, and T. Shimose, "On the Stress-Corrosion Cracking of Ti and Zr in HCl-Methanol Solution," *Corrosion Eng.* 13, 214 (1964).
60. K. Mori, A. Takamura, and T. Shimose, "Stress-Corrosion Cracking of Ti and Zr in HCl-Methanol Solutions," *Corrosion* 22, 29 (1966).
61. E. G. Haney and W. R. Wearmouth, "Effect of 'Pure' Methanol on the Cracking of Titanium," *Corrosion* 25, 87 (1969).
62. B. S. Hickman, J. C. Williams, and H. L. Marcus, "Transgranular and Intergranular Stress-Corrosion Cracking of Titanium Alloys," *J. Aust. Inst. Metals* 14 (No. 3), 138 (1969).
63. M. J. Blackburn and J. A. Feeney, The Boeing Company, Seattle, Wash., unpublished work.
64. T. R. Beck, M. J. Blackburn, W. H. Smyrl, and M. O. Speidel, *Stress-Corrosion Cracking of Titanium Alloys: Electrochemical Kinetics, SCC Studies With Ti:8-1-1, SCC and Polarization Curves in Molten Salts, Liquid Metal Embrittlement, and SCC Studies With Other Titanium Alloys*, Contract NAS 7-489, Quarterly Progress Report 14, The Boeing Company, Seattle, Wash., Dec. 1969.
65. H. R. Herrigel, "Titanium U-Bends in Organic Liquids: Effect of Inhibitors," in "Accelerated Crack Propagation of Titanium by Methanol, Halogenated Hydrocarbons, and Other Solutions," DMIC Memorandum 228, Battelle Mem. Inst., Columbus, Ohio, Mar. 6, 1967, p. 16.
66. G. Sandoz, "Effects of Some Organics on the Stress Corrosion Susceptibility of Some Organics on the Stress Corrosion Susceptibility of Some titanium Alloys," in "Accelerated Crack Propagation of Titanium by Methanol, Halogenated Hydrocarbons, and Other Solutions," DMIC Memorandum 228, Battelle Mem. Inst., Columbus, Ohio, Mar. 6, 1967, p. 10.
67. G. Sandoz, "Subcritical Crack Propagation in Ti-8Al-1Mo-1V Alloy in Organic Environments, Salt Water, and Inert Environments," *Proceedings of Conference on Fundamental Aspects of Stress Corrosion Cracking*, (R. W. Staehle et al., eds.), National Assoc. Corrosion Eng., Houston, Texas, 1969, p. 684.
68. K. E. Weber, J. S. Fritzen, D. S. Cowgill, and W. C. Gillchriest, "Similarities in Titanium Stress-Corrosion Cracking Processes in Salt Water and in Carbon Tetrachloride," in "Accelerated Crack Propagation of Titanium by Methanol, Halogenated Hydrocarbons, and Other Solutions," DMIC Memorandum 228, Battelle Mem. Inst., Columbus, Ohio, Mar. 6, 1967, p. 39.
69. C. C. Seastrom and R. A. Gorski, "The Influence of Flurocarbon Solvents on Titanium Alloys," in "Accelerated Crack Propagation of Titanium by Methanol, Halogenated Hydrocarbons, and Other Solutions," DMIC

Memorandum 228, Battelle Mem. Inst., Columbus, Ohio, Mar. 6, 1967, p. 20.

70. S. V. Glorioso, "Lunar Module Pressure Vessel Operating Criteria," Specification SE-V-0024, NASA/MSC, Houston, Texas, Oct. 1968.
71. C. F. Tiffany and J. N. Masters, *Investigation of the Flaw Growth Characteristics of Ti-6Al-4V Titanium Used in Apollo Spacecraft Pressure Vessels*, NASA CR-65586, The Boeing Company, Seattle, Wash., Mar. 1967.
72. C. F. Tiffany, J. N. Masters, and W. D. Bixler, *Flaw Growth of 6Al-4V Titanium in a Freon TF Environment*, Final Report, NASA Contract 9-8809, The Boeing Company, Seattle, Wash., Apr. 1969.
73. S. P. Rideout, M. R. Louthan, and C. L. Selby, "Basic Mechanisms of Stress-Corrosion Cracking of Titanium," *Stress Corrosion Cracking of Titanium*, ASTM STP 397, Amer. Soc. Testing Mater., Philadelphia, Pa., 1968, p. 137.
74. R. S. Ondrejcin, *Chlorine Gas and Fluoride Ion in Hot-Salt Stress-Corrosion Cracking of Titanium-Aluminum Alloys*, Report DP(NASA)-1179, E. I. du Pont de Nemours and Co., Savannah River Laboratory, Aiken, S.C. (1969).
75. H. L. Logan, "Studies of Hot-Salt Cracking of the Titanium-8%Al-1%Mo-1%V Alloy," *Proceedings of Conference on Fundamental Aspects of Stress Corrosion Cracking* (R. W. Staehle et al., eds.), National Assoc. Corrosion Eng., Houston, Texas, 1969, p. 662.
76. H. L. Logan, M. J. McBee, G. M. Ugiansky, C. J. Bechtoldt, and B. T. Sanderson, "Stress-Corrosion Cracking of Titanium," *Stress-Corrosion Cracking of Titanium*, ASTM STP 397, Amer. Soc. Testing Mater., Philadelphia, Pa., 1966, p. 215.
77. S. P. Rideout, R. S. Ondrejcin, M. R. Louthan, and D. E. Rawl, "The Role of Moisture and Hydrogen in Hot-Salt Cracking of Titanium Alloys," *Proceedings of Conference on Fundamental Aspects of Stress Corrosion Cracking*, (R. W. Staehle et al., eds.), National Assoc. Corrosion Eng., Houston, Texas, 1969, p. 650.
78. G. J. Heimerl, D. N. Braski, D. M. Royster, and H. B. Dexter, "Salt Stress Corrosion of Ti-8Al-1Mo-1V Alloy Sheet at Elevated Temperatures," *Stress-Corrosion Cracking of Titanium*, ASTM STP 397, Amer. Soc. Testing Mater., Philadelphia, Pa., 1966, p. 194.
79. S. P. Rideout, R. S. Ondrejcin, and M. R. Louthan, Jr., "Hot-Salt Stress-Corrosion Cracking of Titanium Alloys," *The Science, Technology, and Application of Titanium* (R. I. Jaffee and N. E. Promisel, eds.) New York, Pergamon Press, 1970, p. 307.
80. H. R. Gray, "Hot-Salt Stress Corrosion of a Titanium Alloy: Generation of Hydrogen and Its Embrittling Effect," *Corrosion* **25**, 337 (1969).
81. W. K. Boyd, "Stress-Corrosion Cracking of Titanium and Its Alloys," *Proceedings of Conference on Fundamental Aspects of Stress Corrosion*

*Cracking*, (R. W. Staehle et al., eds.). National Assoc. Corrosion Eng., Houston, Texas, 1969, p. 593.

82. V. C. Petersen, "Hot-Salt Stress Corrosion of Titanium: A Review of the Problem and Methods for Improving the Resistance of Titanium," paper presented at AIME Spring Meeting, Las Vegas, May 1970.
83. J. D. Jackson and W. K. Boyd, "Corrosion of Titanium," DMIC Memorandum 218, Battelle Mem. Inst., Columbus, Ohio, Sept. 1, 1966.
84. Hercules Incorporated, Hercules, California, private communication.
85. J. D. Jackson, W. K. Boyd, and R. W. Staehle, "Stress Corrosion of Ti-6Al-4V in Liquid Nitrogen Tetroxide," DMIC Technical Note, Defense Metals Information Center, Battelle Mem. Inst., Columbus, Ohio, Apr. 11, 1966.
86. C. F. Tiffany, J. N. Masters, and R. C. Shah, "Fracture Mechanics Assessment of Apollo Launch Vehicle and Spacecraft Pressure Vessels," Boeing Document No. D2-114248-1, The Boeing Company, Seattle, Wash., Jan. 1969.
87. W. Smyrl and M. J. Blackburn, to be published.
88. H. A. Johnson, "Stress Cracking of Titanium," Technical Memorandum WCRT TM56-97, Wright Air Development Center, Wright-Patterson AFB, Ohio, 1956.
89. W. M. Robertson, "Embrittlement of Titanium by Liquid Cadmium," *Met. Trans.* 1, 2607 (1970).
90. A. R. C. Westwood, C. M. Preece, and M. H. Kamadar, "Adsorption-Induced Brittle Fracture in Liquid Metal Environments," to be published in *A Treatise on Brittle Fracture*, (H. Liebowitz, ed.). New York, Academic Press.
91. D. N. Fager and W. F. Spurr, "Solid Cadmium Embrittlement: Part I Titanium Alloys," Boeing Document D6-22691, The Boeing Company, Seattle, Wash., undated.
92. *Nuclear Fuels and Materials Development*, 2d ed., Report TID-11295, USAEC, Washington, D.C., Sept. 1962
93. J. B. Hollowell, J. G. Dunleavy, and W. K. Boyd, "Liquid-Metal Embrittlement," DMIC Technical Note, Battelle Mem. Inst., Columbus, Ohio, Apr. 9, 1965.
94. R. E. Duttweiler, R. R. Wagner, and K. C. Antony, "An Investigation of Stress-Corrosion Failures in Titanium Compressor Components," *Stress-Corrosion Cracking of Titanium*, ASTM STP 397, Amer. Soc. Testing Mater., Philadelphia, Pa., 1966, p. 152.
95. G. Martin, "Investigation of Long-Term Exposure Effects Under Stress of Two Titanium Structural Alloys," *Stress-Corrosion Cracking in Titanium*, ASTM STP 397, Amer. Soc. Testing Mater., Philadelphia, Pa., 1966, p. 95.
96. D. N. Braski, "Preliminary Investigation of Effect of Environmental Factors on Salt Stress-Corrosion Cracking of Ti-8Al-1Mo-1V at Elevated

Temperatures," Technical Memorandum TMX-1048, NASA, Langley Research Center, Langley Station, Hampton, Va., Dec. 1964.

97. R. E. Adams and E. von Tiesenhausen, "Study of Stress Cracking of Commercial Titanium Alloys," *Proceedings of Conference on Fundamental Aspects of Stress Corrosion Cracking*, (R. W. Staehle et al., eds.), National Assoc. Corrosion Eng., Houston, Texas, 1969, p. 691.
98. R. S. Ondrejcin and M. R. Louthan, *Role of Hydrogen Chloride in Hot-Salt Stress-Corrosion Cracking of Titanium-Aluminum Alloys,* Report DP(NASA)-1130, E. I. du Pont de Nemours and Co., Savannah River Lab., Aiken, S.C., Dec. 1967.
99. D. N. Williams and D. J. Maykuth, *Reactions of Titanium with Gaseous Hydrogen at Ambient Temperatures*, DMIC Technical Note, Battelle Mem. Inst., Columbus, Ohio, Feb. 4, 1966.
100. D. N. Williams, B. G. Koehl, and E. S. Bartlett, "The Reaction of Titanium with Hydrogen Gas at Ambient Temperatures," *J. Less-Common Metals* **19**, 385 (1969).
101. R. J. Walter and W. T. Chandler, *Effects of High-Pressure Hydrogen on Metals at Ambient Temperatures*, Final Report NAS 8-19, NASA, Oct. 1969.
102. H. L. Marcus, B. S. Hickman, J. C. Williams, G. Garmong, and P. Stocker, "Slow Crack Growth in Ti Alloys Exposed to Low Pressures of $H_2$ Gas," paper presented at AIME Spring Meeting, Las Vegas, May 1970.
103. R. J. Walter and W. T. Chandler, "Metallography of Alloys Fractured in Gaseous Hydrogen Environments," paper presented at AIME Spring Meeting, Las Vegas, May 1970.
104. H. G. Nelson and D. P. Williams, "Environmental Hydrogen Embrittlement of Ti-6Al-4V," paper presented at AIME Spring Meeting, Las Vegas, May 1970.
105. J. R. Ambrose and J. Kruger, "The Stress Corrosion of Ti and Ti-8Al-1Mo-1V in Methanol Vapour," *Corrosion Sci.* **8**, 119 (1968).
106. A. J. Sedriks, P. W. Slattery, and E. N. Pugh, "Stress Corrosion Cracking of Alpha Titanium in Non Aqueous Environments," in *Proceedings of Conference on Fundamental Aspects of Stress Corrosion Cracking* (R. W. Staehle et al., eds.) National Assoc. Corrosion Eng., Houston, Texas, 1969, p. 673.
107. G. Sanderson and J. C. Scully, "The Stress Corrosion of Ti Alloys in Methanolic Solutions," *Corrosion Sci.* **8** (No. 7), 541 (1968).
108. I. R. Lane and J. L. Cavallaro, "Metallurgical and Mechanical Aspects of the Sea-Water Stress Corrosion of Titanium," *Applications Related Phenomena in Titanium Alloys*, ASTM STP 432, Amer. Soc. Testing Mater., Philadelphia, Pa., 1968, p. 147.
109. J. L. Cavallaro and R. C. Wilcox, "The Embrittlement of Ti-7Al and Ti-8Al Alloys in Sea Water," paper presented at AIME Spring Meeting, Las Vegas, May 1970.

110. S. R. Seagle, R. R. Seeley, and C. S. Hall, "The Influence of Composition and Heat Treatment on the Aqueous Stress Corrosion of Titanium," *Applications Related Phenomena in Titanium Alloys*, ASTM STP 432, Amer. Soc. Testing Mater., Philadelphia, Pa., 1968, p. 170.
111. G. Raucher, The Boeing Company, private communication.
112. T. L. MacKay, C. B. Gilpin, and N. A. Tiner, "Stress-Corrosion Cracking of Titanium Alloys at Ambient Temperatures in Aqueous Solutions," Contract NAS 7-488, Report SM-49105-F1, McDonnell Douglas Corp. Santa Monica, Cal., July 1967.
113. P. Finden, "Comparative Data Titanium Alloy Screening Tests," Boeing Document No. D6-24541-TN, The Boeing Company, Seattle, Washington.
114. J. C. Williams, H. L. Marcus, and B. S. Hickman, "The Influence of Microstructure on the Stress Corrosion Susceptibility of Titanium Alloys," in *Stress Corrosion Mechanisms in Titanium Alloys* (R. F. Hochman and J. C. Scully, eds.), to be published by National Assoc. Corrosion Eng.
115. T. R. Beck and M. J. Blackburn, *Stress-Corrosion Cracking of Titanium Alloys: SCC of Titanium: 8%Mn Alloy; Pitting Corrosion of Aluminum and Mass-Transport-Kinetic Model for SCC of Titanium*, Progress Report 7, Contract NAS 7-489, The Boeing Company, Seattle, Wash., Apr. 1968.
116. L. R. Hall and R. W. Finger, *Stress Corrosion Cracking of Tank Materials*, Final Report Contract NAS 3-12003, The Boeing Company, Seattle, Wash., 1971.
117. R. H. Olsen, R. R. Boyer, H. A. Moreen, A. L. Wingert, W. E. Quist, W. F. Spurr, F. L. Parkinson, and P. Finden, "Metallurgical and Fractographic Analysis of Ti-6Al-4V," Boeing Document MLER G-8842-70-24 (Part I), The Boeing Company, Dec. 1970.
118. R. R. Boyer, H. A. Moreen, R. H. Olsen, and A. L. Wingert, "Metallurgical and Fractographic Analysis of Ti-6Al-4V," Boeing Document MLER 6-8842-71-3 (Part II), Boeing Company, Feb. 1971.
119. H. R. Smith, data reported in "ARPA Coupling Program on Stress-Corrosion Cracking (Seventh Quarterly Report)", NRL Memorandum Report 1941, Oct. 1968, p. 14.
120. J. V. Scanlan and G. J. Chambers, "Forgings in Titanium Alloys." *The Science, Technology, and Application of Titanium* (R. I. Jaffee and N. E. Promisel, eds.), New York, Pergamon Press, 1970, p. 79.
121. J. B. Guernsey, V. C. Petersen, and F. H. Froes, "The Characteristics and Properties of a Heat Treatable Beta Titanium Alloy, Beta III," to be published in Metallurgical Transactions.
122. P. T. Finden, The Boeing Company, Seattle, private communication.
123. R. E. Curtis and P. T. Finden, "Titanium Alloy Development," Boeing Document D6-22997-1, The Boeing Company, Seattle, Wash., July 1969.
124. J. C. Williams, "Some Observations on the Stress-Corrosion Cracking of Three Titanium Alloys," *Trans. Amer. Soc. Metals* **60**, 646 (1967).

125. D. A. Meyn and G. Sandoz, "Fractography and Crystallography of Subcritical Crack Propagation in High-Strength Titanium Alloys," *Trans. AIME* **245**, 1253 (1969).
126. R. W. Staehle, "Comments on the History, Engineering, and Science of Stress Corrosion Cracking," *Proceedings of Conference on Fundamental Aspects of Stress Corrosion Cracking* (R. W. Staehle et al., eds.), National Assoc. Corrosion Eng., Houston, Texas, 1969, p. 3.
127. Discussion by W. W. Gerberich and J. Katz of paper by D. T. Powell and J. C. Scully in *Fracture 1969: Proceedings of the Second International Conference on Fracture*, (P. L. Pratt, ed.), Chapman and Hall, London, 1969, p. 919.
128. D. A. Meyn, "Effect of Crack Tip Stress Intensity on the Mechanism of Stress-Corrosion Cracking of Titanium-6Al-4V in Methanol," *Corrosion Sci.* **7**, 721 (1967).
129. D. N. Fager, "Methanol Cracking of Titanium 8Al-1Mo-1V," *Corrosion Sci.* **10**, 175 (1970).
130. J. C. Scully and D. T. Powell, "The Stress Corrosion Cracking Mechanism of α-Titanium Alloys at Room Temperature," *Corrosion Sci.* **10**, 719 (1970).
131. R. V. Turley and C. H. Avery, "Elevated-Temperature Static and Dynamic Sea-Salt Stress Cracking of Titanium Alloys," *Stress-Corrosion Cracking of Titanium*, ASTM STP 397, Amer. Soc. Testing Mater., Philadelphia, Pa., 1966, p. 1.
132. D. E. Piper and D. N. Fager, "The Relative Stress-Corrosion Susceptibility of Titanium Alloys in the Presence of Hot Salt," *Stress-Corrosion Cracking of Titanium*, ASTM STP 397, Amer. Soc. Testing Mater., Philadelphia, Pa., 1966, p. 31.
133. M. J. Donachie, W. P. Danesi, and A. A. Pinkowish, "Effect of Salt Atmosphere on Crack Sensitivity of Commercial Titanium Alloys at 600°-900°F," *Stress-Corrosion Cracking of Titanium*, ASTM STP 397, Amer. Soc. Testing Mater., Philadelphia, Pa., 1966, p. 179.
134. R. L. Kirchner and E. J. Ripling, "The Diffusion of Corrosion Products in Hot-Salt Stress-Corrosion Cracking of Titanium," *Stress-Corrosion Cracking of Titanium*, ASTM STP 397, Amer. Soc. Testing Mater., Philadelphia, Pa., 1966, p. 230.
135. G. Sanderson and J. C. Scully, "The Stress Corrosion of Titanium Alloys in Aqueous Magnesium Chloride Solution at 154°C," *Corrosion* **24**, 75 (1968).
136. H. Schardin, "Velocity Effects in Fracture," in *Fracture* (B. L. Averback, D. K. Felbeck, G. T. Hahn, and D. A. Thomas, eds.), John Wiley, New York, 1959.
137. M. O. Speidel, "Effect of Stress and Environment on Velocity and Branching of Subcritical Cracks," presented at AIME Spring Meeting, Las Vegas, May 1970.

138. D. J. Maykuth, "Residual Stresses, Stress Relief and Annealing of Titanium and Titanium Alloys," DMIC Memorandum 523, Battelle Mem. Inst., Columbus, Ohio, July 1968.
139. D. G. Howden, J. E. Mortland, and R. E. Monroe, *Joining Technology*, Section 4, Aircraft Designers Manual for Titanium and Titanium Alloys, Technical Report AFML-TR-67-142 Air Force Material Laboratories, Mar. 1967.
140. R. W. Judy, Jr., and R. J. Goode, *Stress-Corrosion Cracking Characteristics of Alloys of Titanium in Salt Water*, NRL Report 6564, Naval Research Laboratory, Washington, D.C., July 21, 1967.

# INDEX